A CHARACTERISATION OF

THE ELECTRO-RHEOLOGICAL EFFECT

by

Douglas Alan Brooks

A dissertation submitted to the Imperial College of Science and Technology in accordance with the requirements for the degree of Doctor of Philosophy.

BIBL. LONDIN. UNIV.

MEMORANDUM

The work described in this dissertation was carried out under the auspices of the Department of Chemical Engineering and Chemical Technology of the Imperial College of Science and Technology, guided by and under the supervision of, Dr.B.J.Briscoe. The work is original except where reference is made in the text. No part of this work has been submitted for a degree at this or any other university.

ACKNOWLEDGEMENTS

I would like to take this opportunity to thank my supervisor, Dr.B.J.Briscoe, who has consistently guided, assisted and supported my efforts for the duration of this study. I would also like to thank Dr.G.C.Maitland who, during the early period of this study, acted as my supervisor.

Similar sentiments are offered to Mr A.Gerrish, my industrial supervisor, who has been a stalwart, not only during the course of this study, but during my entire involvement with the subject of electro-rheological fluids.

I am indebted to all the employees at Air-Log Limited, and in particular Mr. G.I.Bach, for offering both financially assistance and unconditional support for the entire endeavour.

To my colleague and friend, Mr.Siva Kandiah, I offer my gratitude, not only for preparing the fluid used, but for being such a conscientious scientist and the source of many ideas.

There are numerous other people who have in a variety of fashions contributed to this study, either directly in offering assistance and support or generally by promoting the field of electro-rheology. Of the many involved I would like especially mention the following, my colleague Dennis Cooper for having the patience to proof read this thesis, Gary Smith for helping construct some of the apparatus, and Oliver Miles for debugging many of the computer programmes.

Finally I would like to mention Mr.L.R.Palmer, the secretary of the Electro-Rheology Research Syndicate Limited who initially suggested the idea of studying for this degree.

This study is dedicated to all people of science who have preceded me and to all those who will succeed me.

I wish you all every success in your endeavours.

ABSTRACT

An electro-rheological (ER) fluid comprised of a lithium polymethacrylate polymer suspended in a halogenated paraffin was characterised under two flow regimes, that of Poiseuille and Couette flow. The characterisation related the electric field induced shear stress to the strength of the applied electric field, the shear rate, the temperature of the fluid, together with the water content and the volume fraction of the dispersed phase. Five water content and three volume fraction fluids were characterised.

In the case of Poiseuille flow a model was developed that related the geometry of the flow path to the induced shear stress. This enabled a further model to be developed that described the relaxation of the shear stress in this flow profile with the shear rate and enabled the behaviour in Couette flow to be correlated to that in Poiseuille flow. A small laminar shear cell was shown to provide complementary data and as such could be used for an initial appraisal of ER fluids.

It was concluded that the basic electrically induced interaction between the particles was independent of the flow regime established and consequently the physics of the interaction was assessed both from an electrical and a structural point of view. It was shown that an elementary "chain" like model coupled with an enhanced dipole-dipole interaction could be used to describe the variation of shear stress with the applied electric field. The variation caused by the shear rate could be explained using these concepts together with a structural kinematics approach. The behaviour of an ER fluid to both the electric field and shear rate could then be described by a four parameter equation.

CONTENTS

CHAPTER ONE
THE TECHNOLOGY OF ELECTRO-RHEOLOGICAL FLUIDS

		Page
1.1	Introduction	21
1.2	Structure of the Thesis	23
1.3	Objectives of the Study and the Research Conducted	25
1.4	General Features of ER Fluids	27
1.5	Some Applications of ER Fluids	33

CHAPTER TWO
THE HISTORY AND POSSIBLE MECHANISMS IN ER FLUIDS

		Page
2.1	Introduction	41
2.2	An Historical Review of ER Fluids	42
	2.2.1 The Early History of ER Fluids	42
	2.2.2 Some Early Mathematical Descriptions	46
2.3	The Electro-Rheological Phenomena	54
	2.3.1 Hydrodynamic Stresses	56
	The Effect of the Particles	56
	Concentrated Suspensions	58
	The Continuous Phase	62
	Shear Fields	63
	2.3.2 Electrical Stresses	65
	The Role of the Particles	65
	2.3.3 Polarisation Processes	70
	2.3.4 Interaction of the Particles and the Electric Field	73
	Non-Hydrodynamic Interactions	73
	Hydrodynamic Interactions	74

CHAPTER THREE
EXPERIMENTAL APPARATUS

		Page
3.1	Introduction	83
3.2	The Valve and Fluid Development Rig	84
	3.2.1 ER Fluid Flow Circuit	84
	The Motor, Controller and Pump Assembly	84
	The Electro-Rheological Valve	87
	The Hydraulic Circuit	88
	3.2.2 The Data Capture Circuit	89
	The High Voltage Power Supply	89
	The Measuring System	89
	3.2.3 The Control Computer and Software	90
	Computer	90
	Disc Drive	90
	Printer	90
	Interface and Digital to Analogue Converter	91
	Control Software	92
3.3	The Electro-Rheological Viscometer	95
	3.3.1 The Electro-Rheological Viscometer	95
	3.3.2 The Control Box and Power Supply	97
	3.3.3 The Control Computer and Software	98
	Computer Control System	98
	Interface	98
	Control Software	99
3.4	The Static Yield Rig	102
3.5	The Contraves Rheomat 115	105
3.6	The ER Fluids and their Manufacture	106
	3.6.1 Constituents	106
	The Continuous Phase	106
	The Dispersed Phase	106
	3.6.2 The Manufacturing Process	107
	3.6.3 Typical Fluid Characteristics	108

CHAPTER FOUR
EXPERIMENTAL RESULTS

		Page
4.1	Introduction	112
4.2	The Valve and Fluid Development Rig	113
	4.2.1 Reduction of Raw Data	113
	4.2.2 Reproducibility of the Results	119
	4.2.3 The Effect of the Valve Geometry	121
	4.2.4 Temperature Effects	122
	4.2.5 Fluid Composition Effects	123
	The Effect of Volume Fraction	123
	The Effect of Water Content	125
4.3	The Electro-Rheological Viscometer	126
	4.3.1 Reproducibility of the Results	126
	4.3.2 The Effect of Geometry	128
	4.3.3 Temperature Effects	129
	4.3.4 Fluid Composition Effects	130
	The Effect of Volume Fraction	131
	The Effect of Water Content	131
4.4	The Static Yield Rig	132
4.5	The Contraves Rheomat 115	134

CHAPTER FIVE
DISCUSSION OF RESULTS

		Page
5.1	Introduction	137
5.2	Modelling of Experimental Data and the Collation of the Equipment	139
5.2.1	Modelling of the Decay of the Stress with the Shear Rate	140
	A Model for Poiseuille Flow	142
5.2.2	Quality of Fit to Experimental Data	145
	The Effect of the Shear Rate Range	147
	Sensitivity and Applicability of the Model	149
	Volume Fraction Dependence	151
	Temperature Dependence	152
	Water Content Dependence	153
5.2.3	Comparison of Data form Three Experimental Devices	153
5.3	Modelling of the Electro-Rheological Effect	158
5.3.1	Chain Geometry and Chain Forces	160
5.3.2	Electrical Interactions between Particles	165
	Practical Considerations of the Electrical Interactions	173
	The Effect of Particle Size	174
5.3.3	A Model for the Electric Field Dependence of the Excess Shear Stress	176
	Electrical Multipoles	177
	Non-Linear Electric Field Effects	181
5.3.4	A Model for the Shear Rate Dependence of the Excess Shear Stress	186
	Structural Kinetic Processes in ER Fluids	190
	A Model for the Electric Field and the Shear Rate Dependence of the Excess Shear Stress	195
5.4	The Conduction Process	199

CHAPTER SIX
CONCLUSIONS

		Page
6.1	General Remarks	204
6.2	Collation of Experimental Apparatus	205
6.3	Descriptive Models of the Electro-Rheological Effect	208

APPENDIX

A1 A List of the Experiments Conducted

A2 References

A3 Figures for Chapters 4 and 5

LIST OF FIGURES

CHAPTER ONE

Figure	Title
1.1	Shear Stress versus Field Strength
1.2	Current Density versus Field Strength
1.3	Shear Stress versus Shear Rate
1.4	Current Density versus Shear Rate
1.5	Shear Stress versus Volume Fraction
1.6	Relative Viscosity versus Volume Fraction
1.7	Electro-Rheological Interactions
1.8	Schematic of Clutch Designs
1.9	4 Valve Bridge Actuator
1.10	Schematic of Damping Strut
1.11	Telescopic Vehicle Damper
1.12	Vibration Spectrum of Vehicles

CHAPTER TWO

Figure	Title
2.1	The Effect of Concentration on Particle Interaction
2.2	Schematic View of the Distribution of Particles around a Central One
2.3	Radial Distribution Function for "A" Solid "B" Concentrated and "C" Dilute Suspensions
2.4	Idealised Flow Profiles
2.5	Structural Changes in Dispersed Systems
2.6	Typical Dielectric Relaxation Process
2.7	Typical Dielectric Spectrum for Interfacial Polarisation
2.8	Motion of a Spheroid
2.9	Interaction of Hydrodynamic and Electric Fields

CHAPTER THREE

Figure	Title
3.1	Block Diagram of Flow Rig
3.2	Cross Section of an ER Valve
3.3	Software Flowchart for Flow Rig
3.4	Schematic of Electro-Rheological Viscometer
3.5	Schematic of Static Yield Rig
3.6	Schematic of Bead Mill
3.7	Particle Size Distribution

CHAPTER FOUR

The following list is divided into sections based on the test equipment with a further division based on the type of test conducted.

Figures suffixed **a** or **b** will be found in Appendix A3 at the end of the thesis.

Valve and Fluid Development Rig

	Figure	Title
Multi Run Tests	1a	Plot of Developed Pressure versus Field Strength
	1b	Plot of Developed Pressure versus Flow Rate
	2a	Plot of Shear Stress versus Field Strength
	2b	Plot of Shear Stress versus Shear Rate
	3a	Plot of Current Density versus Field Strength
	3b	Plot of Current Density versus Shear Rate
Geometry Gap	4a	Plot of Developed Pressure versus Field Strength
	4b	Plot of Developed Pressure versus Flow Rate
	5a	Plot of Shear Stress versus Field Strength
	5b	Plot of Shear Stress versus Shear Rate
	6a	Plot of Current Density versus Field Strength
	6b	Plot of Current Density versus Shear Rate
Geometry Length and Width	7a	Plot of Developed Pressure versus Field Strength
	7b	Plot of Developed Pressure versus Flow Rate
	8a	Plot of Shear Stress versus Field Strength
	8b	Plot of Shear Stress versus Shear Rate
	9a	Plot of Current Density versus Field Strength
	9b	Plot of Current Density versus Shear Rate
Temp.	10a	Plot of Shear Stress versus Field Strength
	10b	Plot of Shear Stress versus Shear Rate
	11a	Plot of Current Density versus Field Strength
	11b	Plot of Current Density versus Shear Rate
Volume Fraction 30°C	12a	Plot of Shear Stress versus Field Strength
	12b	Plot of Shear Stress versus Shear Rate
	13a	Plot of Current Density versus Field Strength
	13b	Plot of Current Density versus Shear Rate
	14a	Plot of Shear Stress versus Shear Rate
	14b	Plot of Normalised Shear Stress versus Shear Rate
	15a	Plot of Shear Stress versus Field Strength
	15b	Plot of Normalised Shear Stress versus Field Strength
	16a	Plot of Normalised Shear Stress versus Field Strength
	16b	Plot of Normalised Shear Stress versus Shear Rate
	17a	Plot of Normalised Shear Stress versus Field Strength
	17b	Plot of Normalised Shear Stress versus Shear Rate

	18a	Plot of Normalised Shear Stress versus Field Strength
	18b	Plot of Normalised Shear Stress versus Shear Rate
	19a	Plot of Normalised Shear Stress versus Shear Rate
	19b	Plot of Normalised Shear Stress versus Shear Rate
Volume	20a	Plot of Shear Stress versus Field Strength
Fraction	20b	Plot of Shear Stress versus Shear Rate
25°C	21a	Plot of Current Density versus Field Strength
	21b	Plot of Current Density versus Shear Rate
	22a	Plot of Normalised Shear Stress versus Field Strength
	22b	Plot of Normalised Shear Stress versus Shear Rate
Volume	23a	Plot of Shear Stress versus Field Strength
Fraction	23b	Plot of Shear Stress versus Shear Rate
20°C	24a	Plot of Current Density versus Field Strength
	24b	Plot of Current Density versus Shear Rate
	25a	Plot of Normalised Shear Stress versus Field Strength
	25b	Plot of Normalised Shear Stress versus Shear Rate
Volume	26a	Plot of Shear Stress versus Field Strength
Fraction	26b	Plot of Shear Stress versus Shear Rate
15°C	27a	Plot of Current Density versus Field Strength
	27b	Plot of Current Density versus Shear Rate
	28a	Plot of Normalised Shear Stress versus Field Strength
	28b	Plot of Normalised Shear Stress versus Shear Rate
Temp.	29a	Plot of Temperature versus Shear Rate
	29b	Plot of Temperature versus Shear Rate
	30a	Plot of Temperature versus Shear Rate
	30b	Plot of Temperature versus Shear Rate
Water	31a	Plot of Shear Stress versus Field Strength
Content	31b	Plot of Shear Stress versus Shear Rate
	32a	Plot of Current Density versus Field Strength
	32b	Plot of Current Density versus Shear Rate
	33a	Plot of Shear Stress versus Field Strength
	33b	Plot of Shear Stress versus Shear Rate
	34a	Plot of Shear Stress versus Field Strength
	34b	Plot of Shear Stress versus Shear Rate
	35a	Plot of Current Density versus Field Strength
	35b	Plot of Current Density versus Shear Rate
	36a	Plot of Shear Stress versus Field Strength
	36b	Plot of Shear Stress versus Shear Rate

Electro-Rheological Viscometer

	Figure	Title
Multi Run Tests	37a	Plot of Total Shear Stress versus Shear Rate
	37b	Plot of Temperature versus Shear Rate
	38a	Plot of Excess Shear Stress versus Field Strength
	38b	Plot of Excess Shear Stress versus Shear Rate
	39a	Plot of Current Density versus Field Strength
	39b	Plot of Current Density versus Shear Rate
Geometry	40a	Plot of Total Shear Stress versus Field Rotor Strength
Length	40b	Plot of Total Shear Stress versus Shear Rate
	41a	Plot of Excess Shear Stress versus Field Strength
	41b	Plot of Excess Shear Stress versus Shear Rate
	42a	Plot of Current Density versus Field Strength
	42b	Plot of Current Density versus Shear Rate
General Form of Data	43a	Plot of Total Shear Stress versus Field Strength
	43b	Plot of Total Shear Stress versus Shear Rate
	44a	Plot of Excess Shear Stress versus Field Strength
	44b	Plot of Excess Shear Stress versus Shear Rate
	45a	Plot of Current Density versus Field Strength
	45b	Plot of Current Density versus Shear Rate
Temp.	46a	Plot of Total Shear Stress versus Field Strength
	46b	Plot of Total Shear Stress versus Shear Rate
	47a	Plot of Excess Shear Stress versus Field Strength
	47b	Plot of Excess Shear Stress versus Shear Rate
Volume Fraction	48a	Plot of Total Shear Stress versus Field Strength
	48b	Plot of Total Shear Stress versus Shear Rate
	49a	Plot of Excess Shear Stress versus Field Strength
	49b	Plot of Excess Shear Stress versus Shear Rate
	50a	Plot of Current Density versus Field Strength
	50b	Plot of Current Density versus Shear Rate
	51a	Plot of Normalised Excess Shear Stress versus Field Strength
	51b	Plot of Normalised Excess Shear Stress versus Shear Rate

Water Content	52a	Plot of Total Shear Stress versus Field Strength
	52b	Plot of Total Shear Stress versus Shear Rate
	53a	Plot of Excess Shear Stress versus Field Strength
	53b	Plot of Excess Shear Stress versus Shear Rate
	54a	Plot of Current Density versus Field Strength
	54b	Plot of Current Density versus Shear Rate

Static Yield Rig and Contraves Viscometer

Figure	Title
55a	Typical Static Yield Plot
55b	Static Yield Data at Various Fields
56a	Current versus Applied Field Data from Static Rig
56b	Relaxation of Static Yield with Time
57a	Typical Viscosity-Shear Rate Curve for an ER Fluid
57b	Viscosity Temperature Characteristic
58a	Log Viscosity Curve. Data from Figure 57b
58b	Comparison of Viscosity as Measured on Three Test Rigs

CHAPTER FIVE

Figure	Title
59	Newtonian Viscosity Measured on Two Test Rigs
60a	Plot of Excess Shear Stress versus Field Strength
60b	Plot of Excess Shear Stress versus Shear Rate
61a	Fit of Proposed Model to Experimental Data
61b	Proposed Model Showing Variation Due to T_y
62a	Proposed Model Showing Variation Due to T_∞
62b	Proposed Model Showing Variation Due to T_r
63	Fit of Model Showing Overlap of Shear Rate Ranges
64a	Fit of Model to Test Data for Valve Gap of 0.516 mm
64b	Fit of Model to Test Data for Valve Gap of 0.763 mm
65a	Fit of Model to Test Data for Valve Gap of 1.012 mm
65b	Fit of Model to Test Data for Three Valve Gaps
66a	Plot of Model Fitted to Three Field Strengths
66b	Plot of Model Fitted to Three Temperatures
67a	Plot of Model Fitted to Three Volume Fractions
67b	Plot of Model Fitted to Three Water Contents
68a	Characterisation of Fluid 50LV/L35180
68b	Characterisation of Fluid 50LV/L35156
69a	Reproducibilty of Flow Data

69b Reproducibility of Fit to Zero Shear Rate Intercept
70a Reproducibility of Fit to Infinite Shear Rate Intercept
70b Reproducibility of Fit to Relaxation Coefficient
71a Mean Characterisation of Fluid Using Six Sets of Data
71b 95% Confidence Limits on Model
72a Zero Shear Rate Intercept for Three Volume Fractions
72b Infinite Shear Rate Intercept for Three Volume Fractions
73a Relaxation Coefficient for Three Volume Fractions
73b Fit of Model to Normalised Volume Fraction Data
74a Zero Shear Rate Intercept at Different Temperatures
74b Infinite Shear Rate Intercept at Different Temperatures
75a Relaxation Coefficient at Different Temperatures
75b Zero Shear Rate Intercept for Three Fluids
76a Infinite Shear Rate Intercept for Three Fluids
76b Relaxation Coefficient for Three Fluids
77a Comparison of Shear Stress from VFDR and ERV
77b Comparison of Shear Stress from VFDR and ERV
78a Comparison of Shear Stress from VFDR and ERV
78b Comparison of Shear Stress from VFDR and ERV
79a Comparison of Shear Stress from VFDR and ERV
79b Comparison of Shear Stress from VFDR and ERV
80a Comparison of Shear Stress from VFDR and ERV
80b Comparison of Shear Stress from VFDR and ERV
81a Comparison of Shear Stress from Three Test Rigs
81b Comparison of Shear Stress from Three Test Rigs
81c Comparison of Shear Stress from Three Test Rigs
82a Zero Shear Stress and Static Yield Stress versus Field Strength
82b Shear Stress Plots for VFDR and SYR
83 Inverse Particle Distance versus Volume Fraction
84 Schematic of Sphere System
85 Equipotential Surfaces Showing Zones of Mutual Attraction and Repulsion
86 Interaction forces versus Volume Fraction
87 Electric Multipole Arrangements
88 Least Squares Fit of Static Shear Stress Data
89 Least Squares Coefficients against Temperature
90 3-D Plot of 50LV/L35135 at Different Temperatures

91	Linearised Shear Stress Shear Rate Dependence
92	Particle Interaction During Shearing
93a	Fit of Excess Shear Stress Data versus Shear Rate
93b	Fit of Excess Shear Stress versus Field Strength
94a	Structural Parameter "a" versus Field Strength
94b	Structural Parameter "b" versus Field Strength
95a	Influence of Structural Parameter on Fit to Data
95b	Influence of Structural Parameter on Fit to Data
96	Experimental and Predicted 3-D Plot of Excess Shear Stress
97	Conductivity Expression Fitted to Experimental Data

LIST OF TABLES

No.	Title	Page
3.1	Table of Valve Dimensions	93
4.1	Straight Line Approximation of No Field Viscosity of ER Fluids	135
5.1	Variation of Fitting Coefficients with Valve Geometry	147
5.2	Statistical Analysis of Flow Model showing 95% Confidence Limits	151
5.3	Model Fit to Three Volume Fractions Normalised Data Also Shown	152
5.4	Electro-Rheological Viscometer Reproducibility	154
5.5	Typical Set of Data at 3.592 kV/mm	154
5.6	Static Yield Rig Reproducibility	156
5.7	Volume Fraction Effect on Particle Chain Formation	163
5.8	Normalised Shear Stress for Different Volume Fractions	164
5.9	Bond Strength for Different Volume Fractions	165
5.10	Particles in Electrode Space	168
5.11	Field Intensification Coefficients	168
5.12	Force Coefficients F_1 to F_5	169
5.13	Force Coefficients F_6 to F_{10}	170
5.14	Calculated Force of Interaction	175
5.15	Effect of Particle Size	176
5.16	Coefficients From Equation 5.36 for Various Volume Fraction Fluids	183
5.17	Coefficients From Equation 5.36 for Various Temperatures	184
5.18	Coefficients From Equation 5.36 for Various Shear Rates	185
5.19	Variation of Conductivity Parameters with Volume Fraction	203

LIST OF SYMBOLS

A_0 and A_1	Truncated multipole coefficients
C	Volume fraction
C_d	Chain density
C_s	Chain strength
E_a	Field Strength at point "a"
E_o	Applied Electric Field Strength
$E_1 \rightarrow E_3$	Field intensification coefficients
F_E	Electric field induced force
F_x	Electric interaction force in x direction
F_z	Electric interaction force in z direction
$F_1 \rightarrow F_{10}$	Force coefficients
G	Shear rate (Couette Flow)
G_p	Pressure gradient down valve (P_{tot}/L)
G_w	Wall shear rate (Poiseuille Flow)
H	Electrode spacing
H(x)	Variable at any given x
H_∞	Value of variable at infinite x
I	Current
J	Current density
L	Electrode length
N_c	Number of chains
N_v	Number of particles/unit volume V
Pa	Pressure in ram, side "a"
Pb	Pressure in ram, side "b"
Pd	Pump pressure
P_e	Field induced pressure drop
P_n	Newtonian pressure drop
P_{tot}	Total pressure drop
Q	Flow rate
Q_1 and Q_2	Charges on particles
R_b	Rotor (bob) radius
R_c	Stator (cup) radius
R_m	Mean radius $\{(R_c+R_b)/2\}$
R, R_1 & R_2	Particle radii
T_E	Electric field induced torque

T_e	Excess shear stress in Couette flow
T_n	Newtonian shear stress in Couette flow
T_r	Characteristic relaxation time
T_t	Total shear stress in Couette flow
T_x	Total stress in fluid
T_y	Shear at zero shear rate (yield stress)
T_∞	Shear stress at infinite shear rate
T(G)	Shear stress as a function of shear rate
T(G)'	Real component of shear stress
T(G)''	Imaginary component of shear stress
U	Velocity of fluid in Poiseuille flow
V_{max}	Maximum volume fraction
V_o	Applied Voltage
W	Mean valve width
X_0	Dimension of fluid plug in Poiseuille flow
X_1	Dimension of fluid plug in Poiseuille flow
$\mathbf{Y}^n$	The matrix expansion of the multipole order n
Z	Counter ion valency
a and b	Material parameters
a	Particle diameter & a mean free path
$a_0 \rightarrow a_n$	Coefficients of the multipoles, electric field non-uniformities and multipole interactions
d_x	Dipole separation distance
e	Electronic charge
g(r)	Radial distribution function
h	Particle centre distance
n_o	Number concentration
n_p	Number of particles
$^n\alpha$	The multipole polarisability of order n
p_o	Average particle density
$p(q,r_e)$	Electric parameter for a spheroid
q	Charge on a particle
q_i	The individual point charges
r	Particle radius
r_e	Equivalent hydrodynamic radius
α	The volume polarisability of the particle
$\alpha(t)$	Relaxation decay factor at time t
$\alpha(0)$	Decay factor at time 0

β	Activation energy
Γ	Structural parameter assigned to the aggregation-deformation-orientation effects
Γ_e	Equilibrium structural parameter
δ	Inter particle distance
ϵ_o	Permittivity of free space
ϵ_r	Relative permittivity
f	Electrohydrodynamic field parameter
K	Debye-Huckel screening parameter
σ	Conductivity
Φ_o	Surface potential
ϕ	Volume fraction
ϕ	Surface charge density
Ω	Rotational speed in rad/sec
ϕ_r	Force between particles
μ	Newtonian viscosity of a fluid
μ_i	Induced dipole moment
$\mu^{(n)}$	Dipole moment of order n

CHAPTER ONE

THE TECHNOLOGY OF ELECTRO-RHEOLOGICAL FLUIDS

1.1 INTRODUCTION

The potential uses of *electro-rheological (ER) fluids* are numerous and their application is expected to bring about fundamental changes in hundreds of everyday devices. When using the fluids the need for complex mechanical interfaces in many hydraulic systems and mechanical devices is removed as direct electrical control of the properties of the fluid is feasible. Braking systems[147*], robotics[152], valves[152], clutches[147], shock absorbers[147], tensioning devices[151], actuators[152], and vibration dampers[146] are applications currently being investigated. Some of the potential advantages of electro-rheological fluids are, rapid response and significant reductions in space and weight requirements, simpler designs and greater reliability. With the formation in 1982 of the Electro-Rheology Research Syndicate Limited the research in the U.K. became more formalised and it is against this background that their has been a resurgence of activity into the subject. This interest has manifested itself in both the technical[10-12] and the national press[13-15] and has also stimulated academic interest[16-18] along with a number of conferences.[151-152]

In this, the first chapter, the following four points will be covered. Initially the structure of the complete thesis will outlined in some depth. This will be followed by details of the objectives of the study and some information regarding the fluids. These particulars are

* Numbers refer to references. Details of which are in the appendix.

followed by an overview of the general features of electro-rheological fluids and the terminology used in the study is introduced. The chapter is concluded with examples of some potential applications of the fluids based upon some elementary design categories. From this chapter a general picture of the technology will have been created and the context of the thesis established.

1.2 STRUCTURE OF THE THESIS

In the remainder of this chapter, as noted in the introduction above, the general features of ER fluids and potential areas for the application of the technology are discussed. This is provided in order to establish the context of the thesis. In the following chapter, chapter two, a detailed historical review of the technology is presented and included are some particulars of the early attempts to mathematically describe the behaviour of these fluids. Attention is drawn to the confusion in terminology that is often associated with the subject**. In the remainder of the chapter the electro-rheological phenomena is discussed in detail in terms of the hydrodynamic and the electrical stresses. This is followed by a section where the polarisation processes in materials are discussed. The final part of this chapter is a discussion on the types of behaviour that result from the interaction of the hydrodynamic and the electrical fields.

Chapter three is devoted to the experimental apparatus used and a description of the electro-rheological fluids manufactured and used for this study. Two principal devices were employed to conduct the experimental studies. One, known as the *Valve and Fluid Development Rig (VFDR)*, was essentially a flow rig for the measurement of the pressure drop characteristics of an ER fluid. The flow regime established is one of *Poiseuille* flow. The other instrument used was a concentric cylinder viscometer known as the *Electro-Rheological Viscometer (ERV)*, the flow regime established being one of *Couette* flow. Two additional devices were utilised and are described. The first was a laboratory shear cell for the screening of fluids, this was known as the *Static Yield Rig*. The second was a conventional concentric cylinder viscometer. The chapter is concluded with a description of the fluids used and a detailed description of their method of manufacture.

** This is particularly apparent in the variety of names used to describe the effect, for example, Winslow fluids and electro-viscous fluids are commonly used terms.

In chapter four particulars of the data is detailed with respect to the main variables studied. These included the geometry of the apparatus, details of the basic compositional variables of the fluid, typically volume fraction and water content. Temperature and aspects of reproducibility and repeatability are also discussed. Some elementary data reduction procedures are included in this section. In the case of the data collected from the Electro-Rheological Viscometer this was a relatively straightforward procedure. For example, speed was reduced to shear rate and torque to a shear stress. In the case of the Valve and Fluid Development Rig the reduction was a little more complex. To convert pressure drops and flow rates into shear stresses and shear rates an assumption was required as to the flow profile along the flow path. This involves some mathematics and has, therefore, been dealt with in some detail.

The discussion of the results, covered by chapter five, has been sub-divided into three sections. In section one data from the experimental apparatus was examined and a method is proposed to enable the behaviour to be consolidated independent of the flow regime established. The second section explored the particle interactions from a structural and an electrical standpoint before these were merged into a general empirical description of the behaviour of the fluids. This empirical expression is related to the some basic physical processes that are considered to occur in the fluid. In the final section a method for the description of the conduction process is outlined. The process discussed is consistent with the physics detailed in the previous section.

The conclusions are drawn in chapter six and several items are collected in the appendix. Included was a list of the experiments conducted on each device, a fully detailed list of the references cited and the majority of the graphically presented experimental data.

1.3 OBJECTIVES OF THE STUDY AND THE RESEARCH CONDUCTED

The work to be described has three primary scientific objectives:-

a) To characterise the rheology of a range of electro-rheological fluids in Couette and Poiseuille flow.

b) To identify the physical parameters relevant to an understanding of the behaviour and to quantify their relation to the electro-rheological characteristics.

c) To use these results to assess the applicability of a simple laboratory shear cell.

The experimental studies described covered a range of shear rates, fluid temperatures, fluid compositions and applied electric field strengths. Each fluid has been evaluated in the three experimental devices, the Valve and Fluid Development Rig (VFDR), the Electro-Rheological Viscometer (ERV) and the Static Yield Rig (SYR). Additional data is provided from other equipment, notably a conventional concentric cylinder viscometer.

Seven fluid compositions were studied and provided the main body of experimental data. In addition data were collected from two additional compositions to augment the presentation. Data was also available from a number of additional fluids that have been studied. The seven fluids are coded on the basis of the continuous phase, the dispersed phase, the dispersed phase volume fraction and its water content. For example the code *50LV/L35156* refered to a continuous phase designated *50LV*, which is in practice a chlorinated paraffin, Cereclor 50LV***, and a dispersed phase designated *L* which has a

*** An ICI Product

volume fraction of *35%* and a water content of *15.6%*. The seven ER fluids used consisted of three volume fractions 30%, 35% and 40% all of water content 18.0% and five water contents of 13.5%, 15.6%, 15.7%, 16.6% and 18.0%, each of 35% volume fraction.

Experiments were carried out in the flow apparatus, the VFDR, on each of the fluids. The number of experiments varied with each composition but essentially three main valve geometries and four temperatures were assessed, data were collected on one fluid with additional geometries. In all 82 separate flow experiments were conducted. The applied electric field was varied from 0 to 3.0 kV/mm although some experimental work was carried out at higher field strengths.

The above fluids were also studied in the Couette apparatus, the ERV, at five different temperatures. The electrical field strength range used was that of the VFDR experiments, 0 to 3.0 kV/mm, and the shear rate range used was from 0 to 3000 sec^{-1}. A total of 48 experiments were carried out.

Finally, a study was also carried out on the SYR and the Contraves viscometer using each of the fluids.

1.4 GENERAL FEATURES OF ER FLUIDS

Electro-rheological (ER) fluids consist of micron sized particles suspended in an electrically insulating continuous phase. They exhibit the property of altering their flow behaviour when subjected to an electric field (E_0). The change that is produced is reversible and occurs in the order of milliseconds. It is from a viscous fluid like state to a plastic semi-solid like state. The particles are generally believed to structure under the influence of the electric field and the assembly created thus develops "solid like" properties. The principle electric field induced structural property is conventionally termed the *yield or excess shear stress*[****], although the more colloquial term, *strength of the fluid*, is often used. It is the ability of the electrically stressed fluid to withstand applied external forces without rupture. The primary requirement of the two main constituents, the continuous and dispersed phases, is that the continuous phase, usually an oil, is a good electrical insulator whilst the particles, or dispersed phase, must possess the ability to electrically polarise in the applied electric field. Polarisation can be achieved by a number of processes and in the case of the fluids discussed in this work is probably due to ion migration through the particle. To achieve this effect a quantity of water is added to the particle and it is hence necessary for the dispersed phase to be hydrophilic in nature. If an alternative method of polarising the particle is adopted, such as electron migration, essentially water free ER fluids can be formulated[1]. The quantity of dispersed phase, expressed on a volume fraction basis, is typically 20% to 40% whilst the water content varies from 10% to 20% of the dispersed phase. These are typical values and the exact quantities will depend upon a number of factors which include the

[****] Throughout this thesis the yield stress is taken to be the stress when the shear rate is zero, that is, the intercept value on the shear stress versus shear rate plots. The excess shear stress is the additional component of stress due to the applied field. It is present at any shear rate.

usage to which the ER fluid is to be put and the chemical nature of the dispersed phase.

The ER effect is both reversible and electric field strength dependent. That is low fields give low yield stresses and high fields give high yield stresses with a continuous smooth transition between the two extremes. An electric current is observed to flow through the fluid when it is subjected to the electric field. This current, which is also electric field strength dependent, is non ohmic in character. The characteristic form of both the shear stress and current dependence are shown schematically in figures 1.1 and 1.2. The trends depicted are typical and the exact forms are dependent upon a number of factors including composition and temperature. The points to be noted in figure 1.1 are the initial curvature at low field strengths with a transition to a more linear form at higher fields. Electric fields less than 1.0 MV/m (1.0 kV/mm)***** are considered "low" whereas the "high" field region extends from about 2.0 kV/mm upwards. The upper limit of field strength, with careful electrode design and a suitable choice of ER fluid can be as high as 10 to 12 kV/mm. However, with such field strengths severe practical difficulties are imposed and a more realistic level is believed to be 3 to 4 kV/mm. The current density, viz figure 1.2, is exponential in form with typical values of current density at room temperature and at 3.0 kV/mm being in the order of 100-500 A/m^2 (1-5 $\mu A/cm^2$). In addition, to withstanding forces under static conditions, that is, when no shearing occurs, the electric field induced strength fluids is also retained when shear is applied; to a first approximation they resemble Bingham fluids. The shear rate dependence of the stress shear is also electric field strength dependent and thus the classic Bingham fluid behaviour is not retained. Figure 1.3 shows a linerised form of this behaviour in schematic outline. The behaviour

***** S.I. units are used for the first occurrence. Following this more practical unit are used. For example MV/m becomes kV/mm.

with no applied electric field is essentially Newtonian but as the electric field strength is increased the rate of change of shear stress with shear rate becomes less positive and eventually becomes negative. This does not imply that the viscosity is negative, rather that the additional component of shear stress due to the applied electric field depends upon both the electric field *and* the shear rate. This additional component is defined as the *excess shear stress*, it is the total shear stress at any given shear rate minus the Newtonian shear stress at the same shear rate. It can be deduced from figure 1.3 that the excess shear stress falls with shear rate and that the excess shear stress is dependent upon a dynamic structural balance. A balance, that is, between the forces holding the structure together, derived from the electric field, and the forces destroying the structure, derived from the shear forces. If figure 1.4 is considered it can be seen that the current is also dependent on the shear rate. It is decreased as the shear rate is increased. The "strength" of the structure can be increased by strengthening the interaction between the particles or by increasing the concentration of the particles. The dependence of the ER effect on the concentration is shown, in outline, in figure 1.5. The increased concentration naturally has consequences, primarily in the Newtonian flow properties. This is depicted in figure 1.6 which shows the relative viscosity plotted against the volume fraction.

The properties described above are the most important group, although for the hydrophilic polymer based fluids, the water content is also a significant variable. Other factors play roles of varying importance. Temperature, for example, does not significantly alter the yield stress but has a significant influence on the conductivity. It is probably this feature, the rapid rise in current consumption with temperature, that currently places a limit on the practical application of ER fluids. Of equal importance in many applications are the dynamic capabilities of the fluids.

ELECTRO-RHEOLOGICAL FLUID PARAMETERS

Shear Stress vs.Field Strength

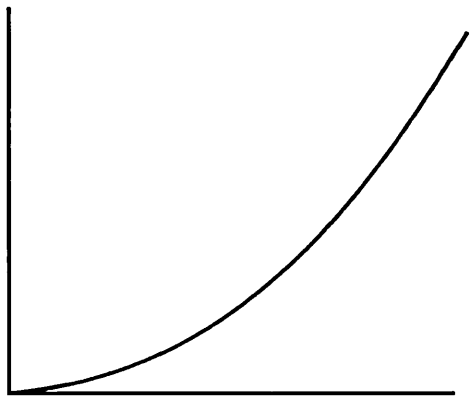


Figure 1.1

Current Density vs.Field Strength

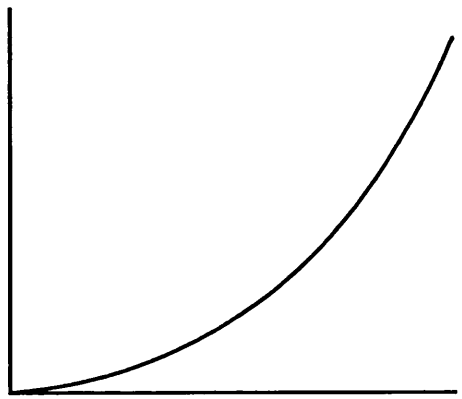


Figure 1.2

Shear Stress vs.Shear Rate

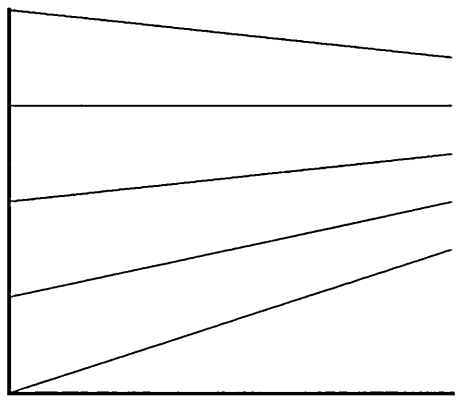


Figure 1.3

Current Density vs.Shear Rate

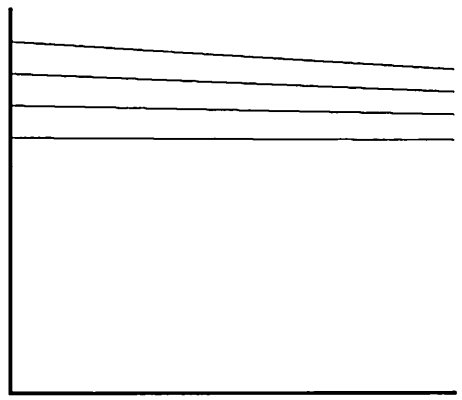


Figure 1.4

Shear Stress vs.Volume Fraction

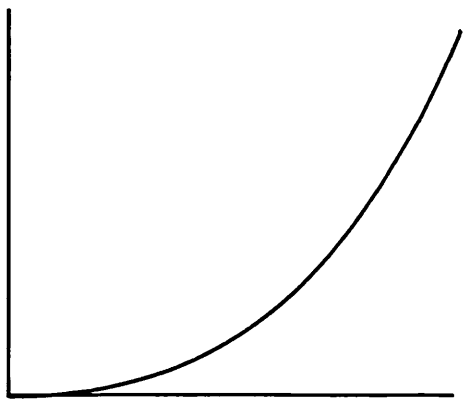


Figure 1.5

Relative Viscosity vs.Volume Fraction

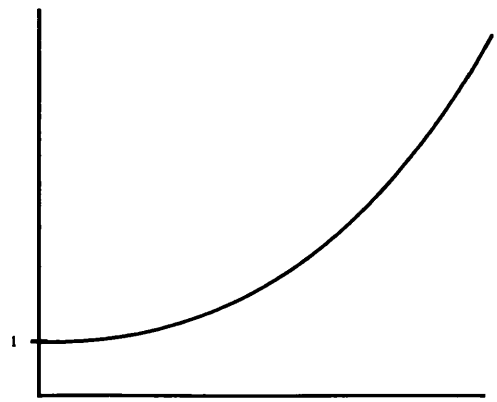


Figure 1.6

Some modulation of the applied electric field to induce a corresponding variation in the ER strength is required in many applications. The change results in an alteration of transmitted torque, developed pressure or damping characteristics. Knowledge of the rate at which such changes can be effected is necessary. This is important from both the mechanical design of the device and the design of the power supply to drive the device. The latter aspect is reflected in the fact that any ER device will exhibit some capacitance and any changes in the dielectric constant with frequency will alter this capacitance.

It is apparent that there are many factors of significance in the investigation and application of ER fluids and, in figure 1.7, a global overview of these factors and their interaction is presented. Not only is the range extensive, data and techniques are also required from a number of disciplines in order to provide a basic understanding of the phenomena involved.

There is now a broad acceptance of the merits of a polarisation mechanism that creates the electrostatic interactions which form a three dimensional matrix structure that resists applied stresses. The problem of defining the electrostatic interaction is complicated due to the complex surface properties of the dispersed phase, the mutually induced polarisation of the particles and the structural complexity of a concentrated suspension. To tackle the problem either the micro-rheology can be investigated so that the force of interaction between the dispersed particles can be calculated. This can then be summated across the suspension and the rheological behaviour of the system obtained. Or, alternatively, the study can be directed at the macro-rheology of the suspensions and the character of the micro-rheology deduced. The advantage of the second approach is that data are generated that are directly applicable to engineering applications. In practice both routes are followed simultaneously as any understanding that is developed must be consistent with both approaches.

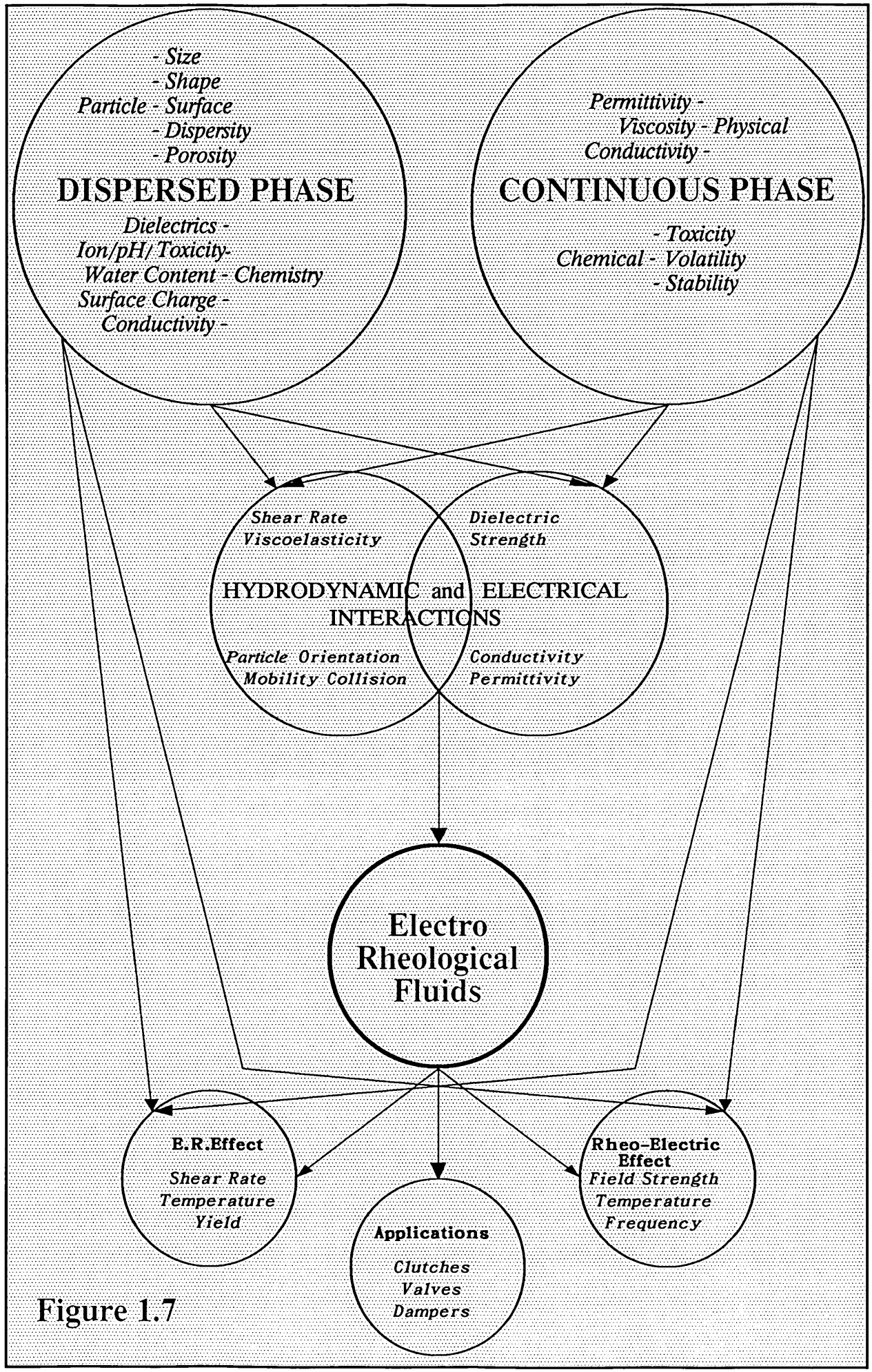

- Size
- Shape
Particle - Surface
- Dispersity
- Porosity
DISPERSED PHASE
Dielectrics -
Ion/pH/ Toxicity-
Water Content - Chemistry
Surface Charge -
Conductivity -
Permittivity -
Viscosity - Physical
Conductivity -
CONTINUOUS PHASE
- Toxicity
Chemical - Volatility
- Stability
Shear Rate
Viscoelasticity
Dielectric
Strength
HYDRODYNAMIC and ELECTRICAL
INTERACTIONS
Particle Orientation
Mobility Collision
Conductivity
Permittivity
Electro
Rheological
Fluids
E.R.Effect
Shear Rate
Temperature
Yield
Applications
Clutches
Valves
Dampers
Rheo-Electric
Effect
Field Strength
Temperature
Frequency

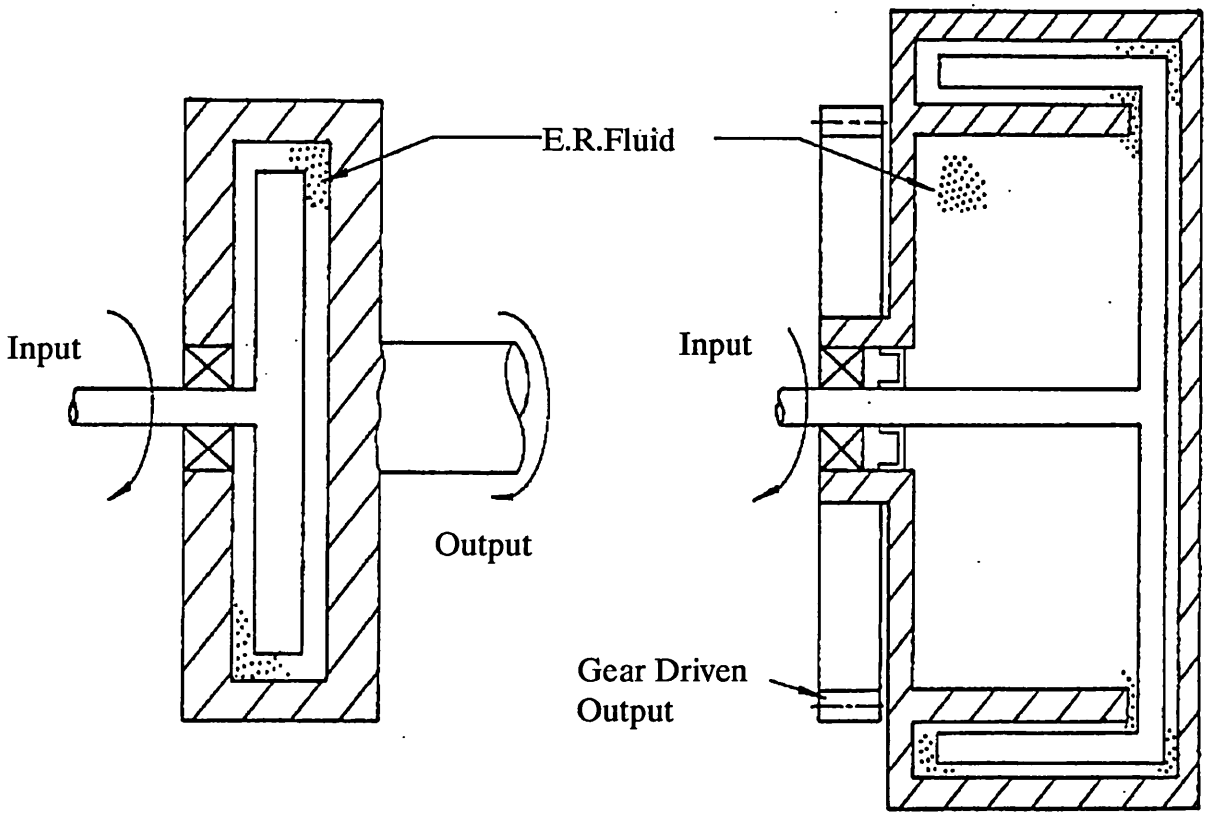
Figure 1.7

1.5 SOME APPLICATION OF ER FLUIDS

The consideration of the engineering modes of operation is more readily facilitated if they are classified into four main types, static situations, clutches type devices, flow based systems and damping applications. The static mode of operation is where the fluid is contained and offers either a low Newtonian resistance or a high electric field induced resistance to motion. If the yield stress of the fluid is exceeded by the applied stress or the applied electric field is removed the structure fails and an action can be performed. Typical devices in this category are release mechanisms and programmable safety catches. This mode of operation is usually termed the *Static Mode*. The second mode is where the fluid is constrained and sheared. This is termed the *Clutch Mode* of operation where Couette flow is usually established. The final detailed design of a clutch will depend on a number of factors which do not materially affect the basic concept of clutch devices and will not therefore be considered here. Two configurations are usually considered, that of the concentric cylinder and that of the parallel plate. Both schemes are shown in figure 1.8. Either design relies on the induced shear stress of the fluid to transmit a torque. The magnitude of the torque transmitted is a function of the shear stress and the clutch plate area and in the case of the concentric cylinder device it is also a function of the cylinder diameter. The minimum torque transmitted is the viscous torque and the maximum is that due to the maximum yield strength of the fluid plus the viscous torque. It should be noted that it is quite feasible to adjust the relative motion of the driven plate from zero, assuming the viscous torque to be insufficient for any transmitted motion, to the speed of the driver plate, that is a fully engaged position, entirely through electrical control of the fluid state. Evidently one can control the speed or control the

torque[129] and this depends on the variable chosen as the feedback element in the control circuit. As the engagement of the clutch is electrical, as is the control circuit, there is no requirement for any mechanical interface. The salient point in clutch designs is that the fluid is continuously sheared. It is also apparent that as a condition of zero shear rate is approached the behaviour approximates the static case.

Figure 1.8 Schematic of Clutch Designs

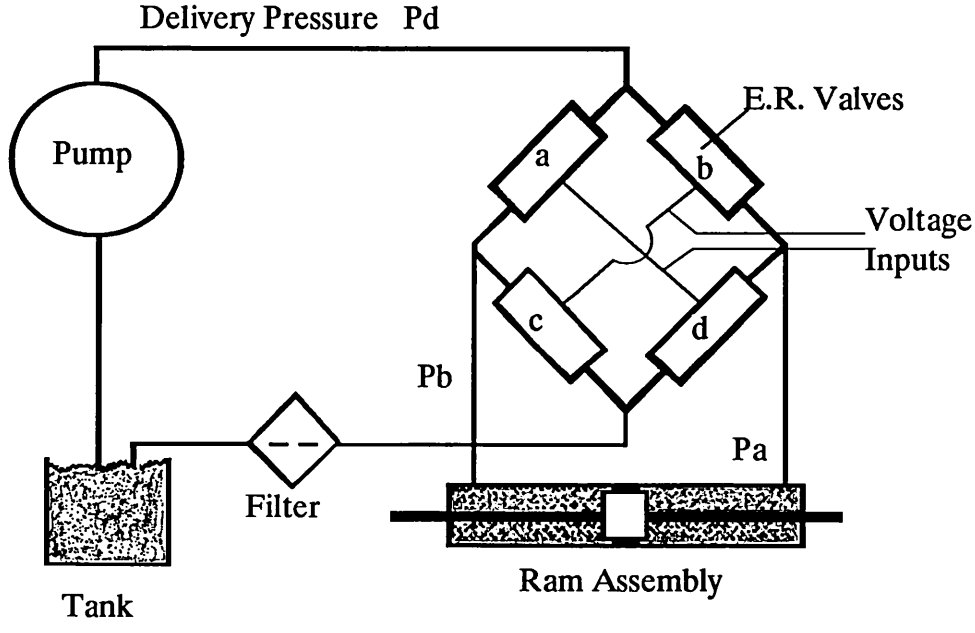


Parallel Plate Design

Concentric Cylinder Design

The next classification is where the fluid is forced around a system, usually by a pump, through a flow restriction. The flow geometry used is often an annular design with dimensions such that the flow regime can be taken as plane parallel or Poiseuille flow. The control element in this case is normally termed a valve and consequently the descriptive term often used is the *Valve Mode*. An electro-rheological valve will provide a restriction to the passage of the fluid due to the Newtonian pressure drop and the component induced by the electric field. For systems in which ER valves are used an external source to create the flow is required, ER valves are used to control this flow, the flow restriction created results in an increased pressure upstream of the valve and this in turn can be used to perform some action. The simplest arrangement that can be considered is a basic four valve bridge arrangement as shown in figure 1.9.

Figure 1.9 4 Valve Bridge Actuator



If the bridge is balanced with equal voltages on each of the four valves the pressure drop down each valve is the same and no differential pressure is generated across the piston, or ram, i.e. Pa=Pb. If the voltage on valves "a" and "d" is increased the bridge balance is upset and an increased pressure occurs which is met by the pump, Pd. If at the same time the voltage is removed from valve "b" and "c" the fluid can readily flow out of the low pressure side of the ram to the tank. In this case Pa>Pb and the piston will be moved to the left. If the reverse voltage condition is made, "a" and "d" low with "b" and "c" high, motion is in the opposite direction as Pb>Pa. The ER valves can be local to the ram or remote with conventional hydraulic connections. Both arrangements have been manufactured and evaluated. Control can be exercised over the position, velocity or the thrust developed, with a conventional feedback control circuit similar to the clutch design. The advantages are the same in that the control is totally electronic. The thrust generated is the product of the piston area and the developed pressure and as it is feasible for pressure drops in the region of 60 Bar (1,000 psi) to be produced down a valve of some 100 cm (4 in) length significant thrusts can be developed. Of considerable interest in this mode is the speed at which this pressure reversal can be induced. The fluids can be caused to change their state in a few milliseconds. It has been demonstrated that pressures of 40 to 60 Bar can be modulated at frequencies in the order of 200 to 300 Hz[19]. Through careful design a high frequency vibrator[151] has been built and subsequently evaluated to explore the limitations of the frequency of the fluid. The vibrator operated from dc to a frequency of 1,000 Hz and was capable of thrusts in the order of 90,000 N (20,000 lbf).

Other work has been conducted on the control of ER actuator systems using different forms of high voltage signalling techniques. Typically, pulse width modulated (PWM) and linear systems have been evaluated. Applications

considered for this type of operation are servo-valve systems and damping systems.

The final area, that of damping, is of interest as it can, dependent on the internal configuration of the damper, operate either as a valve type system, a clutch type system, a static system or even a combination of these regimes. Figure 1.10 shows a damping strut that relied on the shear properties of the fluid alone. Control is exercised by altering the shear strength between the plates and it can therefore be operated either in the static mode at zero shear rates or in a clutch type mode when vibrated. For the damper shown in figure 1.11 the fluid is effectively pumped by the motion and a force is developed on the damper piston related to the pressure drop along the piston length. With no electric field applied this is due to the viscous component and it can be operated as a conventional hydraulic telescopic damper. Unlike the conventional damper of this type it is possible to "lock" the position of the piston using the shear forces as well as having electronically controlled damping properties. The current area of greatest interest is in vibration isolation, especial in the automotive industry. In figure 1.12 the typical automotive vibration problem areas are highlighted and it is apparent that vibrations derived from the engine are the most difficult to isolate. A considerable effort is being expended in isolating and controlling these vibrations using sophisticated oil filled engine mounts. Great potential is offered by using ER fluids in this area as the possibility is presented of far greater control over the vibration spectrum.

These four usage modes are covered by three flow regimes and it the behaviour of ER fluids in these regimes that is dealt with in this study. The annular flow mode is investigated using an item of equipment known as the Valve and Fluid Development Rig (VFDR) a full description of which is in section 3.2. The main elements of this device are a pressure source, a pump, and a precision valve

arrangement which acts effectively as a tube viscometer. A purpose built Couette cell, known as the Electro-Rheological Viscometer (ERV), capable of measuring the shear stresses generated by ER fluids at shear rates commensurate with application devices, is used to quantify the Clutch mode. The static mode was studied using a small shear cell, the Static Yield Rig (SYR), that enabled rapid screening of samples to be made.

Figure 1.10 Schematic of Damping Strut

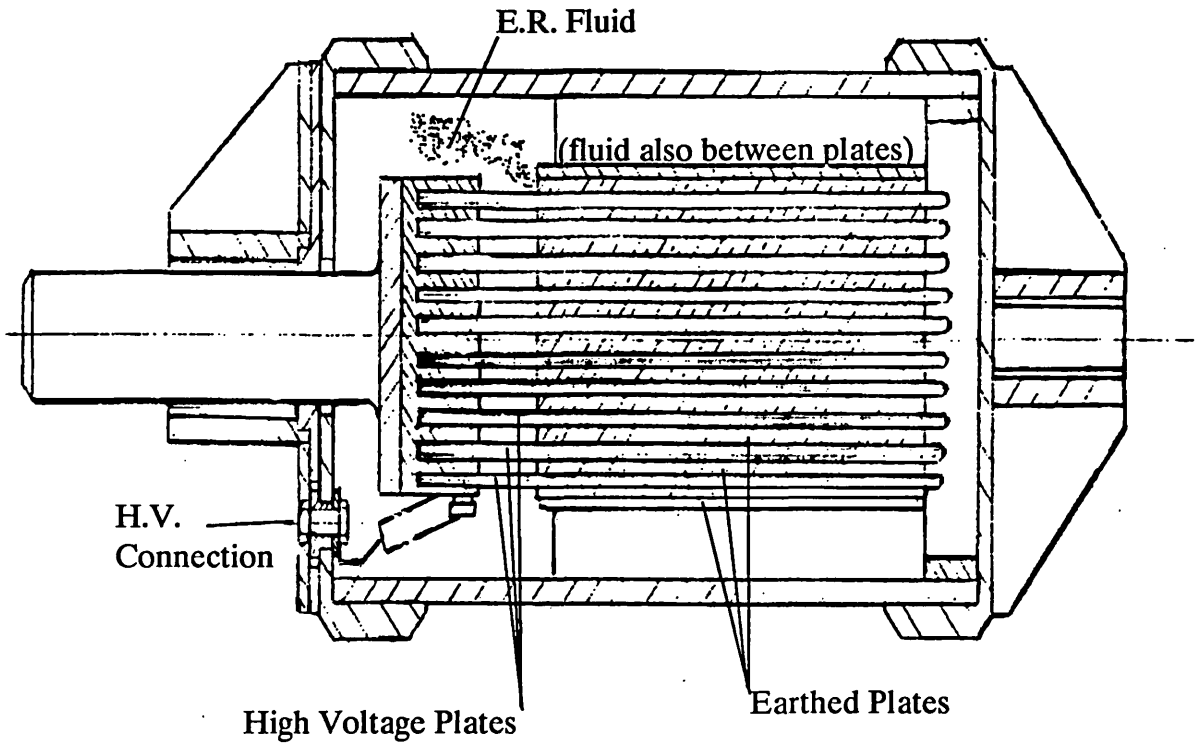


Figure 1.11 Telescopic Vehicle Damper

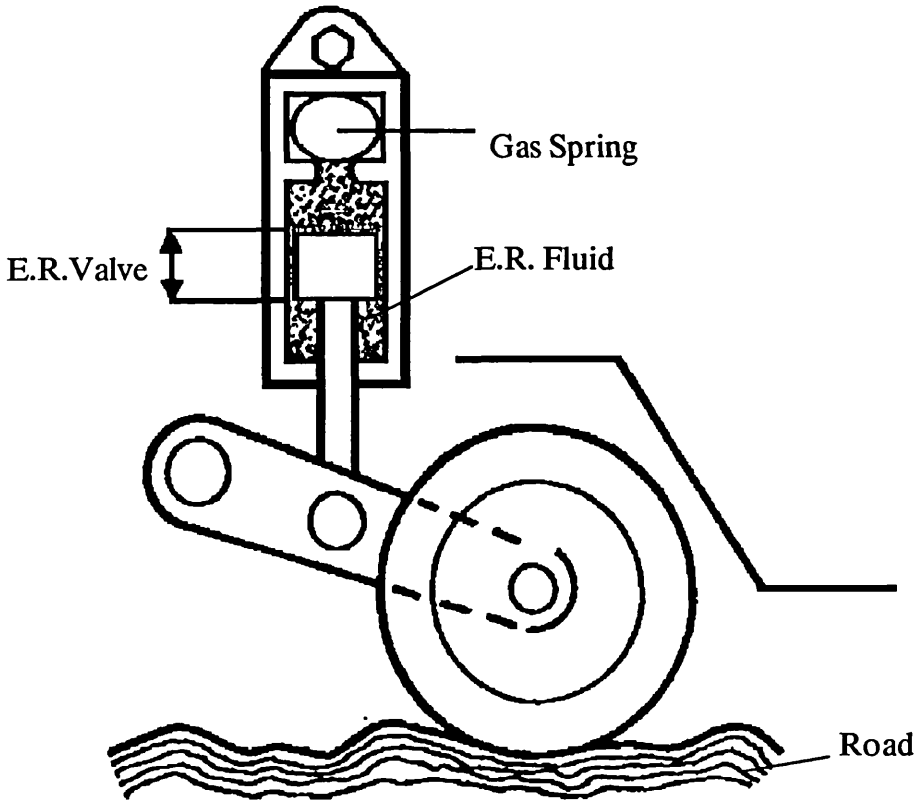
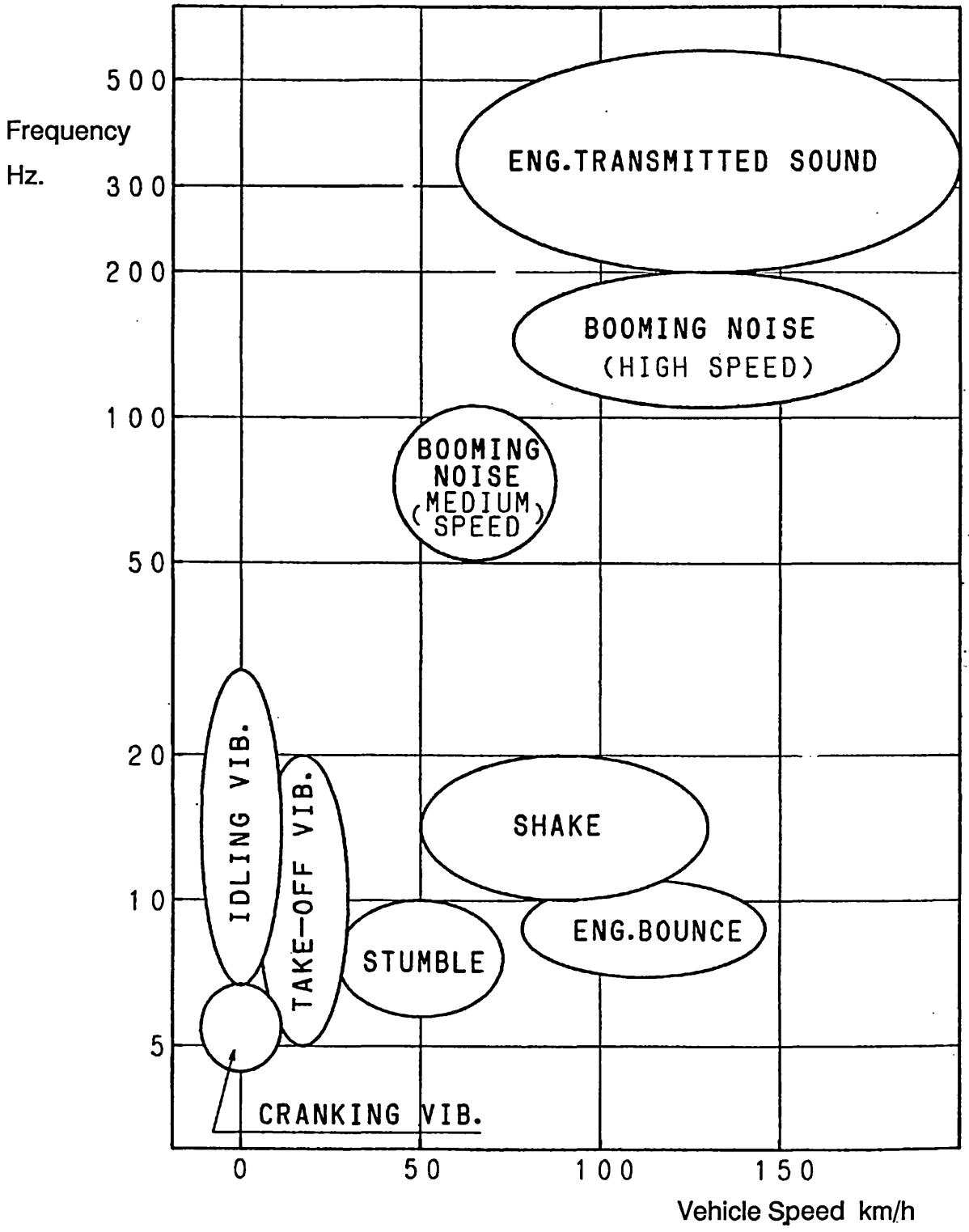


Figure 1.12 Vibration Spectrum of Vehicles



CHAPTER TWO

THE HISTORY AND POSSIBLE MECHANISMS IN ER FLUIDS

2.1 INTRODUCTION

The chapter is sub-divided into two main sections. The historical perspective, presented first, consists of two sub-sections. Initially the history of ER fluids is discussed and reference is made to the individuals involved and the research carried out. This is followed, in the second sub-section, by an overview of some of the mathematical descriptions put forward and used to describe the phenomena.

In the second section a more detailed consideration of the phenomenon of the ER effect is presented. Specific reference is made to the hydrodynamic interactions, that is, the effects due to the shear field on the particle and the role of the morphology of the particle. Next the electrical interactions which are thought to occur in these systems are considered. This is followed by a discussion of the polarisation processes in materials and the chapter is concluded with a section on the types of behaviour anticipated when both hydrodynamic and electrical stresses occur in fluid systems.

2.2 AN HISTORICAL REVIEW OF ER FLUIDS

In general the history of ER fluids, in relation to the development of the fluids themselves, has followed two routes. The early activity in North America and Russia concentrated, almost exclusively, on silica and other inorganic materials. In the UK, the research rapidly identified the shortcomings of these materials. The outcome of which was the development of a range of organic and polymeric materials. The salts of polymethacrylic acid, and in particular the lithium salt, proved to be the most successful. The measurement of success being based on a progressive increase in the yield strength of the system coupled with a substantial reduction in the current flow.

2.2.1 THE EARLY HISTORY OF ER FLUIDS

The discovery of ER fluids is attributed to an American, Willis M. Winslow during 1939, although most of his published work is dated around 1947[2-5]. Most early descriptions of the effect during this period and immediately afterwards carry his name. He conducted extensive experimental work on fluid formulations and devices using the fluids and was the originator of several patents, both on fluid formulations and applications utilising the effect. The effect was studied extensively in North America during the early 1960's where it was then termed the electro-viscous effect. This being based on the erroneous assumption that the applied electric field resulted in an increased viscosity of the suspension rather than a change in the rheology of the suspension. Work was continued in the USA by Klass and Martinek[6,83] who published a number of papers and took out several patents in the sixties. In a fairly comprehensive investigation of the subject they looked at the effect of both ac and dc fields on the fluid behaviour utilising a modified concentric cylinder viscometer. Their results showed that the ER

effect increased with an increased volume fraction of the disperse phase, an increased electric field strength and temperature but decreased with increased shear rate and electric field frequency. A mechanism for the effect based on the polarisation of the diffuse region of the double layer and the subsequent interaction of these polarised regions was proposed. A square law relationship between the induced shear stress and applied electric field was indicated. A paper by Phillips and Auslander[7], also in the USA, in 1971 is notable in that it introduced for the first time the concept of a voltage controlled Bingham yield stress. They also attempted to quantify the dynamic response of these fluids.

It was during this period that the Russian interest in the subject commenced and a number of publications emerged. The paper published in 1970 Deinega[9] was significant because it used the term *electro-rheology* for the first time, prior to this, as noted above, the terms *Winslow effect* or *electro-viscosity* were used to describe the phenomena. Deinega's paper also sub-divided the subject into three main areas which allowed a more clear distinction to be seen amongst the various topics being investigated at that time.

These sub-divisions were as follows:-

a) A study of the effect of electrical charges on the dispersed phase, this was essentially a study of the *electro-viscous effects*.

b) A study of the effect of mechanical deformation on the structure and electrical properties of the suspension. Changes of dielectric properties, conductivity, ultrasonic transmission and optical properties are termed *rheo-electric effects* and *rheo-optic effects*.

c) A study of the effect of electric fields on the structure and rheology of the suspension. The rapid and reversible change in the rheology is termed the *electro-rheological effects*.

This terminology has since been adopted by the majority of workers in the field. Deinega's research also led him to conclude that polarisation and the interaction of polarised particles were the major factors controlling the ER effect.

It is clear that by the early 1970's there was a significant activity by the Russians. In addition to Deinega[20-22] the names of Dukhin[23-29], Shilov[30-33], Shul'man[34-39], Gleb[40], and Vlodavets[41] amongst others, are prominent. Several papers presented descriptions of measuring equipment that indicated that the basic measuring modes had been established[42-47].

Research into the subject of electro-rheological fluids commenced in the UK in 1969 with research by Laser Engineering (Development) Limited and Sheffield University. Sheffield were mainly concerned with the development of new ER fluids and a series of patents[48-50] chronicle the research at the University which was directed at the development of new fluids using polymers for the dispersed phase. It was out of this activity that fluids based on the lithium salt of polymethacrylic acid, as the dispersed phase, were established as a most effective, and potentially commercial, ER fluid. The above patents also contained details of methods for characterising the strength of the effect and ways of expressing the conductivity of the system. Stangroom, at Sheffield, was the main research worker and his extensive review[51] on ER fluids, contained a description of his "water bridging" theory. He suggested that a quantity of absorbed water was forced out by the electric field and provided a "bridge" between the particles. However, simple calculations revealed that there is insufficient water in the polymer for the necessary "bridge" material to be provided. In addition the recent

development of ER fluids that are water free and polarised through electron migration undermines the credibility of the "bride" model. This model is, therefore, probably untenable.

The involvement of Laser Engineering (Development) Limited during this time was with the design, manufacture and evaluation of possible engineering devices. In 1979 Laser commenced the manufacture of pilot quantities of the lithium polymethacrylate based ER fluid for commercial exploitation.

In Japan, a paper by Uejima[52] in 1972 dealt will ER fluids in Couette flow together with some aspects of the dielectric behaviour. The polarisation of double layers was again proposed as the mechanism for the ER effect and the concept of a Bingham fluid was used. Work by Sugimoto[53] in 1977 resulted in the development of ER fluids with ion exchange resins as the dispersed phase. He also examined the effect of electric fields by considering the shape of the particles and concluded that the spherical shape of ion exchange resin particles as compared to the irregular shape of other materials allowed greater electric fields to be applied before breakdown occurred.

Applications directed research was being carried out by Matsumura of Kawasaki Heavy Industries, Sugimoto under the aegis of the Ministry of Labour and Honda and Sasada at the Tokyo Institute of Technology. Sasada[54,55] et al and Honda[56-63] et al produced a series of papers concerned with the change in viscosity with electric field of polymer colloids and suspensions. In some of the suspensions water was used as the continuous phase. The observation was made that, on the basis of a polarisation mechanism, only the electric field was required for the structure formation, that is, current flow was not essential. The paper by Kawasaki[64] is of interest as it dealt with the resistive properties of polymers and dispersions as a result of their moisture content.

A series of papers by the Russian, Estrela-L'opis[65-67] examined firstly, for a dilute concentration, the energy interaction of a pair of spherical particles in an external electric field using the DLVO (Derjaguin and Landau, Verwey and Overbeek) theory. He subsequently, took multipole polarisation into account. Later he studied the effect of adding water to the system which is of particular interest as the system was similar to an ER fluid. There had been a steady output of publications on the subject by the Russians and between 1970 and 1981, 52 papers and 23 patents had been published. A number of publications by Shul'man[35-38] covered a variety of aspects ranging from an extensive list of applications to the description of the formation of structure, in both a qualitative and quantitative manner. The latter paper pertained to the dynamics of chain-like structures in Couette flow and referred to a square law dependence on electric field. The other papers dealt with the question of the effect of foreign material or impurities and were especially significant as they indicated the requirement to understand the practical problems and limitations of an ER fluid with respect to their resistance to contamination.

Very little recent published work has appeared in the USA. However Johnson and Melcher, and Melcher and Dietz[68-70] produced papers between the years of 1975 and 1978 and described studies carried out on electrified fluidised beds using sand and moist air. It was interesting to note that similar expressions were developed for the generation of shear stress and that a primary role was given to the effect of the dielectric nature of the two phases.

2.2.2 SOME EARLY MATHEMATICAL DESCRIPTIONS

If the basic fluid characteristics as presented in figures 1.1 to 1.6 are reconsidered some of the arguments over the basic mechanism of the electro-rheological effect can be indicated. The "strength" of an ER fluid in its activated state is usually described by

adopting the rheological concept of a Bingham fluid, where the material will support a stress up to a prescribed level. Beyond this it yields and then flows to an extent dependent on external stress. The level of this excess stress is dependent on the strength of the electric field applied to the fluid, other factors such as composition and temperature being constant. The nature of the relationship between electric field and the excess shear stress has been the focal point of investigation since the phenomenon of electro-rheology was first encountered. There is general agreement that the yield point is increased with an increased applied electric field. Klass and Martinek[83] concluded that the electro-rheological yield stress is proportional to the square of the electric field strength (and inversely proportional to the shear rate). Many workers, generally tend to favour a square law dependency, as might be expected from an electrostatic model of particle interaction, and contest the notion that the increase is simply linear from some threshold value of voltage. Some sources[71] have preferred to describe the relationship as sigmoidal.

Shul'man[38] promulgated a square law dependence. In a paper published in 1982, for example, the attractive force F, between particles is given as:-

$$F = \pi \epsilon_o \epsilon_r V_0^2 r / 2\delta \qquad \text{---- (2.1)}$$

where V_0 is the applied voltage
δ the interparticle distance
r the particle radius
and ϵ_0 and ϵ_r are the permittivity of free space and the relative permittivity

This lead to an expression explicitly relating the electric field E_0, to the yield strength T_y:-

$$T_y = 0.13 k C \epsilon_0 \epsilon_r E_0^2 \qquad \text{---- (2.2)}$$

where C is the volume fraction of the suspension
and k a dimensionless group.

It should be noted that whilst the electric field is of comparable magnitude to that currently taken as typical the parameters of the fluid are not. For example, the particle radius used in the Russian work was 0.1 micron as compared with 3 to 5 microns of contemporary systems. In addition the volume fraction was in the order of a few percent compared with 30% to 40% for recent systems. At such low volume fraction particle-particle interactions are not going to be significant and it is, therefore, not possible for this type of expression to be utilised.

A similar expression to 2.2 is quoted by Deinega[9] which in this case takes into account, to some extent, particle-particle interactions. The expression for the change, now expressed in terms of *viscosity* $\delta\mu$, is:-

$$\delta\mu = C\epsilon_0\epsilon_r E_0^2(f-g)/\pi\delta \qquad \text{---- (2.3)}$$

The parameter C was the volume fraction of the particles and f and g are dimensionless quantities which characterised the mutual polarisation of the particles as they approach one another. Both parameters were functions of the distance between the particles. In this case concentrations are of the order of 25%. This lack of clarity and distinction between viscosity and yield stress is quite common in early papers and great care is required in interpreting the data.

Chertkova[72] et al using a similar concentration of dispersion also found a square law dependence of the yield stress on the electric field where an ac electric field of 0.8 kV/mm was operated at a frequency of 300 Hz.

Several other workers, however, assign a linear dependence. Stangroom[51] in 1978 showed that the yield point varied linearly with voltage gradient, as did Marson[73].

Early work by Laser Engineering (Development) Limited indicated that results could be described by a linear dependence, but this representation was satisfactory only above a threshold value of electric field. This approach has been extended to include a wide range of different fluids, although in nearly all cases the linear dependency applied over only a restricted range of voltages.

The current flow has been examined by a number of workers. Lovett[74,75] tackled the problem of defining the conduction process in ER fluids. He showed how a statistical mechanical approach could be of value in interpreting empirical data relating voltage, current and temperature and demonstrated that a continuous function could and did describe a discontinuous process. From the two probabilities of motion, with and against the potential gradient (electric field) the current density was determined and found to involve a sinh function.

This resulted in the expression:-

$$J=Ae^{-\beta/kT}\sinh(aqE_0/kT) \qquad \text{---- (2.4)}$$

where A is a constant of proportionality
β is an activation energy
k is Boltzmanns constant
T the temperature in °K
a the mean free path
and q the electronic charge

That this expression accurately described the physical situation is confirmed by the excellent fit of data to this expression.

Davies[76], of the ERA, has carried out an investigation aimed at establishing whether a Hall effect could be measured in ER fluids. Measurements of conduction in several fluids were made with no discernible effect on the concurrent application low electric fields and very high perpendicular magnetic fields. As no Hall effect was detected it was concluded that conductivity parallel to the

BIBL. LONDIN. UNIV.

electric field direction was much greater than that perpendicular to the applied electric field. This observation corroborates with the notion of chains of particles in the fluid that not only provide a network for the conduction process but also for the generation of the induced yield stress. The lack of orthogonal conductivity also implied that the extent of cross linkage between chains was small. Very little work has been reported on the analogous situation with the mechanical properties but measurement of, for example, strength and the modulus in directions perpendicular and parallel to the applied electric field could yield some useful and interesting information.

Further discussion of the mechanisms involved in the transfer of charge in ER fluids is provided in an internal report from Laser[78] for lithium polymethacrylate particles suspended in Cereclor, a chlorinated paraffin supplied by ICI Limited. In this case it is argued that the partial solvation of Li^+ ions assisted their movement in the presence of external electric fields and the movement of these ions can be characterised using the surface conductance theory of Deryagin and Dukhin[77]. The movement of the solvated ion in the polymer phase being also the origin of the charge transfer could well account for the polarisation of the particle. Thereafter a number of process could be responsible for charge transfer between adjacent particles. The suggestion that the rate of charge transfer is related to the current is not surprising. As the external electric field is increased, the current and the effect are increased in a similar fashion. In general, observations relating the current and the yield stress support the idea that the particles in the fluid form "chains" in the electric field and both the yield stress and current would be expected to be roughly proportional to the number of connections between particles. It was on the basis of this model of an inter-electrode bridge of particles that Shul'mam[38] et al formulated the expression

relating the shear stress to the volume fraction for dilute systems. Jansons and Rallison[81] pointed out that at higher volume fractions the notion of separated chains is lost and that the number of connections between the particles would be greatly increased.

The dielectric characteristic of the fluids are important in determining the prevailing mechanism and a number of investigations have been made in this area. It is possible, in principle, for the processes occurring in a disperse system to be observed on the basis of dielectric measurements. There have been, for instance, investigations in which the effect of coagulation processes on dielectric properties have been studied, as well as the orientation of the particles under the effect of the hydrodynamic flow. The permittivity of a disperse system is characterised by its polarisation under the influence of an external electric field, modified by both bulk and surface properties. Dipoles in a material are oriented by the application of an electric field. For polar materials dipole alignment takes place, for materials with no permanent dipole these are induced. Induced dipole moments are an important electro-physical characteristic of disperse particles especially in relation to ER fluids since they cause dipole-dipole attractive forces which leads to aggregation and structure formation in an electric field.

Brooks[79] has examined the frequency response of ER fluids at different polarising voltages and found that the electrical permittivity is frequency dependent. It reduced as the frequency increased. The effect of the voltage was most significant at frequencies below 100 Hz and a loss peak was noted at approximately 150 Hz. Although the relaxation time was difficult to assess it was felt to be around 1 to 2 milliseconds which could be approximated to the observed mechanical time constant of the system. The correlation of the dynamic mechanical response to the electrical phenomena is also apparent in the general shape

of the relative permittivity curve, which corresponds to the mechanical case. The response to ac fields seems, therefore, to reflect to some extent the dynamics of the structural interactions. The combination of alternating electric field and shear fields has been the subject of a number of investigators. Amongst them, Block[80] has studied the topic of flow modified dielectric properties where the time element of polarisation is particularly relevant. Using the measurement technique of flow modified permittivity (FMP) the permittivity of a fluid is measured at various shear rates with electric fields of different frequencies. Particles tend to rotate in order to keep the polarisation vector parallel to the applied electric field and a current is developed which flows tangentially within the spinning particle. Since the particles have a resistive component this current gives rise to an energy loss which is manifested as a force opposing the flow. Characteristic maxima are observed in the permittivity-frequency curves which are associated with a resonance between the shear induced rotation rate and the frequency of the alternating electric field.

In addition to the interest in the dielectric properties of the fluid and its solid phase component some attention has also been paid to the features of the continuous phase. There does not, however, appear to be a simple relationship between the permittivity of the continuous phase and the ER effect. Block found that for semi-conducting polymer materials dispersed in various liquids there was an increase in ER strength with increased permittivity. Sugimoto[53], in contrast, measured the size of the ER effect for nine different carrier media with permittivities varying from 3.62 to 6.47 and could find no clear trend that related the ER effect to the dielectric property in question. Stangroom[51] also viewed the question of the relevance of permittivity and his work suggested that this property was not the important feature of the continuous phase. These materials were actually chosen for

their practical convenience, low viscosity, high boiling point, low freezing point and high density (to prevent settling of the disperse phase) and minimal toxicity.

2.3 THE ELECTRO-RHEOLOGICAL PHENOMENA

The behaviour of the dispersed phase in an ER fluid has been studied (Winslow[2], Davies[76], Shul'man[37], Stangroom[82] etc.,) visually. The observations of these dilute systems has demonstrated that without an electric field the particles moved easily past one another. When an electric field was applied they aggregated to form chains that stretched between the electrodes. Fluid flow only occurred when sufficient stress was applied to break up this formation. Once flow had taken place the structure was seen to be continually breaking and reforming. To develop an understanding of the behaviour of an ER fluid the interaction between the hydrodynamics of the system and the external electric field impressed on the fluid needs to be considered. Both hydrodynamic and electric fields will induce forces and torques on a particle in a continuous medium and it is the magnitude and interaction of these quantities that dictate the observed behaviour of an ER fluid. Arp[107-109] has identified a dimensionless parameter, f, that is essentially a measure of the ratio of the electrical stresses to the shear stresses. From a consideration of this function and its square the possible behaviour modes of an ER fluid in terms that are conventionally adopted can be highlighted. These are detailed in table 2.1. For example if this function is infinite then this is the case of $E_0 \neq 0$ and the shear rate, $G = 0$, this is typically the "Static Yield Case" and the motion of particles in only an electric field is described. The chemical interaction between the particle and continuous phase is not explicitly covered by Arp's work.

TABLE 2.1 Significance of the Function "f"

Condition	Significance
$f < 0$	describes the motion of oblate spheres when $r_e<1$, $P(q,r_e)>0$, $E_0\neq0$ and $G\neq0$.
$f = 0$	i) describes the motion of spheres when $r_e=1$, $E_0\neq0$ and $G\neq0$.
and	ii) describes the motion of spheroids in simple shear when $E_0=0$ and $G\neq0$.
$f > 0$	describes the motion of prolate spheres when $r_e>1$, $P(q,r_e)<0$, $E_0\neq0$ and $G\neq0$.
$f^2 = 0$	simple shear alone with no electric forces $E_0\neq0$ and $G\neq0$.
$0 < f^2 < 1$	subcritical field; spheroids motion is periodic and the effect of shear dominates where $E_0\neq0$ and $G\neq0$.
$f^2 = 1$	critical field; spheroids stop rotating where $E_0\neq0$ and $G\neq0$.
$f^2 > 1$	supercritical field; spheroids stop rotating and effect of electric field is dominant where $E_0\neq0$ and $G\neq0$.
$f^2 = \infty$	describes the motion of spheroids in electric fields alone $E_0\neq0$ and $G=0$.

Notes:-

$r_e<1$	is the equivalent hydrodynamic axis ratio
$P(q,r_e)$	is an electric parameter function for a spheroid >0 for $r_e<1$ and <0 for $r_e>1$.
E_0	is the applied electric field
G	is the shear rate

2.3.1 HYDRODYNAMIC STRESSES

The hydrodynamic stresses experienced by a suspension are due to three prime components, the particles, the continuous phase and the shear field applied. Conventionally, the study of the effect of the particles on the hydrodynamic stresses has been developed from the assumption of model particles that are spherical, monodisperse, hard, uncharged, the number density of which is such that the resulting suspension can be considered dilute. The dispersed phase in an ER fluid by contrast are ill defined particles, polydisperse, are charged and concentrated. Consequently these fluids represent materials which are far from the ideal system.

The Effect of the Particles

The type of disperse system under consideration can be effectively defined by the particle size. Solid particles dispersed in a continuous liquid medium are called suspensions or dispersions. Mewis[1131] has defined these explicitly as follows.

> 1) Suspension: a two phase system of buoyant particulate solid, not colloidal, distributed in a continuous liquid.
>
> 2) Dispersion: a two phase solid-liquid system, the solid particles of which are colloidal. This discriminates between suspensions and dispersions.
>
> 3) Aggregate: a tight cluster of particles, strongly held together, so that it cannot be separated in a given rheological experiment.
>
> 4) Floc or flocculate: a loose, thermodynamically metastable, structure of colloidal particles. A floc may be destroyed, to a greater or lesser extent, by the application of stresses in a given rheological experiment and may reform when the stresses are removed.

The important division is evidently between a suspension and a dispersion. Thadros[132] in common with most workers in this field have defined a colloidal size range based on the difference between the number of "surface" and "interior" molecules. The lower limit is quite often set at 1 nm, whilst the upper limit is taken at 1000 nm (1 micron) on the assumption that there is still a significant proportion of the atoms or molecules at the surface. Using these considerations the conventional colloidal range is put at 1 nm to 1000 nm. Systems that have a significant number of particles above the 1 micron size are termed suspensions. There is no clear upper limit to the maximum size of a particle in a suspension, the limit is usually dictated by that encountered in practice and is conventionally set around the tens of microns. The particle size range of a typical ER fluid is 2-25 micron diameter with a mean diameter of 6-12 micron. Thus the systems are clearly suspensions and not colloidal dispersions. Explanations treating ER fluids as colloidal systems and describing them as such could be, potentially, very misleading. However, there are many aspects of such an analysis that are instructive in an assessment of the behaviour of ER fluids. The most important is in terms of the conduction process. Using the classic Debye-Huckel expression the thickness of an electrical double layer K, can be evaluated:-

$$K^2 = e^2 n_o z^2 / \epsilon_o \epsilon_r kT \qquad \text{---- (2.5)}$$

where e is the elementary charge
n_o is the concentration
z is the valency
k is Boltzmann Constant
and T the temperature

A diffuse layer thickness, based on a concentration[133] of $1.525*10^{-3}$ mols/cm^3, of $1*10^{-7}$ m can be calculated. The system is therefore one of large particles with relatively thin diffuse double layers.

The effect of particle shape on the hydrodynamics is well described for various standard shapes. These are the sphere, the spheroid, both oblate and prolate, the rod and the disc. Arbitrary shapes are not accurately defined. The defining hydrodynamic parameter is the equivalent axis ratio r_e, which is the ratio of the maximum to the minimum axis. Thus for a sphere $r_e = 1$ and for a rod $r_e > 1$. It is therefore conceived that a suspension of arbitrary particles could be modelled as a summation of equivalent axis ratios, Adler[126-127] has made some studies in this area although the results are still inconclusive.

The viscosity of the suspension is also significantly affected by the particle shape, the particle surface charge and their polydispersity. The viscosity is also affected by the volume fraction of the disperse phase and various attempts have been made to model the effect.

Concentrated Suspensions

At this stage it is useful to indicate the difference between a dilute and a concentrated system. A system is considered dilute if the particles do not "see" each other until a collision occurs, that is the average particle separation is greater than the range of the interparticle force. Time averaged quantities are essentially independent. As the particle number concentration is increased, the volume of space occupied by the particles is increased and consequently the probability of particle-particle interaction is increased. The forces between the particles play a dominant role in determining the properties of the system. Eventually a situation is reached when the suspensions behaves like a solid due to the order imposed by the concentration. Again the time average quantities of the system are independent. Between these two extremes concentrations, the dilute and the solid, lie the concentrated suspensions. The interactions are many bodied in nature and motion is restricted, the particles "see" each other within a relatively short time

scale. It is therefore of some importance to understand exactly what the system is and why it is difficult to extrapolate from dilute, time independent suspensions, to concentrated suspensions where the properties are not time independent. What is required is knowledge of how the motion of a particle is modified by the interaction with the neighbouring particles and the time scale of the interactions. Similarly knowledge is required of the spatial arrangement of the particles to assess the temporal aspects. It should be clear that the concept of a concentrated suspension is dependent on the number and the interaction of the particles. Consequently a low volume fraction, highly interactive system will behave like a concentrated system. Figure 2.1 depicts the effects of the concentration and the interaction on the suspension behaviour.

Figure 2.1 The Effect of Concentration and Particle Interaction

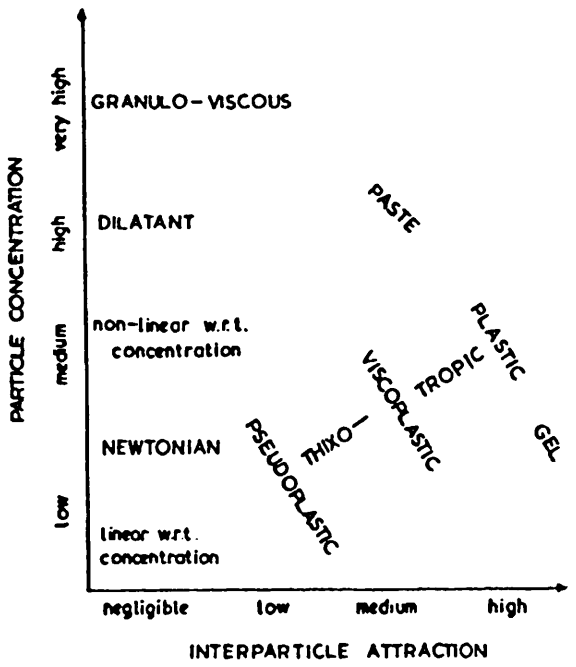
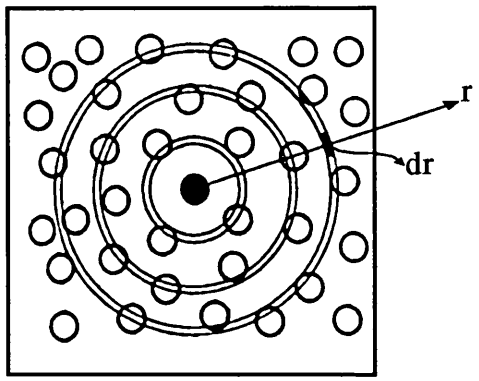
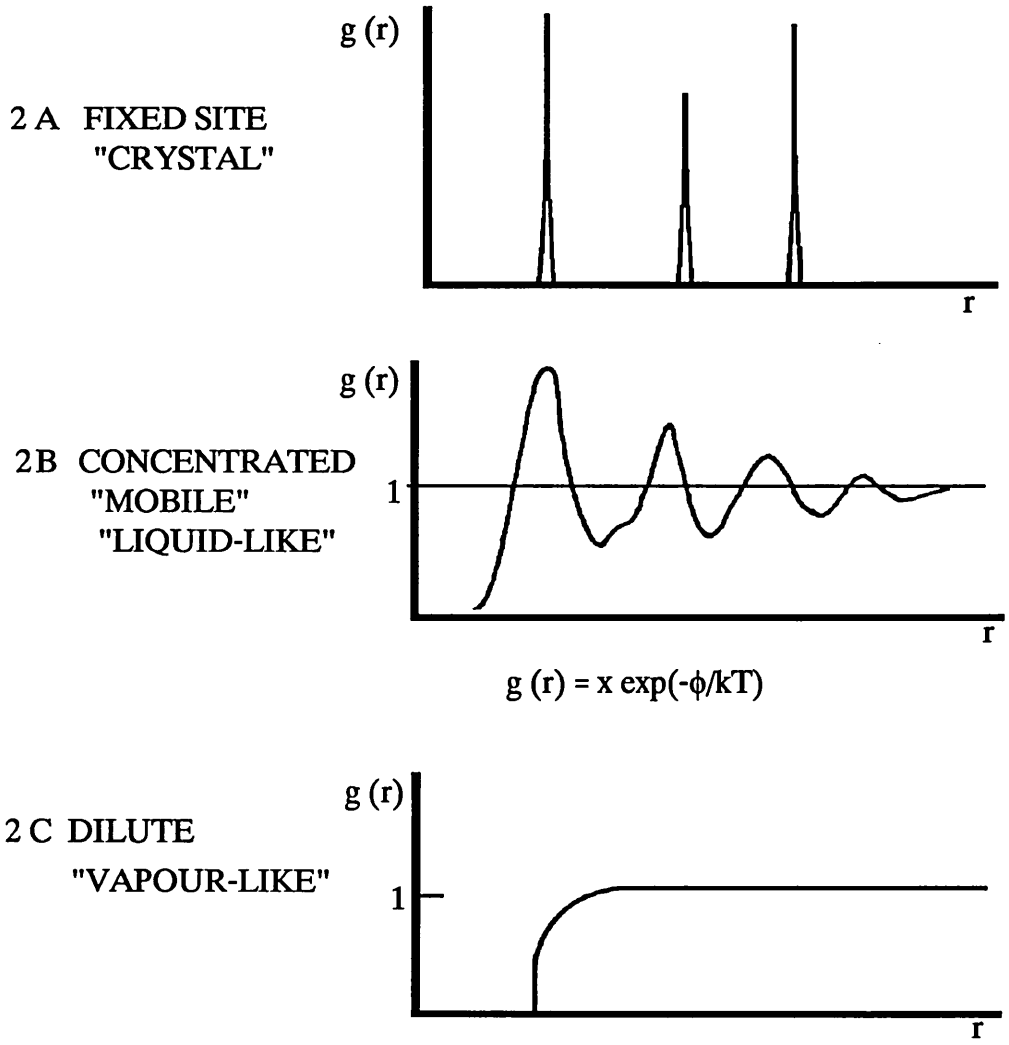


Figure2.2 Schematic View of the Distribution of Particles around a Central One



The most popular method used to describe the structure of a suspension is through the radial distribution function. A fluid of volume V, contains N particles and the average number density is defined as p_o=N/V. Consider figure 2.2 which depicts an assembly of particles. An arbitrary particle, shaded, is in the centre of a number of concentric cells. It is apparent that in the immediate vicinity of the central particle an unoccupied space exists. As the distance, r, from the particle is increased the number of particles with centres in a shell of thickness dr varies. The number density p(r) therefore varies with r and the distribution of the particles is thus described. The number density will have two limiting values, 0 as r goes to 2R, where R is the particle radius, and p_o as r goes to infinity. The radial distribution function is the ratio of p(r) to p_o. Therefore the function $g(r) = p(r)/p_o$, as $g(r) \rightarrow 0$ as $r \rightarrow 2R$ and $g(r) \rightarrow 1$ as $r \rightarrow \infty$.

Figure 2.3 Radial Distribution Function for "A" Solid, "B" Concentrated and "C" Dilute Suspensions



Radial Distribution Function

If g(r) is plotted against r the difference between dilute, concentrated and solid like suspensions can be indicated. In figure 2.3c, a dilute system is shown where g(r) rapidly increases from zero at r = 2R to a maximum value of one, beyond the first shell. Thus, for a dilute system there is no structure and the particles are uniformly and randomly distributed throughout the system. In the case of the solid like system, figure 2.3a, distinct peaks are shown by the function similar to those of atomic and molecular crystals. That is, the spatial arrangement of the particles is essentially fixed and a strong structure is evident. In the case of the concentrated systems there is a pronounced first peak followed by a number of oscillatory peaks eventually damping out to unity, after four or five particle diameters. The peaks also tend to become broader. The radial distribution function may be related to the force between particles by $g(r) = \exp(-\phi_r/kT)$ where ϕ_r is the sum of the simple pair potential and a perturbation term. The pair potential, in colloidal systems, is the summation of the various interactive terms such as electrostatic interactions, steric interactions and van de Waals interactions. Similar interactive terms for ER fluids need to be developed. Typically it would be necessary to consider dipole-dipole interactions, steric interactions and induced dipole interactions.

The Continuous Phase

Apart from the obvious aspects of continuous phase properties, such as high dielectric strength, chemical stability and low toxicity the precise role of the chemical formulation on the ER effect is not well understood. Data are scant and for a variety of reasons unreliable. Evidently the majority of "oily" liquids will function as the continuous phase for an ER fluids, however, it does appear that the halogenated oils give enhanced ER effects but as to why this is so is difficult to ascertain. A systematic study of well defined oils with detailed

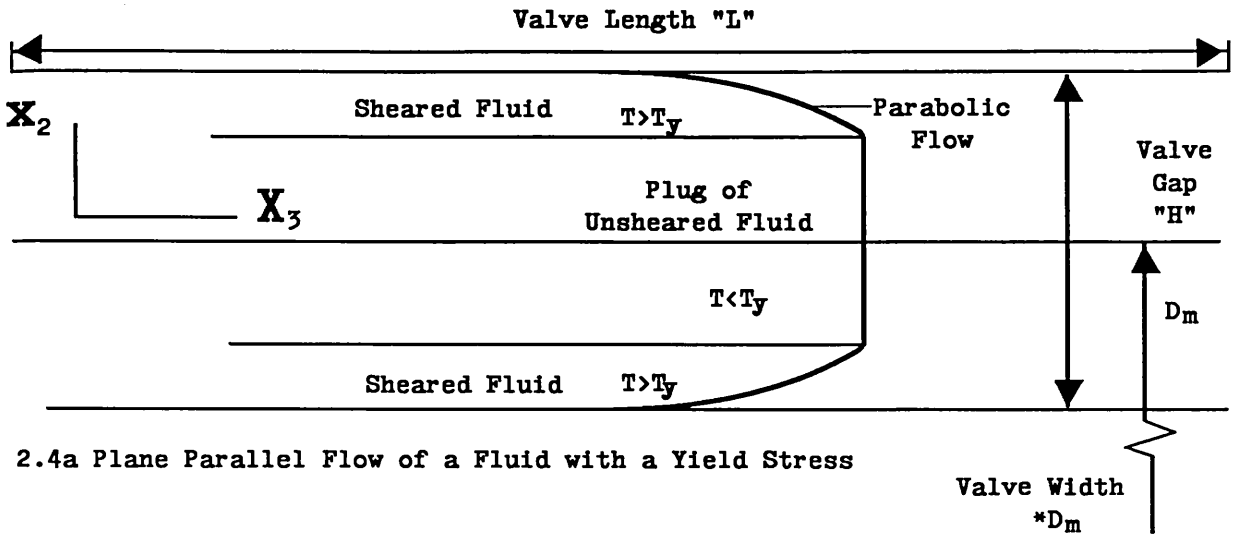
knowledge of their properties, especially electric and dielectric, is needed.

The other main variable is the viscosity of the continuous phase. In conventional suspension studies where the Newtonian viscosity is the main concern this is accommodated by using the relative viscosity. That is, the suspension viscosity divided by the continuous phase viscosity. In the case of ER fluids, interactive effects with the continuous phase viscosity may well be observed, especially in relation to the time dependence of the effect. Experiments with silicone oils of different viscosities were inconclusive and further work will be required here[142].

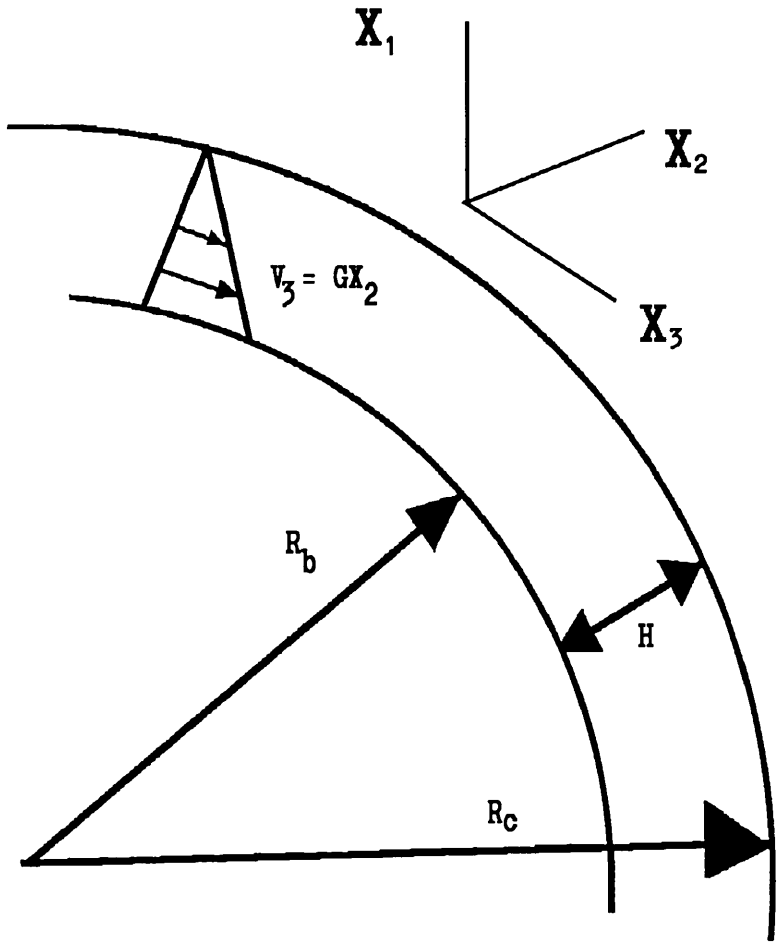
Shear Fields

The form of the shear fields imposed on ER fluid tend to be of two types, Couette flow and Poiseuille flow. These are shown diagrammatically in figure 2.4. Other forms of shear field, extensional flows, for example, have not been considered.

Figure 2.4 Idealised Flow Profiles



2.4a Plane Parallel Flow of a Fluid with a Yield Stress



2.4b Couette Flow showing Coordinate System

2.3.2 ELECTRICAL STRESSES

When an electric field is applied to an ER fluid a number of phenomena are produced. A current flows, which is a non-linear function of the electric field; the permittivity is changed in an electric field dependent manner, and a number of electrokinetic effects are observed. These effects are additional to the main one, the structural change that results in the ER effect itself.

There is of course no ER effect without the existence of a finite number of particles. Similarly the conductivity of the continuous phase is extremely low compared to that of an active ER fluid. Therefore the particles themselves cause an increased conductivity of the suspension either directly or by introducing ionic species into the continuous phase. In a manner similar to the view given of the hydrodynamic stresses, the electrical stresses can be examined by considering the particles.

The Role of the Particles

Materials can be classed in terms of their conductance, the measured term being conductivity, σ, expressed in Sm^{-1}. The spread of conductivities in materials is very large with materials being considered insulators if $\sigma < 10^{-10}$ and metallic if $\sigma > 10^{6}$ Sm^{-1}. Semi-conducting materials are taken to lie in the range 10^{+2} to 10^{-8} Sm^{-1}. For electrical conductance to occur it is necessary for there to be a charged species to act as the charge carrier and for this species to be mobile in the material. An ER fluid, being composed of two phases, makes it necessary for the charge carriers and their mobilities in both the continuous and the dispersed phases to be considered. The dispersed phase used in this work, lithium polymethacrylate, is a non-conducting material in the dry condition. It is rendered conductive by the addition of a small quantity of water with a resultant conductivity in the range of 10^{-6} to 10^{-9} Sm^{-1}. It is required to state a range as the

conductivity is dependent upon the quantity of water in the polymer and the electric field applied to the polymer. It should be stressed that the stated conductivity is referred to that of the dispersed phase only, not the ER fluid itself. The conductivity of the continuous phase is in the order of 10^{-11} Sm^{-1} and is an insulator. An ER fluid can therefore be considered as a suspension of particles of high conductivity in a continuous phase of low conductivity.

Perhaps the most contentious issue is by what mechanism the charge is transferred from particle to particle and implicit in this argument is whether or not the particles come into contact. Considering the "touching" argument first. If the particles touch, charge can easily be transferred. However if the suspension volume fraction is increased to near the maximum packing density the system should behave as a freely conducting system. Similarly it should be possible to form complete chains of conducting particles across an electrode gap and effectively "short out" the electrical circuit. As this is clearly not the case it can be concluded that the particles do not touch. This seems reasonable from a colloidal point of view in that the particles, being charged, will repel each other due to their electrostatic forces. In addition the dispersed phase is manufactured by using lithium hydroxide to neutralise polymethacrylic acid, an acid which is sometimes used to stabilise latex[84]. There remains an estimated 10% free acid in the final product and this will tend to form a sterically repulsive layer on the particle, thereby preventing their touching[85]. This argument is further strengthened by considering the particle suspended in an alternative continuous phase. If we choose a silicone oil it is observed that the suspension is now highly thixotropic and far more stable than in the hydrocarbon oil. This condition is attributed to improved steric stabilisation due to the silicone oil being a better solvent for polymethacrylate than the hydrocarbon oil. A

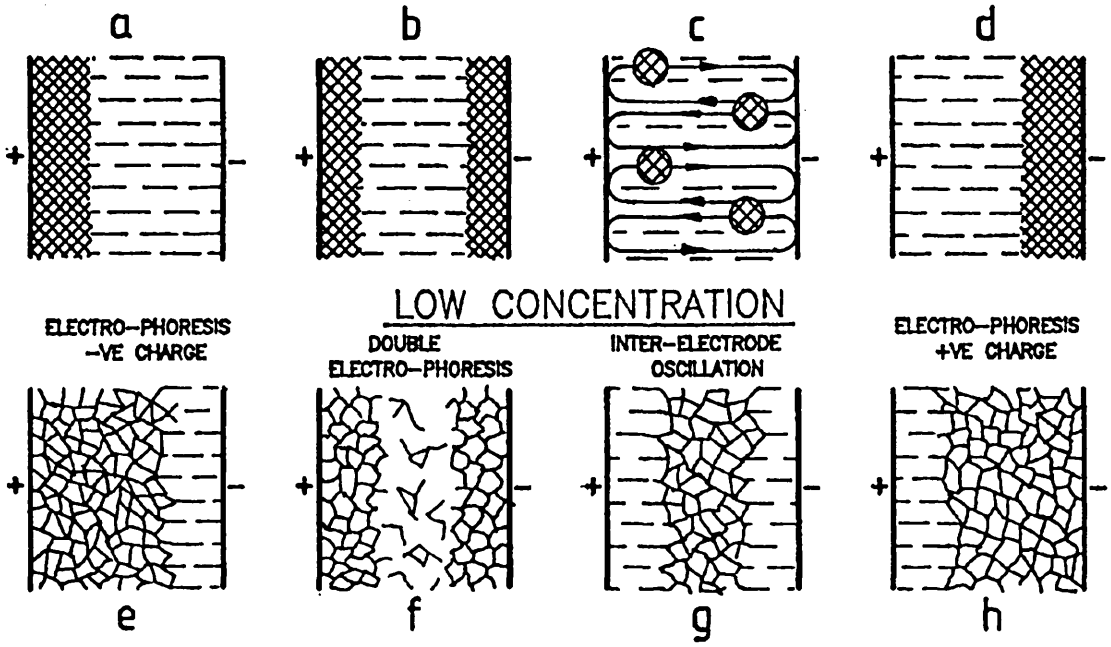
good general reference on stabilisation can be found in "Stabilisation of Colloidal Dispersions by Polymer Adsorption" by Sato and Ruch[86]. It is strongly suggested by this discussion that the particles do not come into direct contact. What is then required is a process whereby the charges can be transferred between the particles via the insulating liquid. There are a number of possible mechanisms, with current flow due to ionic impurities being the most common in insulating organic liquids[87]; coupled, in the case of ER fluids, with an electric field intensification due to the presence of the particles. By way of example, using the diffuse layer thickness previously evaluated, and assuming that the low potential Poisson-Boltzmann relationship of $\phi = \epsilon_0\epsilon_r K\Phi_0$ is applicable then the charge density, ϕ, can be calculated, giving the result $2.6*10^{-5}$ C/m^2. Assuming a particle radius of 5 micron the number of charges per particle can be calculated at approximately 50,000. That is, with every particle introduced into the fluid 50,000 charges are associated with the particle diffuse double layer and are potentially able to take part in the conduction process.

The application of an electric field to a suspension of particles in a continuous phase will result in a variety of motions. If the particle is free to move, the motion is termed electro-phoresis; if the particle is stationary, the fluid motion is termed electro-osmosis. The electric field induces motion by the combined action of the electric field on the particle's surface charge and the space charge in the liquid. Any polarisation of the space charge is offset by the migration of the charges in the electric field. The generic name for these motions is electrokinetic phenomena. In the case of ER fluids it is necessary for the structural changes due to particle polarisation to be considered. Deinega[9] proposed a characterisation based on electrokinetic, polarisation and concentration effects. Figure 2.5 shows the proposed characterisation. It is split into two main sections, that due to electrokinetic phenomena and that due to

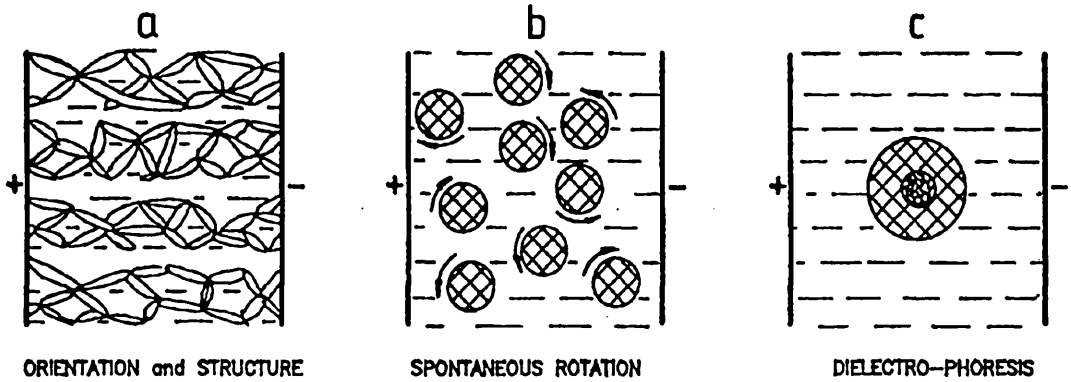
polarisation phenomena. Electro-rheology is primarily concerned with polarisation effects although it is apparent and can be demonstrated that the electrokinetic phenomena will occur within the same fluid composition. Electrokinetic effects, analogous to the electrophoresis effects of aqueous systems are described in parts a to d of the figure. Electrophoresis measurements have been taken for the fluid described in this work and the surface potentials in the order of 42 to 45mV were measured[17]. It should be noted here that conventional electrophoresis cells are not able to measure these potentials as the mobility of the particles is extremely small; some six orders of magnitude less than aqueous systems. The electrophoresis of negatively and positively charged species are shown in sketch a and d, the effects of concentration indicated by e and h. In sketch b the effect of both +ve and -ve particle charges is shown. Part c is the result of particles being charged at one electrode and depositing the charge at the opposite electrode, this is occasionally termed the "bouncing balls" effect. Parts f and g are the extensions at higher concentration where particle to particle interactions occur. Other useful general references are available on the electro-kinetic effects, Melcher[89] and Saville[90], where macroscopic electrical and electrokinetic effects are discussed respectively.

The polarisation effects are shown in the last three sketches. In reverse order these are dielectrophoresis, which as implied by the name is the dielectric equivalent of electrophoresis and is the movement of particles into areas of high electric field. Spontaneous rotation of particles can occur if the induced dipole moment of the particle is misaligned with respect to the electric field direction. This effect has been used to induce rotation in a small concentric cylinder cell[88]. Finally polarisation can result in reversible structural changes so that the rheological properties of the fluid are significantly altered; this effect is the electro-rheological effect.

STRUCTURAL CHANGES IN DISPERSED SYSTEMS



a–h Effect of Concentration and Particle Charge



a–c Effects Associated With Polarisation

Figure 2.5

2.3.3 POLARISATION PROCESSES

A material can respond to an electric field because it contains charges than can be displaced. This can be pictured as the formation of dipole chains which align parallel to the electric field and bind countercharges to the electrodes. The density of the neutralised surface charge is represented by the polarisation which can be taken as the dipole moment per unit volume of the material. Furthermore, the dipole moment, or more strictly the average dipole moment, is assumed to be proportional to the local electric field strength. The constant of proportionality is the *polarisability* of the material. The local electric field will differ from the applied electric field due to the polarisation of the surrounding dielectric medium and in the case of suspensions the surface characteristics of the particles.

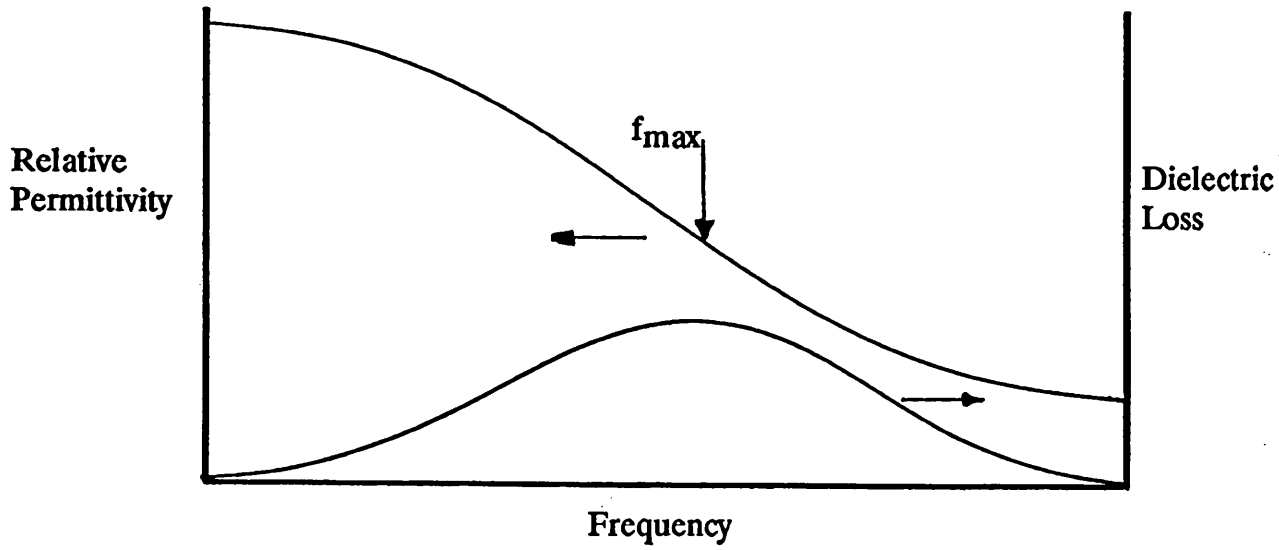


Figure 2.6 Typical Dielectric Relaxation Process

The net polarisability of a material is conventionally taken as the sum of four mechanisms. The first is called electronic polarisability and results from the displacement of the electronic cloud surrounding an atom. The second is known as atomic polarisation and is the

result of two adjacent atoms being displaced to form a dipole. Thirdly there is orientational polarisation due to the rotation of a dipole in an applied electric field and finally interfacial polarisation due to the movement of charges in a material that are accumulated at an interface or defect. Electronic and atomic polarisation operate at a time scale of the order of 10^{-15} seconds and are not considered applicable to this study.

For a dielectric to polarise a finite time is required. When subjected to an alternating applied electric field the resulting phase shift in the polarisation results in a characteristic relaxation spectrum as shown in figure 2.6. The permittivity of a dielectric is therefore complex, the real part of which is represented by the storage component which is out of phase with the electric field and the imaginary component, which is in phase, is termed the loss component. The real component is the relative permittivity and the imaginary component is called the dielectric loss. The ratio of the imaginary to real is the loss tangent and is the ratio of the energy dissipated to the energy stored per cycle.

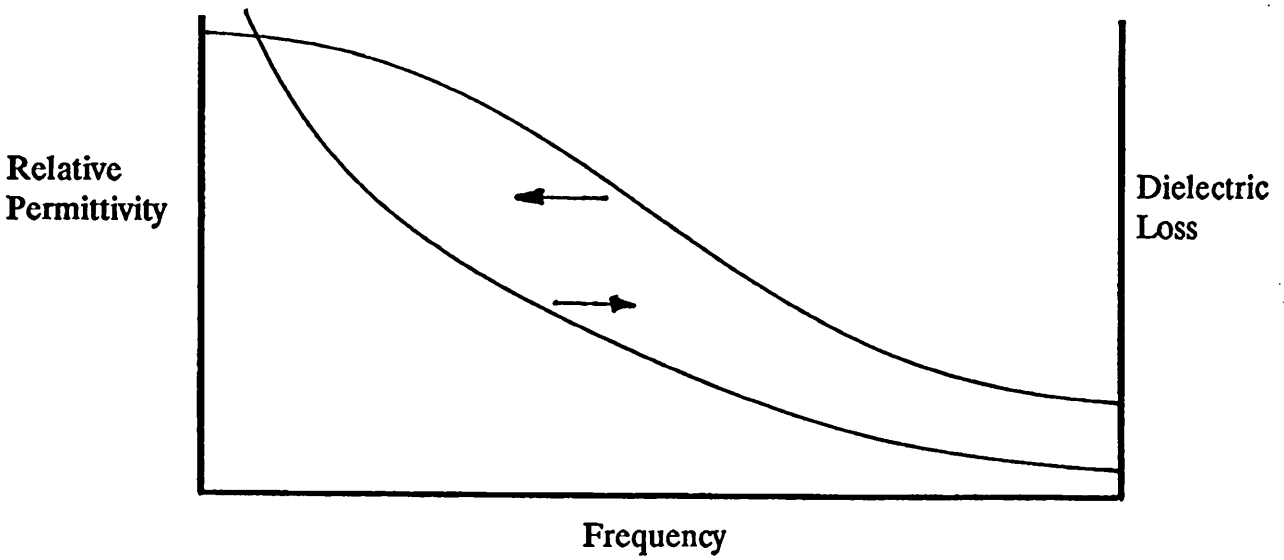


Figure 2.7 Typical Dielectric Spectrum for Interfacial Polarisation

Debye[90] pioneered the basic theory of dielectric relaxation behaviour and characterised the relaxation process by a single exponential decay. Most dielectric materials however show multiple relaxations and the loss peak, which is broader than predicted, is often asymmetric. So far no distinctions have been identified between orientational and interfacial polarisation although from the brief descriptions of the two processes they are evidently quite different. If we consider interfacial polarisation it is apparent that as charges are accumulated at an interface an appropriate model will be that of a conventional two-layer capacitor. This model is known as the Maxwell-Wagner model. The expression for the real part of the permittivity is the same as that for orientational polarisation but the second term has an additional component inversely proportional to the frequency. This means that as the frequency goes to zero the losses go to infinity, see figure 2.7. Thus, by consideration of the loss process interfacial polarisation and orientational polarisation can be distinguished. For an interfacial polarisation the loss process goes to infinity as the frequency goes to zero. This trend towards infinity has been shown in ER fluids by Kelly[71] and it can be concluded therefore, that the process being dealt with is an interfacial polarisation mechanism. The loss component will be increased as the frequency is decreased but it is often masked by the conductivity which is also increased as the frequency is decreased. Often interfacial polarisation cannot be clearly demonstrated from simple static permittivity measurements. Other techniques, notably flow modified permittivity (FMP), need to be used. The Maxwell-Wagner model was developed for spheres of given permittivity and conductivity in a continuous medium of known permittivity and negligible conductivity. The derived equations show that as the conductivity of the spheres is increased the loss peak would shift to higher frequencies. The analysis was developed further to include shape and it

was shown that the loss peak was enhanced and shifted to lower frequencies as the asymmetry of the particles was increased and when the particle axis lay in the electric field direction. The trend in the loss peak of moving to higher frequency as the conductivity of the particles is increased, has been shown to hold for ER fluids[92].

2.3.4 INTERACTION OF THE PARTICLES AND THE ELECTRIC FIELD

Additional dissipation stresses are caused by particles suspended in a Newtonian fluid during flow and result in an increased viscosity. Suspensions may exhibit one or more of the following properties:-

a) an unbounded viscosity at low shear stresses, i.e. a yield stress

b) time and strain dependent properties

c) shear thickening and shear thinning

and d) elasticity

These effects are related to the structures generated by the interactions between the particles causing reorientations and redistribution of the particles and the structure. Both the particle interactions and the non-hydrodynamic interactions need to be considered.

Non-Hydrodynamic Interactions

These are the Brownian forces and the electrical forces which result from the surface charges and the van de Waals forces. As indicated above these are primarily colloidal type forces operating on particles below 1 micron. The importance of non-hydrodynamic forces will be diminished as the particle size is increased and for suspensions of particles with diameters greater than 10

micron the behaviour is mainly determined by the hydrodynamic forces.

Hydrodynamic Interactions

Included under this heading are the interaction of particles which result in a changed velocity distribution in the vicinity of other particles and direct particle-particle interactions. The interactions result in the continuous formation and destruction of particle clusters. The clusters are translated, rotated and oscillated as the suspension is sheared. Clearly the orientation of the particles is changed as the suspension is sheared and the possibility of anisotropy of the suspension structure under certain flows exists.

The single isolated sphere in a simple shear field, 2.8a, translates at the velocity V_3 of the suspending liquid at distance X_2. It is also rotated around the X_1 axis with an angular velocity G/2, assuming no slip, where G is the shear rate. This rotation is of considerable significance when the particle is non-spherical as the angular velocity is variable and results in preferred orientations of particles. The single sphere is the starting point for the considerations of the interactions. The next step in increased complexity is the interaction of two spheres in simple shear.

This was extensively studied by Mason[93-106] et al and represents the simplest of a series of orthokinetic rate processes. Orthokinetic phenomena result from the particle movements caused by the flow of the fluid medium in which they are dispersed, these movements are regular. By contrast perikinetic phenomena are those originating from Brownian translation and/or rotation and being thermally induced follow random statistics. As noted earlier these different motions are essentially size dependent and this study is concerned primarily with the orthokinetic flow processes.

Figure 2.8 Motion of Spheroid

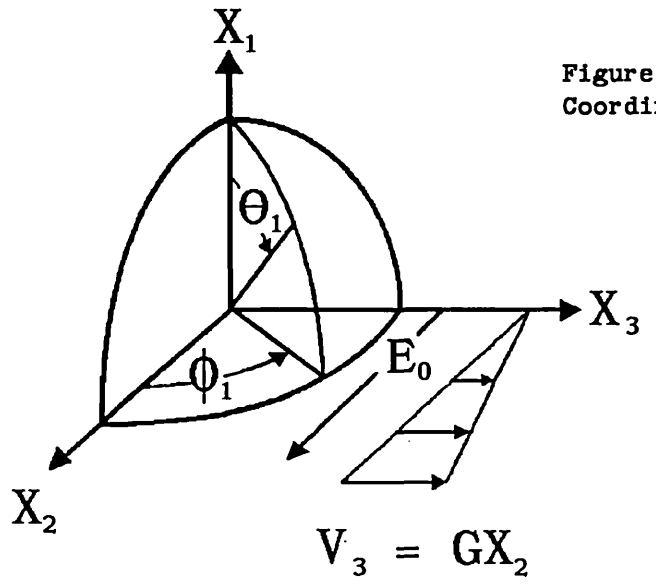


Figure 2.8a
Coordinate System

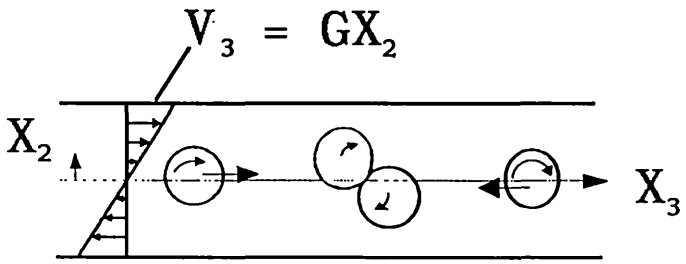


Figure 2.8b
Othokinetic Collision of
Two Spheres

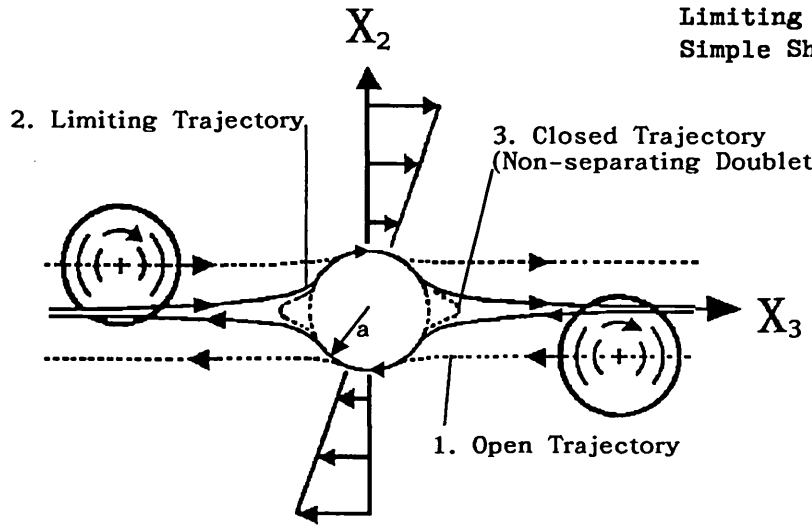


Figure 2.8c
Limiting Trajectories in
Simple Shear

Figure 2.8b shows the orthokinetic collision of two spheres and the resulting collision doublet that is formed. The collision frequency of the particles is related to the number density of the particles, the size of the particles and the shear rate. The full details of these interactions have been worked out for the case of two uncharged spheres and confirmed experimentally. The results, summarised in figure 2.8c, allows for two types of doublet, one transient and one non separating. It should be borne in mind that although the case may be a non separating kind, the particles are not considered to touch and a separation distance of $4*10^{-5}*a$, a being the particle radius, has been calculated[111]. The type of doublet formed depends only on the paths of approach. A permanent doublet once formed should therefore be permanent, however they are often separated due to the following processes. Collision from another particle forming a triplet and consequent fracture of the group; interaction of other forces, van der Waals forces or external fields, Brownian diffusion and surface roughness.

As the concentration is increased the number of triple and higher order collisions is significantly increased. As n-body collisions, (n>3), are unsymmetrical there is a resultant displacement along the X_2 and X_1 axes which will result in significant migration of the particles.

When the electric and hydrodynamic fields are coupled, a variety of electrohydrodynamic (EHD) effects are observed. These have been extensively studied by Arp[107-109]. Under the combined fields each individual particle is coupled to these fields and the surrounding liquid by interfacial stresses. As a result of the forces and torques from both the electrical and hydrodynamic fields a variety of phenomena are often observed. Included in these are electric and optical birefringence, dichroism and angular light scattering as well as the electro-rheological and rheo-electric effects. All are the result of particle

orientation, both translation and rotation, and particle-particle interactions in the applied electric field. As the position and orientation of the particles are changed their electrohydrodynamic environment is altered. Consequently different stresses will act at the particle surfaces due to the variations in the flow and the electric fields. Disturbances due to the motions of the particles themselves will also effect the stresses. Arp[110] in a wide ranging review has highlighted these factors and the interactions. These are shown in figure 2.9. The arrows are uni- or bi-directional and depend upon whether or not the factors are mutually interdependent. For example, the electrical stresses and polarisation are mutually interdependent whereas the dielectric constant and the polarisation are not mutually interdependent. In general, particle motions are linked to the interfacial stresses via the particle forces and torques but particle motions influence the flow and electric fields and hence the stresses.

For dilute systems of rigid symmetrical particles Okagawa[111] obtained expressions for the angular velocities of a particle in the combined fields. The rotation and alignment of the spheroid was found to depend on a function, f, where:-

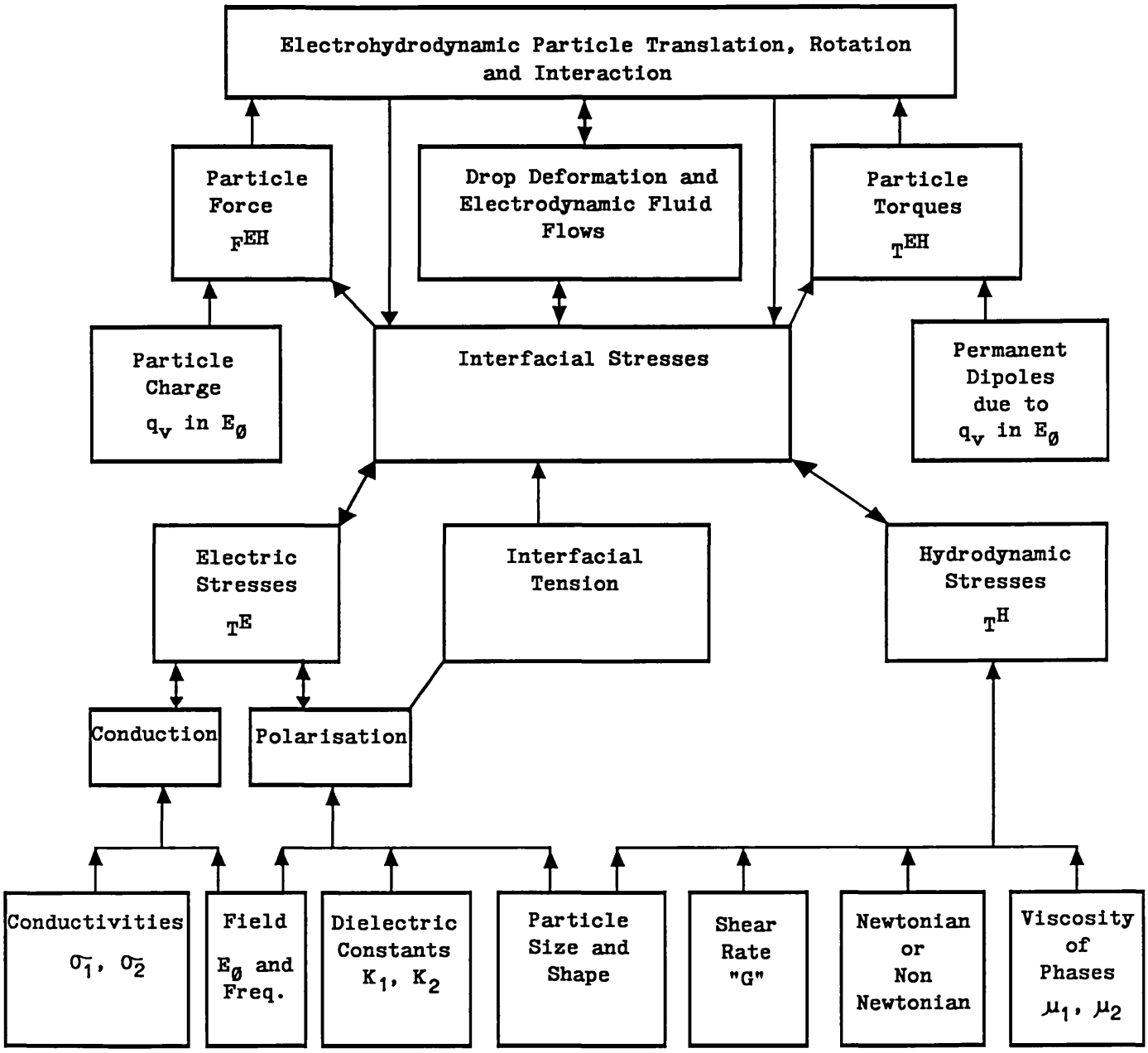
$$f \approx \epsilon_o \epsilon_r E_o^2 / \mu G \qquad \text{---- (2.6)}$$

and was, in essence, a measure of the ratio of the electrical to shear stresses. The function, f, is seen to depend upon the electric field squared, indicating that the effects are independent of polarity, the shear rate, the continuous phase Newtonian viscosity, the dielectric constant and a function that characterises the effect of induced polarisation on the motion. It was assumed that no permanent dipole exists. If this were not the case a linear dependence on polarity would be observed. The function f can be used to characterise the behaviour of particles in combined fields and its square, f^2, enables three different

regimes to be distinguished. Thus $f^2 = 1$ is termed a *critical field*, $f^2 > 1$ a *super-critical field* and $f^2 < 1$ a *sub-critical field*. These are shown in table 2.2. If the suspension is subjected to shear alone, $E_0 = 0$ and $f^2 = 0$ then the period of rotation is given by the formula for the rotation of a spheroid $T = 2\pi(r_e + r_e^{-1})/G$ where r_e is the equivalent hydrodynamic radius. As a critical field condition is approached, i.e. when $f^2 \rightarrow 1$, the rotation period becomes infinite and the particle stops spinning. At this point and beyond into the super-critical field condition, the particles assume a steady orientation and motion induced field disturbances cease.

It is indicated from the above analysis that particles will behave differently in shear alone, in electric field alone and when both are applied simultaneously. Davis[133-134] has calculated the mutually induced electric forces between two spheres in a uniform electric field. Particle motions are due to the dielectrophoresis forces arising from the non-uniformity of the electric field in the vicinity of the sphere. The forces developed can be attractive or repulsive depending upon the orientation of the line of centres of the particles. It is therefore expected that whilst a shear field alone does not induce any aggregation of a suspension the effect of combined fields will result in some form of aggregation. Such aggregation has been observed by Mason[107] where two particles are seen to form a doublet that is permanent as long as the electric field is applied. The doublet is able to attract a third particle which in general is out of alignment with the doublet centre and the triplet formed is bent. Similarly a fourth, fifth, sixth etc. particle can be attracted to form the chain like structure observed in dilute ER fluids. Once the electric field is removed the shear field can break up the chain formation.

Figure 2.9 Interaction of Hydrodynamic and Electric Fields



It is therefore possible, in principle, to accurately model the behaviour of a dilute model ER fluid system from a knowledge of the rotation, translation and capture of the particles and the resulting development of chain-like structures. In practice, however, ER fluids are far from ideal systems. At present spherical polymer particles that exhibit the ER effect cannot be manufactured. ER fluids are usually manufactured by the comminution of the polymeric material in a mill of some description. Consequently the particles are irregular and polydisperse. In addition ER fluids are used as concentrated suspensions for which the underlying principles, whilst being recognised, cannot be quantified in order to calculate the detailed structure of the suspensions. Even so, it is useful to highlight the principles of the structural formation process and deformation so that the empirical observations can be assessed in general terms.

It is apparent that when stable physical bonds are formed between particles the possibility exists for the formation of stable structures. To a first approximation two networks can be envisaged, a linear growth leading to chain like formations and a random growth which leads to a more spherically shaped cluster. The chain formation could be developed into a complex three dimensional network and at high concentration there would be little difference between the two. Graham and Bird[113-115] studied particle clusters in flow experiments using Information Theory techniques and predicted the suspension viscosity quite accurately. They concluded that the most applicable packing arrangement for concentrated suspensions was a close packed hexagonal arrangement. Kamphuis[116] et al using a network model similar to the elastic floc model of Frith and Hunter[117-123] explained the rheological properties of concentrated suspensions including the elastic response, the stress overshoot and the shear rate dependence. This network model consists of an assembly of chains of

particles packed close together with branches and links so that a three dimensional mesh is formed. The particles are close together due to attractive forces yet the configuration extends throughout the available space. In this case the structure is evolved from the balance of the structural build-up due to inter-particle forces and collisions and the structural break-down due to the shear forces. However, the characteristics of such creation and fracture processes are very specific to the nature of the dispersed system under consideration and need to be based on physical system properties such as the nature of the interactive forces, the flow characteristics and the shear rate. The creation of chains will depend on the rate of collision induced by the flow, the diffusion process and interactive forces and will be dependent, therefore, on the particle number density, the deformation history and the rate of deformation. For the network to be fractured it will be necessary for the force transmitted by the chain, the chain density, their orientation and length and the deformation history to be considered. It is therefore apparent that such a situation to be accurately defined is a very difficult, if not impossible, problem. There are two basic ways of proceeding. Firstly to fit model stress curves to the experimental data and for information concerning the structural dynamics and interactive forces to be extracted. Secondly, if the three dimensional structure of the system is known, to fit the experimental data to system models and hence the interactive forces can be obtained. Conversely the interactive forces can be used together with the experimental data to derive the structure. In the second case it is necessary for knowledge of the structural kinetics to be available.

In this chapter the principle processes involved in the properties of ER fluids have been reviewed and it is apparent that the subject spans many disciplines. It is also evident that, even without an applied electric field the understanding of the properties of concentrated

polydisperse systems is limited and that the most appropriate way of progressing is by experiment and the interpretation of the data.

CHAPTER 3

EXPERIMENTAL APPARATUS

3.1 INTRODUCTION

This chapter has six sections that fall naturally into two main parts. In the first part, sections 3.1 to 3.5, the experimental equipment used for the generation of the data is discussed. The second part, section 3.6, the fluids used in the study are detailed. A comprehensive list of the experiments performed are included in the appendix. There were three main items of equipment used in this work. These are referred to as the Valve and Fluid Development Rig (VFDR), which was a flow device where an ER fluid is forced along a flow path that can be approximated to plane parallel flow. Pressure drop measurement were taken in conjunction with flow rates. The second device was known as the Electro-Rheological Viscometer (ERV) in which Couette flow was established and measurements of torque and rotational speed are taken. Finally, the Static Yield Rig (SYR), where simple shear was established and the load required to shear the fluid measured. These devices were supplemented by one other additional item of equipment, a conventional concentric cylinder viscometer, a Contraves Rheomat 115.

3.2 THE VALVE AND FLUID DEVELOPMENT RIG

The Valve and Fluid Development Rig (VFDR) was a fully automated research apparatus in which electro-rheological fluids and valve geometries were assessed. The apparatus, shown in block diagram form in figure 3.1, can be conveniently split into three parts, the first being the hydraulic circuit which uses, wherever possible, conventional hydraulic components. Next was the data capture circuit which, as implied by the name, handles all the measurements, under computer control. Finally there was the computer hardware and the associated control software. The basic principle of this apparatus was to measure the pressure dropped through a valve at different conditions of flow, applied electric field and temperature. The valve geometry could then be varied. Finally a different ER fluid could be used and the sequence repeated.

3.2.1 ER FLUID FLOW CIRCUIT

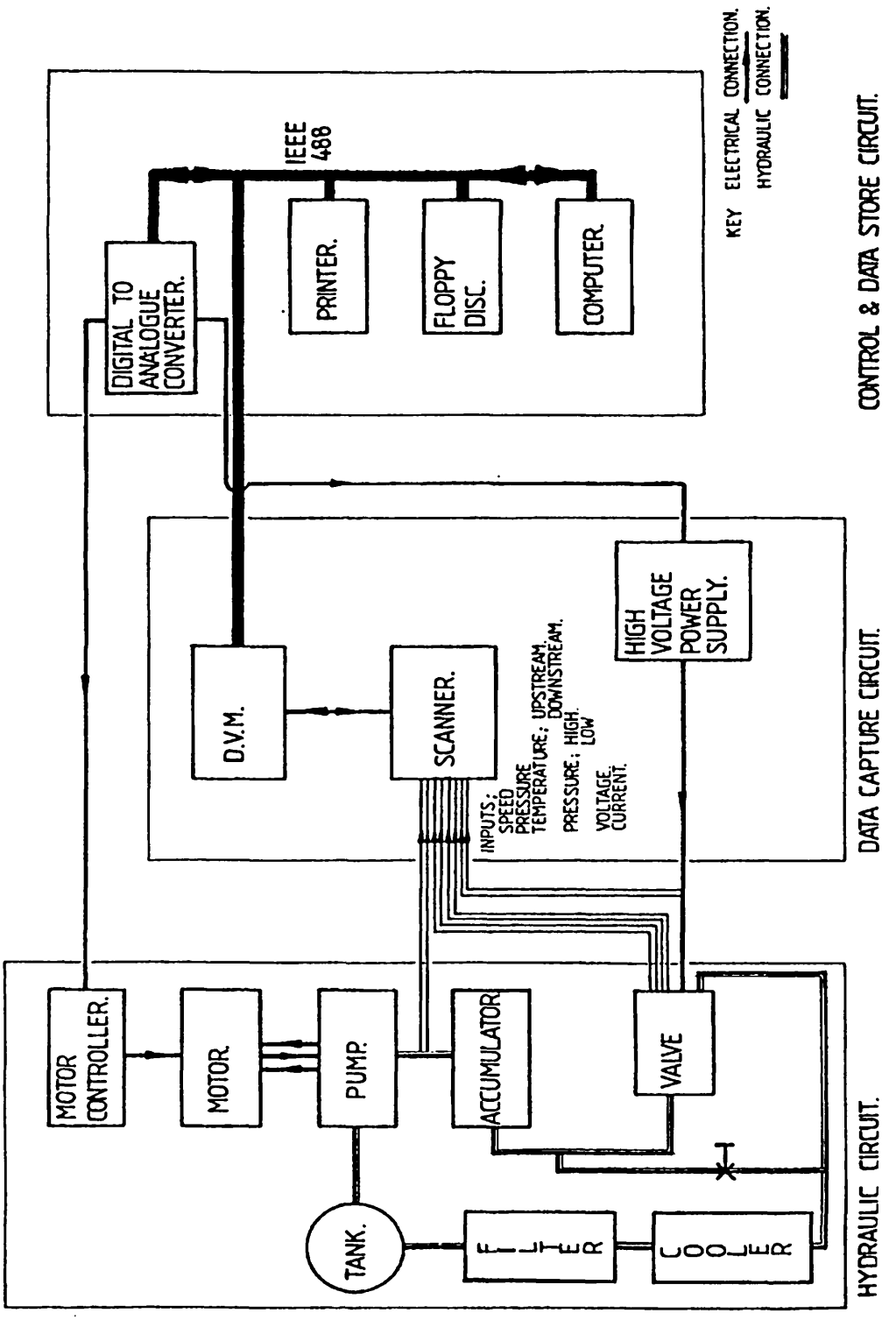
The hydraulic circuit was straightforward, and consisted of a variable speed motor driving the pump. The fluid, was passed through an accumulator, then through the ER valve, and finally to the tank via a cooler and filter. The tank was triple skinned with the two inner skins providing a flow path for a coolant and the outer skins providing a space for an insulating layer. The tank could be evacuated or alternatively purged with nitrogen. It was fitted with a stirrer to keep the ER fluid particles in suspension at all times.

The Motor, Controller and Pump Assembly

The motor was a fan cooled dc shunt wound unit manufactured by Mawdsley Limited and was rated at 4.1 kW with a maximum speed of 2,000 rev/min. The controller, a Saftronics DC2S unit, was a thyristor type controller which provided a fixed excitation voltage and a varying armature voltage. The control circuit was isolated from the drive

circuit enabling remote speed control. The armature voltage provided a feedback signal to the control circuit which provided a speed control over a 20:1 range. Other features included a maximum and a minimum speed adjustment, a maximum current limit and current stability adjustment together with protection for over temperature and stalled conditions. In-house modifications included changeover switching for local or remote operation and the provision of a remote speed signal input. The pump was a Hydracell D4 unit manufactured by Wanner Engineering and delivered a maximum flow rate of 15 litres/min at a pressure of 60 bar. It was a three cylinder axial piston oil pump in which the pumping action of the pistons was transferred through hydraulic cells to the pumped fluid. The hydraulic cells are isolated from the pumped fluid by means of three membranes. Pressure was maintained in the system by poppet valves that were self aligning, self cleaning and self seating. The hydraulic circuit was separated from the pumping circuit and virtually any fluid or suspension could be handled. ER fluids are pumped with ease and studies had shown that the pump suffers negligible wear. The pump was a positive displacement device and the flow rate was varied by the pump speed. If an increased delivery pressure was demanded a slight fall in the flow rate was observed, this was compensated by the controller and the software to some extent, but by monitoring both the pump pressure and the pump speed the flow rate could be accurately calculated. The pump speed was monitored by an Orbit Controls Limited digital tachometer deriving an input signal from a 60 tooth wheel fitted to the pump shaft. A frequency to digital converter provided an analogue signal for the data acquisition circuit.

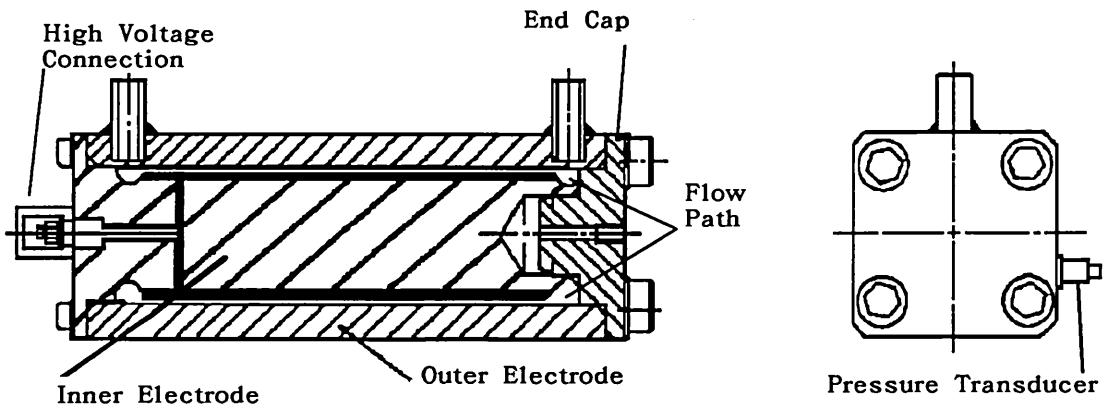
Figure 3.1 Block Diagram of Flow Rig



The Electro-Rheological Valve

The ER valve used in this study is shown schematically in figure 3.2. This design was evolved from a number of previous designs. The valve consisted of an inner electrode assembly, an outer earthed electrode and an end cap. The inner electrode was of interest, it consisted of a mild steel sleeved tufnol rod relieved at both ends to provide a smooth flow entry and exit to the electrode length. The steel sleeve, which was the high voltage electrode with an internal high voltage connection, was ground concentric to a location collar at one end and a counterbored centring hole at the other end. The end cap was suitably machined to locate into this hole. It also had a location collar similar to the inner electrode. The outer body was simply a square tube with a suitably finished hole through its centre; tapped holes are provided to secure the end cap and the inner electrode assembly. The design was elegant, simple, reliable, and could be cleaned and changed with particular ease. The concentricity was readily maintained and the attention to detail at the electrode edges are such that electric field strengths in excess of 12 kV/mm can be maintained.

Figure 3.2 Cross Section of an ER Valve



Four tapped holes are provided in the body to give access to the fluid flow path immediately before and after the electrode length. Two of these holes were used by miniature pressure transducers and directly accessed the flow path, thereby eliminating errors in the measured pressure due to any entry and exit losses. The transducers in question were Kulite, stainless steel, electron beam welded strain gauge devices. They were very rugged and capable of tolerating 100% over-range without being damaged. Linearity and hystersis were less than 1% of full scale with a repeatability of 0.25%. The low pressure units (100 psi) had a natural frequency of 80 kHz and the high pressure units (1000 psi) one of 225 kHz; output was a nominal 75 mV. Each transducer was supplied with its own calibration certificate. The other two holes were used by miniature, fast acting type T thermocouples. The temperature being measured by two Farnell DTT2 digital thermometers. These have a range of -15°C to 199.9°C, a resolution of 0.1°C with an accuracy of 0.1°C plus 1 digit. The units also provided an analogue output of 10mV/°C.

The Hydraulic Circuit

The remainder of the hydraulic circuit was conventional hydraulics. A piston accumulator followed the pump and efficiently eliminated the ripple from the pump outlet. Standard fittings connected the ER valve to the circuit. There then followed a conventional water/oil cooler and a large mesh (250 micron) filter. The filter outlet drained into the tank which had a capacity of approximately 5 litres. Temperature control was exercised using a Haake KT 40-4 cryostat. This had an operating range of -40°C to 40°C with a cooling capacity of 5,000 watts at 20°C and a heating capacity of 2,000 watts. The control head was a precision "Antidrift" unit specifically designed for the cryostat.

3.2.2 THE DATA CAPTURE CIRCUIT

Included in this circuit are the high voltage source, the measuring instrument and a scanner. Also included are miscellaneous circuits to drive the pressure transducers.

The High Voltage Power Supply

The power supply used was a standard high voltage laboratory unit manufactured by Hartley Measurements Limited. The unit operated in the voltage programmed mode and provided up to 5 kV at 20 mA. It was fitted with a remote input module requiring 5 volts for 5 kV output. Current and voltage monitoring was accomplished internally and was available as a 100 μA signal. Other features included a remote inhibit of the output, polarity changing and short-circuit proof design.

The Measuring System

The heart of the data capture circuit was a Solartron 7055 microprocessor voltmeter. The unit was equipped with an IEEE 488 communication bus and a processing interface which also included an RS232C interface. Accuracy was 0.002% plus 1 digit of the input scale, the unit was auto-ranging from 10mV to 1000 volts. Input sensitivity on the bottom range was 1 μV and 10mV on the upper range. Maximum reading rate without the filter was 330 readings per second, falling to 6 per second with the filter in. A Solartron 7010 scanner complemented the voltmeter. This unit was designed to accompany the 7055 voltmeter and derived both its power and timing signals from the voltmeter. All control signals were provided by the voltmeter which in turn received them from the system controller, usually a computer or a terminal. The scanner provided 16 channels, each 4 wire plus guard, and generated

a reading rate of 130 per second with less than 1 μV error due to switching noise.

Additional components were dc power supplies to drive the pressure transducer plus BNC sockets for external monitoring of signals.

3.2.3 THE CONTROL COMPUTER AND SOFTWARE

The experimental apparatus was automated and controlled via a computer on the IEEE 488 bus system. The following components form the system.

Computer

The computer was a Commodore PET machine with 32k of ram running Basic 4. It was fitted with an additional 8k of ram dedicated to the screen thus giving access to the individual pixels of the monitor. This gave a screen resolution of 400 by 200 points enabling reasonable graphics presentation of collected data.

Disc Drive

The disc drive was a Commodore 4040 with dual drives of 170k storage each. It was used for the storage of the collected data enabling additional processing at a later time.

Printer

The printer was again a Commodore machine; a 4022P bi-directional printer operating at 100 characters per second. Being a dot matrix machine it was possible for the screen graphics to be reproduced in bit image form on the printer.

Interface and Digital to Analogue Converter

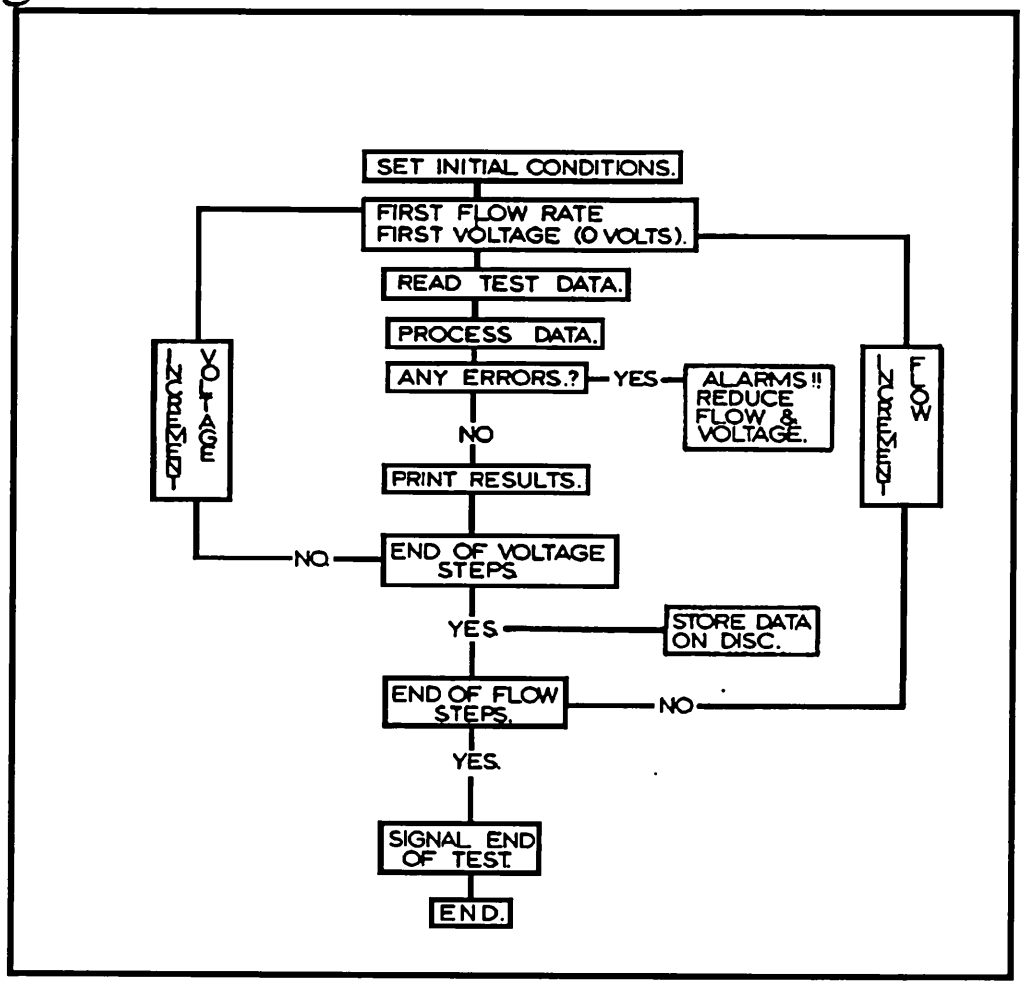
This was a 3D Designs, 8 channel, 8 bit resolution machine and was used to control the pump speed, the high voltage output, the inhibit signals and the alarm circuits. The maximum output was 5 volts with an accuracy of 0.5%.

Control Software

Data was collected on the apparatus of the pressure drop characteristics for a particular geometry against variables of flow rate and voltage. Other parameters are monitored, including temperature and current. The hardware described above in this section operated on the IEEE 488 bus and is interconnected with the voltmeter on the same bus system. The control software was designed to collect and store data as well as monitoring the system in terms of its integrity, for example, possible dangerous or erroneous conditions of pressures, flow rate and/or temperature. Included in the software procedure was a certain amount of data reduction. The general pattern of the programme is indicated by the flow chart, figure 3.3. The initial conditions are set as the first operation, these included details of the valve geometry, voltage and flow rate ranges and a subroutine that measured all the system zero errors so that all subsequent measurements are compensated. The programme commenced with the first, lowest, flow rate and increments the voltage from zero to the pre-determined maximum in steps that can be linear or a programmed function. At each voltage setting the following variables were read:-

a) Voltage Output
b) Current Drawn
c) Upstream Pressure
d) Downstream Pressure
e) Upstream Temperature
f) Downstream Temperature
g) Pump Speed
h) Pump Pressure

Figure 3.3 Software Flowchart for Flow Rig



Each reading was taken in sequence and 10 sequences were taken i.e. 80 readings being taken at the unfiltered scanner rate of 0.62 seconds. Each set was then averaged to provide 8 data points.

The next step was the reduction of the analogue readings to their engineering equivalents. Typically the analogue pressure signals were reduced to a pressure and the pump speed and pump pressure to a flow rate. Included in this step was the reduction of the pressure drop, via the valve geometry and a Bingham model, to a yield stress. The data were then printed to the printer. The voltage was incremented until the desired maximum voltage was reached, typically some 15 steps were used. When this stage was reached the entire set of data were transferred to disc,

the data arrays were re-set to zero and the sequence was repeated at a new flow rate; typically 11 flow rates were used. Additional features included data checking and system integrity checking at each voltage step, computation of the viscosity of the fluid and the wall shear rate at each flow setting, a theoretical modelling of the experimental conductivity data at each voltage set and a flushing procedure to fully mix the fluid prior to the next flow set. Once all the data have been stored a least squares fit of the pressure and flow data occurs, fitting the data to a Bingham model that did not assume prior values of either viscosity or of a yield stress. This was different from the computation that occurs during execution of the control programme, where a viscosity from the no voltage reading was assumed for all voltage steps.

TABLE 3.1 TABLE OF VALVE DIMENSIONS

Body Internal Diameter		Electrode External Diameter	Gap		Valve Length Electrode	Shear Rate Range
50.015	a	47.991	1.012 mm	a	150	600 - 5000
		48.489	0.763 mm	b	150	1000 - 8000
		48.983	0.516 mm	c	150	2500 - 21000
		48.983	0.516 mm	d	150	2500 - 21000
		48.466	0.775 mm	e	100	600 - 5000
		48.466	0.775 mm	f	100	600 - 5000
50.013	b	48.489	0.762 mm	g	150	600 - 5000
50.055	c	48.489	0.783 mm	h	150	600 - 5000
30.005	d	28.386	0.810 mm	i	60	1700 - 14000
		28.594	0.706 mm	j	60	2300 - 18000
		28.785	0.610 mm	k	60	3000 - 25000
		28.989	0.508 mm	l	60	4000 - 36000

Body (a) used with electrodes a,b,c and e.
Bodies (b) and (c) used with electrodes c and d, e and f, g and h to give pairs for response studies.
Body (g) used with electrodes i,j,k and l

Shear Rate from $G_w = 2\pi Q/H^2W$

where Q, the flow rate, varies from 0.5 to 8 ltr/min
and H valve gap W valve width
D mean diameter G_w wall shear rate

The total time of this procedure was approximately 3 hours during which time a total of 13,200 readings are taken and 1,485 readings are stored along with a description of the fluid, experimental details and description of the valve geometry valve, for additional processing at a later stage. A hard copy of the data was also available from the printer.

3.3 THE ELECTRO-RHEOLOGICAL VISCOMETER

The Electro-Rheological Viscometer (ERV), shown schematically in figure 3.4, was essentially a concentric cylinder viscometer designed to investigate ER fluids. Some significant differences from a conventional viscometer are required to permit this. In particular it was necessary for the low voltage circuits to be isolated and protected from the high voltage circuit. It was also essential for the magnitude of the torque being transmitted to be considered along with the effect of heating in the fluid being investigated. Finally for comparative purposes, with clutch type devices, the viscometer had been designed to be operated at high shear rates, typical values being 3,000 to 5,000 sec^{-1}.

The philosophy of construction and operation of this device was similar to the flow device described above in that it was composed of three main sections. Firstly there was the viscometer itself with its cooling and drive system, next there was the measurement and data transfer system backed up by a computer to control, monitor, process, and store the data that was generated.

3.3.1 THE ELECTRO-RHEOLOGICAL VISCOMETER

The viscometer consisted of a rotor that runs in a jacketed copper cylindrical stator. The stator had a nominal diameter of 28 mm and rotors were available to give nominal radial clearances of 0.5 mm, 0.75 mm and 1.00 mm and length variations of 30 mm, 40 mm and 50 mm. The rotors have one interesting design feature in that the centre was bored out and a 10mm diameter by 100mm length heat pipe was inserted into the hole. The hot end aligned with the rotor body and the cool end aligned with a series of fins that were cooled by both the rotation of the rotor and the flow of air from a miniature fan. The stator was cooled by using circulating mineral oil from a Haake F3-C circulator. With these two features good temperature control was provided

over the range 5°C to 100°C. At temperatures below the atmospheric dew point the entire viscometer can be enclosed in an air tight perspex cover and the air purged with dry nitrogen.

The rotor was held concentric to the stator by the use of a spherical ball that rode in a vee notch in both the bottom of the stator and the rotor. The top of the rotor could be moved relative to the stator by three nylon adjustments screws. A dial test indicator was clamped to the rotor and the tip of the DTI rests on a concentrically machined location collar on the outside of the stator. Following adjustment of the screws and noting the deflection of the DTI concentricity errors of less than 0.05mm can be achieved.

The stator was bolted to a glass filled PTFE disc which was in turn bolted to an R.D.P. Electronics Limited torque transducer. This was a four arm strain gauge bridge device with an output of 15 mV for 1 Nm. The drive motor and feedback tachometer are bolted to a large triangular mounting plate that rides up and down three support pillars. Motion was conveyed to the mounting plate via three toothed belt driven ballscrews that are located inside the support pillars. Microswitches were used to control the limit of movement of the mounting plate. The connection between the drive motor and the rotor was made by a semi-flexible spiral coupling that permits some axial misalignment without excessive side load. The main drive motor was manufactured by Printed Motors Limited. It was a dc servo motor type G12M4T and was rated at 147 watts continuous. The other continuous ratings were a maximum speed of 3,650 rev/min with a maximum torque of 1 Nm. However, the motor can be driven a lot harder depending on cooling and the motor drive amplifier. The maximum pulsed torque was 10 Nm for 50 ms with a maximum power input rating of 500 kW/s. This massive power input gave the motor great acceleration and it could be accelerated from rest to full speed in some 12.5 ms. The tachometer provided an

output of 6 volts per 1000 rev/min and a linearity error of less than 0.05% was quoted. The ripple was less than 3% at 1000 rev/min. The controller, type 4Q 60/9 from Printed Motors, was a 12 kHz 4 quadrant chopper unit with internal presets for top speed, current limit and stability. The unit provided 60 volts at 9 amp continuously and 15 amp peak for 4 seconds. The controller provided input signal and feedback signal conditioning as well as adjustments for both continuous and peak currents. The input balance could be adjusted and a lead-lag compensator was provided. Safety features include logic and power monitoring with fault shutdown, short-circuit protection and over-temperature protection.

3.3.2 THE CONTROL BOX AND THE HIGH VOLTAGE POWER SUPPLY

The power supply used on this device, a Kepco BHK 2000-.01M unit, was of hybrid design giving a high voltage, precision regulated supply with automatic crossover between voltage and current regulation. It was equipped with 10 turn precision voltage and current controls, mode indicator lamps, and output voltage and current meters. Control of the output, up to 2,000 volts at 100mA, could be local or via a remote input signal.

The control, measuring and operation of the viscometer can be effected locally from the control box or remotely via a computer. The control box was split into three sections, the first contains power supplies to drive the torque transducer and the platform motor as well as the relay switching that limits the motion of the platform. The other two sections were similar in that they both utilised the same measuring systems. One section dealt with the voltage and current whilst the other dealt with the torque and speed. The voltage was measured via a resistor dropping chain and the current via a 10 ohm measuring resistor. The low voltage electronics was protected from the high voltage

circuit by a Burr-Brown 3652 optically coupled isolation amplifier. The voltage and speed were measured on two Normailair-Garrett Limited digital panel meters as were the current and torque signals. In the latter case the meter also provided the bridge supply and an analogue output signal.

All the measured signals, including the fluid temperature, which was measured using a Farnell DTT2 thermocouple meter described previously, were available via BNC sockets to drive recording instruments and through multicore cables to the PIP interface that connected the viscometer to the computer. The interface also provided analogue drive signals for the motor speed and the voltage. Remote or local operation was switch selectable.

3.3.3 THE CONTROL COMPUTER AND SOFTWARE

The apparatus was automated and controlled via a computer on the IEEE 488 bus system. The following components form the system.

Computer Control System

The system was identical to that on the VFDR apart from the interface.

Interface

Data transfer and control of the viscometer was carried out via an interface that operated on the IEEE 488 bus. The PIP interface was a microprocessor driven multi-function interface manufactured by Micro Consultants Limited. It was a stand alone unit that incorporated power supplies, the IEEE 488 bus board and an 8 bit analogue to digital converter, with software controllable ranges from 10 mV to 10.24 volts. There were a variety of plug in analogue output and digital input/output cards available as well as cards for battery back-up, internal clock, an RS232 interface and a capacitor scanner. For the control and data

logging of the viscometer two analogue output channels and five analogue input channels were required.

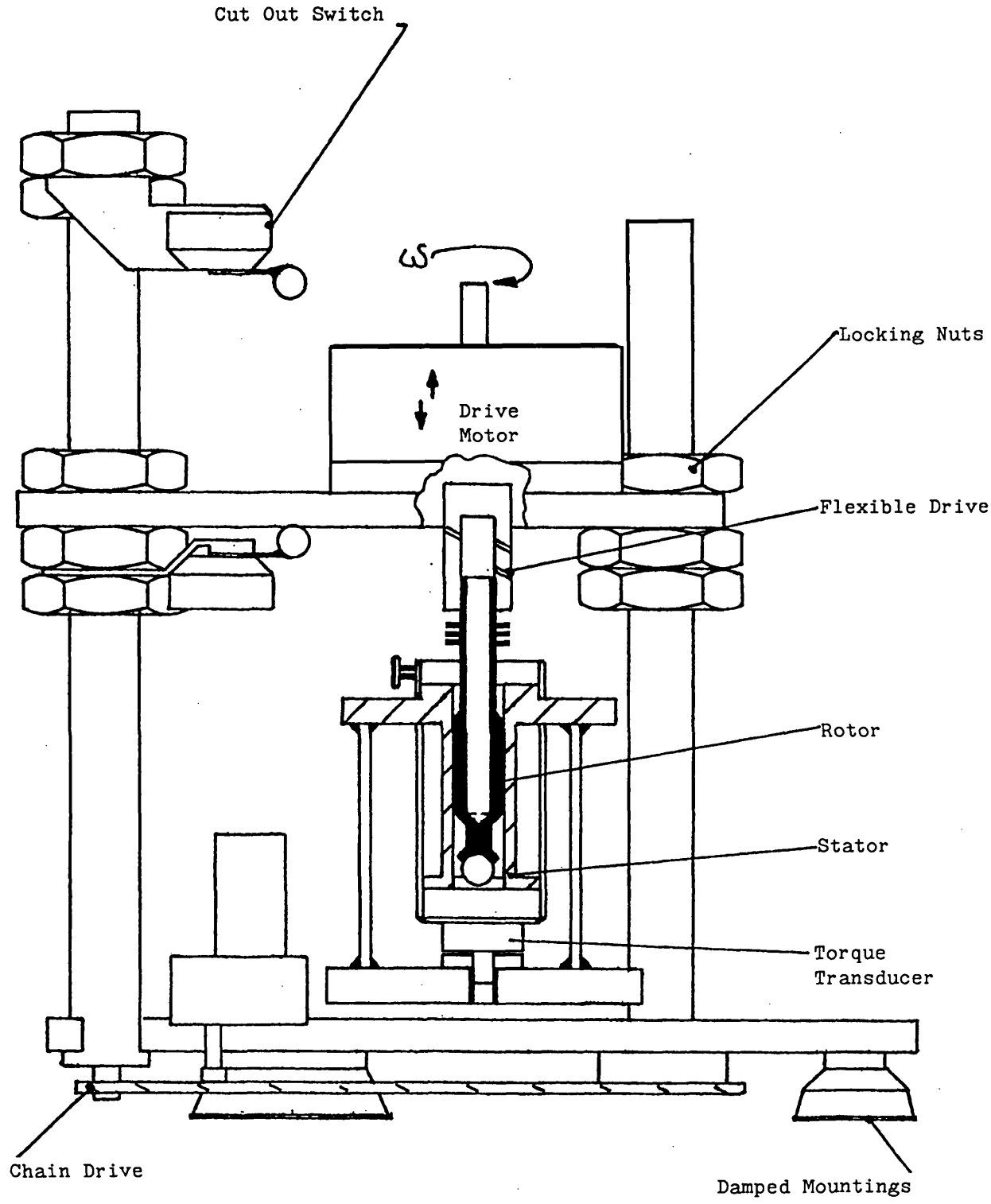
Control Software

The control software followed the same concept as for the VFDR. The programme was fed with details of the rotor used, the voltage range required and the shear rate range required. The viscometer could be operated by stepping through either shear rates or voltages with the option of incrementing the other variable later in the programme. The sequence used was to step the shear rate through a data set and then increment the voltage step. This was the reverse of the VFDR system described earlier. All data are stored for later analysis. The analogue voltage signals are converted at each step e.g. the speeds were converted to a shear rate and the torques were converted into a shear stress. The viscosity was calculated for each set as was the yield stress. There are a variety of features included to improve both the operation and the reliability of the system. The automatic torque error correction was one. Before each data set the viscometer was set to run between 2 to 5 rev/min and the torque was measured some 200 times. This torque was assumed to be the zero torque error and was subtracted from the measured torque; the measurement also provided an indication of the reliability of the results for if the torque error had changed significantly some error had probably been introduced. Other features included a variable number of readings depending on rotor speed thereby improving accuracy at low shear rates, setting the speed to 100 rev/min between each set of readings to ensure temperature stability, variable cooling times which are shear rate dependent so at high rates of shear and high energy input the cooling period was extended. The actual temperature rise was monitored using the Farnell DTT2 thermometer and measurements are taken immediately before the voltage was applied and immediately after it was removed. This ensured

that the effect of the high electric field in the vicinity of the thermocouple does not give spurious readings.

A typical experimental sequence would be to run through 20 shear steps and 15 voltage steps. At each step readings are taken of the voltage, current, speed, torque and temperature. Each set of five readings was taken between 35 and 50 times, the precise number being dependent on the rotor speed; therefore in a typical experiment around 40,000 to 50,000 readings were taken in the space of 1.5 hours. The data was reduced during this time and approximately 1,100 readings were stored for later analysis.

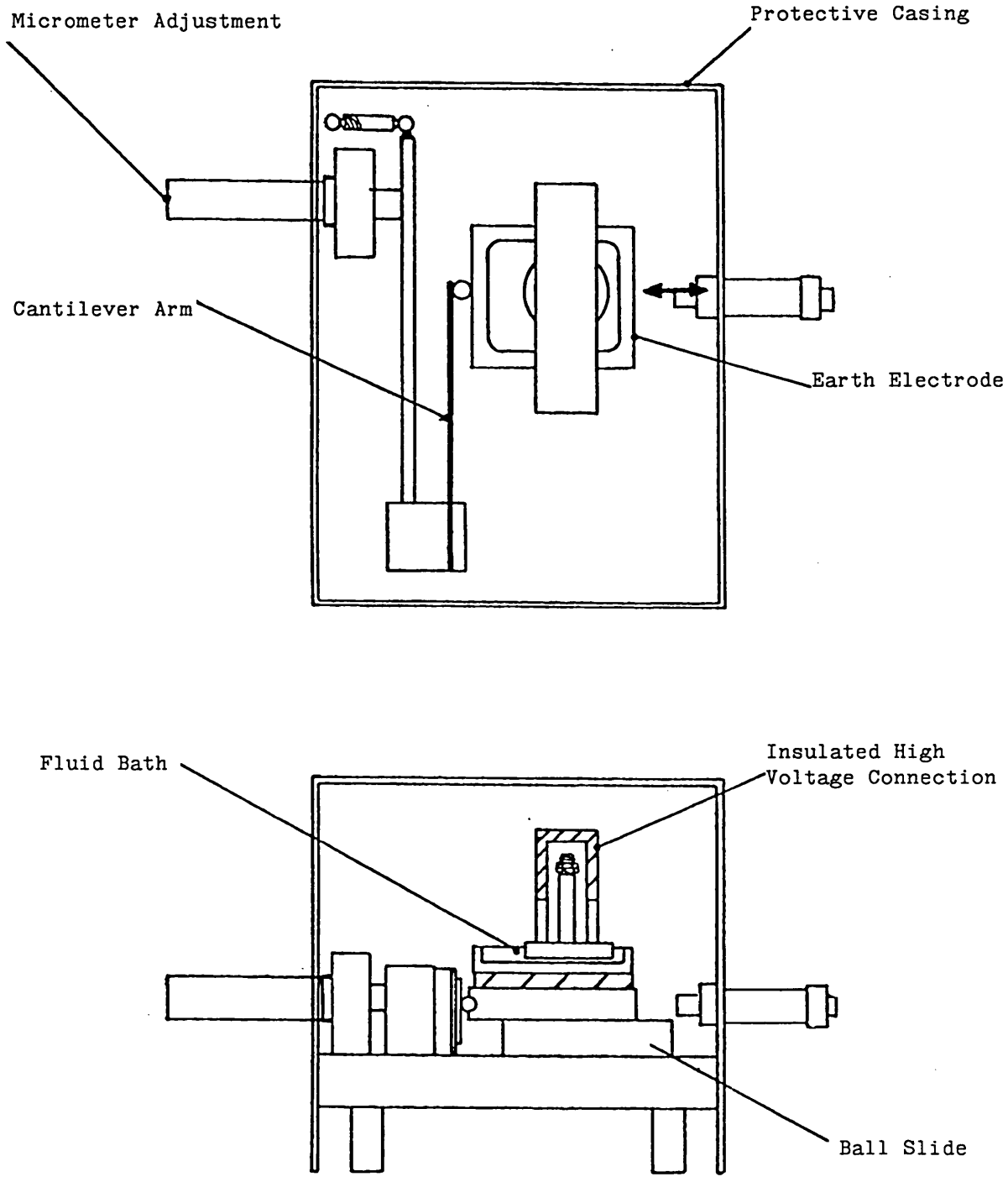
Figure 3.4 Schematic of Electro-Rheological Viscometer



3.4 THE STATIC YIELD RIG

The Static Yield Rig (SYR) was a small laboratory or workshop device for measuring both the electro-rheological effect and the conductivity of an ER fluid. It is shown in schematic form in figure 3.5. The unit was sufficiently accurate to enable details of the zero shear rate yield behaviour of an ER fluids to be provided. The zero shear rate yield behaviour being defined as the stress at which an ER fluid will fail with an electric field applied but under conditions of zero shear rate. The device consisted of a fixed high voltage electrode supported in a gantry above an earthed movable lower electrode. The upper electrode was isolated from the gantry by means of an insulated bush made from glass filled PTFE. Shims under the electrode allowed some flexibility in the electrode gap. The lower electrode was bonded to a thermoelectric cooler which was in turn bonded to a precision ball slide. Changing the polarity of the thermoelectric cooler converted it into a heater and thus permitted temperature control of the device. The lower electrode was shaped like a trough and the fluid to be studied was poured into the trough. Voltage was applied across the fluid between the two electrodes. Turning the micrometer screw loaded the cantilever arm which bore onto the movable lower electrode. The fluid resisted and the load was increased until the fluid yields, whereupon the slide moves. The readings of maximum shear stress and current are noted. The unit was reset, the voltage increased and the sequence repeated. The cantilever arm was instrumented with a four arm strain gauge bridge. A strain gauge conditioning amplifier provided the necessary bridge supply as well as the compensation and conditioning for the bridge. The bridge supply was adjustable as was the zero offset and the gain. This last feature enabled different arms to be used and effects such as creep to be studied.

Figure 3.5 Schematic of Static Yield Rig



The control box was a self contained measuring unit and housed all the necessary equipment for the operation of the apparatus. A temperature controller was also hgoused as was a high voltage power supply capable of delivering 2.5 kV at 4.0 mA. The power supply was short circuit proof and folds back if excessive current was drawn. The power supply was provided with analogue outputs to monitor both the current and the voltage. These were both 10 volts for full scale output. The bridge output was scaled so that 7.5 volts was equivalent to a stress of 20 kPa. There was a switch selectable display showing both analogue and digital signals. The display was scaled in kilovolts 0-2.5 kV, current 0-4 mA and yield stress 0-20 kPa. Included are on-off switching, fusing, a heater boost button, a display hold button and a high voltage logic interrupt that switches off the voltage. Voltage control was either via a local 10 turn potentiometer or a remote 0-5V signal. Four BNC plugs are provided enabling the measured signals for volts, current, stress and temperature, to be fed to an external measuring or recording device.

3.5 THE CONTRAVES RHEOMAT 115

This was a standard viscometer produced by Contraves AG. It was a conventional concentric cylinder device and could be operated over a shear range of 1 to 1000 sec^{-1}. The torque measurement range was from 0 to 50mNm. It was equipped with a selectable low pass filter and hold button. The unit was controlled by a Hewlett Packard 85F computer via a Contraves Rheoanalyser interface. This enabled automatic experimentation on samples as well as graphical presentation of the results, a Hewlett Packard 7225B plotter being used for this purpose. Temperature was controlled using a Haake D8-13 bath and a Haake EK-12 cooler. This could be operated over a range from 0 to 80°C.

3.6 THE ER FLUIDS AND THEIR MANUFACTURE

The ER fluids used in this research have all been manufactured in the same manner with chemicals obtained from the same supplier. Previous work had shown that the fluid manufacturing technique described below produced reliable and reproducible fluids. The fluids are made of two main components, the continuous phase and the dispersed phase, the latter component was itself made from two components.

3.6.1 CONSTITUENTS

The Continuous Phase

The continuous phase, a chlorinated paraffin with a stoichiometry of $C_{12}H_{21}Cl_5$, was a product supplied by I.C.I. and can be obtained under the proprietary name of Cereclor 50LV. It was a pale yellow liquid, stable up to 140°C, and compatible with most metals. It had a density of 1.19 gm/cm^3 at 25°C and a viscosity of 0.80 poise at the same temperature. It was chosen for this study on the grounds of stability, its intrinsic lubrication properties and its general qualities as a continuous phase for ER fluids.

The Dispersed Phase

The dispersed phase was the product of the reaction of lithium hydroxide and polymethacrylic acid. The lithium hydroxide was obtained from B.D.H. Chemicals in the form of 99.5% pure lithium hydroxide monohydrate. It was caustic and an irritant. The polymethacrylic acid was supplied by Allied Colloids under the name of Versicol K13 and was in the form of an 20% aqueous solution. The viscosity at 25°C was 54 poise with a density of 1.07 gm/cm^3. The number average molecular weight was approximately 26,000.

3.6.2 THE MANUFACTURING PROCESS

The manufacture of an ER fluid can be split into four sections, that of neutralising the acid, initial drying of the aqueous solution, secondary drying to the required water content and finally milling so that the size of the particles is reduced.

Lithium hydroxide was added to the polymer acid and mixed well using an industrial mixer. The pH was continuously monitored using a Beckman 31 digital pH meter until a pH of 9.00 was obtained. The material was then mixed for a further 30 minutes and the pH was re-checked.

The aqueous solution was then dried in a Niro Atomiser S-125R spray dryer. The solution was pre-heated to 50°C and then was atomised and mixed with a stream of air heated to 220°C. The water was driven off and after a retention time of 15-30 seconds the dry product was collected. Additional product was collected from the exhaust air stream by a cyclone arrangement. The final water content of the product was dictated by the exhaust temperature and it has been found that a temperature of 90°C was optimum. ER fluids require a well defined quantity of water and therefore a secondary drying stage was required. Before this was attempted the polymer was ground in a Sumeet 842 mill which reduces the "fluffy" polymer to a fine powder. The manufacture is assisted in a number of ways. For example, in the final wet milling stage it eases the flow of the suspension through the mill. Also in the assessment of the water content more surface area is exposed and the error in the measurement is reduced, and finally the secondary drying process is accelerated. The water content was assessed using a Mettler Infra Red dryer. Approximately 1 to 2 grams of polymer are required and a stable reading was obtained in 40 minutes with a heater temperature of 150°C. Repeatability measurements have shown that the instrument can measure the water content to an error of approximately ±0.05%. The water content measured by this technique was not the total water of the polymer.

For example, a measured water content value of 15.5% by the IR dryer when measured using a Karl Fischer technique gave a value of approximately 22% and a value of 26% if elemental analysis is used. The measurement was however repeatable and provided a measurement of the water in the polymer thereby enabling reproducable batches of fluid to be manufactured as required. Secondary drying was achieved in a fluidised bed dryer where a stream of warm air was passed through the polymer for a specified time. The water content was checked and the process repeated until the desired composition was produced.

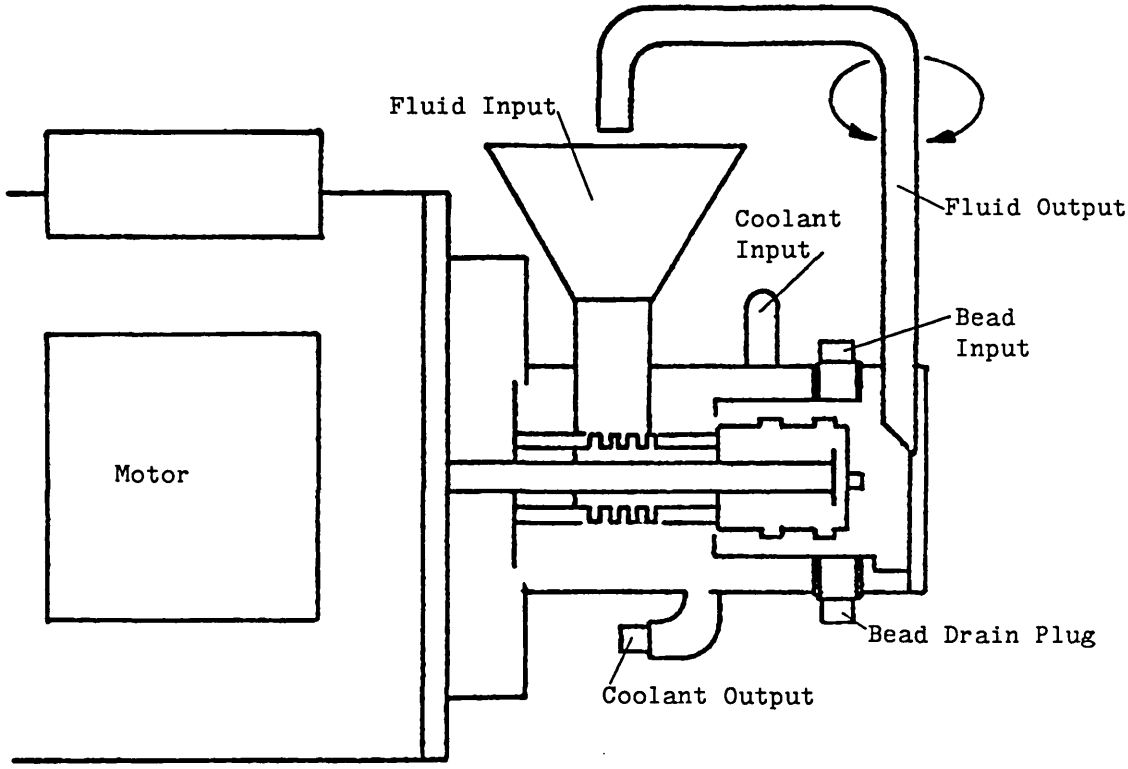
The final stage of the manufacturing process was for a quantity of polymer to be dispersed, according to the volume fraction required, into the continuous phase before the suspension was wet milled. This was achieved in an Eiger Bead mill, shown in figure 3.6. It consisted of a central pumping/agitator shaft which was spun at high speed, 5,000 rev/min, by an electric motor. The fluid was pumped into a chamber where a quantity of glass beads were held. The beads impact on the solid material in the fluid and the size of the particles is reduced. Coolant was circulated in a jacket around the grinding chamber, the temperature being maintained at 60°C.

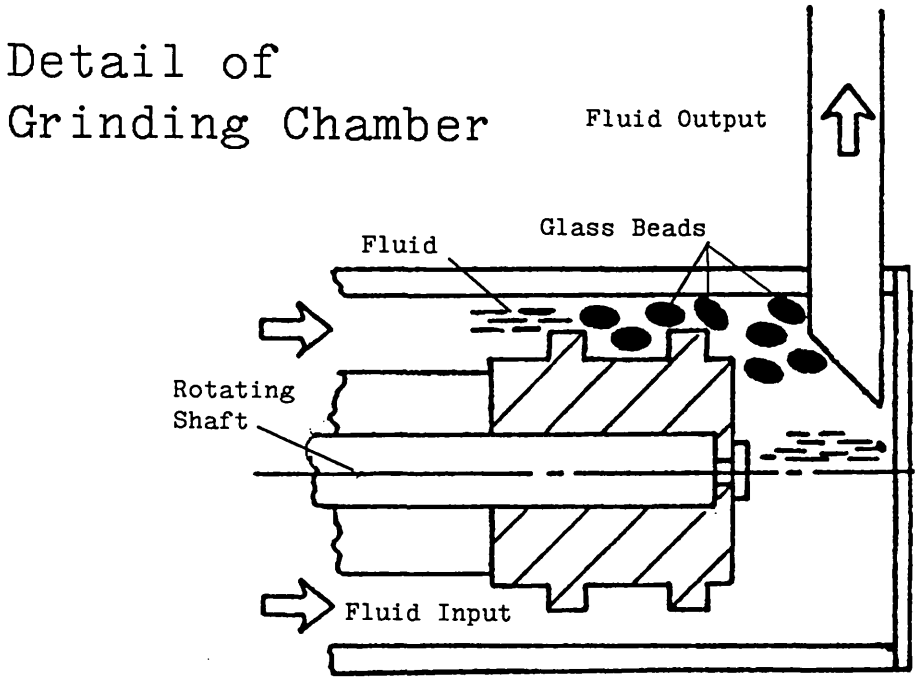
3.6.3 TYPICAL FLUID CHARACTERISTICS

The final product was a suspension of asymmetric particles covering a size range of 2-40 microns with a mean particle diameter of 6-7 micron. Listed below are details of the dispersed phase and the apparatus used to measure the parameters.

Property	Method		Data
Density	Micromeritics Auto Pycnometer		1.454 gm/cm^3
Particle Size	Coulter Counter	range	2-40 micron
		mean	6-7 micron
Surface Area	B.E.T Surface Area		0.589 m^2/gm
Pore Size	Micromeritics Auto-Pore 9200	size	0.537 cc/gm
		area	43.42 m^2/gm
	average pore diameter		0.05 micron

Figure 3.6 Schematic of Eiger Bead Mill





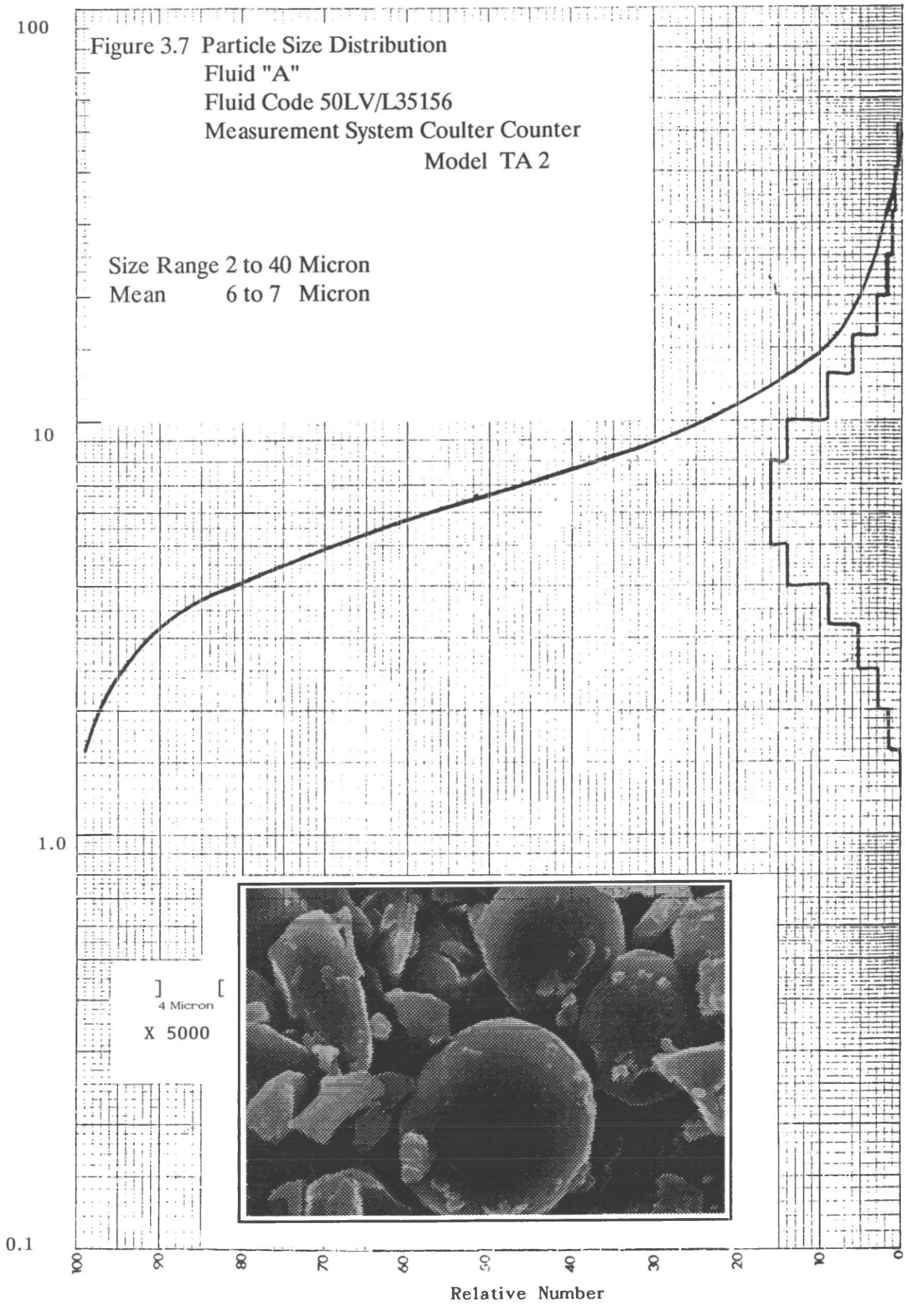
In figure 3.7 a typical particle size distribution for one of the fluids is shown. This, when compared with visual assessment is satisfactory. The inset shows a typical collection of particles.

Each fluid so manufactured was assigned a fluid code as indicated in section 1.3. For example a code of 50LV/L35156 used Cereclor 50LV as the continuous phase, 50LV, and the alphanumerics L35156 designated a polymer, of lithium polymethacrylate, L, at a volume fraction of 35% and water content 15.6%.

The following fluids were manufactured in five litre batches and used in the study.

Code		Description
50LV/L35135	(F)	35% volume fraction 13.5% water
50LV/L35156	(A)	35% volume fraction 15.6% water
50LV/L35157	(B)	35% volume fraction 15.7% water
50LV/L35166	(G)	35% volume fraction 17.4% water
50LV/L35180*	(C)	35% volume fraction 18.0% water
50LV/L30180	(D)	30% volume fraction 18.0% water
50LV/L35180*	(C)	35% volume fraction 18.0% water
50LV/L40180	(E)	35% volume fraction 18.0% water

* These are The same fluid in practice.


Figure 3.7 Particle Size Distribution
Fluid "A"
Fluid Code 50LV/L35156
Measurement System Coulter Counter
Model TA 2
Size Range 2 to 40 Micron
Mean 6 to 7 Micron
100
10
1.0
0.1
] [
4 Micron
X 5000
100
90
80
70
60
50
40
30
20
10
0
Relative Number

CHAPTER 4

EXPERIMENTAL RESULTS

4.1 INTRODUCTION

The following selection of experimental data can be sub-divided into a number of sections. In the first section data from the Valve and Fluid Development Rig (VFDR) is dealt with and it is the most comprehensive section. Data is presented on the reproducibility, geometry, current density and composition of the fluids. This is followed by a section covering data from the Electro-Rheological Viscometer (ERV) and a representative selection of the data is presented. Some acceptable reduction in the quantity of graphical information is introduced based on the extensive data presented in the previous section. In subsequent sections the Static Yield Rig (SYR) and the Contraves Rheomat 115 viscometer are covered.

A general format is followed for all sections, data is presented initially showing the reproducibility of the experiment, followed by the effect of geometric parameters, electrode gap, length and width on the ER behaviour. Temperature is then discussed before concluding with fluid parameters such as volume fraction and water content.

The graphical presentation of the data referred to in this chapter is collected en masse and can be located in appendix A3, this is the final section the thesis.

4.2 THE VALVE AND FLUID DEVELOPMENT RIG

A full description of the VFDR has been presented in section 3.2 and only a brief description is given here. The apparatus consisted of a pressure source, a pump, that forced the fluid at a constant flow rate through an ER valve. The ER valve is of concentric cylinder design and different electrode configurations can be used to give different geometries. Upstream and downstream pressures were measured using miniature pressure transducers located at the entrance to the electrode path thereby reducing the effect of any entrance and exit pressure drop. The pump speed and pump pressure were monitored and the flow rate calculated from these two variables; the calibration being checked using a collection method at regular intervals. The applied voltage and current drawn were measured along with the downstream fluid temperature.

The entire operation of the equipment was computer controlled and consisted of stepping through a voltage range at a fixed flow rate. This sequence was then repeated again at a higher flow rate. Sixteen voltage steps and thirteen flow rate steps were used.

4.2.1 REDUCTION OF RAW DATA

Plots of pressure against flow rate are of practical interest, but to provide data for investigation into valve geometry and fluid behaviour the pressure needs to be reduced to a shear stress and the flow rate to a shear rate. The latter is easily achieved by the following expression[144]:-

$$G_w = \frac{2 * \pi * Q}{H^2 * W} \quad \text{---- (4.1)}$$ *

where G_w is the wall shear rate
Q is the flow rate
H is the valve gap
and W is the valve width

The method by which the developed pressure is reduced to a shear stress is somewhat more complicated. In the simplest case, the Newtonian pressure drop can be evaluated from:-

$$P_n = \frac{12 * \mu * Q * L}{H^3 * W} \quad \text{---- (4.2)}$$

where μ is the Newtonian viscosity
and L is the valve (electrode) length.

The electric field induced pressure drop can be calculated by:-

$$P_e = \frac{2 * T_y * L}{H} \quad \text{---- (4.3)}$$

where T_y is the yield stress due to the applied electric field.

Equation 4.2 has been shown to adequately model the Newtonian component but the use of equation 4.3 will, unfortunately, lead to an error in the order of 20% in the total pressure developed by an ER fluid. A treatment based on

*Equations in boxes are considered significant.

the existence of a yield stress producing a "plug" of unsheared fluid in the valve, has been shown to lead to a more acceptable result.

If figure 2.4a, reproduced below, is considered a general expression for the flow of a fluid with a yield stress down a parallel plate geometry can be developed. The total stress, T_x, in a fluid with a yield stress, T_y, and a Newtonian viscosity, μ, can be described by the following expression.

$$T_x = T_y + \mu \frac{dU}{dX} \qquad \text{---- (4.4)}$$

where U is the fluid velocity.

For flow between plane parallel plates

$$\frac{dT_x}{dX} = - G_p \qquad \text{---- (4.5)}$$

where G_p is the pressure gradient given by P_{tot}/L
and P_{tot} is the total pressure drop

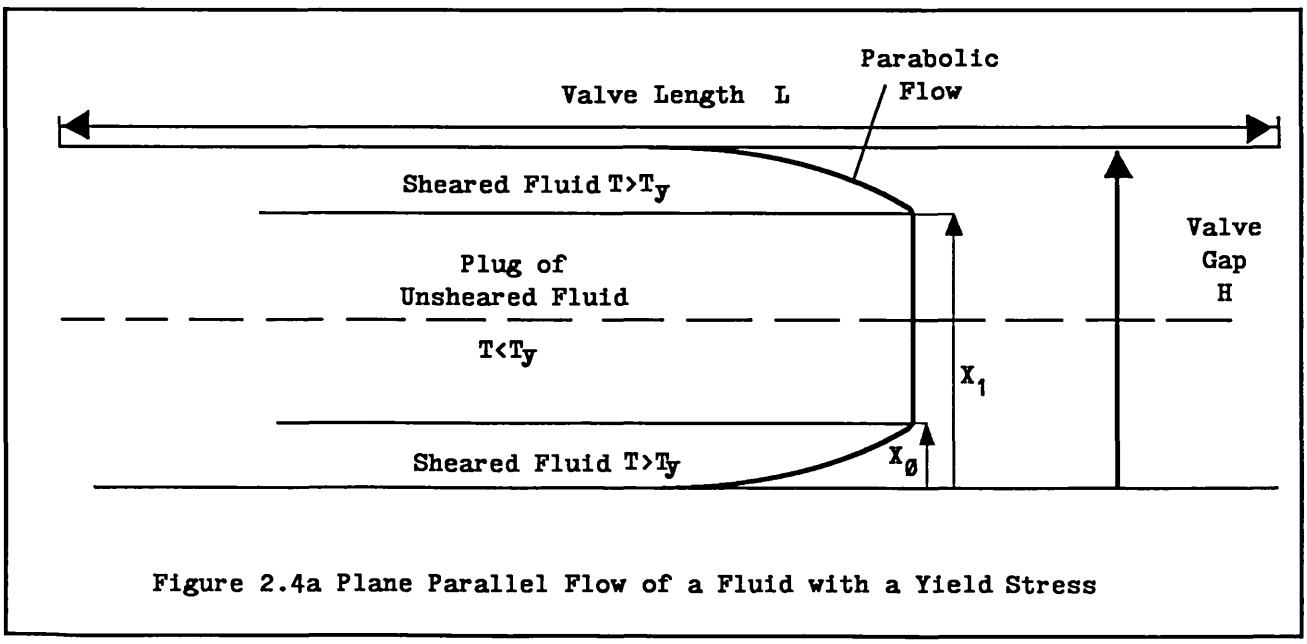


Figure 2.4a Plane Parallel Flow of a Fluid with a Yield Stress

A discontinuity exists at the boundaries of the sheared and the unsheared regions and therefore it is inadvisable for (4.4) to be substituted into (4.5) to form a differential equation as equation (4.4) is only valid if $T_x > T_y$.

It is noted that as the flow profile is symmetrical

$$T_x = 0 \text{ when } X = \frac{H}{2}$$

where X is the distance across the gap.

Equation (4.5) can therefore be integrated to give:-

$$T_x = G_p(H/2 - X) \qquad \text{---- (4.6)}$$

if (4.6) is substituted into (4.4) and re-arranged

$$\frac{dU}{dX} = \frac{1}{\mu}\left(\frac{G_p H}{2} - G_p X - Ty\right) \qquad \text{---- (4.7)}$$

Equation (4.7) is only valid when $T_x > T_y$ which is only valid when $dU/dX > 0$. That is, equation (4.7) will cease to be valid when;

$$T_y = G_p(H/2 - X_0)$$

$$\text{i.e. at } X_0 = \frac{H}{2} - \frac{T_y}{G_p}, \quad \frac{dU}{dX} = 0 \text{ and } T_x = T_y$$

For X between X_0 and X_1, the shear stress is below the yield stress and the fluid will move as a solid plug. The plug being symmetrical about the centre will only vanishes if T_y is zero or G_p is infinite.

Equation (4.7) can be integrated to give:-

$$U = \frac{G_p}{2\mu} X(H - X) - \frac{T_y X}{\mu} \qquad \text{---- (4.8)}$$

This will only be valid if $T_x > T_y$, i.e if $0 < X < X_0$ and by symmetry $X_1 < X < H$. As noted previously in the region $X_0 < X < X_0$ the material moves as a solid plug of fluid with velocity U_0 given by:-

$$U_0 = \frac{G_p}{2\mu} X_0(H - X_0) - \frac{T_y X_0}{\mu} \qquad \text{---- (4.9)}$$

as $X_0 = \frac{H}{2} - \frac{T_y}{G_p}$

it can be substituted to give:-

$$U_0 = \frac{G_p}{2\mu} \left(\frac{H}{2} - \frac{T_y}{G_p}\right)^2 \qquad \text{---- (4.10)}$$

An equation is now required for the pressure gradient along the valve in terms of the flow rate, the yield stress and the valve geometry.

$$Q = \int_0^H W\, U\, dX \qquad \text{---- (4.11)}$$

where W is the valve width

The integration is carried out across three zones, the unsheared plug and the two symmetrical sheared zones either side of the plug.

$$Q = 2W \int_0^{X_0} \left[\frac{G_p}{2\mu} X(H - X) - \frac{T_y X}{\mu}\right] dX + W(X_1 - X_0)U_0$$

Integrate the equation and substitute:-

$$X_0 = \frac{H}{2} - \frac{T_y}{G_p}$$

$$X_1 = \frac{H}{2} - \frac{T_y}{G_p}$$

and U_0 from (4.10) to obtain:-

$$Q = \frac{G_p H^3 W}{12\mu} * \left(1 - \frac{2T_y}{G_p H}\right)^2 * \left(1 + \frac{T_y}{G_p H}\right) \quad \text{---- (4.12)}$$

In practice it is more useful to express (4.12) in the form of pressure drop and flow rate and it is therefore necessary for the expression to be re-arranged as follows.

Let $x = \frac{Ty}{G_p H}$ and $b = \frac{12\mu Q}{G_p H^3 W}$

substitute these into (4.12) to give:-

$b = (1 - 2x)^2 * (1 + x)$ which expands to

$4x^3 - 3x = b - 1$

Using the trigonometric identity

$4\cos^3\theta - 3\cos\theta = \cos 3\theta$

θ can be evaluated as:-

$$\theta = \cos\left(\frac{1}{3}\cos^{-1}(b - 1) + \frac{4\pi}{3}\right) \quad \text{---- (4.13)}^{**}$$

**$4\pi/3$ is chosen as the only physically possible root.

If $G_0 = 12\mu Q/H^3W$, that is, the pressure gradient with no yield stress, then $b = G_0/G_p$. Additionally, it is noted that since $X = T_y/G_pH$, where $G_p = P_{tot}/L$ and $G_0 = P_n/L$, where P_n is the Newtonian pressure drop equation (4.13) can be re-written as:-

$$T_y = \frac{P_{tot}H}{L} \cos\left(\frac{1}{3}\cos^{-1}\left(\frac{P_n}{P_{tot}} - 1\right) + \frac{4\pi}{3}\right) \quad \text{---- (4.14)}$$

Therefore, from measurements of pressure drop with and without the applied electric field, P_{tot} and P_n, in conjunction with details of flow rate and the valve geometry, the yield stress in the case of Poiseuille flow can be determined.

4.2.2 REPRODUCIBILITY OF THE RESULTS

The applied electric field and the shear rate (flow rate) in a device combine and a given ER effect is produced and a current is seen to flow. The experimental sequence outlined above provided data on the effect of both electric field strength and flow rate. For the performance of a fluid to be described adequately both these factors have to be accounted for. In the data that follows on each page two graphs are displayed, the dependent variable being plotted against either electric field strength and flow or shear rate. In figures 1a to 3b the reproducibility of the data is indicated. Five complete sets of data are used and representative data at a fixed shear rate for the electric field strength plots and conversely fixed electric field strength for flow or shear rate plots are shown. The values of these two variables are usually 2200 sec^{-1} and 2.66 kV/mm and the temperature used is usually 30°C.

Figures 1a and 1b show the developed pressure plotted against applied electric field in 1a, and flow rate in

1b. The valve geometry for these results was 0.763 mm gap, 150 mm length and 155.8 mm width. The width of the valve was defined as the mean entrance diameter to the flow path, i.e. $\pi * D_m$, where D_m is the mean diameter of the valve. The nominal temperature was 30°C, but as this is difficult to maintain with the heat generated in the fluid, the following average temperatures resulted for experiments 1 to 5 respectively, 30.9°C, 30.4°C, 30.8°C, 31.0°C, and 29.9°C.

Plots of pressure drop against flow rate are of practical interest, but data is required for investigation into valve geometry and fluid behaviour. The pressure drop has to be expressed as a shear stress and the flow rate as a shear rate. If the two expressions, 4.1 and 4.14, are used, the curves in figures 1a and 1b can be reduced to 2a and 2b, plots of shear stress against electric field strength and shear stress against shear rate. The following data from the flow rig, showing shear stresses, have all been reduced in this manner. The trends presented are typical of ER fluids in this mode of operation.

Finally figures 3a and 3b show current density plotted against electric field strength and shear rate. The exponential form of the plot in figure 3a can be modelled using a sinh function of the form $J = Ae^{-\beta/kT} \sinh(aqE_0/kT)$ where J is the current density and A is a constant of proportionality. The fall of current density with shear rate is also typical of ER fluids. The derivation of this expression is dealt with in more detail in section 5.4

The calculated scatter on the shear stress was approximately ±5% for data presented for both the electric field and shear rate plots. This reduced to approximately ±4% in the case of the current density versus electric field strength plot. Overall the reproducibility was good.

4.2.3 THE EFFECT OF GEOMETRY

The applicability of equation 4.14 was further examined and the influence of the valve geometry on the ER effect was assessed. The results are shown in twelve graphs, 4a to 9b. The first six deal with the effect of the electrode gap and are presented in a form similar to the six graphs shown previously dealing with reproducibility. Figures 4a and 4b show the developed pressure for three gaps of nominal sizes 0.5, 0.75 and 1.0 mm. The trends seen in figures 1a and 1b are repeated here but scaled in a manner dependent upon the gap. In the case of figure 4a it is observed that the pressure developed at zero electric field strength was increased as the gap was reduced, due to the H^3 term in equation 4.2. It was also observed that the pressure developed under an applied electric field was also increased as the gap was decreased. A similar situation is seen in figure 4b. The pressure increased as the gap was reduced. A point to be noted is that for the 0.516 mm electrode gap in this figure the flow rate was reduced so as to control the heat input at the higher shear rates. If the above expression, equation 4.14, for the shear stress necessary to develop the pressure was applied to these graphs they could be reduced to give figures 5a and 5b. It is indicated in these two figures that the effect of the gap can be accounted for by the expression. In the case of the current density, figures 6a and 6b, a similar coalescence of the data was observed although more scatter was apparent on the data due to temperature fluctuations.

In a similar manner the effect of valve length can be eliminated. However, in this case the situation is complicated by the fact that for the valve length of 60 mm the width has also been reduced from 155.8 mm to 93.1 mm. In figures 7a and 7b the data is presented for the developed pressure and it is indicated that as the length is increased the total pressure drop is also increased. The ratio between the 150 mm and the 100 mm is scaled in an approximately linear fashion on the length but in the case of the 60 mm long electrode the scaling is less clear due to the difference in

valve width already mentioned. If the data is reduced to a shear stress and shear rate figures 8a and 8b are produced which show a good correlation for the different geometries. The data given for current density, figures 9a and 9b, are not as good. The effect of the temperature fluctuations can be seen in figure 9a for the case of the 150 and 100 mm lengths. The data was matched up to 2.2 kV/mm but then drifts apart due to the rise in temperature. The deviation in the 60 mm electrode length data is greater, as indicated and it may be that the current density does not directly scale with the valve width.

It has been clearly shown that if the model developed above is used, the pressure generated in an electrically stressed ER fluid can be accurately represented by a shear stress that is both electric field and shear rate dependent. It has also been shown that the model can successfully account for the effects of the valve geometry. It is therefore a relatively straightforward procedure for the pressure developed in an ER valve to be predicted for any given geometry from basic fluid data concerning the shear stress-electric field strength characteristic.

4.2.4 TEMPERATURE EFFECTS

If the temperature of the fluid is reduced the ER characteristics are affected in a number of ways, the most significant of which is the reduction in current density. The shear stress versus shear rate behaviour is also affected, both with and without the applied electric field. That is the Newtonian viscosity is increased as the temperature is decreased and therefore the Newtonian pressure drop is increased. The *total* developed pressure at different temperatures arises from a complex contribution of these sources. However, it has been shown that the developed pressure of any geometry can be reduced using equation 4.14 and presented as shear stress versus applied electric field strength and shear stress versus shear rate plots. This being the case, it is unnecessary for developed pressure against

applied electric field and flow rate at different temperatures to be reproduced, but rather to proceed directly to the reduced data forms. In figures 10a and 10b some typical results are shown. The general trend is similar to that seen in the previous plots although as the temperature is reduced the variation in the shear stress is more exaggerated. The effect of temperature on the current density is shown in figures 11a and 11b where it can be seen that the effect of temperature is very significant. A doubling of current density for approximately every 5 to 6°C temperature rise is observed.

4.2.5 FLUID COMPOSITION EFFECTS

It is now necessary for two basic aspects of fluid composition, volume fraction and water content, to be considered. Volume fraction experiments were conducted on three fluids at 30%, 35% and 40% solid content. These were all of the same water content. Experiments were conducted at different temperatures using different geometries. The water content data are of similar format although in these cases some five water contents at 35% volume fraction were studied.

The Effect of Volume Fraction

The effect of volume fraction is shown in figures 12a to 19b for experiments at a temperature of 30°C. The reduction demonstrated in this set of graphs is extended to three other temperatures, 25°C, 20°C and 15°C in figures 20a to 28b.

If the volume fraction is increased the Newtonian viscosity is increased and the shear stress at any given electric field strength and shear rate condition is also increased. The change of current density is slight and the trends are difficult to identify. The two effects are shown in figures 12a and 12b and 13a and 13b respectively and these trends are apparent at any given combination of shear rate and electric field strength. It is possible for the effect of volume fraction to be scaled by normalising the data. To do

this it is necessary for the individual shear stress to be divided by the maximum shear stress of the experimental set. That is the maximum value of the entire set of data, which is usually found to be at the maximum electric field strength and the minimum shear rate value. Alternatively the individual maximum of the data set under consideration can be used. A data set being defined by a complete set of shear rates at a fixed voltage or a complete set of voltage increments at a fixed shear rate. In the case of the shear rate set this will usually be the value at the minimum shear rate and for the electric field strength set it will be the value at the maximum electric field strength. In figures 14a to 18b the normalisation of the data at different shear rates for a fixed electric field strength and different electric field strengths for a fixed shear rate is shown. In this manner electric field strengths from 1.11 kV/mm to 2.96 kV/mm and shear rates from 1500 sec^{-1} to 7500 sec^{-1} have been covered. It is clear from this presentation that the effect of volume fraction can be normalised so as to be independent of both the electric field strength and the shear rate. The last figures for the 30°C data are 19a and 19b, these two plots show ten electric field strengths varied from 0.81 kV/mm to 2.95 kV/mm. This is virtually the entire experimental set of the 35% fluid. It is apparent that the change of shear stress with shear rate is decreased as the applied electric field is increased. To re-phrase this, the ability of the electric field induced structure to withstand the destructive effects of the shear rate is electric field dependent. The strength of the structural bonds is increased with applied electric field.

A similar normalisation procedure can be applied as the temperature is decreased. In figures 20a to 22b data is presented of shear stress, current density and normalised shear stress plotted against electric field strength and shear rate. These are repeated for 20°C in figures 23a to 23b, and 15°C in figures 26a to 28b. The normalisation becomes progressively worse as the temperature is reduced, and this can be attributed to the difficulties of maintaining constant

temperature. In figures 29a to 30b plots of temperature against shear rate are shown for three fluids. For the plot at 30°C, figure 30b, a good degree of overlap is indicated whereas the temperatures for the 15°C experiments, figure 29a, a progressive separation is observed above 3000 sec^{-1}. The normalised plot, figure 28b reflects this divergence.

The Effect of Water Content

In the final set of graphs the effect of water content on the performance of an ER fluid is dealt with. In figures 31a to 36b the shear stress and current density plots are covered in a similar manner to that used previously. Again the general form of the curve is the same regardless of water content although the response to the electric field and the shear rate varied with the water content. This is particularly clear for the 13.5% water content fluid where less shear stress is developed at any given shear rate. From this it can be concluded that a water content of 13.5% is well below the optimum for an ER fluid of this type. The current density is not significantly effected by the water content except at the maximum value where it is considerably higher. Generally the more water the more responsive is the fluid albeit, at the expense of an increased current flow.

4.3 THE ELECTRO-RHEOLOGICAL VISCOMETER

The Electro-Rheological Viscometer (ERV) has been fully described in section 3.3 and only a brief description will be given here. It was of concentric cylinder design with a stator diameter of approximately 28 mm. Various rotors were available giving different lengths and electrode gaps. The instrument differs from a conventional viscometer in that high electric fields can be applied to the stator in safety. The shear stresses generated are more than in a conventional device and consequently a larger torque sensing element is used. The maximum shear rate is somewhat higher than is commonly encountered so that shear rates found in typical clutch type applications are approximated. The instrument was computer controlled and a typical programme consisted of stepping through a set of shear rates at a fixed voltage before increasing the voltage and repeating the sequence. In practice twenty-one shear rate steps and sixteen electric field strength steps were used. The basic data generated is reported in a similar fashion to that of the previous section. The reproducibility will be dealt with initially before moving on to geometric effects, temperature, volume fraction and water content.

4.3.1 REPRODUCIBILITY OF THE RESULTS

Plots analogous to those presented for the VFDR can be generated in the case of the ERV, the most important being the excess shear stress and the current density. The excess shear stress, T_e, is defined as the difference between the total shear stress, T_t, and the shear stress with no applied electric field, T_n, which is the Newtonian component of the total shear stress. Data are presented in a similar manner to before as pairs of graphs, one plotted against electric field strength and one against shear rate. The computations for shear rate and shear stress were of a standard form for a concentric cylinder viscometer[134]. The calculation of the electric field strength gave the value measured at the stator,

that is, the position where the torque is measured. The shear rate is also referred to the stator.

Shear Rate:-

$$G = 2 * \Omega * R_b^2/(R_c^2 - R_b^2) \qquad \text{----(4.14)}$$

Shear Stress:-

$$T = \text{Torque} / (2 * \pi * R_c^2 * H) \qquad \text{----(4.15)}$$

Electric field Strength:-

$$E_0 = V_0 / \{R_c * \text{Ln}(R_c/R_b)\} \qquad \text{----(4.16)}$$

Current Density:-

$$J = I / (2 * \pi * R_m * H) \qquad \text{----(4.17)}$$

where:-
R_c is the stator (cup) radius R_b is the rotor (bob) radius
R_m is the mean radius $\frac{R_c+R_b}{2}$ Ω is the speed in rad/sec
H is the rotor height and V_0 is the applied voltage

In figures 37a and 37b the data from five experiments are shown. Each experiment is separate, in that a new sample of fluid was introduced into the stator for each experiment. The differences in figure 37a are due mainly to the temperature variation between each experiment. In figure 37b these variations are shown and a slight difference in the Newtonian stress component is noted. If the Newtonian component is subtracted from the total shear stress to give the excess shear stress figure 38b is obtained. Figure 38a is data from the same experiment but plotted against electric field strength. In both plots good reproducibility is shown with approximately ±5% deviation, similar to that obtained from the VFDR. The final pair of graphs, 39a and 39b, are of

current density, and the exponential form similar to those presented for the VFDR data is shown.

4.3.2 THE EFFECT OF GEOMETRY

In the section where data is presented for the VFDR, it has been shown that the data from the VFDR could be analysed using a general expression that related the pressure drop to the electric field induced shear stress. It was further shown that this expression could adequately take into account the geometry of the valve. This was dealt with in some detail in section 4.2.1 and it was concluded that the geometry could be excluded from the data and the ER characteristic could be expressed in terms of a shear stress and a wall shear rate. Consequently, in the interests of reducing the total number of graphs presented it is only necessary for one geometric variable to be considered as an example. It will thereby be indicated that a similar data reduction procedure can be applied to results from Couette flow. The length has been chosen to demonstrate this. In figures 40a and 40b the total shear stress against electric field strength and shear rate for three rotor lengths is shown. If the Newtonian component is subtracted figures 41a and 41b are produced. The reduction of the current density being shown in 42a and 42b. The reproducibility is similar to that for data generated using the VFDR for valve lengths. It is indicated that the fluids in Couette flow gave reproducible data and that the effect of geometry can be effectively removed from measurements. The discussion can, therefore, be centred around parameters such as shear stress, shear rate, electric field strength and current density.

In figures 43a to 45b some three pages of graphs, the three main parameters, shear stress, both total and excess, and current density are shown in the form generally obtained from the apparatus. For the excess shear stress and the current density versus shear rate plots a shear rate dependence similar to that of the VFDR was indicated, whilst the form of the curves are similar the magnitude of the shear

stresses are different. Figure 44a can be compared with figure 2a. At a electric field strength of 2.1 kV/mm the shear stress from the ERV is approximately 2.4 kPa, whereas the value from the VFDR was around 3.7 kPa. Due to the differences in temperature, 50°C, for the ERV and 30°C for the VFDR, a direct comparison of the current densities is not possible. However, as noted previously, the current density doubles every 5 to 6°C, the two situations can be approximated. From figure 45a the current density at 2.1 kV/mm was in the order of 240 $\mu A/cm^2$. The value for the VFDR data, figure 3a, was approximately 32 $\mu A/cm^2$ at 30°C. Assuming a doubling every 6°C the extrapolated current density for the VFDR case will be in the order of 250 $\mu A/cm^2$, which is an acceptable correlation.

4.3.3 TEMPERATURE EFFECTS

The effect of temperature is dealt with in a similar fashion as before, total shear stress being presented in figures 46a and 46b, with excess shear stress in figures 47a and 47b. Again, as in the case of the VFDR data, a similar shape for the plots was observed, that is, a reduction in the excess shear stress at any given shear rate as the temperature was reduced. Poor temperature control is observed for the 10°C data and should be considered unreliable above a shear rate of 1000 sec^{-1}. It is indicated that at zero shear rate the ER effect is, to a first approximation, independent of temperature. It would appear, therefore, that if the temperature is lowered the ability of the electric field induced structure to resist the shear forces is reduced so that at low shear rates where the electric forces dominate the effect of temperature changes are minimal.

4.3.4 FLUID COMPOSITION EFFECTS

The effect of volume fraction and water content are covered in graphs 48a to 54b. The procedure for the volume fraction is similar to that adopted for the VFDR data and is presented in graphs 48a to 51b.

The Effect of Volume Fraction

As the volume fraction is increased the ER effect is also increased along with the current drawn. In figures 48a and 48b the total shear stress plots for the three volume fraction fluids discussed previously is shown. The Newtonian component is higher for higher volume fraction fluids but this can be removed the plots. In figures 49a and 49b it is indicated that the excess shear stress for the fluids was also increased as the volume fraction was increased. The current density was also increased slightly as the volume fraction was raised. This is different from the VFDR situation, see figures 13a and 13b, where no clear trend was observed. The normalisation process developed for the flow data can be applied to the Couette data and the results obtained are shown in figures 51a and 51b. Data are not presented for other electric field and shear rate combinations or temperatures, although the general observation that the reduction applied to data from the VFDR, and shown extensively in the previous section, was equally applicable to data from the ERV. It can be concluded that the shear stress versus shear rate data can be normalised for both Poiseuille flow and Couette flow.

The Effect of Water Content

In the last set of graphs, 52a to 54b, plots of total shear stress, excess shear stress and current density for four fluids of different water content are shown. The dependence of all the parameters on water content was slight, for example, in figure 53b a small increase in the excess shear stress is observed as the water content is increased but this is at the expense of an increased conductivity in the

fluid. Generally, provided extremes of water content are not exceeded, the dependence on water content was slight and if a value between 15.2% and 15.7% is used an effective fluid with minimal conductivity will be produced.

4.4 THE STATIC YIELD RIG

The Static Yield Rig was a simple machine for screening ER fluids. It has been fully described in section 3.4. The typical form of the data obtained from the equipment is shown in figure 55a. Referring to the schematic diagram of the rig, figure 3.5 it can be seen that as the load is applied to the stressed fluid the cantilever will deflect giving an output from the strain gauges. Rather than simply note the value of shear stress obtained prior to the shearing of the fluid, which is often difficult to determine accurately, it is more instructive to plot the strain gauge output as a function of time, these are the traces obtained in figures 55a and 55b. If the trace in figure 55a is considered the generation of the curve can be explained. Initially the slack is taken up by the micrometer, which is motor driven at 5 rev/min, and no stress is recorded. As the micrometer is turned further the load measured by the strain gauges is gradually increased. A critical value is reached at point "a" and the fluid yields. At this failure point the cantilever, which is under load, will shear the fluid until the stress has fallen to a level where the fluid will once again behave as a solid and the motion of the lower electrode is arrested. The micrometer is still being turned by the motor and the load is reapplied to the fluid. The voltage was still applied to the fluid and the shear stress measured will be recovered following a path similar to that of the initial loading. Ideally it would again reach the initial yield point, "a", and be sheared again giving a level sawtooth type trace. What is observed, however, is a steady increase in the magnitude of the shear stress required to cause yielding, and that this value of stress is increased with each successive yielding. It would appear that an asymptotic value of stress would be reached but in practice this is cannot be achieved as the equipment will have reached the end of its travel. The initial yield value can be distinct, as in figure 55a, or subtle as in figure 55b at a electric field strength of 2.86 kV/mm. The fall of stress on

yielding is increased as the voltage is applied due to the larger stress in the fluid and consequently greater strain energy being stored in the beam. Additional data from this rig, particularly in relation to the variation of yield stress with applied electric field and correlation with the other two devices will discussed in more detail in the next chapter.

Figure 56a shows the current recorded at zero shear rate. It can be seen that it is of a similar exponential form to those presented for both the VFDR and the ERV. Current densities are of a similar order of magnitude to the VFDR and the ERV. The final figure related to the SYR is figure 56b. A slight relaxation of the recorded stress is shown after the motion was stopped but whilst the load and voltage are applied. The degrees of relaxation is approximately 5% for both electric field used.

Full details are available for the reproducibility of the rig. These are similar to those already presented. For example the initial yield recorded on five runs using the same fluid sample were, 3.2, 3.1, 3.1, 3.3, and 3.5 kPa (3.24 kPa averaged). Using a fresh fluid sample for each run gave the following results, 2.9, 3.3, 3.3, 3.7, and 3.5 kPa (3.34 kPa averaged). The data indicated that the results are repeatable and reasonably accurate when the simplicity of the equipment is considered.

4.5 THE CONTRAVES RHEOMAT 115

The Contraves Rheomat 115 was a conventional concentric cylinder viscometer and was used to measure the viscous properties of fluid under conditions of no applied electric field. The typical experimental sequence is a ramped speed increment over a period of 240 seconds with 100 data points being collected. The torque and speed are converted into shear stress and shear rate and plots are possible of the flow curve, that is, the shear stress plotted against the shear rate, and/or a conventional viscosity curve. In figure 57a the result for a 35% fluid is presented over a range of 10 to 1000 sec^{-1}. The form of the trace is typical of an ER Fluid suspension with a small degree of shear thinning being apparent. The viscosity at low shear rate is difficult to determine due to the small stress being measured. Figure 57b is a plot of the viscosity measured at 1000 sec^{-1} against temperature. The curve is the normal exponential decay characteristic of any hydrocarbon oil. When the curve is re-plotted in a log-linear form it results in a nominal straight line to which the common approximation yielding the concept of a viscosity index can be applied. This approximation has been evaluated for a number of fluids and is detailed in table 4.1. In the final plot, figure 58b, a comparison of the viscosity measured on the three devices, that is the Electro-Rheological Viscometer, the Valve and Fluid Development Rig and the Rheomat 115 is shown. The values were taken at approximately 1000 sec^{-1} for the two viscometers and at a wall shear rate of 1000 sec^{-1} for the VFDR. The coincidence of the points is extremely good and it is apparent that any of the three rigs can give an accurate measurement of the no field viscosity. It is also implied, from the ability of the VFDR to measure viscosity accurately, that the assumption of plane parallel flow is acceptable, and furthermore that the apparatus can be used as a tube type viscometer if required. This being the case, the viscosity of an ER fluid can be measured at very high wall shear rates, that is, up to 30,000 sec^{-1}.

The no field viscosity of an ER fluid was unremarkable from a rheological standpoint, showing behaviour typical of a slightly interactive suspension. The straight line approximation used to characterise the temperature profile of most Newtonian liquids was acceptable over the limited temperature range considered and indicated that the form of the no field viscosity characteristic is independent of both volume fraction and water content. In case of the influence of the water content it was observed that the magnitude of the no field viscosity was not unaffected, that is the water content does not significantly change the Newtonian viscosity.

TABLE 4.1 STRAIGHT LINE APPROXIMATION OF NO FIELD VISCOSITY OF ER FLUIDS

Fluid		Intercept	Slope
50LV/L35135		2111	.0579
50LV/L35152		2225	.0552
50LV/L35156		2301	.0588
50LV/L35157		2274	.0544
50LV/L35162	*	2255	.0562
50LV/L35166		2234	.0583
50LV/L35180		2275	.0567
50LV/L30180		1846	.0580
50LV/L40180		4109	.0561
50LV/L20162		948	.0589
50LV/L25162		1082	.0555
50LV/L30162		1897	.0577
50LV/L35162	*	2255	.0562
50LV/L40162		4211	.0565

		Intercept	Slope
Mean Values	30% Fluids	1872	.0579
	35% Fluids	2239	.0568
	40% Fluids	4160	.0566
	All Fluids	----	.0570

* Same fluid

From the analysis indicated in table 4.1 above it can be seen that the slope, or viscosity index, was essentially independent of both the volume fraction and the water content. In addition, for fluids of the same volume fraction but different water content the intercept is approximately the same. That is, within experimental error, the viscosity was independent of water content.

This chapter has presented the main body of data concerning the equipment and the fluids tested. Data has been presented in the case of Poiseuille flow on the VFDR and it was shown that the basic data collected from this equipment was pressure and flow rate. This, although useful from a practical viewpoint, did not actually address the key variables. Two mathematical expressions were presented relating the pressure drop to the shear stress and the flow rate to the wall shear rate. The expressions presented accounted for the geometry of the valve and it was shown that the raw data could be reduced to shear stresses and shear rates. Data was presented showing the behaviour at different temperatures and for different fluids. Again the raw data reduced appropriately.

Data from the ERV, Couette flow, was then considered. The reduction for such a geometry was relatively straightforward and results were presented for variations in temperature and fluid composition.

Finally results from the simple shear device, the SYR, were presented together with some supplementary data from the Contraves viscometer.

It was noted that in general the form of the data collected from the three devices, the VFDR, the ERV and the SYR, were the same. That is as the applied electric field is increased the excess shear stress is increased and that shearing the fluid reduced the excess shear stress. However, the magnitudes of the measured excess shear stress, were different. In the next chapter these difference are investigated.

CHAPTER FIVE

DISCUSSION OF RESULTS

5.1 INTRODUCTION

In this chapter, in broad terms, the analysis of the ER effect is detailed and a description of the phenomena in appropriate physical terms is attempted. The chapter is divided into three sections. In the first section the experimental work described in chapter four is assessed. It had been demonstrated that in Poiseuille flow the basic information concerning pressure and flow rate collected from the equipment could be reduced to a more general form of shear stress and shear rate. However, the shear stress data when compared to data in Couette flow, (collected from the ERV), was significantly different in magnitude although the same form was presented. In the first section a model of the Poiseuille flow behaviour is discussed and the parameters collated with both the Couette data and the simple shear data from the Static Yield Rig. It is suggested therefore, that when an ER fluid is used in a different flow regimes it is only necessary to take into account the nature of the flow regime for the observed experimental results to be described. There is no essential contradiction inherent in the changes induced by the electric field whether usage is in Poiseuille flow, Couette flow or in a simple shear situation. The analysis indicated, covered shear rates, fluid temperatures, fluid compositions and applied electric field strengths.

In the second section the above observation was used, that is, the electric field induced stress is independent of the experimental conditions, to enable the interactions between the particles to be explored. It was necessary for two principle components to be considered with respect to the induced shear stress. These were the constructive interactions brought about by the electrical

interactions and the destructive effect of shearing the fluid. Initially consideration has been given to the electrical aspects but before this it was necessary to simplify the geometric arrangement of the particles. A simple "chain" approximation was used so that the details of the arrangement of the particles could be evaluated. The electrical interactions of a pair of isolated particles were then considered. Recognition is given of two possible situations, that where no contact has occurred and that where the particles have touched.

In the following section the polarisation process is detailed and these processes are then expanded to permit an assessment of the complications expected due to the concentrated nature of the particles in an ER fluid.

Having discussed the electrical interactions, attention is directed towards the effect of the shear rate on the induced excess shear stress. A general phenomenological model is used. In the last part of this section the two aspects are brought together and a generic model for the behaviour of ER fluids is presented.

In the final section a model is described for the conduction process in an ER fluid which is consistent with the electrical and structural model discussed in the previous sections.

5.2 MODELLING OF EXPERIMENTAL DATA AND THE COLLATION OF THE EQUIPMENT

The two main items of experimental equipment used to characterise the ER fluids were the VFDR and the ERV. The data presented in chapter 4 indicated that the magnitude of the shear stresses from the two rigs were different even though the same fluid was used, see figures 60a* and 60b. In addition when results from the SYR were described it was indicated that this data was not readily reconcilable with that obtained from either of the two main devices. The viscosity measured, from the Contraves viscometer, however, could be readily related to values obtained from the Valve and Fluid Development Rig, see figure 58b, and excellent agreement was obtained. Indeed, the agreement is good enough to allow the flow rig, the VFDR, to be utilised as a tube viscometer and measurements of the Newtonian viscosity over an extended shear rate range can be made. In figure 59** the viscosity measured by both the Contraves Rheomat 115 and the VFDR is shown. The upper shear rate limit on the Contraves was 1000 sec^{-1} whereas, in the VFDR, this can be extended to 10,000 to 20,000 sec^{-1}. No discontinuity in the data is indicated and the shear thinning, noted previously, continues at the higher shear rates.

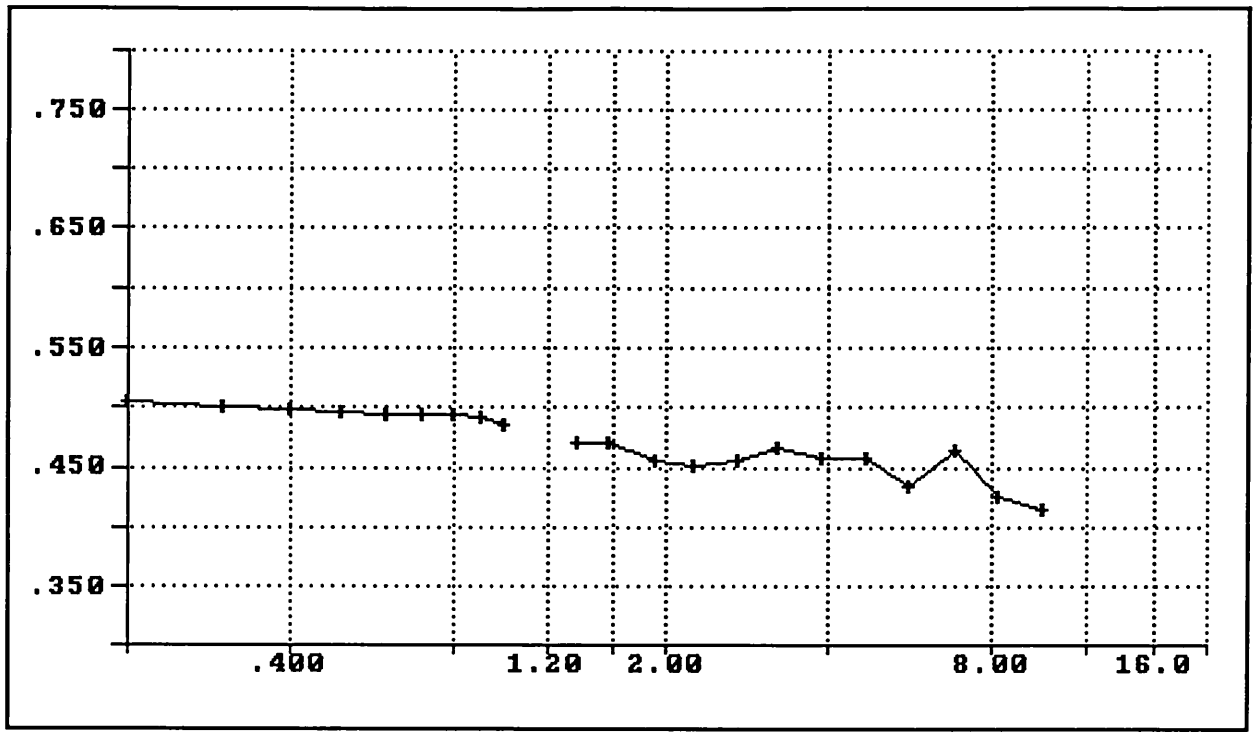
The direct comparison of the shear stress in VFDR and the excess shear stress from the ERV is shown in figures 60a and 60b where the data are plotted against electric field strength and shear rate respectively. It can be seen, that in both cases, the data from the ERV is significantly less than that from the flow rig. The main concern was, therefore, the reconciliation of these anomalies and a correlation of the results from the two items of equipment and, if possible, for data from the SYR to be integrated into the assessment.

---

* Figure numbers suffixed "a" or "b" are located in Appendix A3 at the end of the thesis.

** Figures without a suffix "a" or "b" are located in the body of the text.

FIGURE 59 NEWTONIAN VISCOSITY MEASURED ON TWO TEST RIGS



Fluid 50LV/L35156
Temperature 30 C

X Axis 1*e4 s-1
Y Axis Pas

5.2.1 MODELLING THE DECAY OF THE STRESS WITH THE SHEAR RATE

There is a significant difference between the conditions experienced by an ER fluid in a valve to that experienced by the same fluid in the viscometer under conditions of continuous shear. In the case of an ER fluid subjected to an external electric field in Poiseuille flow the existence of two regions in the flow path is proposed. These are a central plug of unsheared fluid and two centrally symmetrical regions of sheared fluid, these regions are depicted in figure 2.4a. These two regions can be described in terms of the parameter, f, detailed in table 2.1. In the region of sheared fluid the effects of shear dominate and therefore $f^2 < 1$, whereas in the plug region $f^2 > 1$ and evidently at the interface between the regions a situation

exists where $f^2 = 1$. As the shear rate is increased the size of this unsheared fluid plug will be decreased and the region defined by $f^2 < 1$ will be increased. It is apparent that the two sheared regions are similar to those experienced by the fluid in Couette flow, in that shearing will occur across the whole of the fluid. It should be noted that this argument is confined to the case of Poiseuille flow where we are involved in the change of the dimension of the unsheared fluid region due to the increased shear rate. In the case of the fully sheared region a shear rate dependence may also be anticipated. The particles will be rotated by the shear field and a time element will be introduced into the response of an ER fluid in Couette flow. It would therefore be expected that the excess shear stress data obtained from Couette flow experiments will also demonstrate a dependence on the shear rate. Such a dependence can be readily observed in the figures for the ERV, typically figure 47a. In the case of Poiseuille flow the effect measured, i.e. the pressure drop, is due to the restriction in the valve gap presented by the unsheared region and shear dependent changes in the sheared region are of little significance.

As was noted on page 116 the unsheared fluid region will only vanish under two conditions; when the electric field induced shear stress is zero or when the shear rate is infinite. Evidently the first case is trivial and in practice the second case, when $G \rightarrow \infty$ is unobtainable. Superficially then, a correspondence between the two flow situations can never be achieved. However, from an inspection of figure 60b, it is observed that as the shear rate in the flow situation is increased the shear stress measured approximates the low shear rate value of the ERV. The point on the ERV curve marked "a" is similar to the high shear limit of the VFDR curve marked "b". It is necessary, for a model to be developed that is able to relate the experimental data at finite shear rates but allows a mathematical extrapolation to conditions of infinite shear rate. The model is required to have sufficient flexibility so that the variation of the induced shear stress

in Poiseuille flow with geometry shown in figure 5b of chapter 4, with temperature, figure 10b, with volume fraction, figure 20b, and with water content, figure 31b, can be accommodated. Indeed all of the figures related to the flow apparatus, as shown in chapter 4, should be able to be reliable described by the proposed model.

A Model for Poiseuille Flow

The shear stress developed with no electric field applied is approximately Newtonian and it therefore follows that the shear stress - shear rate relationship of an ER fluid can be adequately expressed as;

$$T_x = T_y(G) + \mu G \qquad \text{---- (5.1)}$$

where T_x is the total shear stress at shear rate G
and $T_y(G)$ is the electric field induced yield stress.

This expression is that of equation 4.4 but now the electric field induced component is relaxed so as to be a function of the shear rate.

We will assume that these two components superimpose and that cross product terms such as $T_y(G).\mu G$ can be neglected from the argument. In general the Newtonian component can be subtracted so that an expression for the change of the electric field induced component in Poiseuille flow as a function of the shear rate is required. The reduction of the dimension of the unsheared fluid region will be dependent, with all other parameters being equal, upon the shear rate. For a particle to move from a condition defined by $f^2 > 1$, (where it is electric field dominated), to a condition where it is able to rotate, defined by $f^2 < 1$, (where it is shear rate dominated), a finite period of time will be required. Any variable that is required to follow another variable within a finite time interval will exhibit a relaxation or loss process. Such occurrences are usually found in the frequency domain interpretation of data. Typical occurrences being in

dielectric loss processes, the frequency response analysis of control systems and vibration dynamics.

The general expression for such a system is:-

$$H(x)=H_\infty + \int_0^\infty \alpha(t)e^{jxt}\,dt \qquad \text{---- (5.2)}$$

where $H(x)$ is the value at any given x
H_∞ is the value at infinite x
and $\alpha(t)$ is a decay factor describing the relaxation.

For the case being discussed the independent variable x is the shear rate and the dependent variable is the developed shear stress T(G). The decay factor must be such that as $x \to \infty$, $\alpha(t) \to 0$ will be described. In the case under consideration the change in the shear stress with the shear rate is represented by this decay factor. Many expressions were assessed as to their applicability and the most tractable expression that satisfied the required conditions and also had some direct bearing on the mechanism is the classic single decay expression of:-

$$\alpha(t) = \alpha(0)e^{-t/T_r} \qquad \text{---- (5.3)}$$

where T_r is a characteristic relaxation time.
and $\alpha(0)$ is the value at t = 0

If equation 5.3 is substituted into the general case, 5.2, the following expression is the result.

$$H(x) = H_\infty + \int_0^\infty \alpha(0)\ e^{jxt}\ e^{-t/T_r}\,dt \qquad \text{---- (5.4)}$$

the general variables of H(x) and H_∞ can be replaced with T(G) and T_∞ so that equation 5.4 becomes:-

$$T(G) = T_\infty + \int_0^\infty \alpha(0)\ e^{(jG-1/T_r)t}\,dt \qquad \text{---- (5.5)}$$

It is now required to integrate

$$\int_0^\infty \alpha(0)\ e^{(jG-1/T_r)t}\ dt, \text{ i.e. } \alpha(0)\int_0^\infty e^{(jG-1/T_r)t}\ dt$$

as $\frac{de^{2x}}{dx} = 2e^{2x}$ and therefore $\int_0^\infty e^{2x} = \frac{1}{2}\ e^{2x}$

the integral is therefore

$$\int_0^\infty e^{(jG-1/T_r)t}\ dt = \frac{e^{(jG-1/T_r)t}}{jG-1/T_r}\ \Big|_0^\infty = \frac{e^{jGt}.e^{-t/T_r}}{jG\ -1/T_r}\ \Big|_0^\infty$$

at infinity $e^{(jGt-t/T_r)} = 0$ and at zero $e^{(jGt-t/T_r)} = 1$

Therefore:-

$$\alpha(0)\ \int_0^\infty e^{(jG-1/T_r)t}\ dt = \alpha(0)\{0 - \frac{1}{jG - 1/T_r}\}$$

or $\frac{\alpha(0)}{1/T_r - jG}$ and equation 5.5 can be reduced to:-

$$T(G) = T_\infty + \frac{\alpha(0)}{1/T_r - jG} \qquad \text{---- (5.6)}$$

At G = 0, T(G) = T_y and equation 5.6 becomes:-

$$T_y = T_\infty + T_r\ \alpha(0)$$

which can be substituted into the decay expression, 5.3, to give:-

$$\alpha(t) = \frac{T_y - T_\infty}{T_r}\ e^{-t/T_r} \qquad \text{---- (5.7)}$$

which when substituted into 5.5 produces:-

$$T(G) = T_\infty \int_0^\infty \frac{T_y - T_\infty}{T_r}\ e^{-t/T_r}\ e^{jGt}\ dt \qquad \text{---- (5.8)}$$

Equation 5.8 can be integrated as above to give:-

$$T(G) = T_\infty + \left(\frac{T_y + T_\infty}{T_r}\right) \cdot \frac{1}{1/T_r - jG} \qquad \text{---- (5.9)}$$

$$\text{i.e. } T(G) = T_\infty + \frac{T_y + T_\infty}{1 - jGT_r} \qquad \text{---- (5.10)}$$

$$\text{or } T(G) = T' - jT''$$

by equating real and imaginary parts it is found that

$$\underline{\text{Real}} \qquad T(G)' = T_\infty + \frac{T_y - T_\infty}{1 + (GT_r)^2} \qquad \text{---- (5.11)}$$

$$\underline{\text{Imaginary}} \qquad T(G)'' = \frac{T_y - T_\infty}{1 + (GT_r)^2} * GT_r \qquad \text{---- (5.12)}$$

The full shear stress shear rate dependence will be given by:-

$$T(G) = T(G)' + \mu G$$

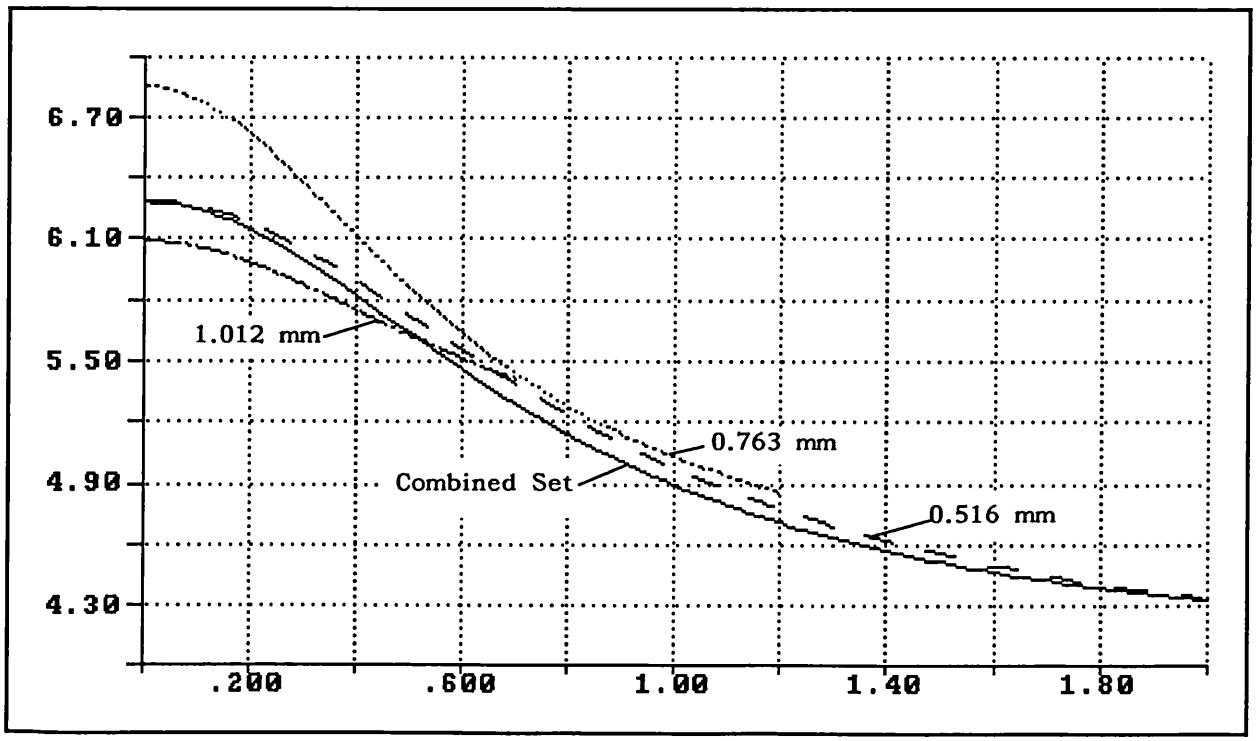
where μ is the Newtonian no field yield stress
and $T(G)'$ is described by the three parameters;
T_y, the shear stress at zero shear rate
T_∞, the shear stress at infinite shear rate
and T_r, a characteristic relaxation time.

5.2.2 QUALITY OF FIT TO EXPERIMENTAL DATA

Having developed a model based on a single relaxation process it is instructive for the manner in which the shear stress versus shear rate response of an ER fluid is effected by changes in the three coefficients. It is also required that the quality of the fit is explored and indicated. The curve fitting can be conducted on data from any particular geometry and in figure 61a the typical fit to one set of data is shown. To fit this model to the experimental

data required an iterative least squares fitting routine as the expression could not be linearised. The manner in which the shape of the curves are effected by the coefficients is shown in figures 61b to 62b where values are chosen for the coefficients similar to those obtained from the curve fitting but rounded up to convenient numbers. The Newtonian, or no field component μG, has been subtracted from all the following data. This is common to all data unless explicitly stated to the contrary. In figure 61b the zero shear rate shear stress, T_y, is varied with T_∞ and T_r held constant. It is indicated by the plot that as T_y is increased the values at low shear rates are increased and the fall to the high shear rate values exaggerated. In figure 62a the changes in T_∞, the infinite or high shear rate term, are shown. The response is again effected in this case by an alteration in the final value of the curve at higher shear rates. Finally, in figure 62b, the effect of varying the relaxation time, T_r, is shown and it is indicated that this coefficient has a marked effect on the shape of the response. As the relaxation coefficient is increased the more dramatic the effects of the shear rate are on the fluid.

FIGURE 63 FIT OF MODEL SHOWING OVERLAP OF SHEAR RATE RANGES



Fluid 50LV/L35157
Temperature 30 C

X Axis 1*e4 s-1
Y Axis kPa

The Effect of the Shear Rate Range

Preliminary analysis of the results has indicated that the model is sensitive to the shear rate range and that a single set of data generated from one geometry is insufficient for the experimental results to be covered in sufficient detail. Similar shaped curves are be produced from the fluid being studied under similar conditions of electric field and flow rate but different geometries gave slightly different values to the coefficients of the equation. This is clearly indicated by figure 63 shown above. The data used to generate this graph are that from figures 64a to 65a and also that detailed as the first set of data in table 5.1.

TABLE 5.1 VARIATION OF FITTING COEFFICIENTS WITH VALVE GEOMETRY

50LV/L35157 30°C 3.05kV/mm	Shear Rate	T_y	T_∞	T_r
1.012 mm gap	780 to 6000	6.09	4.79	1.49
0.763 mm gap	1160 to 10550	6.85	4.32	1.16
0.516 mm gap	1364 to 21790	6.29	3.95	1.13
Combined set	780 to 21790	6.28	4.02	1.24
50LV/L35166				
30°C 2.95kV/mm	**Shear Rate**	T_y	T_∞	T_r
1.012 mm gap	980 to 5320	6.98	4.95	5.14
0.763 mm gap	1400 to 9100	6.69	4.38	2.40
0.516 mm gap	1930 to 13100	6.96	3.55	1.03
Combined set	980 to 13100	6.51	4.65	1.95
50LV/L30180				
30°C 2.95kV/mm	**Shear Rate**	T_y	T_∞	T_r
1.012 mm gap	930 to 6100	4.53	3.63	2.37
0.763 mm gap	1640 to 11320	4.27	3.00	1.21
0.516 mm gap	3300 to 14000	4.69	3.17	0.82
Combined set	930 to 14000	4.31	3.21	0.91
50LV/L30180				
15°C 2.95kV/mm	**Shear Rate**	T_y	T_∞	T_r
1.012 mm gap	930 to 6100	3.39	1.53	4.36
0.763 mm gap	1640 to 11320	3.27	0.86	3.08
0.516 mm gap	3300 to 14000	3.69	1.05	2.44
Combined set	930 to 14000	3.26	1.14	2.88

In the table above, table 5.1, the coefficients have been obtained from three geometries and are listed together with a fit using the data from all three geometries; this is listed in the table as the "combined set". A slight discrepancy between the values is observed. This variation can be explained if the relationship between flow rate and the shear rate is considered. Starting with the largest gap, over any given flow rate range, the shear rate range is fixed. As the gap is reduced the shear rate range is increased, due to the H^2 term in equation 4.1. The approximate shear rate ranges for the three gaps in question are also shown in the table and as can be seen these vary considerable, although in all cases the flow rate is only varied between approximately 1 and 6 ltr/min.

In addition there is a predominance of data points at the lower flow rates as the flow rate increment used was not linear. Whilst there is a certain amount of overlap between the shear rates of each geometry there is a tendency for each geometry to emphasis a different aspect of the flow curve. The largest gap, low shear rate experiment, was more able to identify the zero shear rate coefficient. The smallest gap, which gave the highest shear rate, is more able to identify the infinite shear rate coefficient. The 0.763 mm gap provided the most reasonable fit over all the data as well as identifying the relaxation coefficient, T_r, reasonably well. For the entire flow curve to be accurately characterised it is appropriate to study each fluid with the three geometries available and then fitting the expression to combined set of data. This effectively trebles the amount of experimental work that is required to accurately model the flow in an ER valve, however, a more acceptable result is produced.

In the three figures, 64a to 65a, the fit to the data using single geometries of 0.516 mm, 0.763 mm, and 1.012 mm respectively are shown. In figure 65b the fit when all three geometries are combined is shown. As can be observed, the fit to any geometry is good and the dependence upon the shear rate range can be clearly identified. The scatter on the

data is presented in figure 65a. Note that each geometry is not separately identified.

Sensitivity and Applicability of the Model

The proposed model must be able to fit the data and be able to account for the changes due to the applied electric field. This is shown in figure 66a for three different electric field strengths, the fit is acceptable. The next plot, figure 66b, is for different temperatures and again an acceptable fit is obtained. In this case it is noted that not only is the magnitude of the stress different the shape of the curves are also temperature dependent. Referring back to the idealised shape of the curves presented in figures 61b to 62b, particularly figure 62b, it is indicated that as the temperature is decreased the relaxation coefficient will be increased, that is, the fluid is less able to withstand the effects of shear as the fluid is cooled. The two figures 67a and 67b show that the model can also be used to describe fluids of different volume fractions and different water contents. It can therefore be concluded that a model, based on a single exponential decay term, is capable of describing the experimental data with respect to water content, volume fraction, temperature and electric field strength.

It is possible for any fluid, at one temperature, to be represented as a family of curves at different electric field strengths similar to those shown in figure 66a. Alternatively the behaviour of the fluid can be described by the three coefficients but now plotted against the electric field strength. It is evident that these coefficients will be a function of electric field strength in that the induced shear stress is a function of electric field strength. The entire shear stress versus electric field strength response of a fluid can be completely characterised by these three coefficients when plotted against electric field strength. In figures 68a and 68b such a characterisation for two different fluids at the same temperature is shown and as can be observed the entire behaviour of an ER fluid in Poiseuille flow can be

depicted on a single graph. It is noted that the relaxation coefficient is approximately the same for both plots, an observation that can also be applied to the zero shear intercept value. The difference between the two fluids is mainly in the values for the infinite shear stress, which, referring to figure 62a, will cause a considerable alteration in the shape of the shear stress versus shear rate characteristic of the fluid.

Before these aspects are investigated in a little more detail the errors and limits in the model need to be identified. The data from six flow experiments has been used with fluid 50LV/L35180. The experiments in question were VFDR 99 to 103 and VFDR 119 and the temperature was approximately 30°C. In figure 69a a plot of the shear stress plotted against shear rate for three of these experiments is shown and very good reproducibility is indicated. A statistical analysis of the flow data was carried out and the results are presented in Table 5.2.

The fit to the coefficients using the model is shown for the three experiments of figure 69a, in figures 69b to 70b. The zero shear rate intercept is by far the best and only a small amount of scatter is noted. It can be concluded that this limit can be clearly identified. In figure 70a the infinite shear rate intercept is presented and slightly more scatter is shown although the value is clearly identified. The relaxation coefficient is evidently more susceptible to variation, as shown in figure 70b. By putting a 95% confidence limit on the mean values has enabled a plot to be generated showing the scatter band of the fluid. This is shown in figure 71b, and the probable error on the shear stress is ± 0.1 kPa at low shear rates rising to ± 0.22 kPa at high shear rates. The final figure, 71a, is the mean of the six experiments used to generate table 5.2. If this is compared with figure 68a, which shows one of these experiments, it can be seen that multiple experiments produce smoother results and also flatten the relaxation coefficient. It is suggested that the relaxation coefficient may well be independent of electric field strength.

TABLE 5.2 STATISTICAL ANALYSIS OF FLOW MODEL SHOWING 95% CONFIDENCE LIMITS

Field kV/mm	Zero Shear Value kPa		Infinite Shear kPa		Relaxation mS	
	T_y	Limit	T_∞	Limit	T_r	Limit
0.44	0.111	0.030	0.043	0.025	0.048	0.0189
0.81	0.509	0.033	0.169	0.036	0.232	0.0361
1.12	1.035	0.031	0.296	0.130	0.183	0.0383
1.43	1.725	0.043	0.706	0.203	0.167	0.0343
1.66	2.315	0.053	1.042	0.432	0.182	0.0632
1.89	2.958	0.059	1.471	0.378	0.176	0.0562
2.10	3.560	0.063	2.154	0.224	0.175	0.0457
2.26	4.044	0.092	2.583	0.151	0.174	0.0324
2.41	4.550	0.074	3.024	0.191	0.175	0.0289
2.56	5.032	0.114	3.590	0.245	0.182	0.0346
2.67	5.345	0.072	3.847	0.150	0.178	0.0282
2.77	5.674	0.077	4.155	0.129	0.184	0.0247
2.87	6.111	0.088	4.458	0.157	0.193	0.0291
2.95	6.313	0.098	4.701	0.263	0.192	0.0116
3.03	6.713	0.123	4.984	0.289	0.228	0.0282

Fluid 50LV/L35180
Temp 30°C

Valve Geometry Length 150 mm
Width 156 mm
Gap .763 mm

Volume Fraction Dependence

The dependence of the three descriptive parameters on volume fraction is shown in figures 72a to 73b. As expected from the experimental data presented in chapter 4 the values of both the zero and the infinite shear rate intercepts are increased as the volume fraction is increased. The relaxation coefficient, however, appears to be constant although rather a lot of scatter on the plot is observed, particularly on the 40% fluid. It was shown that the volume fraction could be normalised by dividing the data at any given electric field strength by the maximum stress across the shear rate. If this process was carried out the three volume fraction sets of data superimpose adequately. In a similar manner the data can be normalised, but now using the zero shear rate intercept for each volume fraction as the normalising factor. The results of this procedure are shown in figure 73b and table 5.3.

TABLE 5.3 MODEL FITTED TO THREE VOLUME FRACTIONS NORMALISED DATA ALSO SHOWN

Fluid	T_y	T_∞	T_r
50LV/L40180	8.48	6.68	1.797
50LV/L35180	6.51	4.86	1.869
50LV/L30180	4.65	3.66	1.892
Normalised 40%	1	0.788	1.797
Normalised 35%	1	0.746	1.869
Normalised 30%	1	0.788	1.892

Temperature Dependence

The dependence of the behaviour of the fluid is shown in figures 74a to 75b. As the temperature is decreased all the three coefficients fall, that is, not only is less shear stress developed in the fluid for any given voltage but the shear stress falls more rapidly to the infinite shear rate value as the shear rate is increased. The relaxation coefficient has therefore increased. In addition the value of the stress at infinite shear rate has decreased as the temperature has fallen. The temperature change clearly has a significant effect on the stress developed in the fluid, this is clearly indicated by figure 10b. The above three graphs detailed the results for the fluid with the variables of applied electric field and shear rate being used. Similar plots were generated for fluids with different volume fractions and different water contents. In all cases data has been utilised from experiments on three geometries as opposed to a single geometry. This has improved the precision of the data.

Water Content Dependence

The dependence of water content is shown in figures 75b to 76b. The zero shear rate intercept would appear to be independent of water content, a small dependence is indicated on the infinite shear rate intercept. It is increased as the water content is increased. The relaxation term would also appear to be sensibly independent of the water content. These results are slightly different to those of figures 68a and 68b, which were for a single gap, the plots now being generated with data taken from all three geometries. This results in a more accurate characterisation and the potential limitations of only using a limited shear rate range is indicated.

5.2.3 COMPARISON OF DATA FROM THREE EXPERIMENTAL DEVICES

It has been postulated that the infinite shear stress approximates the conditions experienced in the ERV at conditions of low shear rate where the fluid is being continuously sheared. It is necessary, therefore, for this correlation to be demonstrated for a number of different fluids, both in relation to volume fraction and water content and for any given fluid, at different temperatures. The eight figures, 77a to 80b, show the comparison for the conditions outlined. The volume fraction dependence, at constant temperature, is shown in figures 77a to 78a. The correlation at different temperatures, for a 35% volume fraction fluid, is shown in figures 77a and 78b and for a 40% volume fraction fluid in figures 77b, 79a and 79b at temperatures of 30°C, 20°C and 10°C respectively. Three different water contents at 30°C and at 35% volume fraction are shown in figures 77a, 80a and 80b. With the exception of figure 80a, the correlation between the two devices is excellent. For example the maximum difference between the plots in figure 77a is approximately 0.3 kPa at 1.5 kV/mm. The analysis, as shown in table 5.2, exhibited a scatter on the infinite shear rate value of ± 0.20

kPa, at this electric field strength. The typical scatter for data from the ERV, shown below in table 5.4 at a temperature of 30°C and at 1.5 kV/mm is in the order of ± 0.08 kPa. Consequently, the deviations shown in these figures, are well within the scatter bands observed for the experimental work.

TABLE 5.4 ELECTRO-RHEOLOGICAL VISCOMETER REPRODUCIBILITY***

Field kV/mm	Yield Stress Max.	Min.	kPa Mean	Std.Dev.	95% Limit
0.000	0.0	0.0	0.00	-	-
0.214	0.04	0.00	0.01	0.018	0.010
0.602	0.26	0.19	0.21	0.014	0.008
0.904	0.62	0.53	0.55	0.028	0.016
1.199	1.08	0.94	0.97	0.044	0.023
1.499	1.58	1.36	1.41	0.146	0.084
1.798	2.16	1.86	1.99	0.079	0.045
2.099	2.78	2.53	2.58	0.099	0.057
2.394	3.44	3.00	3.18	0.121	0.069
2.694	4.07	3.57	3.81	0.142	0.081
2.994	4.62	4.23	4.46	0.123	0.070
3.296	5.32	4.87	5.14	0.147	0.084
3.592	6.08	5.51	5.82	0.176	0.100

Fluid 50LV/L35180 Temp 30 °C Rotor 40.00 mm
Shear Rate 136 sec^{-1} Gap 0.536 mm

TABLE 5.5 TYPICAL SET OF DATA AT 3.592 kV/mm

Test No.	Shear Stress kPa	Test No.	Shear Stress kPa
1	5.91	2	5.80
3	6.01	4	5.65
5	6.08	6	5.64
7	5.75	8	5.51
9	5.94	10	5.97
11	5.79		

Mean 5.82 kPa Std.Dev. 0.176 95% Limit 0.10

***These experiments were carried out at a fixed shear rate with the applied electric field being varied. Eleven separate experiments conducted.

Before the comparison of the data from the experimental devices is left it will be necessary for an indication to be given as to whether the Static Yield Rig (SYR) can also be used to determine the performance of an ER fluid. It has been noted that ER fluids, when subjected to shear in the SYR, exhibited an initial yield point and then the shear stress progressively increased as the experiment was continued, see figures 55a and 55b. It is suggested that this is due to a more favoured rearrangement of the structure whilst under the effect of an external electric field. The final yield is approximately 1.5 times that of the initial yield value at point "a" on figure 55a. It is difficult to be precise about the location of this point as the final value is reached asymptotically and, in addition, at higher electric fields the value appears to be beyond the travel of the machine. It is postulated that of these two shear stress values the initial yield corresponds both to the infinite shear value in flow and the continuous shear rate value from the ERV, and that the maximum value corresponds to the zero shear rate value from the flow data. Initially, however, the reproducibility of the data from the SYR needs to be assessed. Six experiments were conducted using a fresh sample for each experiment in table 5.6 the results of these reproducibility experiments are shown.

The data for the mean yield stress from table 5.6 together with data for this fluid at the same temperature from the other two devices is shown in figure 81a. The data from the ERV and VFDR is taken from figure 77a, and it can be seen that the SYR data falls along the same path as these data. Indicated by the two graphs of figure 81b and 81c is the correlation for a different volume fraction fluid and a different water content fluid. Finally in figures 82a and 82b, the zero shear rate stress value from the flow data is plotted together with the maximum shear value from the SYR for the fluid shown in figure 81a and for the 15.6% water content fluid at 30°C in figure 82b. The correspondence of the data is good and it is indicated that the SYR can be used for the initial appraisal of an ER fluid.

TABLE 5.6 STATIC YIELD RIG REPRODUCIBILITY

Field Strength kV/mm	Yield Stress kPa Max.	Min.	Mean	Std.Dev.	95% Limit
0.000	0.0	0.0	0.00	-	-
0.286	0.1	0.1	0.10	-	-
0.571	0.5	0.2	0.30	0.10	0.09
0.857	0.7	0.5	0.58	0.09	0.08
1.143	1.0	0.8	0.90	0.08	0.74
1.429	1.6	1.2	1.38	0.15	0.13
1.714	2.1	1.6	1.87	0.16	0.15
2.000	2.9	2.1	2.45	0.24	0.22
2.286	3.4	2.5	2.93	0.33	0.30
2.571	4.0	3.0	3.50	0.31	0.28
2.857	4.6	3.6	3.93	0.31	0.28
3.143	5.2	3.9	4.70	0.42	0.38
3.429	5.1	4.4	5.09	0.53	0.48

Fluid 50LV/L35180
Temp. 30 °C
Gap 0.7 mm

The initial area that required resolution was stated to be an assessment of the experimental methods used and from that gain confidence in the reliability of the data generated. This having been completed attempts were made to correlate the fluid behaviour in the two main flow regimes and to include into this an assessment a small laboratory shear cell. The data available from these instruments was sufficiently different and tested over a wide enough operational context to enable the development of some empirical constituitive equations for the behaviour of the fluid. The development of these generic expressions enabled the two flow regimes, Couette and Poiseuille flow, to be consolidated and scaling factors to be evaluated.

The next stage is for these generic expressions to be assessed in terms of some of the basic physical properties and to expound some plausible mechanisms for the ER effect. The objective is the development of an understanding of the mechanism by which the electric field induces a shear stress

in the fluid. The route is for the interaction between particles to be attributed to an interfacial polarisation type process. Central to this process is the structure that has evolved under the influence of the electric field and a three dimensional network structure based on "chains" of spherical particles will be used.

5.3 MODELLING OF THE ELECTRO-RHEOLOGICAL EFFECT

As asymmetric particles under shear can be characterised by an equivalent hydrodynamic radius it can be assumed, at least in the hydrodynamic case, that the particles are effectively spherical. Details of the interactions can therefore be computed. Such an investigation forms the majority of this section and a simple "chain-like" structural model is discussed along with the interaction between two spherical particles in the external electric field. Forces are calculated which are shown to be of the correct order of magnitude. The dependence on the external electric field of the induced shear stress is discussed and it is indicated that a simple E_0^2 dependence is most unlikely to arise in practice due to the complex nature of the polarisation mechanism. Finally the dependence of the shear stress on the shear rate is investigated and additional comments are made.

An ER fluid with no electric field applied is virtually Newtonian. A small degree of shear thinning is noted but other than that the behaviour is relatively unremarkable from a rheological view. When an electric field is applied the behaviour changes dramatically and the fluid responds as an elastic solid to small amplitude motions and approximates a Bingham fluid at large amplitude motions. An ER fluid is a suspensions in which the particle-particle interactions govern the rheology and it is to those interactions that attention is now turned. In most aqueous suspensions attractive dispersion forces result in a primary minimum whose depth, according to the classical Hamaker treatment, depends upon a material constant, A, the particle radius, r, and the minimum separation distance, δ. As this attraction would, in general, result in rapid flocculation long range electrostatic repulsion forces are introduced to provide stability. For non-aqueous suspensions stability is usually attained by the adsorption of polymer molecules on the surface of the particles resulting in a steric barrier some 1 nm to 10 nm

thick. In colloidal systems Brownian motions are significant, these can be characterised by the time required for a particle to diffuse a distance comparable to its radius. The time, given by $6\pi\mu r^3/kT$, scales on the radius cubed and it therefore becomes excessive as the radius of the particle is increased. The particles in an ER fluid are of such a size that the diffusion time is very large and therefore Brownian motion can be considered insignificant.

For the study of inter-particle interactions it is necessary that the particle positions are specified within a given volume of fluid. The suspension structure can, therefore, only be determined in a statistical sense. In the case of dilute systems when three-body and higher-order interactions can be neglected, the probalistic representation given by the pair distribution function is valid. As the volume fraction is increased the validity of this approach declines and above, approximately 20% volume fraction, multi-particle interactions occur and this approach is rendered invalid. Fortunately the macroscopic consequences of the pair interactions are mimicked, in a general fashion, by more concentrated systems and much information can be gleaned from a study based on pair distributions.

A number of techniques have been developed to study multi-particle interactions. Monte Carlo and Molecular Dynamic[143] simulation procedures can be used to predict suspension properties by tracking particle motion and velocity vectors. An equilibrium microstructure is developed and the pair distribution function is calculated by ensemble averaging. Structural model, of the cell or lattice type also depend on pairwise additivity but, by definition, assume a structural rather than a statistically developed one. Good agreement is often obtained between Monte Carlo simulation studies and cell models of ordered structures. The problems introduced if a pairwise additivity procedure is used can be avoided if the so called self consistent field approximation is employed. In this case a spherical unit cell, consisting of a charged rigid sphere is surrounded by a fluid cell, with a

continuum having the mechanical and electrical properties of the bulk suspension. The response of this ensemble to the imposed shear and electric fields is governed by classical conservation equations and boundary conditions. Analytical solutions for the fields are obtained and then volume averaged to determine the bulk properties.

Many difficulties are experienced when attempting to model concentrated suspensions. Whilst the hydrodynamics of a system of dilute rigid spheres is tractable, with and without an electric field, the situation becomes progressively more complicated as a practical formulation for the suspension is approached. The next stage to be considered with respect to complexity is that of unequal spheres subjected to hydrodynamic fields. This can be formulated but progressing a further stage to that of unequal asymmetric particles is not, as yet, feasible. The solution of the electric field equations is even more limited and solutions are only available for a limited number of conditions. Consequently a detailed mathematical description of the ER fluids used in this research, is not only beyond the scope of this work, it is, as yet, not possible. However, from a consideration of the general requirements of both the structure and the influence of the electrical interaction that result in the ER effect a great deal can be discovered. The results can then be compared with known experimental data. Such a structural/electrical approach should enable data to be scaled with volume fraction and the applied electric field. The details of the assessment should also enable the dependence of the excess shear stress on shear rate to be explained.

5.3.1 CHAIN GEOMETRY AND CHAIN FORCES

If a typical ER fluid is considered and some simplifying assumptions applied some particulars of the chains that are seen to form under the influence of an external electric field can be postulated. Assuming the particles in the fluid are spheres of 6 μm diameter, this being the mean diameter previously measured, one cubic centimetre of a 35%

volume fraction fluid will contain approximately $3.1*e^9$ particles. The ERV contains some 2.8 cc of fluid in the electrode spacing and therefore $8.7*e^9$ particles would occupy the region. The mean surface separation, δ, of these spherical particles can be calculated, using equation 5.14, and is calculated at 1.1 μm. The viscometer gap was 0.536 mm, and therefore some 75 particles will be required to span the electrode gap. The number of chains can therefore be estimated as $1.2*e^8$.

At an applied electric field of 2.0 kV/mm some 2 kPa (2000 N/m^2) is supported by this structure, which over the viscometer electrode area of 35 cm^2, implies that a load in the order of approximately 7 N is supported. Each "chain" therefore, is required on average to support a load of approximately $6.0*e^{-8}$ N. This simple chain arrangement can be explored with respect to volume fraction. In a volume, V, the number of particles will be given by:-

$$N_v = 6V\phi/\pi a^3 \qquad \text{---- (5.13)}$$

where ϕ is the volume fraction
and a is the diameter of the particle

The surface separation of the particles can be calculated from equation 5.14 where the maximum packing fraction, V_{max}, will be 52% for a simple cubic arrangement, 62% for a body centred cubic arrangement and 74% for a close packed arrangement. In practice a maximum packing fraction of 58% was evaluated by centrifuging various volume fraction fluids and measuring the degree of separation. This figure is used in conjunction with equation 5.14 to permit the data presented in table 5.7 to be generated.

$$\delta = a\{(V_{max}/\phi)^{1/3} - 1\} \qquad \text{---- (5.14)}$$

The simplest method to enable the number of chains to be calculated is to divide the number of particles, n_p, by the number required to form a chain. If the number of

particles to form a chain is taken as the electrode gap divided by the particle diameter, $n_p = H/a$, it is implicitly assumed that the particles touch rather than being located at some lattice site dictated by equation 5.14. Evaluating the chain density using these two approaches will lead to different values. These values are shown in the last two columns of table 5.7. The chain density on the simpler basis will be given by:-

$$N_c = N/n_p \quad \text{or} \quad 6V\phi/\pi a^2 H \qquad \text{---- (5.15)}$$

As V/H is the effective area the chain density per unit area will be:-

$$C_d = 6\phi/\pi a^2 \qquad \text{---- (5.16)}$$

whereas the chain density based on a packing fraction of 58% will result in the following expression:-

$$C_d = 6\phi(V_{max}/\phi)^{1/3}/\pi a^2 \qquad \text{---- (5.17)}$$

These differences are illustrated in the data shown in table 5.7. The two chain densities being defined as "simple" and "full" for the above two cases. It is apparent that the differences are most significant at lower volume fractions.

In figure 83 a plot of $1/\delta$, the inverse separation distance, against volume fraction is shown, data has been superimposed from the SYR experiments. This data has been modified to scale to the curve by taking an arbitrary volume fraction as a normalising factor and the remaining data reduced by this value. In table 5.8 the reduction is shown when the 35% volume fraction value is used as the normalising factor.

TABLE 5.7 VOLUME FRACTION EFFECT ON PARTICLE CHAIN FORMATION

ϕ	δ μm	$1/\delta$	$(V_{max}/\phi)^{1/3}$	N /cm^3 *e^9	C_d /cm^2 full *e^8	simple *e^8
0	∞	-----	-----	----	----	----
5	7.58	0.132	2.264	0.44	0.59	0.26
10	4.78	0.209	1.797	0.88	0.95	0.53
15	3.42	0.293	1.570	1.33	1.25	0.80
20	2.56	0.391	1.426	1.77	1.51	1.06
25	1.94	0.515	1.324	2.21	1.76	1.33
30	1.48	0.678	1.246	2.65	1.98	1.60
35	1.10	0.909	1.183	3.10	2.20	1.86
40	0.79	1.264	1.132	3.54	2.40	2.12
45	0.53	1.888	1.088	3.99	2.60	2.39
50	0.30	3.286	1.051	4.42	2.79	2.65
55	0.11	9.332	1.017	4.86	2.97	2.92
58	0.00	∞	1.000	5.13	3.08	3.08

A factor of 100 is used in the detailed calculations to account for the volume, V, being in cm^3, the gap, H, being in mm and the particle size is in μm. To arrive at the number of chains for any given electrode gap simply multiply C_d by the gap in mm.

FIGURE 83 INVERSE PARTICLE DISTANCE versus VOLUME FRACTION

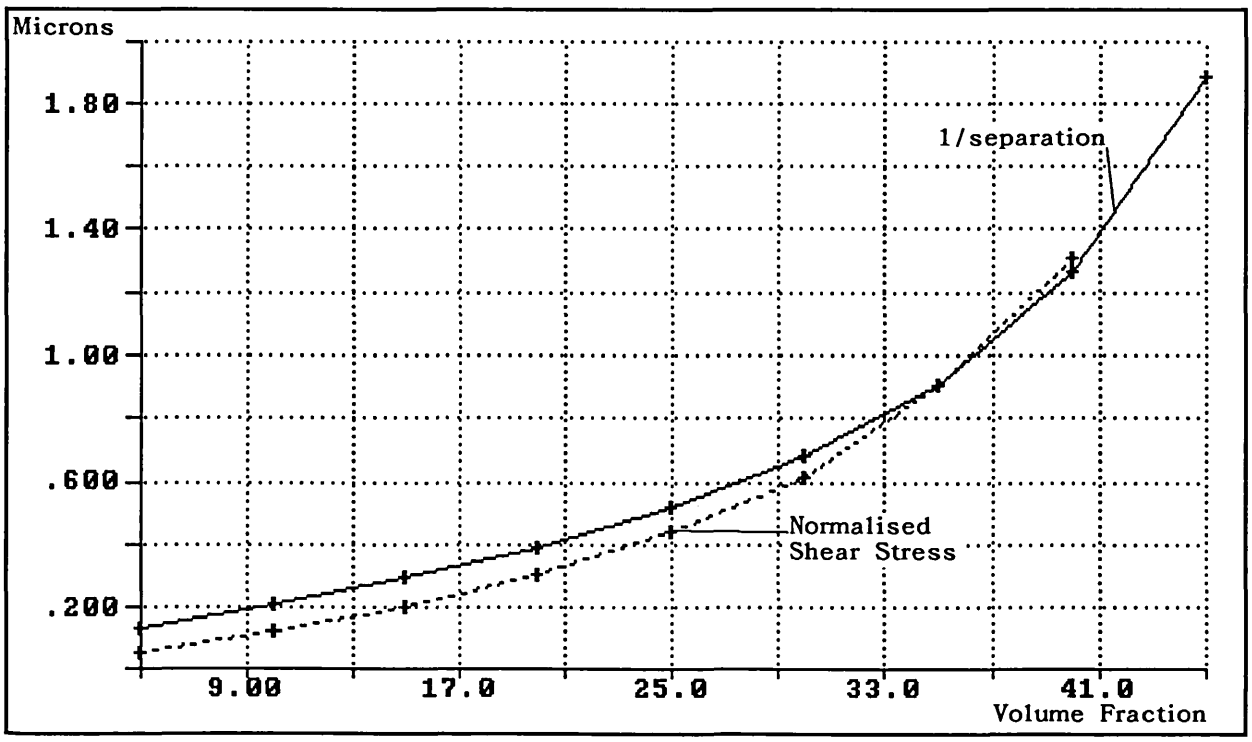


TABLE 5.8 NORMALISED SHEAR STRESS FOR DIFFERENT VOLUME FRACTIONS

V/V	0	5	10	15	20	25	30	35	40
T_y	0	.229	.548	.868	1.32	1.92	2.65	3.93	5.67
T_n	0	.053	.127	.201	.305	.444	.613	.909	1.31
$1/\delta$	0	.132	.209	.293	.391	.515	.678	.909	1.26

Fluid 50LV/L35180 at 30°C and 2.86kV/mm
Normalised to 35% volume fraction

As can be observed the scaling on $1/\delta$ is good, especially when the simplifying assumptions regarding both the nature of the particles and the structure that is assumed to form is taken into consideration. It is therefore reasoned that in order for a first order calculation to be pursued that the increased ER effect, as the volume fraction is increased, is due to the particles being brought closer together. If it is assumed that the stress transmitted by an ER fluid is supported equally by each "chain" the strength of each bond can be estimated by simply dividing the load supported by the chain density. It is implied by this argument that the strength of the interparticle bond is the same in both tension and shear. This is, in all probability, not the case. However, by analogy with the strength of solids where the ratio between strength in tension and strength in shear is approximated to 2:1. and if it is assumed that a similar ratio holds for an electrically stressed ER fluid the problem reduces to a factor of 2 whereas the situation being studied is an "order of magnitude" situation. If the data from table 5.8 is taken and the chain density data from table 5.7 used with the gap and area taken into account the chain strength, C_s, can be evaluated. In table 5.9 the results are shown. Other parameter in the table relate to electric field intensification and are discussed later.

TABLE 5.9 BOND STRENGTH FOR DIFFERENT VOLUME FRACTIONS

v/v	δ/r	C_s Chain Strength Newtons	E_3 Field Intensification		C_s/E_3 $R_1=R_2$
0	----	----	----	----	----
5	2.52	$0.254 * 10^{-7}$	3.16	5.31	.080
10	1.59	$0.377 * 10^{-7}$	3.39	6.03	.111
15	1.14	$0.453 * 10^{-7}$	3.63	7.08	.124
20	0.853	$0.573 * 10^{-7}$	3.80	7.59	.151
25	0.647	$0.712 * 10^{-7}$	4.22	8.51	.168
30	0.493	$0.874 * 10^{-7}$	4.57	10.00	.191
35	0.367	$1.166 * 10^{-7}$	5.37	11.48	.217
40	0.263	$1.542 * 10^{-7}$	6.68	13.49	.231
			R1=R2	$R_1=10R_2$	

C_s is the chain strength and is computed from the excess shear stress being divided by the number of chains evaluated using equation 5.17.
E_3 is the electric field intensification factor calculated by Davis[135] using equations 5.18 and table 5.11. The intensification is shown for equal spheres and unequal spheres of a 10:1 radial ratio.

5.3.2 ELECTRICAL INTERACTIONS BETWEEN PARTICLES

The strength of the bond between adjacent particles has now been estimated. The next step is for the interactions caused by the applied electric field to be identified. It is necessary for two cases to be distinguished, one where the particles remain separated and the other where they touch.

The solution to the problem of calculating the force between two charged conducting spheres, see figure 84, in an electric field has been tackled by Davis[135]. The complete solution to the problem is contained in his paper and the problem was stated as follows. "Given two conducting spheres of specified and (in general) unequal radii, separated by a specified distance and bearing given charges, in an impressed electric field that is uniform at a great distance from the conductors: find the electric field strength at the surfaces of the conductors and the forces acting on the conductors". The two sphere boundary value problem was solved and expressions were derived for the electric field strength and the force components. The method used required changing the

expressions were derived for the electric field strength and the force components. The method used required changing the Cartesian coordinate system to the bispherical coordinate system. Vlodavets tackled the same problem but used a consecutive imaging technique[41]. The information produced by this method results in a small difference in the magnitude of the force coefficients due to a different summation procedure. Davis's technique is more complete, giving components in both the x and z direction as well as electric field intensification data. This approach will therefore, be applied in some detail to ER fluids.

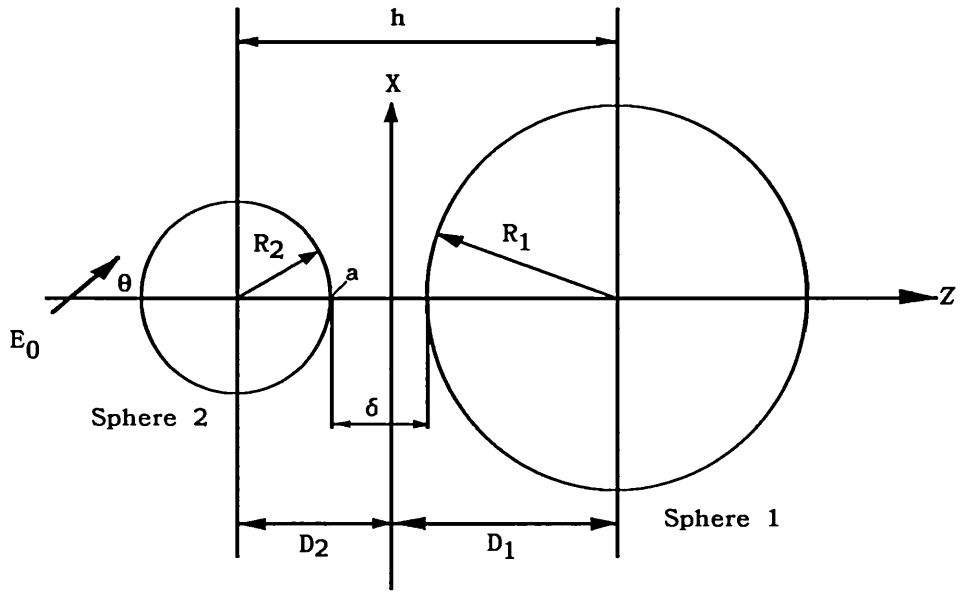


FIGURE 84 SCHEMATIC OF SPHERE SYSTEM

The electric field strength is computed at point "a" on the smaller sphere, see figure 84, which is in most cases the maximum electric field between the two spheres. This electric field is computed as:-

$$E_a = \frac{1}{\epsilon R_2^2} (E_1Q_1 + E_2Q_2) + E_3E_0 \cos\theta \quad \text{---- (5.18)}$$

where θ is the angle between the electric field and particle centres
Q_1 and Q_2 are the charges on the spheres
E_0 is the applied electric field strength
and E_a is the electric field at point "a"
E_1, E_2 and E_3 are complicated series.

The values for E_1, E_2 and E_3 are summarised in table 5.11 for a number of particle separation distances and particle size ratios.

In general the electric field is offset by the angle θ to the particle centres and it is necessary for expressions to be evaluated for the force in both the x direction and in the z direction. These expressions are as follows:-

$$F_z = \{\epsilon R_2^2 E_0^2 (F_1\cos^2\theta + F_2\sin^2\theta) + E_0\cos\theta(F_3Q_1 + F_4Q_2) + \frac{1}{\epsilon R_2^2}(F_5Q_1^2 + F_6Q_1Q_2 + F_7Q_2^2)\} + E_0Q_2\cos\theta \quad \text{---- (5.19)}$$

$$F_x = \{\epsilon R_2^2 E_0^2 F_8 \sin 2\theta + E_0\sin\theta(F_9Q_1 + F_{10}Q_2)\} + E_0Q_2\sin\theta \quad \text{---- (5.20)}$$

Again, the coefficients F_1, F_2 .... F_{10} are complicated series expressions and specific examples are shown in tables 5.12 and 5.13. These coefficients, $E_1 \rightarrow E_3$ and $F_1 \rightarrow F_{10}$, depend only on the relative geometry, that is the radii of the spheres and the separation distance of the spheres. The

applied electric field, E_0, and the charges, Q_1 and Q_2, have been separated out and therefore the expressions can be applied to any given situation of particle charge and applied electric field.

TABLE 5.10 PARTICLES IN ELECTRODE SPACE

V/V	30	35	40
No.*e^9	4.92	5.75	6.57

TABLE 5.11 FIELD INTENSIFICATION COEFFICIENTS

	δ/R_2	E_1*10^9	E_2*10^9	E_3
$R_1=R_2$	10.00	-.2169	9.000	3.004
	1.000	-6.089	9.846	3.718
	0.100	-37.69	37.69	14.17
	0.010	-252.3	252.3	92.48
	0.001	-1905	1905	696.7
$R_1=2R_2$	10.00	-.1827	9.000	3.027
	1.000	-2.832	10.66	4.741
	0.100	-13.01	43.79	18.16
	0.010	-84.78	291.6	117.2
	0.001	-639.5	2204	883.4
$R_1=5R_2$	10.00	-.1170	9.000	3.215
	1.000	-.7488	11.53	6.556
	0.100	-2.618	46.19	22.03
	0.010	-16.37	299.3	137.5
	0.001	-121.8	2235	1022
$R_1=10R_2$	10.00	-.0666	9.018	3.733
	1.000	-.2295	11.81	7.753
	0.100	-.7110	45.95	23.75
	0.010	-4.347	293.3	145.4
	0.001	-32.12	2174	1073

δ is the particle separation distance and R_1 and R_2 are the radii of the spheres.
E_1, E_2 and E_3 are the coefficients of equation 5.18 and define the maximum local electric field.

The two coefficients F_1 and F_2, are proportional to E_0^2 and result from the polarising action of the applied electric field on the particles. F_3 and F_4 result from the polarisation of the net charge and F_5, F_6 and F_7 represent the coulombic repulsion terms. If the spheres carry no net charge, $Q_1=Q_2=0$, then only terms in E_0^2 would be relevant, in practice this is virtually the case for the ER fluids used because, although the particles are charged, the charge per particle is small and can, in the first instance, be neglected. If no electric field is applied, $E_0=0$, but the particles carry net charges only the quadratic term remains. If both situations are relevant, an applied electric field and net charges, all coefficients are involved and the solution is case dependent. Using the force coefficients, F_i, the forces can be evaluated and similarly the electric field intensification can be evaluated.

TABLE 5.12 FORCE COEFFICIENTS F_1 TO F_5

	δ/R_2	F_1*10^{-9}	F_2*10^{-9}	F_3	F_4	F_5*10^{9}
$R_1=R_2$	10.00	.00003	-.00002	-.0012	.00116	.00007
	1.000	.0103	-.0037	-.0951	.09510	.0909
	0.100	.1556	-.0105	-.9741	.9741	1.380
	0.010	1.060	-.0115	-5.994	5.994	8.337
	0.001	6.610	-.0116	-36.39	36.39	49.97
$R_1=2R_2$	10.00	.00018	-.00084	-.00093	.00730	.00005
	1.000	.0309	-.0759	-.0576	.3063	.0204
	0.100	.3484	-.1436	-.5370	2.128	.2196
	0.010	2.288	-.1505	-3.356	11.97	1.228
	0.001	14.18	-.1511	-20.59	71.46	7.469
$R_1=5R_2$	10.00	.0013	-.0006	-.0006	.0611	.00005
	1.000	.0714	-.0103	-.0191	.8537	.0013
	0.100	.5900	-.0115	-.1436	.3.617	.0087
	0.010	3.848	-.0114	-.9203	18.17	.0550
	0.001	23.67	-.0114	-5.641	105.0	.3360
$R_1=10R_2$	10.00	.0042	-.0015	-.0003	.2162	.00004
	1.000	.0854	-.0064	-.0055	1.322	.00009
	0.100	.6808	-.0054	-.0411	4.336	.00062
	0.010	4.598	-.0052	-.2757	20.60	.00414
	0.001	28.31	-.0051	-1.696	116.9	.02540

TABLE 5.13 FORCE COEFFICIENTS F_6 TO F_{10}

	δ/R_2	F_6*10^9	F_7*10^9	F_8	F_9	F_{10}
$R_1=R_2$	10.00	-.0630	.00007	-.00001	.0006	-.0006
	1.000	-.1031	.0909	-.0043	.0407	-.0407
	0.100	-4.079	1.379	-.0250	.1736	-.1736
	0.010	-18.05	8.337	-.0417	.2707	-.2707
	0.001	-101.3	49.97	-.0517	.3260	-.3260
$R_1=2R_2$	10.00	-.0531	.00004	-.00009	.0005	-.0036
	1.000	-.5958	.2295	-.0115	.0203	-.1330
	0.100	-2.090	2.679	-.0450	.0706	-.3717
	0.010	-9.261	15.17	-.0689	.1058	-.5066
	0.001	-52.34	89.51	-.0831	.1264	-.5793
$R_1=5R_2$	10.00	-.0351	.00025	-.00065	.0003	-.0305
	1.000	-.1980	.4446	-.0213	.0053	-.3765
	0.100	-.5427	3.824	-.0512	.0124	-.6470
	0.010	-2.279	20.09	-.0708	.0171	-.7555
	0.001	-12.62	115.2	-.0826	.0199	-.8098
$R_1=10R_2$	10.00	-.0198	.0066	-.0018	.0001	-.1080
	1.000	-.0675	.5427	-.0214	.0013	-.5893
	0.100	-.1593	4.127	-.0393	.0024	-.7965
	0.010	-.6462	21.03	-.0516	.0031	-.8657
	0.001	-3.532	118.9	-.0593	.0036	-.8990

Data consistent in :- Length - Meters, Field - Volts/Meter, Charge - Coulomb, Force - Newton

For completeness the force on the second sphere can be evaluated from:-

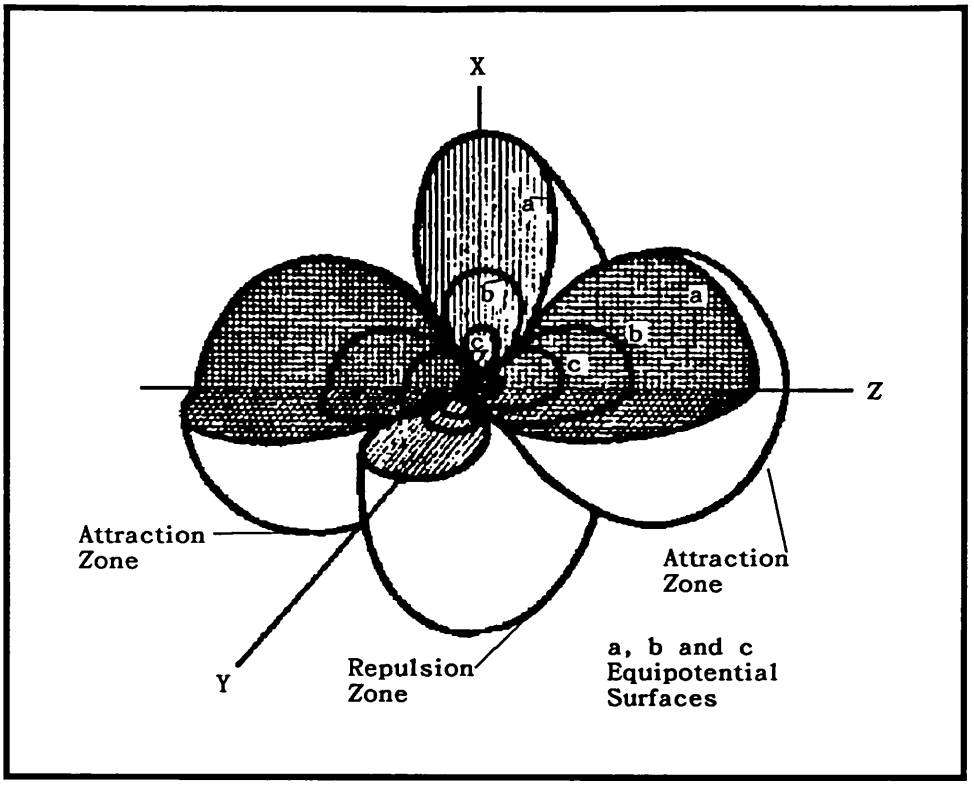
$$F(1) = E_0(Q_1 + Q_2) - F(2) \qquad \text{---- (5.21)}$$

Two assumptions are made in the analysis, that the conductors are spherical and that they are perfect conductors. Davis[136] subsequently investigated the latter point by considering the case of a non-conducting sphere with a dielectric constant K. Two cases were considered, that when the sphere was separated a distance, s, from a grounded conducting plane and that when the sphere has a point charge at its centre, a solution which applies equally to the case of

two identical separate spheres separated by 2s and carrying net charges +Q and -Q. Results were presented graphically for a number of different dielectrics and it was concluded that the theory for perfect conductors, solved previously and outlined above, was equally applicable for non-conducting spheres with dielectric constants above 81. The dielectric constant of water is 81 and was important in Davis's work as it was related to processes in the formation of clouds. Deviations were only apparent below a separation distance of 0.01 of the sphere radius and the maximum error was believed to be less than 0.5%.

Vlodavets, as mentioned earlier, obtained an interactive expression similar to that of Davis but evaluated the force coefficients by the method of consecutive imaging. The expression he obtained only gives the first two terms of equation 5.19, that is, the effects due to charges on the particles were not included. Direct comparison of the coefficients has indicated only small difference using this technique. Vlodavets also considered the surfaces of equipotential around each particle and demonstrated that three clear zones existed, these are shown in figure 85. These are, in effect, the interactions identified by Davis as F_z and F_x. One zone, approximately toroidal in shape, is of mutual repulsion and surrounds the particle in a plane perpendicular to the electric field direction whereas the other two zones are of attraction and are nearly spherical in shape. These two zones are located both sides of the particle in a direction parallel to the applied electric field. It is therefore clear that in such a configuration alignment to the electric field direction will be encouraged, an observed trend, and also that charge transfer parallel to the applied electric field will be encouraged but that charge transfer perpendicular to the applied electric field will be prevented. Such a situation has been shown to exist in ER fluids by the experiments, referred to earlier to measure the Hall effect[76].

FIGURE 85 EQUIPOTENTIAL SURFACES SHOWING ZONES OF MUTAL ATTRACTION AND REPULSION



Vlodavets also considered the case of zero separation, that is the case when the particles come into contact. O'Meara[137] has considered this case in greater detail. For the case of touching spheres the force in the z direction is given by:-

$$F_z = -4\pi\epsilon a^2 E_0^2 (F_1 \cos^2\theta + F_2 \sin^2\theta) + E_0 Q F_3 \cos\theta - Q^2 F_4 / 4\pi\epsilon a^2 \qquad \text{---- (5.22)}$$

where Q is the total charge on the spheres.

In contrast to the previous case for uncharged spheres the interaction is repulsive. Furthermore, it is suggested by the equation that the interaction may be either attractive or repulsive. This will be dependent on whether or not a net charge is in existence together with the relative size of the spheres. Consideration is also required with

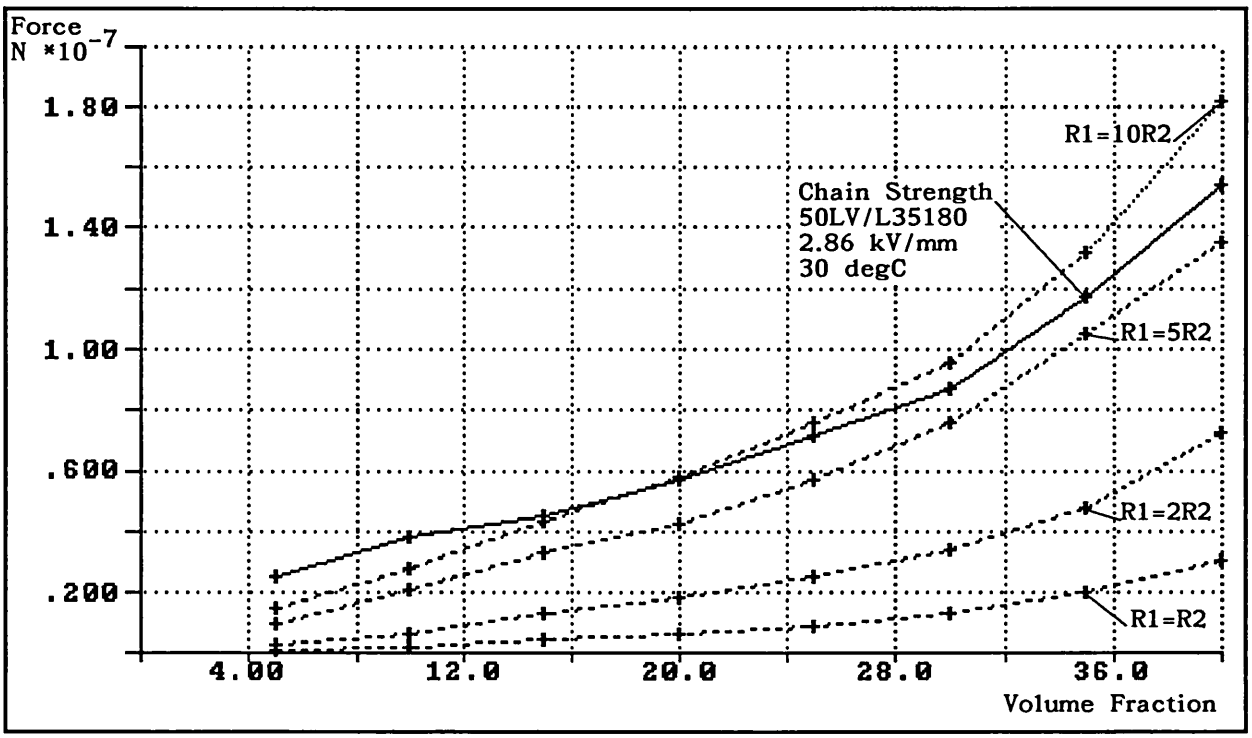
respect to the magnitude of the charge on the particle and electric field orientation with respect to the centres of the particles. It is therefore necessary that the two cases be distinguished.

Practical Considerations of the Electrical Interactions

The work of Davis has enabled the electric field intensification to be evaluated at different volume fractions. For an ER fluid with a volume fraction of 35% the electric field intensification is for equal sized spheres, from table 5.9, some five times the linear electric field gradient given by the voltage drop over the separation distance. This is increased to some twelve times when the ratio of the sphere diameters is 10:1. That is, if the dielectric strength of the continuous phase, E_{max}, is taken as 80 to 120 MV/m the maximum sustainable applied electric field E_0 will be in the order of 16 to 24 kV/mm when $R_1=R_2$ falling to 7 to 10 kV/mm when $R_1=10R_2$. In either case significantly greater than that applied in practice. Typically electric fields of 3 to 5 kV/mm being used. In addition Block[138] has conducted experiments where the particles of an ER fluid are embedded in rubber. Measurements of the elasticity of the rubber have indicated that it is changed with the applied electric field and it was concluded that there was no need for the particles to move or to come into contact to give rise to an ER effect. Coupling these arguments with the probable existence of a steric layer at the surface of the particles it is concluded that the particles do not have to touch for the effect to be generated and in all probability it is concluded that they do not touch. The interaction forces between the particles are, therefore, best expressed using the equations developed by Davis, that is equations 5.19 and 5.20. Some further simplifying assumptions are required for this limited assessment. It is assumed that there is no net charge on the particle and that the electric field lines are parallel to the z axis. This being the case $\sin\theta = 0$ and $\cos\theta = 1$. Values for the force coefficient F_1 from table 5.12 have been interpolated graphically for

different ratios of δ/R and different size ratios. The graphical interpolation is assisted if natural logarithms of both axis are taken. Having evaluated the values of the coefficient the force between the particles can be calculated and compared with the estimated chain force that was computed from the shear stress data. These results are presented in table 5.14 and figure 86 where it can be seen that the fit is reasonable and it is progressively improved as the size ratio of the interacting particles is increased.

FIGURE 86 INTERACTION FORCES versus VOLUME FRACTION



The Effect of Particle Size

It should be noted that the development of the chain density assumed equal sized spheres and as a consequence if unequal spheres are used both the interparticle distance and the chain density will be changed. Such a further development of this limited model is unnecessary as the main objective was

to show that the ER effect would scale with volume fraction in a manner that indicated that the only interaction required was an electrostatic one developed from the charge separation caused by a polarisation of the particle. This has been comfortable demonstrated and for a further expansion of the model to be accomplished data will be required from fluids of well defined particle size and shape. It is suggested by the analysis that the ER effect will be enhanced by having a variety of particle sizes rather than having a monodisperse system.

TABLE 5.14 CALCULATED FORCES OF INTERACTION

V/V	δ/R	$R_1=R_2$ Force N 10^{-8}	$R_1=2R_2$ Force N 10^{-8}	$R_1=5R_2$ Force N 10^{-7}	$R_1=10R_2$ Force N 10^{-7}	C_s Force N 10^{-7}
5	2.52	.076	.295	.095	.151	.254
10	1.59	.209	.670	.206	.275	.377
15	1.14	.426	1.28	.330	.436	.453
20	.853	.632	1.82	.426	.575	.573
25	.647	.909	2.51	.574	.758	.712
30	.493	1.35	3.39	.756	.955	.874
35	.367	1.99	4.78	1.05	1.32	1.17
40	.263	3.01	7.23	1.35	1.82	1.54

If equation 5.19 is considered and the previous simplifying assumptions are applied the equation becomes:-

$$F_z = \epsilon R_2^2 E_0^2 F_1 \cos^2\theta \qquad \text{---- (5.23)}$$

It is apparent that if the particle size is increased an enhanced electrostatic force between two spheres will take place. This being due to the R^2 term in the equation. Such a modification would, however, alter also the chain density, the separation distance and the electric field intensification. An assessment can be made of the effect on the interactive forces between two equal sized spheres at a

fixed volume fraction as the particle size is changed. The shear stress transmitted by the number of chains formed at that particular particle size can then be computed. In table 5.15 data is presented for a number of particle radii. What is observed is that as the particle size is increased the chain density per unit area is rapidly decreased and although the interactive forces are increased the shear stress remains the same. The importance of the structural model used to represent an ER fluid is highlighted by such an investigation, for although the electrical interactive force is increased some 25 times the shear stress is unaffected if a simple chain type geometry is retained.

TABLE 5.15 EFFECT OF PARTICLE SIZE

Size Dia μm	Density $Cd*10^{8}$	Force $N*10^{-8}$	Stress C_d*N
6	2.197	1.995	4.38
10	0.791	5.542	4.38
14	0.403	10.86	4.38
18	0.244	17.95	4.38
22	0.163	26.83	4.38
26	0.117	37.47	4.38
30	0.088	49.88	4.38

5.3.3 A MODEL FOR THE ELECTRIC FIELD DEPENDENCE OF THE EXCESS SHEAR STRESS

The above description of the interaction of two spherical particles in an external electric field has indicated that the variation of the force, and consequently the yield stress, between adjacent particles will scale as E_0^2. However, if the data is looked at carefully, figure 88 for example, it is seen that this is not the case. This deviation can be explained when it is appreciated that the analysis was developed using the assumption that the charge distribution within the particle was fixed and uneffected by either the

presence of the external electric field or by any interaction with a neighbouring systems of charges, i.e. other particles. Any electric charge distribution will be modified by the action of an external electric field, that is, the charges will move relative to each other and the system will be polarised. Whilst this may be of little significance in many cases, an ER fluid is chosen specifically for the polarisation to be enhanced. Additionally an ER fluid is manufactured to have a great number particles in close proximity. Any electric field distortion around one particle will effect the neighbouring particles and the induced polarisation due to the external electric field will be augmented by a mutually induced polarisation due to the presence of the neighbouring particles. Consequently an E_0^2 type interaction would only be expected to occur at low volume fractions and low electric fields. As both the volume fraction and the electric field are increased a progressively more complex form of the polarisation interactions takes place.

Electrical Multipoles

At the simplest level it can be assumed that the induced dipole moment, μ_i, is proportional to the electric field strength inducing it:-

$$\mu_i = \alpha E_0 \qquad \text{---- (5.24)}$$

where α is the volume polarisability of the particle. (α has an SI unit of $C^2m^2J^{-1}$).

In the general case of either charged systems or permanent dipoles the increasing complexity of the polarisation interactions can be assessed as a series of multipolar approximations. The simplest being a monopole, given by the total charge of the system, that is:-

$$q = \Sigma\, q_i \qquad \text{---- (5.25)}$$

where q_i represents the individual point charges of the system.

The summation can be positive, negative or neutral when the positive charges are equalled by the negative charges. The next level of complexity is the conventional electric dipole where two charges of opposite sign are separated by a distance, d_x, giving a general expression for the dipole moment of:-

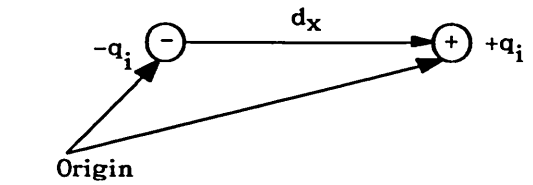
$$\mu = \Sigma\ q_i\ d_x \qquad \text{---- (5.26)}$$

The electric quadrupole is a characteristic of a surface charge distribution as opposed to monopoles and dipoles which are used to characterise a point and a linear charge distribution respectively. A quadrupole is conceived as two dipoles displaced by a small distance d_y. The quadrupole moment, when represented in matrix form has nine components. Increasing the complexity still further is the octupole, covering three dimensional space with 27 components followed by the hexadecapole with some 81 components. It is apparent that the complexity is increased in the ratio of 1 : 2 : 4 : 8 : 16 etc. and it is therefore possible for any multipole polarisation to be represented by a 2^n-pole system so that:-

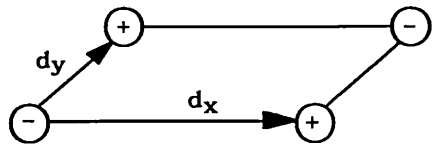
$$\mu^{(n)} = \Sigma\ q_i\ d_i\ \mathbf{Y}^{(n)} \qquad \text{---- (5.27)}$$

where $\mathbf{Y}^n$ is the matrix expansion of the multipole.

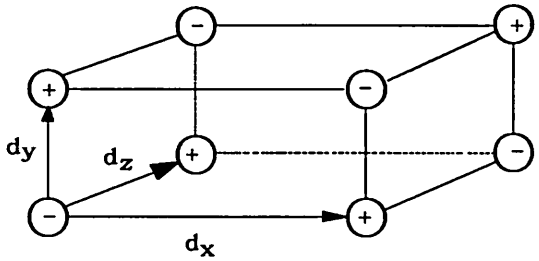
The schematic arrangements for a dipole and the quadrupole are shown in figure 87. In the case of a practical ER fluid, also shown schematically in figure 87, the charges are shown as point charges located at the centres of the particles. It is apparent that the induced polarisation will be very complicated as neighbouring particles will have both attractive and repulsive force components.



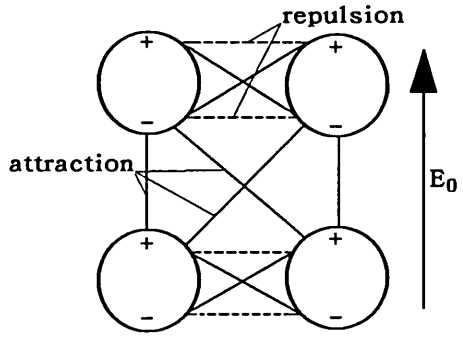
An Electric Dipole



An Electric Quadrupole



An Electric Octupole



Simple ER Fluid Multipole

FIGURE 87 ELECTRIC MULTIPOLE ARRANGEMENTS

The induced dipole moment, equation 5.24, can likewise be expressed in a general fashion as an induced 2^n-pole moment so that:-

$$\mu_i^{(n)} = {}^n\alpha E_o \qquad \text{---- (5.28)}$$

where ${}^n\alpha$ defines the multipole polarisability of order n with respect to the uniform electric field E_0.

If n = 1 the induced dipole moment is obtained, when n = 2 the induced quadrupole moment is obtained, when n = 3 the induced octupole moment is obtained and so forth. In general the inducing electric field, E_0, will not be locally uniform due to the distribution of the particles and the effect of particle shape. In general the induced multipole moment, equation 5.28, is augmented by terms induced by the electric field gradient dE_0/dx, the gradient of the gradient

d^2E_0/dx^2 and so forth. The liner dipole moment, μ_i, can therefore replaced by:-

$$\mu_i^{(1)} = {}^1\alpha E^0 + \frac{1}{3} {}^1\alpha \frac{dE_0}{dx} + \frac{1}{15} {}^1\alpha \frac{d^2E_0}{dx^2} \ldots \quad \text{---- (5.29)}$$

That is the dipole moment is augmented by a dipole polarisation due to the electric field gradient, a dipole moment due to the gradient of the electric field gradient and so on. Similarly the quadrupole, where n = 2, will be replaced by:-

$$\mu_i^{(2)} = {}^2\alpha E_0 + \frac{1}{3} {}^2\alpha \frac{dE_0}{dx} + \frac{1}{15} {}^2\alpha \frac{d^2E_0}{dx^2} \ldots \text{ -- (5.30)}$$

and the octupole, where n = 3, can be likewise expanded and a general expression of the form developed:-

$$\mu^{(n)} = \Sigma_{n=1}^{\infty} \frac{2^n\, n!}{(2n)!} {}^n\alpha \frac{d^nE_0}{dx^n} \quad \text{---- (5.31)}$$

In weak electric fields the dipole polarisation is electric field independent. However at high electric fields it may become electric field dependent. Equation 5.25 can be rewritten as:-

$$\mu_i = \alpha(E_0)\ E_0 \quad \text{---- (5.32)}$$

where $\alpha(E_0)$ is now a function of the electric field strength.

It is usual for $\alpha(E_0)$ to be expressed as a series expansion of the form:-

$$\alpha(E_0) = \alpha(0) + \beta E_0 + \epsilon E_0^2 + \ldots \quad \text{---- (5.33)}$$

where $\alpha(0)$ is the linear polarisability and β and ϵ are the so called hyperpolarisabilities.

What is apparent from these discussions is that an adequate description of the ER effect is most unlikely to be

provided by the simple dipole-dipole interaction. The closer a description of a practical ER fluid is attempted the greater the level of sophistication required for the polarisation mechanism. At this stage such a detailed exploration is unwarranted as currently little is known regarding the polarisability of the particles, the electric field dependence of the polarisation or the way in which irregular shaped particles could be included into the general expressions. Whereas simple dipole-dipole interactions can be scaled as E_0^2, multipole interactions will have to be represented by a complex series expansion where the multipoles, the electric field distortions and electric field dependent polarisability are reflected. Such an analysis is not attempted in this research but it is instructive for the relationship of the shear stress to be considered with respect to the applied electric field in the light of the preceding discussion.

Non-Linear Electric Field Effects

The ER effect is taken to result from the interaction of particles that have an induced polarisation. Whereas non-linear polarisation mechanisms are evident at a molecular level it is considered improbable that they will occur at the particulate level. Consequently it can be assumed that the volume polarisability will be independent of the applied electric field and that the series expression described by equation 5.33 is unnecessary. However, it is apparent that a simple E_0^2 dependence can not be applied, see figure 88, and that a more complex dependence is required. If both the multipole polarisation and the non-uniformity of the electric field as expressed by equations 5.29 to 5.31 are considered the multipole polarisation and the electric field non-uniformities can be included into a single expression. On this basis the ER effect should be related to the applied electric field by an expression of the form:-

$$T_y = a_0 E_0^2 + a_1 \frac{dE_0}{dx}.E_0 + a_2 \frac{d^2E_0}{dx^2}.E_0 + .. \quad -- (5.35)$$

where $a_0 \rightarrow a_n$ are coefficients encompassing the multipoles, electric field non-uniformities and the interaction of the multipoles.

What is now required is some notion as to the most appropriate term for such a series to be truncated. Curve fitting of the data to the above function has indicated that only the first two terms are significant. The truncation being based on fitting expression 5.35 to the shear stress data presented in tables 5.4 and 5.6.

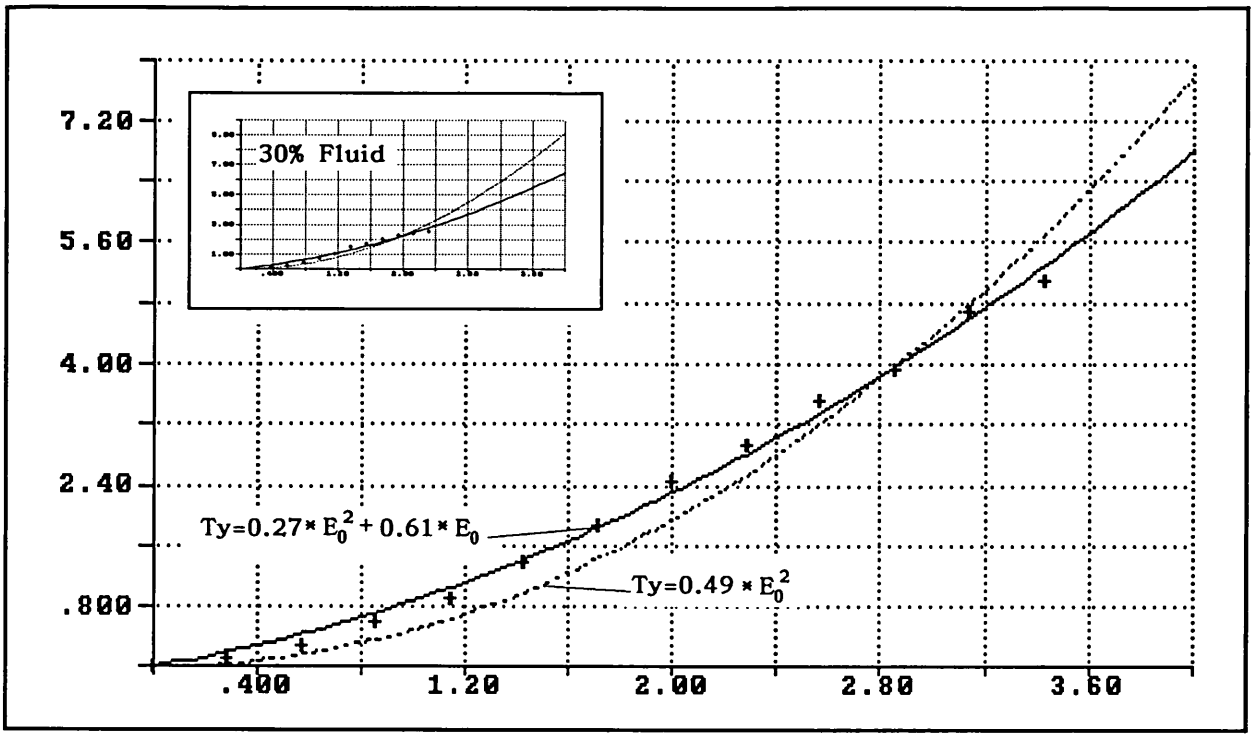
That is, equation 5.35 can be reformulated as:-

$$T_y = A_0 E_0^2 + A_1 E_0 \quad ---- (5.36)$$

It is assumed that the electric field gradient is a constant value which can be incorporated into the coefficient A_1.

In figure 88 a plot is shown of the experimental data from table 5.6 together with a least squares fit to an E_0^2 dependence and a fit based on equation 5.36. As can be observed an E_0^2 dependence has imposed an exaggerated curvature so that at the higher electric field strengths the strength achieved by the fluid is considerable over estimated. This aspect is further identified by the inset graph of figure 88 which shows the fit for a 30% fluid where again an over estimate is predicted by an E_0^2 dependence. Detailed below, in tables 5.16 and 5.17, are the two coefficients, A_0 and A_1, for a number of different fluids at different fluid temperatures and shear rates. The acceptability of the fit is represented by two terms, the sum of the squared residuals, Err^2, and the correlation coefficient, R. As can be noted, the fit is generally very good.

FIGURE 88 LEAST SQUARES FIT OF STATIC SHEAR STRESS DATA



Fluid 50LV/L35180
Temperature 30 degC

X Axis kV/mm
Y Axis kPa

TABLE 5.16 COEFFICIENTS FROM EQUATION 5.36 FOR VARIOUS VOLUME FRACTION FLUIDS

	30%	35%	40%	30%	35%	40%
A_0	0.267	0.451	0.420	0.193	0.386	0.410
A_1	0.258	0.166	0.665	0.291	0.221	0.613
Err^2	0.057	0.100	0.082	0.034	0.073	0.120
R	0.996	0.996	0.998	0.997	0.997	0.997

Shear Rate 270 sec^{-1} Shear Rate 1270 sec^{-1}
Fluids 50LV/L30180 Temperature 30°C
50LV/L35180
50LV/L40180

TABLE 5.17 COEFFICIENTS FROM EQUATION 5.36 FOR VARIOUS TEMPERATURES

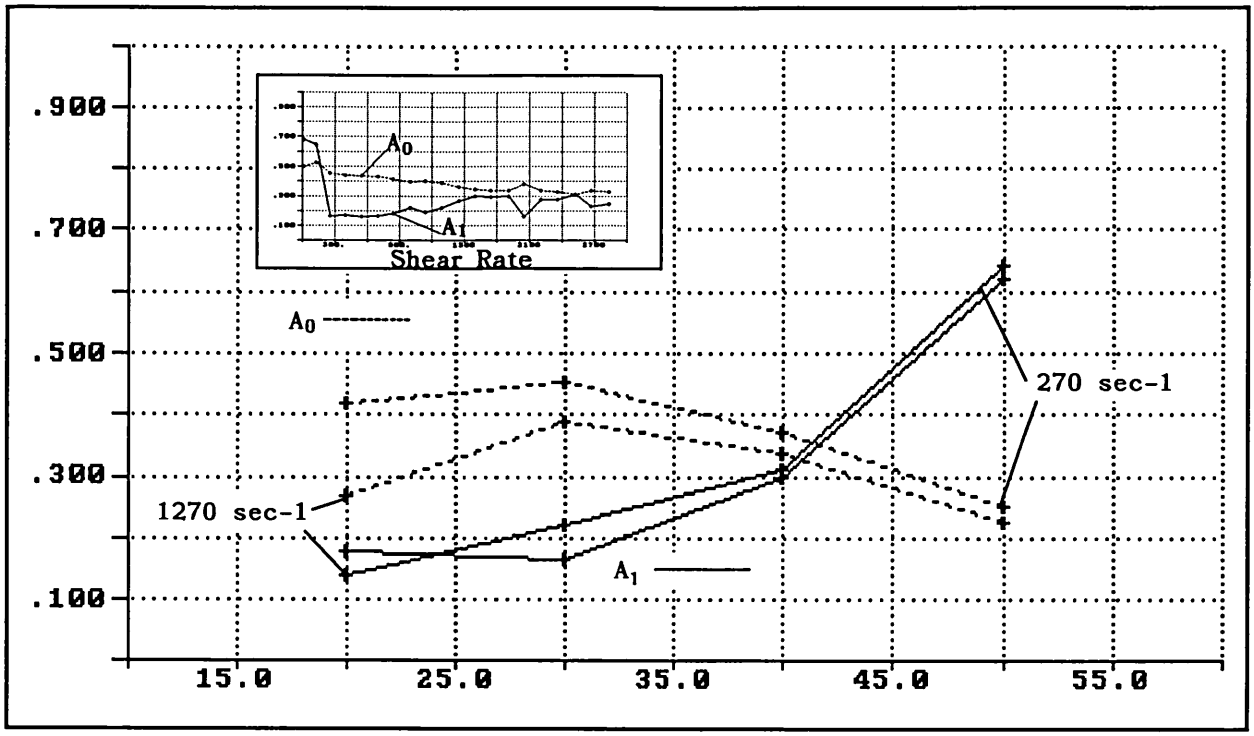
	20°C	30°C	40°C	50°C
A_0	0.420	0.451	0.370	0.249
A_1	0.177	0.166	0.296	0.621
Err^2	0.006	0.100	0.199	0.345
R	0.999	0.996	0.992	0.988
Shear Rate 270 sec^{-1}			Fluid 50LV/L35180	

	20°C	30°C	40°C	50°C
A_0	0.267	0.386	0.335	0.226
A_1	0.138	0.221	0.310	0.642
Err^2	0.028	0.073	0.051	0.267
R	0.997	0.997	0.997	0.990
Shear Rate 1270 sec^{-1}			Fluid 50LV/L35180	

	20°C	30°C	40°C	50°C
A_0	0.432	0.336	0.292	0.128
A_1	0.113	0.275	0.399	0.828
Err^2	0.032	0.069	0.048	0.227
R	0.996	0.997	0.998	0.992
Shear Rate 2270 sec^{-1}			Fluid 50LV/L35180 Data from the ERV	

It is suggested that the variation of shear stress induced by the applied electric field can be adequately represented by the expression presented as equation 5.36. The fit to the experimental data is acceptable in the majority of cases. Some trends are apparent in the data presented in tables 5.16 and 5.17 although some difficulty is experienced in isolating these trends. For example, if the change of the coefficients A_0 and A_1 with temperature is considered it is suggested from the data in table 5.17 that A_0 will fall as the temperature is increased and that A_1 will be increased as the temperature is increased. Additional data is required with respect to temperature although some trends, as shown in figure 89, can be clearly observed. A dependence on shear rate was also observed, as shown by the inset and detailed in table 5.18. This will be discussed in the next section.

FIGURE 89 LEAST SQUARES COEFFICIENTS AGAINST TEMPERATURE



Fluid 50LV/L35180 X Axis degC

TABLE 5.18 COEFFICIENTS FROM EQUATION 5.36 FOR VARIOUS SHEAR RATES

G	22	128	259	398	538
A_0	0.501	0.524	0.451	0.441	0.434
A_1	0.680	0.644	0.165	0.167	0.160
Err^2	0.173	0.173	0.100	0.093	0.075
R	0.993	0.994	0.996	0.996	0.997
G	693	836	984	1135	1294
A_0	0.430	0.415	0.395	0.399	0.386
A_1	0.163	0.184	0.220	0.190	0.221
Err^2	0.087	0.076	0.082	0.077	0.073
R	0.997	0.997	0.996	0.996	0.997
G	1433	1590	1743	1905	2049
A_0	0.361	0.345	0.336	0.335	0.378
A_1	0.269	0.299	0.294	0.299	0.159
Err^2	0.069	0.073	0.070	0.076	0.109
R	0.997	0.997	0.997	0.996	0.994
G	2206	2363	2514	2672	2834
A_0	0.335	0.328	0.311	0.338	0.326
A_1	0.275	0.278	0.310	0.230	0.248
Err^2	0.069	0.076	0.064	0.072	0.062
R	0.996	0.996	0.997	0.996	0.997

5.3.4 A MODEL FOR THE SHEAR RATE DEPENDENCE OF THE EXCESS SHEAR STRESS

When the variation of shear stress with the wall shear rate in Poiseuille was discussed, in section 5.2.1, it was suggested that the electric field induced shear stress would be expected to vary with shear rate in the two fully sheared regions either side of the central plug. It was suggested that the conditions in a Couette cell were similar to these two sheared regions. A cursory glance at typical data from the ERV has indicated that this was the case. This was subsequently confirmed in detail in section 5.2.3. It was also noted that in Couette flow the excess shear stress would be expected to be a function of the shear rate. The variation of excess shear stress with shear rate will probably be electric field dependent, figure 44b, probably water content dependent and certainly temperature dependent, figure 47b. The shear dependent behaviour, particularly at the lower temperatures, is clearly not a simple linear function of the shear rate and some means of expressing such a variation is required.

In general it can be assumed that the excess shear stress is the result of the sum of two components, an electric field induced force, F_E, and an electric field induced torque, T_E. If the fluid is sheared the particles will spin, and give rise to a rotation rate of G/2 for spherical particles. If an external electric field is applied the particles will be polarised and the effect of the electric field will be to try to align the polarisation vector of the particle. There will then be an interaction with the shear rate induced rotation. Such a phenomena gives rise to a number of observable resonant type characteristics, among them a flow modified permittivity[145]. However, this contribution to the ER effect is slight, being only a modifying component as an externally applied shear rate is required for a torque to be generated. Even though only a small component, it would be expected to be manifested as a resonant peak in the shear stress versus shear

rate profiles, the position of which, should in principle be, determinable from dielectric data.

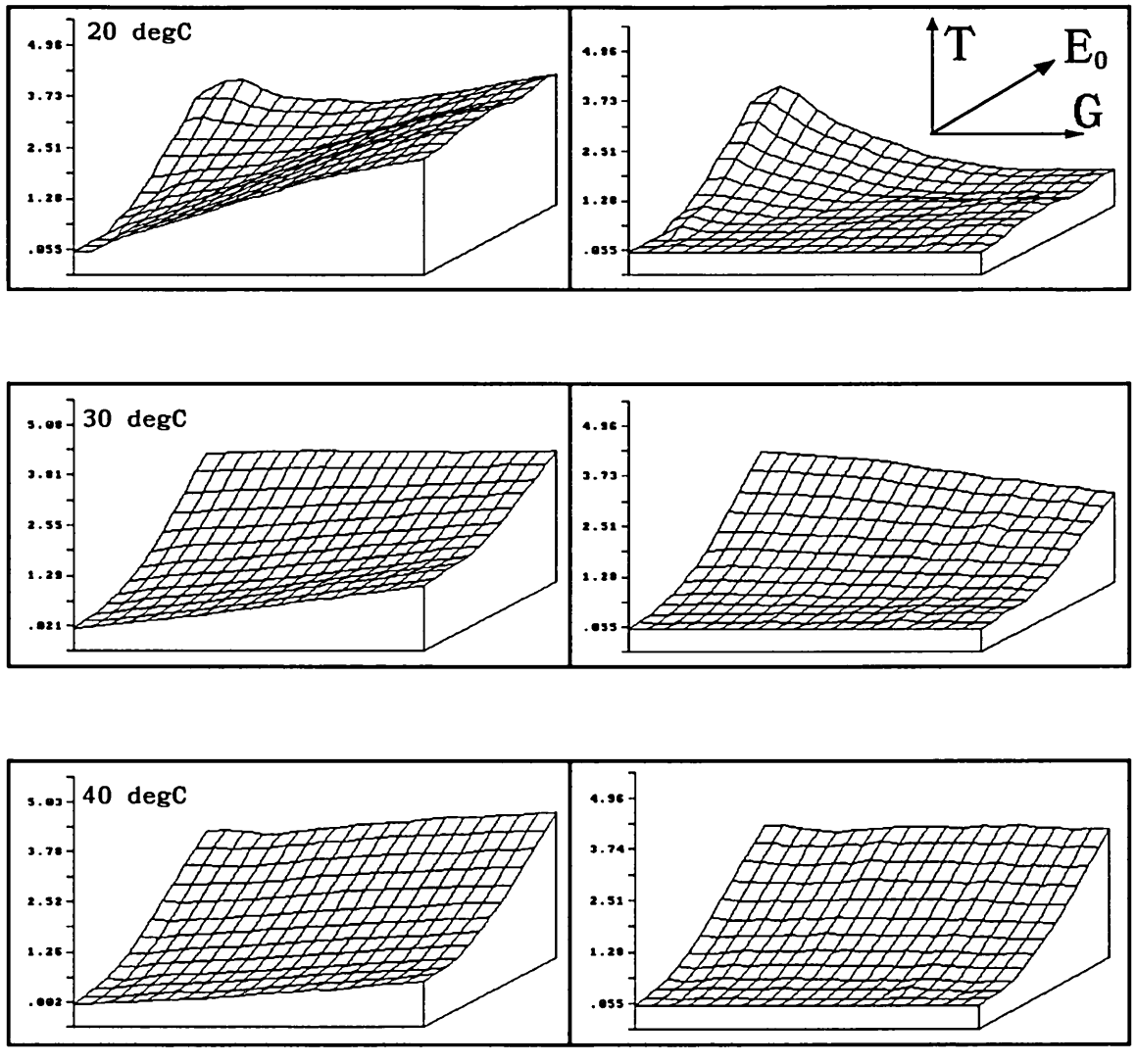


FIGURE 90 3-D PLOTS OF 50LV/L35135 AT DIFFERENT TEMPERATURES

The variation of excess shear stress with shear rate can be most readily visualised by the use of three dimensional plots as shown in figure 90. Data are presented for the fluid coded 50LV/L35135 at three temperatures. Plots of the total and the excess shear stress are presented. The shear rate has been varied from approximately 22 to 3000 sec^{-1} in 19 equal increments in the x direction. The electric field strength being varied from 0 to 2.34 kV/mm in 12 increments and is shown in the z direction. The stress is in the y direction. The plots of total shear stress indicated an approximately Newtonian behaviour at zero electric field with the shear stress being increased as the electric field was increased at all shear rates. It is clearly indicated by the plots of excess shear stress that the stress component falls as the shear rate is increased.

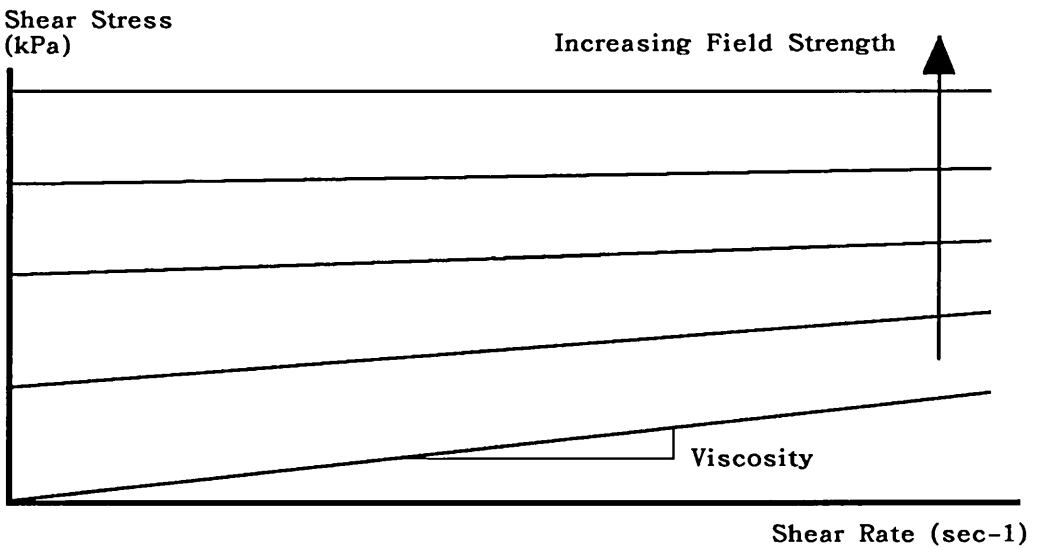


FIGURE 91 LINEARISED SHEAR STRESS SHEAR RATE DEPENDENCE

This reduction is clearly a function of temperature, and an increased temperature results in a decreased stress. These variations can, as an initial approximation, be linearised and are shown in figure 91. The general characteristics can be described as follows:-

a) At zero voltage, the behaviour can be approximated as Newtonian.

b) At low electric field strengths the slope dT_t/dE is positive.

c) As the electric field strength is increased the slope is decreased.

d) As the electric field strength is increased, at constant shear rate, the excess shear stress is increased.

e) With an electric field applied the fluid will support a non- vanishing shear stress; a yield stress is exhibited.

It follows from a) and c) that the slope can under certain circumstances be negative but must subsequently become positive as the Newtonian component will progressively be increased, especially at higher shear rates. Such a phenomenon is observed for the 20°C plot where the fall of the electric field induced shear stress is of sufficient magnitude for the total stress to fall with shear rate before the Newtonian component is increased to such a magnitude as to cause a positive slope in the data.

In the study of the rheology of non-Newtonian fluids such a progressive reduction, usually in the viscosity, is attributed to a breakdown of structure in the fluid. This is frequently expressed as a series with four steps:-

a) a breakdown of gel-like structures, or possibly some shear induced aggregation.

b) a gradual orientation and deformation of aggregates.

c) a progressive breakdown of aggregates into small units leading to individual particles.

d) possible deformation of particles and/or orientation of individual particles.

These steps will have different relaxation times which are decreased in magnitude as the breakdown is progressed. In the case of concentrated suspensions other factors, such as fluid trapping and deformation by crowding may be important. For polydisperse systems the amount of fluid trapping is small as the interstitial spaces are occupied by the smaller particles.

Structural Kinetic Processes in ER Fluids

If the highly simplified ER fluid structure shown in figure 92 is considered some details of these effects can be illuminated. Two adjacent sequences of particles in three successive time increments, A, B, and C are represented. The top particle sequence is taken to have a velocity dU with respect to the lower sequence. As the sequences move from configuration A) towards configuration B) the particles will be moved towards a condition of closest approach as displayed in arrangement B). Interactive forces between the particles, for example particles "1" and "A" will be increased whilst the forces between "1" and "B" will be decreased, and so on along the sequence. At position B) the arrangement of the particles corresponds to a position of closest approach and this will correspond to the local maximum electric field and therefore the local maximum particle interaction. As the shearing is progressed, position C) is reached, and the bond between "1" and "A" is weakened as the bond between "2" and "A" is being formed.

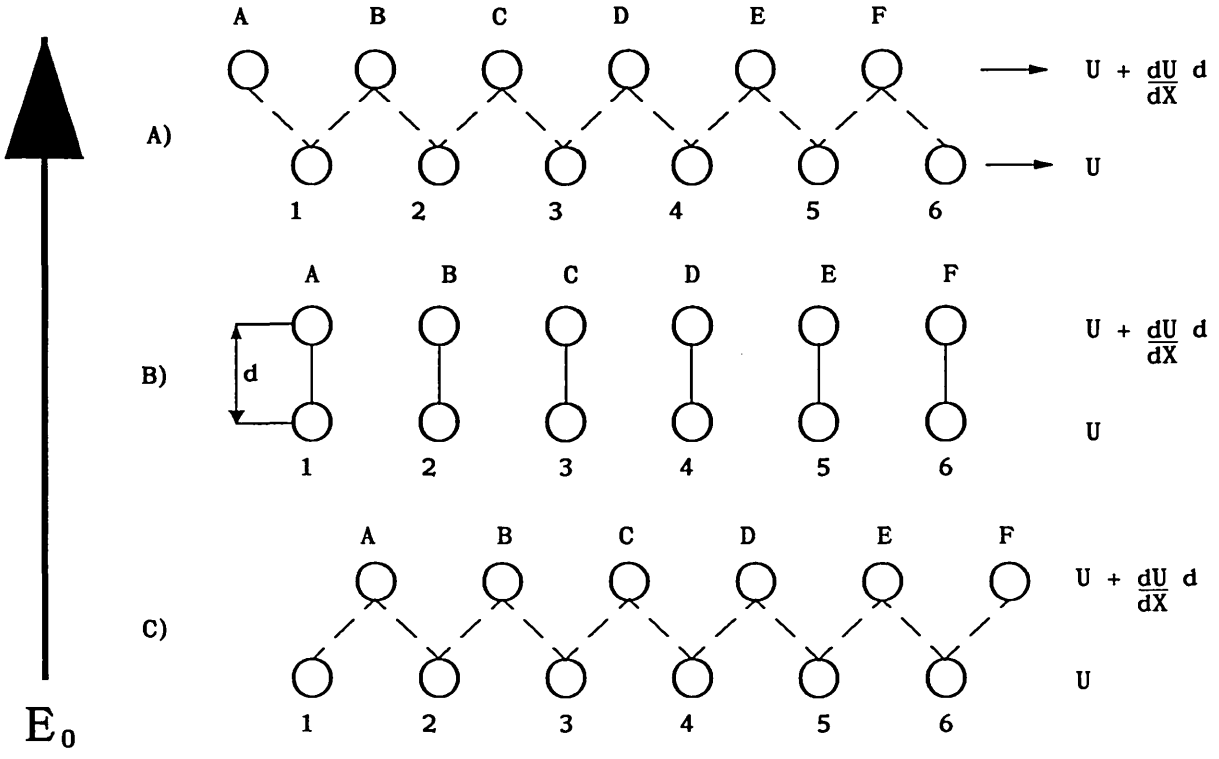


FIGURE 92 PARTICLE TRANSLATION DURING SHEARING

Clearly some such process of structural development and structural break-up must occur as the fluid is sheared for <u>if</u> the bonds cannot survive the effects of the shear rate there will be no electric field induced shear stress during shear. When the fluid is sheared the particles will be rotated and translated and if the shear rate is maintained the particles will be moved past each other to a position which is identical to the start position but now shifted in the direction of the shear field.

The development of the interaction between the particles must occur in a finite time period. When a shear rate is applied to the fluid the time available for the interaction will be changed, progressively getting smaller as the shear rate is increased, and must inevitably result in a fall of excess shear stress with increased shear rate. A structural kinetics approach is often applied to the change of rheological properties with time and with shear rate; such an

approach can be readily adapted to the ER fluid case. Given that the above description is highly simplified, and if it is assumed that not all the structural units are identical, the conventional approach can be applied and a structural parameter, Γ, assigned to these aggregation-deformation-orientation effects. A general framework using such a phenomenological model was developed by Cheng and Evans[138] who concluded that the behaviour can be described by two equations:-

$$T_y = f(G,\Gamma) \qquad \text{---- (5.37)}$$

$$\text{and} \quad \frac{d\Gamma}{dt} = g(G,\Gamma) \qquad \text{---- (5.38)}$$

where G is the shear rate and Γ is the structural parameter

such that $0 \leq \Gamma \leq 1$.

These equations, although originally developed for thixotropic suspensions, were later extended to include suspensions exhibiting a yield stress. They indicated that the shear stress is not constant but depends on the shear rate and a structural state prevailing at any time in the suspension which is represented by the parameter Γ. The manner in which the structure is changed is given by the rate equation in which it is stated that the rate of change of the structure will depends on the shear rate and the current structure. Positive values of $d\Gamma/dt$ indicated that structural build-up will take place and negative values indicated that structural breakdown will occur. If either $d\Gamma/dt$ or the function g is zero then structural build-up will equal the structural breakdown and a equilibrium situation will exist. In this case, $\Gamma = \Gamma_e$ and equation 5.37 can be re-written as:-

$$T_y = f(G,\Gamma_e) \qquad \text{---- (5.39)}$$

The approach for handling experimental data is to take polynomial expressions of increasing order and in this instance it is sufficient to restrict the order to one. This is the development proposed by Moore[139]. He postulated that the rate of breakdown of the suspension structure was proportional to the structural level and the shear rate, whereas the structural build-up was assumed to be independent of the shear rate but proportional to the amount of structure capable of being built-up, that is (1-Γ). Equation 5.38 can now be re-written as:-

$$\frac{d\Gamma}{dt} = a\,(1-\Gamma) - b\,\Gamma\,G \qquad \text{---- (5.40)}$$

At equilibrium $d\Gamma/dt = 0$ and the equilibrium structural parameter is given by:-

$$\Gamma_e = \frac{a}{a + bG} \qquad \text{---- (5.41)}$$

giving the equilibrium shear stress as:-

$$T_e = \frac{a\,T_y}{a + bG} \qquad \text{---- (5.42)}$$

where a and b are material parameters that represent the structural build-up and the structural breakdown.

Figure 93a is a typical fit of the experimental data for one fluid at two fluid temperatures and one electric field strength, the fit shown is reasonable. This interpretation can be extended to all values of electric field strength and the three parameters can then be plotted as a function of electric field strength, as shown in figures 93b to 94b. A number of interesting features can be noted if these three graphs are examined. Firstly, the variation of the excess shear stress against electric field strength is sensibly independent of temperature and can be adequately modelled using expression 5.36. This is, in effect a re-iteration of the previously noted behaviour of the static yield rig. Secondly, the parameter "a" is effectively independent of electric field

strength although some difficulty is experienced in evaluating this parameter. This is discussed below. Thirdly, in figure 94b, the variation in "b" with temperature is significant and can be shown most effectively on a logarithmic plot. Taking "b" to be electric field independent, the averaged values at 20, 30 and 40°C are $5.5*e^{-4}$, $1.49*e^{-4}$ and $0.14*e^{-4}$ respectively. As noted above a problem exists in determining the values for "a" and "b" for it is found that the fitting is fairly insensitive to "a" and variations in "a" can be accommodated by changes in "b". For example in figure 95a the data at 1.95 kV/mm for a temperature of 40°C is shown together with lines for the following parameters;

$a = 0.3, 0.5, 0.7$ and $b = 9.2*e^{-6}$
with an excess shear stress, T_y, of 2.05 kPa

In figure 95b, data from the above fluid at 20°C is shown with curves for the case where the yield stress is fixed at 2.05 kPa and "a" at 0.3, 0.5 or 0.7. The fit then rests on the value of "b". It was discovered that "b" took numerical values of $6.2*e^{-4}$, $10.3*e^{-4}$ and $14.5*e^{-4}$ for the three cases. The resulting curves, however, are indistinguishable from each other and differences are very difficult to detect.

Additional analysis of data from other fluids has indicated that similar results to those discussed above occur. For example, the fluid designated 50LV/L35180, which is at the opposite extreme in terms of water content to the above fluid was considered. A similar coalescence of data was indicated with the excess shear stress being independent of temperature, and values of "a" around the 0.4 to 0.8 being returned. The values of "b" are essentially constant with applied electric field but again are seen to fall significantly as the temperature is increased. The averaged values of "b" for this fluid are, at 20°C, $2.86*e^{-4}$, at 30°C, $2.96*e^{-5}$ and at 40°C a value of $5.84*e^{-6}$ is obtained. Clearly there is a requirement for data to be obtained from the rate of structural build-up with time before a fuller description of these expressions and their detailed applicability to ER fluids can be assessed.

A Model for the Electric Field and the Shear Rate Dependence of the Excess Shear Stress

It is possible for the effect of both shear and electric field strength to be combined and a 3-D plot created, similar to figure 90, for both the experimental data and the theoretical prediction. Using equation 5.36 and equation 5.42 the variation of the excess shear stress with electric field strength and shear rate can be mapped out. The governing equation for this being:-

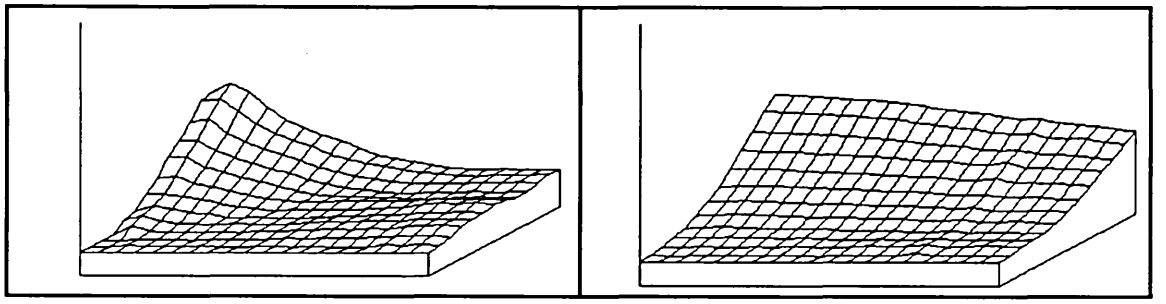
$$T_e(G,E_0) = \frac{aA_0E_0^2 + A_1E_0}{a + bG} \qquad \text{---- (5.43)}$$

where a and b are structural parameters and A_0 and A_1 characterise the particle polarisation.

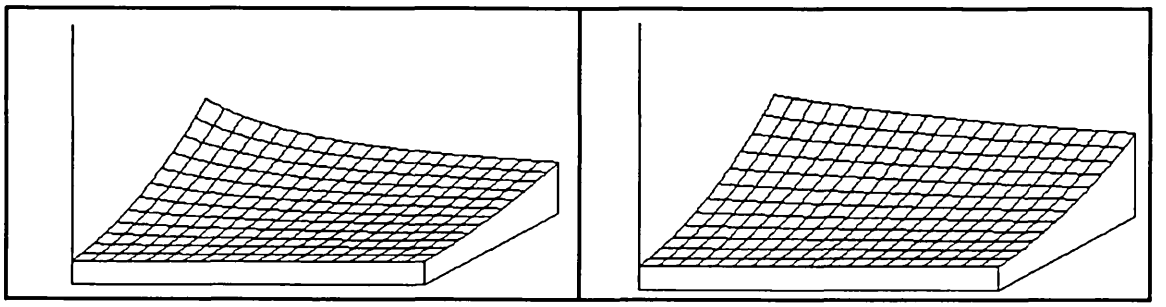
Using averaged values of 0.35 for "a" and $5.2*e^{-4}$ for "b" and taking A_0 as 0.503 and A_1 as 0.41 the surface shown in figure 96 can be generated. The values of shear rate and electric field strength increment are the same as those for the experimental data shown in figure 90. As one would expect the fitted expression maps out a much smoother surface but it is apparent that this relatively simple expression enables the desired profile to be generated.

It would appear that the behaviour of an ER fluid when subjected to different electric field strengths and shear rates can be described using the expression given in equation 5.43. Of the four coefficients A_0 and A_1 stem directly from the interaction of charged spheres given by Davis, although it is necessary for the simple polarisation terms to be expanded to take into account the multipole polarisation due to the electric field and the gradient of the electric field. Implicit in the discussion was an assumption as to the

structure formed by the particles under the applied electric field, that is, one of chains. The complexity of chain formation in the electric field of concentrated asymmetric particles rendered a detailed exposition impossible and this inability can also be extended to the multipole polarisation mechanism. It is apparent that it is not a practical possibility to predict, from these initial assumptions, the behaviour of an ER fluid. The preceding analysis has indicated that the experimental data can be scaled with the parameters used and it is suggested that additional constants, e.g ϵ_r, could be removed from the coefficients. Additional experimental data on the effect of the dielectric constant of the continuous phase on the behaviour of ER fluids will be required.



Experimental Data of Excess Shear Stress versus Shear Rate and Field Strength
20 degC 30 degC



Prediction based on Equations 5.36 and 5.41
20 degC 30 degC

FIGURE 96 EXPERIMENTAL AND PREDICTED 3-D PLOT OF EXCESS SHEAR STRESS

Parameters "a" and "b" in equation 5.43 are features of the dynamics of the structure formation and must be linked directly to the form of the structure that is evolved with time. Due to the nature of the structural equilibrium expression "b" must have dimensions of time, it can therefore be assumed to be the relaxation time of the particle interaction. Again more detailed data is required, specifically with different polymer systems. In addition, as noted, it is difficult to evaluate "a" or "b" to any high level of confidence. To do this extensive dynamic measurements are required on the rate of build-up and break-down of the structure.

At this stage it could be argued that the four coefficients are merely fitting parameters. In part, this is a fair argument, although it is necessary for the immense difficulty in expanding each coefficient to a more elementary form to be considered. Within the basic formulation of the problem, a significant amount of diverse data has been accommodated. However, substantially more data is required in specific areas to enable each of the coefficients to be expanded. A major source of data would be generated from an investigation as to the role of particle size and shape. Unfortunately there are a number of practical problems to be overcome before an ER active dispersed phase of controlled size and shape can be manufactured. If a range of spherical particles could be manufactured a much clearer understanding of the structure that is created, the polarisation mechanism that occurs and the interaction that results, could be realised.

This examination of ER fluids has indicated that the strength of the fluid is controlled by the polarisation and the structure that evolves. In addition, the rheological dependence of the fluid has been shown to be a function of the structure and of the relaxation of the interparticle forces. There are a number of additional components that add complexity to the issue, such as the torque component and the need to ensure that the fluid in the Couette cell is fully

sheared, but these are relatively small details compared to the overriding electric field induced component that is the ER effect itself. As a final point in the discussion it is useful to comment on an inherent electrical effect, that although not essential to the generation of the shear stress has profound practical implications, that is the conductivity of the fluid under an applied electric field.

5.4 THE CONDUCTION PROCESS

At room temperature solid insulators have, for most practical purposes, a negligible conductivity; dielectric liquids however, always retain a considerable conductivity and at higher electric field strengths, 5 to 10 kV/mm, the conductivity is often so large as to render them commercially unusable. The conduction is usually understood to be electrochemical in nature, and a number of reactions have been identified. For example a molecular species can undergo a reduction process and give rise to a radical ion, this reaction is common in nitrobenzene. Alternatively water oxidation at the anode is commonly observed, $H_2O \rightarrow e + H^+ + OH$, although the resulting injection of protons is irregular and often not reproducible. In the case of an ER fluid numerous sources of charge exist, water in the polymer, impurity species in the continuous phase and disperse phase as well a charge injection at the electrodes.

It is implied by the simple fact that the current flows that a charge is transported and that this current flow is the product of the total transported charge and the drift velocity of the charges. There are a number of possibilities as to the nature of both the charge and the charge carrier and these will be combined, the assembly being referred to as a *particle-charge*. The particle-charge is subjected to a number of influences, being charged it is electric field dependent, that is, it will preferentially drift with respect to the external electric field. Similarly the particle-charge is influenced by the chemistry of the system. Some activation energy, α, is required to move the particle-charge. Finally the particle-charge is subjected to thermal energy. Provided that the activation energy is exceeded by the sum of the thermal and electrical energies the particle-charge will move with a net drift velocity in the direction of the applied electric field and a current will flow. At this stage is apparent that if additional fields are applied to the system, specifically a perpendicular hydrodynamic field, typical of

the shear field in a Couette cell, the net current flow will be modified.

Empirically the current versus temperature profile can be approximated by a Boltzmann type curve. If it is assumed that the energy is distributed amongst the particle-charges on the basis of a Boltzmann distribution with an associated charge of, q, the particle-charge in an electric field, E_0, will gain energy proportional to qE_0. The particle-charge will have some mean free path, a, which will depend on the structure of the system. In being moved a distance, a, the energy gained will be aqE_0. If the activation energy is exceeded by this energy plus the thermal energy after the particle-charge has moved the mean free path distance the particle-charge will continue in the conduction process and a net current flow will be observed. It is assumed that no electrical energy is required to charge the particle-charge. If such additional energy is required the total electrical energy available would be reduced and as such would represent a reduction in the magnitude of the aqE_0 term.

The probability that a particle-charge will be enabled to "move up" the potential gradient will be proportional to $\exp\{(-\alpha - aqE_0)/kT\}$ and the probability that the particle-charge will "move down" the potential gradient will be proportional to $\exp\{(-\alpha + aqE_0)/kT\}$ where k is Boltzmanns constant and T is the absolute temperature. The net current flow will be the difference of these two probabilities. This can be written as:-

$$J = De^{-\alpha/kT} \sinh(aqE_0/kT) \qquad \text{---- (5.44)}$$

where J is the current density
and D is a constant of proportionality.

At low values of E_0 where $\sinh(aqE_0/kT)$ can be approximated to aqE_0/kT it is found that:-

$$J = \frac{DaqE_0}{kT} \exp^{-\alpha/kT} \qquad \text{---- (5.45)}$$

That is, the conduction is ohmic at low E_0 whilst at the higher electric fields $\sinh(aqE_0/kT)$ can be approximated to $e^{(aqE_0)/2}$ and the conduction will be exponential in form. Equation 5.44 is in fact a specific case of the Butler-Volmer equation for interfacial charge transfer where the symmetry factor, β, has been assigned a value of 0.5. This is the commonly accepted practice for most single electron exchange reactions[140-141]. This straightforward explanation of the conduction process could be further expanded but at this stage it is only necessary to examine some of the terms of equation 5.44 with respect to the experimental data.

The experimental apparatus used was a purpose built conductivity cell with the usual precautions of guard rings and high impedance measuring equipment. At high temperatures and high electric fields the Joule heating can be sufficient for errors to be introduced in the currents measured. These can be readily corrected by plotting the log of the current against the electric field, that is using the high electric field approximation to correct the data. The data can then be fitted to the expression:-

$$J = A \sinh(BE_0) \qquad \text{---- (5.46)}$$

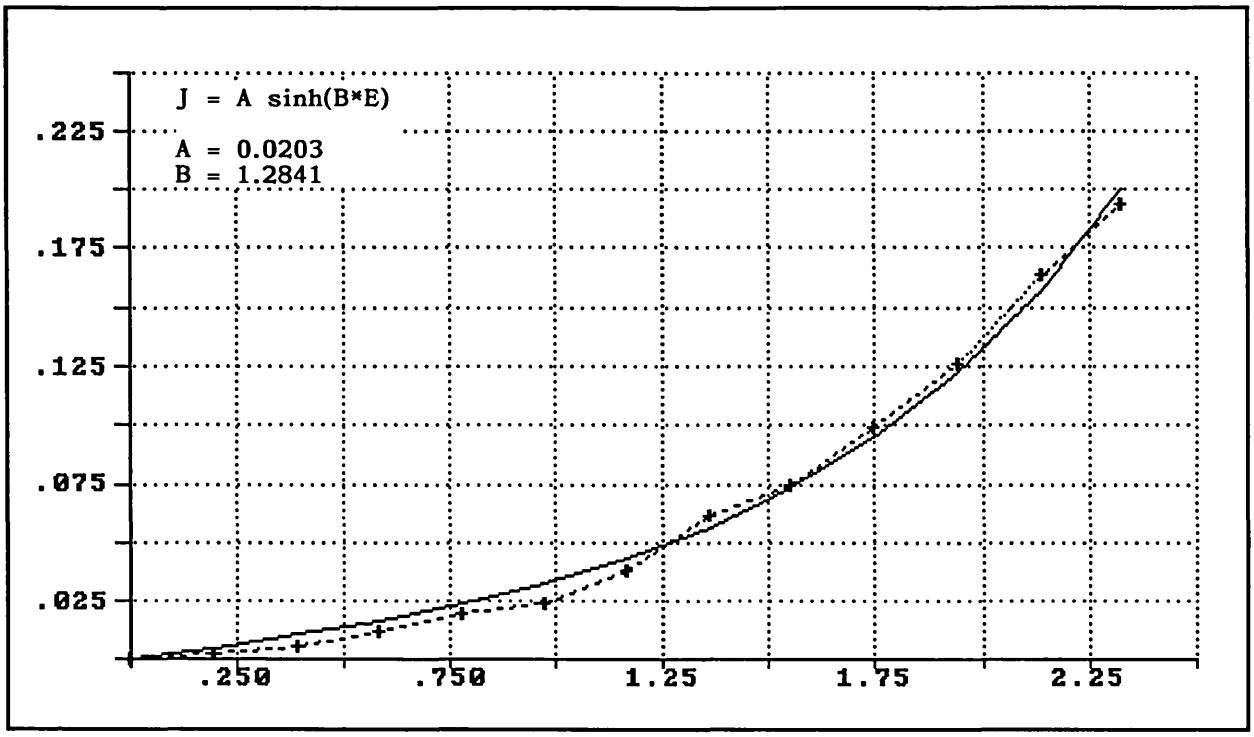
where $A = D\, e^{-\alpha/kT}$

and $B = aqE_0/kT$

Figure 97 shows a typical plot, the data fitting is good. Conductivity measurements were made at a variety of temperatures and the constant of proportionality, D, the activation energy, α, and the mean free path, a, evaluated. The proportionality constant and the activation energy are calculated from the slope and intercept of Ln A plotted against the reciprocal of the temperature in °K. The intercept

is the constant of proportionality and is assumed to be the total number of free charges in the system. The slope is the activation energy.

FIGURE 97 CONDUCTIVITY EXPRESSION FITTED TO EXPERIMENTAL DATA



Fluid 50LV/L35180
Temperature 40 degC

X Axis kV/mm
Y Axis mA/cm2

If the coefficients are considered individually commencing with the proportionality term, D, the effect on the current flow can be noted. As D is increased the total current will be increased; it is simply a multiplying factor linked to the total number of conducting species that can take part in the process. The activation energy term is the exponential term, so that the current will be decreased as the activation energy is raised; that is, as the resistance to movement is increased. The mean free path, as it is decreased, will give a reduced current flow. This is because the velocity of the charge carrier, being the product of the mean free path or jump distance and the jump frequency, will be reduced. The values for the proportionality constant are large and can be

meaningfully assumed to be related to the number of charge carriers. The possible errors on the proportionality term are also large as temperatures are normally measured between 0°C and 90°C and the extrapolation is to 0°K. The values for the activation energy are of a realistic nature. From the second coefficient, B, the mean free path, a, can be calculated and some summary data is shown in table 5.19.

TABLE 5.19 VARIATION OF CONDUCTIVITY PARAMETERS WITH VOLUME FRACTION

Fluid	D	α (eV)	a (mm)
50LV/L10180	$1.08e^{9}$	0.572	$1.38e^{-8}$
50LV/L20180	$5.09e^{12}$	0.864	$1.77e^{-8}$
50LV/L30180	$1.80e^{13}$	0.904	$1.91e^{-8}$
50LV/L40180	$1.31e^{15}$	1.053	$2.04e^{-8}$
Temperature 30 °C			

It is not intended to pursue this exposition any further at this stage. It is apparent that if the model presented is used the conductivity process in an ER fluid can be characterised and numerical estimates of the coefficients provided which are consistent with known practice. As a final point it should be noted that the fall in current flow with shear rate can be explained on two counts. Initially the conductive paths, as demonstrated by the Hall effects experiments[76], exist only perpendicular to the applied electric field. That is they exist because the structure that results in the ER effect exists. As has been shown the effectiveness of this structure and the stability of the links that make the structure are reduced with the increase in the shear rate. It would therefore be anticipated that a fall of the current flow with the shear rate would be observed, this is demonstrated in figure 39b. In addition the carrier velocity will have a component in the direction of shear rate and hence the component parallel to the electric field will be decreased, hence the current flow will be decreased with shear rate.

CHAPTER SIX

CONCLUSIONS

6.1 GENERAL REMARKS

Electro-Rheological fluids lend themselves to the rapid and relatively easy generation of significant quantities of experimental data. To a large extent it is this characteristic together with the extensive array of testing methods potentially available that has added confusion to the explanation of the phenomena. When the often ambiguous terminology used to describe the behaviour is coupled with the above difficulties a very muddled, and frequently contradictory, picture emerges. One of the main aspects of this study was, therefore, the evaluation and characterisation of a number of fluids in the two most commonly used and well defined flow regimes, that of Couette flow and that of Poiseuille flow. The fluids themselves were typical of the materials employed in practice, both in terms of water content and volume fraction of the dispersed phase. They were a credible and reproducible material with practical applicability. This type of material has been produced in quantity and the manufacturing techniques are well established. From the seven fluids manufactured a considerable body of experimental data was obtained and this was used to facilitate an understanding into the behaviour of the fluid and the possible underlying mechanisms that result in the ER effect.

6.2 COLLATION OF EXPERIMENTAL APPARATUS

Initially, an assessment of the behaviour of ER fluids in Poiseuille flow was made. From the basic measurements of the pressure drop through an ER valve of known geometry, at a given flow rate and field strength, an expression was developed that described the behaviour, equation 4.14. The primary variables in the resultant expression were the wall shear rate and the excess shear stress. The geometry of the flow path was incorporated into the model thereby permitting the prediction of the flow characteristics of an ER fluid through an arbitrary valve arrangement.

The analysis of the data suggested that the effects of volume fraction could be normalised using the excess shear stress at zero shear rate. The stresses were then seen to be independent of volume fraction and a universal curve could be produced. The change of excess shear stress with shear rate was therefore, unaffected by the volume fraction of the fluid.

The effects in flow were shown not to influenced to any significant extent by the water content of the fluid and in most cases a water content that gave minimum current flow was desired.

The temperature had a more significant effect on the excess shear stress developed. Generally, the lower the temperature the less ER effect was produced and the more rapid was the fall of the excess shear stress with the shear rate.

The data indicated that the excess shear stress induced by the applied electric field decreased as the shear rate was increased. A model was developed, equation 5.11, and the reduction could be accounted for if a single relaxation coefficient was used.

The model had three parameters, and these were:-

T_y, the excess shear stress at zero shear rate

T_∞, the excess shear stress at infinite shear rate

and T_r, a characteristic relaxation time.

The difference between the two shear stress values, T_y and T_∞, was suggested to be a result of a different structural arrangement of the dispersed phase brought about by the shear rate induced motion of the particles. In both cases the same electrically induced interactions occurred but preferred orientations, to a more favourable alignment with respect to the electric field, imparted different values.

The parameter, f, which was essentially a ratio of the electric and hydrodynamic forces was discussed in relation to the relaxation process. The relaxation parameter, characterised by the coefficient T_r, could then be explained in terms of the erosion of particles from a region where the parameter $f^2 > 1$, the plug, to a region where $f^2 < 1$, the sheared region.

The collation of the data from the three devices was shown to be possible when it was recognised that different conditions were being experienced by the fluid in each of the three situations. It was shown that the infinite shear rate value, T_∞, corresponded to the value obtained at conditions of continuous shear in the Couette device, and in all probability, the initial yield value from the laminar shear cell, the Static Yield Rig (SYR). It was noted that whilst the SYR could be used to assess fluids for a possible ER effect it had severe limitations in relation to the accuracy of the data it provided. The zero shear rate value, T_y, was shown to correspond to the maximum value from the SYR, again the comments concerning the accuracy of the SYR should be noted.

It was proposed that the maximum excess shear stress value was the result of the most favoured structural arrangement under the electric field and that such an arrangement was progressively destroyed by the action of the shear forces until the excess shear stress at an infinite shear rate was obtained. This value in Poiseuille flow was a mathematical extrapolation to an infinite wall shear rate. The relaxation coefficient described the rate at which this change occurred.

It was concluded that there was no essential difference in the electrical interactions under different flow conditions. Data concerning the effectiveness of an ER fluid in either of the two main configurations could be used to predict some of the behaviour in the other configuration. Data from the SYR could be used, with caution, to make an initial prediction of the behaviour of an ER fluid in either of the two main flow regimes. It was therefore practical for the data from the various experimental conditions to be used to develop an explanation of the electrically induced interactions between the particles.

6.3 DESCRIPTIVE MODELS OF THE ELECTRO-RHEOLOGICAL EFFECT

A number of generic expressions were developed in terms of basic physical properties and plausible mechanisms thought to be operative in ER fluids. It was concluded that the development of the excess shear stress by the electric field could be attributed to the mutual interaction between particles as a result of an interfacial polarisation process. Central to the effect generated was the structure that evolved due to this interaction for the structure influenced the degree of polarisation and hence the interaction between adjacent particles. It was concluded that a three dimensional network structure was the most probable configuration. If it was assumed that the particles were spherical it was shown that a simple chain like structure of different sized particles would scale to the measured ER effect. The difficulties in the evaluation of these interaction for a polydisperse network system of irregular particles was noted. It was also noted that for such a modelling technique to be successful considerable computing power would be required. Additionally, a great deal more research would be required beforehand, both on the electrical and hydrodynamic interaction of irregular particles, before such a modelling exercise could be attempted.

The initial stage in the development of the generic expressions was the assessment of a simplified arrangement based on the formation of "chains" of spherical particles. The magnitude of the forces required to produce the excess shear stress was then evaluated. The excess shear stress, suitable normalised, was shown to scale on the particle separation distance. The computed chain forces were compared with the electric interaction forces derived from the work of Davis[135]. It was indicated that forces of the correct magnitude were obtained. It was suggested that the electrical interaction

forces would vary as the particle size distribution became polydisperse. However, as this concurrently altered the number of "chains" the resulting excess shear stress generated remained constant.

The profile of the excess shear stress versus field strength curve was discussed. On a rudimentary level a dependence on E_0^2 would be expected. However, as a result of the close proximity of the particles additional terms were required for the profile to be adequately described. In general additional terms are required that are related to the magnitude of the applied electric field, the gradient of the electric field and the other higher order gradients. Another expansion is required for terms that are related to the multipolar interaction of the particles. An enlargement of the description of the effect incorporating these two expansions would result in a complicated series expression. Curve fitting of the expression to the experimental data indicated that truncation after two terms was appropriate and that a two parameter model adequately described the behaviour, this was equation 5.36. Additional data are required to establish the effect of temperature and in addition data is required regarding different fluid compositions so that the parameters can be refined further. It should then be possible to isolate the effects of the field non-uniformity and that of multipole polarisation.

As noted above in relation to the effect of particle size, the "strength" of an ER fluid is closely linked with the structure that is evolved under the constructive, structure building, effect of the electric field. The "strength" was equated to the excess shear stress and it was therefore, not surprising that a reduction in the excess shear stress was observed when a shear rate, that tended to destroy the structure, was applied. The reduction in the excess shear stress was modelled within a structural kinetics framework and a first order two parameter model was developed that described

the behaviour reasonably faithfully, this was equation 5.42. Some difficulty was noted in obtaining precise values for the two parameters.

The two models were subsequently combined into a four parameter expression and it was indicated that both the electric field and the shear rate dependence of an ER fluid could be represented by the expression. This was equation 5.43 and is shown below.

$$T_e(G,E_0) = \frac{aA_0E_0^2 + A_1E_0}{a + bG}$$

where a and b are structural parameters and A_0 and A_1 characterise the particle polarisation.

Finally the conduction process was assessed. An electrochemical type analysis was used and a model was presented that represented the conductive behaviour extremely well, equation 5.44. The parameters of the model were related to the number of charge carriers in the system, an activation energy and a mean free path. The parameters were of appropriate values and were consistent with known processes.

Information from additional experimental studies on conduction[76] coupled with the attraction and exclusion zones of the form proposed by Vlodavets[41], page 172, has indicated that the conductive process and the development of a chain type structure are complementary and consistent phenomena.

It has been concluded that if a simple chain type model, coupled with a particle interaction based on an interfacial polarisation process, were used the ER effect could be adequately characterised. Additional terms are required to the simple dipole-dipole interaction, primarily from the non-uniform interparticle fields and the multipole polarisation.

If a structural kinetics approach was used the effects of the shear rate could be accommodated into a straightforward expression.

Finally, these two processes were incorporated into a four parameter equation. The equation characterised the dependence of the excess shear stress on both the applied electric field and the shear rate.

APPENDIX

A1 LIST OF THE EXPERIMENTS CONDUCTED

The following list details the experiments that were conducted on the VFDR and the ERV. Details of the temperature and geometry, of the valve in the case of the flow device and the rotor in the case of the viscometer are also provided. Also indicated in the list are the fluid codes used and a supplementary letter in brackets which indicated the order in which the fluids were studied in the VFDR.

Flow Experiments Conducted

Fluid	Test No.	Ave.Temp °C	Gap mm	Length mm	
Fluid "A"					
50LV/L35156	VFDR 74	29.69	.763	.150	
	VFDR 75	24.27	.763	.150	
	VFDR 76	21.00	.763	.150	
	VFDR 77	28.92	.763	.150	
	VFDR 78	34.94	.763	.150	
	VFDR 79	29.28	1.012	.150	
	VFDR 80	21.15	1.012	.150	
	VFDR 81	26.08	1.012	.150	
	VFDR 82	20.97	.516	.150	
	VFDR 83	29.95	.516	.150	
	VFDR 84	25.44	.516	.150	
	VFDR 85	34.96	.516	.150	12 Expts.

Fluid	Test No.	Ave.Temp °C	Gap mm	Length mm	
Fluid "B"					
50LV/L35157	VFDR 86	29.27	.763	.150	
	VFDR 87	20.64	.763	.150	
	VFDR 88	25.62	.763	.150	
	VFDR 89	30.90	.763	.150	
	VFDR 90	34.40	.763	.150	
	VFDR 91	20.80	1.012	.150	
	VFDR 92	25.50	1.012	.150	
	VFDR 93	30.40	1.012	.150	
	VFDR 94	34.30	1.012	.150	
	VFDR 95	21.03	.516	.150	
	VFDR 96	25.40	.516	.150	
	VFDR 97	30.30	.516	.150	
	VFDR 98	34.30	.516	.150	13 Expts.

Fluid	Test No.	Ave.Temp °C	Gap mm	Length mm	
Fluid "C" 50LV/L35180	VFDR 99	30.93	.763	.150	
	VFDR 100	30.43	.763	.150	
	VFDR 101	30.78	.763	.150	
	VFDR 102	31.04	.763	.150	
	VFDR 103	29.85	.763	.150	
	VFDR 104	25.76	.763	.150	
	VFDR 105	20.16	.763	.150	
	VFDR 106	15.70	.763	.150	
	VFDR 107	30.57	1.012	.150	
	VFDR 108	25.21	1.012	.150	
	VFDR 109	20.17	1.012	.150	
	VFDR 110	15.49	1.012	.150	
	VFDR 111	30.45	.516	.150	
	VFDR 112	25.67	.516	.150	
	VFDR 113	20.70	.516	.150	
	VFDR 114	15.60	.516	.150	
	VFDR 115	30.79	.516	.150	
	VFDR 116	25.05	.516	.150	
	VFDR 117	21.04	.516	.150	
	VFDR 119	29.83	.763	.150	20 Expts.

Fluid	Test No.	Ave.Temp °C	Gap mm	Length mm	
Fluid "C" 50LV/L35180	VFDR 120	29.38	.775	.100	
	VFDR 121	29.66	.775	.100	
	VFDR 122	29.44	.775	.100	
	VFDR 123	29.73	.810	.060	
	VFDR 124	34.53	.810	.060	
	VFDR 125	40.39	.810	.060	
	VFDR 126	21.93	.810	.060	
	VFDR 127	20.53	.810	.060	
	VFDR 128	20.31	.610	.060	
	VFDR 129	20.19	.610	.060	30 Expts.

Fluid	Test No.	Ave.Temp °C	Gap mm	Length mm	
Fluid "D" 50LV/L30180	VFDR 133	29.46	.763	.150	
	VFDR 134	30.49	.763	.150	
	VFDR 135	25.49	.763	.150	
	VFDR 136	20.26	.763	.150	
	VFDR 137	15.19	.763	.150	
	VFDR 138	30.15	1.012	.150	
	VFDR 139	25.74	1.012	.150	
	VFDR 140	20.53	1.012	.150	
	VFDR 141	15.31	1.012	.150	
	VFDR 142	30.73	.516	.150	
	VFDR 144	20.69	.516	.150	
	VFDR 145	15.26	.516	.150	
	VFDR 146	31.08	.516	.150	
	VFDR 147	30.88	.763	.150	
	VFDR 148	30.71	.775	.100	
	VFDR 149	26.27	.763	.150	
	VFDR 150	21.14	.763	.150	
	VFDR 151	15.02	.763	.150	18 Expts.

Fluid	Test No.	Ave.Temp °C	Gap mm	Length mm	
Fluid "E"					
50LV/L40180	VFDR 152	31.03	.763	.150	
	VFDR 153	26.11	.763	.150	
	VFDR 154	20.95	.763	.150	
	VFDR 155	15.72	.763	.150	
	VFDR 156	29.99	1.012	.150	
	VFDR 157	24.88	1.012	.150	
	VFDR 158	20.91	1.012	.150	
	VFDR 159	15.18	1.012	.150	
	VFDR 160	10.89	1.012	.150	9 Expts.

Fluid	Test No.	Ave.Temp °C	Gap mm	Length mm	
Fluid "F"					
50LV/L35135	VFDR 161	30.02	1.012	.150	
	VFDR 162	29.96	.763	.150	
	VFDR 163	30.63	.516	.150	
	VFDR 164	30.69	.775	.100	
	VFDR 165	30.25	.710	.060	
	VFDR 166	30.60	.710	.060	
	VFDR 167	40.71	.710	.060	
	VFDR 168	20.83	.710	.060	
	VFDR 169	51.39	.810	.060	
	VFDR 170	51.06	.810	.060	
	VFDR 171	40.77	.810	.060	
	VFDR 172	30.47	.810	.060	
	VFDR 173	20.98	.810	.060	
	VFDR 174	10.12	.810	.060	
	VFDR 175	21.74	.810	.060	15 Expts.

Fluid	Test No.	Ave.Temp °C	Gap mm	Length mm	
Fluid "G"					
50LV/L35166	VFDR 176	30.84	.516	.150	
	VFDR 177	21.06	.516	.150	
	VFDR 178	11.77	.516	.150	
	VFDR 179	11.85	.763	.150	
	VFDR 180	10.26	.763	.150	
	VFDR 181	22.03	.763	.150	
	VFDR 182	29.74	.763	.150	
	VFDR 183	31.02	1.012	.150	
	VFDR 184	21.04	1.012	.150	
	VFDR 185	10.54	1.012	.150	10 Expts.

Viscometer Experiments Conducted

The following experiments were conducted in the ERV

Fluid	Test	Temp	Length	Gap	File Name
Fluid "A"		°C	mm	mm	
50LV/L35156	C1	30	50	.530	1-71-C1
	C2	30	40	.536	1-71-C2
	C3	30	30	.540	1-71-C3
	P10	30	50	.530	1-69-P10
	P11	36	50	.530	1-69-P11
	P12	40	40	.536	1-70-P12
	P13	50	40	.536	1-70-P13
	P14	60	40	.536	1-71-P14
	P15	20	40	.536	1-71-P15
	P16	11	40	.536	1-71-P16
	C1	50	40	.536	1-36-C1
	C2	50	40	.536	1-36-C2
	C3	50	40	.536	1-36-C3
	C4	50	40	.536	1-36-C4
	T5	50	40	.536	1-36-T5
	T5	50	40	.536	1-43-T5
	T4	40	40	.536	1-43-T4
	T3	30	40	.536	1-43-T3
	T2	20	40	.536	1-43-T2
20 Expts.	T1	10	40	.536	1-43-T1

Fluid	Test	Temp	Length	Gap	File Name
Fluid "B"		°C	mm	mm	
50LV/L35157	P17	30	50	.530	1-72-P17
	P18	40	50	.530	1-72-P18
	P19	40	40	.540	1-72-P19
	P20	35	40	.530	1-63-P20
	P22	25	40	.530	1-63-P22
	P23	20	40	.536	1-73-P23
7 Expts.	P24	15	40	.536	1-73-P24

Fluid	Test	Temp	Length	Gap	File Name
Fluid "C"		°C	mm	mm	
50LV/L35180	T5	50	40	.536	1-41-T5
	T4	40	40	.536	1-41-T4
	T3	30	40	.536	1-41-T3
	T2	20	40	.536	1-41-T2
5 Expts.	T1	10	40	.536	1-41-T1

Fluid	Test	Temp	Length	Gap	File Name
Fluid "D"		°C	mm	mm	
50LV/L30180	T5	50	40	.536	1-40-T5
	T4	40	40	.536	1-40-T4
	T3	30	40	.536	1-40-T3
	T2	20	40	.536	1-40-T2
5 Expts.	T1	10	40	.536	1-40-T1

Fluid	Test	Temp	Length	Gap	File Name
Fluid "E"		°C	mm	mm	
50LV/L40180	T5	50	40	.536	1-42-T5
	T4	40	40	.536	1-42-T4
	T3	30	40	.536	1-42-T3
	T2	20	40	.536	1-42-T2
5 Expts.	T1	10	40	.536	1-42-T1

Fluid	Test	Temp	Length	Gap	File Name
Fluid "F"		°C	mm	mm	
50LV/L35135	T5	50	40	.536	1-56-T5
	T4	40	40	.536	1-56-T4
	T3	30	40	.536	1-56-T3
	T2	20	40	.536	1-56-T2
	T5	50	40	.536	1-44-T5
	T4	40	40	.536	1-44-T4
	T3	30	40	.536	1-44-T3
8 Expts.	T2	20	40	.536	1-44-T2

Fluid	Test	Temp	Length	Gap	File Name
Fluid "G"		°C	mm	mm	
50LV/L35166	T5	50	40	.536	1-55-T5
	T4	40	40	.536	1-55-T4
	T3	30	40	.536	1-55-T3
	T2	20	40	.536	1-55-T2
5 Expts.	T1	10	40	.536	1-55-T1

Data was also available from the following experiments:-

Fluid	Test	Temp	Length	Gap	File Name
Fluid		°C	mm	mm	
50LV/L40180	T5	50	40	.536	2-24-T5
	T4	40	40	.536	2-24-T4
	T3	30	40	.536	2-24-T3
	T2	20	40	.536	2-24-T2
5 Expts.	T1	10	40	.536	2-24-T1

Fluid	Test	Temp	Length	Gap	File Name
Fluid		°C	mm	mm	
50LV/L35180	T5	50	40	.536	2-25-T5
	T4	40	40	.536	2-25-T4
	T3	30	40	.536	2-25-T3
	T2	20	40	.536	2-25-T2
5 Expts.	T1	10	40	.536	2-25-T1

Fluid	Test	Temp	Length	Gap	File Name
Fluid		°C	mm	mm	
50LV/L30180	T5	50	40	.536	2-26-T5
	T4	40	40	.536	2-26-T4
	T3	30	40	.536	2-26-T3
	T2	20	40	.536	2-26-T2
5 Expts.	T1	10	40	.536	2-26-T1

Fluid	Test	Temp	Length	Gap	File Name
Fluid		°C	mm	mm	
50LV/L25180	T5	50	40	.536	2-27-T5
	T4	40	40	.536	2-27-T4
	T3	30	40	.536	2-27-T3
	T2	20	40	.536	2-27-T2
5 Expts.	T1	10	40	.536	2-27-T1

Fluid	Test	Temp	Length	Gap	File Name
Fluid		°C	mm	mm	
50LV/L20180	T5	50	40	.536	2-28-T5
	T4	40	40	.536	2-28-T4
	T3	30	40	.536	2-28-T3
	T2	20	40	.536	2-28-T2
5 Expts.	T1	10	40	.536	2-28-T1

Fluid	Test	Temp	Length	Gap	File Name
Fluid		°C	mm	mm	
50LV/L15180	T5	50	40	.536	2-29-T5
	T4	40	40	.536	2-29-T4
	T3	30	40	.536	2-29-T3
	T2	20	40	.536	2-29-T2
5 Expts.	T1	10	40	.536	2-29-T1

In total 107 individual experiments were carried out on the fluids in the VFDR and 55 experiments in the ERV. Data were also available from 30 other studies on diluted samples of fluid "E", giving data covering a volume fraction range of 40% to 15% in steps of 5% volume fraction.

A2 REFERENCES

1 Block H Dielectric Properties of Fluids and their Relation to Electro-Rheology IEE Colloquium Electrically Active Fluids 1985
The Inst. Elec. Eng. Feb 1985 Digest No 1985/14

2 Winslow M W U.S. Patent No 2,417,850 1947

3 Winslow M W U.S. Patent No 2,661,596 1953

4 Winslow M W U.S. Patent No 2,886,151 1959

5 Winslow M W U.S. Patent No 3.047.507 1962

6 Klass D L and Martinek T W Electroviscous Fluids 1: Rheological Properties
J of Appl.Phys. Vol 38 No 1 1967 67-74

7 Phillips R W and Auslander D M The Electroplastic Flow Modulator
Meas.& in Sci.& Ind. Symo.Proc.Pittsburg 1971 1243-1251

8 Arguelles J,Martin H R and Pick R A Theoretical Model For Steady Electroviscous Flow Between Parallel Plates
J of Mech.Eng.Sci. Vol 16 No 4 1974 232-239

9 Deinega Yu F The Electrorheology of Dispersed Systems
Inzh-Fiz.Zh. Vol 18 No 6 1970 994-999

10 Brooks D A Electro-Rheological Devices
Chartered Mechanical Engineer Sept.1982 91-93

11 Scott D and Yamaguchi J Solidifying Fluid Transforms Clutches and Flow Valves
Auto.Eng 1983 Vol 91 No.11 61-66

12 Stangroom J E Control Systems based on Electro-Rheological Fluids
Inst. & Cont. Eng. June 1986 66-67

13 Fishlock D A New Era in Molecular Electronics
Financial Times 13th Feb. 1985

14 Fishlock D Kitchen Chemists get Cooking
Financial Times 26th Feb. 1985

15 Science Editor Electro-Rheological Fluids Solid Results
The Economist 5-11 Dec. 1987

16 Sprecher A F, Carlson J D and Conrad H Electrorheology at Small Strain Rates of Suspensions of Silica Particles in Silicone Oil
Matl.& Sci.Eng V95 Nov 1987 p187-197

17 Brooks D A, Goodwin J, Hjelm C, Marshall L and Zukoski C Visco-Elastic Studies on an Electro-rheological Fluid Coll.& Surf. 18 (1986) 293-312

18 Sproston J L,Stevens N G and Page I M An Investigation of Torque Transmission Using Electrically Stressed Dielectric Fluids Inst.Phy.Conf. Series No 66 Electrostatics 83 53-58

19 Stevens N G,Sproston J L and Stanway R Experimental Investigation of a Simple Electroviscous Damper J.of Electrostatics 15 2 1984 275-283

20 Deinega Yu F,Kovganich N Ya and Popko K K Electrokinetic and Polarisation Phenomena in Hydrocarbon Dispersed Systems Electrochem Ind. Process & Bio. No1 1979 38-42

21 Deinega Yu F,Popko K K and Kovganich N Ya Temperature Dependence of the Electroviscous Effect and Dielectric Parameters of Suspensions of Hydrated Substances in Hydrocarbons Heat Trans.Soviet Res. Vol 10 No 1 1978 50-56

22 Kovganich N Ya,Deinega Yu F and Popko K K Electrorheological and Dielectric Investigations of Hydrocarbon Suspensions of Clayey Materials Ukra.Khim.Zh. Vol 44 No 2 1978 209-212

23 Dukhin S S and Shilov V N Dielectric Phenomena and the Double Layer in Disperse Systems and Polyelectrolytes Wiley & Sons 1974

24 Dukhin S S Dielectric Properties of Disperse Systems Surface & Colloid Sci. Ed. E Matijevic Vol 3 1973 83-165

25 Derjaguin B V and Dukhin S S Nonequilibrium Double Layer and Electrokinetic Phenomena Surf.& Colloid Sci.Ed E Matijevic Vol 7 1974 322-330

26 Derjaguin B V,Dukhin S S and Shilov V N Kinetic Aspects of Electrochemistry of Disperse Systems Advan.in Colloid and Interface Sci. 13 1980 141-152

27 Dukhin S S,Sorokina T S and Chelidze T L Film-Effect Theory of Low-Frequency-Dispersion Dielectric Permeability of a Moistened Coarse-Dispersed System Koll.Zh. Vol 31 No6 1969 823-830

28 Dukhin S S and Shilov V N Theory of Static Polarisation of the Diffuse Part of the Double Layer of Spherical Particles Koll.Zh. Vol 31 No 5 1969 706-713

29 Dukhin S S,Shilov V N and Yeremova Yu Ya Induced Dipole Moments of Colloid Particles
Hung.Proc.Conf.Colloid 1975 Vol 1 1975 349-356

30 Shilov V N and Dukhin S S Theory of Low Frequency Dispersion of Dielectric Permittivity in Suspensions of Spherical Colloidal Particles due to Double Layer Polarisation
Koll.Zh. Vol32 No2 1970 293-300

31 Shilov V N and Dukhin S S Theory of Polarization of the Diffuse Part of a Thin Double Layer of a Spherical Particle in an Alternating Electrical Field
Koll.Zh. Vol 32 No 1 1970 117-123

32 Shilov V N,Sonntag H and Ichenskii V I Induced Dipole Moment in a Spherical,Nonconducting Particle
Koll.Zh. Vol 42 No 4 1980 715-723

33 Shilov V N Polarisation Interaction and Electrocoagulation 1.Expression of the Force of Dispersed Interaction in an Electric Field by Way of an Induced Dipole Moment
Koll.Zh. Vol 42 No 6 1980 1160-1165

34 Lykov A V,Shul'man Z P,Gorodkin R G and Matsepuro A D Mechanical Behaviour of Electroviscous Nonaqueous Disperse Systems in Shear Flow in a Transverse Electric Field
Inzh-Fiz Zh Vol 18 No 6 1971 979-986

35 Shul'man Z P and Korobko E V Study of Electrorheological Effect During Flow of Dielectric Suspensions in a Horizontal Coaxially Cylindrical Capacitor
Inzh-Fiz. Zh. Vol 26 No 5 1977 820-824

36 Shul'man Z P,Gorodkin R G,Korobko E V and Gleb V K The Electrorheological Effect and its Possible Uses
J of Non-Newt.Fluid Mech. 8 1981 29-41

37 Shul'man Z P,Matsepuro A D and Khusid B M Structure Formation of Electro-Rheological Suspensions in an Electric Field. 1. Qualitative Considerations
Vestsi Akad.Navuk Belar.SSR No 3 1977 116-121

38 Shul'man Z P,Khusid B M and Matsepuro A D Structure Formation of Electro-Rheological Suspensions in an Electric Field. 2. Quantitative Considerations
Vestsi Akad.Navuk Belar.SSR No 3 1977 122-127

39 Efimov B F,Shul'man Z P and Gorodkin R G The Effect of Certain Foreign Material Inclusions on the Qualitative Characterstics of Highly-Concentrated Electro-Rheological Suspensions
Vestsi Akad.Navuk Belar.SSR No 4 1976

40 Gleb V K and Demchuk S A Effect of an Electric Field on the Discharge of Polydispersions from a Slotted Vertical Plane-Parallel Channel
Inzh-Fiz Zh Vol 23 No 4 1972 681-685

41 Vlodavets I N,Vorob'eva T A and Grivtsov A G Special Features of Dispersed-Phase Particle Interactions in Alternating Electric Fields
Koll.Zh. Vol 36 No 6 1974 1046-1053

42 Kovganich N Ya,Deinega Yu F,Popko K K and Petruk A S The Influence of Electric Field Frequency on the Viscosity-Increase Effect of Dispersed Systems
Ukra.Khim.Zh. Vol 43 No 12 1977 1237-1240

43 Petrzhik G G,Trapeznikov A A,Makarova E V,Nikiforov V P and Davletshin R A Apparatus for Electrorheological Studies
Russian J of Phys.Chem. 47(10) 1973 1522-1524

44 Malov V A,Kalminskaya I A and Lavrov I S Measurement of the Force Acting on Particles Located in an Inhomogeneous Electric Field
Koll.Zh. Vol 36 No 5 1974 971-974

45 Shor G I,Lapin V P ,Likhterov S D and Shkol'nikov V M Electroviscous Effects in Lubricating Oils
Khim. i Tekh.Topl. i Masel No 6 1975 41-44

46 Likhterov S D,Shor G I ,Lapin V P and Fufaev A A Electroviscous Effect in Oils with Additives
Khim. i Tekh.Topl. i Masel No 1 1980 43-45

47 Petrzhik G G,Chertkova O A and Trapeznikov A A An Electrorheological Formulation
Russian Patent No 715596 1977

48 Stangroom J E U.K. Patent No 1,501,635 1978

49 Stangroom J E U.K. Patent No 1,570,234 1980

50 Stangroom J E Provisional Patent No 8,118,885 1982

51 Stangroom J E A Review of Observations on, and Theories Concerning, Electro-Rheological Fluids
Sheff.Univ Report

52 Uejima H Dielectric Mechanism and Rheological Properties of Electro-Fluids
Jap.J.of Appl.Phy. Vol 11 No 3 1972 319-326

53 Sugimoto N Winslow Effect in Ionic Exchange Resin Dispersions
Bulletin JSME Vol 20 No 149 1977 1476-1483

54 Sasada T,Kamijo K and Kishi T On the Electroviscous Effect in Single Phase Liquids
Proc.Cong. on Materials Res. 1974 224-227

55 Sasada T,Kishi T and Kamijo K On the Electroviscous Effect in Colloidal Liquids
Proc.Cong. on Material Res. 1974 228-231

56 Honda T,Kurosawa K and Sasada T A.C. Characterstics of the Electroviscous Effect
Jap.J. of Appl.Phy. Vol 19 No 8 1980 1463-1466

57 Honda T,Kurosawa K and Sasada T Transient Pressure-Drop Fluctuations in Electroviscous Effect
Jap.J. of Appl.Phy. Vol 18 No 11 1979 2059-2063

58 Honda T and Sasada T Electroviscous Effect in Chloroform
Jap.J.of Appl.Phy. Vol 18 No 8 1979 1663-1664

59 Honda T and Sasada T Electroviscous Effect in Liquids of Low Permittivity
Jap.J.of Appl.Phy. Vol 18 No 8 1979 1605-1606

60 Honda T,Sasada T and Sakamoto T Electroviscous Effect in Non-Polar Liquids
Jap.J.of Appl.Phy. Vol 18 No 6 1979 1031-1037

61 Honda T and Sasada T The Electroviscous Effect of Water
Jap.J.of Appl.Phy. Vol 18 No 3 1979 675-676

62 Honda T and Sasada T The Mechanism of Electroviscosity 1. Electrodynamic Effect on Polar Liquids
Jap.J.of Appl.Phy. Vol 16 No 10 1977 1175-1783

63 Honda T and Sasada T The Mechanism of Electroviscosity 2. Conductivity Effect of Dielectric Liquids on Electroviscosity
Jap.J.of Appl.Phy. Vol 16 No 10 1977 1785-1791

64 Kawasaki K On the Variation of Electrical Resistance of a Polymer as a Function of the Extent and Nature of Sorbed Water
J.of Colloid Sci. 16 1961 405-440

65 Estrela-L'opis V R,Dukhin S S and Shilov V N Energy of Interaction of Two Spherical Colloid Particles in an External Electric Field
Koll.Zh. Vol 36 No 6 1974 1140-1144

66 Estrela-L'opis V R and Shilov V N Polarisation Interaction and Electrocoagulation Part 1
Koll.Zh. Vol 43 No 4 1981 733-740

67 Estrela-L'opis V R and Gavrilyuk A I Polarisation Interaction and Electrocoagulation
Koll.Zh. Vol 43 No 5 1981 945-951

68 Johnson T W and Melcher J R Electromechanics of Electrofluidized Beds
Ind.Eng.Chem.Fundam. Vol 14 No 3 1975

69 Dietz P W and Melcher J R Interparticle Electrical Forces in Packed and Fluidized Beds
Ind.Eng.Chem.Fundam. Vol 17 No 1 1978

70 Dietz P W and Melcher J R Momentum Transfer in Electrofluidized Beds
Amer.Inst.Chem.Eng. Vol 74 74 No 175 1978

71 Kelly J Studies in Electro-Rheology
MSc Thesis University of Liverpool 1985

72 Chertkova O A,Petrzhik G G and Trapeznikov A A Influence of Nature of Surfactant on the Electrorheological Effect in Nonaqueous Dispersions
Col. J. USSR Vol 44 No 1 1982 68-74

73 Marson E An Investigation into the Mechanism of an Electroviscous Fluid
PhD.Thesis Sheffield Univ. 1974

74 Lovett C A Note Concerning the Conduction Mechanism in Electroviscous Fluids
Report 672/11/1 Laser Eng. (Dev.) Ltd. March 1977

75 Lovett C Fundamental Mechanisms in Electroviscous Fluids
Report 672/11/2 Laser Eng. (Dev.) Ltd. April 1977

76 Davis D K Electrical Characterstics of Electro-Rheological Fluids
ERA Report No 83 0010 1983

77 Derjaguin B V and Dukhin S S The Theory of Surface Conductance
Koll.Zh. Vol 31 No 3 1968 350-358

78 Brooks D A Electro-Rheological Research
Report 046/10 Laser Eng. (Dev.) Ltd. June 1983

79 Brooks D A A Treatise on the Electro-Rheological Effect
Laser Eng. (Dev.) Ltd 1981

80 Block H The Nature and Application of Electrical Phenomena in Polymers
Adv. in Polymer Sci. No.33 1979

81 Jansons K M and Rallison J M Electro-Rheological Fluid Dynamics
ERRS Report

82 Stangroom J E Electrorheological Fluids
Phys.Tech. Vol 14 1983 290-296

83 Klass D L and Martinek T W Electroviscous Fluids 2:Electrical Properties
J of Appl.Phys Vol 38 No1 1967 75-80

84 Daniels W E Enos C T Iacoviella J G Frost J H Vanderhoff J and Ahmed S M
Polymer Colloids Vol 2 ed Fitch R M Plenum Press (1980)

85 Hjelm C Studies on an Electro-Rheological Fluid
M.Sc. Thesis Bristol University

86 Sato T and Ruch R Stabilisation of Colloidal Dispersions by Polymer Adsorption
Surfactant Science Series Vol 9 (1980)

87 Gallagher T J Simple Dielectric Liquids
Oxford University Press (1975)

88 Shul'man Z P,Gorodkin R G & Kuz,min V A Some Factors Affecting the Rotation of a Dielectric in an Electrorheological Medium
Inz.Fiz Z Vol 23 No 5 1972 1403-1405

89 Melcher J R Electric Fields and Forces in Semi-Insulating Liquids
J of Electrostatics 2 (1976) 121-132

90 Saville D A Electrokinetic Effects with Small Particles
Ann.Rev.Fluid Mech. 1977 9 p321-337

91 Debye P Polar Molecules New York (1929)

92 Block H Investigation into Electro-Viscous Materials at Liverpool University
Internal Report 1981

93 Mason S G Orthokinetic Phenomena in Dispersed Systems
J of Colloid and Interface Sci. Vol 58 No 2 1977 275-285

94 van de Ven T G M and Mason S G The Microrheology of Colloidal Dispersions:4 Pairs of Interacting Spheres in Flow
J of Colloid and Interface Sci. Vol 57 No 3 1976 505-516

95 van de Ven T G M and Mason S G The Microrheology of Colloidal Dispersions:5 Primary and Secondary Doublets of Spheres in Shear Flow
J of Colloid and Interface Sci. Vol 57 No 3 1976 517-534

96 van de Ven T G M and Mason S G The Microrheology of Colloidal Dispersions:6 Chains of Spheres in Shear Flow Spheres in Shear Flow
J of Colloid and Interface Sci. Vol 57 No 3 1976 535-546

97 Arp P A and Mason S G The Kinetics of Flowing Dispersions:8 Doublets of Rigid Spheres (Theroetical)
J of Colloid and Interface Sci. Vol 61 No 1 1977 21-43

98 Arp P A and Mason S G The Kinetics of Flowing Dispersions:9 Doublets of Rigid Spheres (Experimental)
J of Colloid and Interface Sci. Vol 61 No 1 1977 44-61

99 Okagawa A Cox R G and Mason S G The Kinetics of Flowing Dispersions:VI Transient Orientation and Rheological Phenomena of Rods and Discs in Shear Flow
J of Colloid and Interface Sci. Vol 45 No 2 1973 303-329

100 Okagawa A Cox R G and Mason S G The Kinetics of Flowing Dispersions:VII Oscillatory Behaviour of Rods and Discs in Shear Flow
J of Colloid and Interface Sci. Vol 45 No 2 1973 330-358

101 Okagawa A Cox R G and Mason S G The Kinetics of Flowing Dispersions:X Oscillation in Optical Properties of Streaming Suspensions of Spheroids
J of Colloid and Interface Sci. Vol 71 No 1 1979 11-17

102 Okagawa A Cox R G and Mason S G The Kinetics of Flowing Dispersions:12 Some Effects of Nonuniform Shear
J of Colloid and Interface Sci. Vol 71 No 1 1979 11-17

103 van de Ven T G and Mason S G The Microrheology of Colloid Dispersions:7 Orthokinetic Doublet Formation of Spheres
Colloid and Polymer Sci. 255 1977 468-479

104 Chaffey C E and Mason S G Particle Behaviour in Shear and Electric Fields:5 Effect on Suspension Viscosity
J of Colloid and Interface Sci. Vol 27 No 1 1978 115-126

105 Chaffey C E and Mason S G Particle Behaviour in Shear and Electric Fields:4 The Viscosity of Suspensions of Nonrotating Ellipsoids.
J of Colloid Sci. 20 1965 330-340

106 Cerda C M, Foister R T and Mason S G Rheoptical Transients in Sheared Suspensions:3 Effect of Brownian Motion on Oblate Spheres
J of Colloid and Interface Sci. Vol 85 No 1 1982 87-100

107 Arp P A and Mason S G Particle Behaviour in Shear and Electric Fields. VIII:Interactions of Pairs of Conducting Spheres (Theoretical)
Colloid & Polymer Sci. 255 1977 566-584

108 Arp P A and Mason S G Particle Behaviour in Shear and Electric Fields. IX:Interactions of Pairs of Conducting Spheres (Experimental)
Colloid & Polymer Sci. 255 1977 980-993

109 Arp P A and Mason S G Chains of Spheres in Shear and Electric Fields
Colloid & Polymer Sci. 255 1977 1165-1173

110 Arp P A Foister R T and Mason S G Some Electrodynamic Effects in Fluid Dispersions
Advs.Coll.& Inter.Sci. 12 1980 295-356

111 Okagawa A, Cox R G and Mason S G Particle Behaviour in Shear and Electric Fields V1 The Microrheology of Rigid Spheroids
J of Col and Int. Sci. Vol 47 No 2 1974 536-567

112 Okagawa A, and Mason S G Particle Behaviour in Shear and Electric Fields V11 Orientation Distribution of Cylinders
J of Col. and Int. Sci Vol 47 No 2 1974 568-587

113 Graham A L and Bird R B Particle Clusters in Concentrated Suspensions 1 Experimental Observations of Particle Clusters
Ind.Eng.Chem.Fund. 1984 23 406-410

114 Graham A L and Bird R B Particle Clusters in Concentrated Suspensions 2 Information Theory and Particle Clusters
Ind.Eng.Chem.Fund. 1984 23 411-420

115 Graham A L and Bird R B Particle Clusters in Concentrated Suspensions 3 Prediction of Suspension Viscosity
Ind.Eng.Chem.Fund. 1984 23 420-425

116 Kamphuis H, Jongschaap R J J and Mijnlieff P F
A Transient-Network Model Describing the Rheological Behaviour of Concentrated Dispersions
Rheo.Acta. 23 329-344 (1984)

117 Frith B A and Hunter R J Flow Properties of Coagulated Colloidal Suspensions:1 Energy Dissipation in Flow Units
J Colloid and Interface Sci. Vol 57 No 2 1976 248-256

118 Frith B A Flow Properties of Coagulated Colloidal Suspensions:2 Experimental Properties of the Flow Curve Parameters
J Colloid and Interface Sci. Vol 57 No 2 1976 257-265

119 Frith B A and Hunter R J Flow Properties of Coagulated Colloidal Suspensions:3 The Elastic Floc Model
J Colloid and Interface Sci. Vol 57 No 2 1976 266-275

120 Hunter R J and Frayne J Couette Behaviour of Coagulated Colloidal Suspensions:4 Effect of Viscosity of the Suspension Medium
J of Colloid and Interface Sci Vol 71 No 1 1979 30-38

121 Hunter R J and Nicol S K The Dependence of Plastic Flow Behaviour of Clay Suspensions on Surface Properties
J of Colloid and Interface Sci. Vol 28 1968 250-259

122 van de Ven T G and Hunter R J Viscoelastic Properties of Coagulated Sols.
J of Colloid and Interface Sci. Vol 68 No 1 1979 135-143

123 Frith B A Dynamics of Attracting Spheres in a Laminar Shear Field
Rheo.Acta 19 1980 716-723

124 Wagstaff I and Chaffey C E Shear Thinning and Thickening Rheology:1 Concentrated Acrylic Dispersions
J of Colloid and Interface Sci Vol 59 No 1 1977 53-62.

125 Chaffey C E and Wagstaff I Shear Thinning and Thickening Rheology:2 Volume Fraction and Size of Dispersed Particles
J of Colloid and Interface Sci. Vol 59 No 1 1977 63-75

126 Adler P M Hetrocoagulation in Shear Flow
J of Colloid and Interface Sci. Vol 83 No 1 1981 106-115

127 Adler P M Interaction of Unequal Spheres
J of Colloid and Interface Sci. Vol 83 No 2 1981 491-474

128 Sproston J L A Study of the Properties of Electroviscous Fluids
Univ.Liverpool Report 1984

129 Stanway R, Sproston J L and Stevens N G
Non-Linear Identification of an Electroviscous Vibration Damper
7th IFAC Symp. 1985

130 Deinega Yu F and Vinogradov G V Electric Fields in the Rheology of Disperse Systems
Rheo. Acta 23:636-651 1984

131 Mewis J and Spaull A J B Rheology of Concentrated Dispersions
Advs.Coll. and Int.Sci. 6 (1976) 173-200

132 Tadros Th F Control of the Properties of Suspensions
Colloids and Surfaces 18 (1986) 137-173

133 Marshall L Electrically Induced Charges in the Rheology of Dispersed Systems
Ph.D. Bristol University 1987

134 Van Waser J R, Lyons J W, Kim K Y and Colwell R E
Viscosity and Flow Measurement Wiley 1963

135 Davis M H Two Charged Spherical Conductors in a Uniform Electric Field: Forces and Field Strengths
Quart.Journ.Mech and Appl.Maths Vol XVII 4 1964 p 498-511

136 Davis M H Electrostatic Field and Force on a Dielectric Sphere ear a Conducting Plane.
Amer.Journ.Phys Vol 37 No 1 1969 p 26-29

137 O'Meara D J and Saville D A The Electrical Forces on Two Touching Spheres in a Uniform Field
Quart.Journ.Mech and Appl.Maths Vol XXXIV 1 1981 p 8-26

138 Cheng D C-H and Evans F Phenomenological Characterisation of the Rheological Behaviour of Inelastic Reversible Thixotropic and Antithixotropic Fluids
Brit.J.Appl.Phys 1956 16 p1599

139 Moore F The Rheology of Ceramic Slips and Bodies
Trans.Brit.Ceram.Soc. 58 1959 p470

140 Bockeris J O'M and Reddy A K N Modern Electrochemistry Vol 1 Plenum/Rosetta 1977

141 Bockeris J O'M and Reddy A K N Modern Electrochemistry Vol 2 Plenum/Rosetta 1977

142 Shaw C P Electro-Rheology M.Sc. Thesis Cranfield Institute of Technology 1987

143 Heyes D M Rheology of Molecular Liquids and Concentrated Suspensions by Microscopic Dynamical Simulations
J of Non.Newt.Fluid Mech. 27 (1988) p 47-85

144 Peel D Electroviscous Control of Dampers
Departmental Report 89 May 1977

145 Block H and Kelly J P Electro-rheology - A Review Article
J Phys.D Appl.Phys 21 (1988) p 1661-1677

146 Duclos T G An Externally Tunable Hydraulic Mount which Uses Electro-Rheological Fluid
SAE Technical Paper 870963 1988

147 Duclos T G Design of Devices Using Electro-Rheological Fluids
SAE Paper 881134 1988

148 Bullough W A and Foxon M B A Proportionate Coulomb and Viscosity Damped Isoltation System
J of Sound and Vibration (1978) 56(1) p 35-44

149 Adriani P M and Gast A P A Microscopic Model of Electrorheology
Phys.Fluids 31 (10) 1988 p 2757-2768

150 Stevens N G, Sproston J L and Stanway R On the Mechanical Properties of Electro-Rheological Fluids
Trans ASME Vol 54 1987 p 456-458

151 Smart Fluids - A New Route to Advanced Hydraulic Systems/Devices
Technical Insights Seminar March 9th 1989

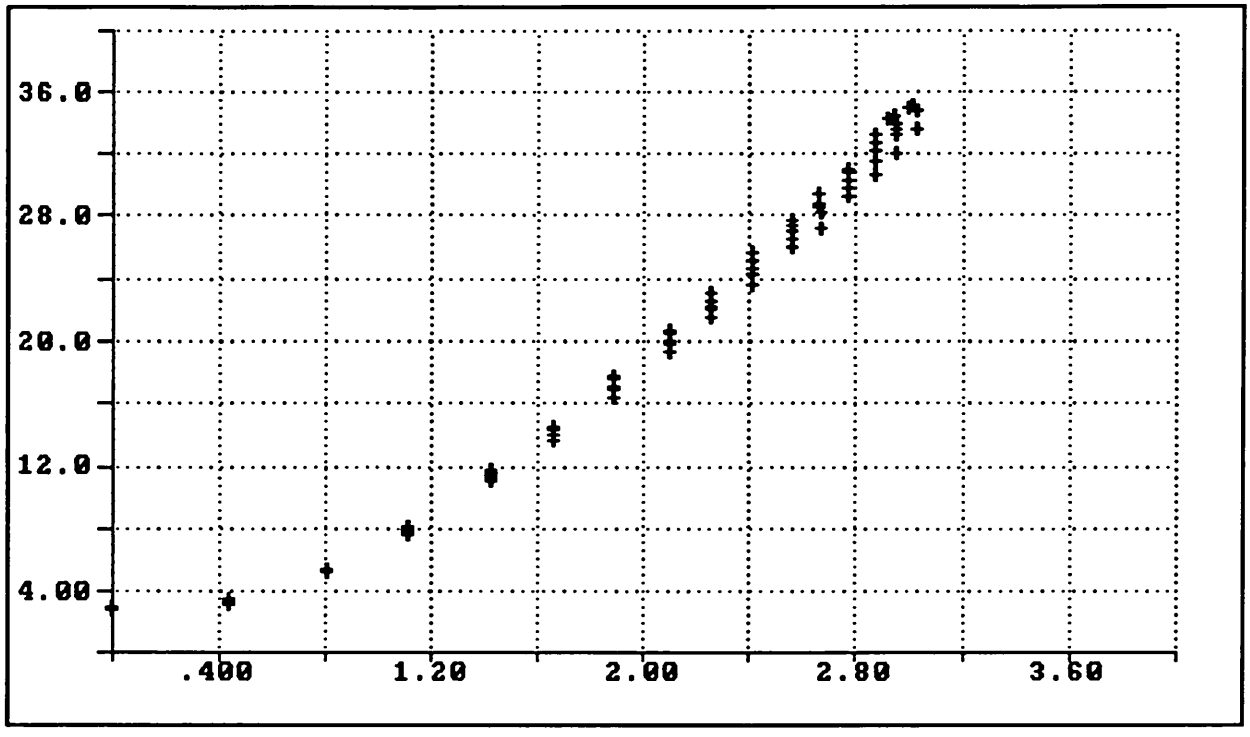
A3 GRAPHICAL DATA FOR CHAPTER 4 AND CHAPTER 5

In the following 83 pages the basic graphs relevant to chapters four and five are displayed. The graphs are presented to the general format of two graphs to each page. In relation to the list of figures, pages 10 to 16, only those graphs suffixed either by an **"a"** or by a **"b"** are to be found in this section.

In the first 58 pages graphs are shown for chapter four. In these graphs the basic data is shown for the two main experimental devices, the Poiseuille flow device, the Valve and Fluid Development Rig (VFDR) and the Couette Viscometer, the Electro-Rheological Viscometer (ERV). Additional data is presented for the laminar shear cell, the Static Yield Rig (SYR) and the Contraves Viscometer. Indicated by the legends are the x axes and the y axes together with the fluid being studied, the test temperature and the experimental apparatus used to generate the data.

In the next 25 pages graphs are shown for chapter five. These are of a similar form to those of chapter four. However, the data presented is related to comparisons between fluids, experimental apparatus and experimental conditions together with an examination of the various models proposed. Specific graphs more relevant to the course of the discussion are embedded within the text.

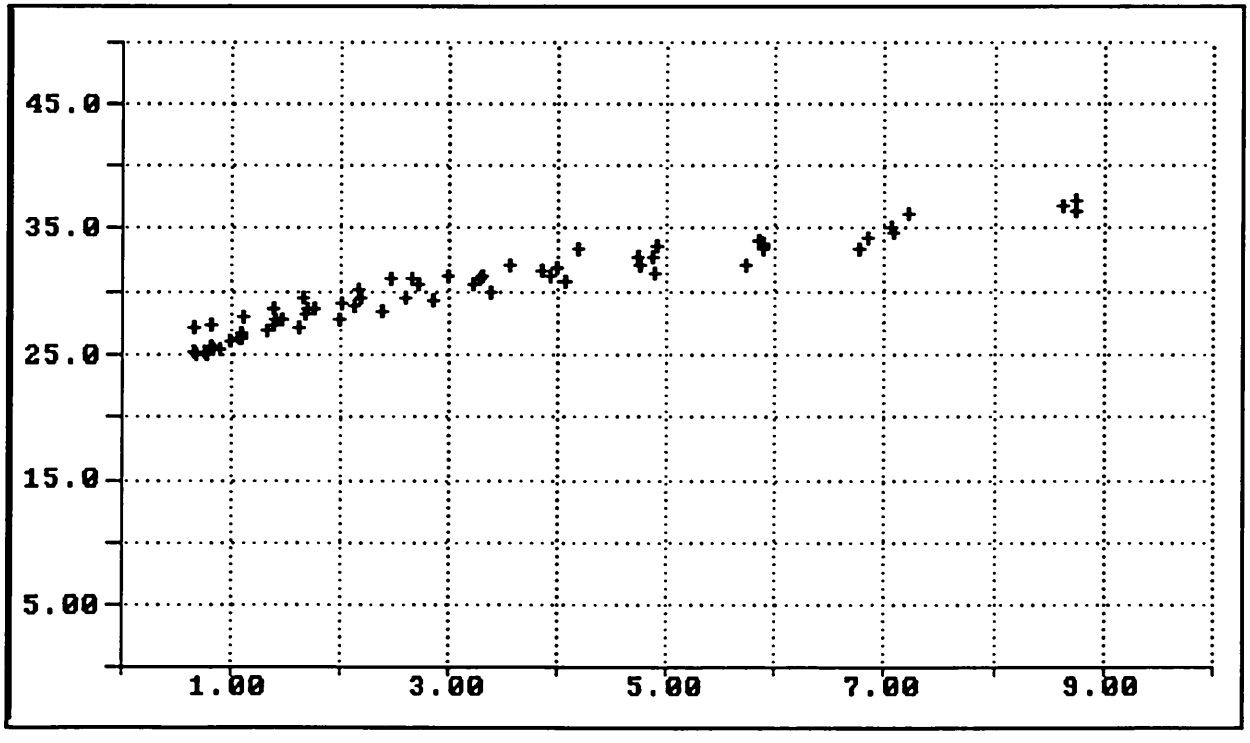
FIGURE 1a PLOT OF DEVELOPED PRESSURE versus FIELD STRENGTH



Fluid 50LV/L35180
Temperature 30 degC
Shear Rate 2200 sec-1

X Axis kV/mm
Y Axis Bar
Flow Rig

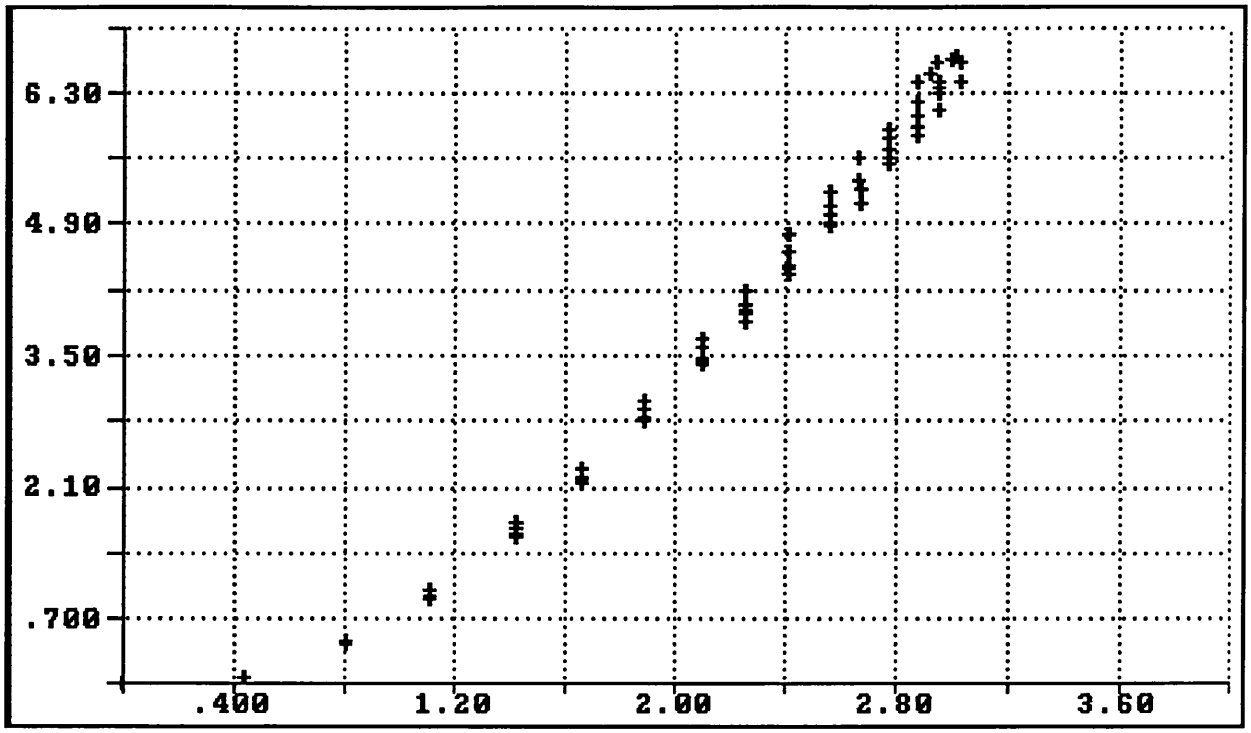
FIGURE 1b PLOT OF DEVELOPED PRESSURE versus FLOW RATE



Fluid 50LV/L35180
Temperature 30 degC
Field 2.66 kV/mm

X Axis Ltr/Min
Y Axis Bar
Flow Rig

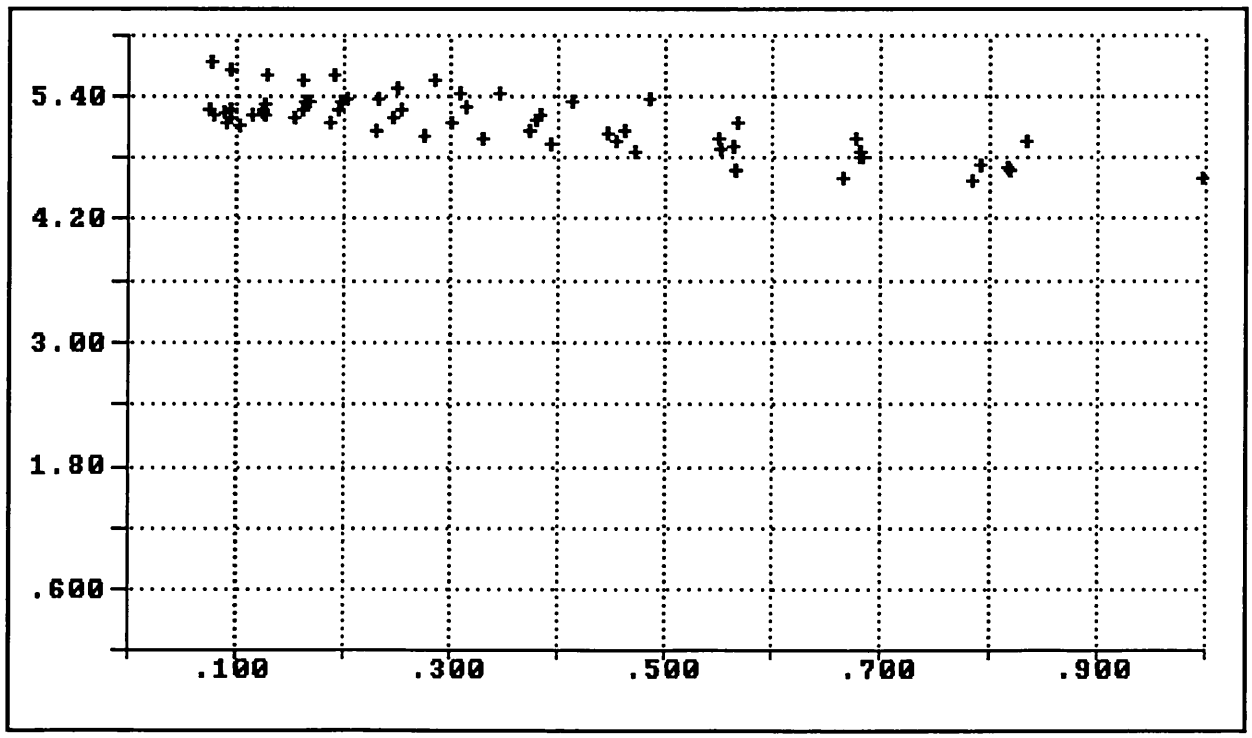
FIGURE 2a PLOT OF SHEAR STRESS versus FIELD STRENGTH



Fluid 50LV/L35180
Temperature 30 degC
Shear Rate 2200 sec-1

X Axis kV/mm
Y Axis kPa
Flow Rig

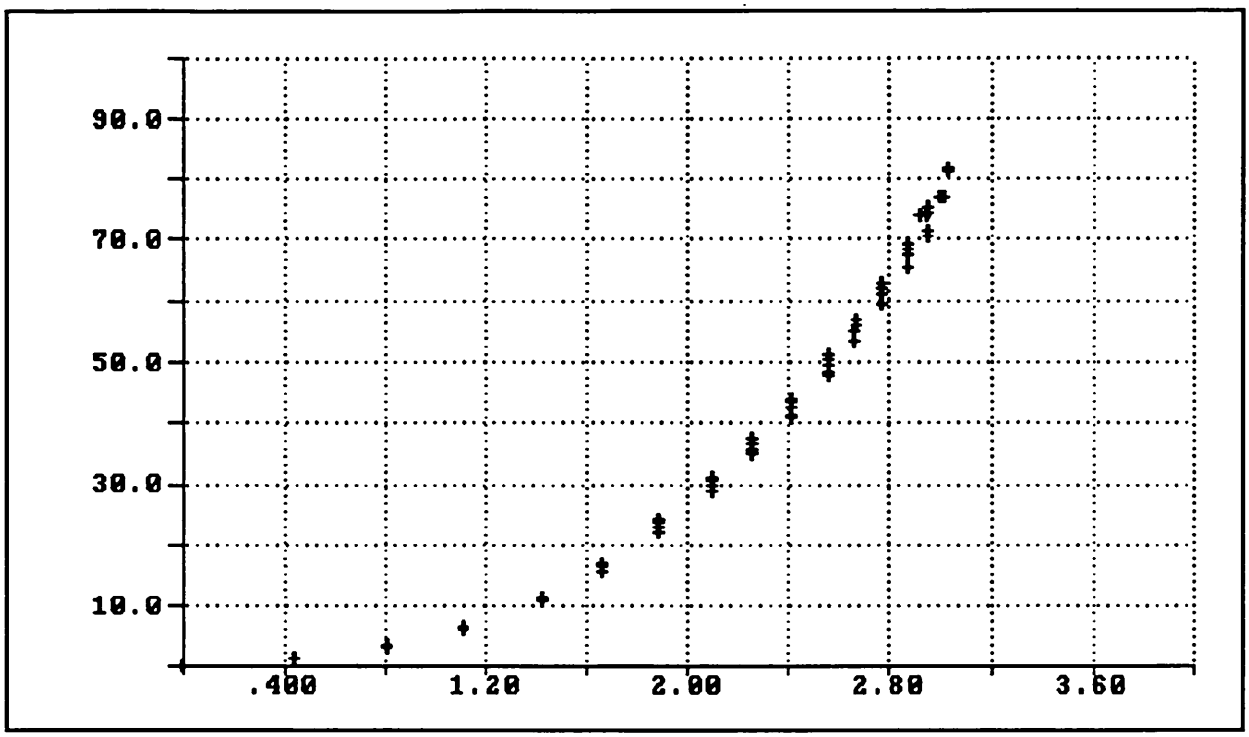
FIGURE 2b PLOT OF SHEAR STRESS versus SHEAR RATE



Fluid 50LV/L35180
Temperature 30 degC
Field 2.66 kV/mm

X Axis 1*e4 s-1
Y Axis kPa
Flow Rig

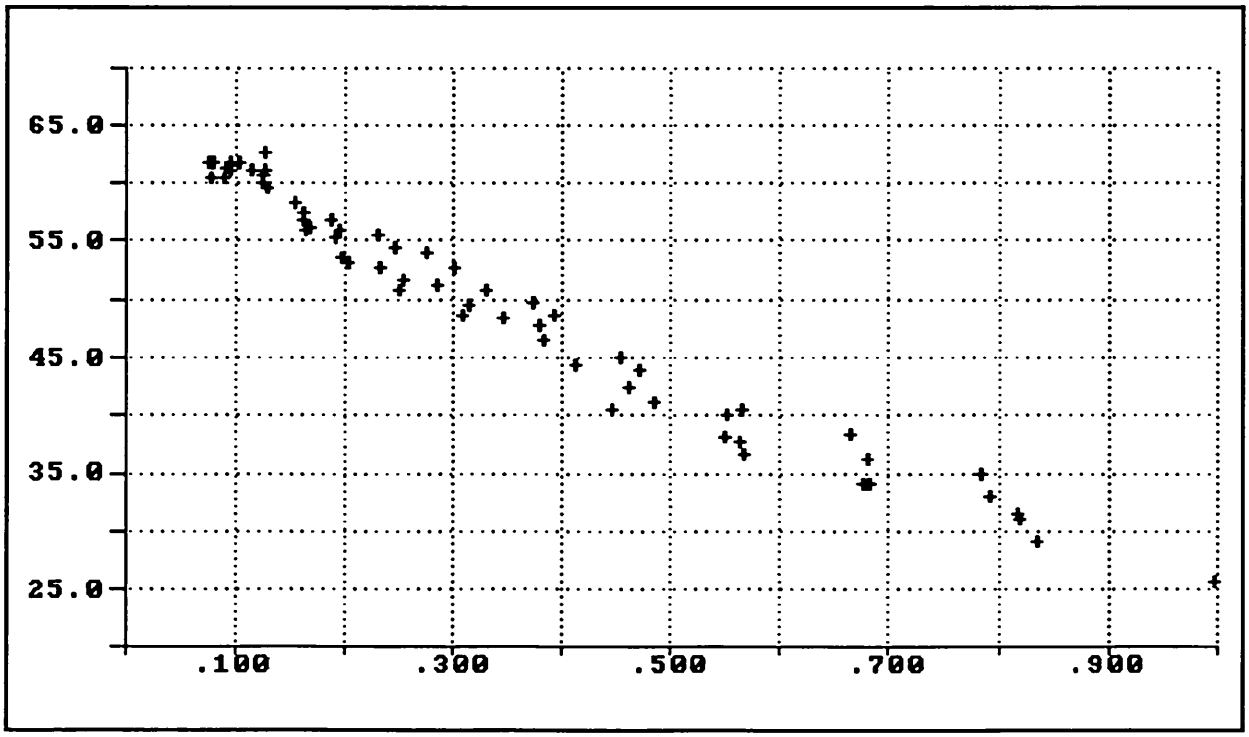
FIGURE 3a PLOT OF CURRENT DENSITY versus FIELD STRENGTH



Fluid 50LV/L35180
Temperature 30 degC
Shear Rate 2200 sec-1

X Axis kV/mm
Y Axis uA/cm2
Flow Rig

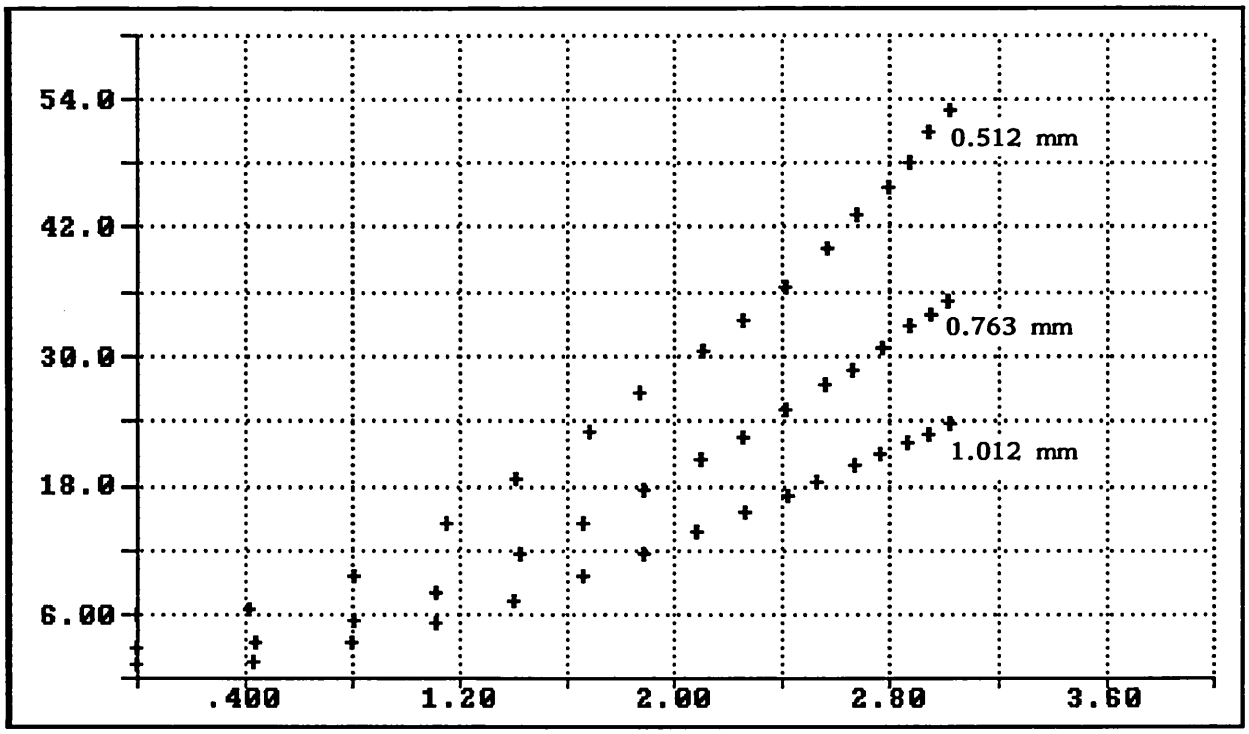
FIGURE 3b PLOT OF CURRENT DENSITY versus SHEAR RATE



Fluid 50LV/L35180
Temperature 30 degC
Field 2.66 kV/mm

X Axis 1*e4 s-1
Y Axis uA/cm2
Flow Rig

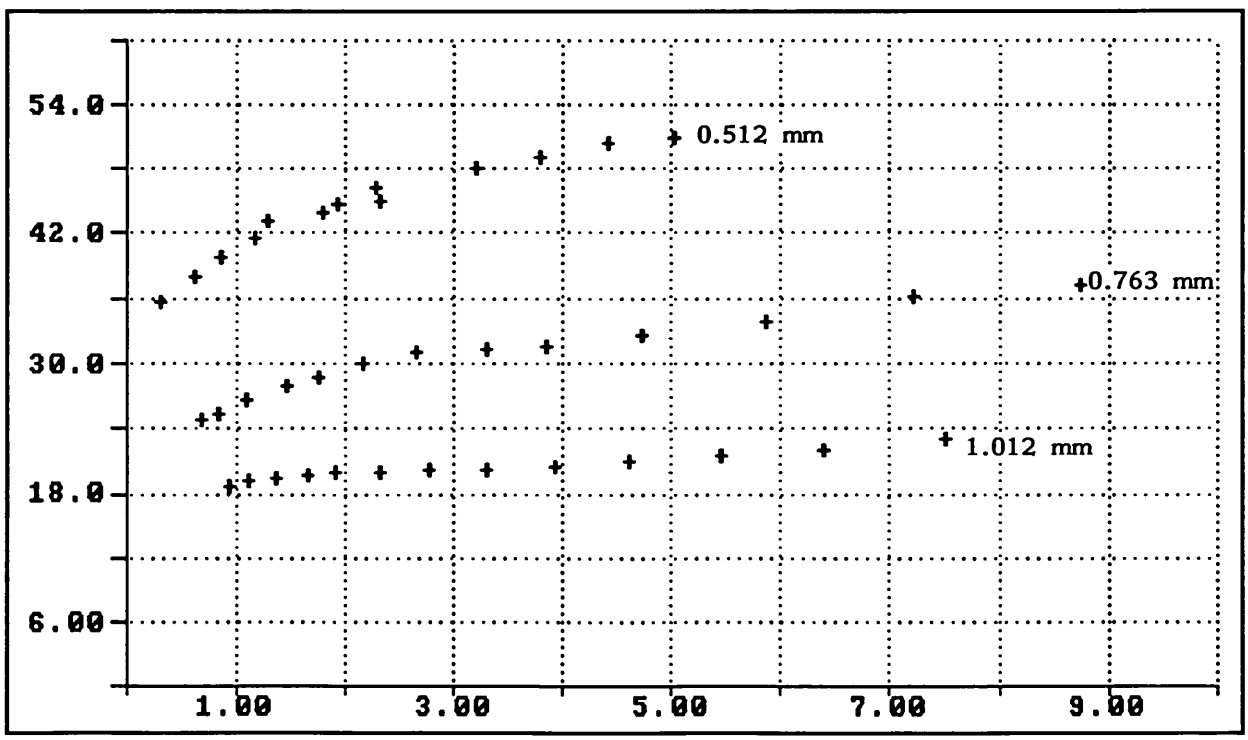
FIGURE 4a PLOT OF DEVELOPED PRESSURE versus FIELD STRENGTH



Fluid 50LV/L35180
Temperature 30 degC
Shear Rate 2200 sec-1

X Axis kV/mm
Y Axis Bar
Flow Rig

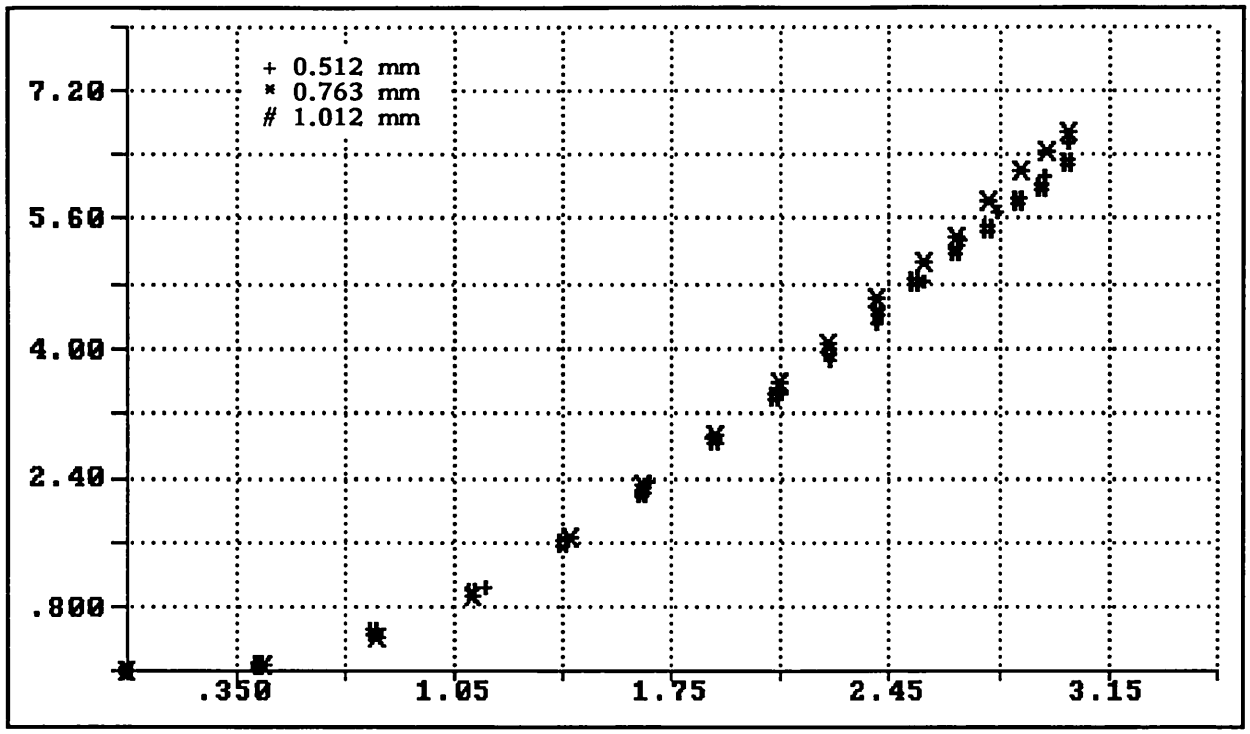
FIGURE 4b PLOT OF DEVELOPED PRESSURE versus FLOW RATE



Fluid 50LV/L35180
Temperature 30 degC
Field 2.66 kV/mm

X Axis Ltr/Min
Y Axis Bar
Flow Rig

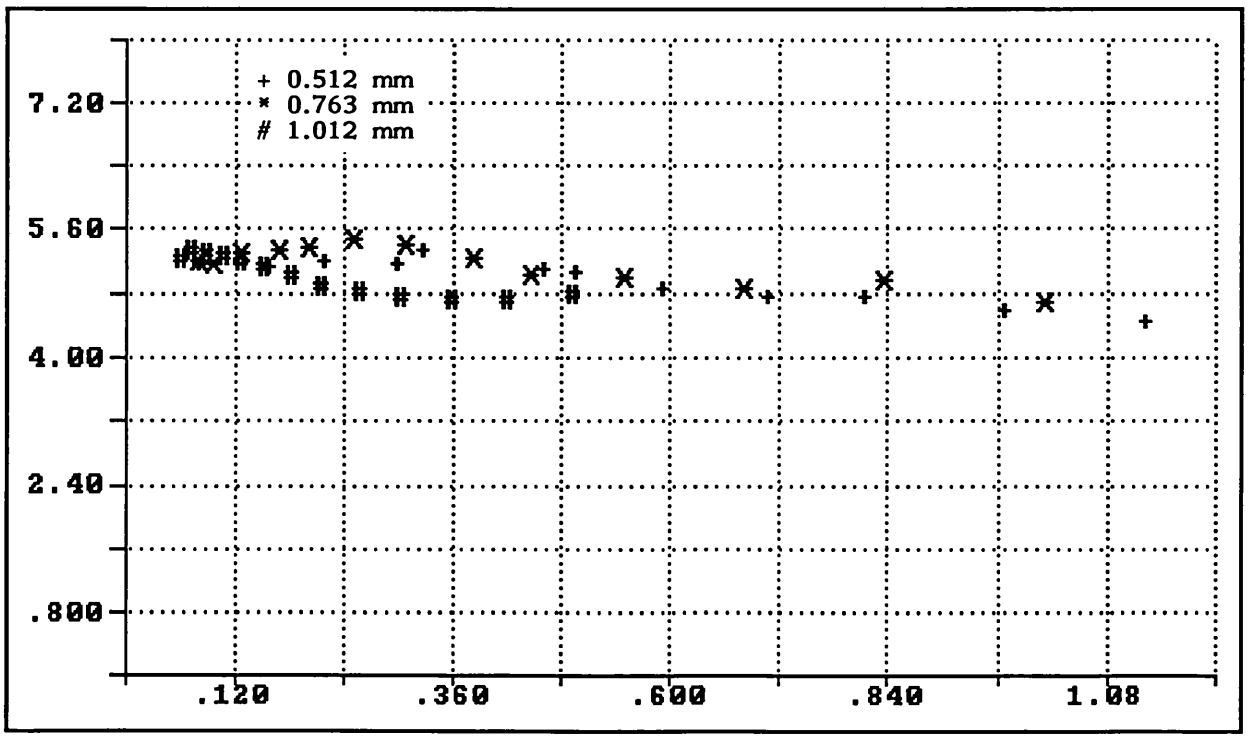
FIGURE 5a PLOT OF SHEAR STRESS versus FIELD STRENGTH



Fluid 50LV/L35180
Temperature 30 degC
Shear Rate 2200 sec-1

X Axis kV/mm
Y Axis kPa
Flow Rig

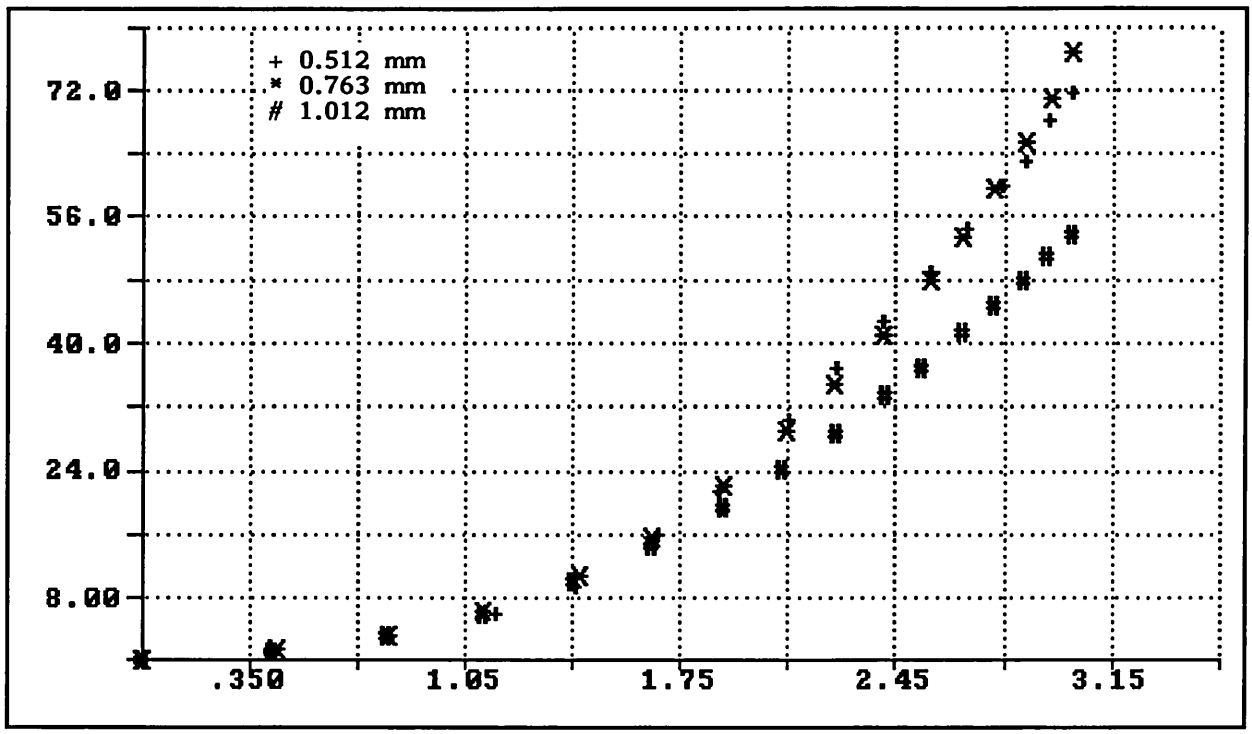
FIGURE 5b PLOT OF SHEAR STRESS versus SHEAR RATE



Fluid 50LV/L35180
Temperature 30 degC
Field 2.66 kV/mm

X Axis 1*e4 s-1
Y Axis kPa
Flow Rig

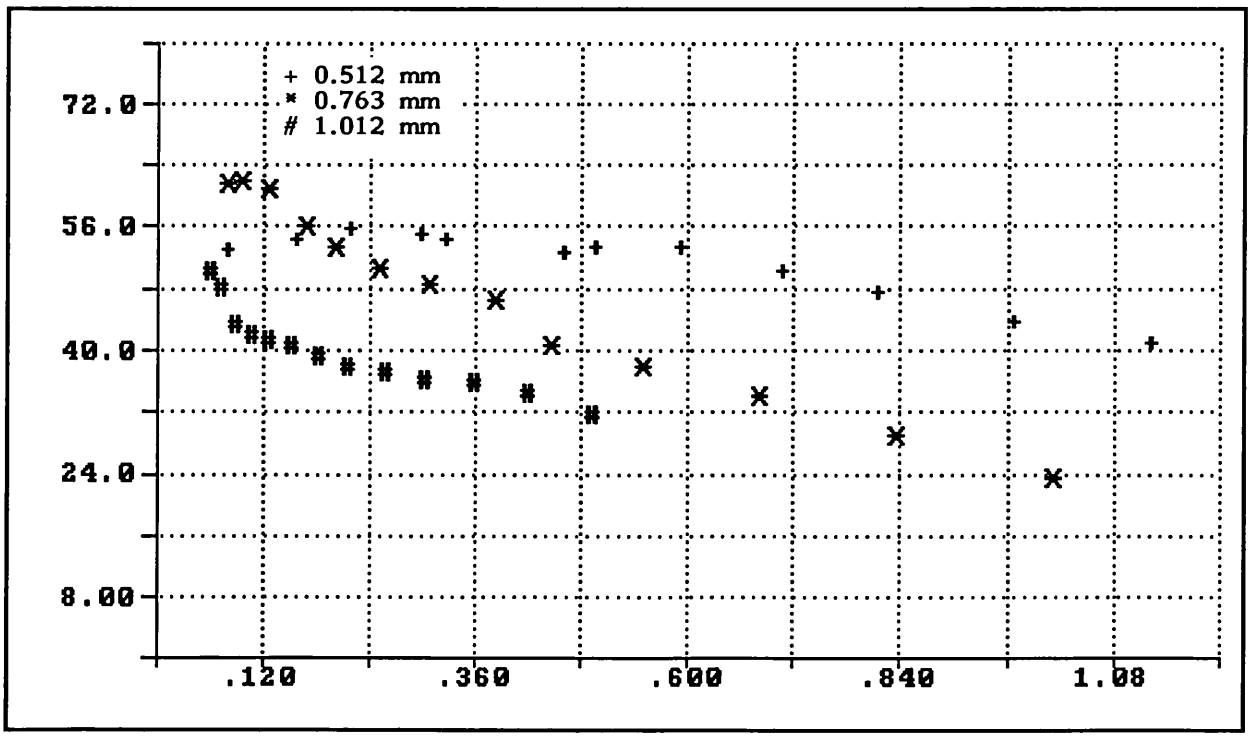
FIGURE 6a PLOT OF CURRENT DENSITY versus FIELD STRENGTH



Fluid 50LV/L35180
Temperature 30 degC
Shear Rate 2200 sec-1

X Axis kV/mm
Y Axis uA/cm2
Flow Rig

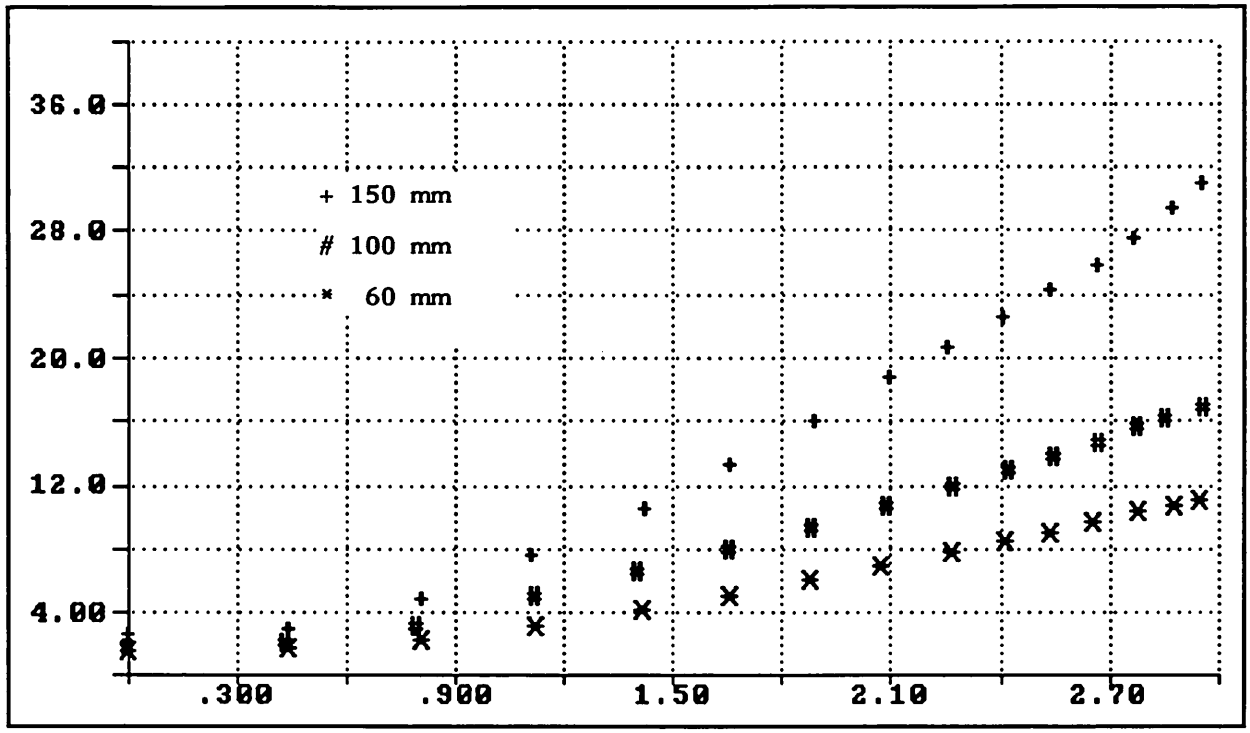
FIGURE 6b PLOT OF CURRENT DENSITY versus SHEAR RATE



Fluid 50LV/L35180
Temperature 30 degC
Field 2.66 kV/mm

X Axis 1*e4 s-1
Y Axis uA/cm2
Flow Rig

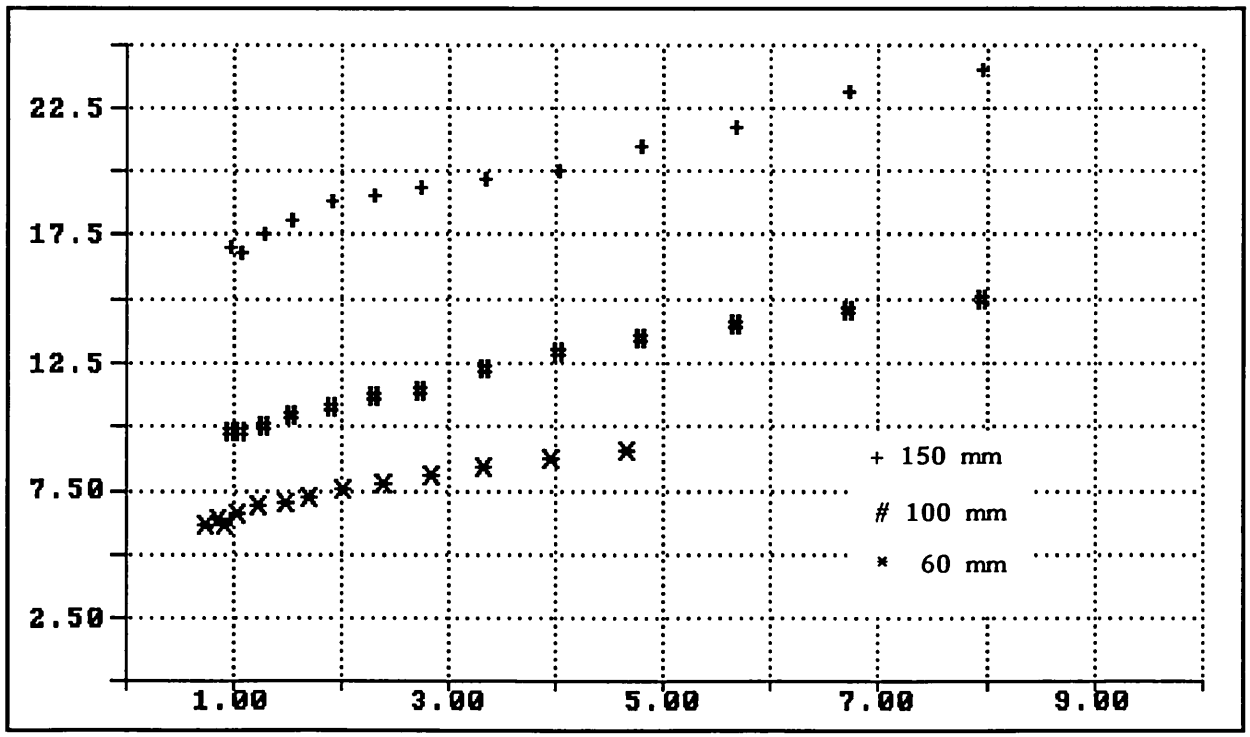
FIGURE 7a PLOT OF DEVELOPED PRESSURE versus FIELD STRENGTH



Fluid 50LV/L35180
Temperature 30 degC
Shear Rate 2200 sec-1

X Axis kV/mm
Y Axis Bar
Flow Rig

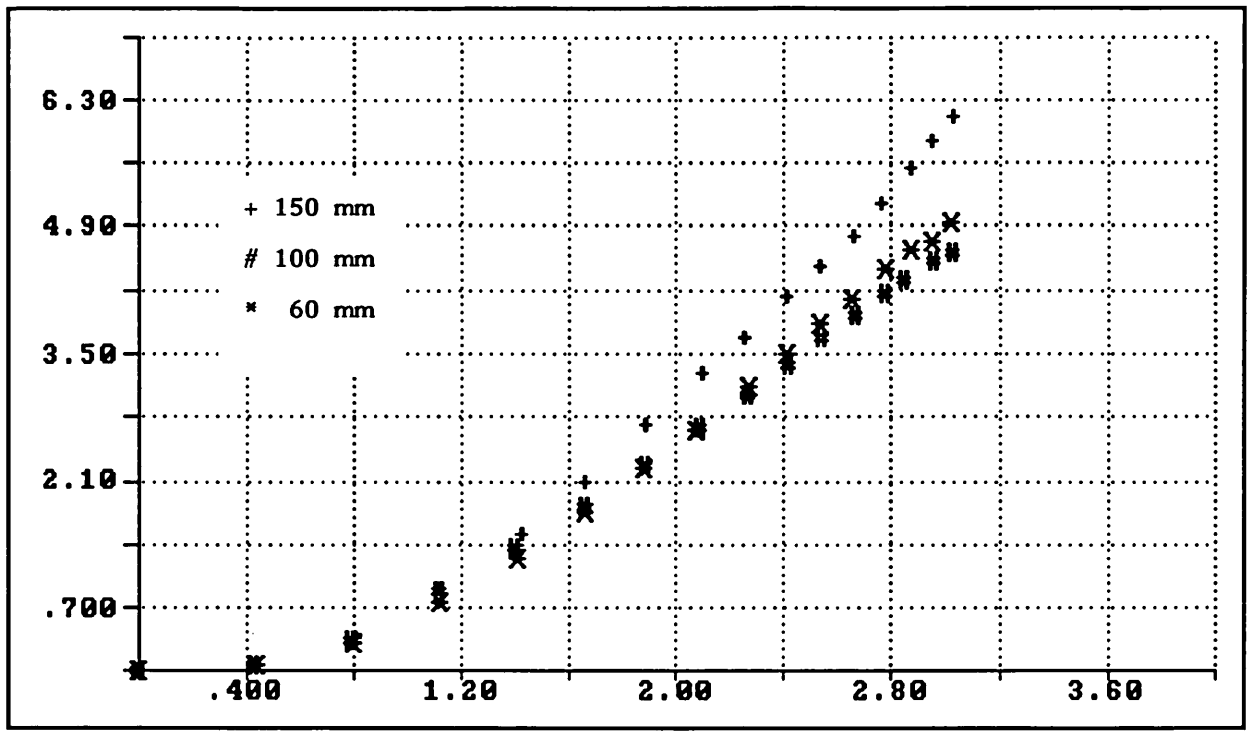
FIGURE 7b PLOT OF DEVELOPED PRESSURE versus FLOW RATE



Fluid 50LV/L35180
Temperature 30 degC
Field 2.11 kV/mm

X Axis Ltr/Min
Y Axis Bar
Flow Rig

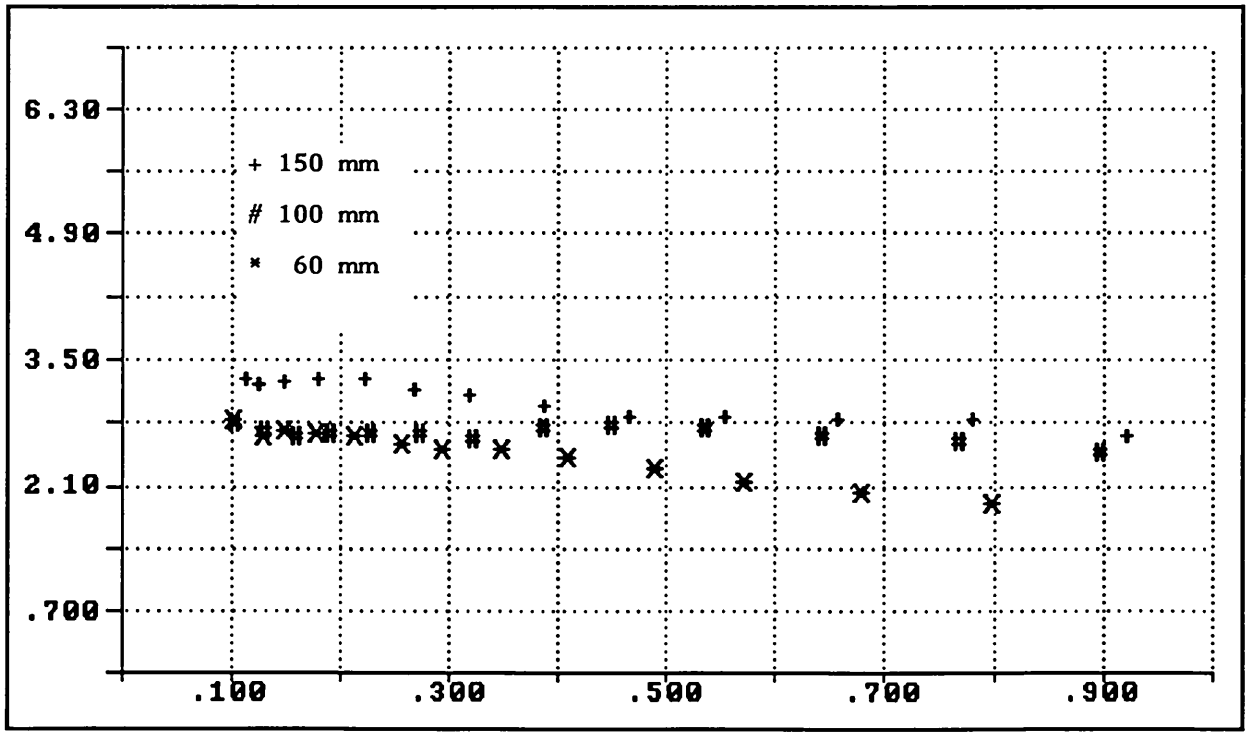
FIGURE 8a PLOT OF SHEAR STRESS versus FIELD STRENGTH



Fluid 50LV/L35180
Temperature 30 degC
Shear Rate 2200 sec-1

X Axis kV/mm
Y Axis kPa
Flow Rig

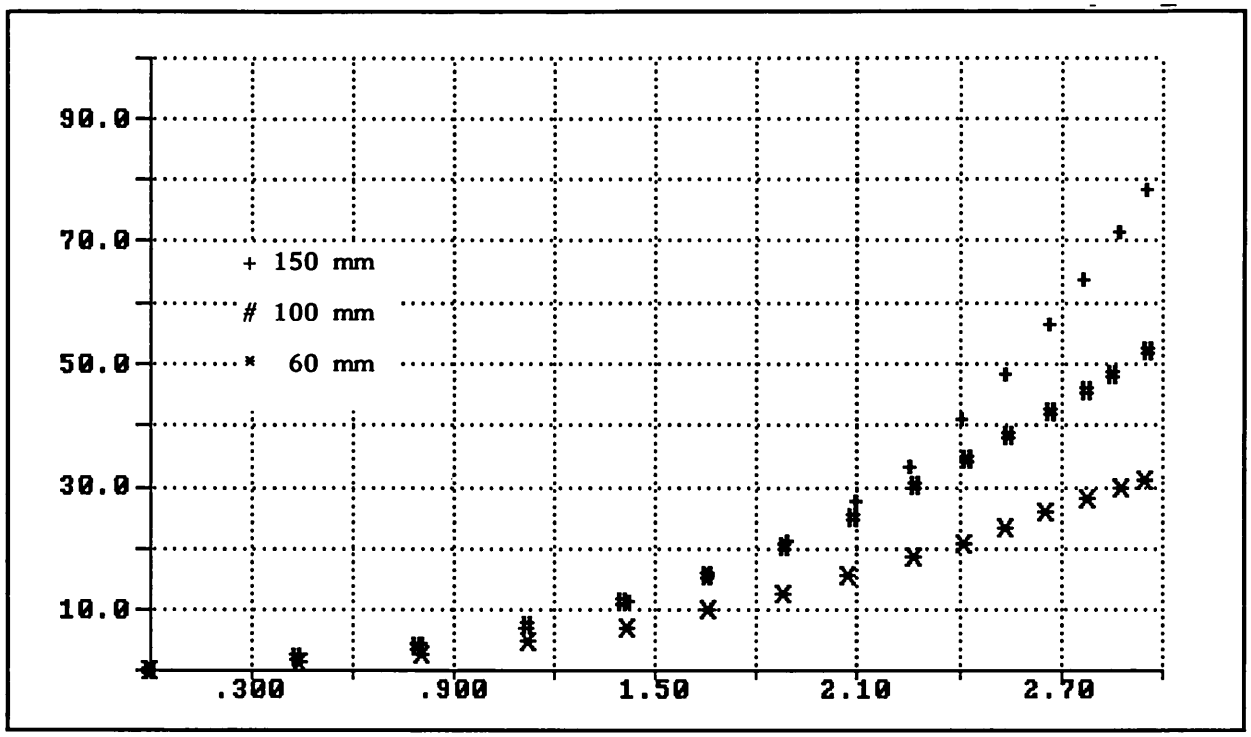
FIGURE 8b PLOT OF SHEAR STRESS versus SHEAR RATE



Fluid 50LV/L35180
Temperature 30 degC
Field 2.11 kV/mm

X Axis 1*e4 s-1
Y Axis kPa
Flow Rig

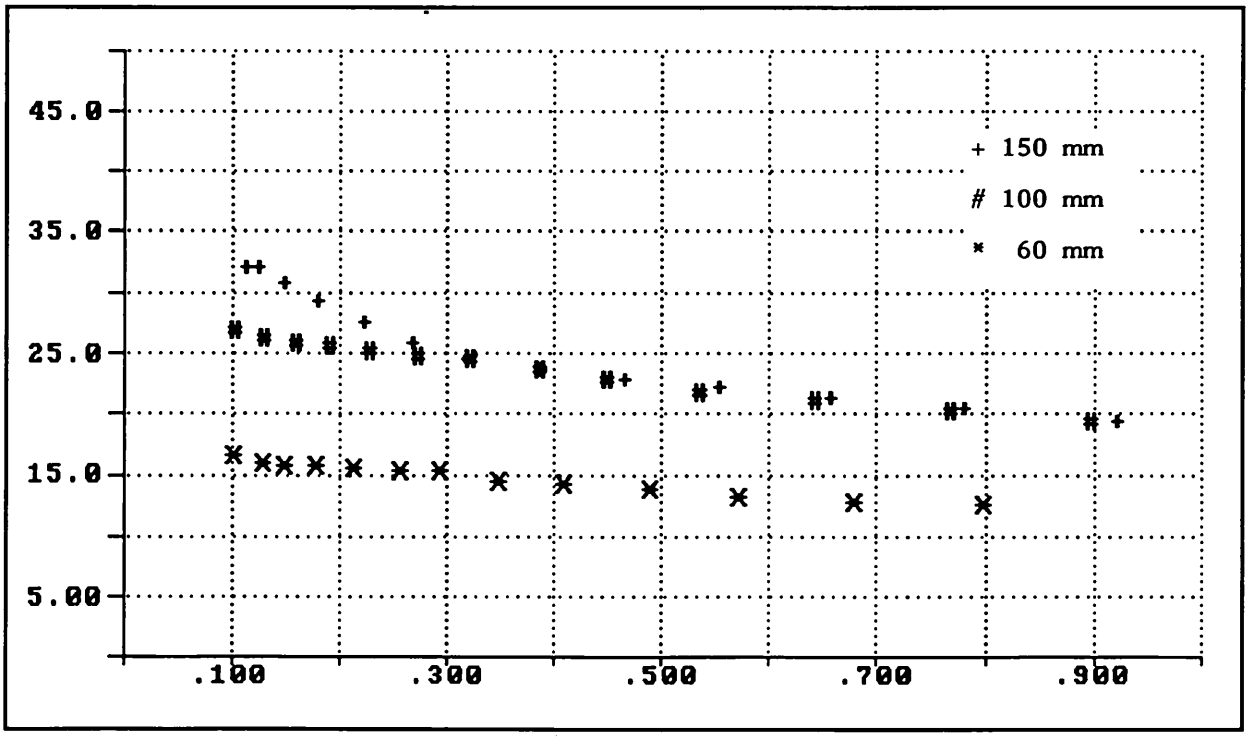
FIGURE 9a PLOT OF CURRENT DENSITY versus FIELD STRENGTH



Fluid 50LV/L35180
Temperature 30 degC
Shear Rate 2200 sec-1

X Axis kV/mm
Y Axis uA/cm2
Flow Rig

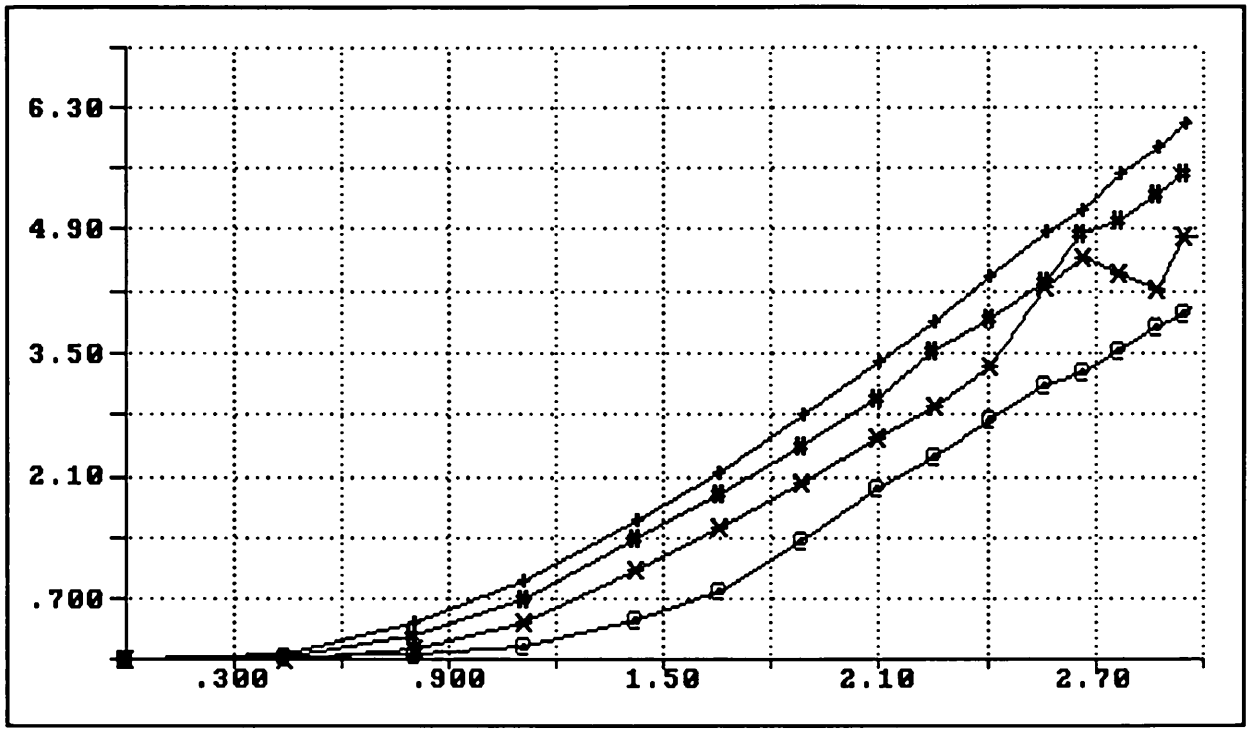
FIGURE 9b PLOT OF CURRENT DENSITY versus SHEAR RATE



Fluid 50LV/L35180
Temperature 30 degC
Field 2.11 kV/mm

X Axis 1*e4 s-1
Y Axis uA/cm2
Flow Rig

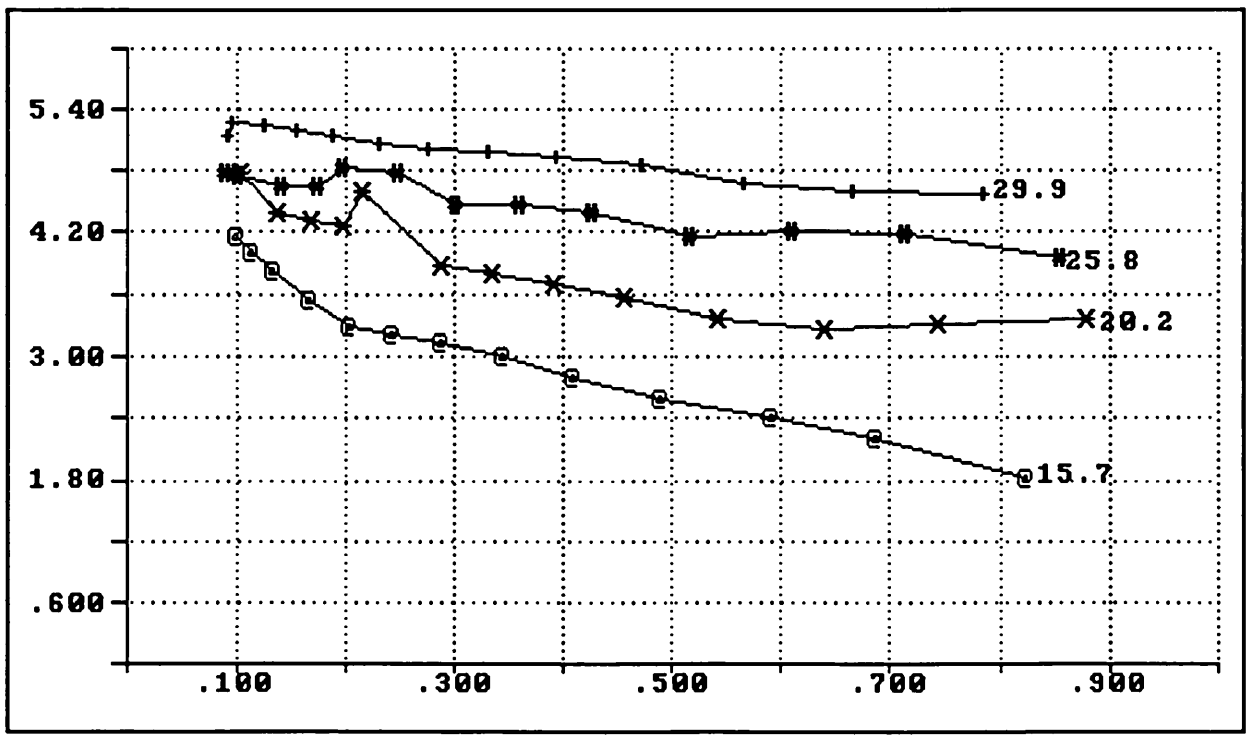
FIGURE 10a PLOT OF SHEAR STRESS versus FIELD STRENGTH



Fluid 50LV/L35180
Temperature 30 degC
Shear Rate 2200 sec-1

X Axis kV/mm
Y Axis kPa
Flow Rig

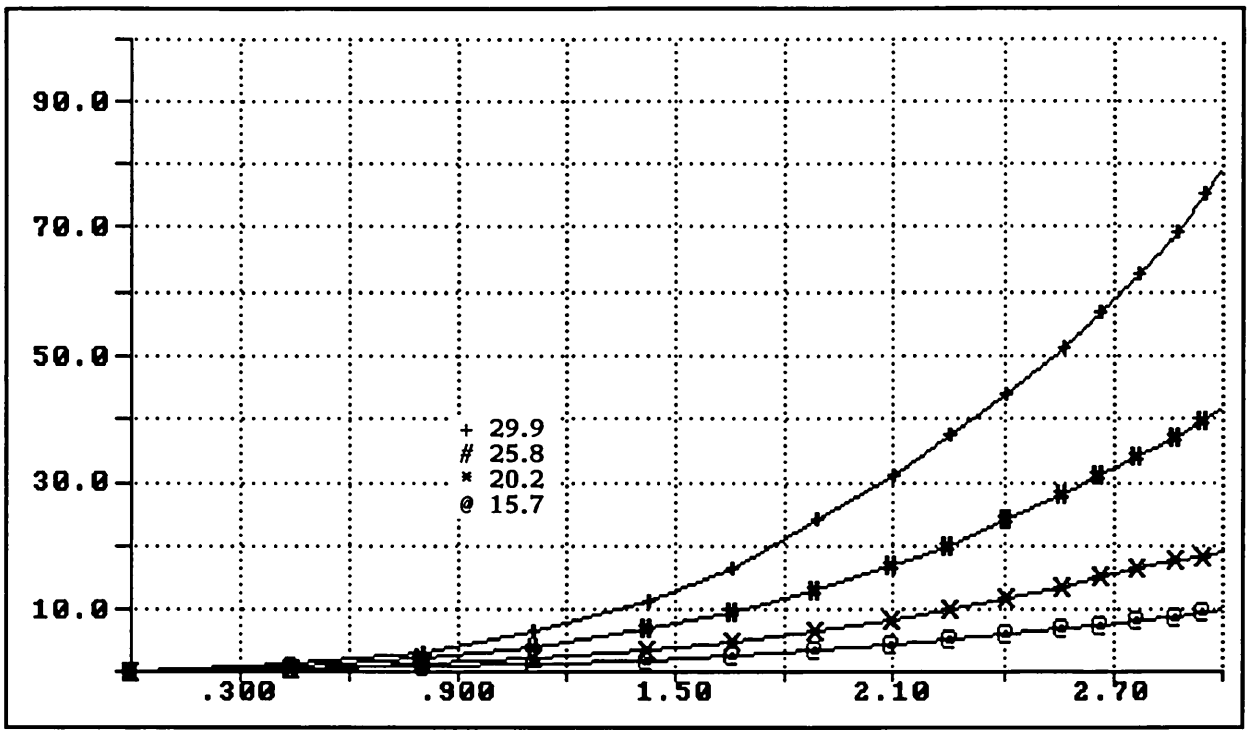
FIGURE 10b PLOT OF SHEAR STRESS versus SHEAR RATE



Fluid 50LV/L35180
Temperature 30 degC
Field 2.66 kV/mm

X Axis 1*e4 s-1
Y Axis kPa
Flow Rig

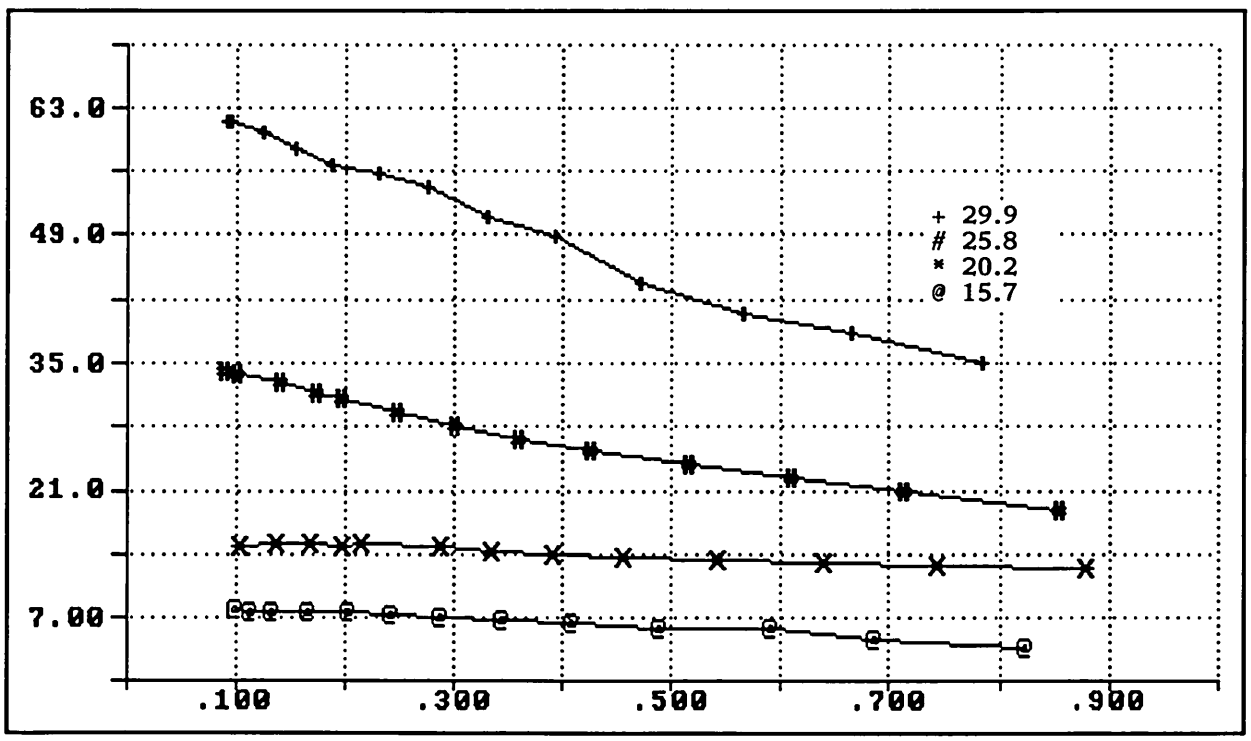
FIGURE 11a PLOT OF CURRENT DENSITY versus FIELD STRENGTH



Fluid 50LV/L35180
Temperature 30 degC
Shear Rate 2200 sec-1

X Axis kV/mm
Y Axis uA/cm2
Flow Rig

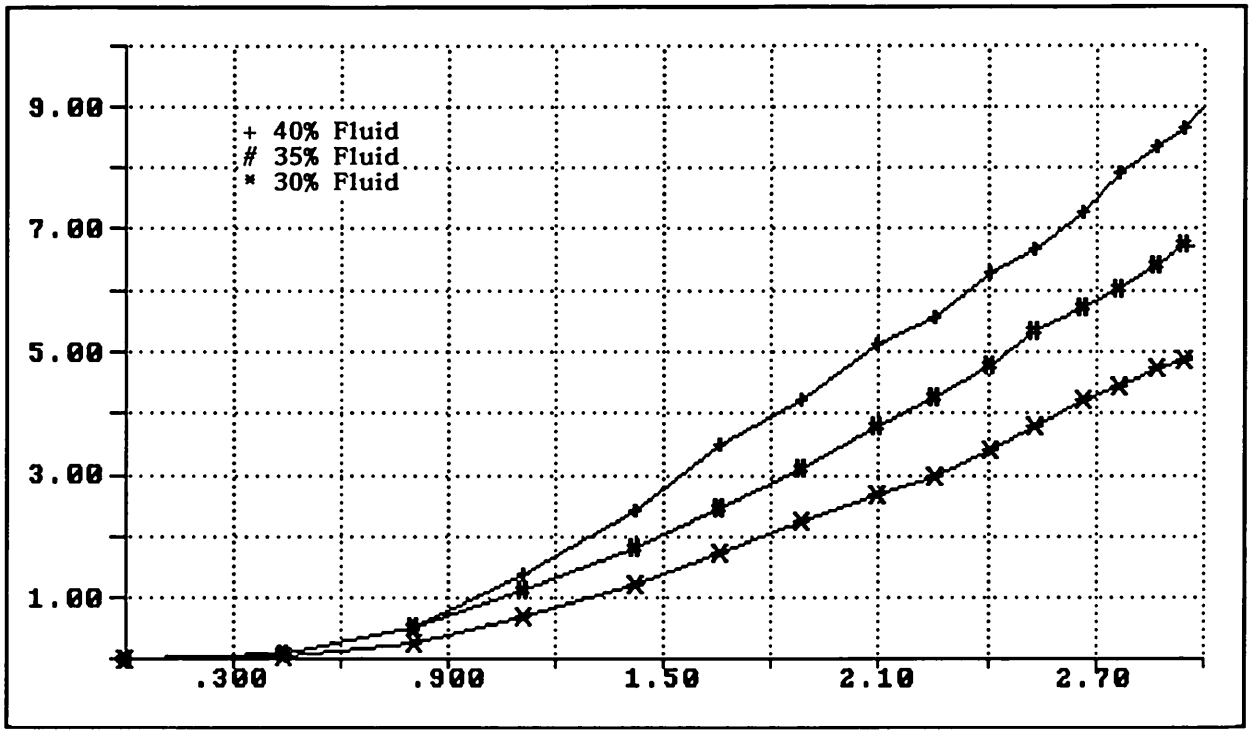
FIGURE 11b PLOT OF CURRENT DENSITY versus SHEAR RATE



Fluid 50LV/L35180
Temperature 30 degC
Field 2.66 kV/mm

X Axis 1*e4 s-1
Y Axis uA/cm2
Flow Rig

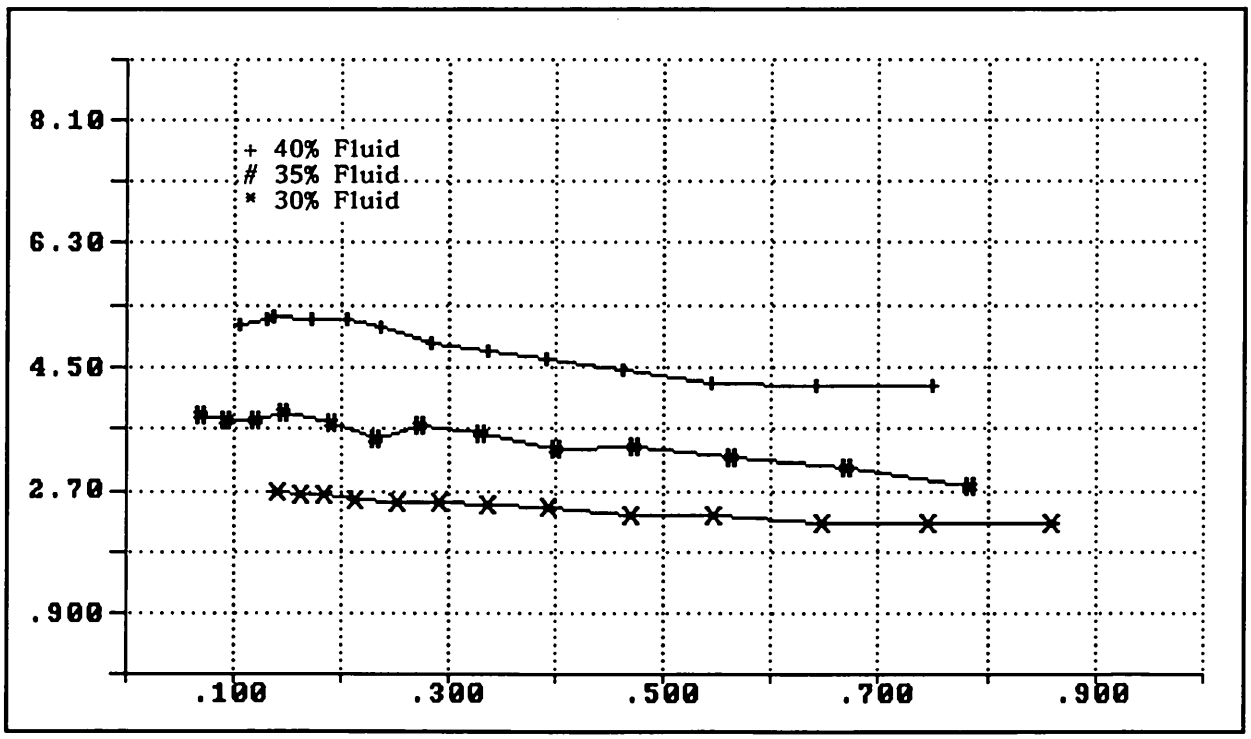
FIGURE 12a PLOT OF SHEAR STRESS versus FIELD STRENGTH



Fluids 50LV based
Temperature 30 degC
Shear Rate 1500 sec-1

X Axis kV/mm
Y Axis kPa
Flow Rig

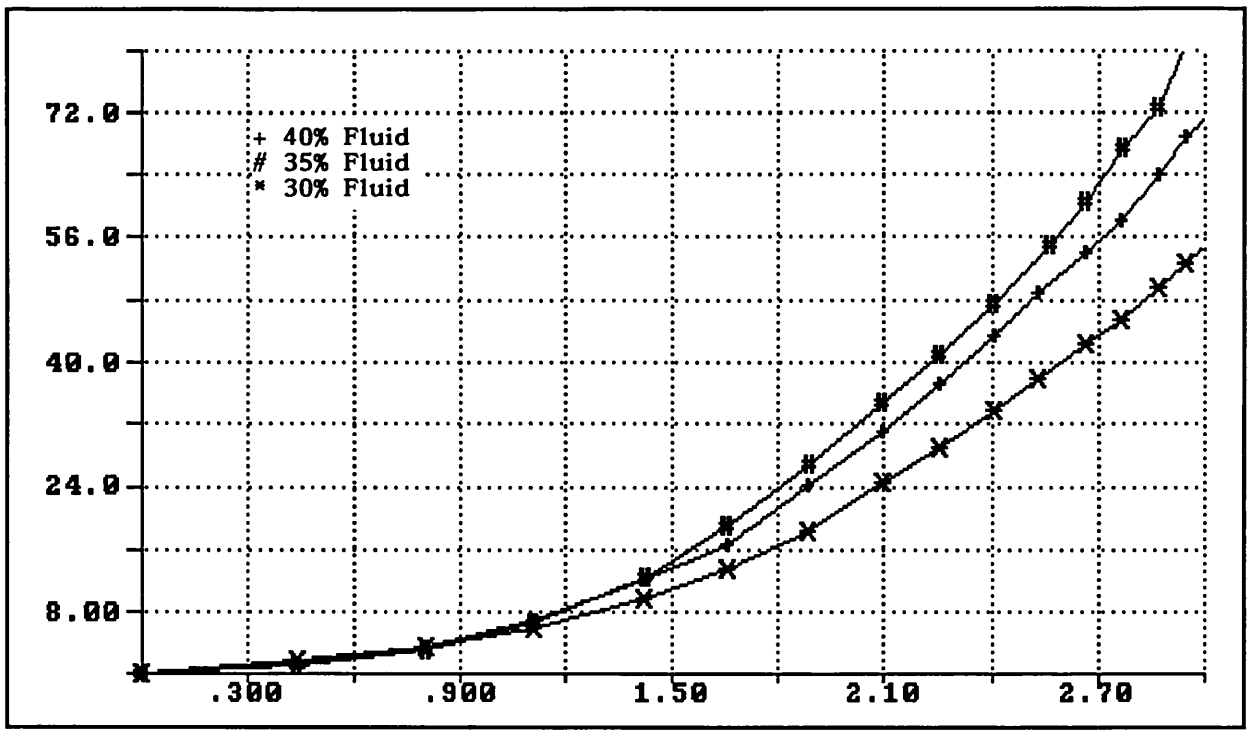
FIGURE 12b PLOT OF SHEAR STRESS versus SHEAR RATE



Fluids 50LV based
Temperature 30 degC
Field 2.11 kV/mm

X Axis 1*e4 s-1
Y Axis kPa
Flow Rig

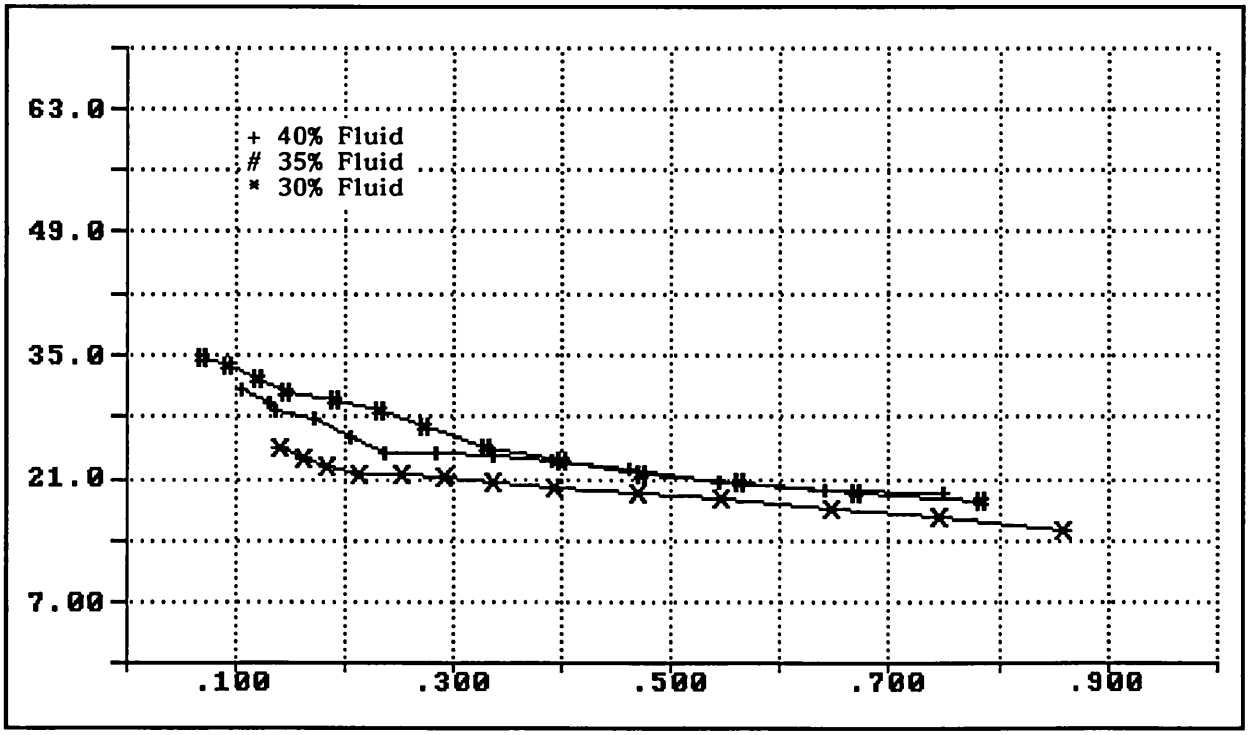
FIGURE 13a PLOT OF CURRENT DENSITY versus FIELD STRENGTH



Fluids 50LV based
Temperature 30 degC
Shear Rate 1500 sec-1

X Axis kV/mm
Y Axis uA/cm2
Flow Rig

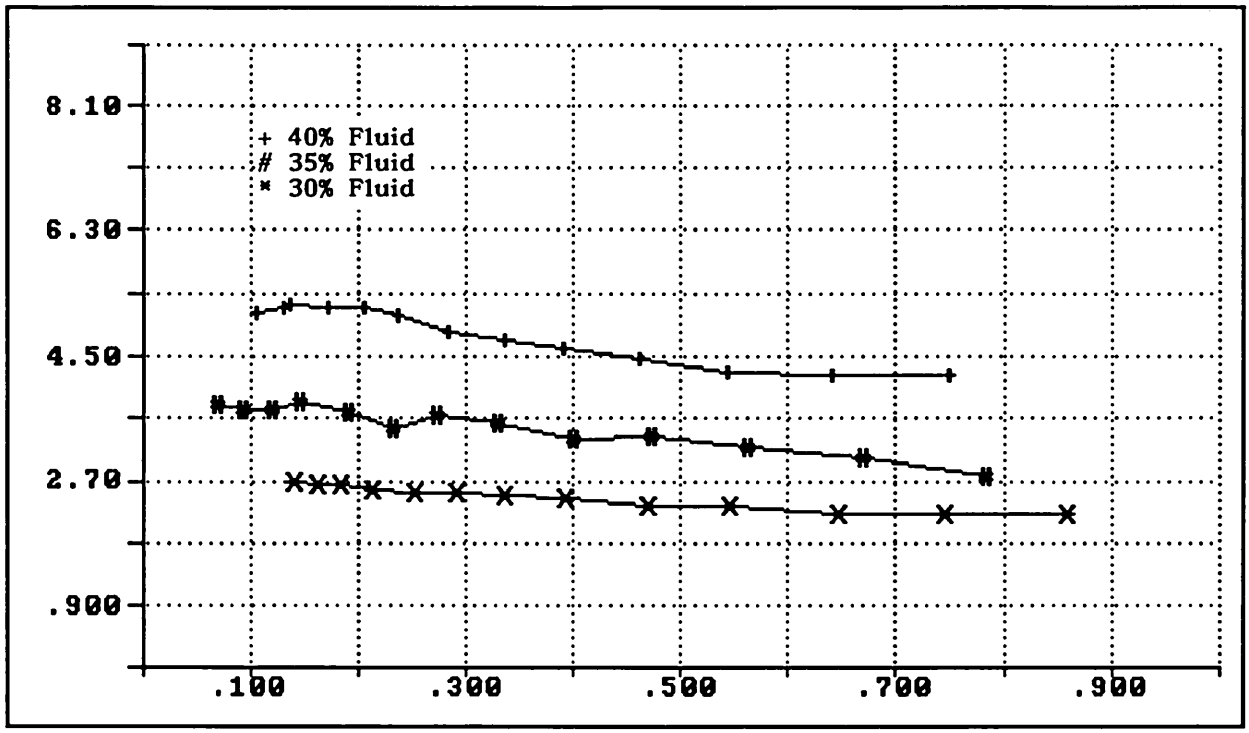
FIGURE 13b PLOT OF CURRENT DENSITY versus SHEAR RATE



Fluids 50LV based
Temperature 30 degC
Field 2.11 kV/mm

X Axis 1*e4 s-1
Y Axis uA/cm2
Flow Rig

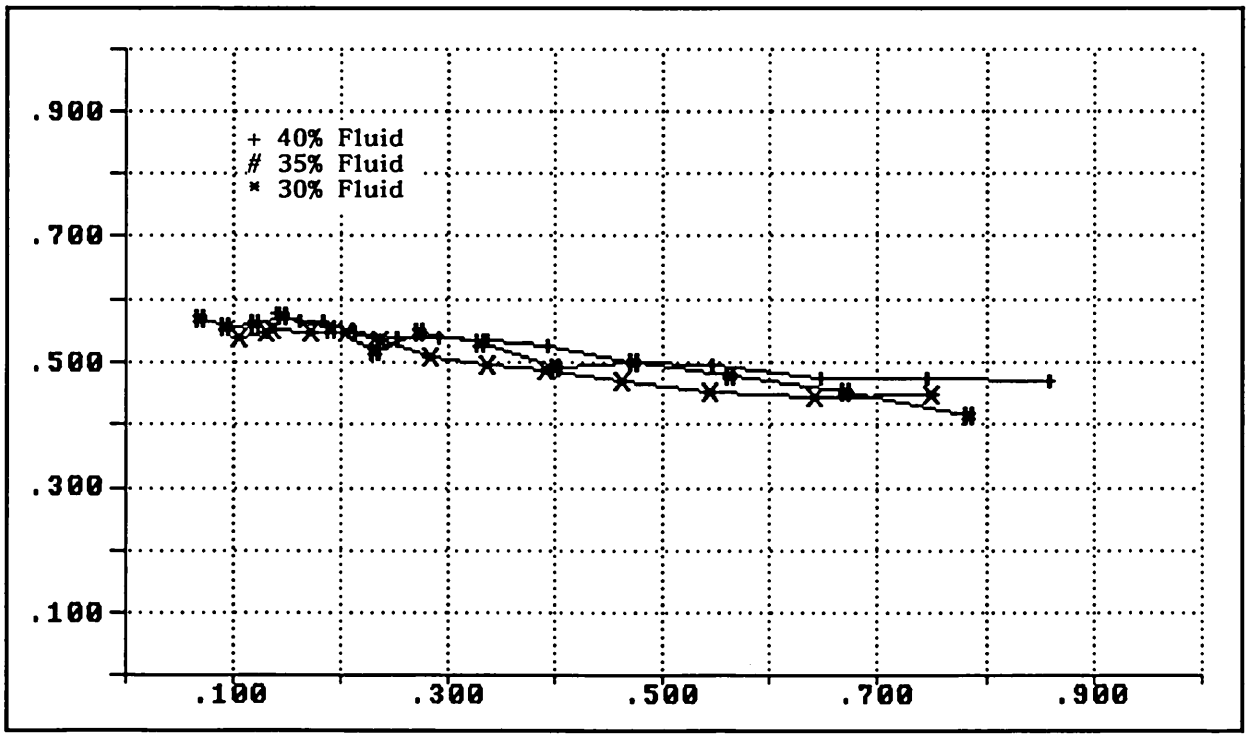
FIGURE 14a PLOT OF SHEAR STRESS versus SHEAR RATE



Fluids 50LV based
Temperature 30 degC
Field 2.11 kV/mm

X Axis 10e4*s-1
Y Axis kPa
Flow Rig

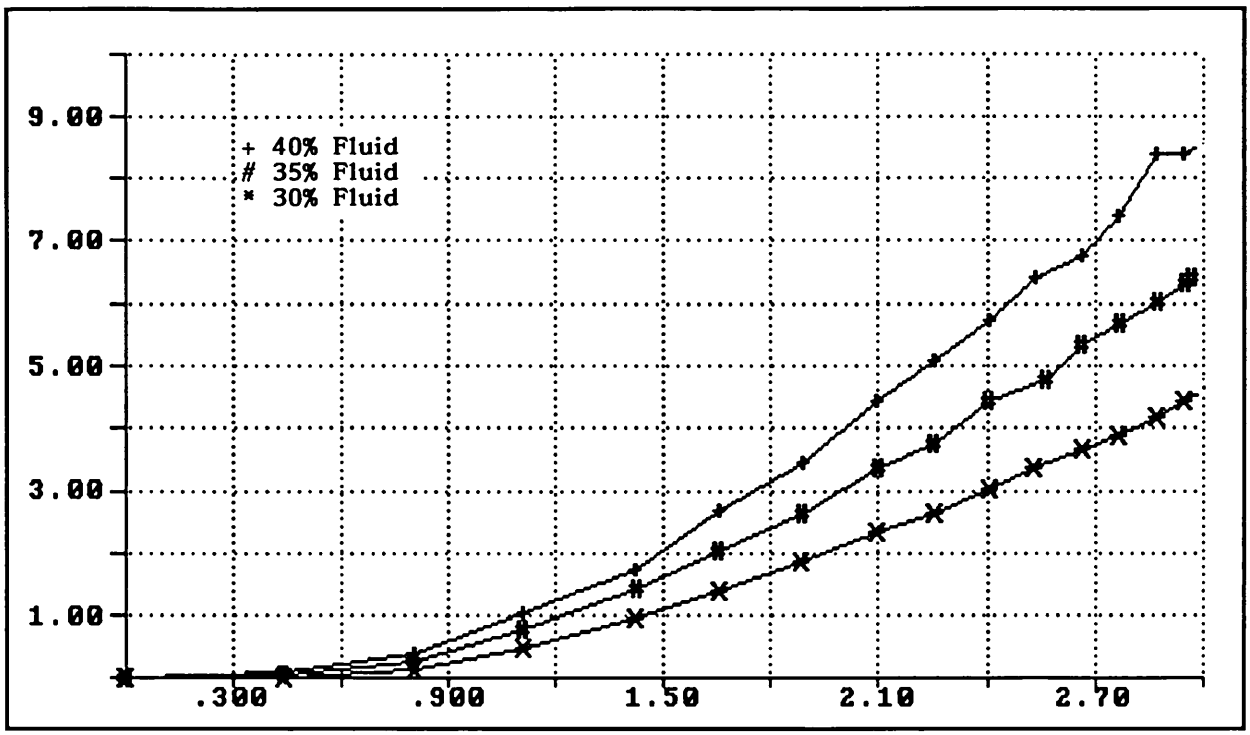
FIGURE 14b PLOT OF NORMALISED SHEAR STRESS versus SHEAR RATE



Fluids 50LV based
Temperature 30 degC
Field 2.11 kV/mm

X Axis 1*e4 s-1
Y Axis kPa Norm
Flow Rig

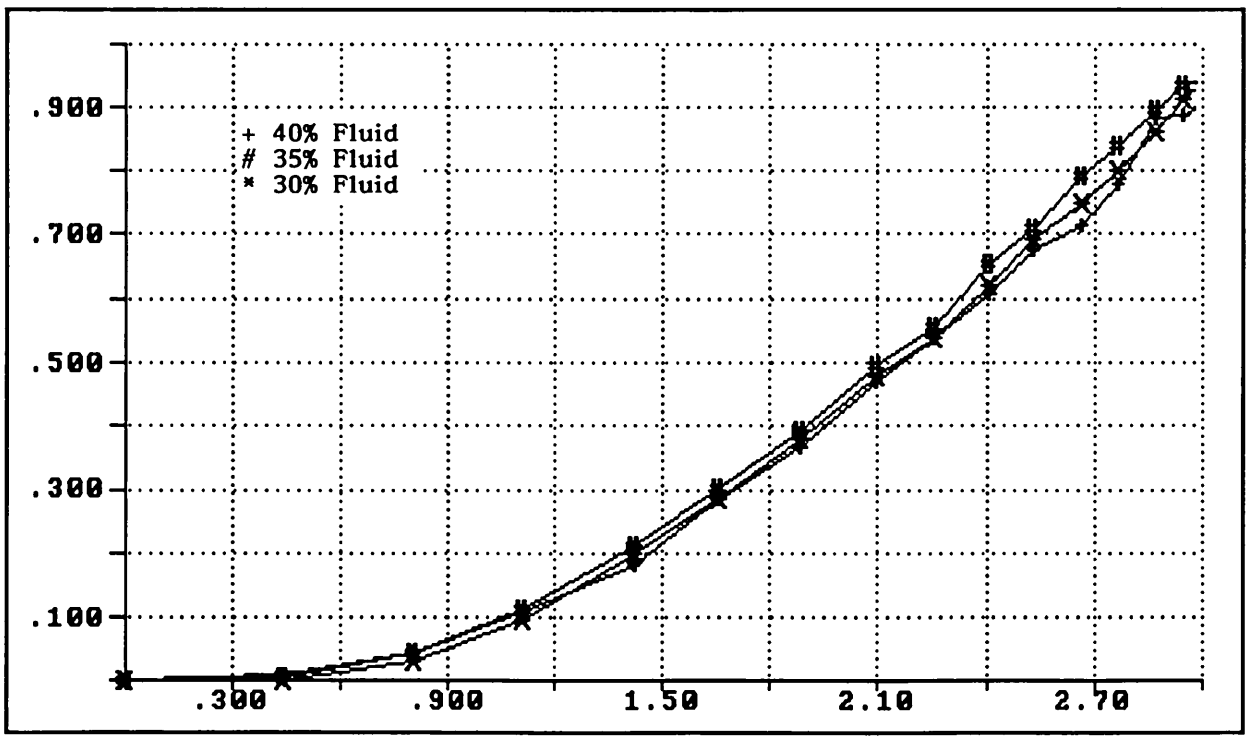
FIGURE 15a PLOT OF SHEAR STRESS versus FIELD STRENGTH



Fluids 50LV based
Temperature 30 degC
Shear Rate 4750 sec-1

X Axis kV/mm
Y Axis kPa
Flow Rig

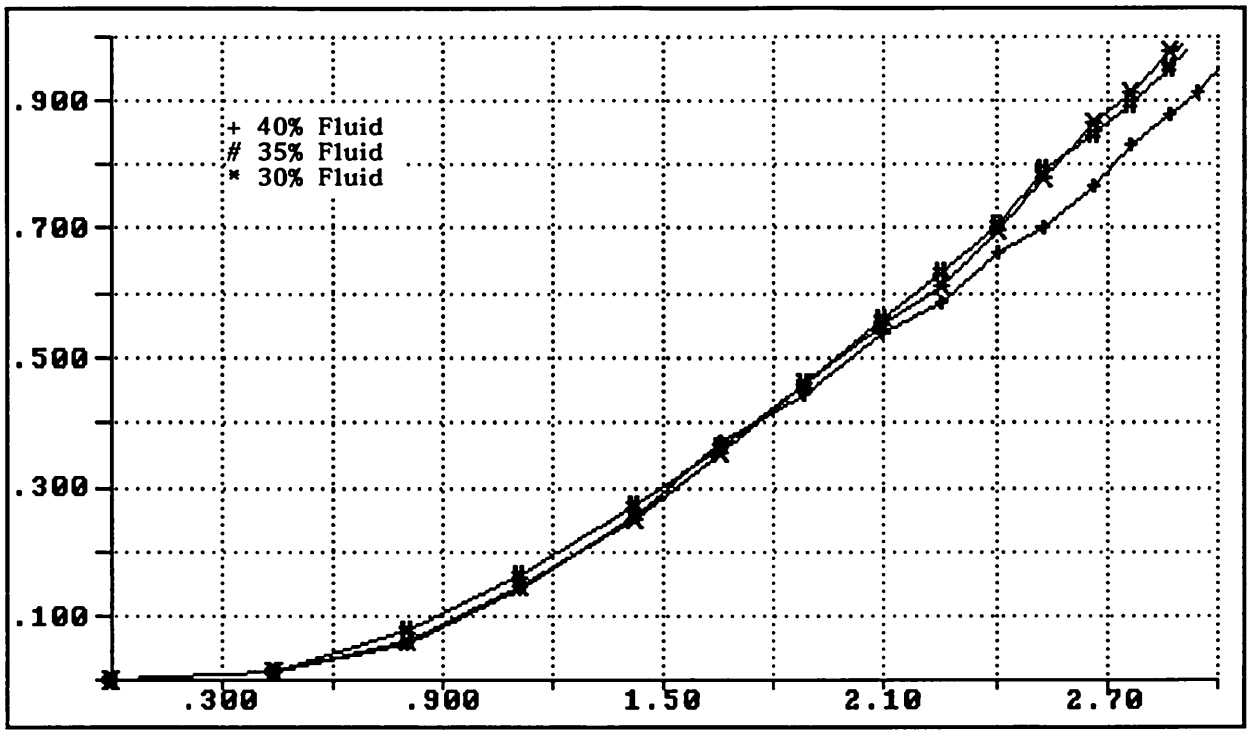
FIGURE 15b PLOT OF NORMALISED SHEAR STRESS versus FIELD STRENGTH



Fluids 50LV based
Temperature 30 degC
Shear Rate 4750 sec-1

X Axis kV/mm
Y Axis kPa Norm
Flow Rig

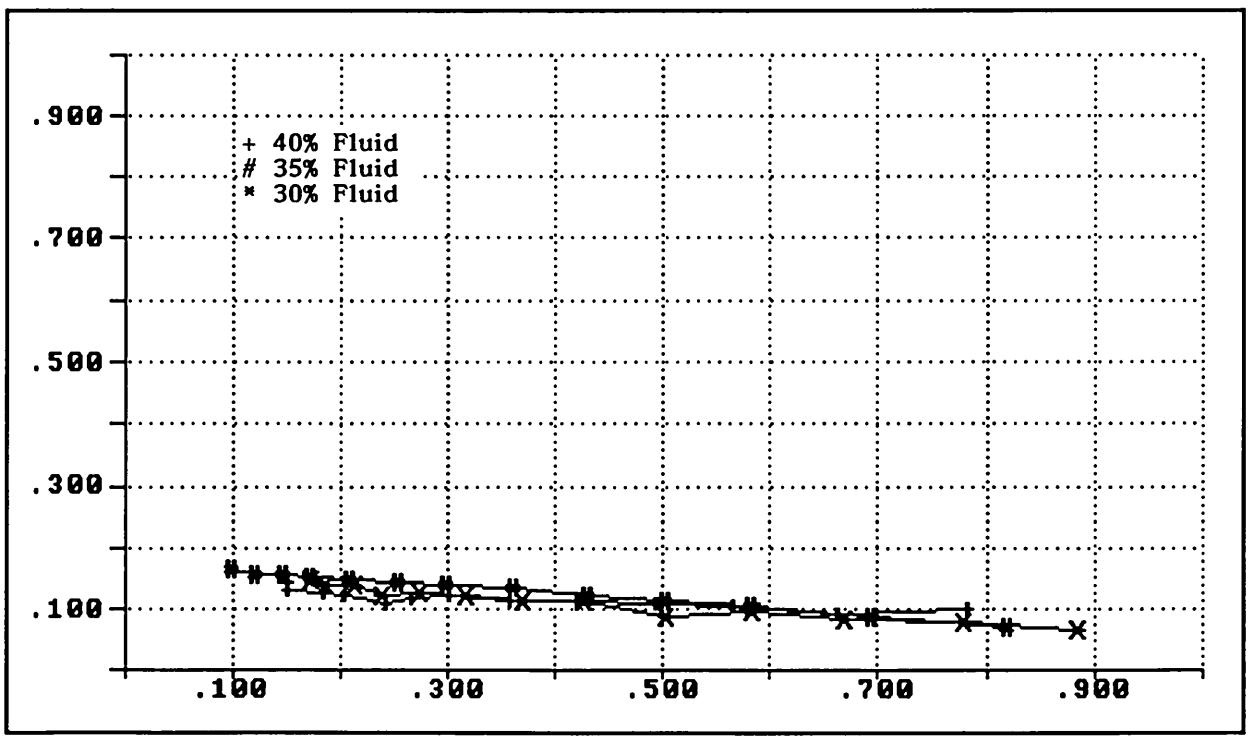
FIGURE 16a PLOT OF NORMALISED SHEAR STRESS versus FIELD STRENGTH



Fluids 50LV based
Temperature 30 degC
Shear Rate 1500 sec-1

X Axis kV/mm
Y Axis kPa Norm
Flow Rig

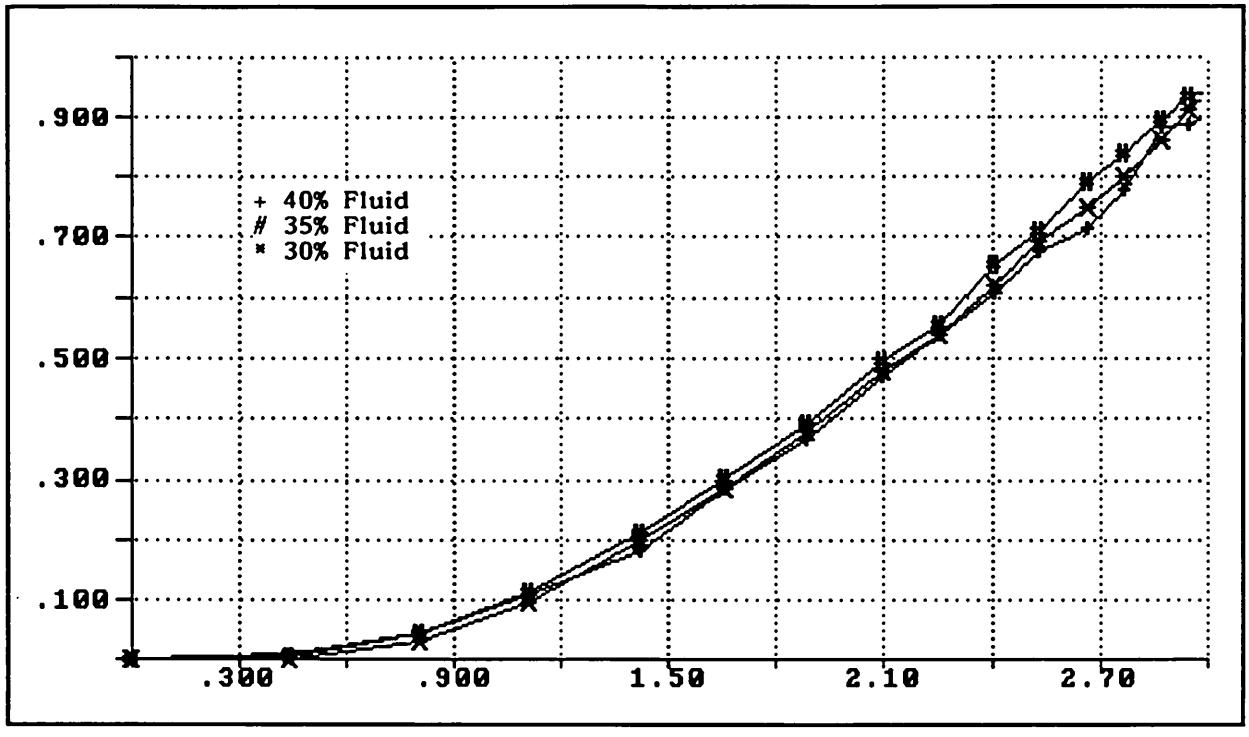
FIGURE 16b PLOT OF NORMALISED SHEAR STRESS versus SHEAR RATE



Fluids 50LV based
Temperature 30 degC
Field 1.11 kV/mm

X Axis 1*e4 s-1
Y Axis kPa Norm
Flow Rig

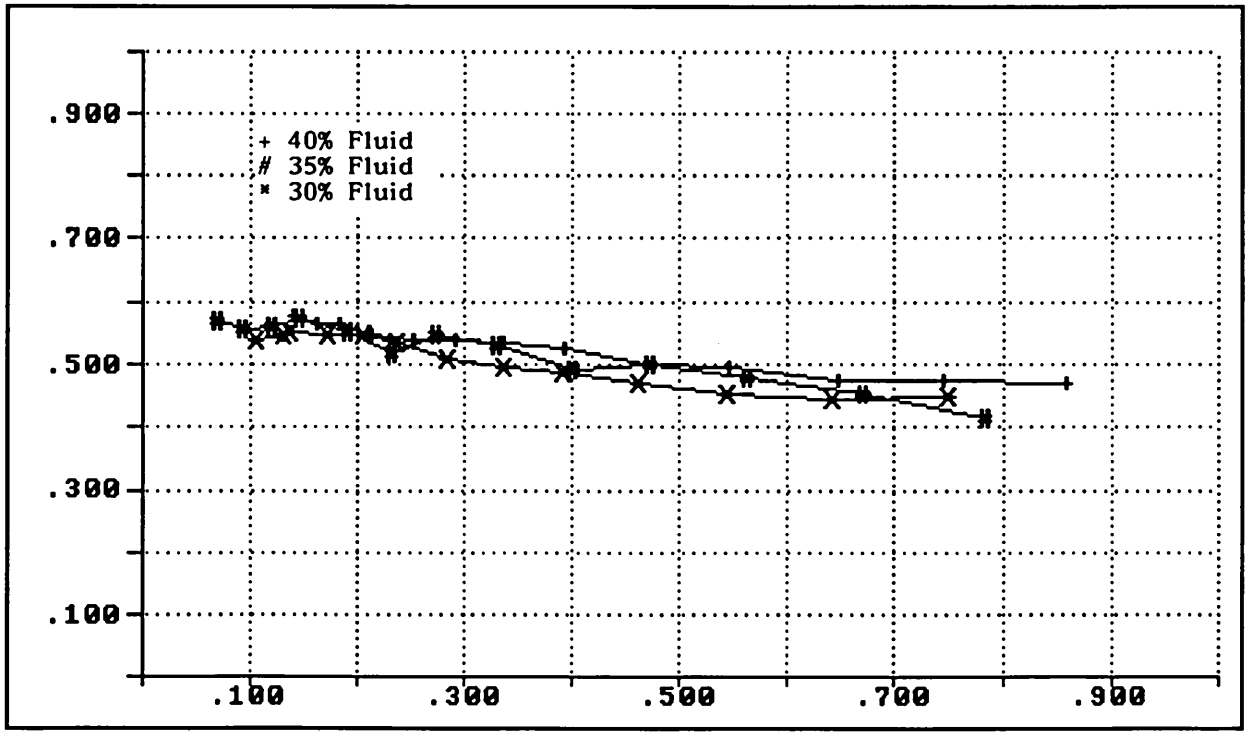
FIGURE 17a PLOT OF NORMALISED SHEAR STRESS versus FIELD STRENGTH



Fluids 50LV based
Temperature 30 degC
Shear Rate 4750 sec-1

X Axis kV/mm
Y Axis kPa Norm
Flow Rig

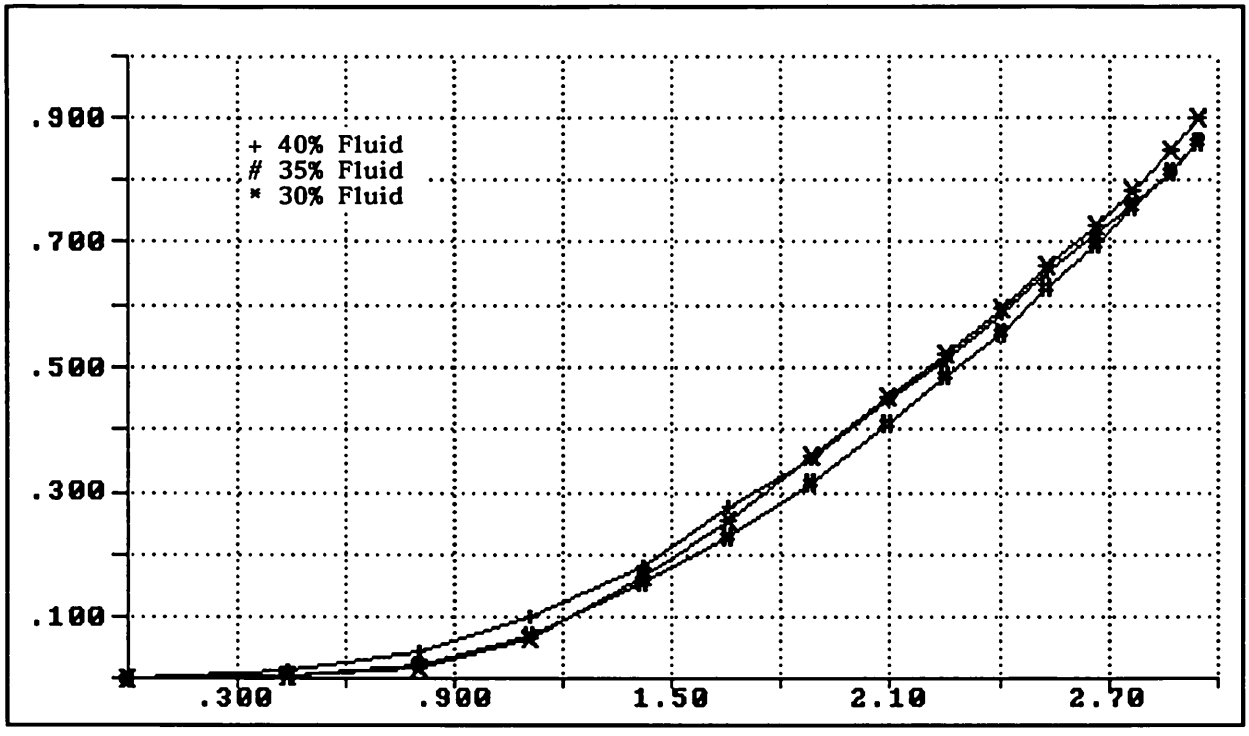
FIGURE 17b PLOT OF NORMALISED SHEAR STRESS versus SHEAR RATE



Fluids 50LV based
Temperature 30 degC
Field 2.11 kV/mm

X Axis 1*e4 s-1
Y Axis kPa Norm
Flow Rig

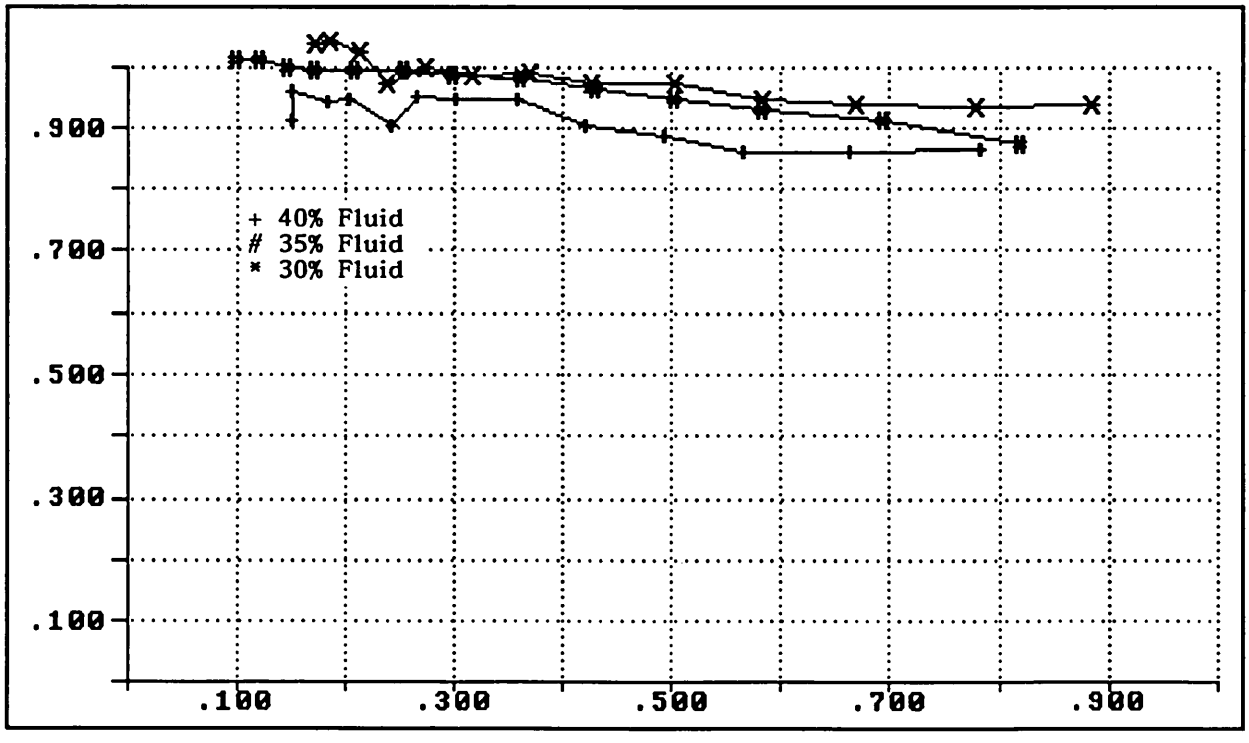
FIGURE 18a PLOT OF NORMALISED SHEAR STRESS versus FIELD STRENGTH



Fluids 50LV based
Temperature 30 degC
Shear Rate 7500 sec-1

X Axis kV/mm
Y Axis kPa Norm
Flow Rig

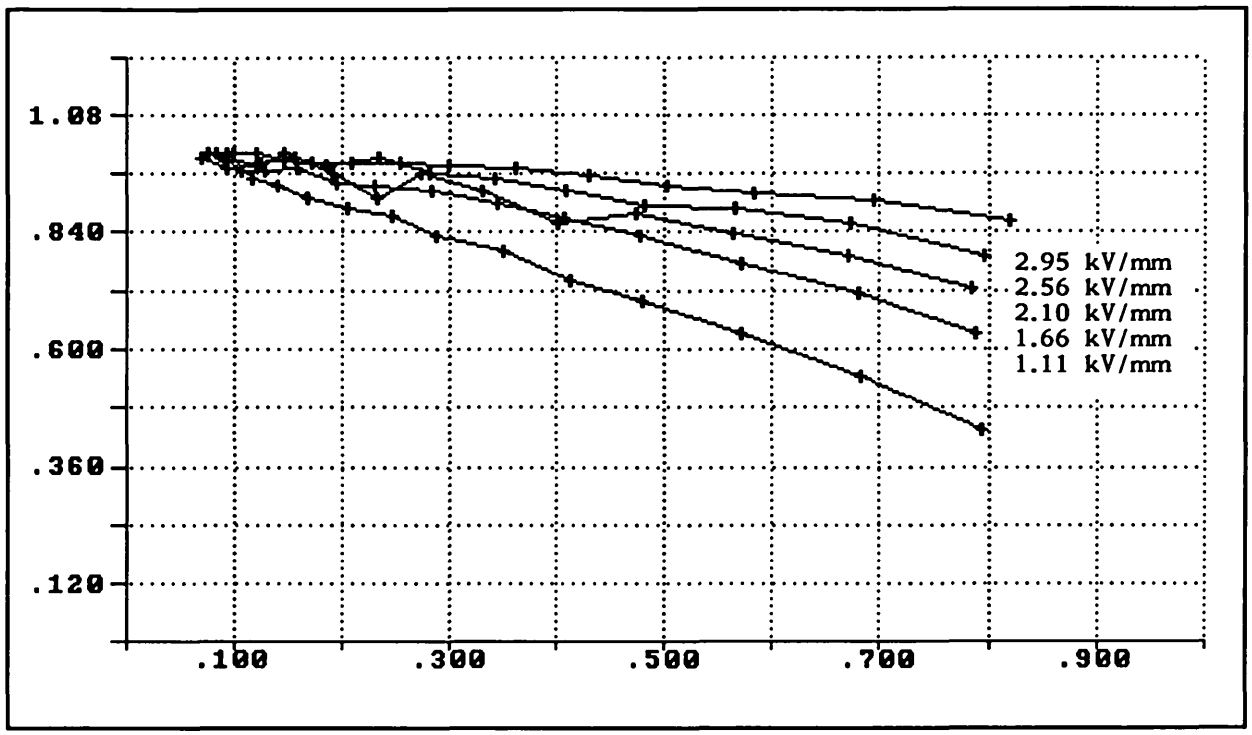
FIGURE 18b PLOT OF NORMALISED SHEAR STRESS versus SHEAR RATE



Fluids 50LV based
Temperature 30 degC
Field 2.96 kV/mm

X Axis 1*e4 s-1
Y Axis kPa Norm
Flow Rig

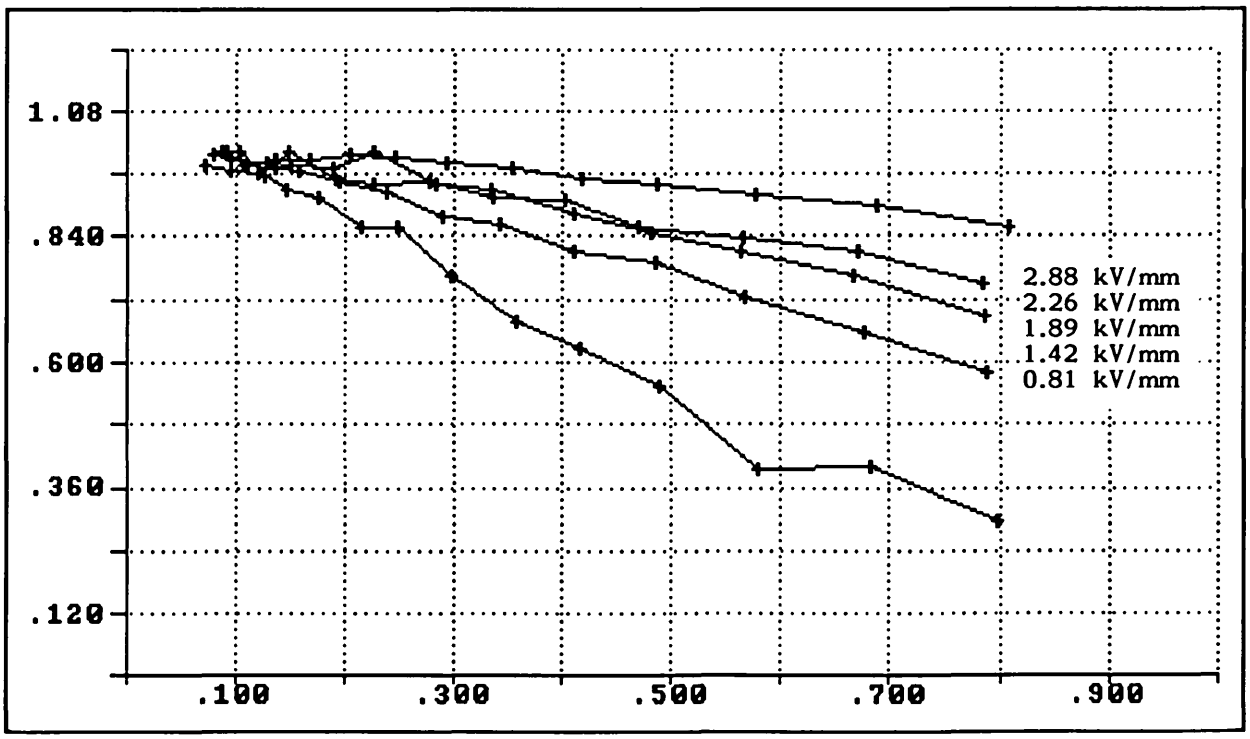
FIGURE 19a PLOT OF NORMALISED SHEAR STRESS versus SHEAR RATE



Fluid 50LV/L35180
Temperature 30 degC
Fields 1.11 to 2.9

X Axis 10e4*s-1
Y Axis kPa Norm
Flow Rig

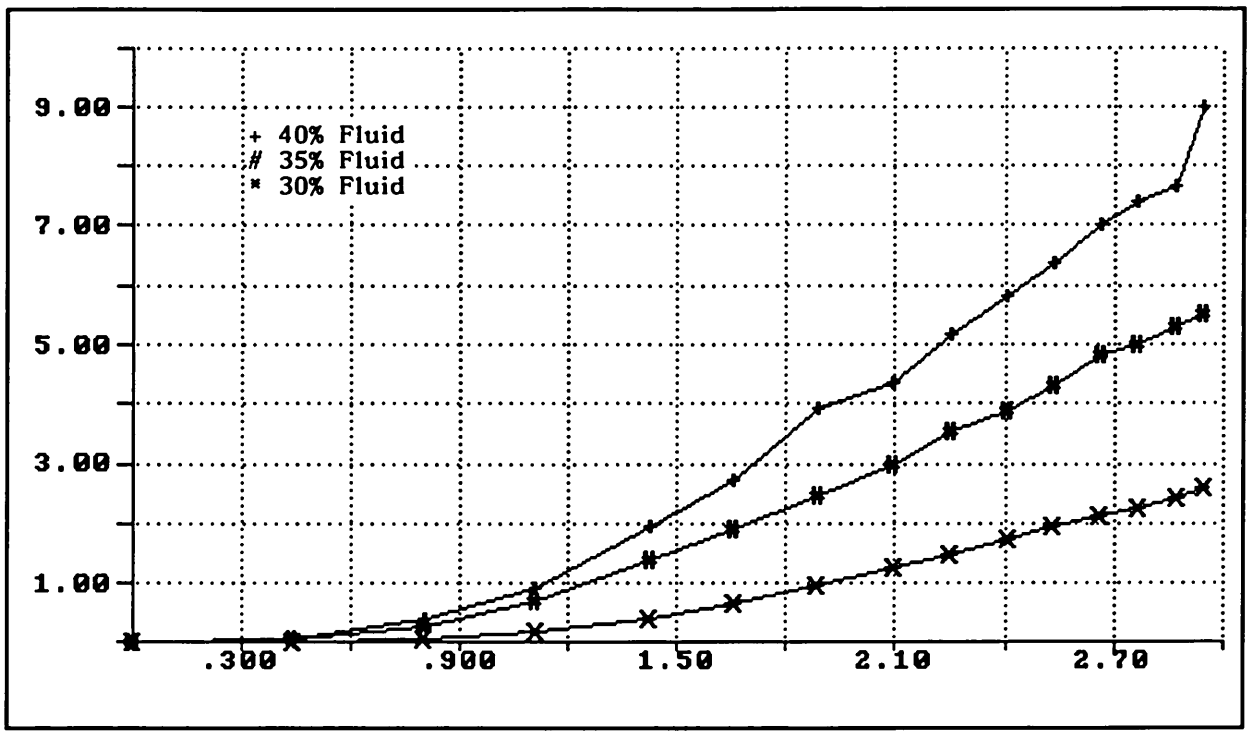
FIGURE 19b PLOT OF NORMALISED SHEAR STRESS versus SHEAR RATE



Fluid 50LV/L35180
Temperature 30 degC
Fields 0.81 to 2.9

X Axis 1*e4 s-1
Y Axis kPa Norm
Flow Rig

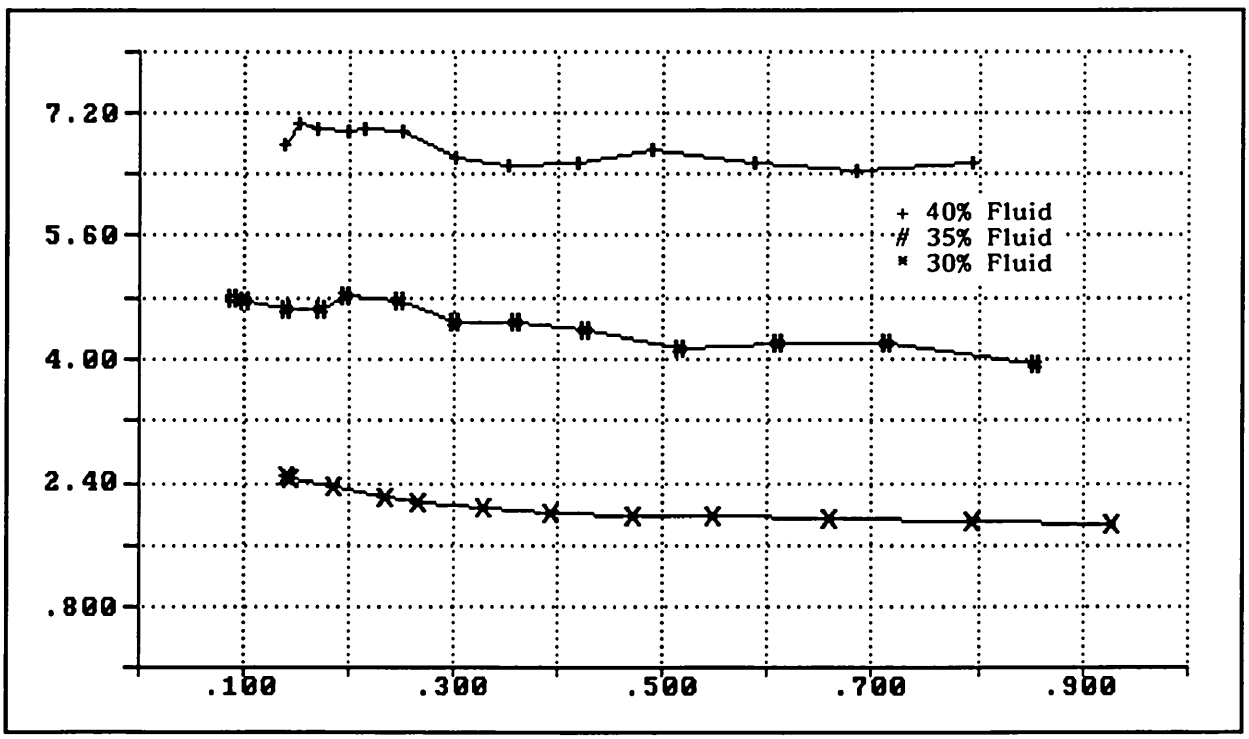
FIGURE 20a PLOT OF SHEAR STRESS versus FIELD STRENGTH



Fluids 50LV based
Temperature 25 degC
Shear Rate 2200 sec-1

X Axis kV/mm
Y Axis kPa
Flow Rig

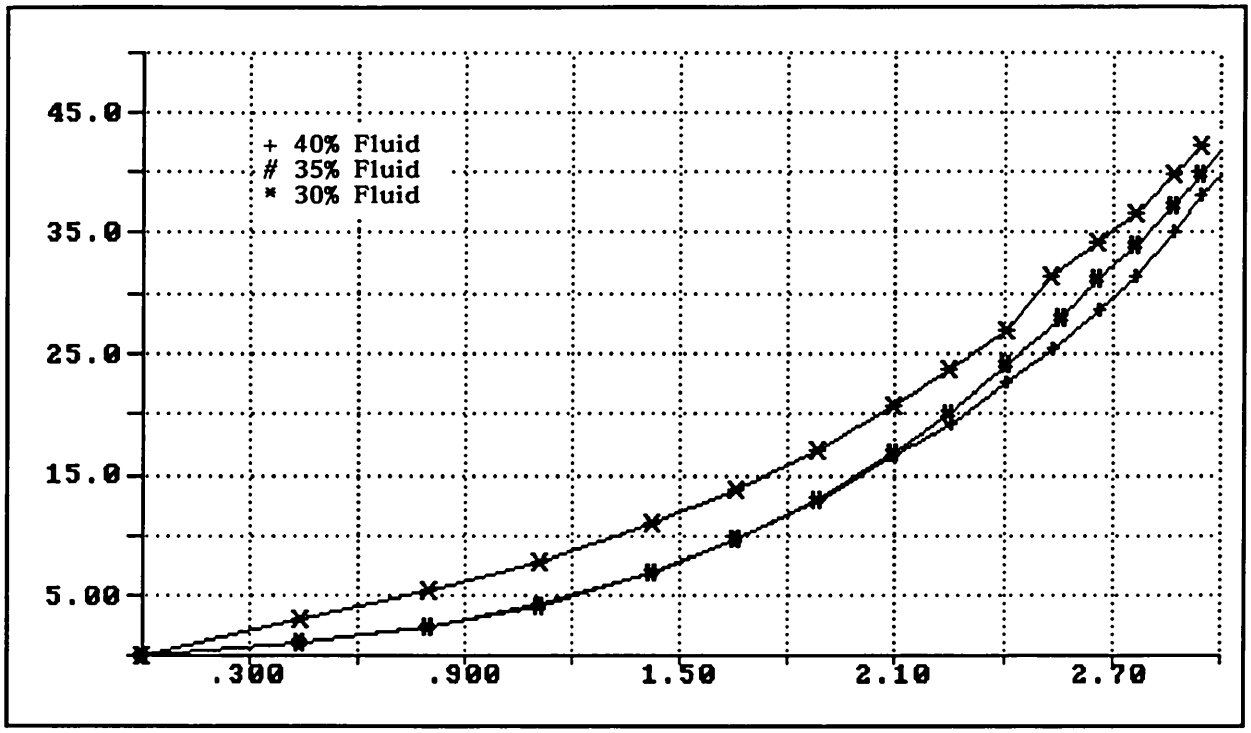
FIGURE 20b PLOT OF SHEAR STRESS versus SHEAR RATE



Fluids 50LV based
Temperature 25 degC
Field 2.66 kV/mm

X Axis 1*e4 s-1
Y Axis kPa
Flow Rig

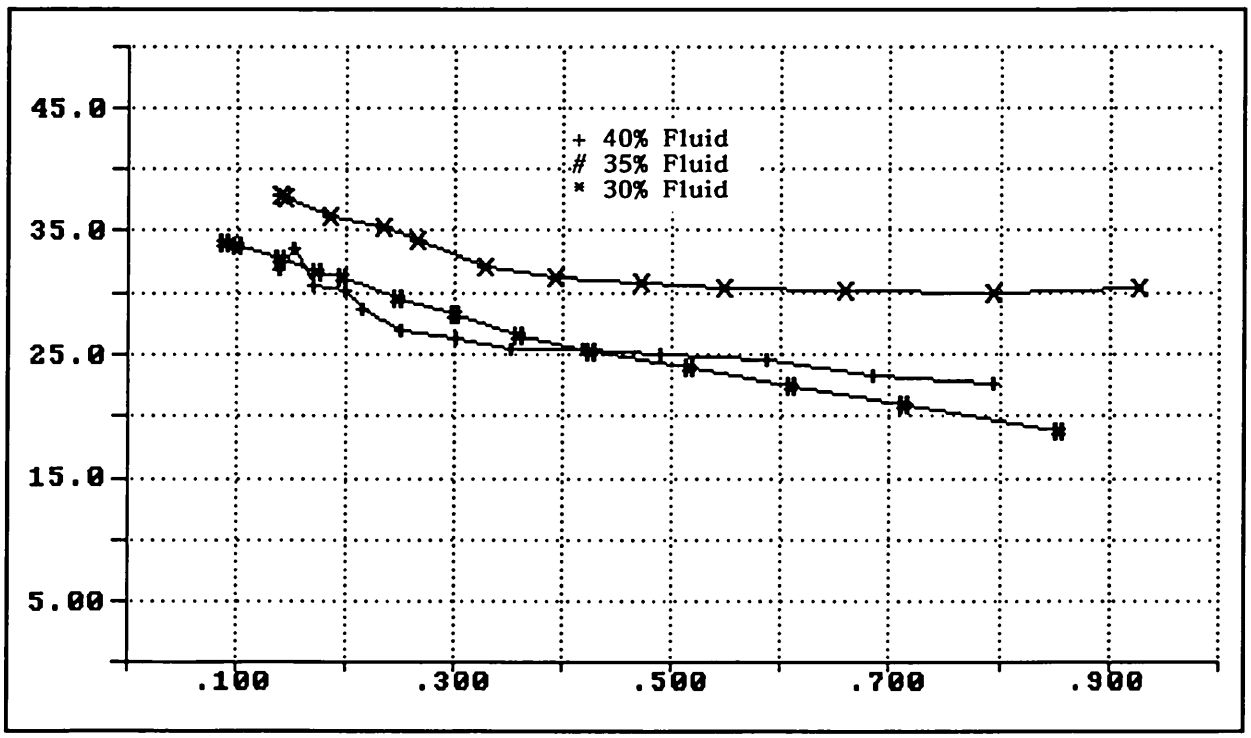
FIGURE 21a PLOT OF CURRENT DENSITY versus FIELD STRENGTH



Fluids 50LV based
Temperature 25 degC
Shear Rate 2200 sec-1

X Axis kV/mm
Y Axis uA/cm2
Flow Rig

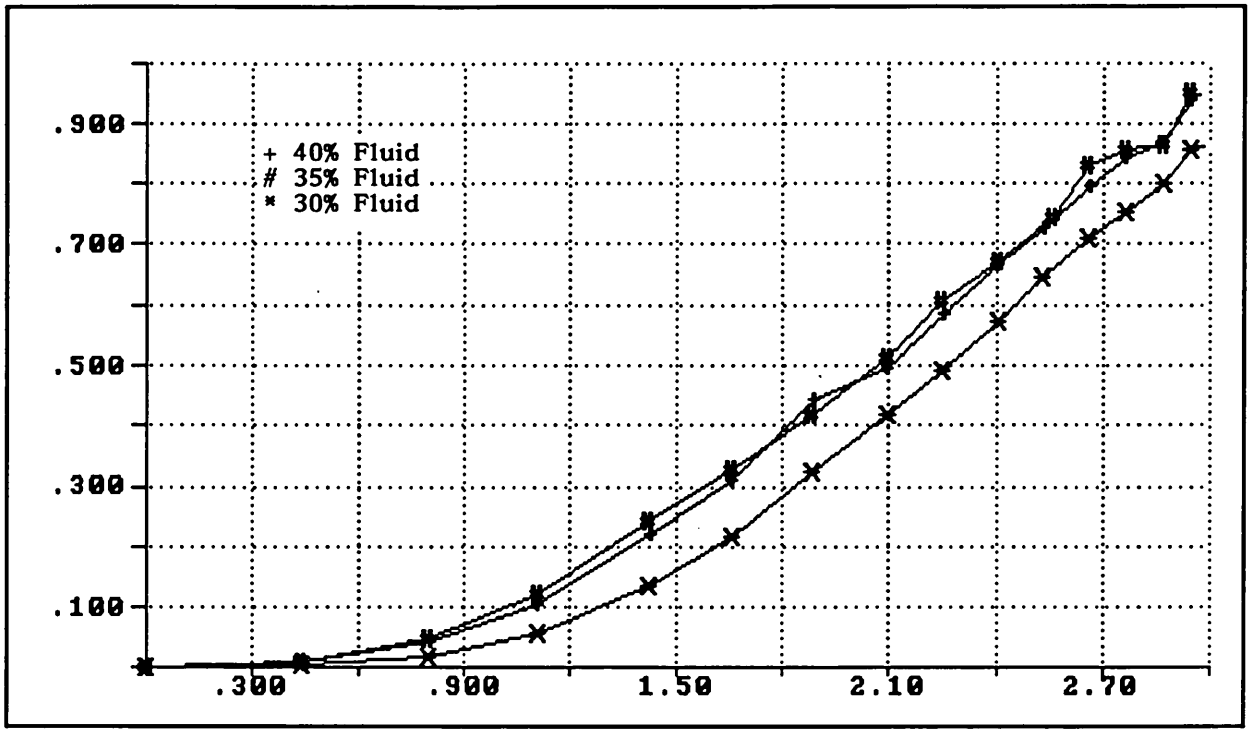
FIGURE 21b PLOT OF CURRENT DENSITY versus SHEAR RATE



Fluids 50LV based
Temperature 25 degC
Field 2.66 kV/mm

X Axis 1*e4 s-1
Y Axis uA/cm2
Flow Rig

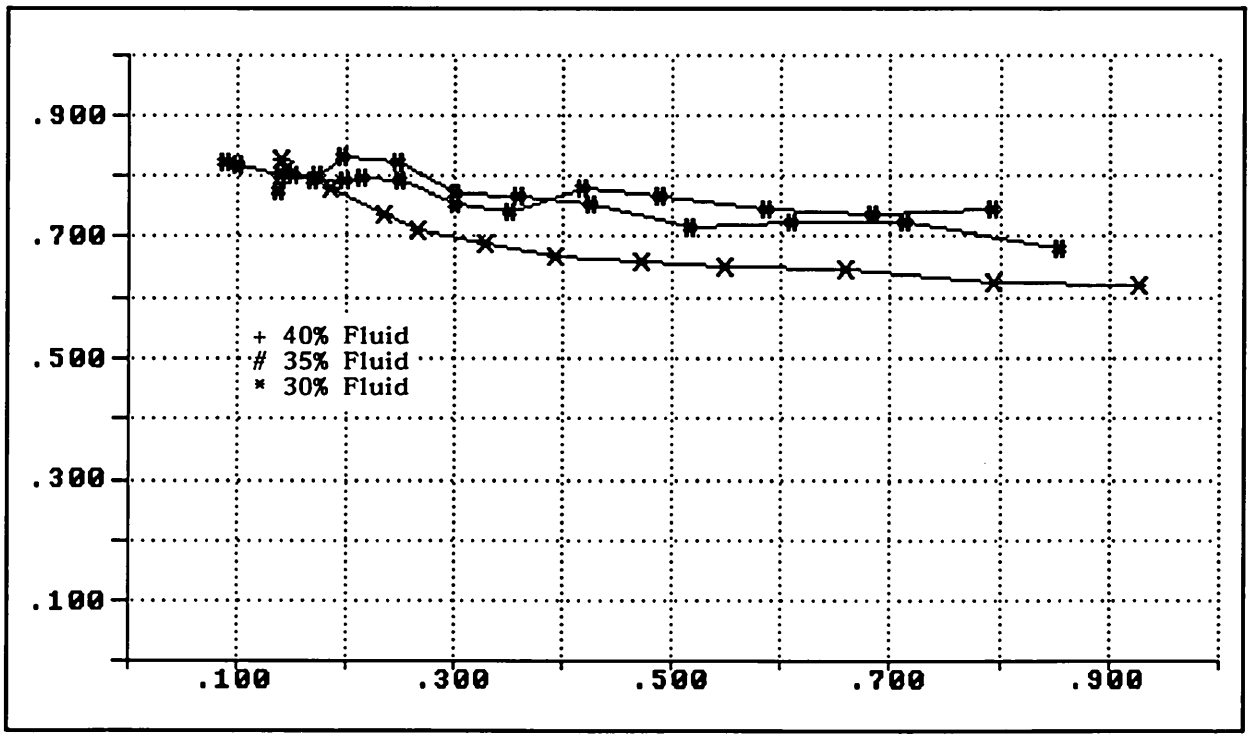
FIGURE 22a PLOT OF NORMALISED SHEAR STRESS versus FIELD STRENGTH



Fluids 50LV based
Temperature 25 degC
Shear Rate 2200 sec-1

X Axis kV/mm
Y Axis kPa Norm
Flow Rig

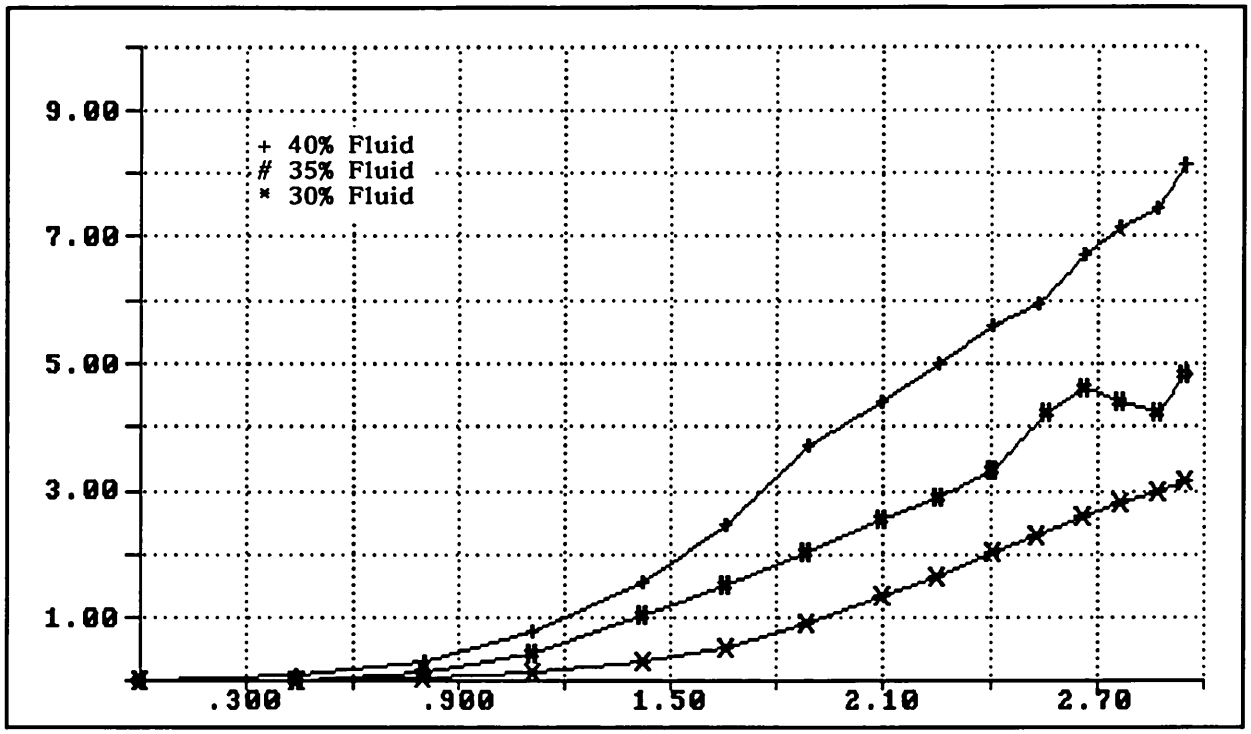
FIGURE 22b PLOT OF NORMALISED SHEAR STRESS versus SHEAR RATE



Fluids 50LV based
Temperature 25 degC
Field 2.66 kV/mm

X Axis 1*e4 s-1
Y Axis kPa Norm
Flow Rig

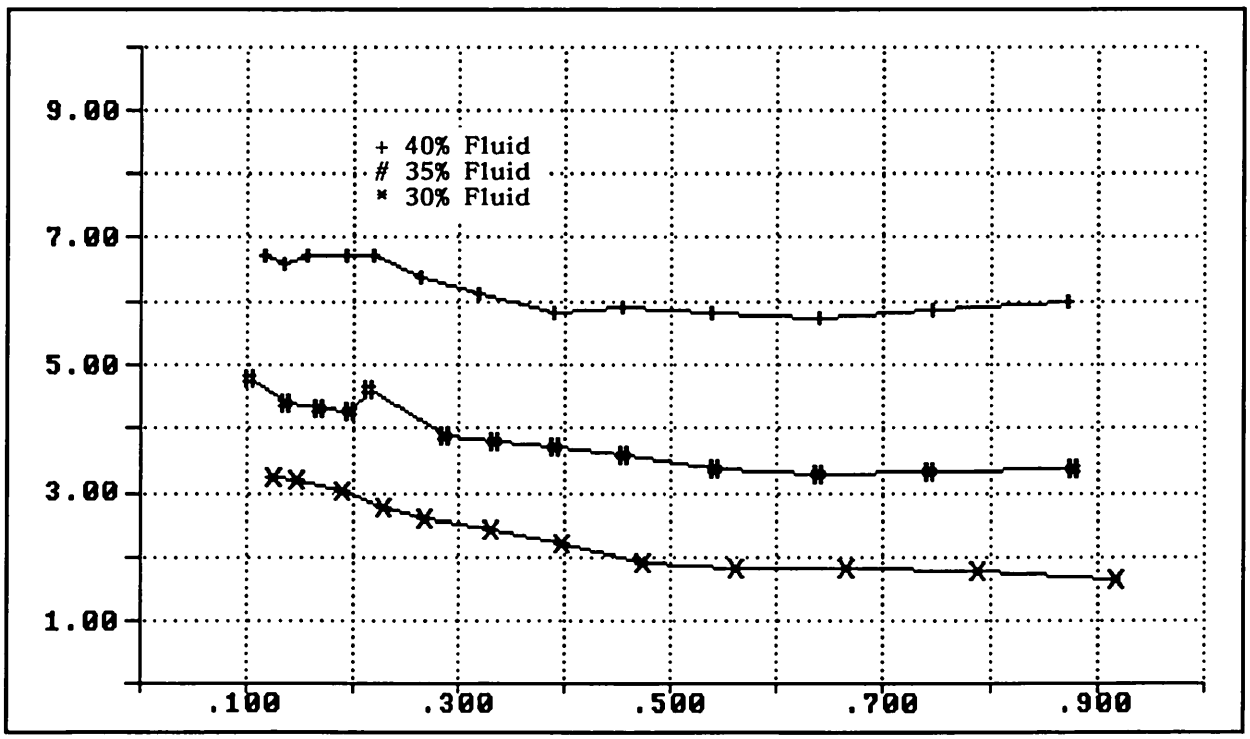
FIGURE 23a PLOT OF SHEAR STRESS versus FIELD STRENGTH



Fluids 50LV based
Temperature 20 degC
Shear Rate 2200 sec-1

X Axis kV/mm
Y Axis kPa
Flow Rig

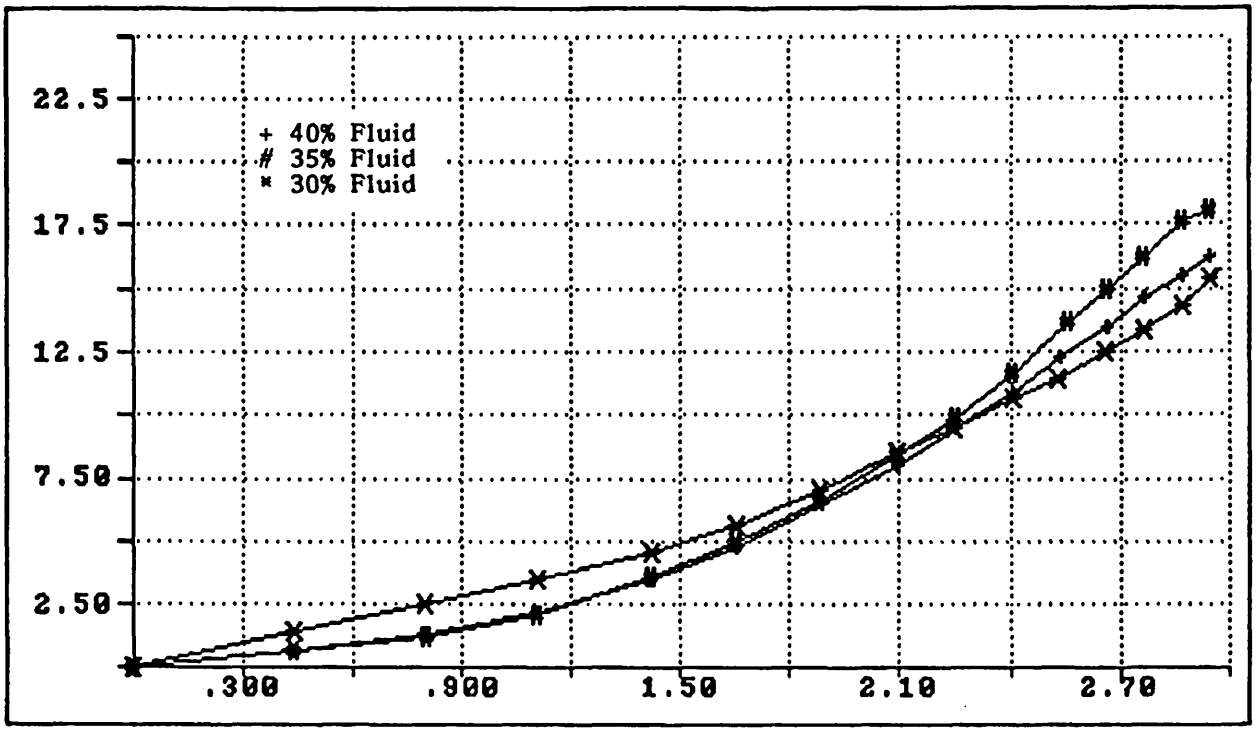
FIGURE 23b PLOT OF SHEAR STRESS versus SHEAR RATE



Fluids 50LV based
Temperature 20 degC
Field 2.66 kV/mm

X Axis 1*e4 s-1
Y Axis kPa
Flow Rig

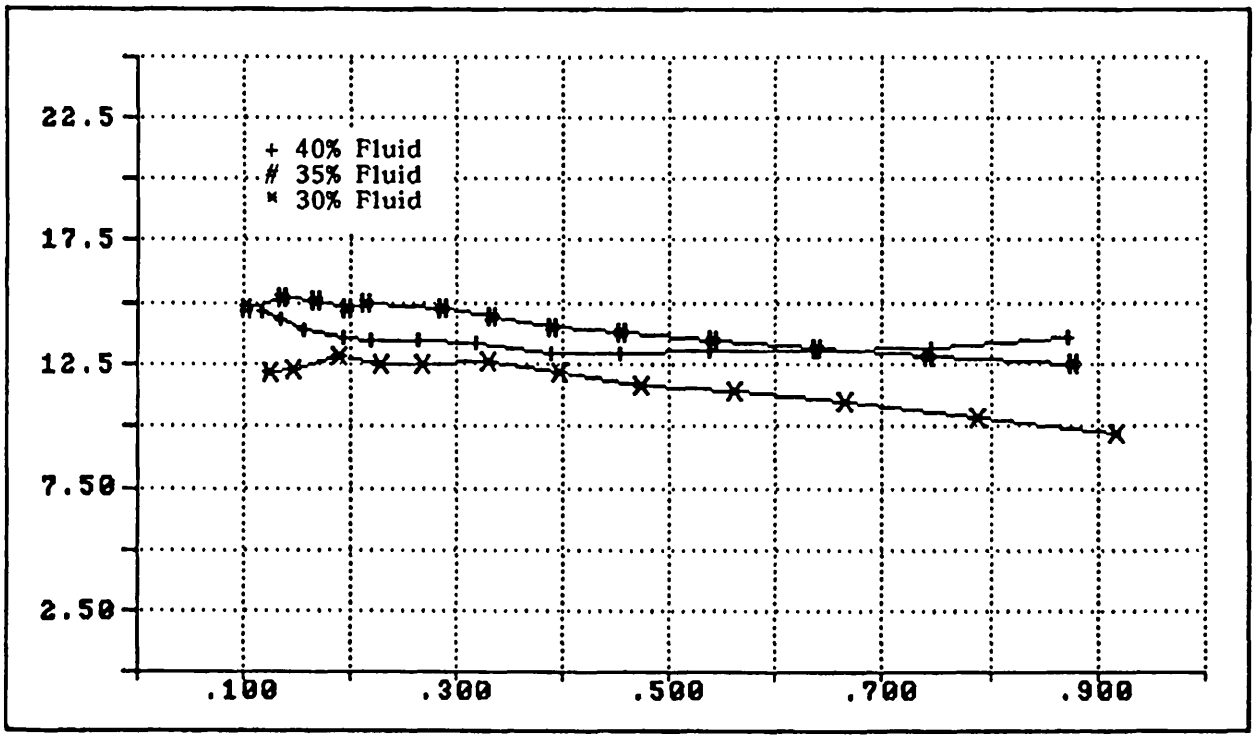
FIGURE 24a PLOT OF CURRENT DENSITY versus FIELD STRENGTH



Fluids 50LV based
Temperature 20 degC
Shear Rate 2200 sec-1

X Axis kV/mm
Y Axis uA/cm2
Flow Rig

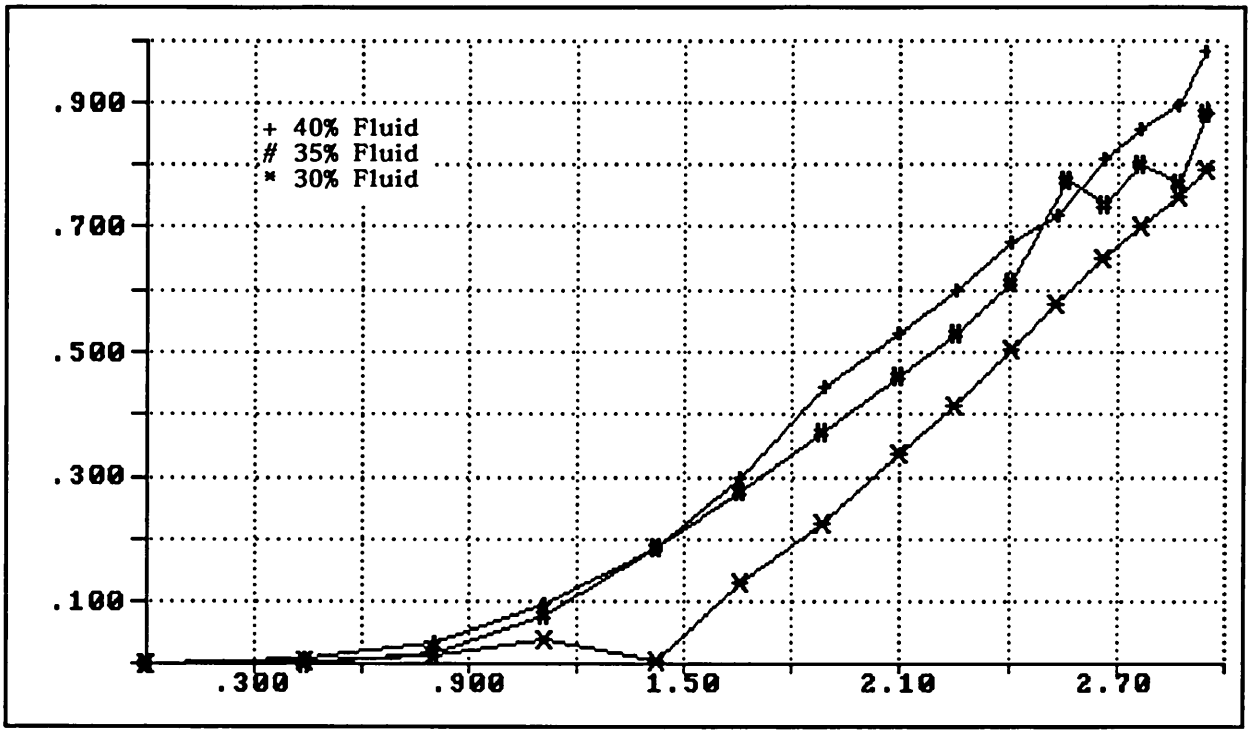
FIGURE 24b PLOT OF CURRENT DENSITY versus SHEAR RATE



Fluids 50LV based
Temperature 20 degC
Field 2.66 kV/mm

X Axis 1* e4 s-1
Y Axis uA/cm2
Flow Rig

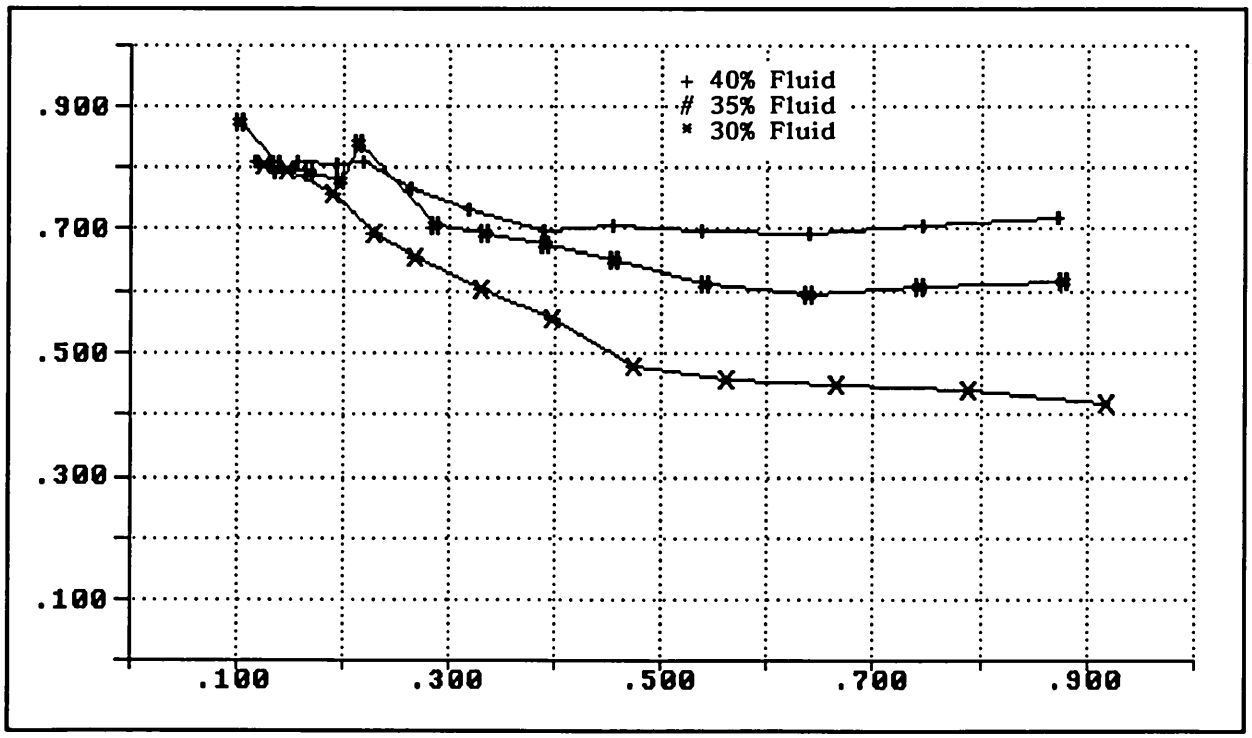
FIGURE 25a PLOT OF NORMALISED SHEAR STRESS versus FIELD STRENGTH



Fluids 50LV based
Temperature 20 degC
Shear Rate 2200 sec-1

X Axis kV/mm
Y Axis kPa Norm
Flow Rig

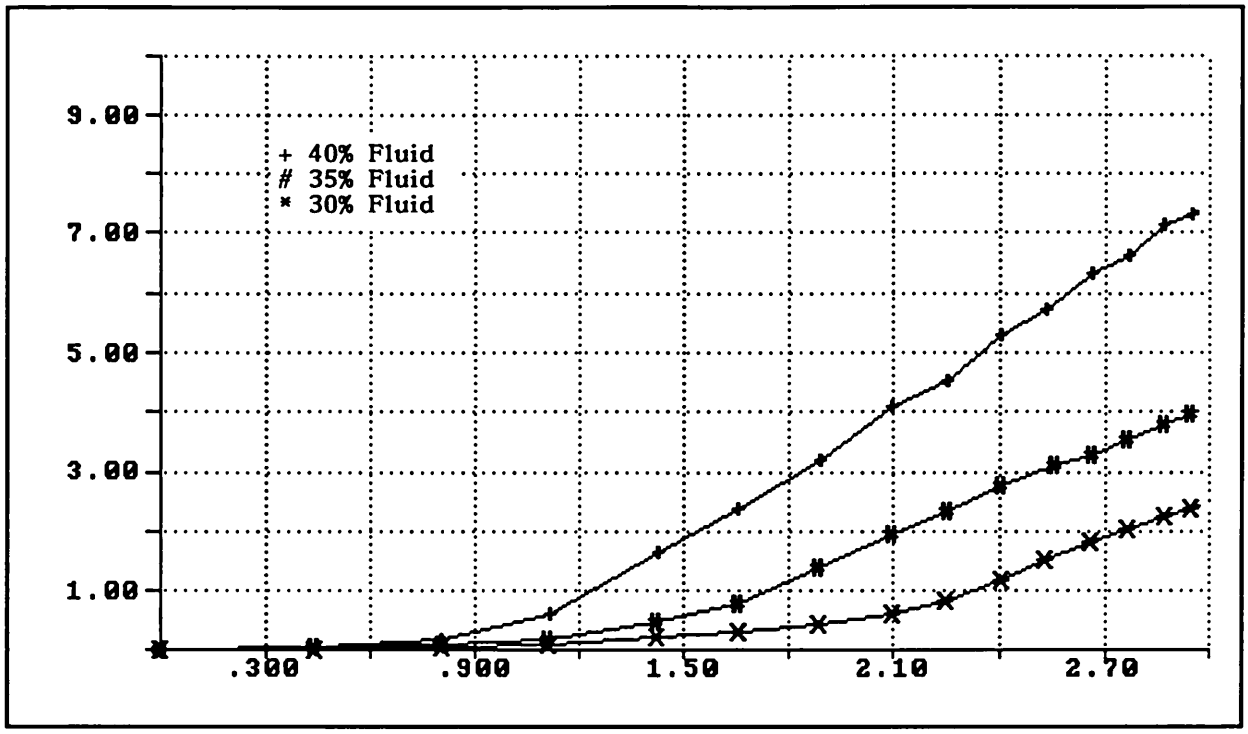
FIGURE 25b PLOT OF NORMALISED SHEAR STRESS versus SHEAR RATE



Fluids 50LV based
Temperature 20 degC
Field 2.66 kV/mm

X Axis 1*e4 s-1
Y Axis kPa Norm
Flow Rig

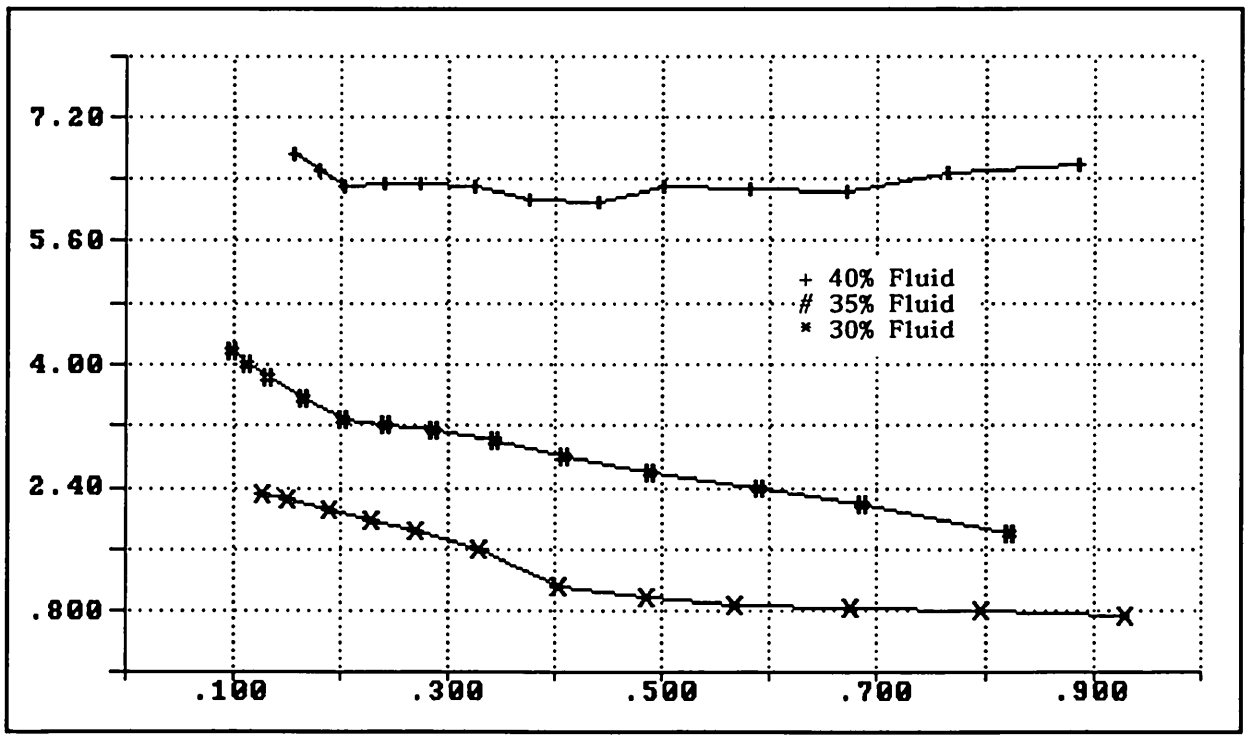
FIGURE 26a PLOT OF SHEAR STRESS versus FIELD STRENGTH



Fluids 50LV based
Temperature 15 degC
Shear Rate 2200 sec-1

X Axis kV/mm
Y Axis kPa
Flow Rig

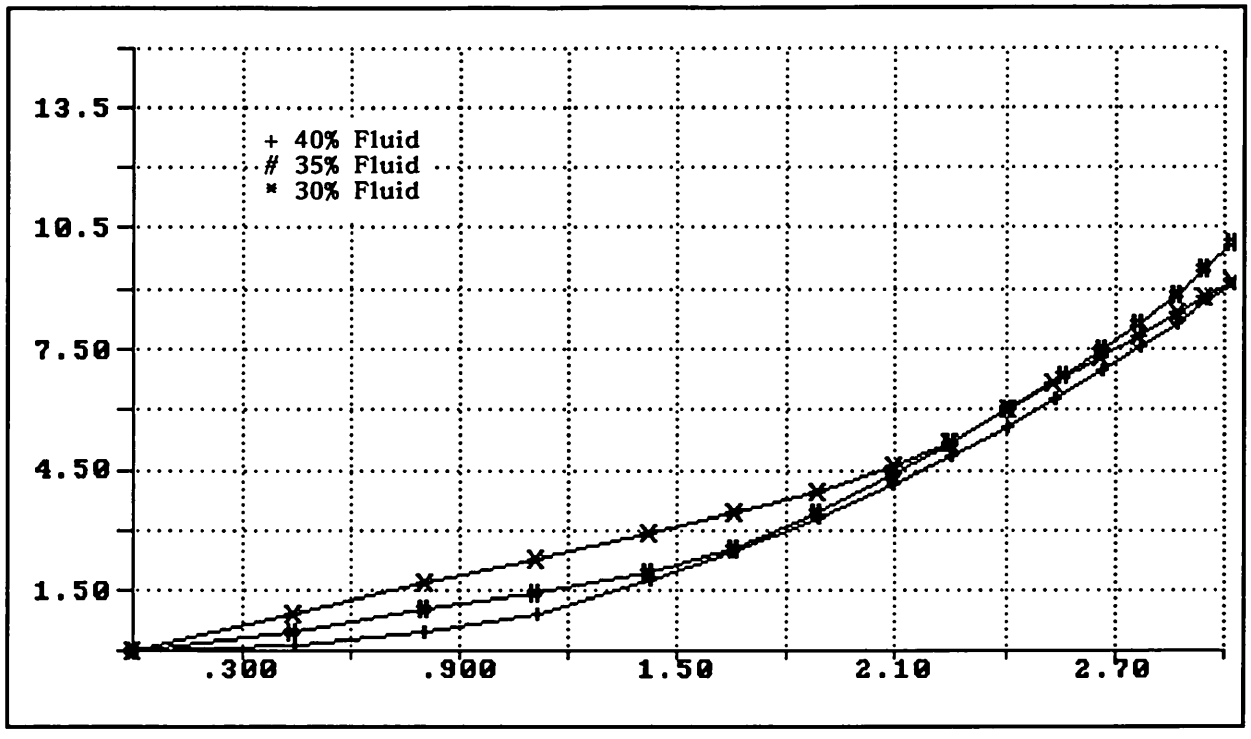
FIGURE 26b PLOT OF SHEAR STRESS versus SHEAR RATE



Fluids 50LV based
Temperature 15 degC
Field 2.66 kV/mm

X Axis 1*e4 s-1
Y Axis kPa
Flow Rig

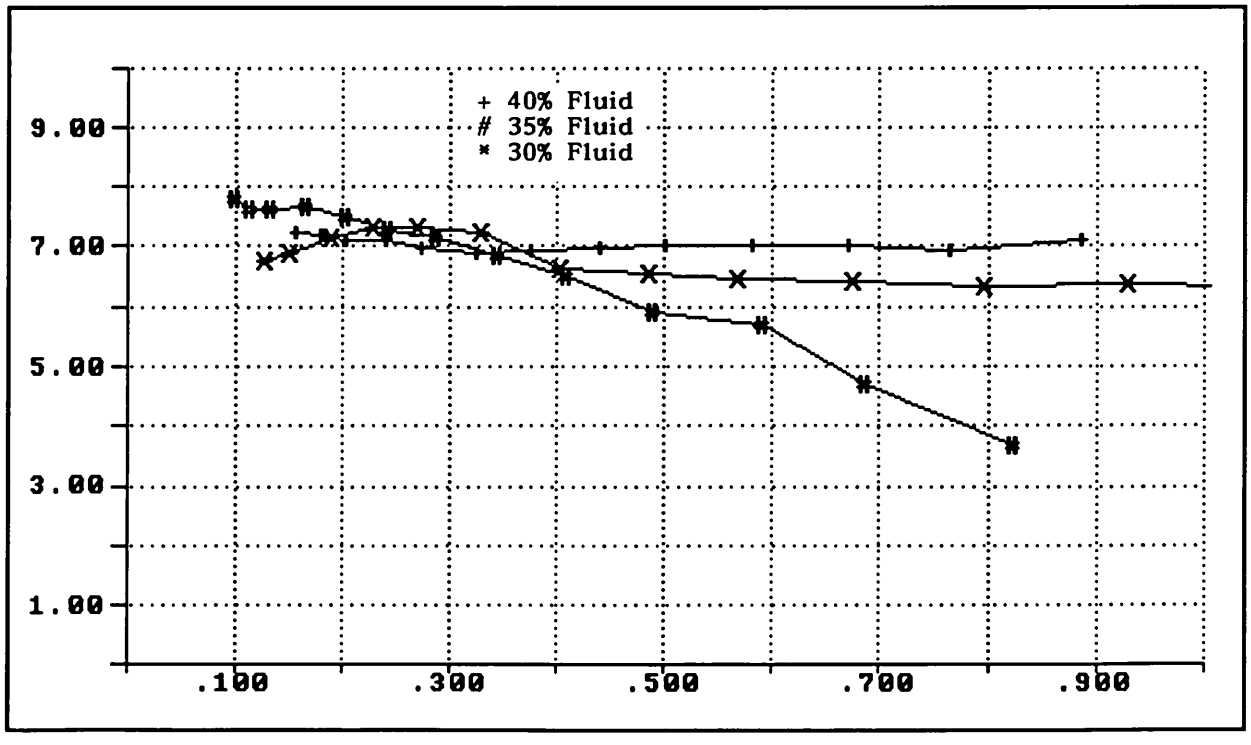
FIGURE 27a PLOT OF CURRENT DENSITY versus FIELD STRENGTH



Fluids 50LV based
Temperature 15 degC
Shear Rate 2200 sec-1

X Axis kV/mm
Y Axis uA/cm2
Flow Rig

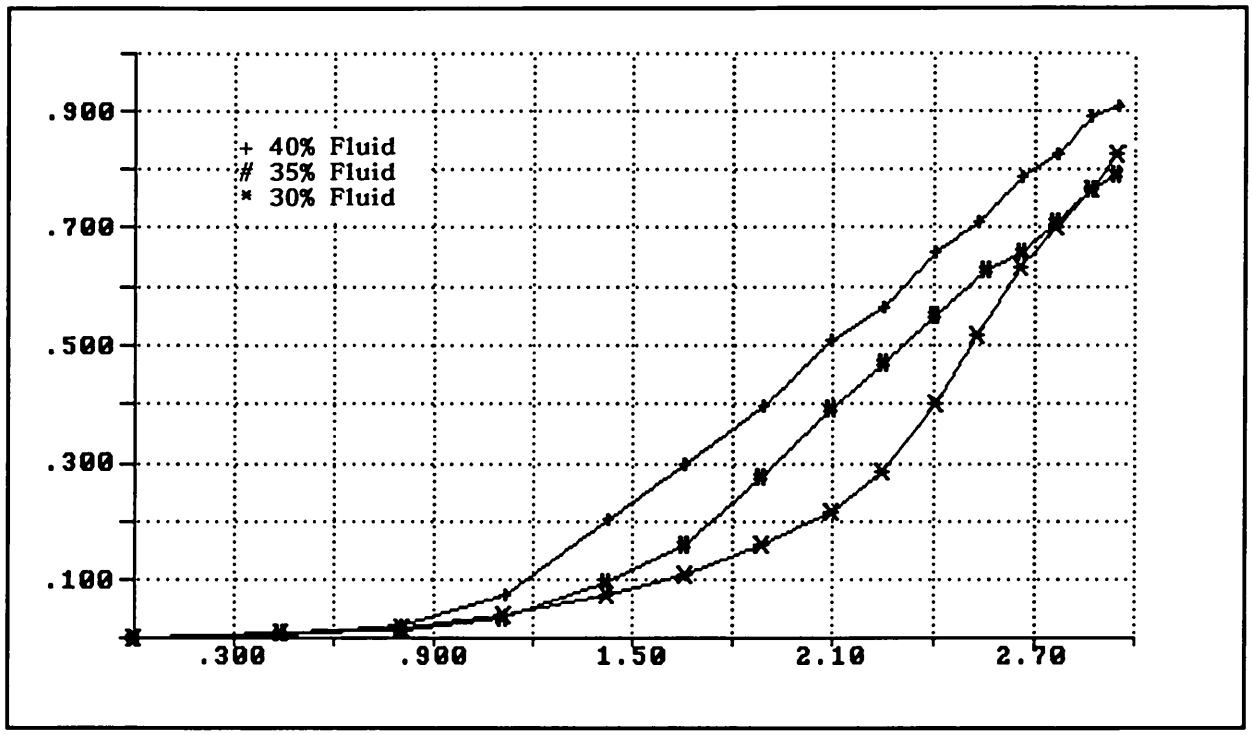
FIGURE 27b PLOT OF CURRENT DENSITY versus SHEAR RATE



Fluids 50LV based
Temperature 15 degC
Field 2.66 kV/mm

X Axis 1*e4 s-1
Y Axis uA/cm2
Flow Rig

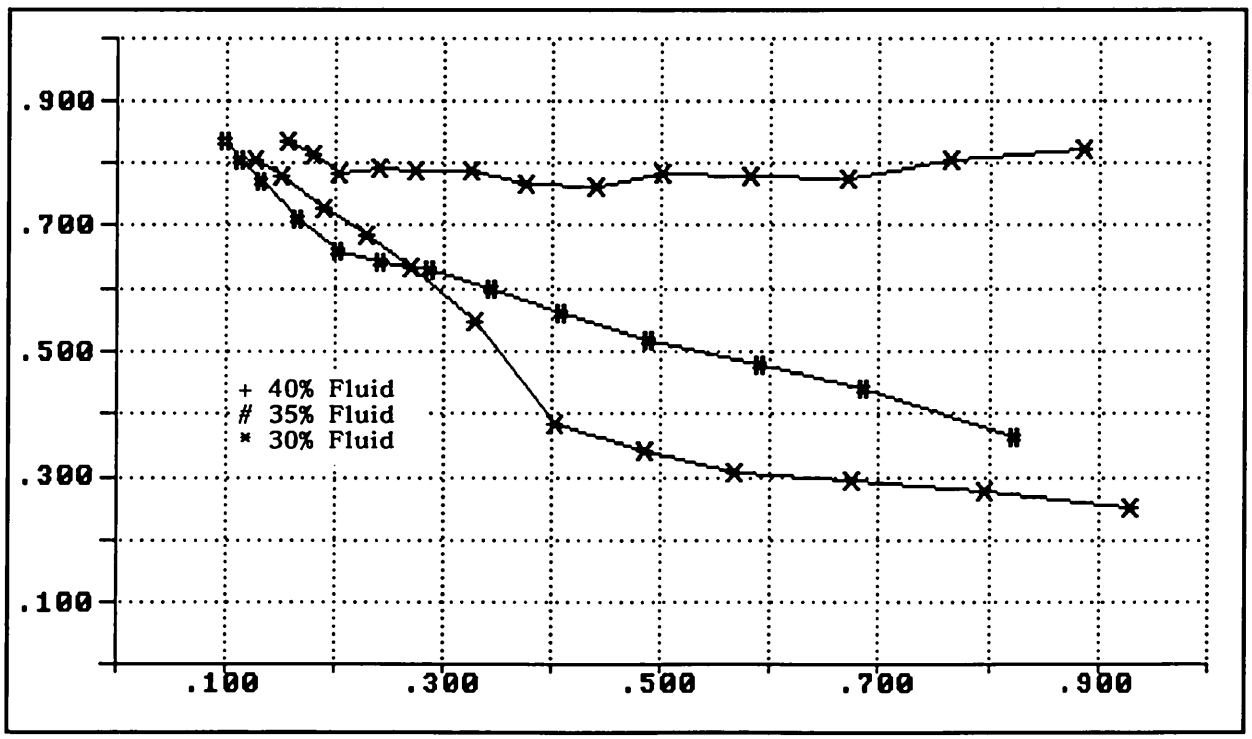
FIGURE 28a PLOT OF NORMALISED SHEAR STRESS versus FIELD STRENGTH



Fluids 50LV based
Temperature 15 degC
Shear Rate 2200 sec-1

X Axis kV/mm
Y Axis kPa Norm
Flow Rig

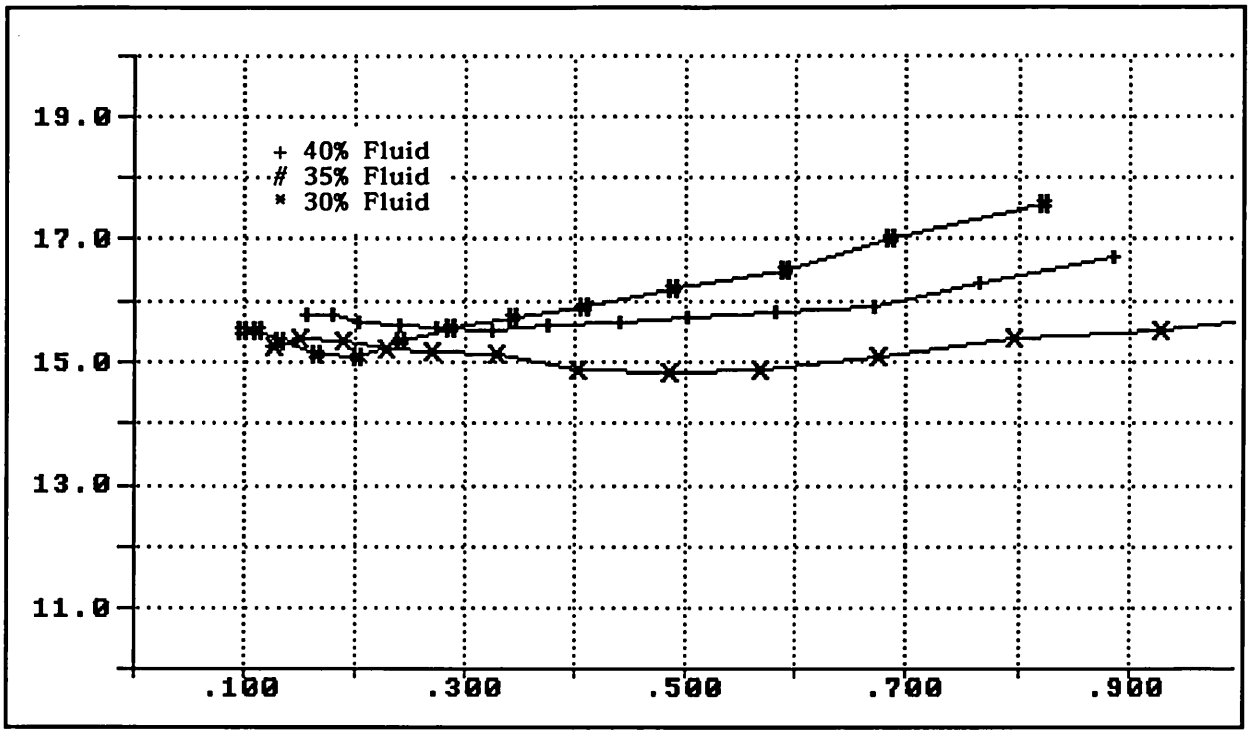
FIGURE 28b PLOT OF NORMALISED SHEAR STRESS versus SHEAR RATE



Fluids 50LV based
Temperature 15 degC
Field 2.66 kV/mm

X Axis 1*e4 s-1
Y Axis kPa Norm
Flow Rig

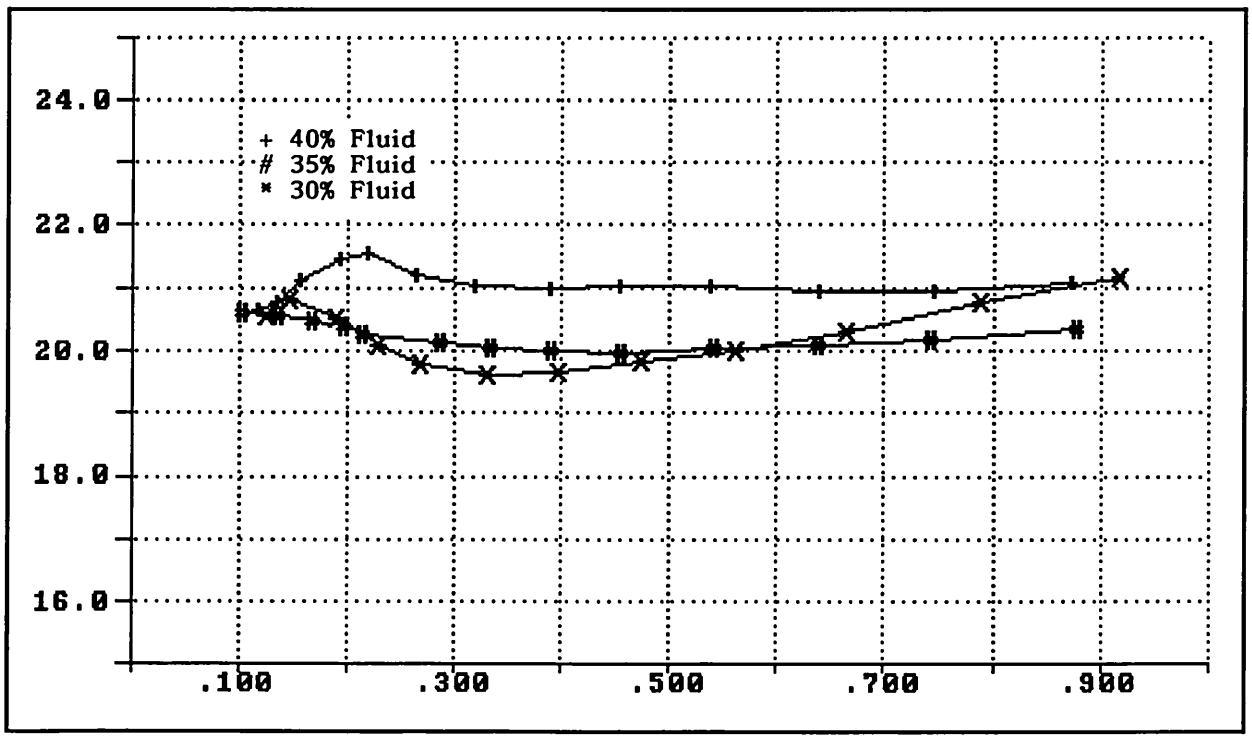
FIGURE 29a PLOT OF TEMPERATURE versus SHEAR RATE



Fluids 50LV based
Temperature 15 degC
Field 2.66 kV/mm

X Axis 10e4*s-1
Y Axis degC
Flow Rig

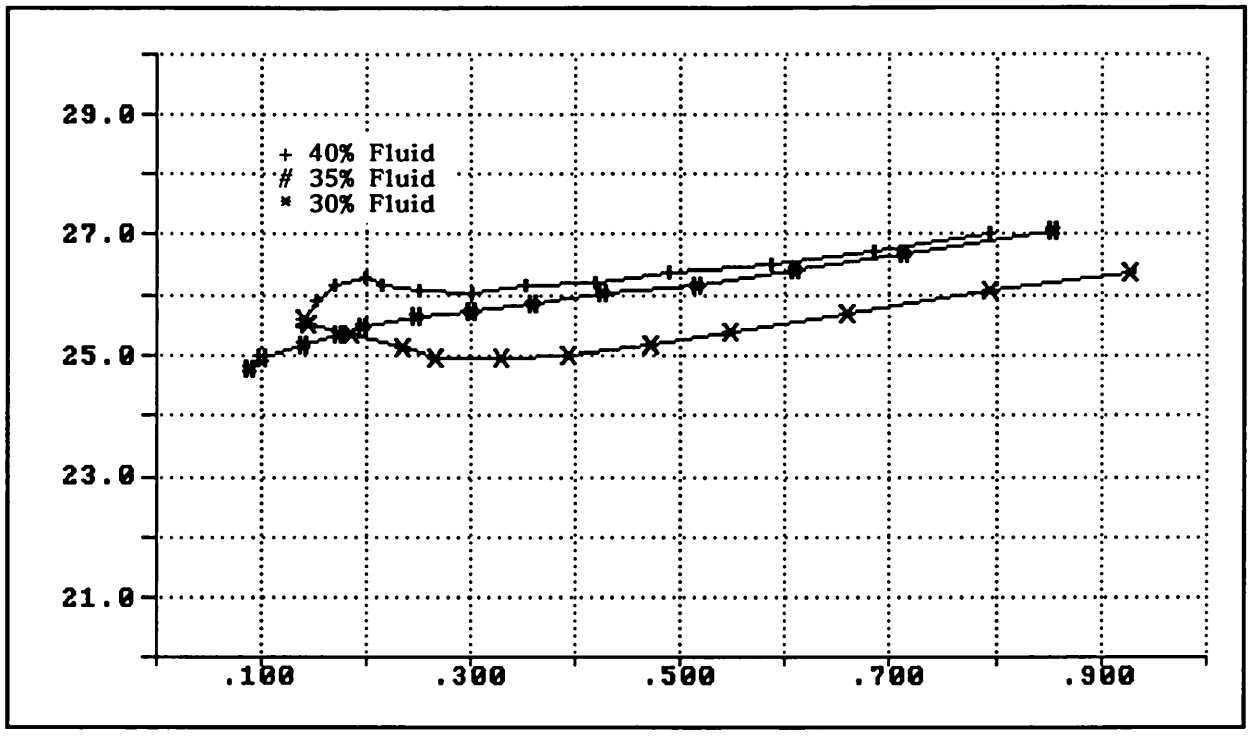
FIGURE 29b PLOT OF TEMPERATURE versus SHEAR RATE



Fluids 50LV based
Temperature 20 degC
Field 2.66 kV/mm

X Axis 1*e4 s-1
Y Axis degC
Flow Rig

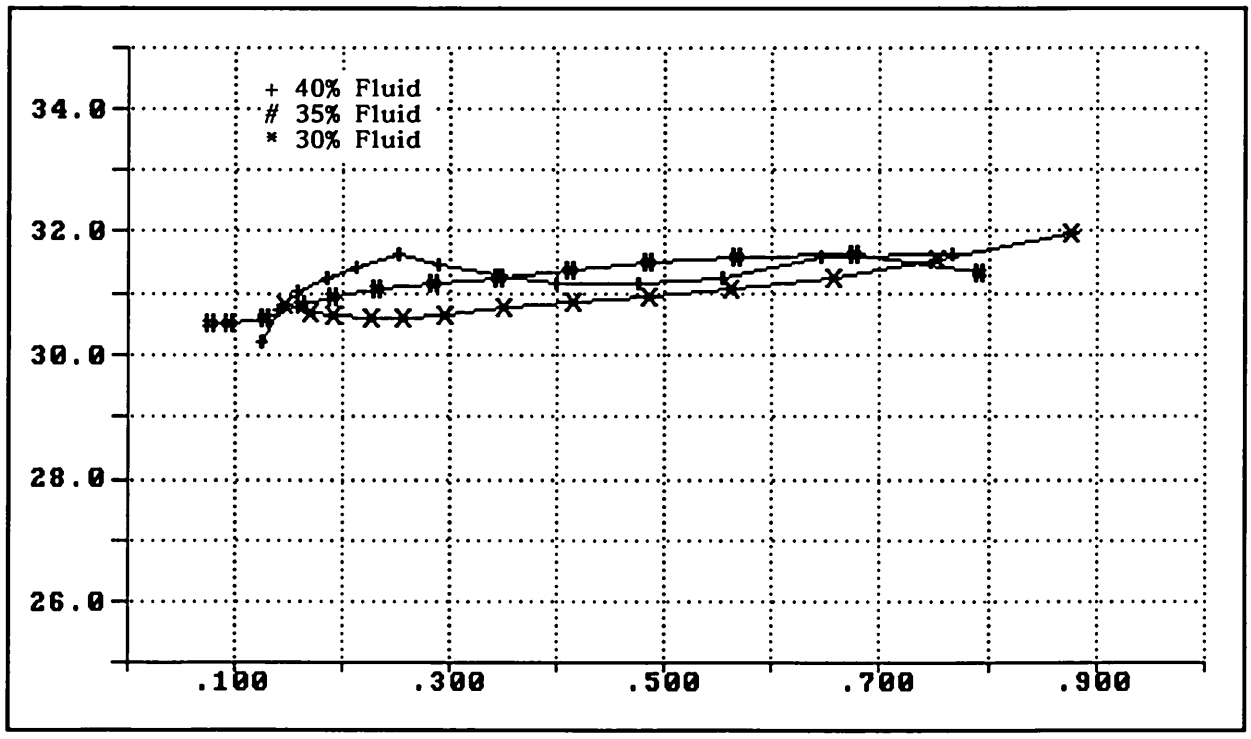
FIGURE 30a PLOT OF TEMPERATURE versus SHEAR RATE



Fluids 50LV based
Temperature 25 degC
Field 2.66 kV/mm

X Axis 10e4*s-1
Y Axis degC
Flow Rig

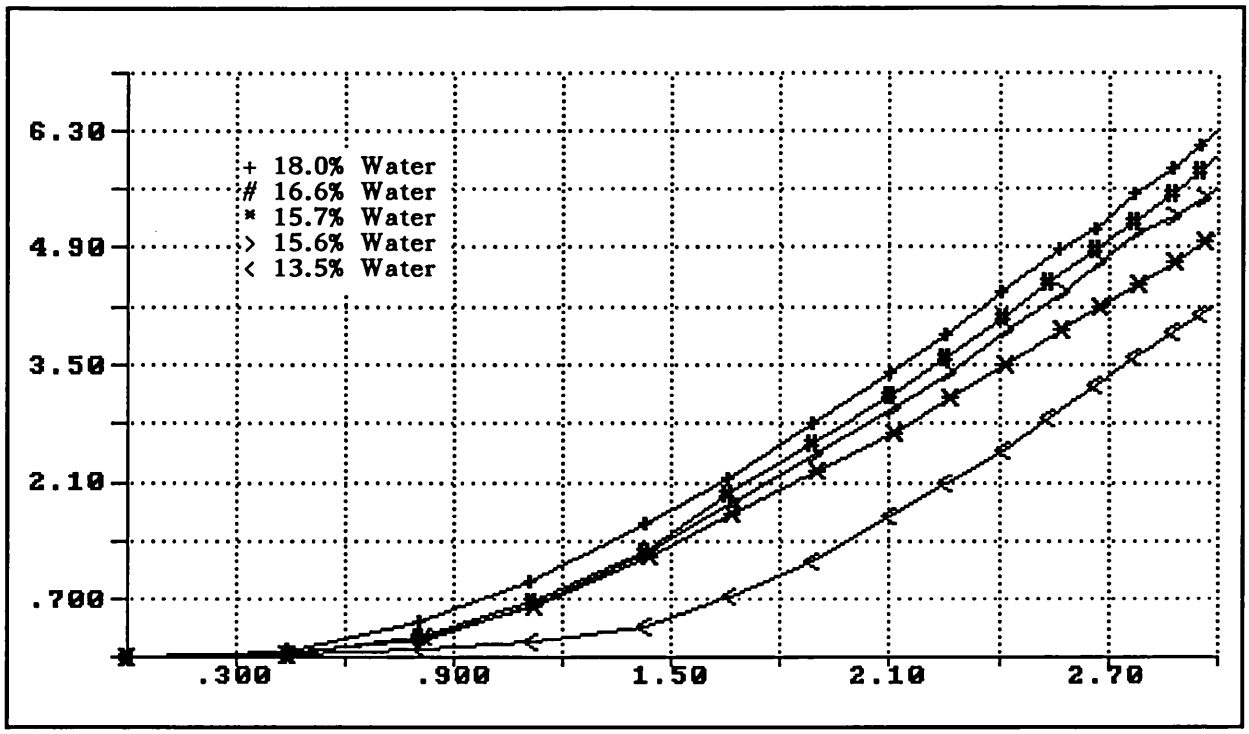
FIGURE 30b PLOT OF TEMPERATURE versus SHEAR RATE



Fluids 50LV based
Temperature 30 degC
Field 2.66 kV/mm

X Axis 1*e4 s-1
Y Axis degC
Flow Rig

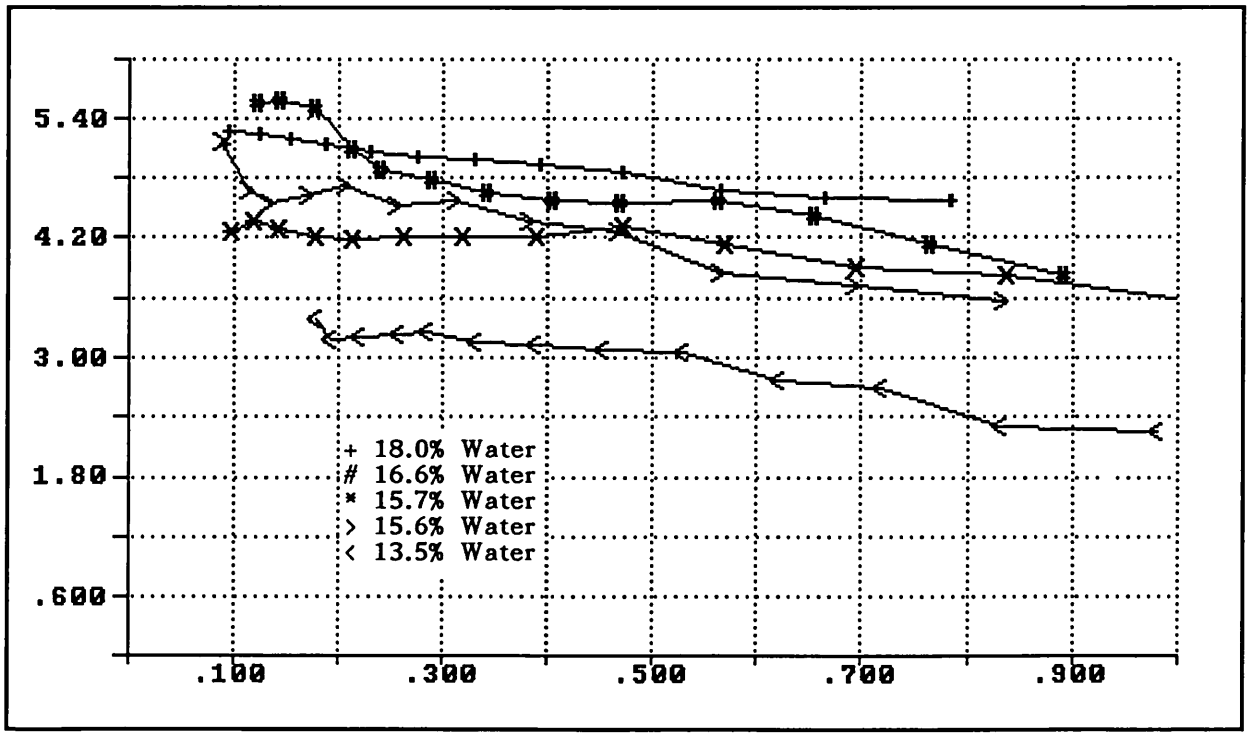
FIGURE 31a PLOT OF SHEAR STRESS versus FIELD STRENGTH



Fluids 50LV Based
Temperature 30 C
Shear Rate 2200 sec-1

X Axis kV/mm
Y Axis kPa
Flow Rig

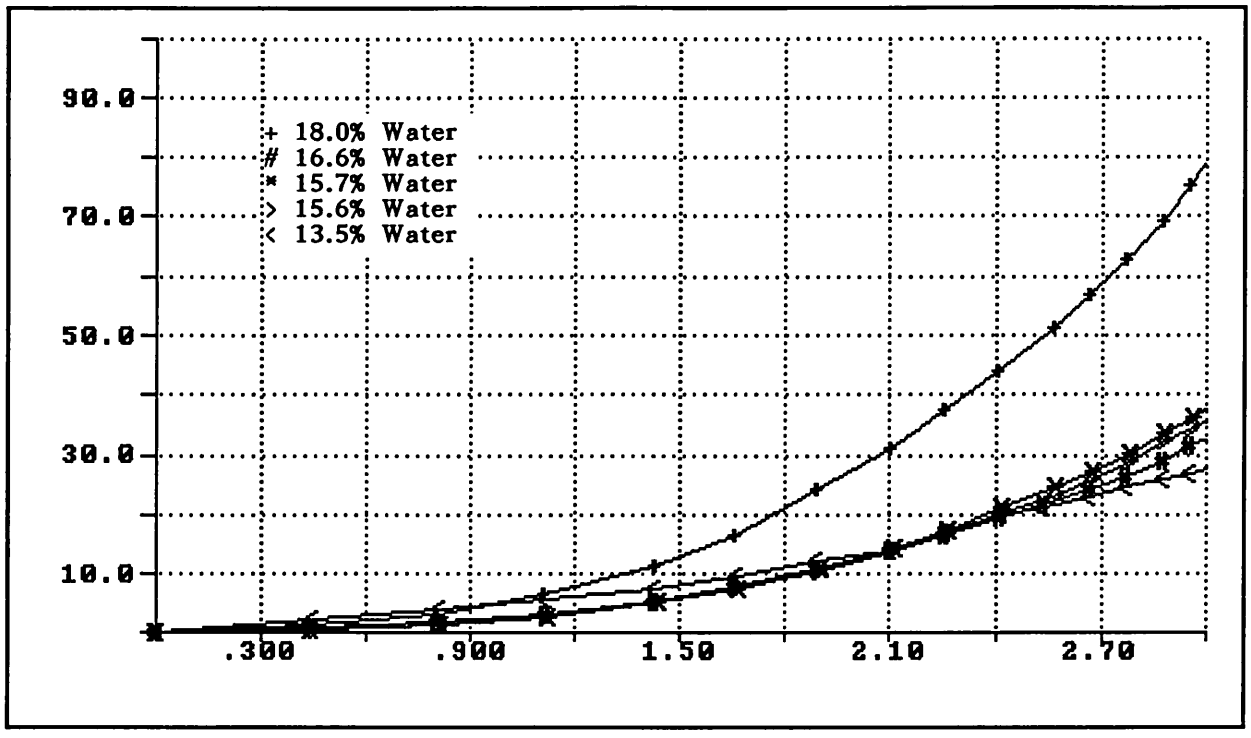
FIGURE 31b PLOT OF SHEAR STRESS versus SHEAR RATE



Fluids 50LV Based
Temperature 30 C
Field 2.66 kV/mm

X Axis 1*e4 s-1
Y Axis kPa
Flow Rig

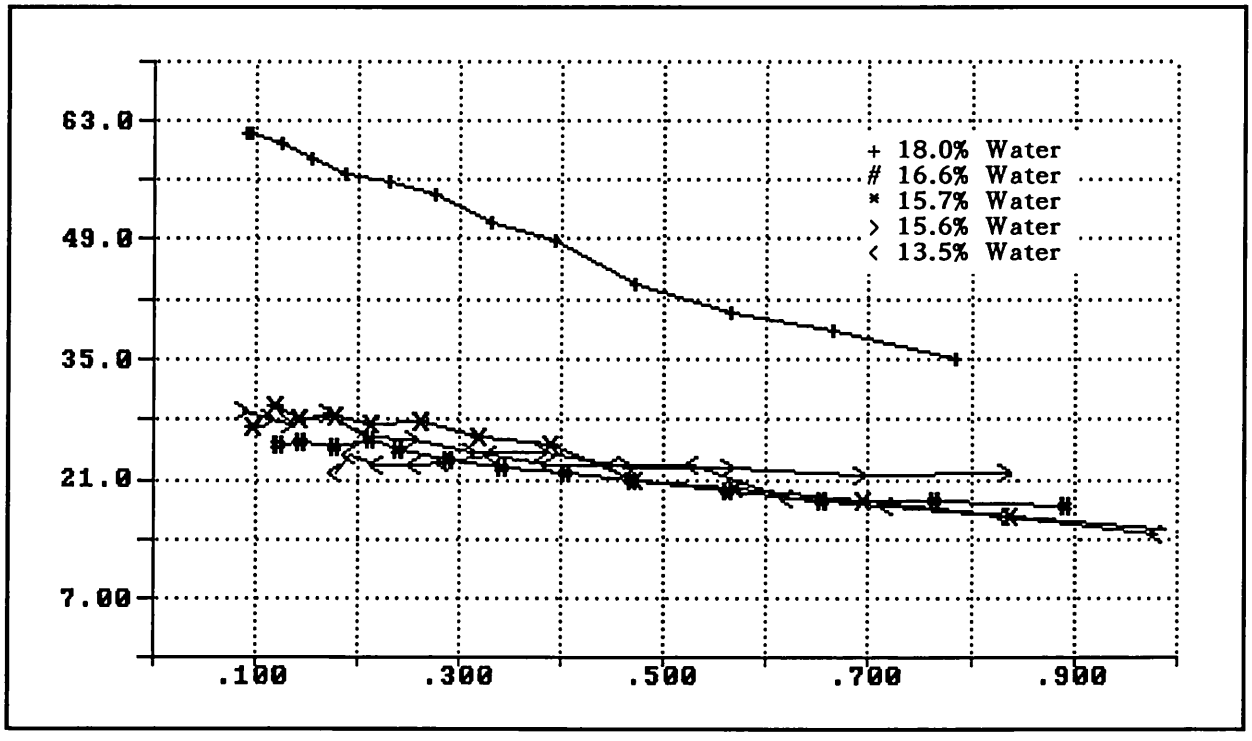
FIGURE 32a PLOT OF CURRENT DENSITY versus FIELD STRENGTH



Fluids 50LV Based
Temperature 30 C
Shear Rate 2200 sec-1

X Axis kV/mm
Y Axis uA/cm2
Flow Rig

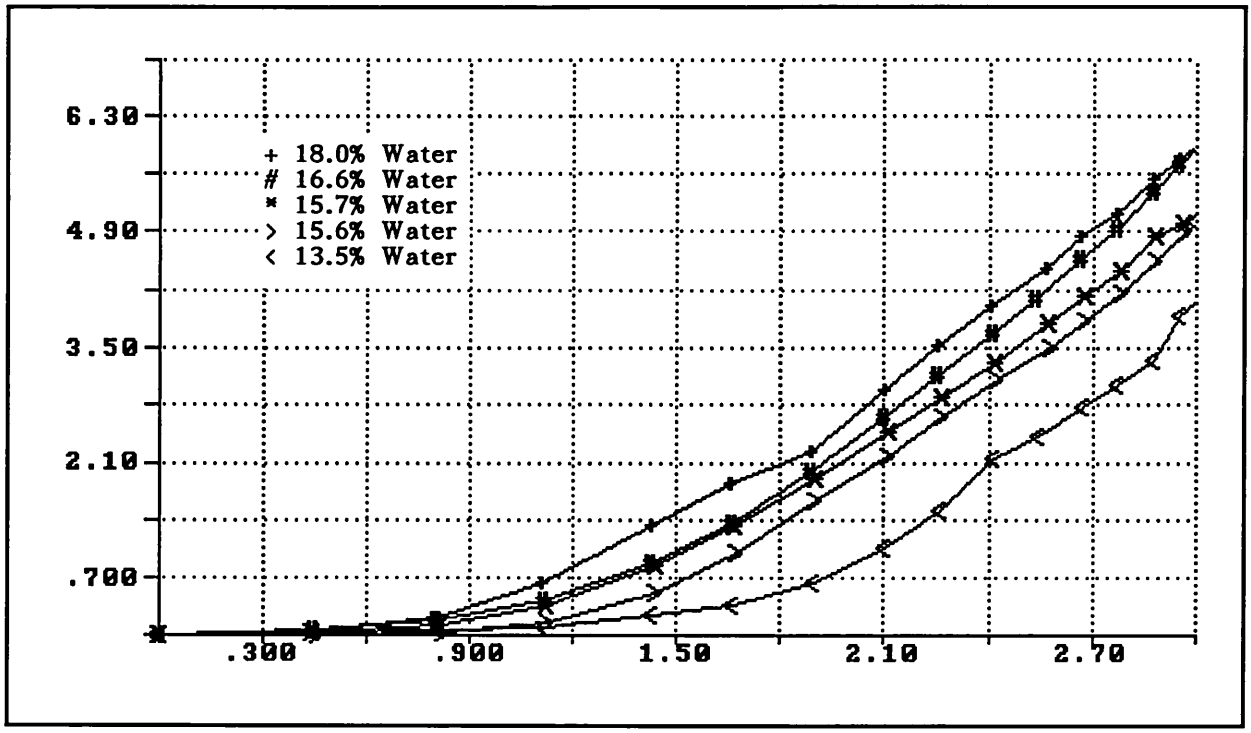
FIGURE 32b PLOT OF CURRENT DENSITY versus SHEAR RATE



Fluids 50LV Based
Temperature 30 C
Field 2.66 kV/mm

X Axis 1*e4 s-1
Y Axis uA/cm2
Flow Rig

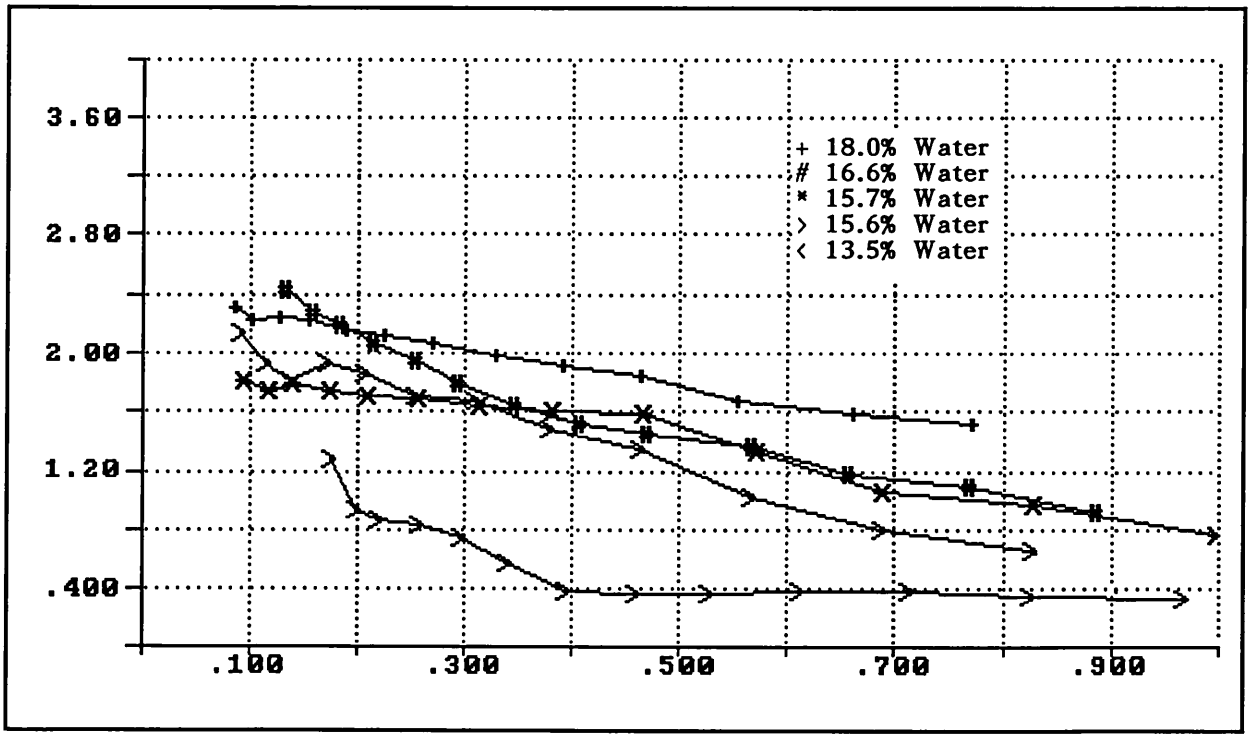
FIGURE 33a PLOT OF SHEAR STRESS versus FIELD STRENGTH



Fluids 50LV Based
Temperature 30 C
Shear Rate 5750 sec-1

X Axis kV/mm
Y Axis kPa
Flow Rig

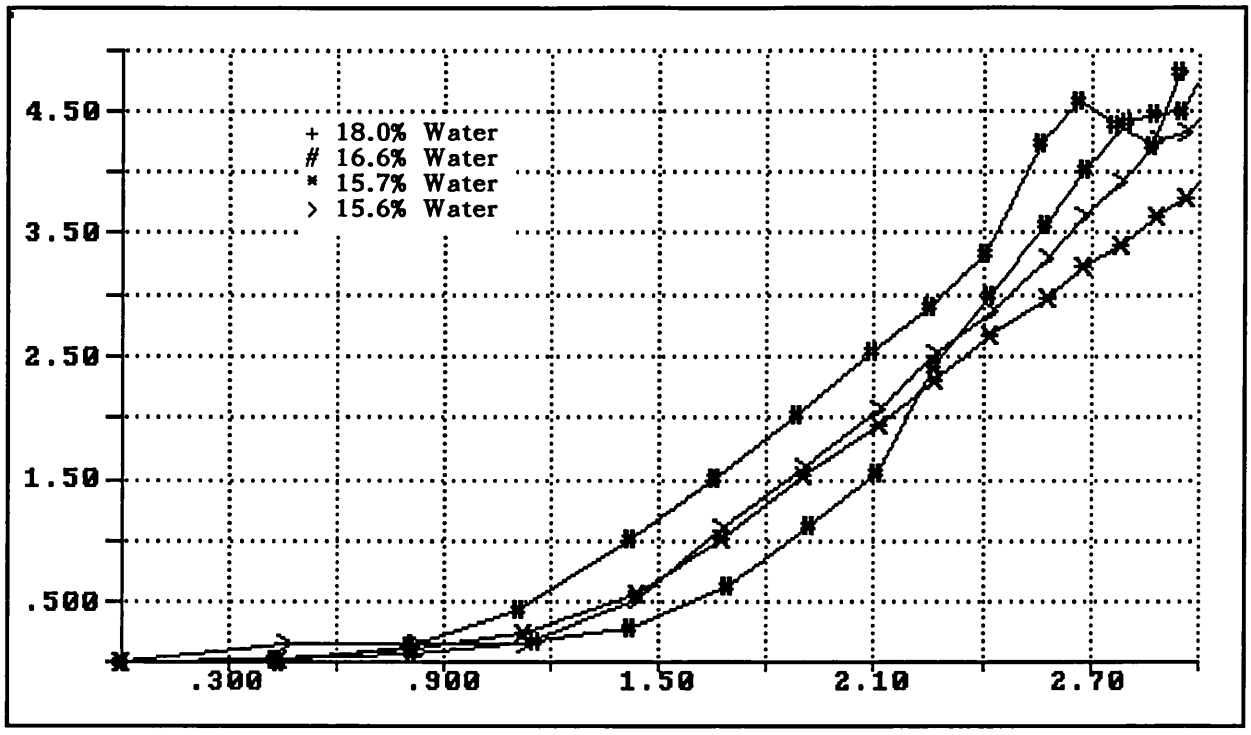
FIGURE 33b PLOT OF SHEAR STRESS versus SHEAR RATE



Fluids 50LV Based
Temperature 30 C
Field 1.66 kV/mm

X Axis 1*e4 s-1
Y Axis kPa
Flow Rig

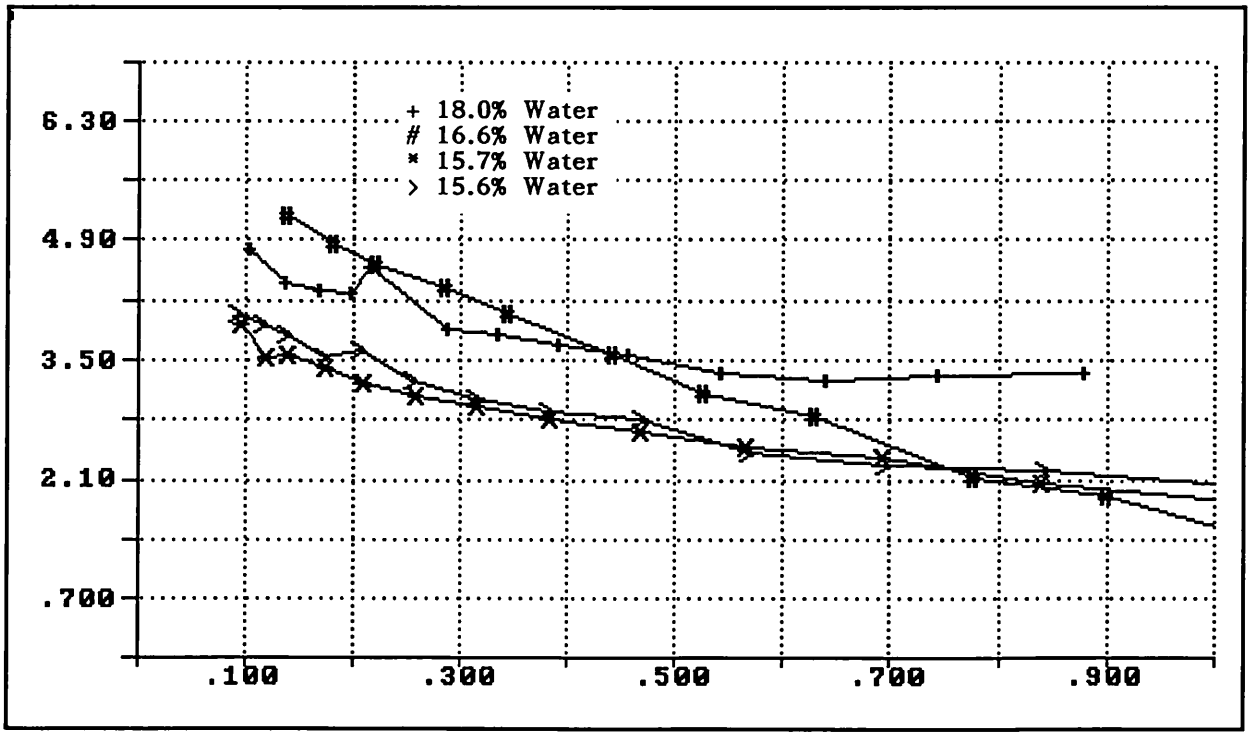
FIGURE 34a PLOT OF SHEAR STRESS versus FIELD STRENGTH



Fluids 50LV Based
Temperature 20 C
Shear Rate 2200 sec-1

X Axis kV/mm
Y Axis kPa
Flow Rig

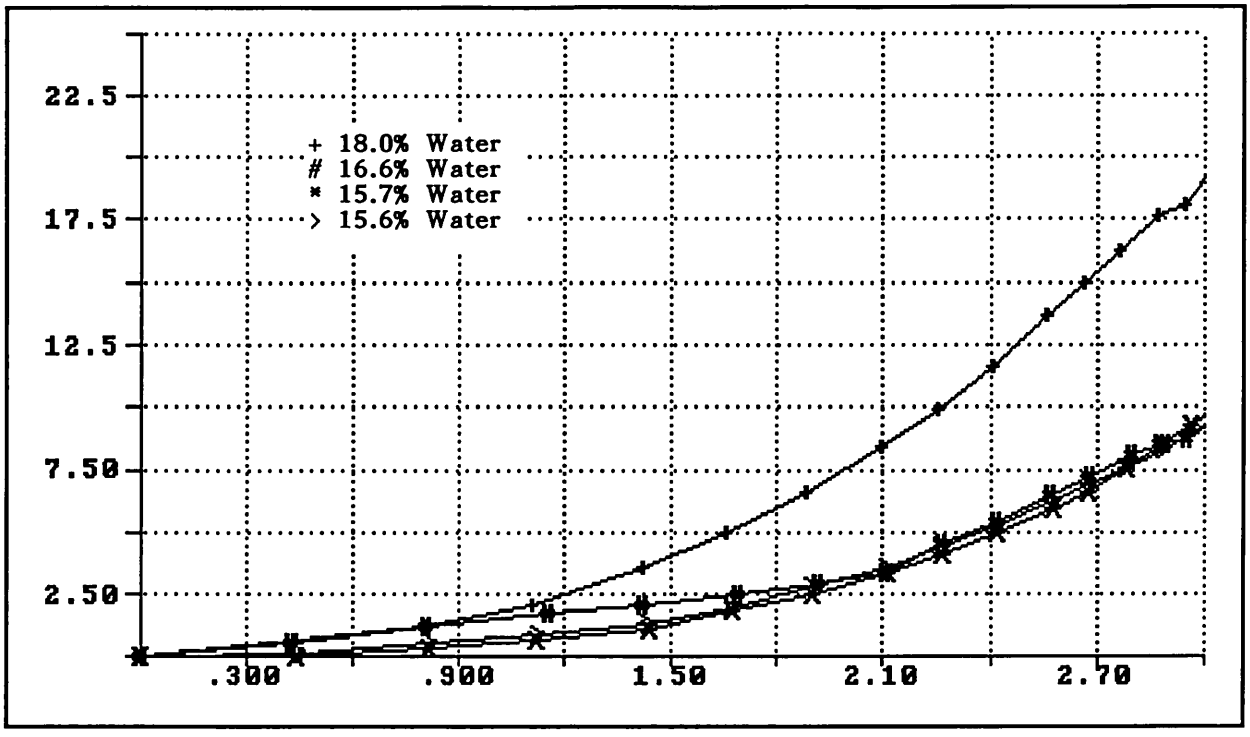
FIGURE 34b PLOT OF SHEAR STRESS versus SHEAR RATE



Fluids 50LV Based
Temperature 20 C
Field 2.66 kV/mm

X Axis 1*e4 s-1
Y Axis kPa
Flow Rig

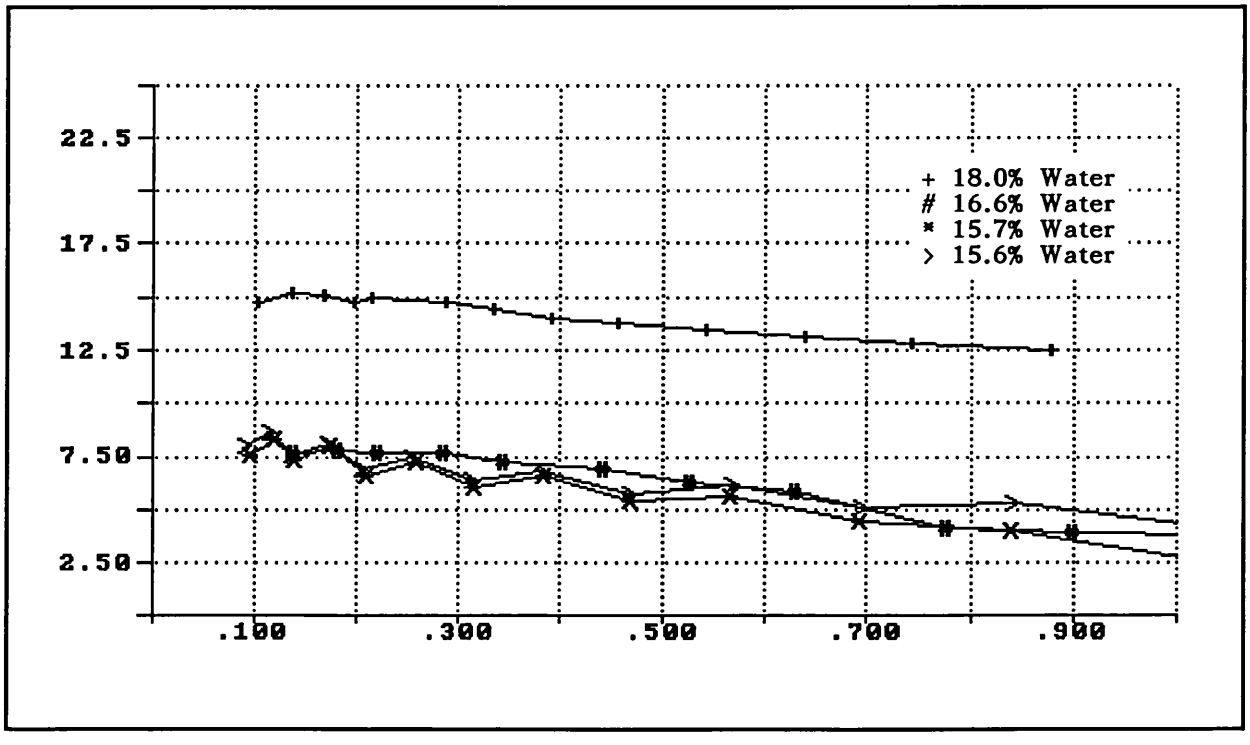
FIGURE 35a PLOT OF CURRENT DENSITY versus FIELD STRENGTH



Fluids 50LV Based
Temperature 20 C
Shear Rate 2200 sec-1

X Axis kV/mm
Y Axis uA/cm2
Flow Rig

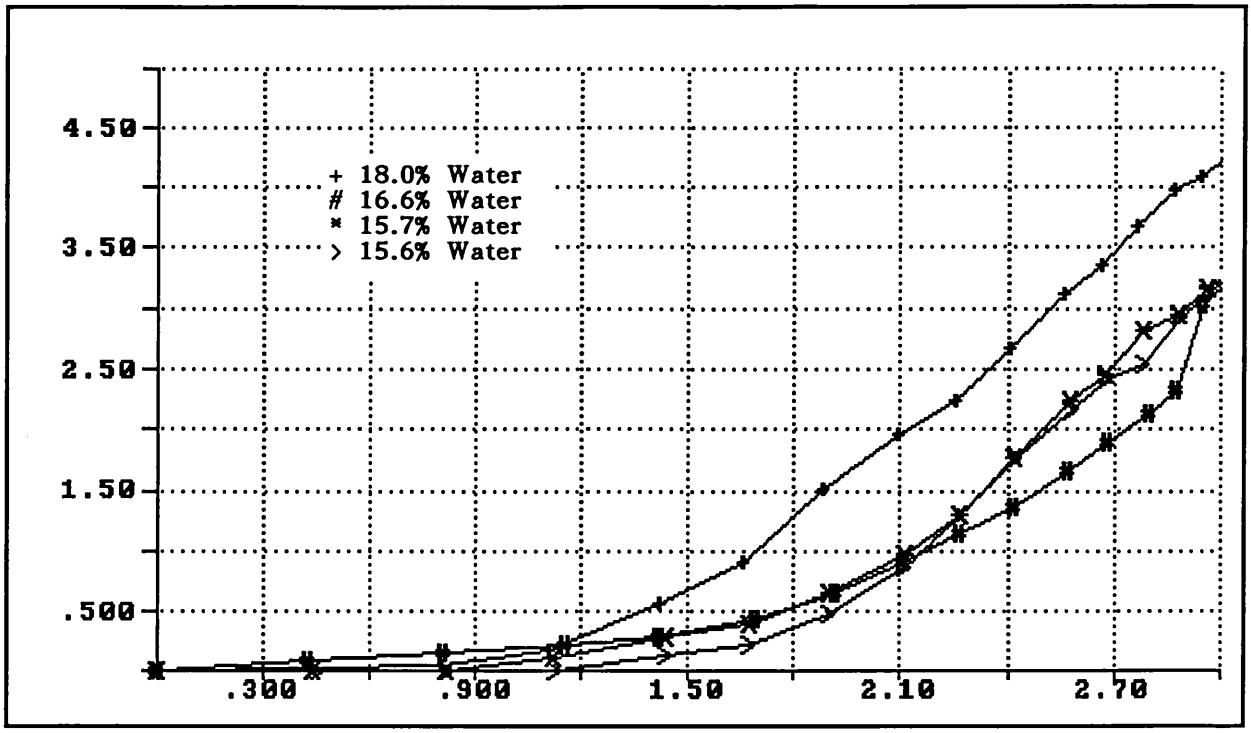
FIGURE 35b PLOT OF CURRENT DENSITY versus SHEAR RATE



Fluids 50LV Based
Temperature 20 C
Field 2.66 kV/mm

X Axis 1*e4 s-1
Y Axis uA/cm2
Flow Rig

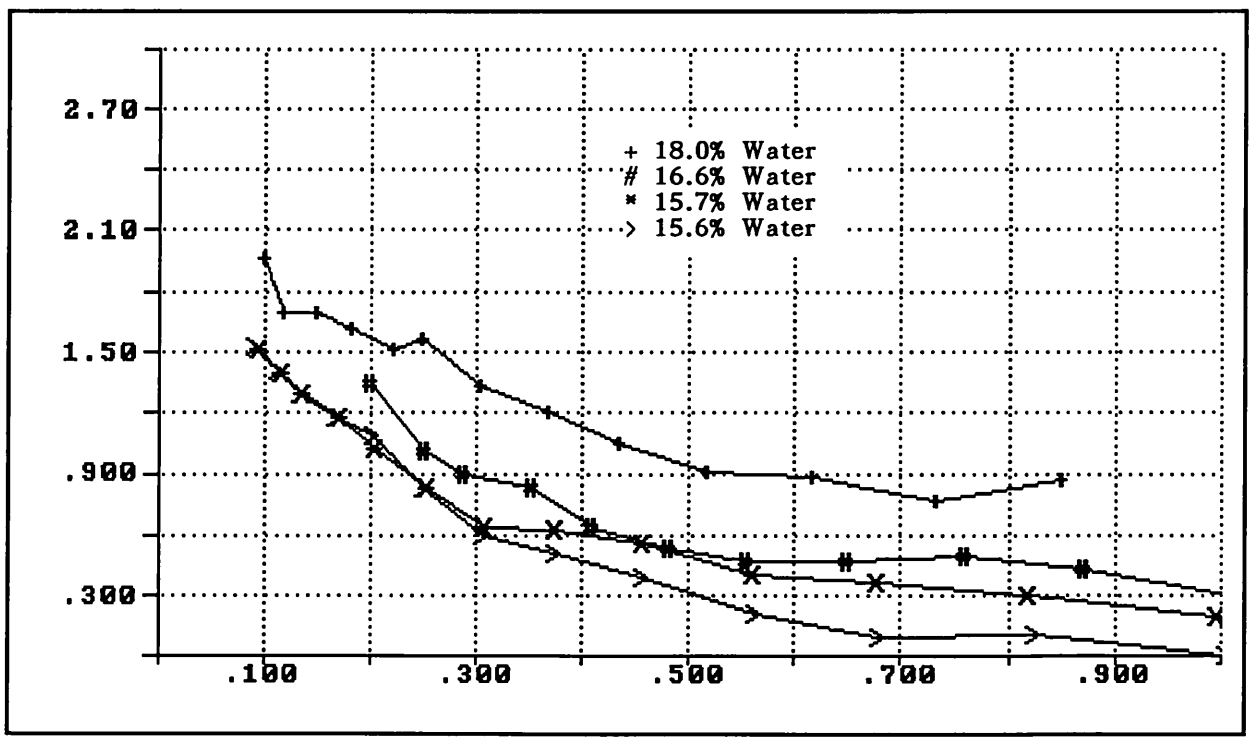
FIGURE 36a PLOT OF SHEAR STRESS versus FIELD STRENGTH



Fluids 50LV Based
Temperature 20 C
Shear Rate 5750 sec-1

X Axis kV/mm
Y Axis kPa
Flow Rig

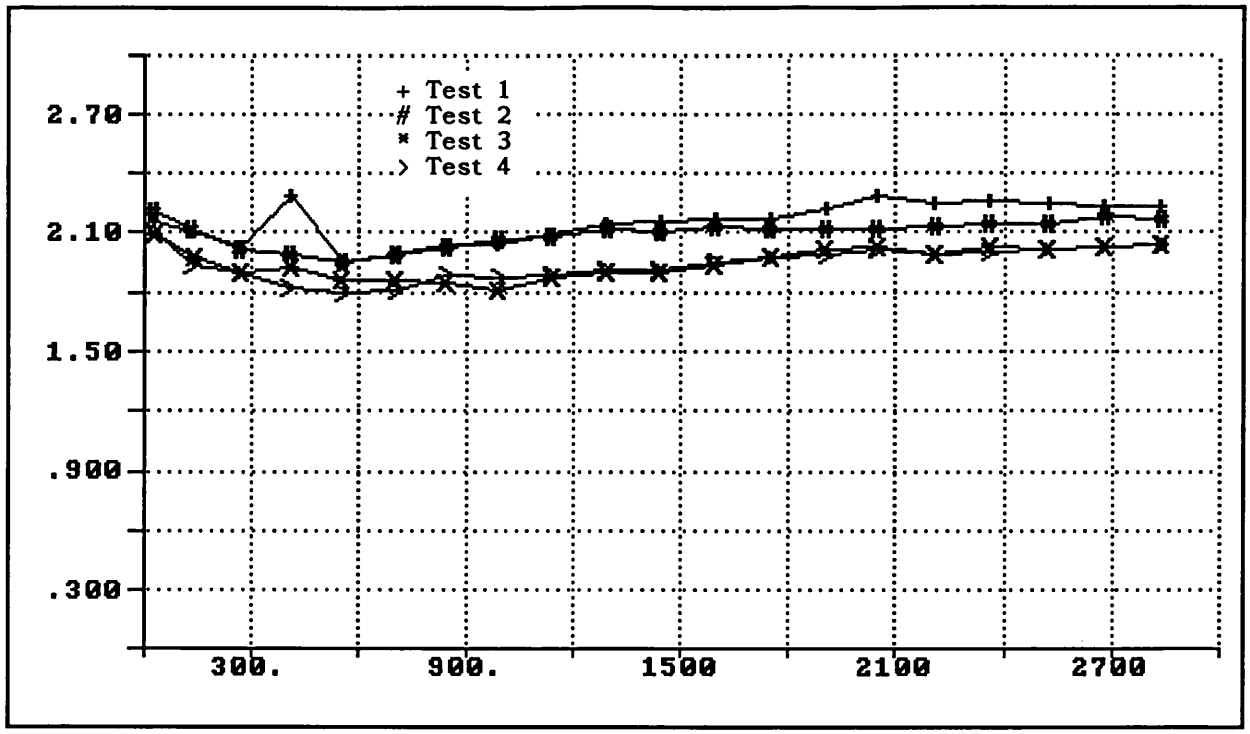
FIGURE 36b PLOT OF SHEAR STRESS versus SHEAR RATE



Fluids 50LV Based
Temperature 20 C
Field 1.66 kV/mm

X Axis 1*e4 s-1
Y Axis kPa
Flow Rig

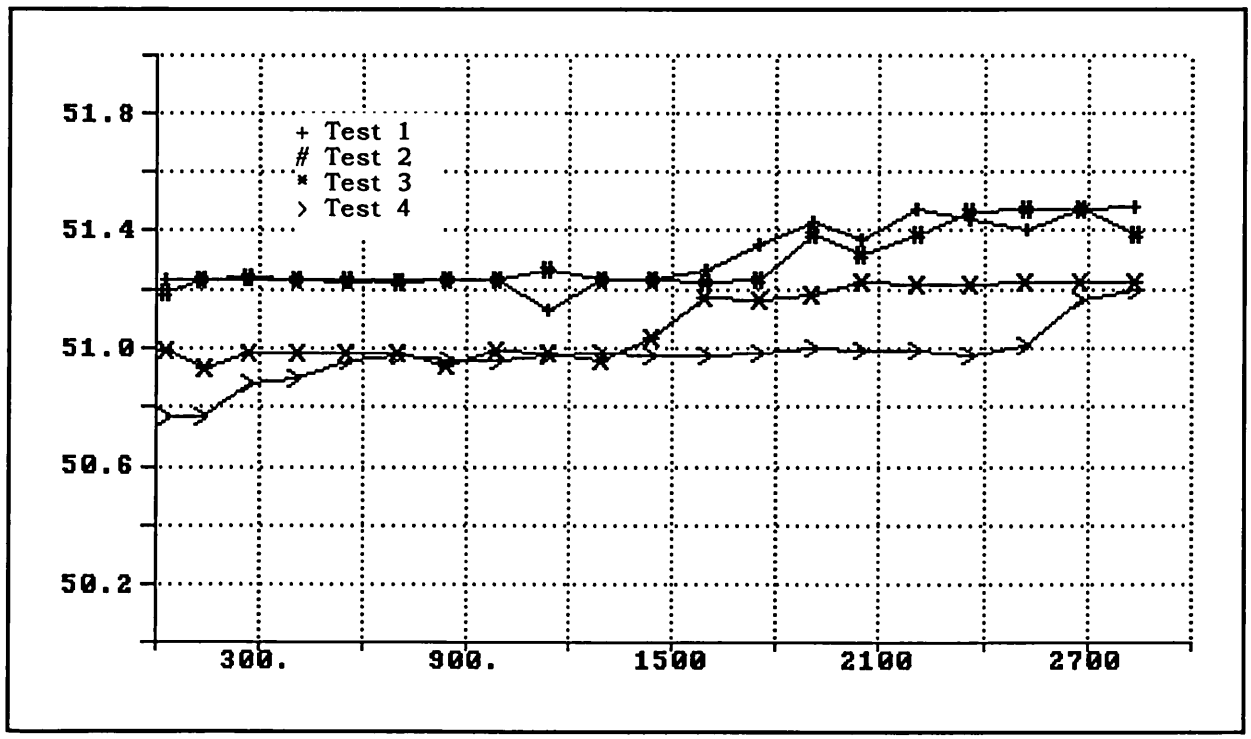
FIGURE 37a PLOT OF TOTAL SHEAR STRESS versus SHEAR RATE



Fluid 50LV/L35156
Temperature 50 C
Field 1.95 kV/mm

X Axis sec-1
Y Axis kPa
E.R.V.

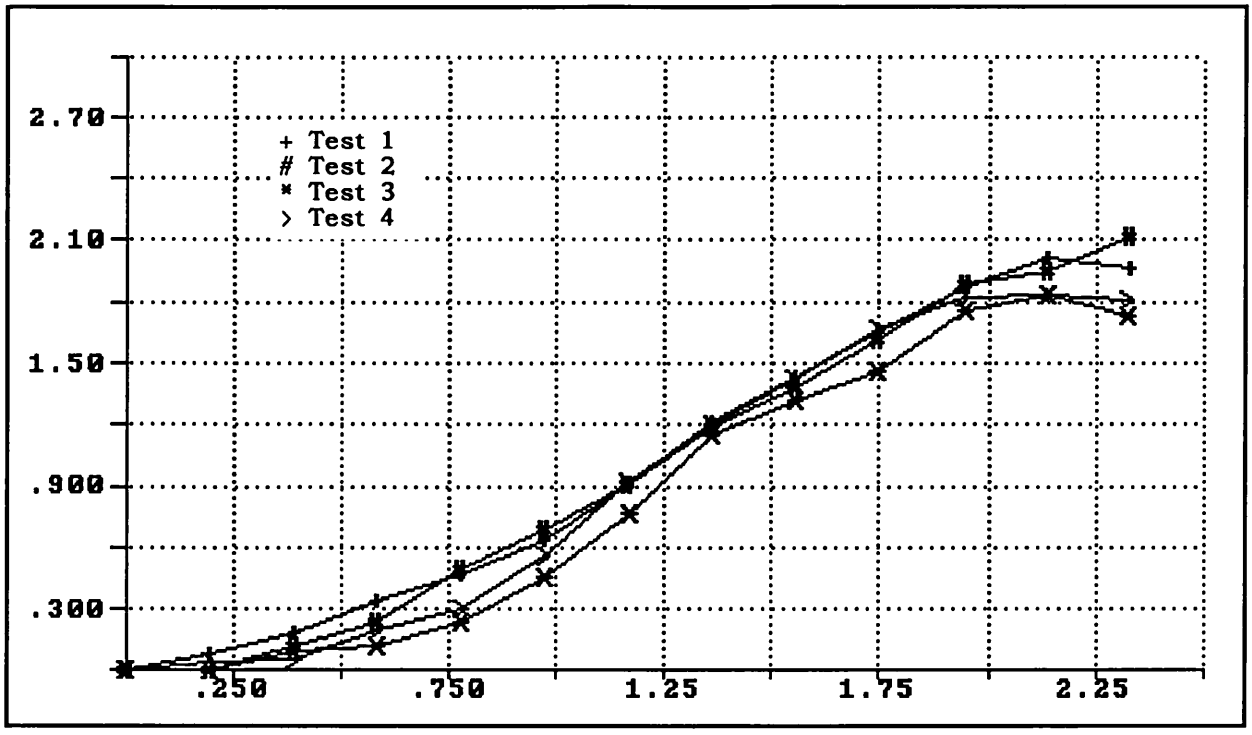
FIGURE 37b PLOT OF TEMPERATURE versus SHEAR RATE



Fluid 50LV/L35156
Temperature 50 C
Field 1.95 kV/mm

X Axis sec-1
Y Axis degC
E.R.V.

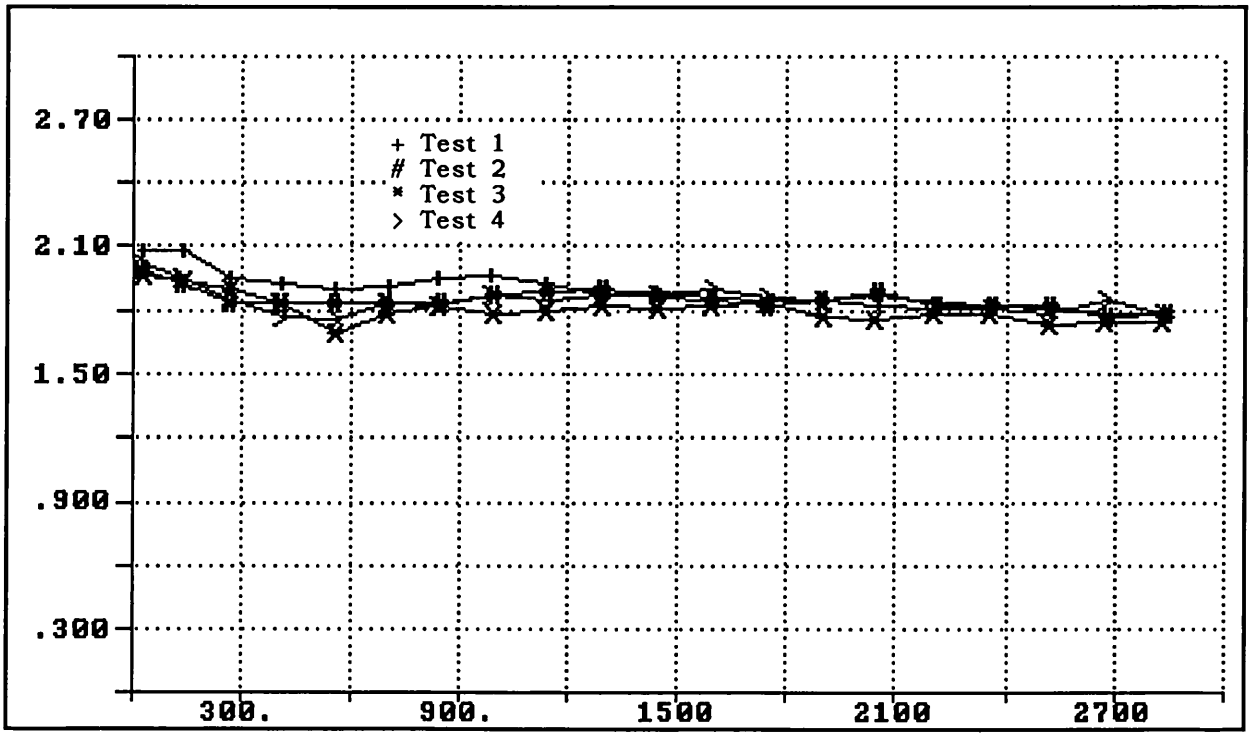
FIGURE 38a PLOT OF EXCESS SHEAR STRESS versus FIELD STRENGTH



Fluid 50LV/L35156
Temperature 50 degC
Shear Rate 465 sec-1

X Axis kV/mm
Y Axis kPa
E.R.V.

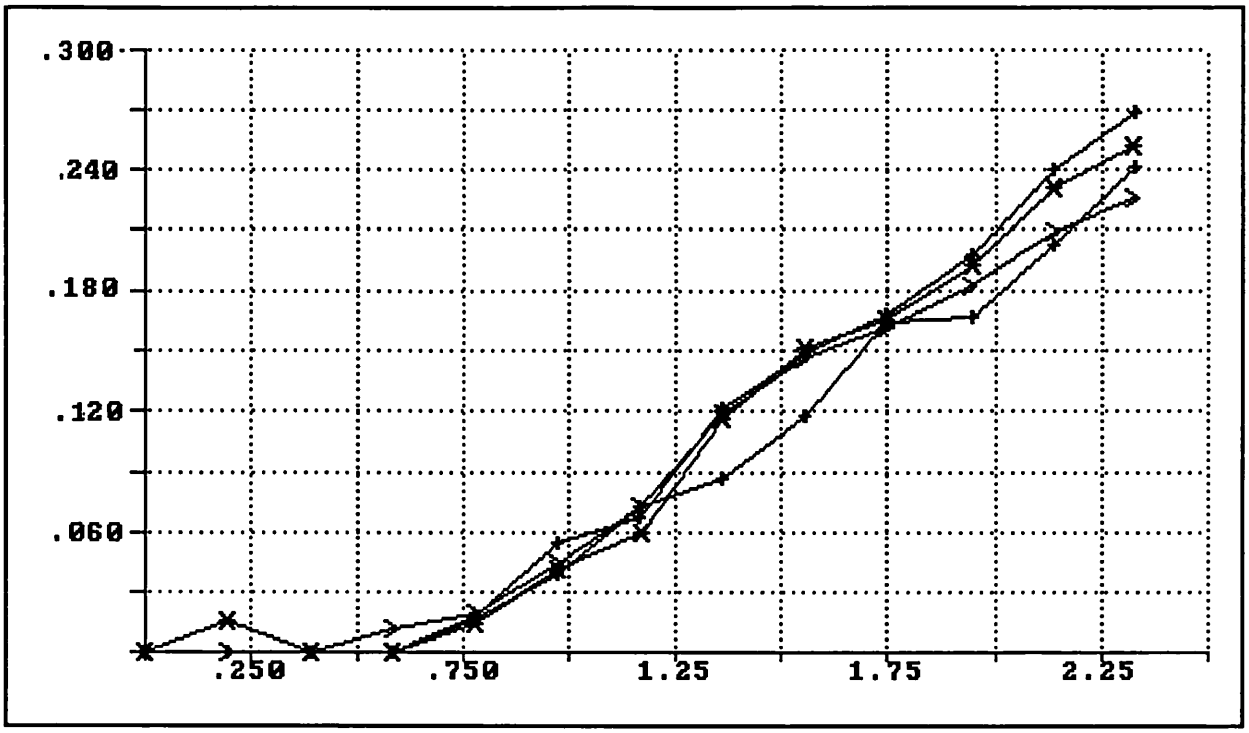
FIGURE 38b PLOT OF EXCESS SHEAR STRESS versus SHEAR RATE



Fluid 50LV/L35156
Temperature 50 degC
Field 1.95 kV/mm

X Axis sec-1
Y Axis kPa
E.R.V.

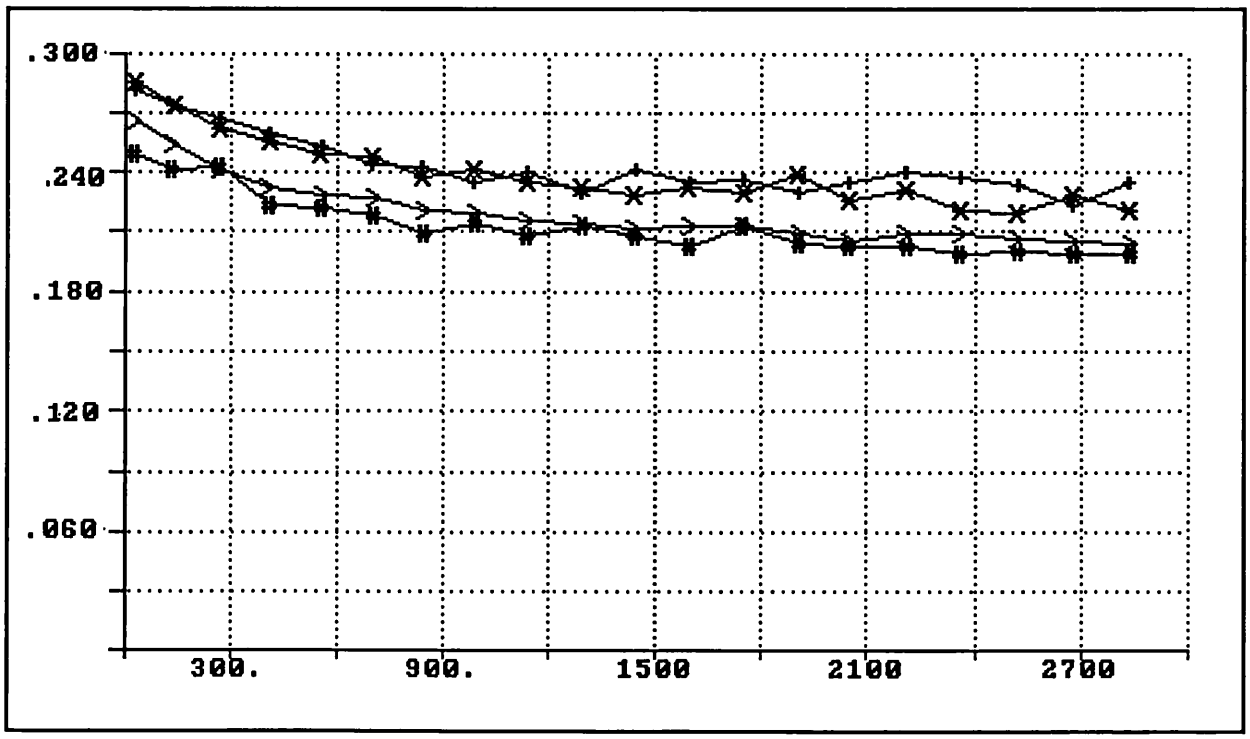
FIGURE 39a PLOT OF CURRENT DENSITY versus FIELD STRENGTH



Fluid 50LV/L35156
Temperature 50 C
Shear Rate 465 sec-1

X Axis kV/mm
Y Axis mA/cm2
E.R.V.

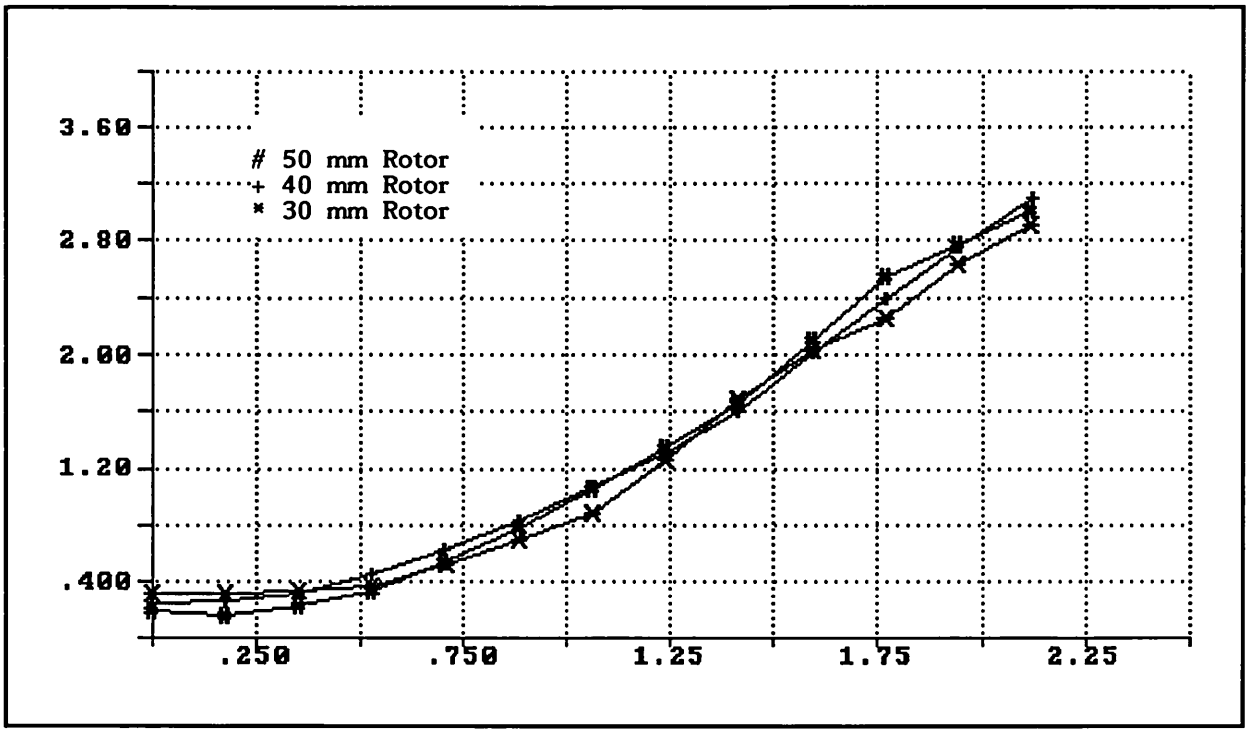
FIGURE 39b PLOT OF CURRENT DENSITY versus SHEAR RATE



Fluid 50LV/L35156
Temperature 50 C
Field 1.95 kV/mm

X Axis sec-1
Y Axis mA/cm2
E.R.V.

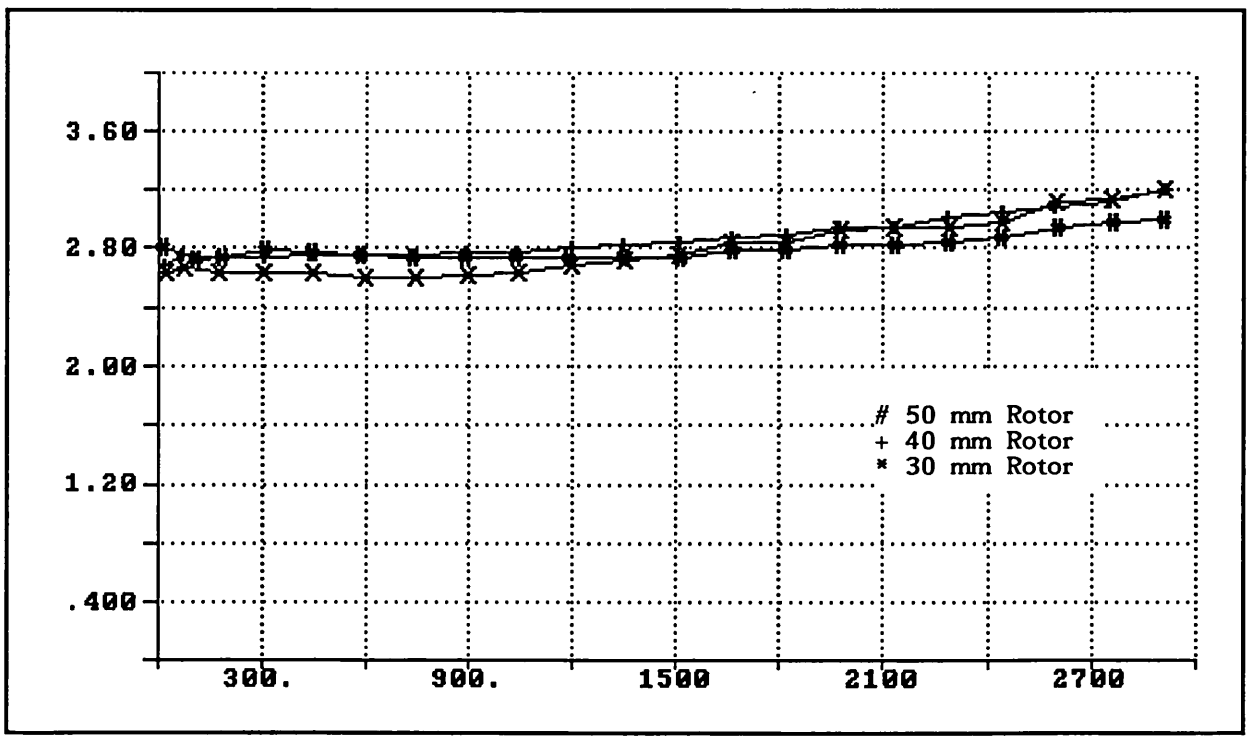
FIGURE 40a PLOT OF TOTAL SHEAR STRESS versus FIELD STRENGTH



Fluid 50LV/L35156
Temperature 30 C
Shear Rate 465 sec-1

X Axis kV/mm
Y Axis kPa
E.R.V.

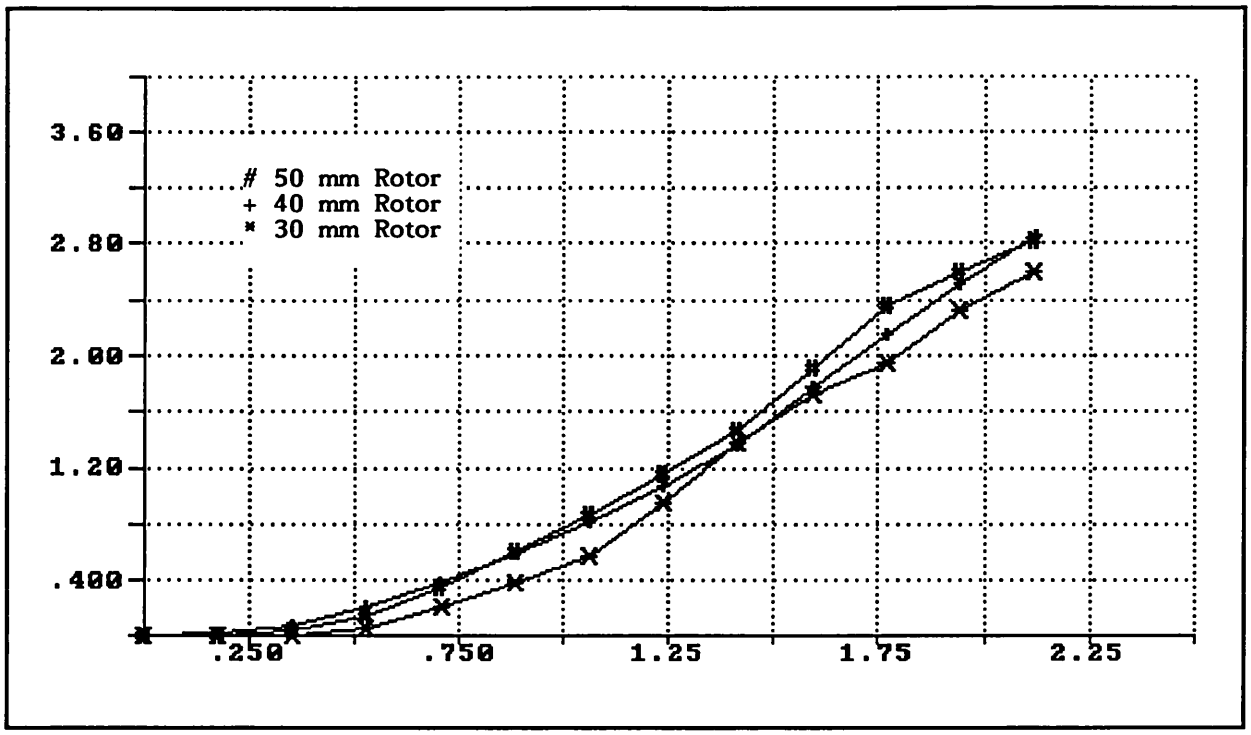
FIGURE 40b PLOT OF TOTAL SHEAR STRESS versus SHEAR RATE



Fluid 50LV/L35156
Temperature 30 C
Field 1.95 kV/mm

X Axis sec-1
Y Axis kPa
E.R.V.

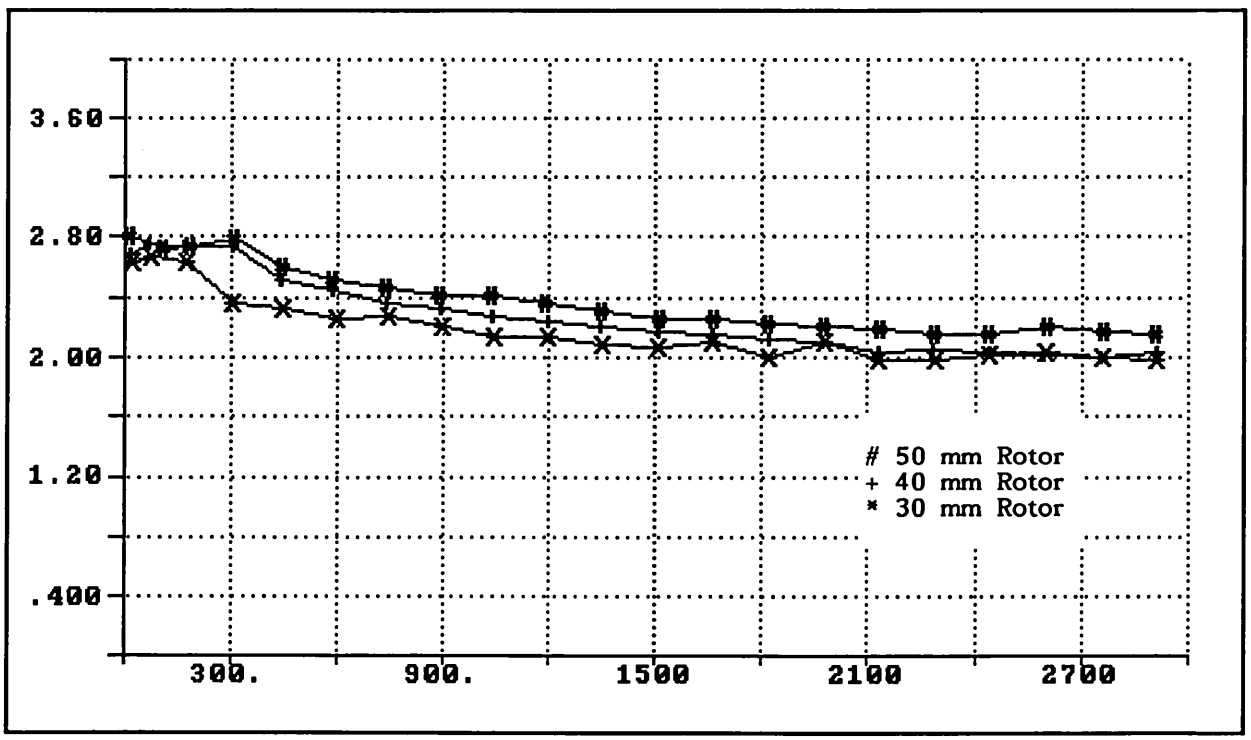
FIGURE 41a PLOT OF EXCESS SHEAR STRESS versus FIELD STRENGTH



Fluid 50LV/L35156
Temperature 30 degC
Shear Rate 465 sec-1

X Axis kV/mm
Y Axis kPa
E.R.V.

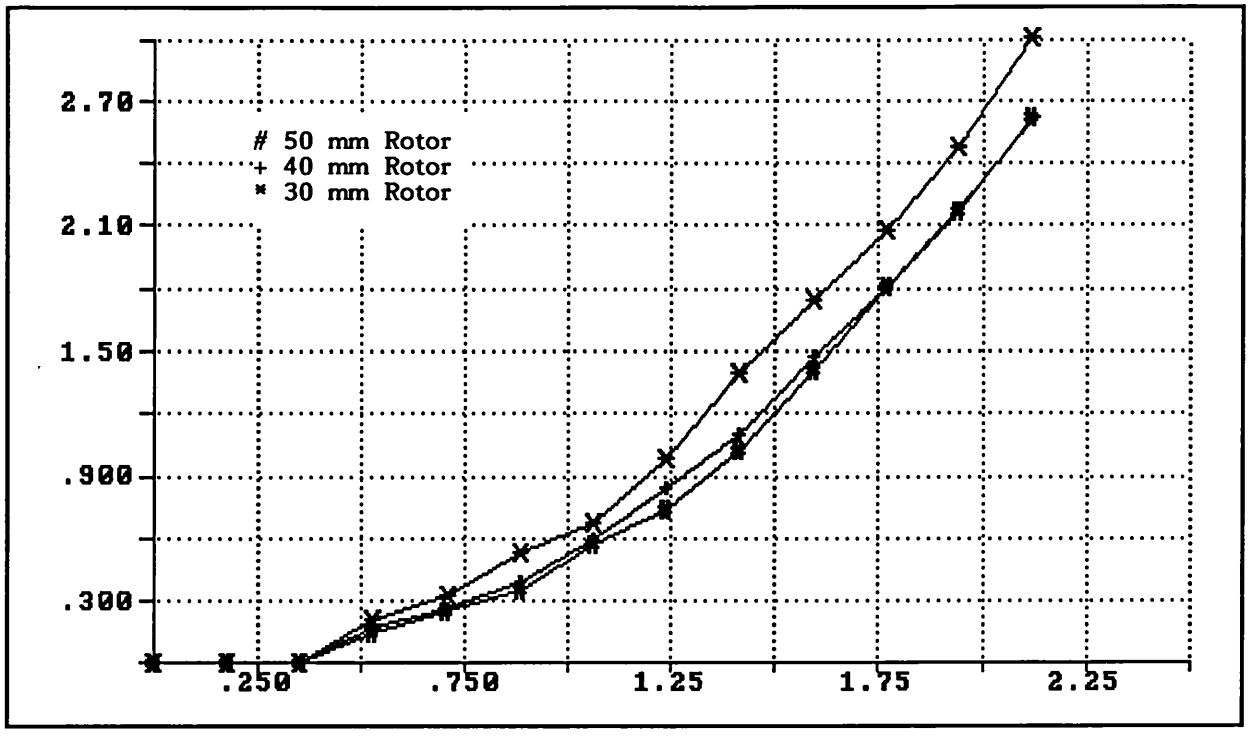
FIGURE 41b PLOT OF EXCESS SHEAR STRESS versus SHEAR RATE



Fluid 50LV/L35156
Temperature 30 degC
Field 1.95 kV/mm

X Axis sec-1
Y Axis kPa
E.R.V.

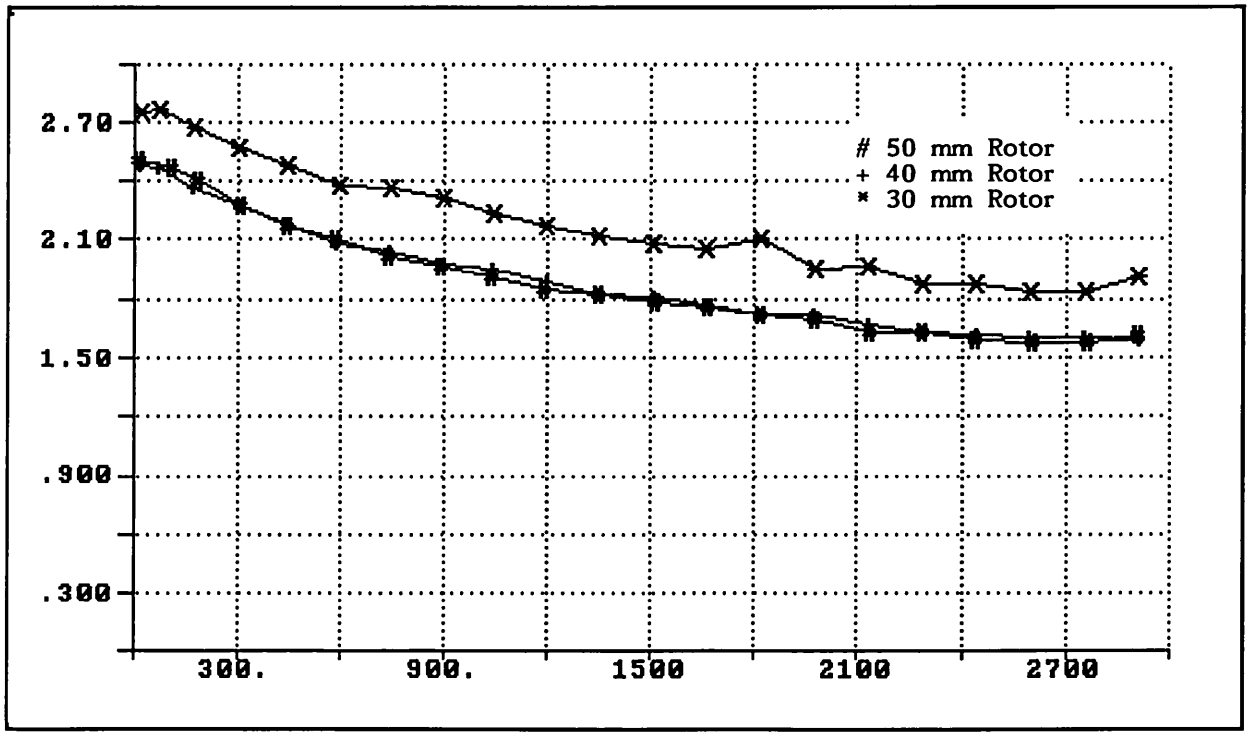
FIGURE 42a PLOT OF CURRENT DENSITY versus FIELD STRENGTH



Fluid 50LV/L35156
Temperature 30 C
Shear Rate 465 sec-1

X Axis kV/mm
Y Axis 10*uA/cm2
E.R.V.

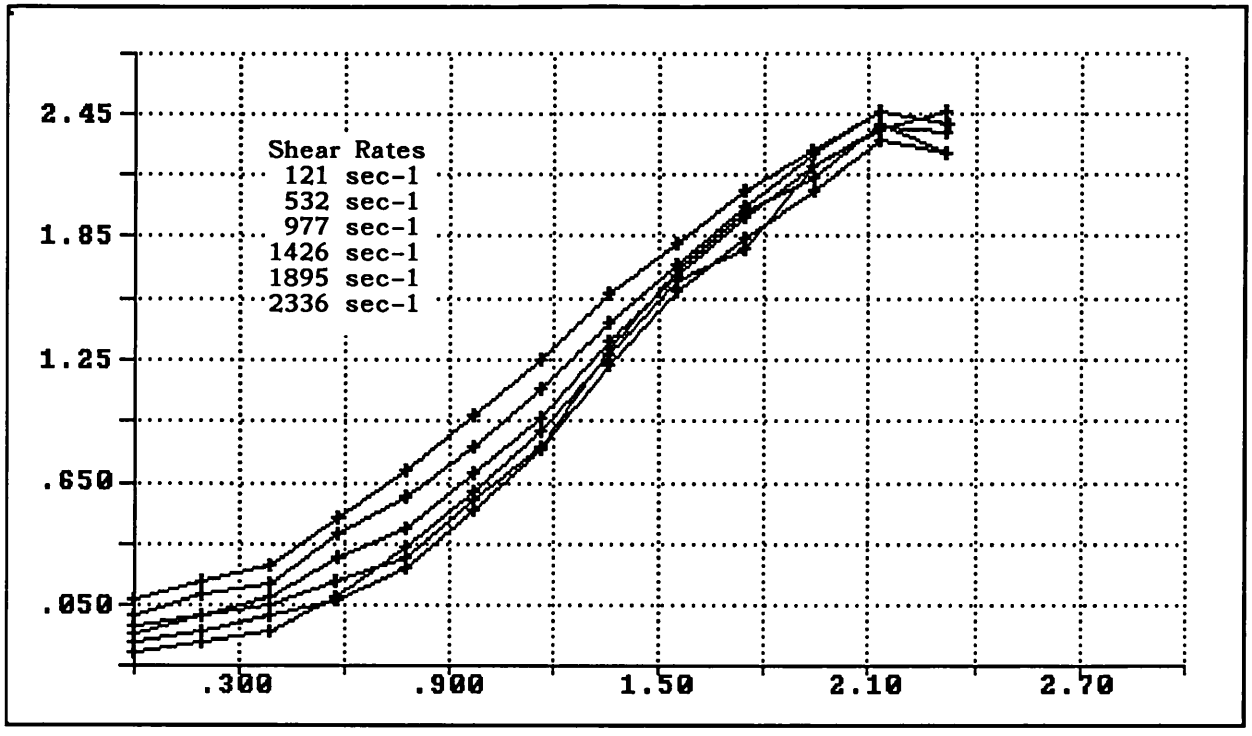
FIGURE 42b PLOT OF CURRENT DENSITY versus SHEAR RATE



Fluid 50LV/L35156
Temperature 30 C
Field 1.95 kV/mm

X Axis 10e4*s-1
Y Axis 10*uA/cm2
E.R.V.

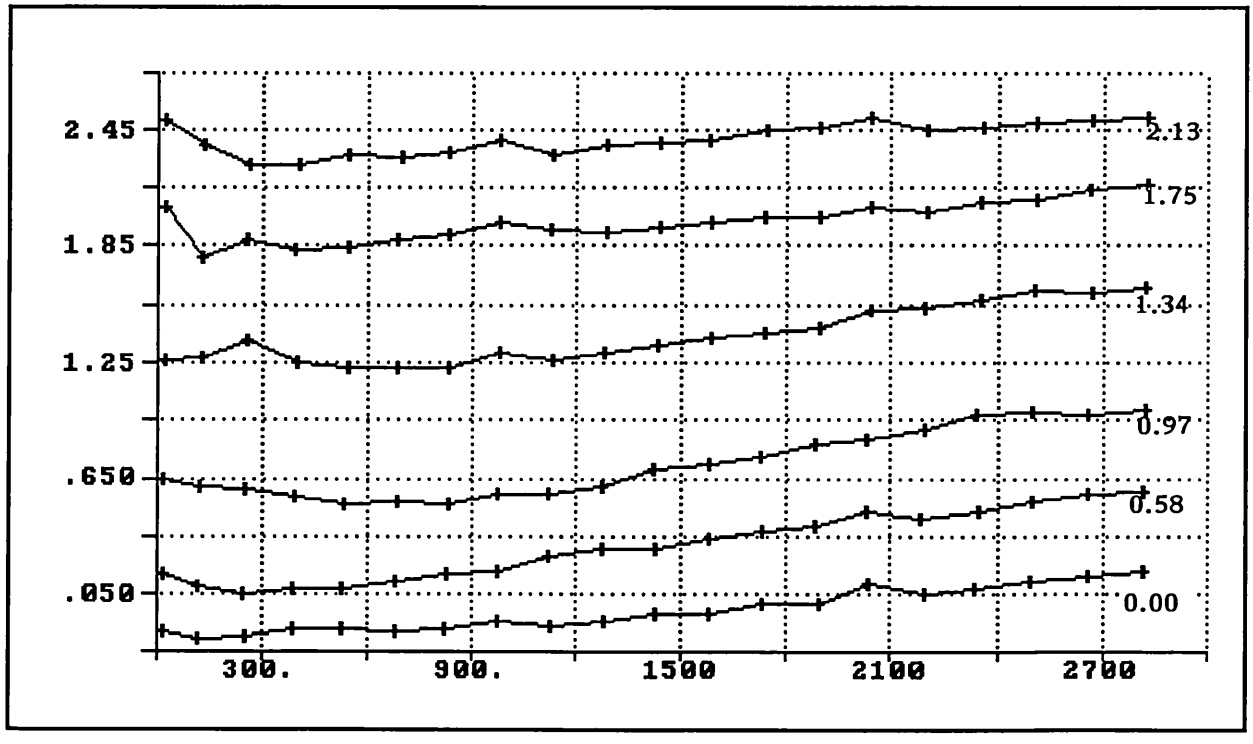
FIGURE 43a PLOT OF TOTAL SHEAR STRESS versus FIELD STRENGTH



Fluid 50LV/L35180
Temperature 50 C
Various Shear Rates

X Axis kV/mm
Y Axis kPa
E.R.V.

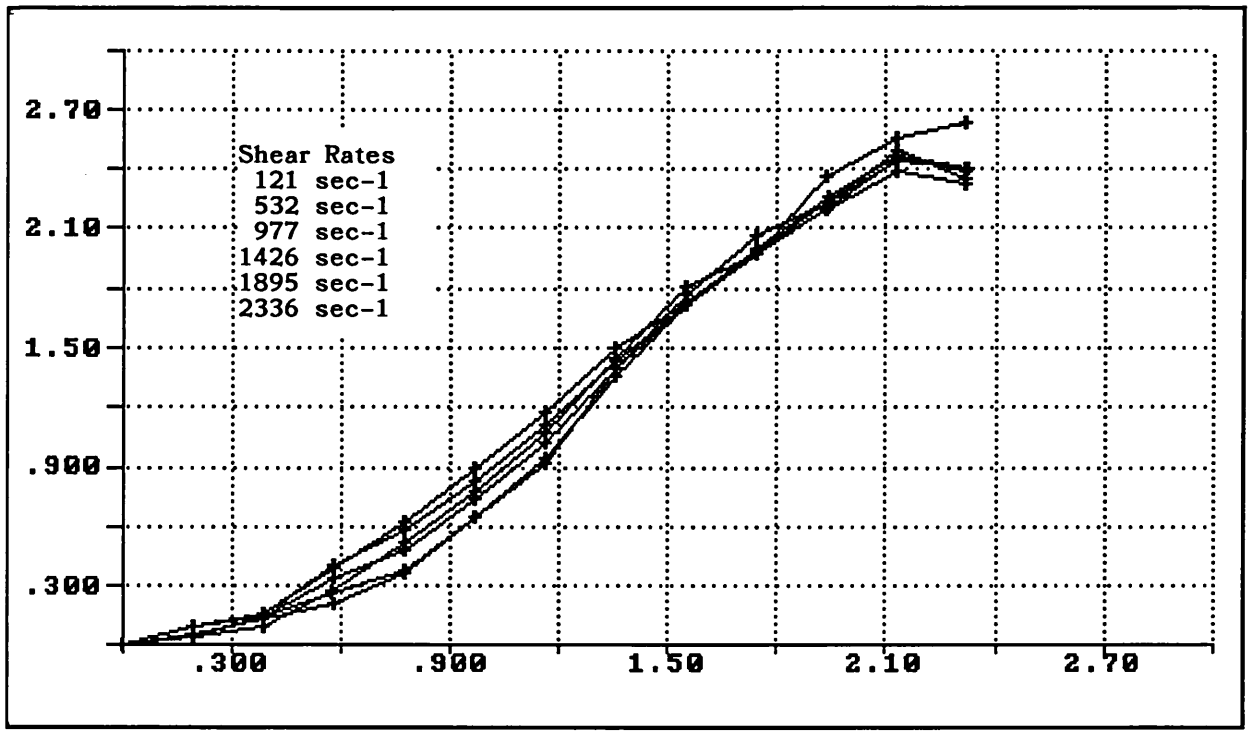
FIGURE 43b PLOT OF TOTAL SHEAR STRESS versus SHEAR RATE



Fluid 50LV/L35180
Temperature 50 C
Various Field Strengths

X Axis sec-1
Y Axis kPa
E.R.V.

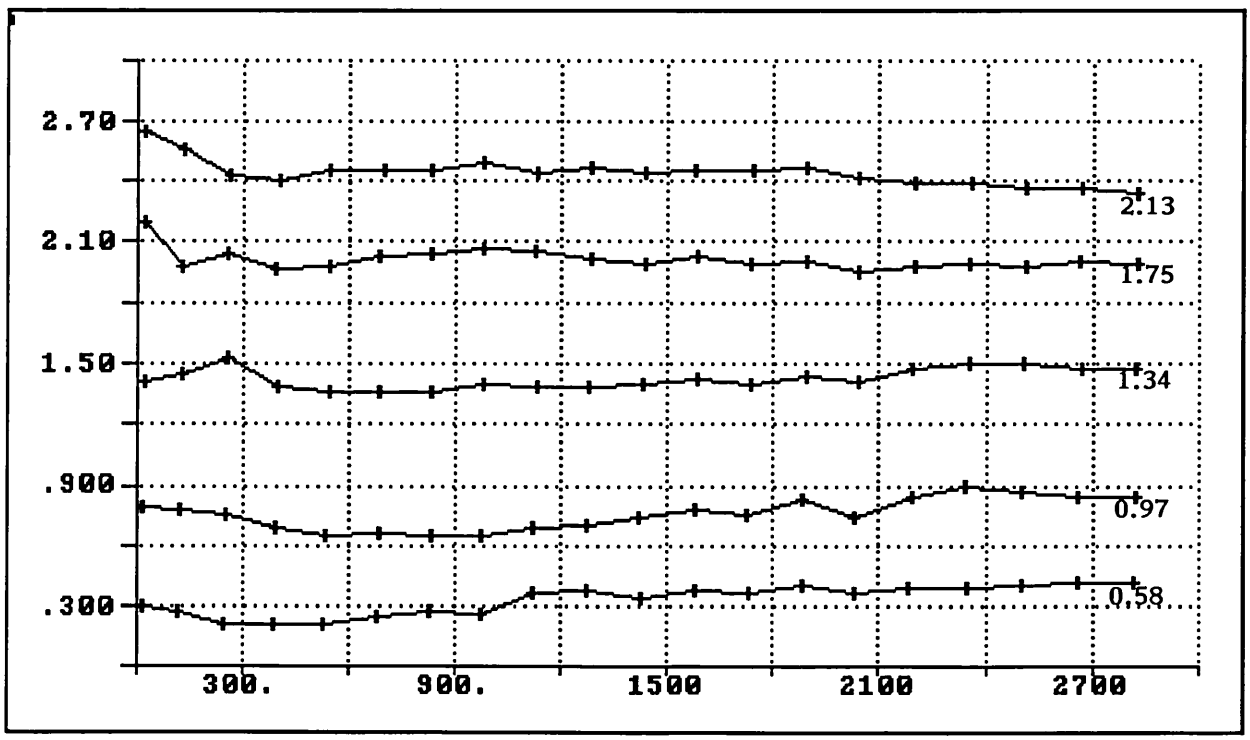
FIGURE 44a PLOT OF EXCESS SHEAR STRESS versus FIELD STRENGTH



Fluid 50LV/L35180
Temperature 50 degC
Various Shear Rates

X Axis kV/mm
Y Axis kPa
E.R.V.

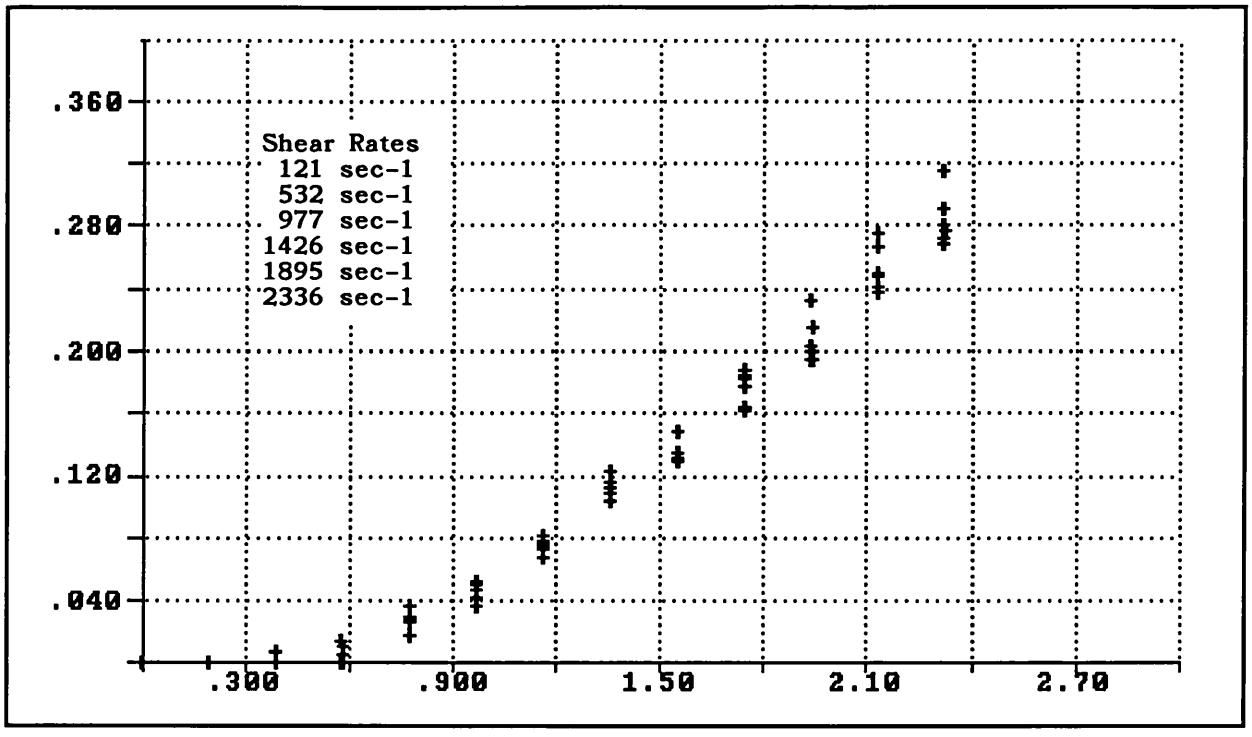
FIGURE 44b PLOT OF EXCESS SHEAR STRESS versus SHEAR RATE



Fluid 50LV/L35180
Temperature 50 degC
Various Field Strengths

X Axis sec-1
Y Axis kPa
E.R.V.

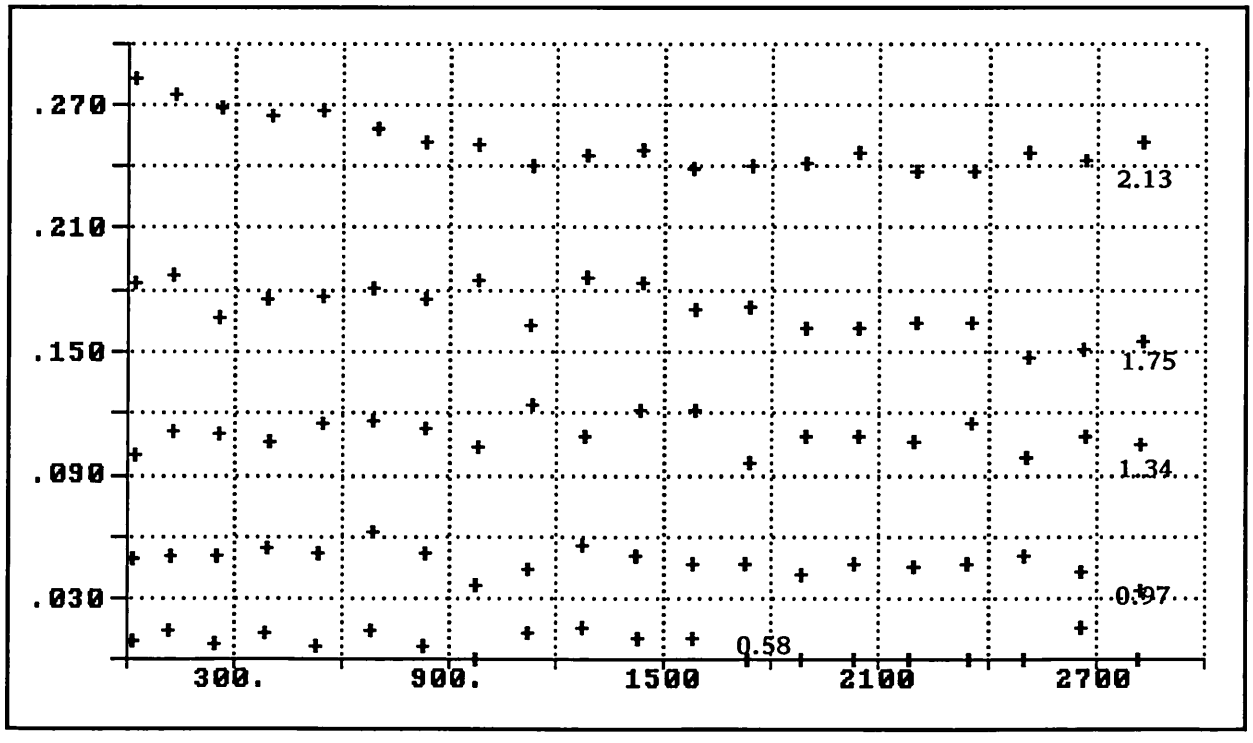
FIGURE 45a PLOT OF CURRENT DENSITY versus FIELD STRENGTH



Fluid 50LV/L35180
Temperature 50 C
Various Shear Rates

X Axis kV/mm
Y Axis mA/cm2
E.R.V.

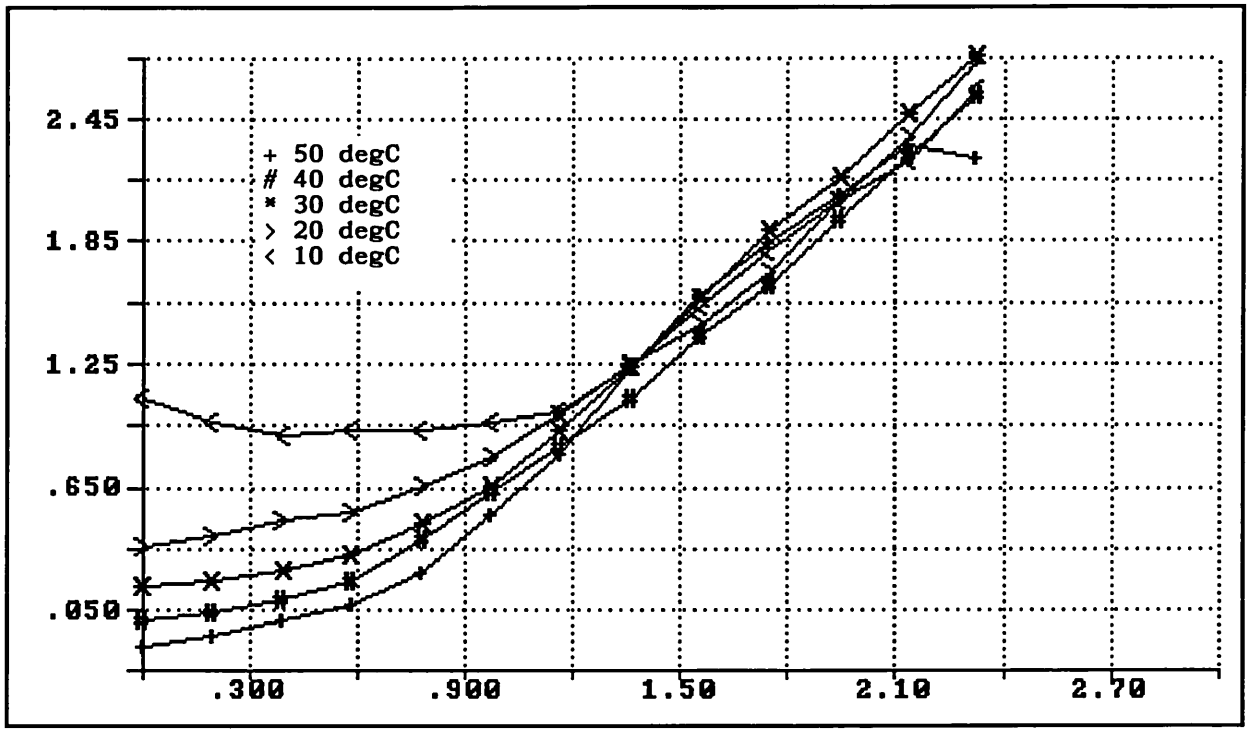
FIGURE 45b PLOT OF CURRENT DENSITY versus SHEAR RATE



Fluid 50LV/L35180
Temperature 50 C
Various Field Strengths

X Axis sec-1
Y Axis mA/cm2
E.R.V.

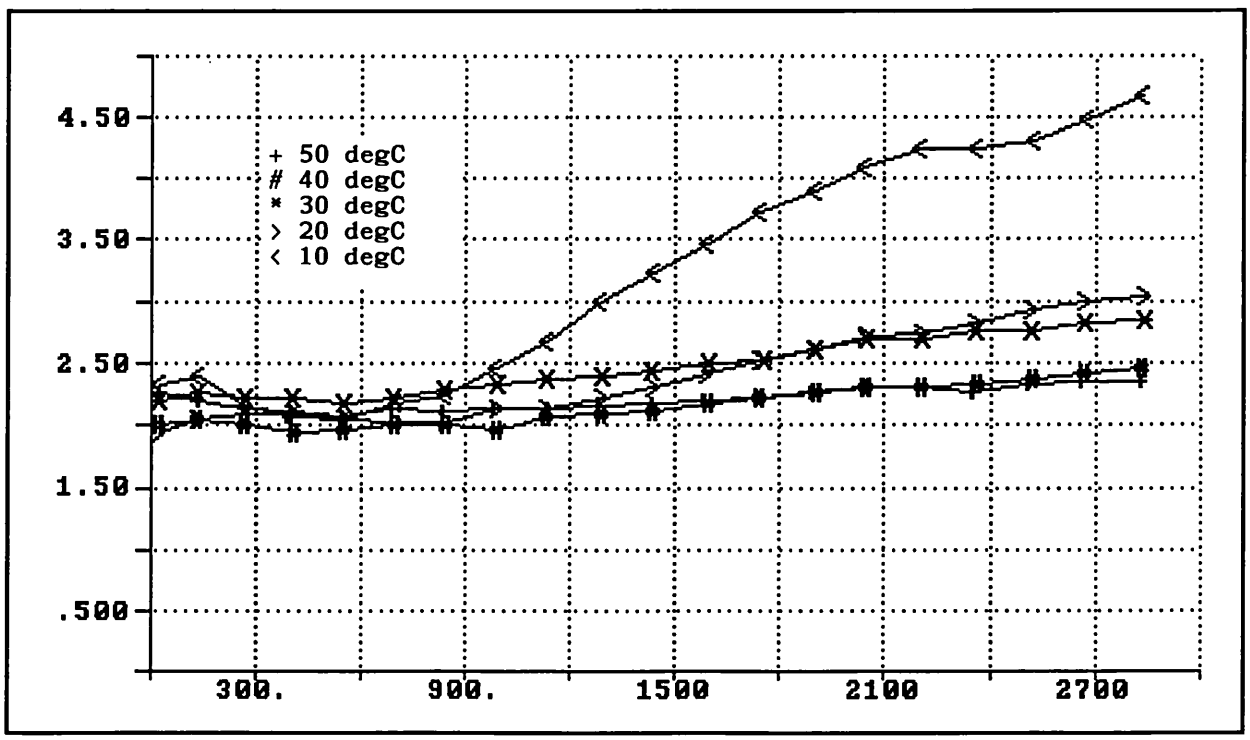
FIGURE 46a PLOT OF TOTAL SHEAR STRESS versus FIELD STRENGTH



Fluid 50LV/L35180
Temperature
Shear Rate 540 sec-1

X Axis kV/mm
Y Axis kPa
E.R.V.

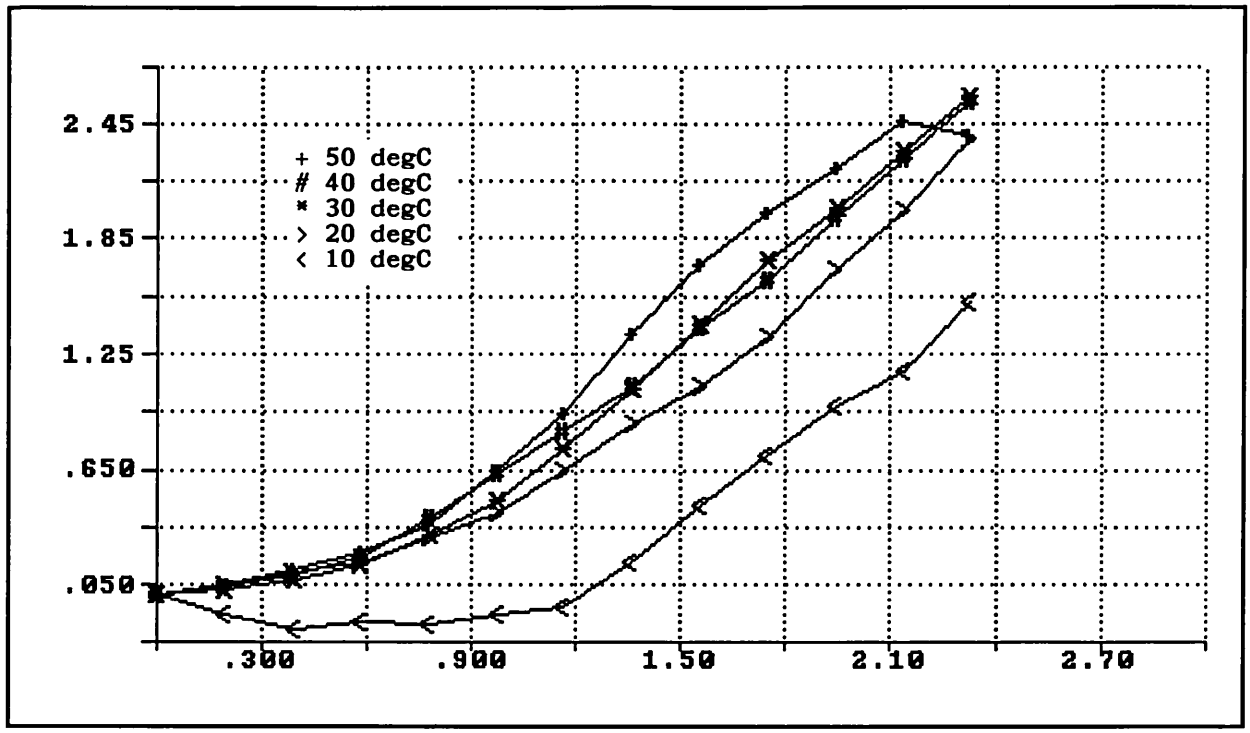
FIGURE 46b PLOT OF TOTAL SHEAR STRESS versus SHEAR RATE



Fluid 50LV/L35180
Temperature
Field 1.94 kV/mm

X Axis sec-1
Y Axis kPa
E.R.V.

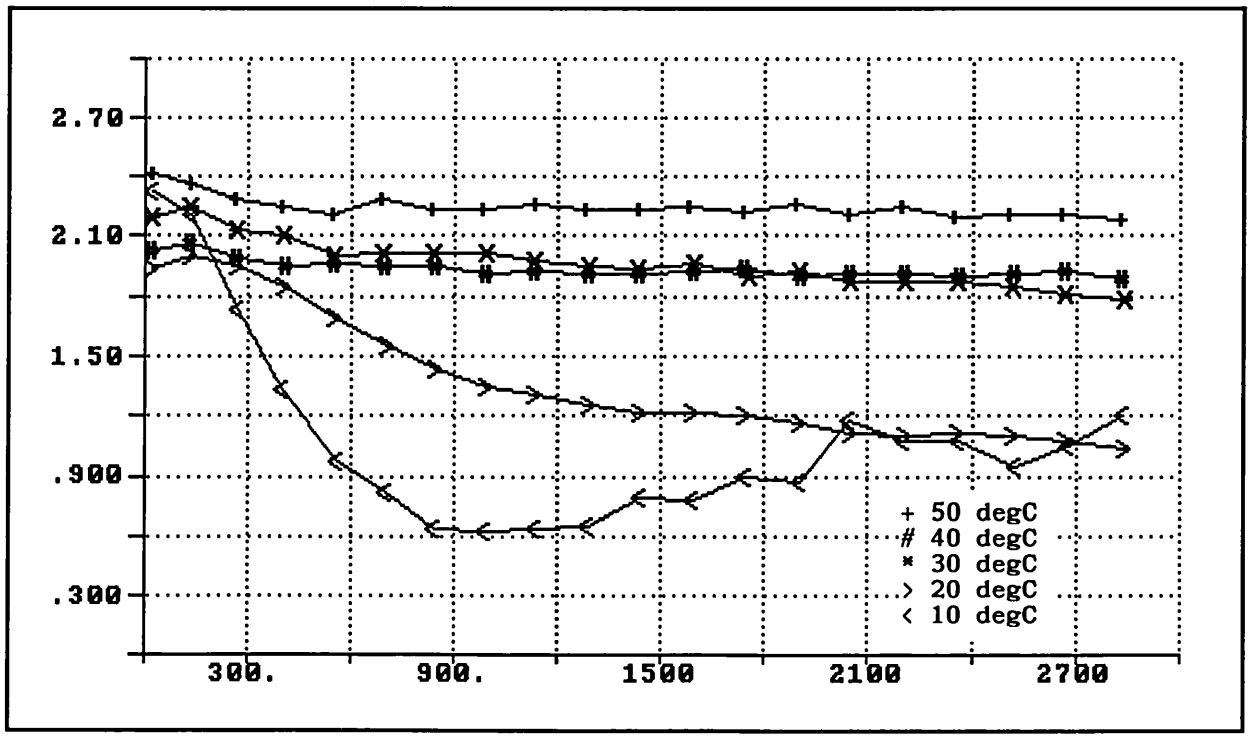
FIGURE 47a PLOT OF EXCESS SHEAR STRESS versus FIELD STRENGTH



Fluid 50LV/L35180
Temperature
Shear Rate 540 sec-1

X Axis kV/mm
Y Axis kPa
E.R.V.

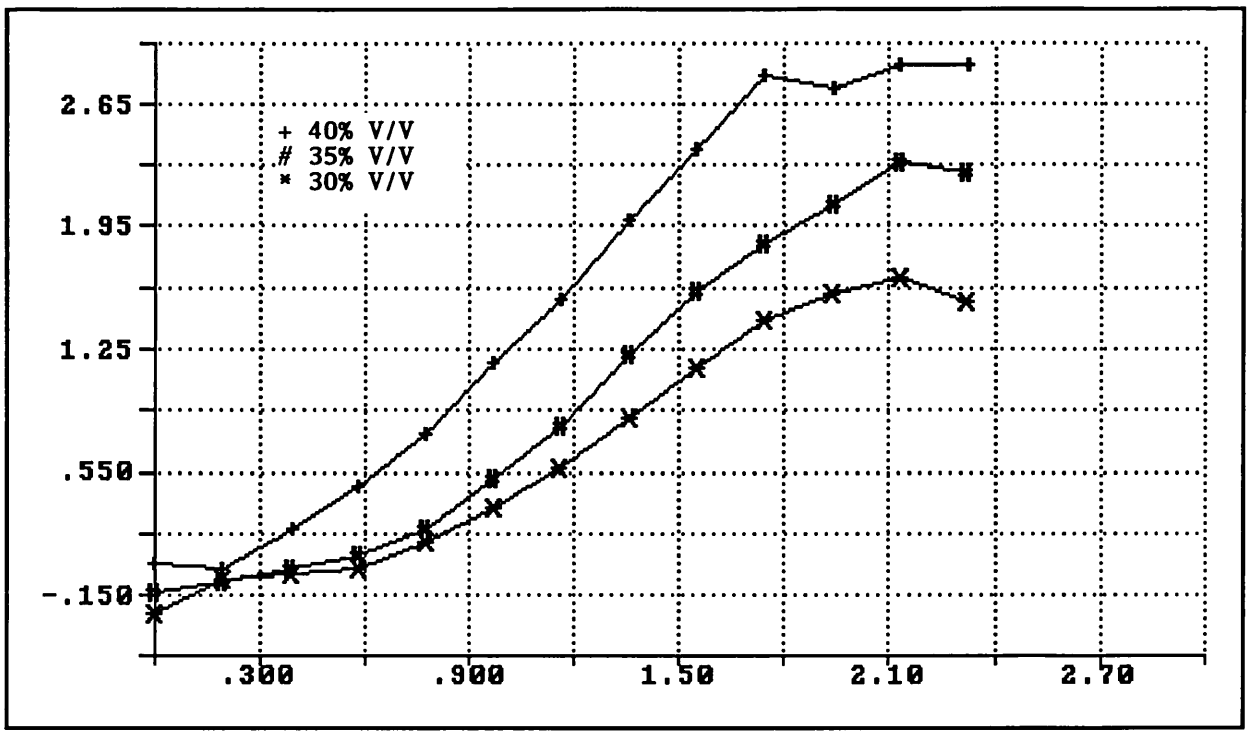
FIGURE 47b PLOT OF EXCESS SHEAR STRESS versus SHEAR RATE



Fluid 50LV/L35180
Temperature
Field 1.94 kV/mm

X Axis sec-1
Y Axis kPa
E.R.V.

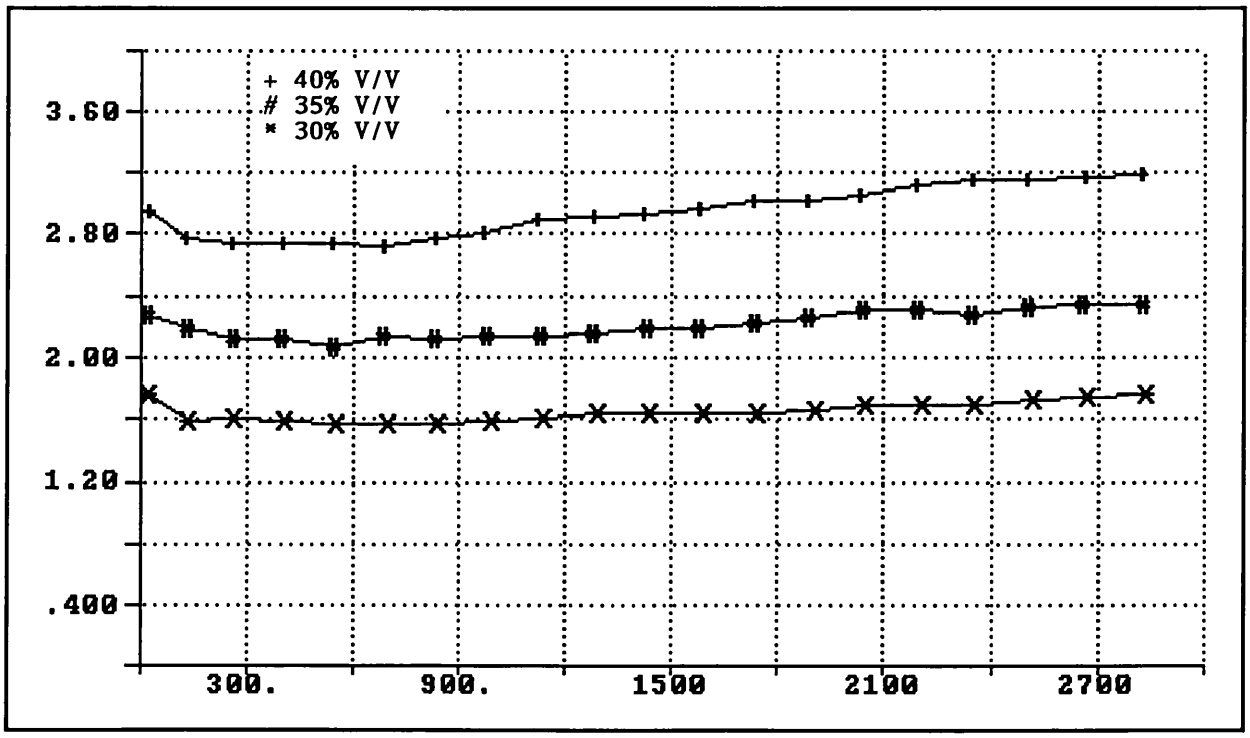
FIGURE 48a PLOT OF TOTAL SHEAR STRESS versus FIELD STRENGTH



Fluids 50LV Based
Temperature 50 C
Shear Rate 540 sec-1

X Axis kV/mm
Y Axis kPa
E.R.V.

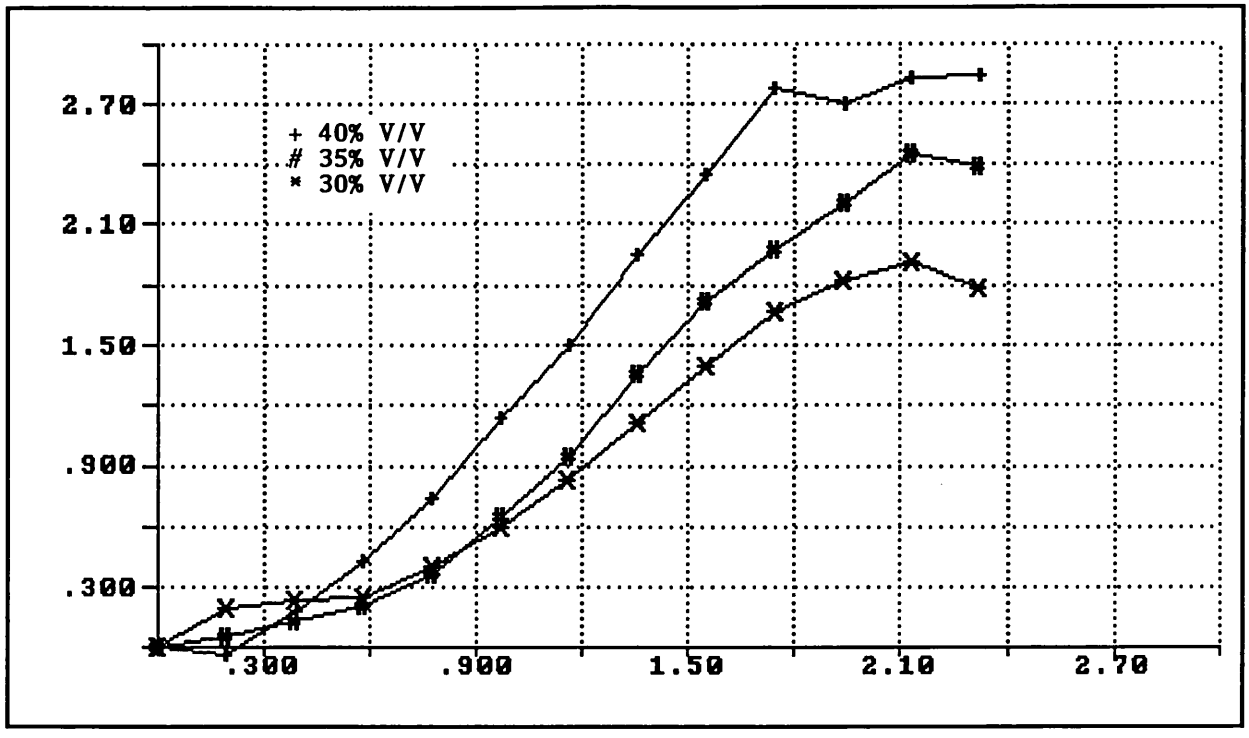
FIGURE 48b PLOT OF TOTAL SHEAR STRESS versus SHEAR RATE



Fluids 50LV Based
Temperature 50 C
Field 1.94 kV/mm

X Axis sec-1
Y Axis kPa
E.R.V.

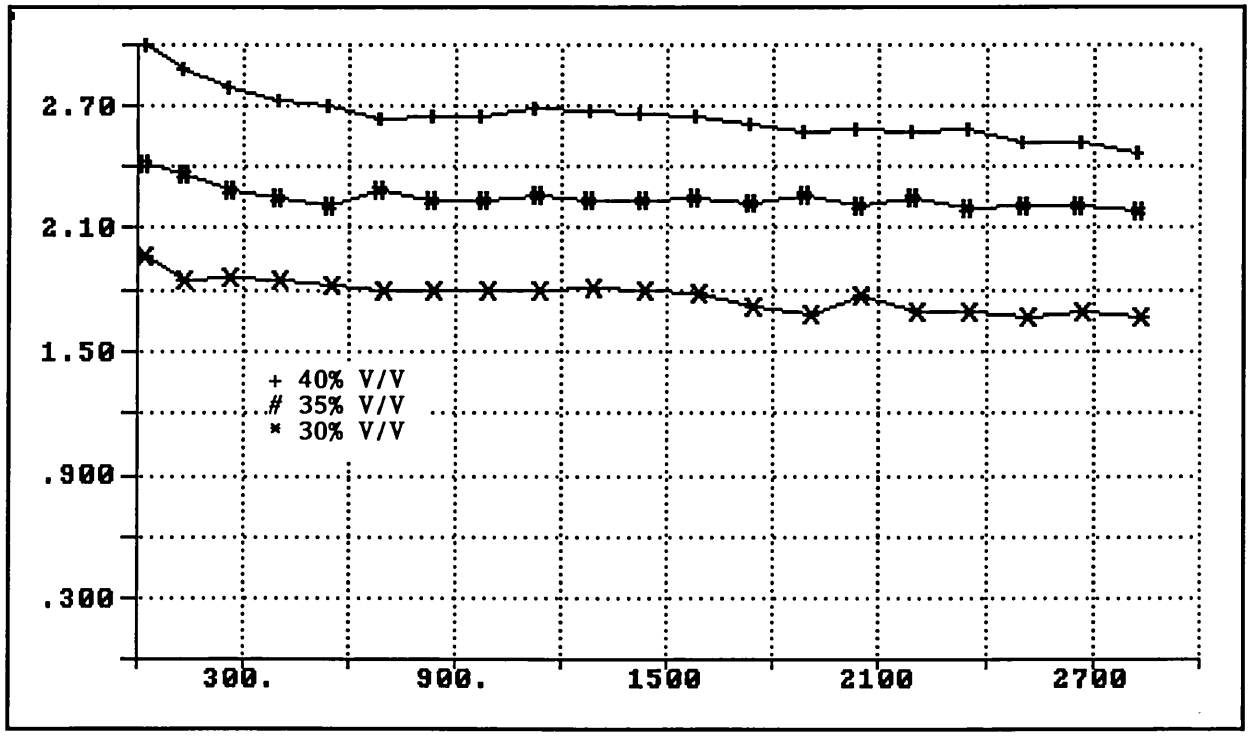
FIGURE 49a PLOT OF EXCESS SHEAR STRESS versus FIELD STRENGTH



Fluids 50LV Based
Temperature 50 degC
Shear Rate 540 sec-1

X Axis kV/mm
Y Axis kPa
E.R.V.

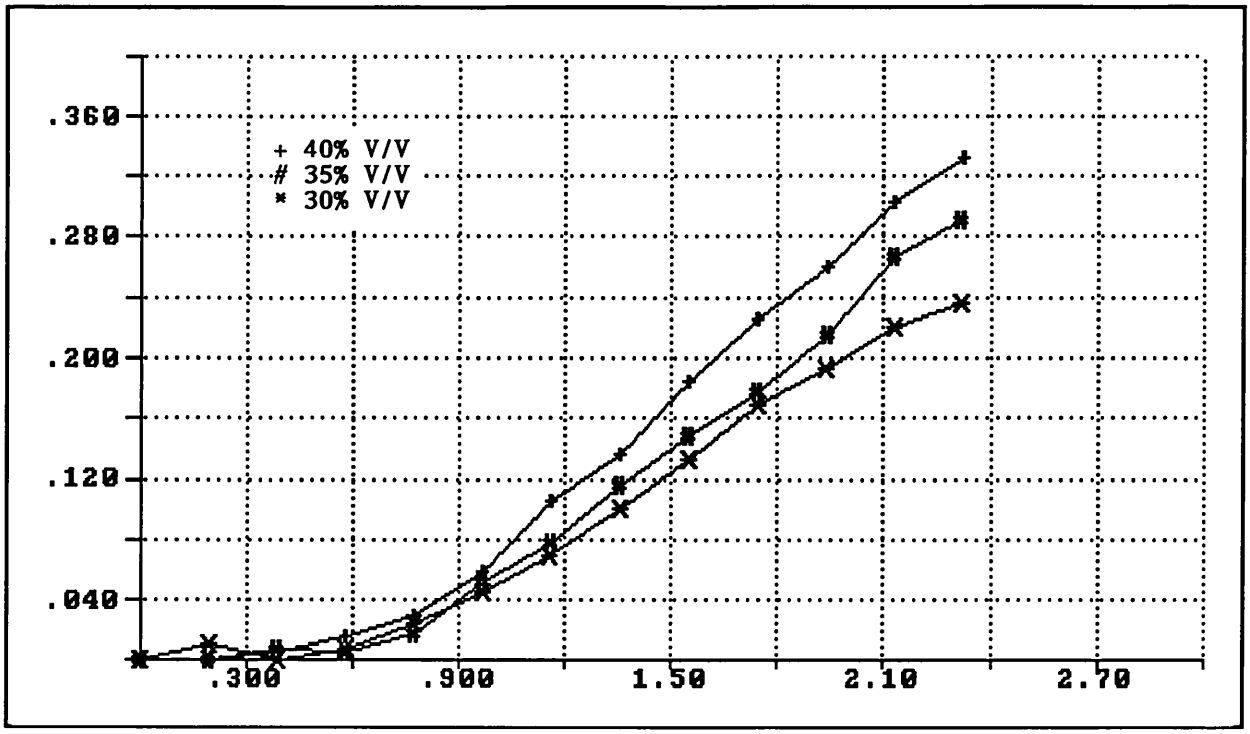
FIGURE 49b PLOT OF EXCESS SHEAR STRESS versus SHEAR RATE



Fluids 50LV Based
Temperature 50 degC
Field 1.94 kV/mm

X Axis sec-1
Y Axis kPa
E.R.V.

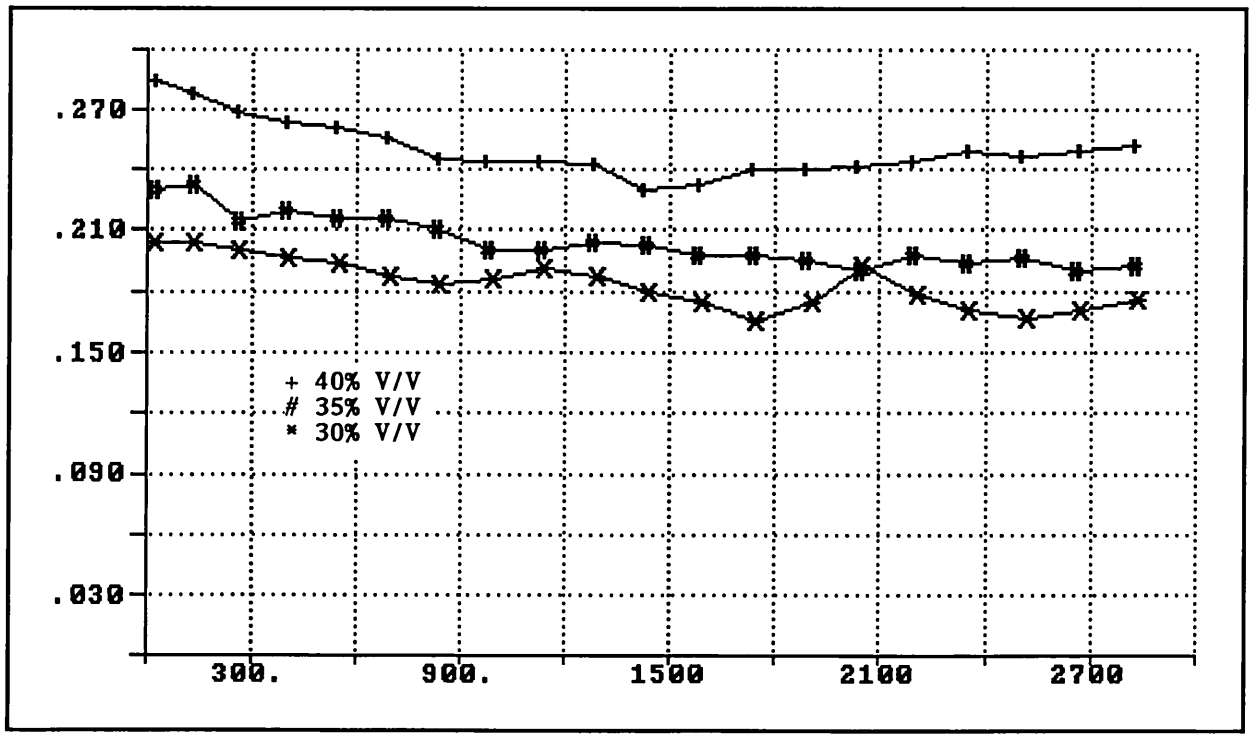
FIGURE 50a PLOT OF CURRENT DENSITY versus FIELD STRENGTH



Fluids 50LV Based
Temperature 50 C
Shear Rate 540 sec-1

X Axis kV/mm
Y Axis mA/cm2
E.R.V.

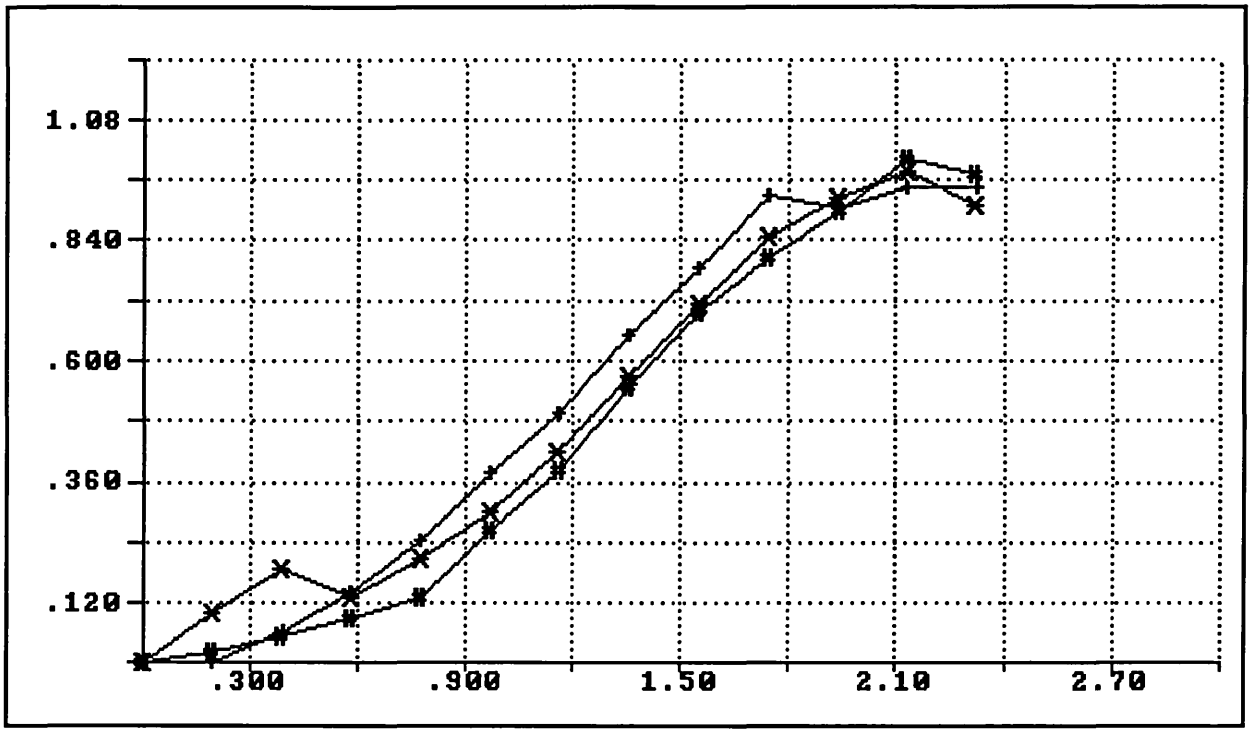
FIGURE 50b PLOT OF CURRENT DENSITY versus SHEAR RATE



Fluids 50LV Based
Temperature 50 C
Field 1.94 kV/mm

X Axis sec-1
Y Axis mA/cm2
E.R.V.

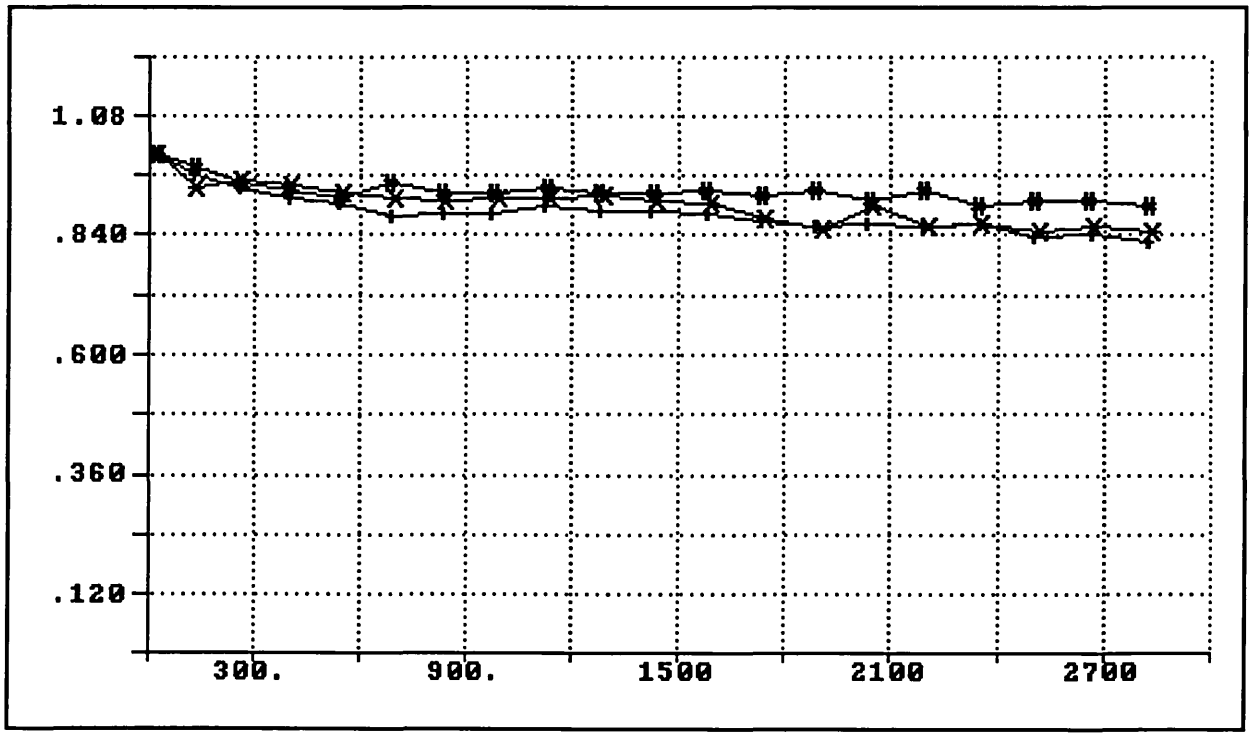
FIGURE 51a PLOT OF NORMALISED EXCESS SHEAR STRESS versus FIELD



Fluids 50LV Based
Temperature 50 degC
Shear Rate 540 sec-1

X Axis kV/mm
Y Axis kPa Norm
E.R.V.

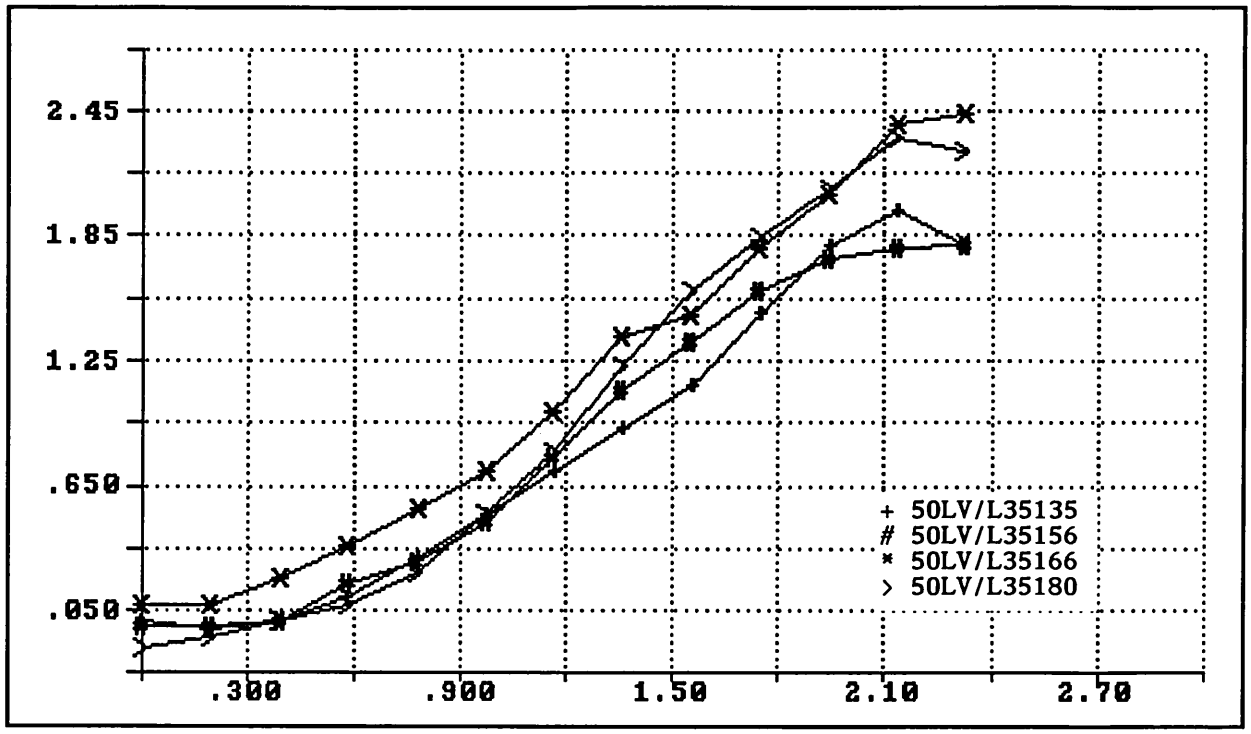
FIGURE 51b PLOT OF NORMALISED EXCESS SHEAR STRESS vs SHEAR RATE



Fluids 50LV Based
Temperature 50 degC
Field 1.94 kV/mm

X Axis sec-1
Y Axis kPa Norm
E.R.V.

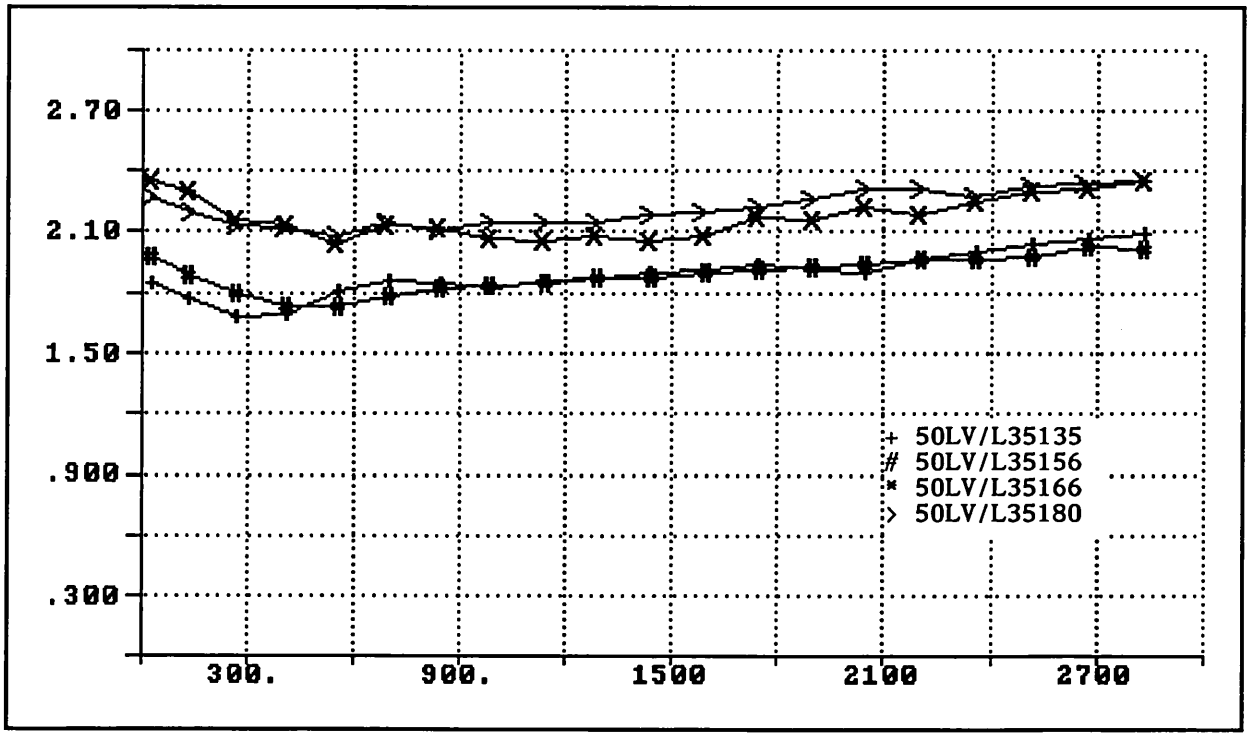
FIGURE 52a PLOT OF TOTAL SHEAR STRESS versus FIELD STRENGTH



Fluids 50LV Based
Temperature 50 C
Shear Rate 540 sec-1

X Axis kV/mm
Y Axis kPa
E.R.V.

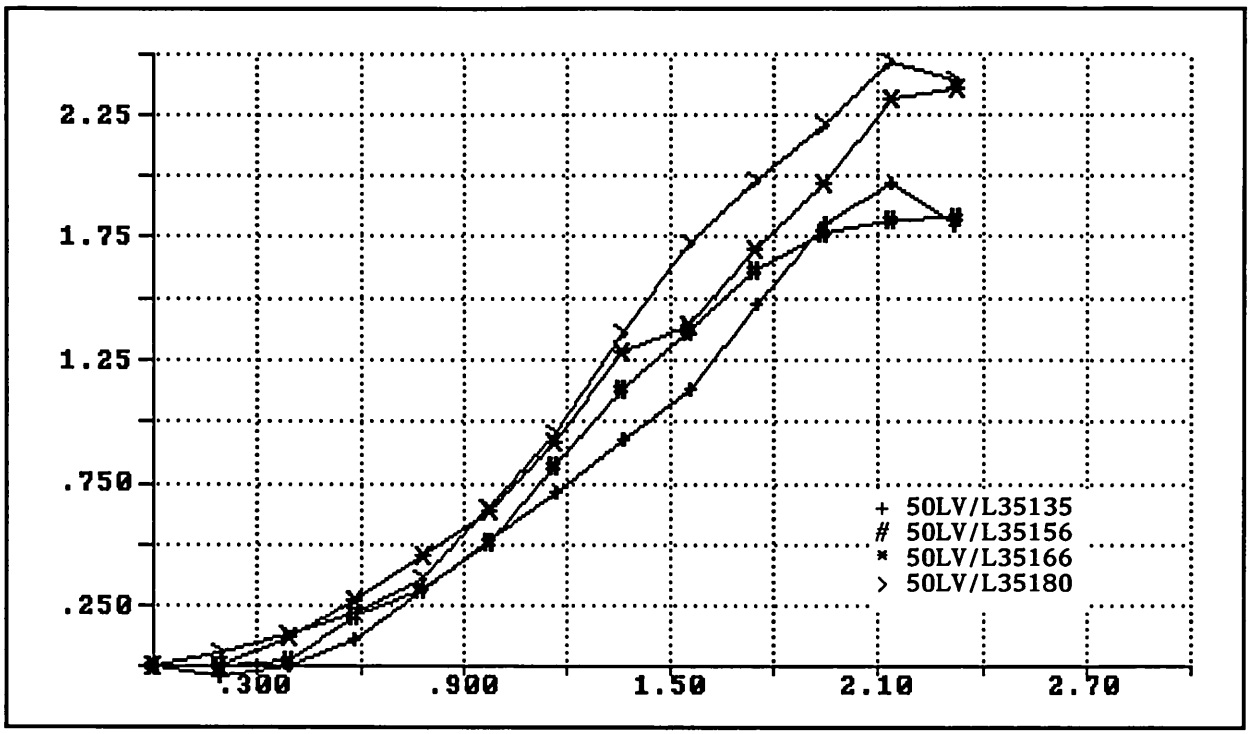
FIGURE 52b PLOT OF TOTAL SHEAR STRESS versus SHEAR RATE



Fluids 50LV Based
Temperature 50 C
Field 1.94 kV/mm

X Axis sec-1
Y Axis kPa
E.R.V.

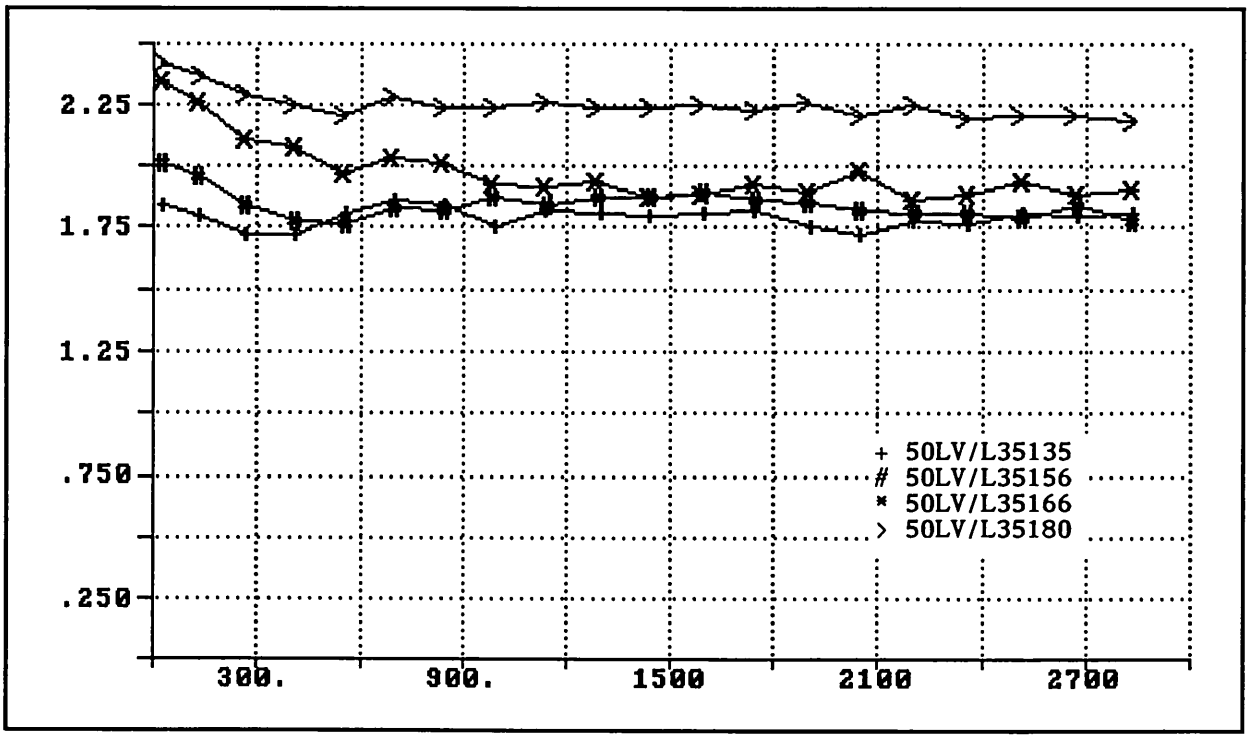
FIGURE 53a PLOT OF EXCESS SHEAR STRESS versus FIELD STRENGTH



Fluids 50LV Based
Temperature 50 degC
Shear Rate 540 sec-1

X Axis kV/mm
Y Axis kPa
E.R.V.

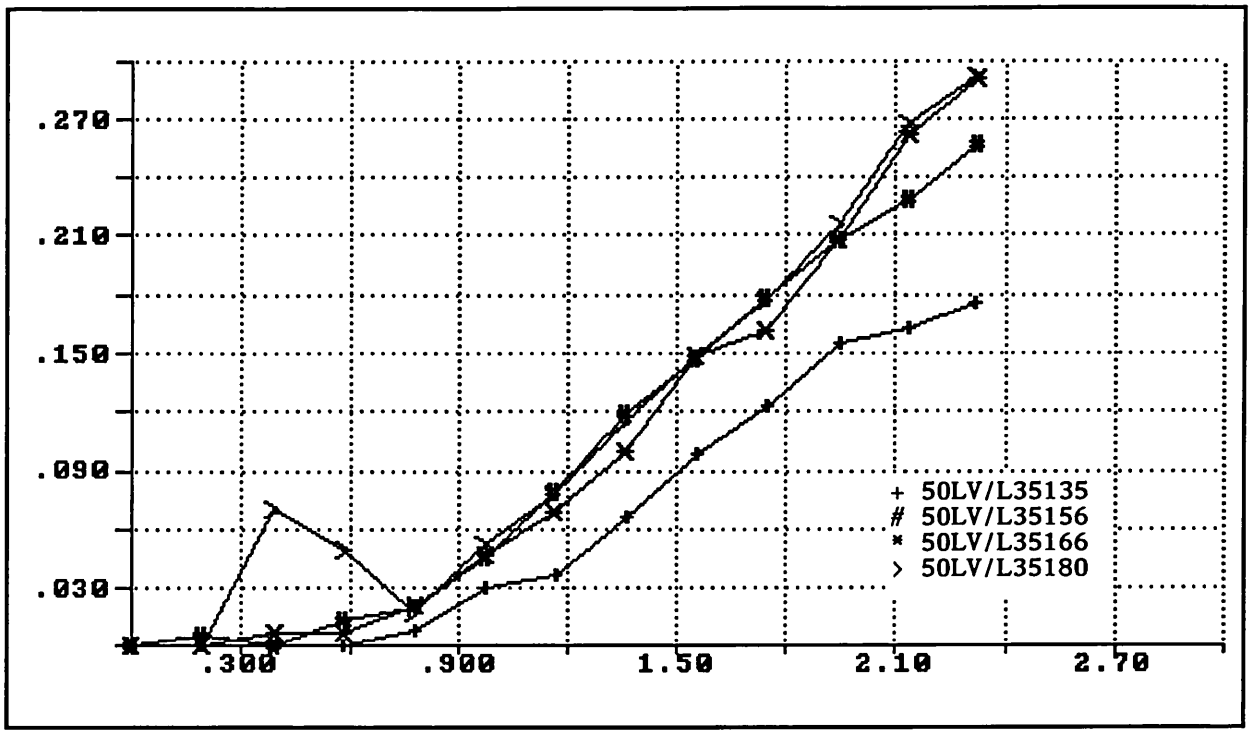
FIGURE 53b PLOT OF EXCESS SHEAR STRESS versus SHEAR RATE



Fluids 50LV Based
Temperature 50 degC
Field 1.94 kV/mm

X Axis sec-1
Y Axis kPa
E.R.V.

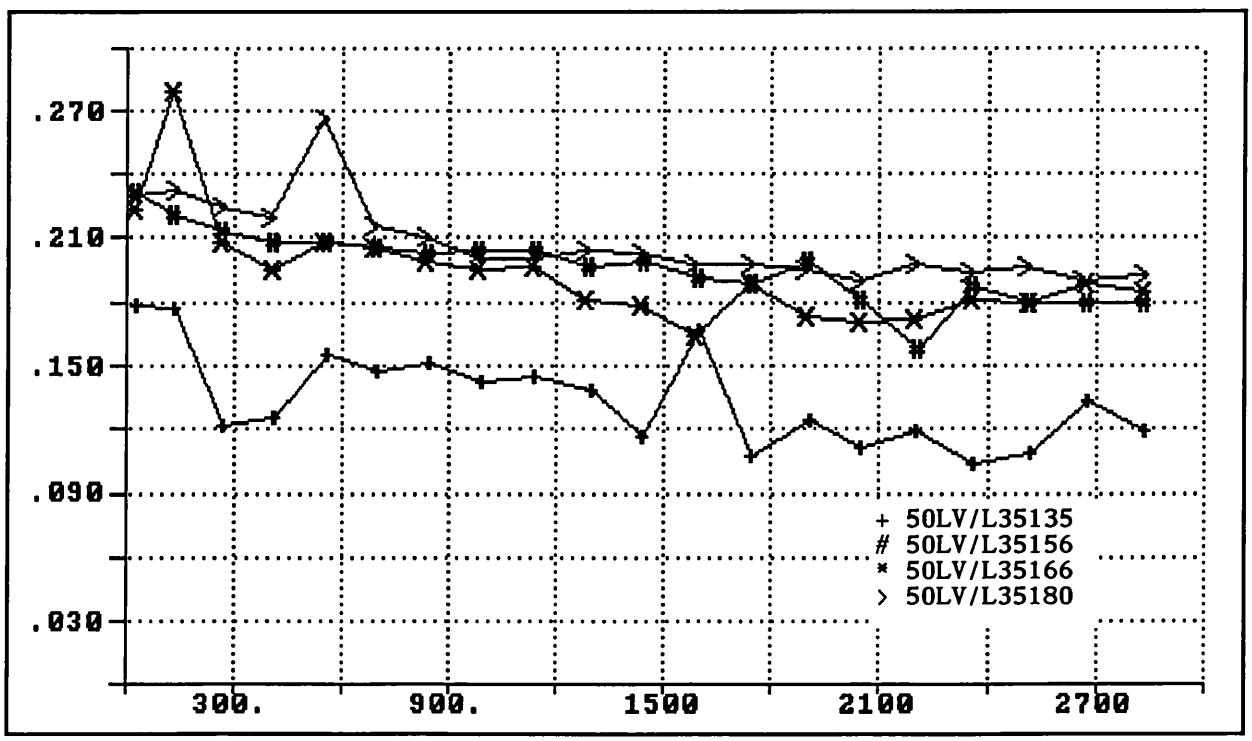
FIGURE 54a PLOT OF CURRENT DENSITY versus FIELD STRENGTH



Fluids 50LV Based
Temperature 50 C
Shear Rate 540 sec-1

X Axis kV/mm
Y Axis mA/cm2
E.R.V.

FIGURE 54b PLOT OF CURRENT DENSITY versus SHEAR RATE



Fluids 50LV Based
Temperature 50 C
Field 1.94 kV/mm

X Axis sec-1
Y Axis mA/cm2
E.R.V.

Figure 55a Typical Static Yield Rig Plot

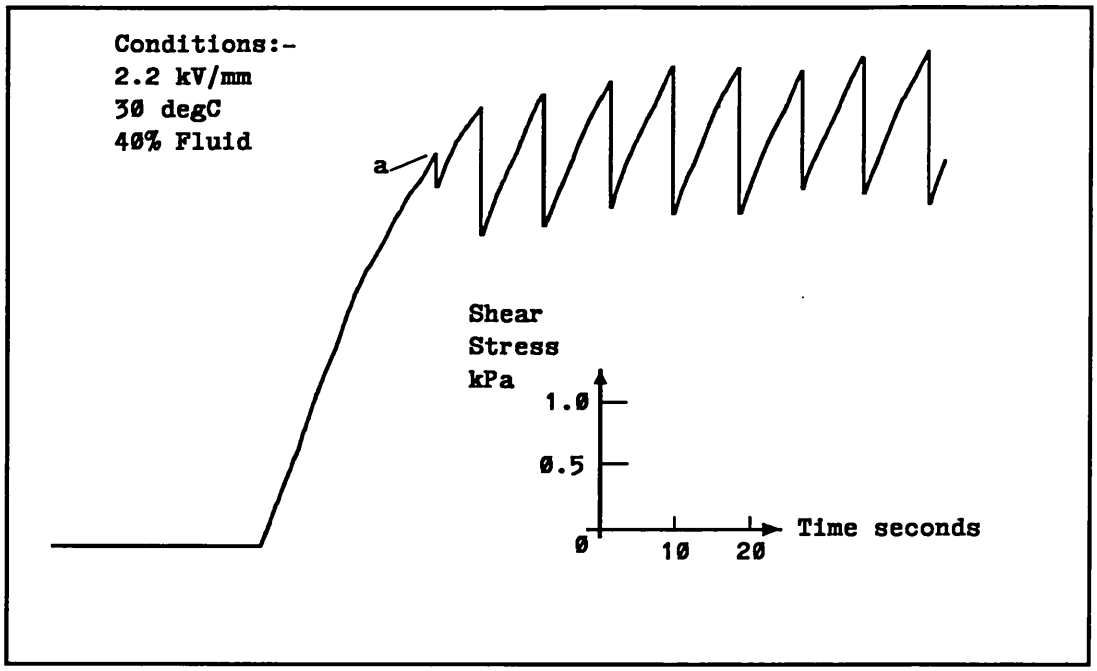


Figure 55b Static Yield Rig Data at Various Fields

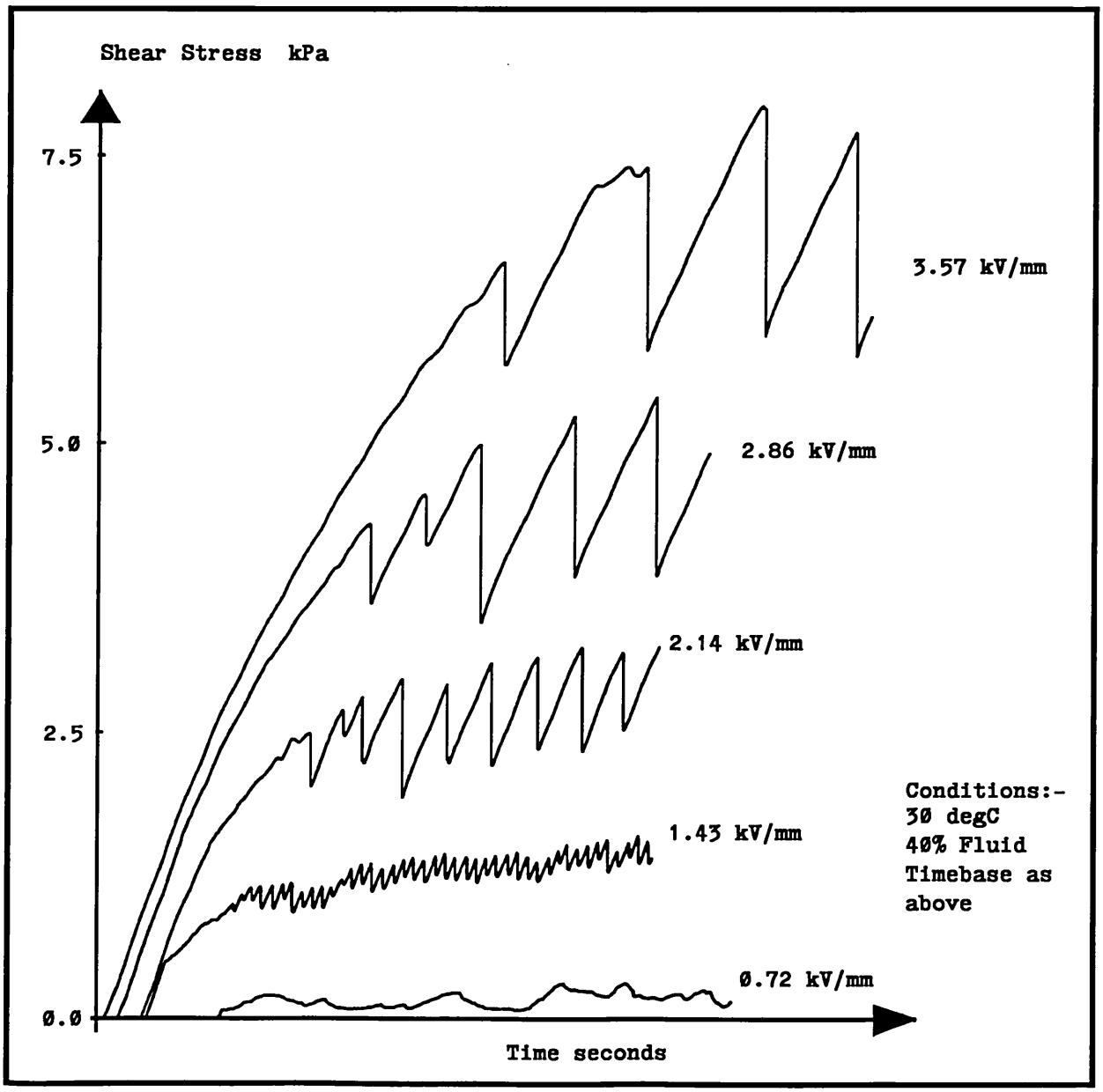


Figure 56a Current versus Applied Field Data from Static Rig

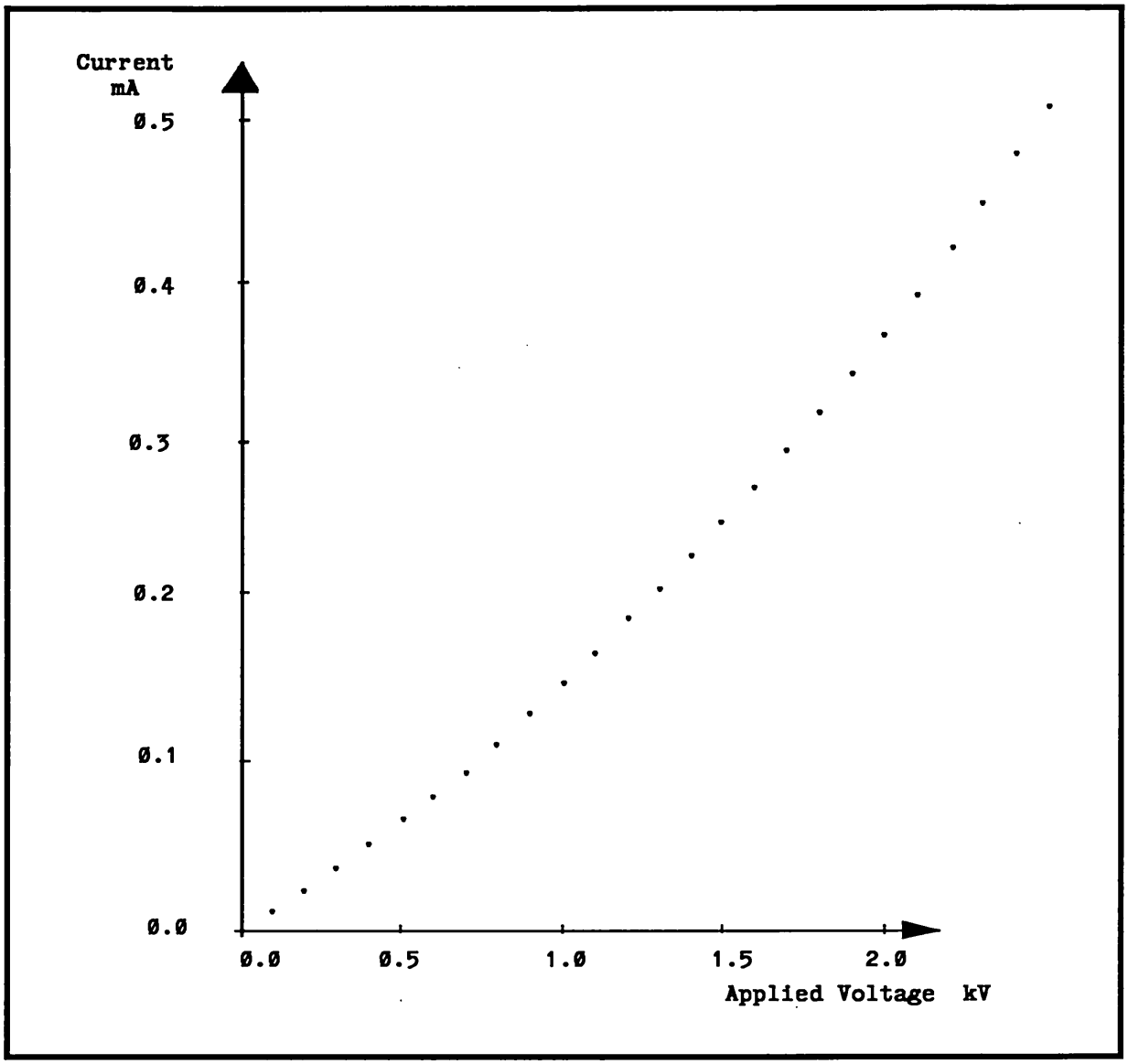


Figure 56b Relaxation of Static Yield with Time

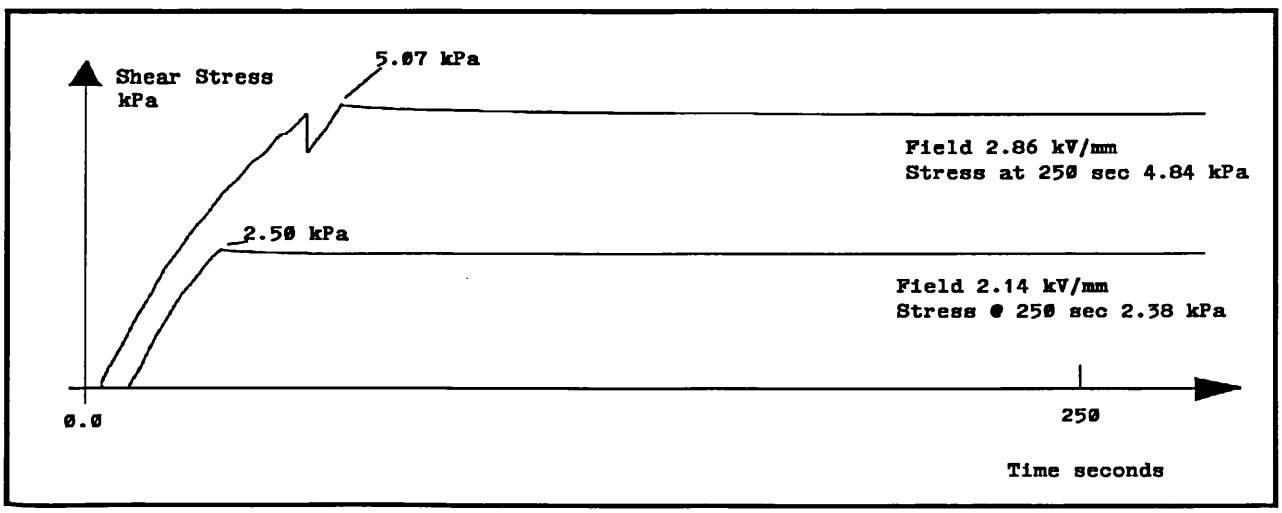


Figure 57a Typical Viscosity-Shear Rate Curve for an ER Fluid

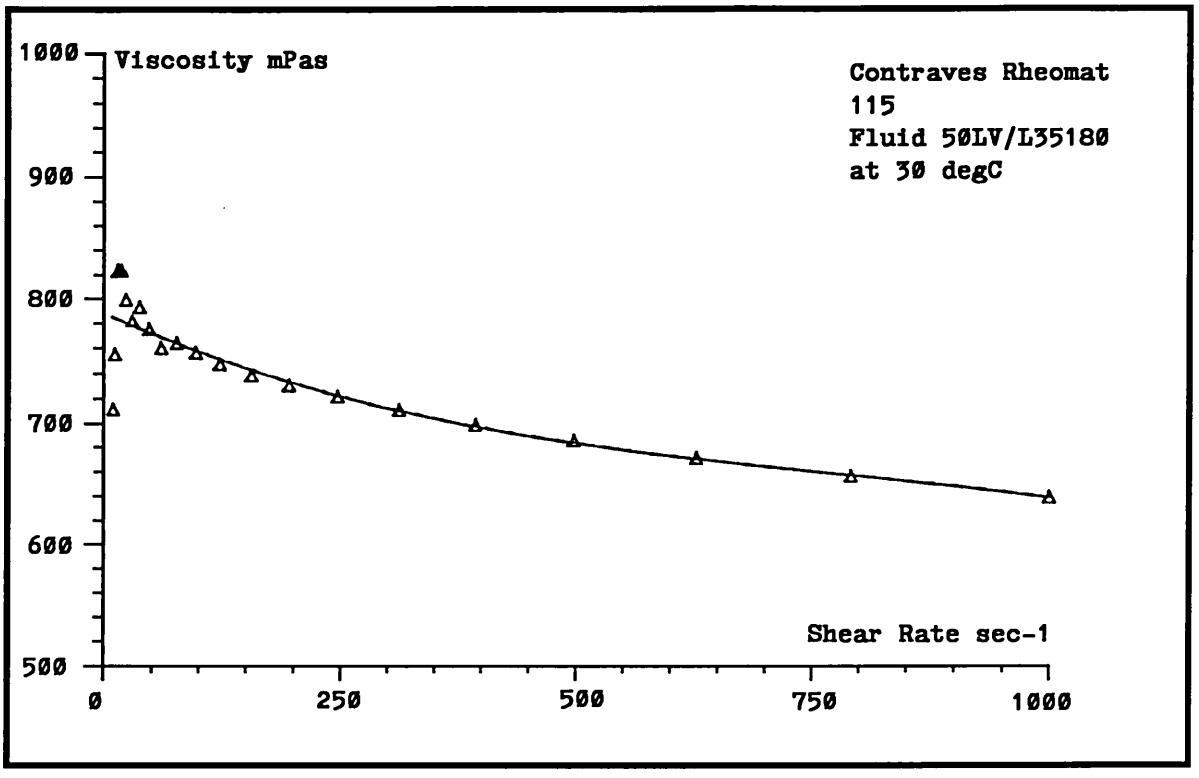


Figure 57b Viscosity Temperature Characteristic

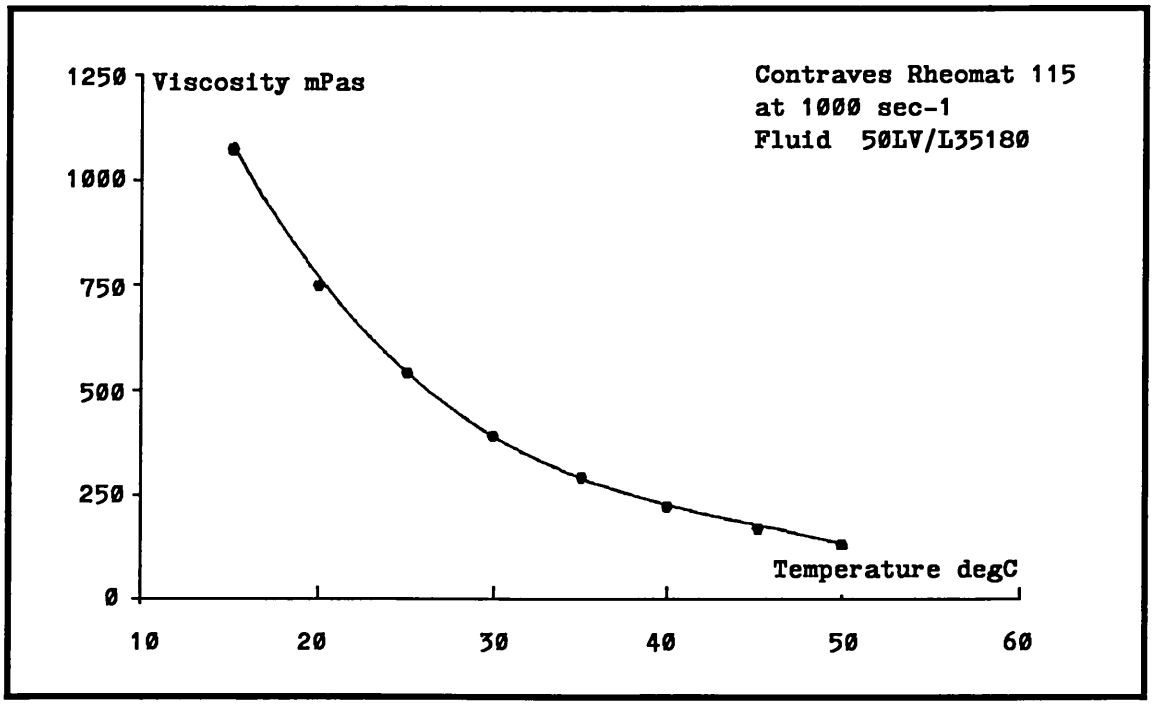


Figure 58a Log Viscosity Curve. Data from Figure 57b

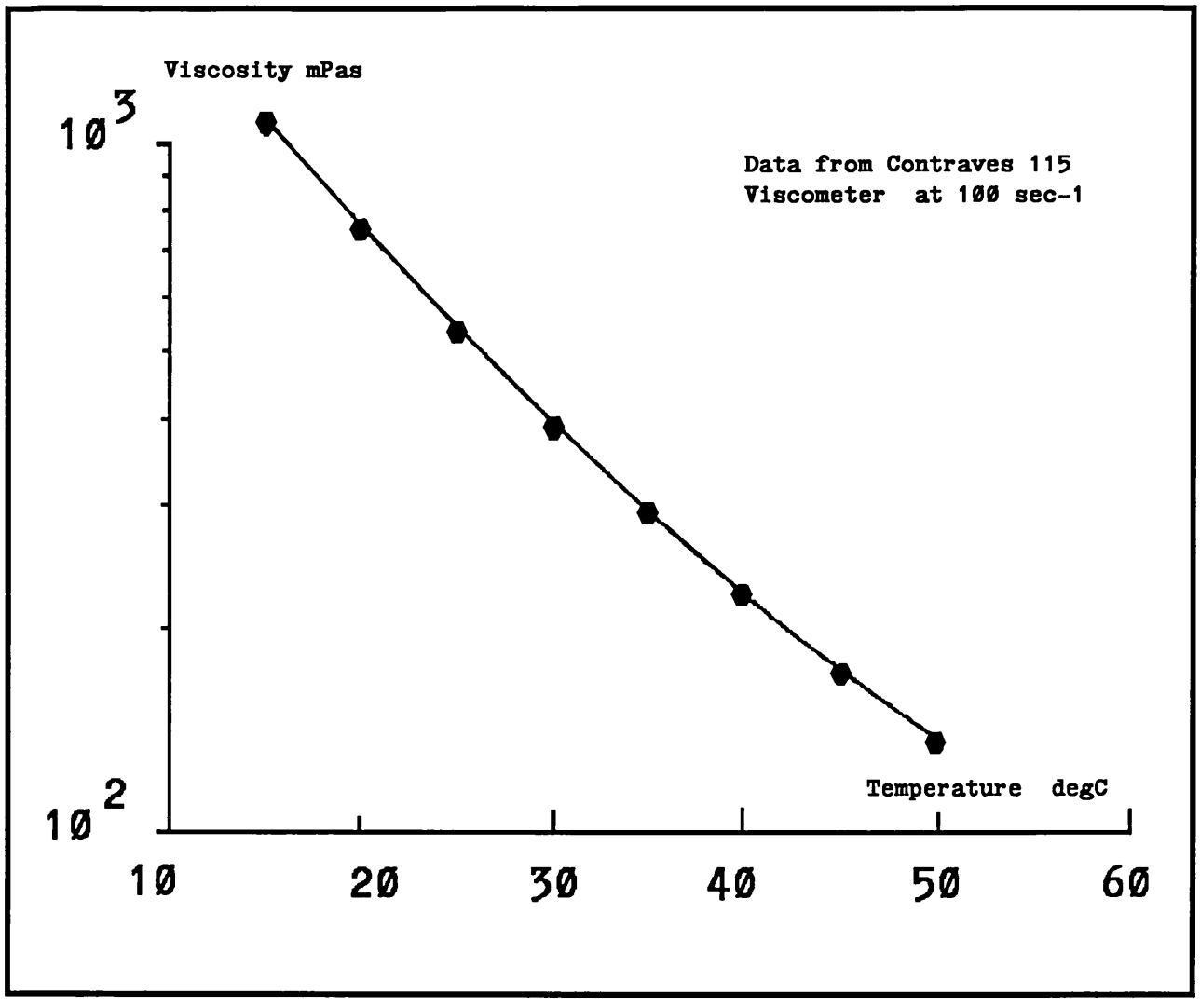


Figure 58b Comparison of Viscosity as Measured on Three Test Rigs

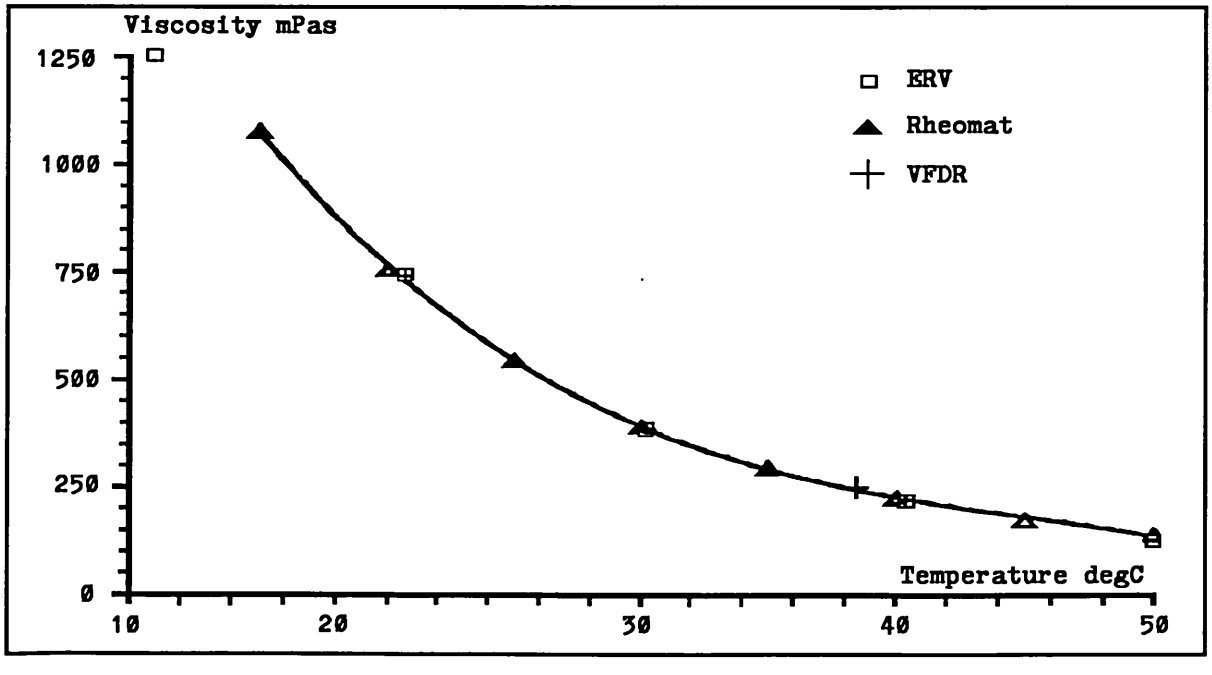
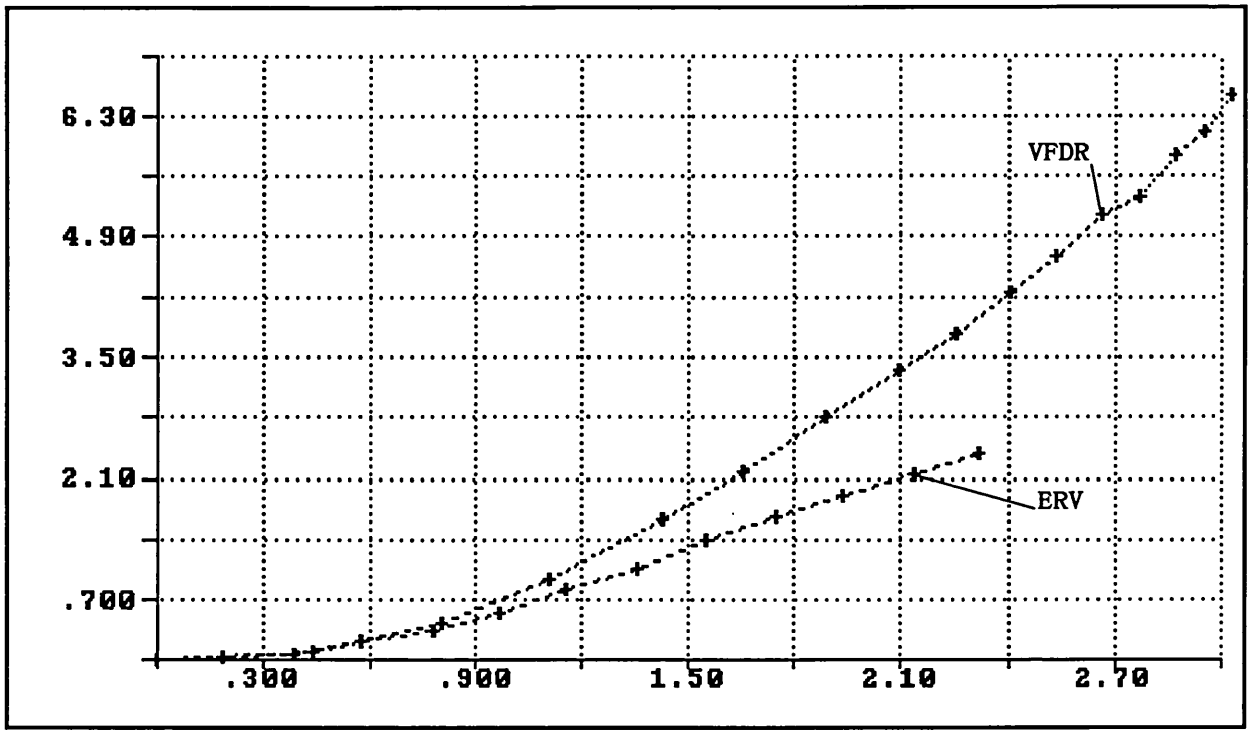


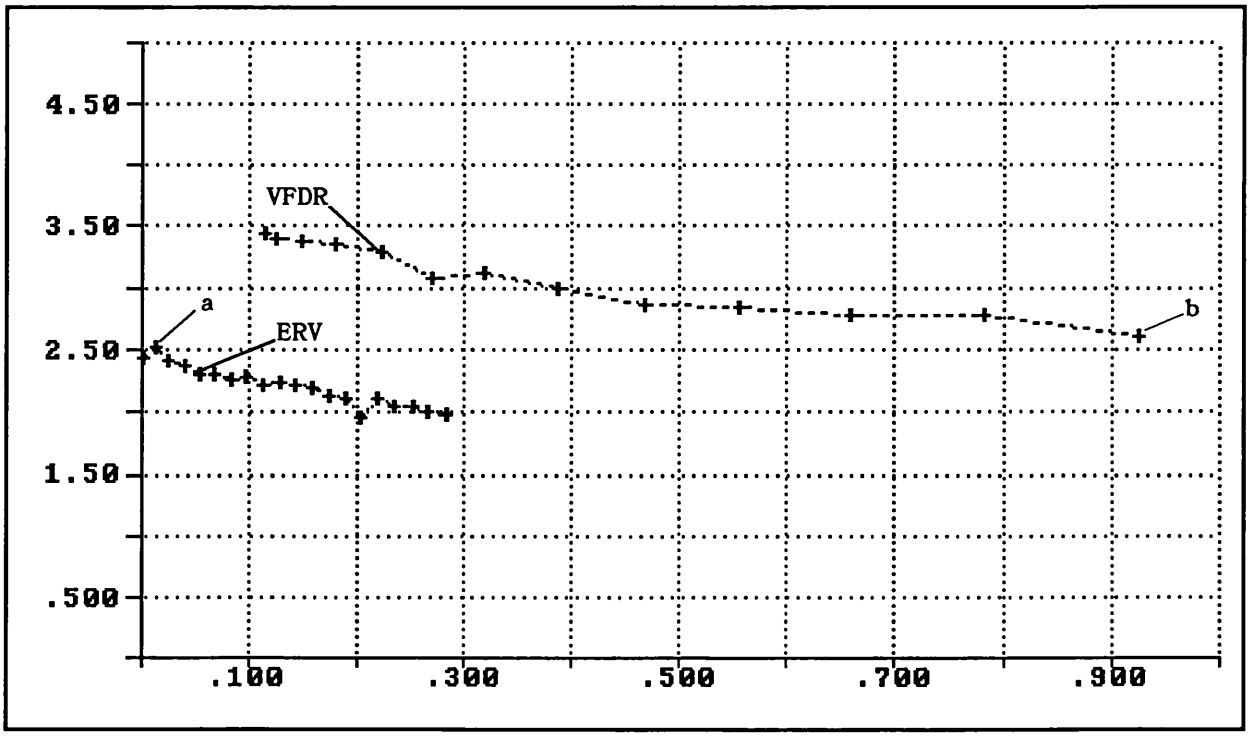
FIGURE 60a PLOT OF EXCESS SHEAR STRESS versus FIELD STRENGTH



Fluid 50LV/L35180
Temperature 30 C
Shear Rate 1750 sec-1

X Axis kV/mm
Y Axis kPa

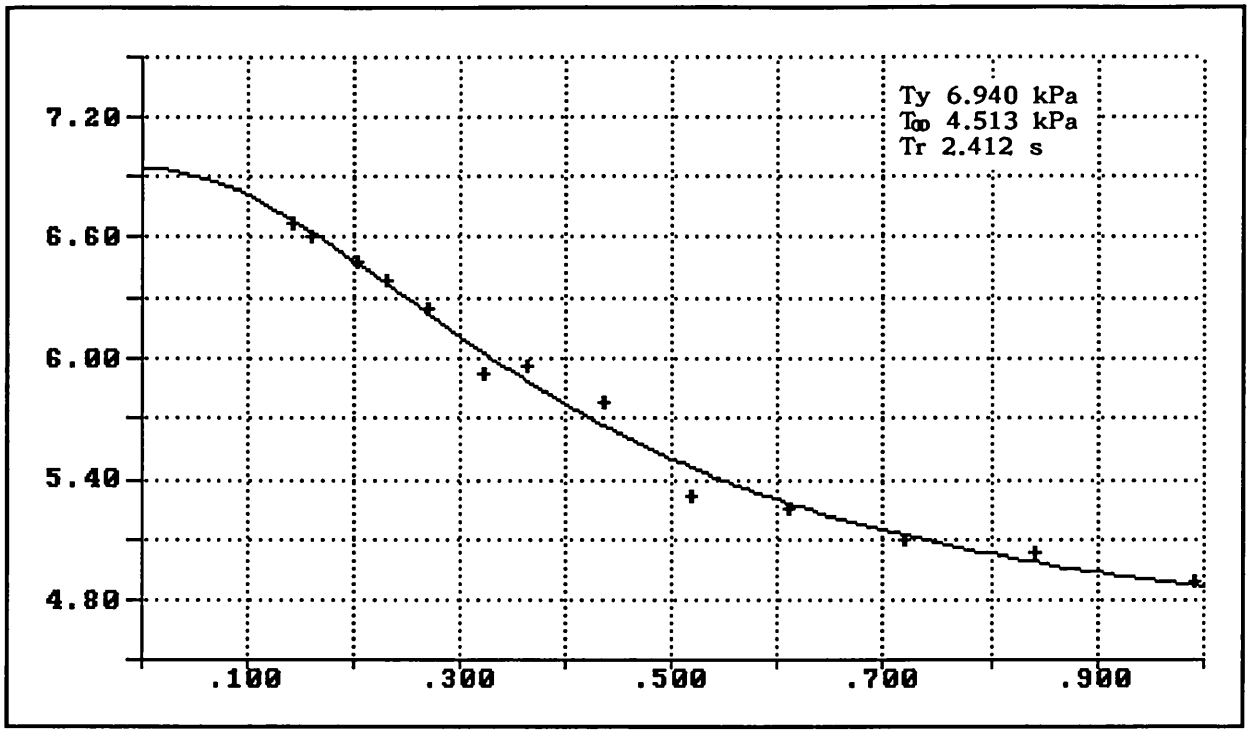
FIGURE 60b PLOT OF EXCESS SHEAR STRESS versus SHEAR RATE



Fluid 50LV/L35180
Temperature 30 C
Field 2.14 kV/mm

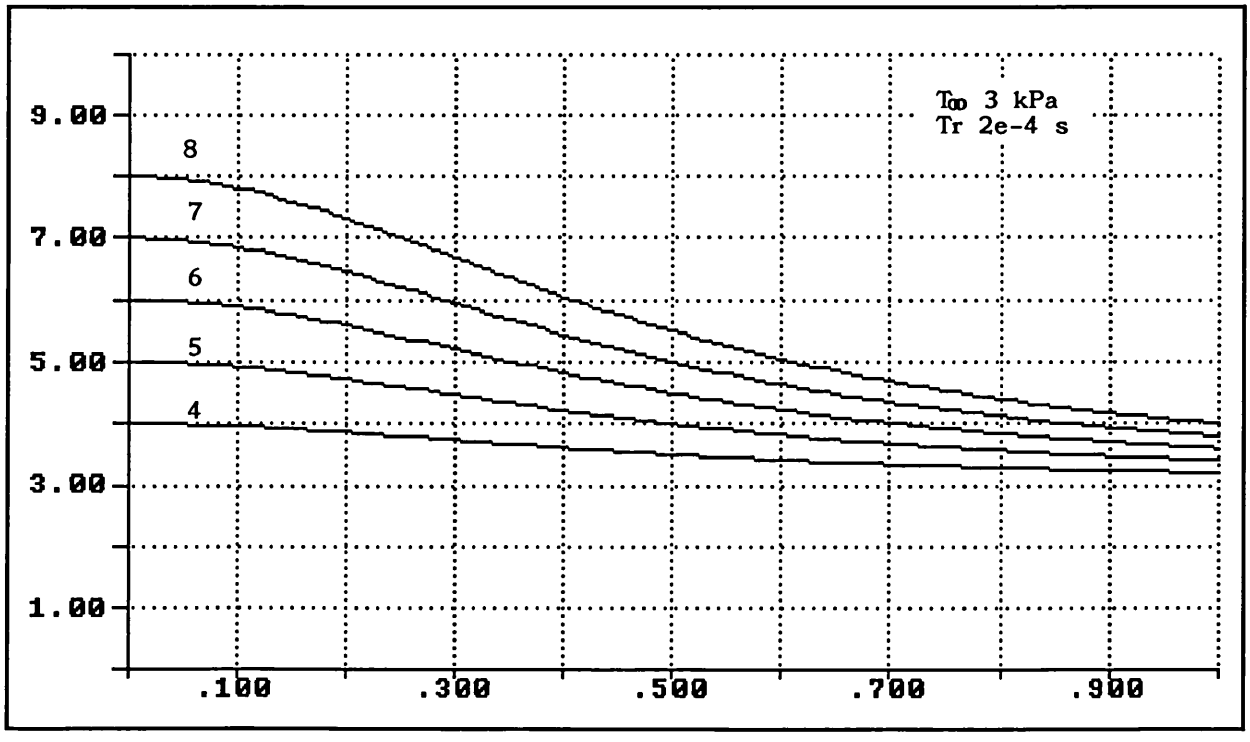
X Axis 1*e4 s-1
Y Axis kPa

FIGURE 61a FIT OF PROPOSED MODEL TO EXPERIMENTAL DATA



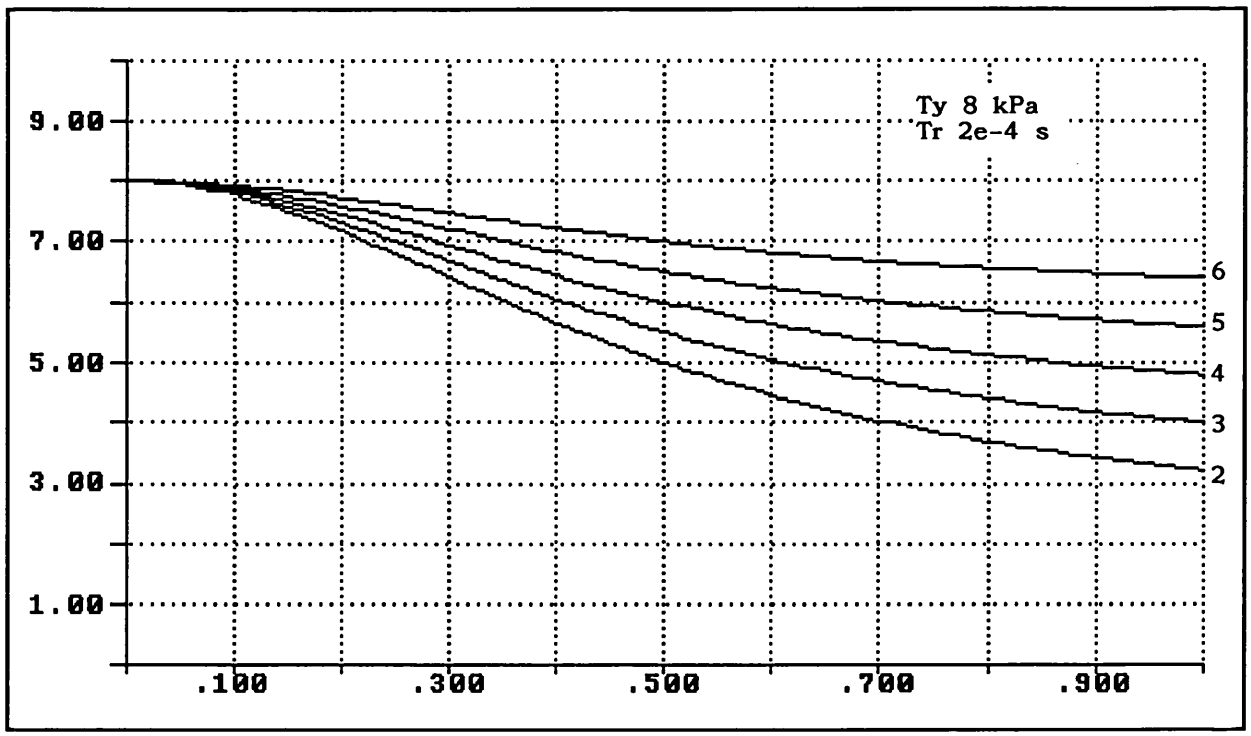
Fluid	50LV/L35180	X Axis 1*e4 s-1
Field	3.05 kV/mm	Y Axis kPa
Gap	0.763 mm	Temperature 30 C

FIGURE 61b PROPOSED MODEL SHOWING VARIATION DUE TO Ty



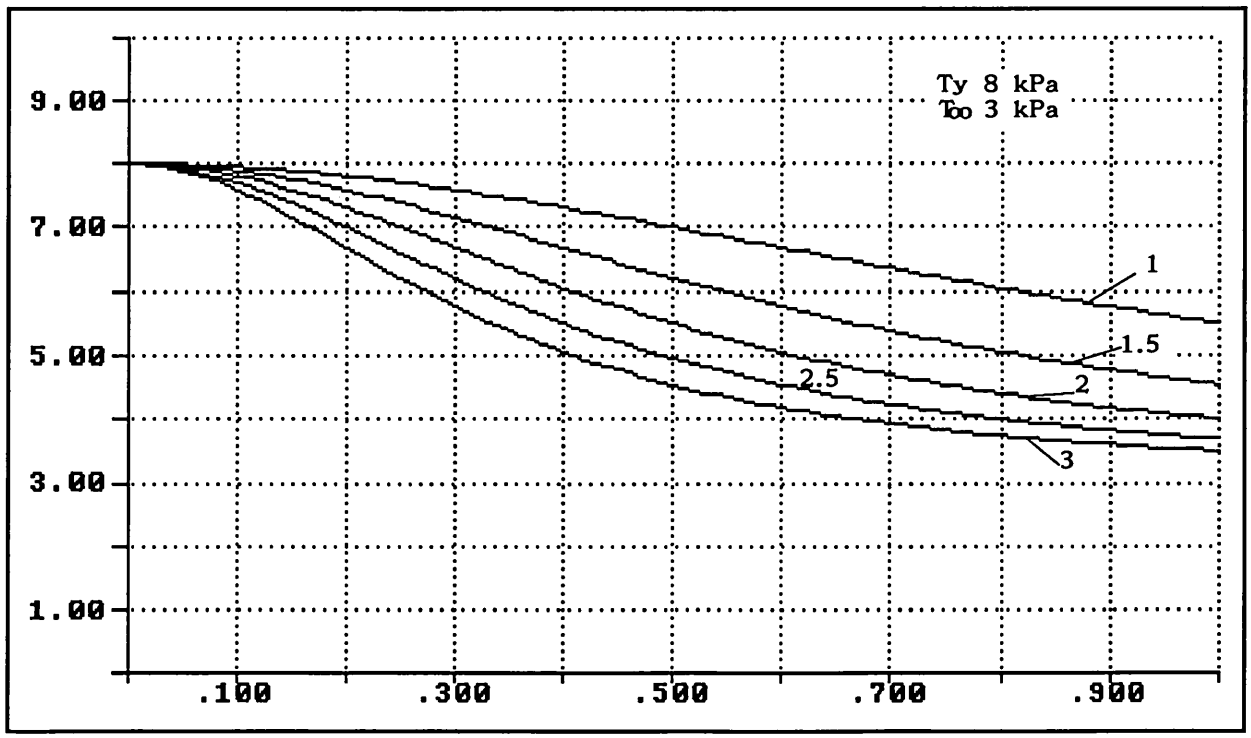
X Axis 1*e4 s-1
Y Axis kPa

FIGURE 62a PROPOSED MODEL SHOWING VARIATION DUE TO τ_{oo}



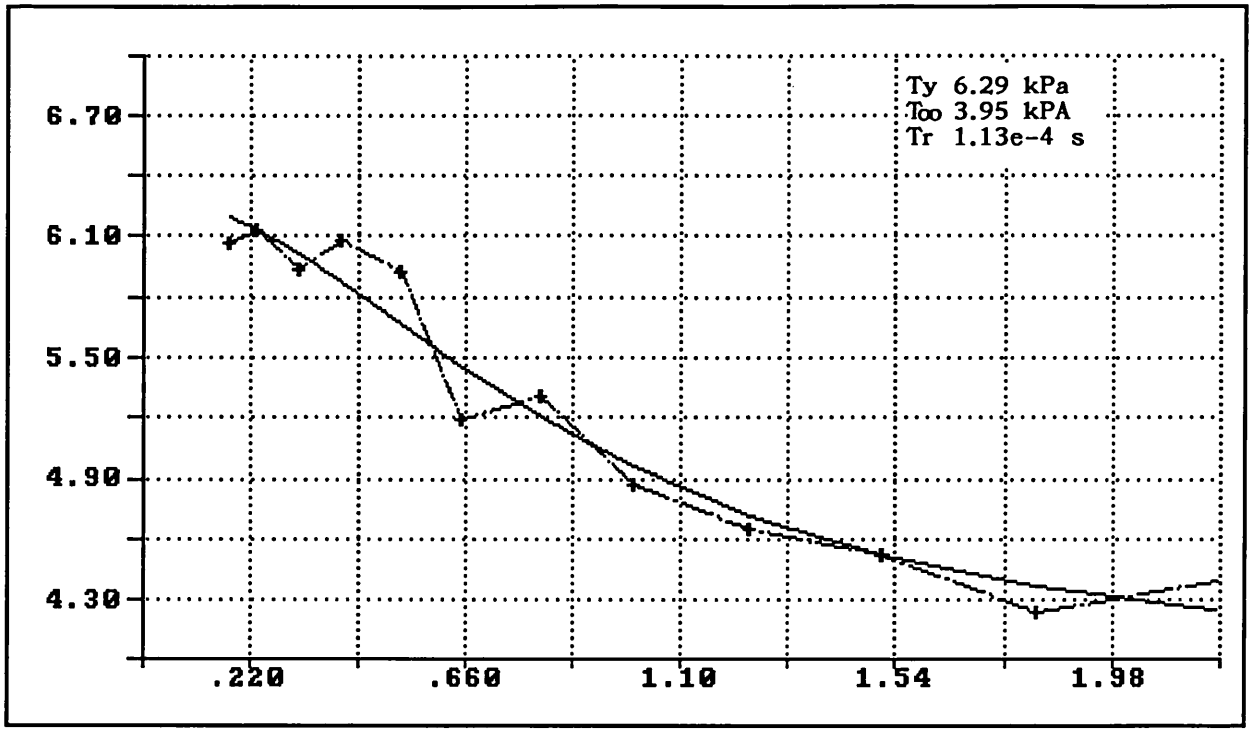
X Axis 1*e4 s-1
Y Axis kPa

FIGURE 62b PROPOSED MODEL SHOWING VARIATION DUE TO Tr



X Axis 1*e4 s-1
Y Axis kPa

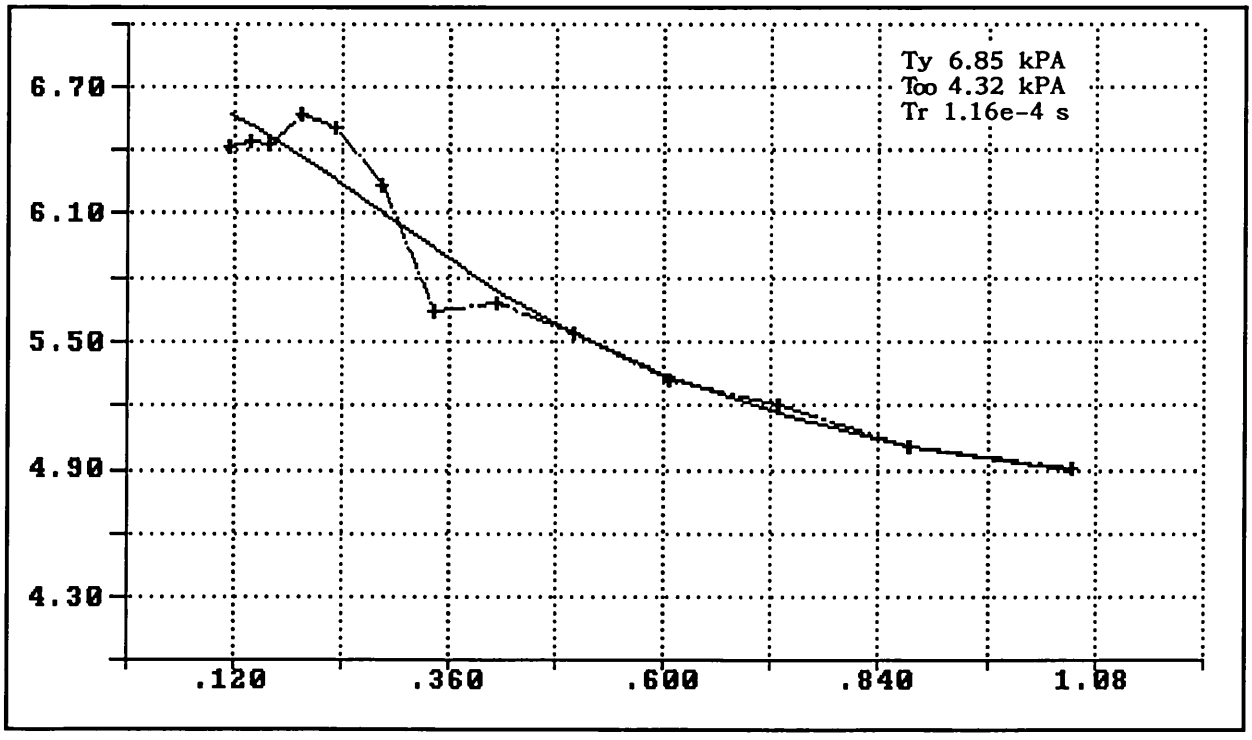
FIGURE 64a FIT OF MODEL TO TEST DATA FOR VALVE GAP OF 0.516 MM



Fluid 50LV/L35157
Temperature 30 C
Gap 0.516 mm

X Axis 1*e4 s-1
Y Axis kPa
Flow Rig

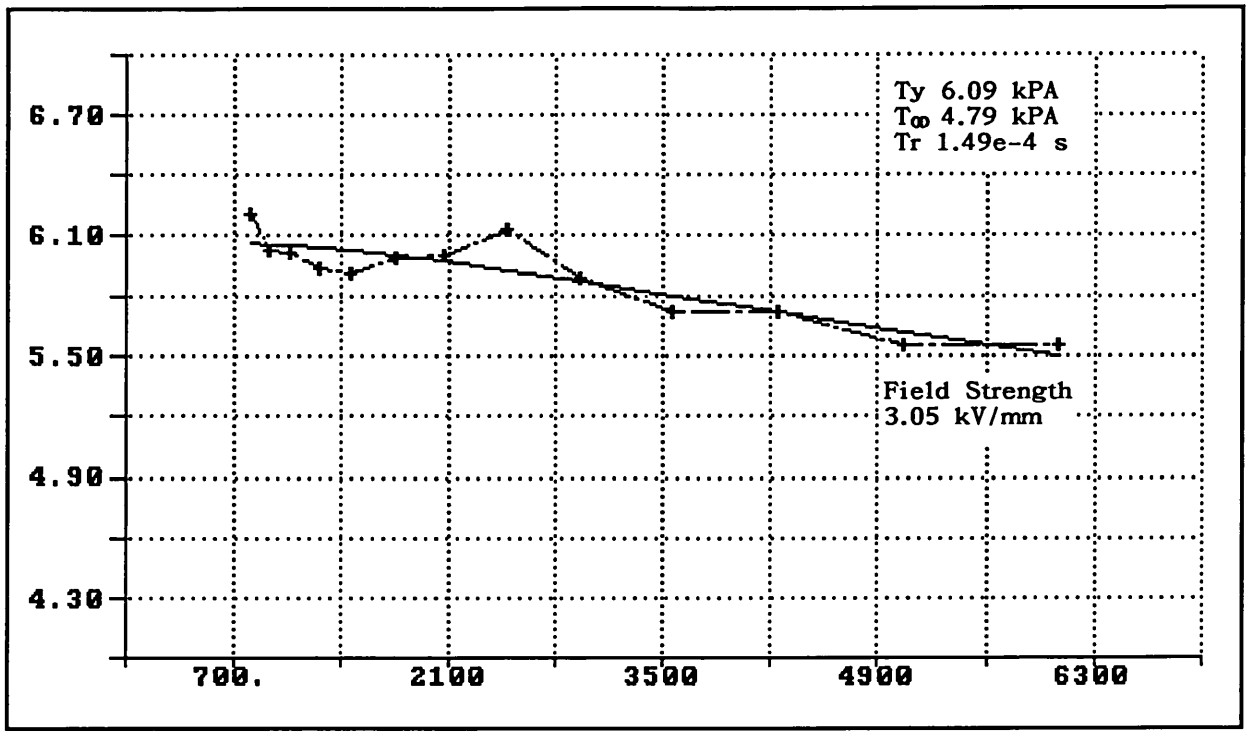
FIGURE 64b FIT OF MODEL TO TEST DATA FOR VALVE GAP OF 0.763 MM



Fluid 50LV/L35157
Temperature 30 C
Gap 0.763 mm

X Axis 1*e4 s-1
Y Axis kPa
Flow Rig

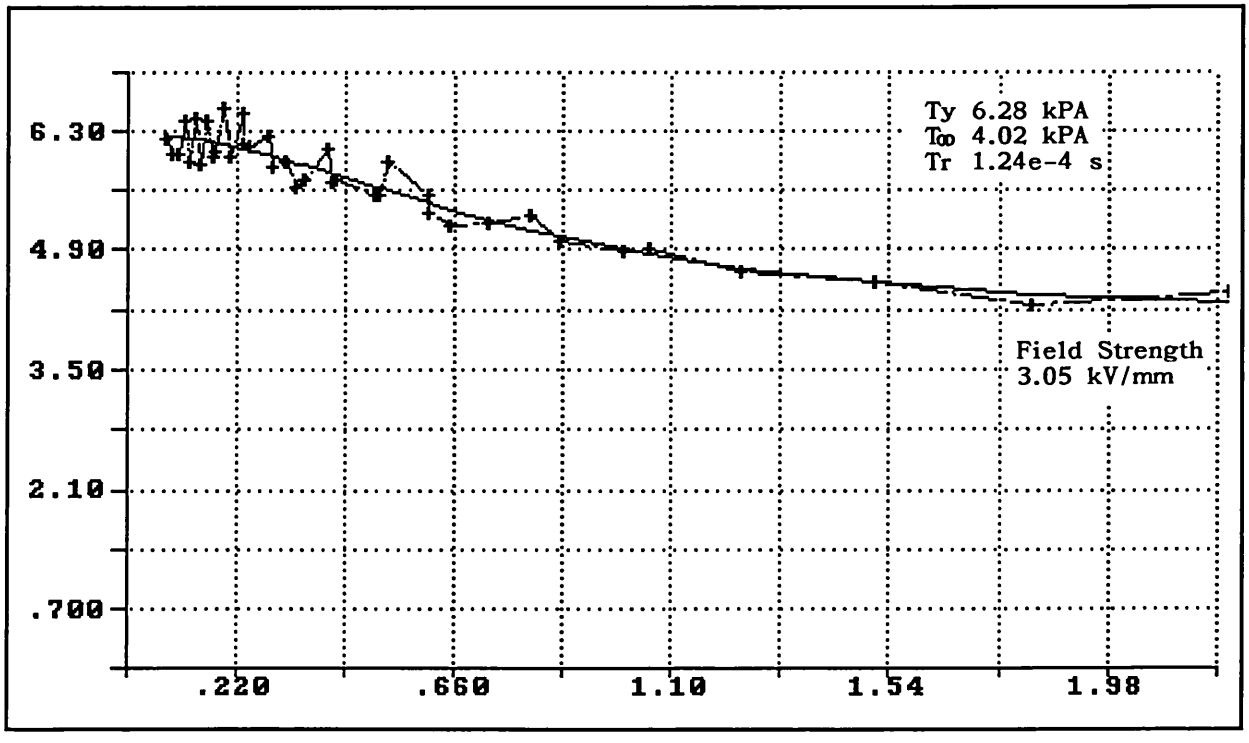
FIGURE 65a FIT OF MODEL TO TEST DATA FOR VALVE GAP OF 1.012 MM



Fluid 50LV/L35157
Temperature 30 C
Gap 1.012 mm

X Axis s-1
Y Axis kPa
Flow Rig

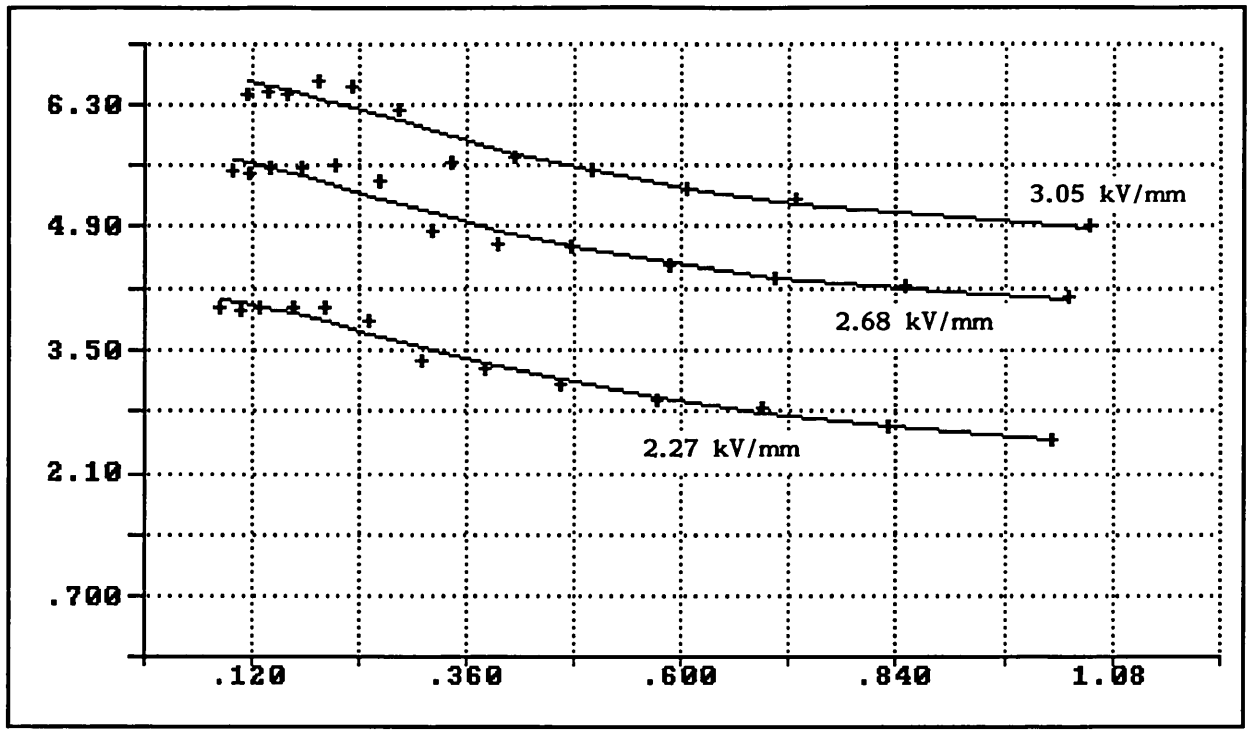
FIGURE 65b FIT OF MODEL TO TEST DATA FOR THREE VALVE GAPS



Fluid 50LV/L35157
Temperature 30 C

X Axis 1*e4 s-1
Y Axis kPa

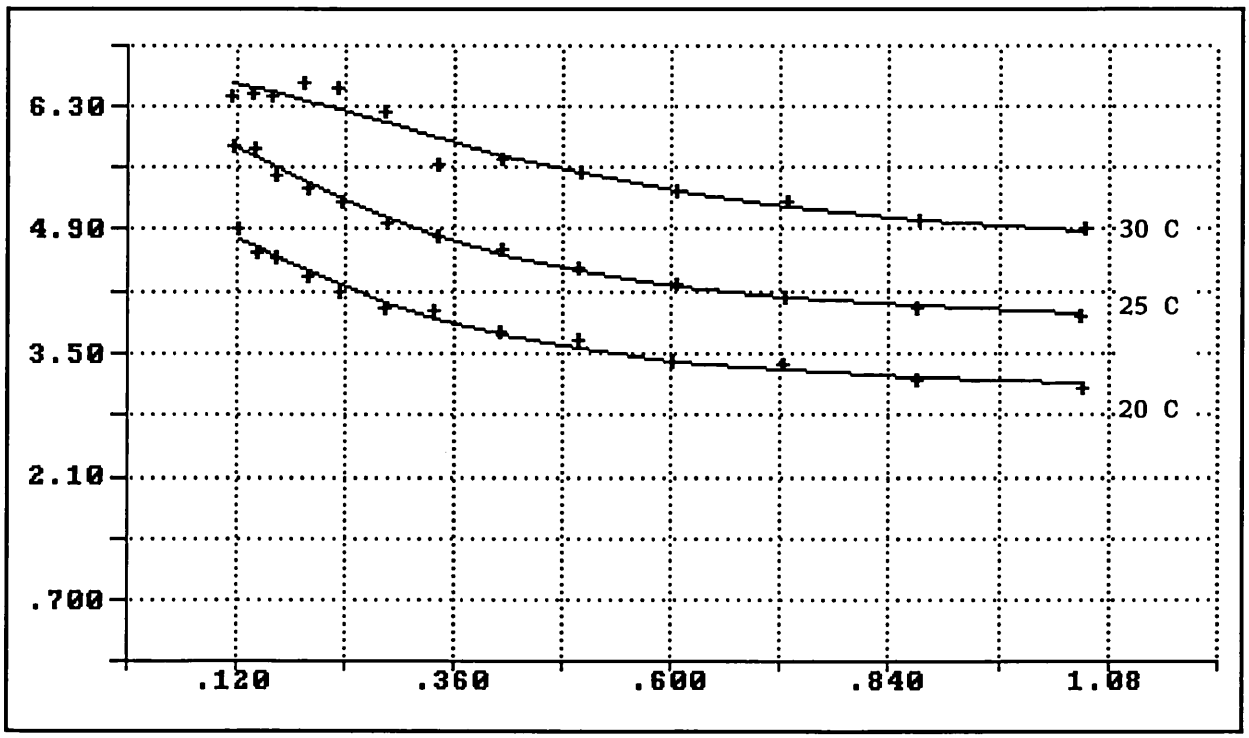
FIGURE 66a PLOT OF MODEL FITTED TO THREE FIELD STRENGTHS



Fluid 50LV/L35157
Temperature 30 C
Gap 0.763 mm

X Axis 1*e4 s-1
Y Axis kPa
Flow Rig

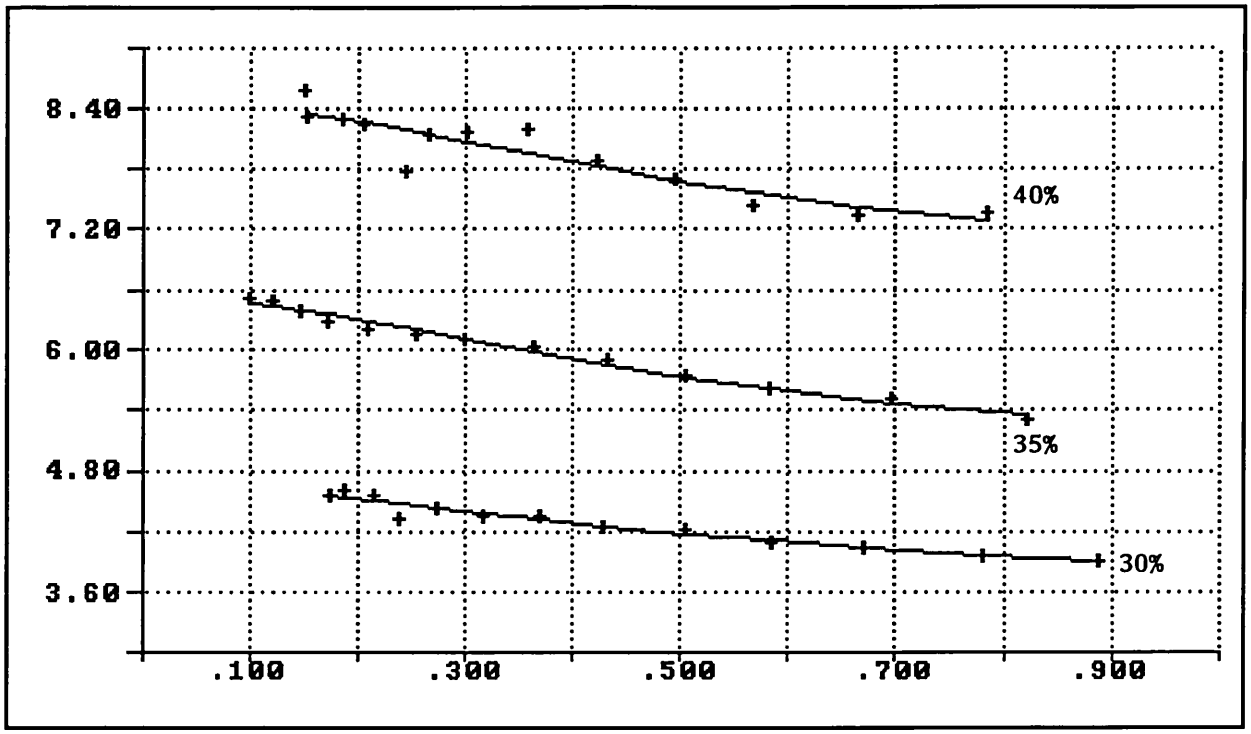
FIGURE 66b PLOT OF MODEL FITTED TO THREE TEMPERATURES



Fluid 50LV/L35157
Field 3.05 kV/mm
Gap 0.763 mm

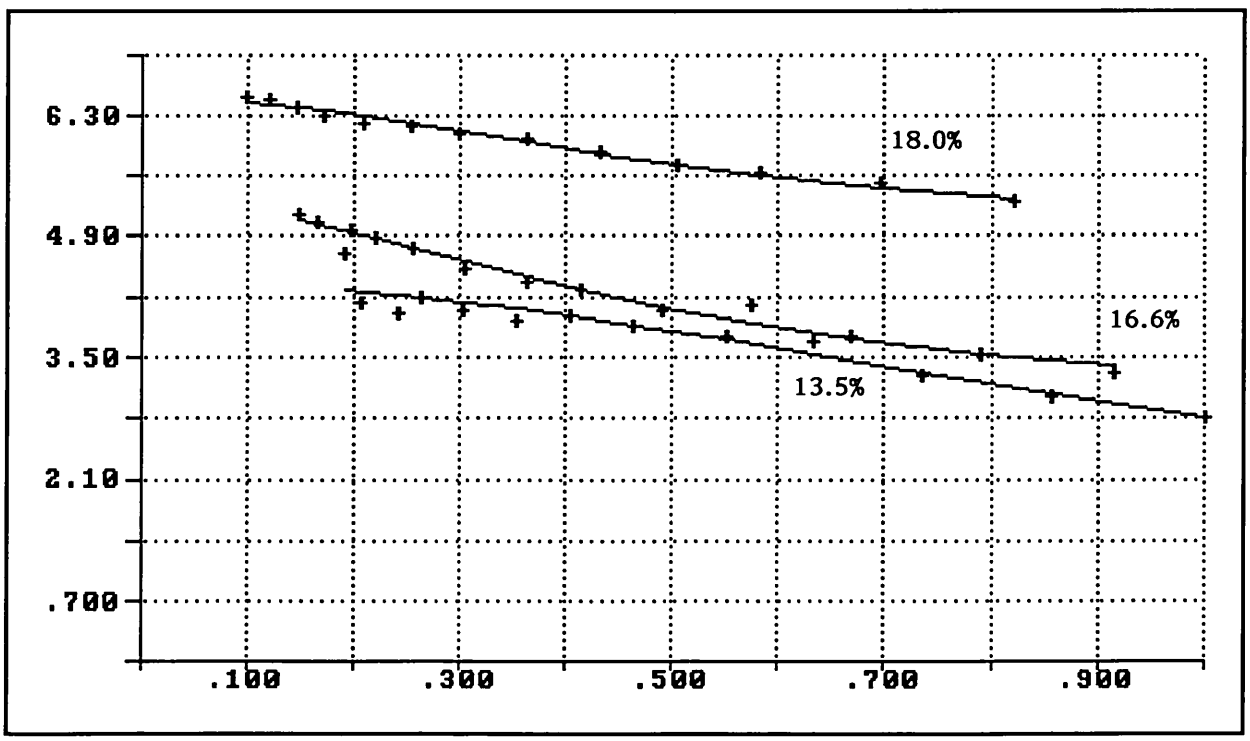
X Axis 1*e4 s-1
Y Axis kPa
Flow Rig

FIGURE 67a PLOT OF MODEL FITTED TO THREE VOLUME FRACTIONS



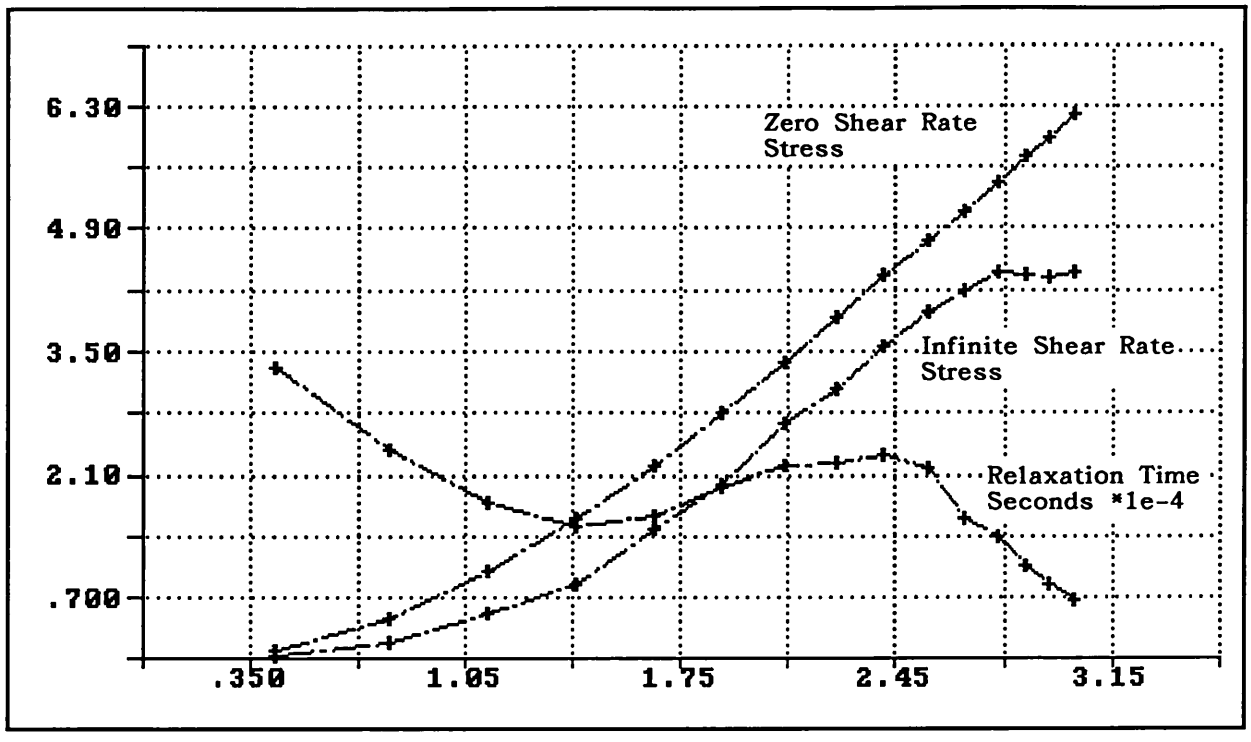
Fluids	50LV Based	X Axis 1*e4 s-1
Field	2.95 kV/mm	Y Axis kPa
Gap	0.763 mm	Temperature 30 C

FIGURE 67b PLOT OF MODEL FITTED TO THREE WATER CONTENTS



Fluids	50LV Based	X Axis 1*e4 s-1
Field	2.95 kV/mm	Y Axis kPa
Gap	0.763 mm	Temperature 30 C

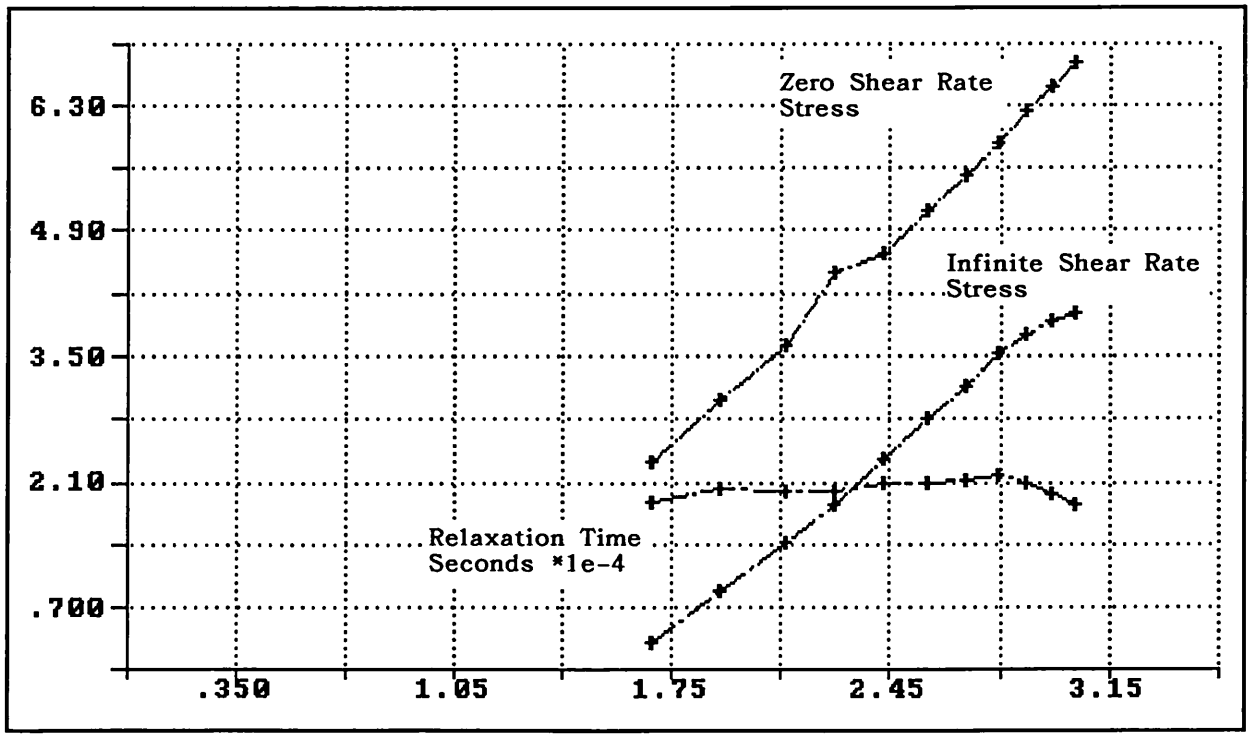
FIGURE 68a CHARACTERISATION OF FLUID 50LV/L35180



Temperature 30 C
Gap 0.763 mm

X Axis kV/mm
Y Axis kPa

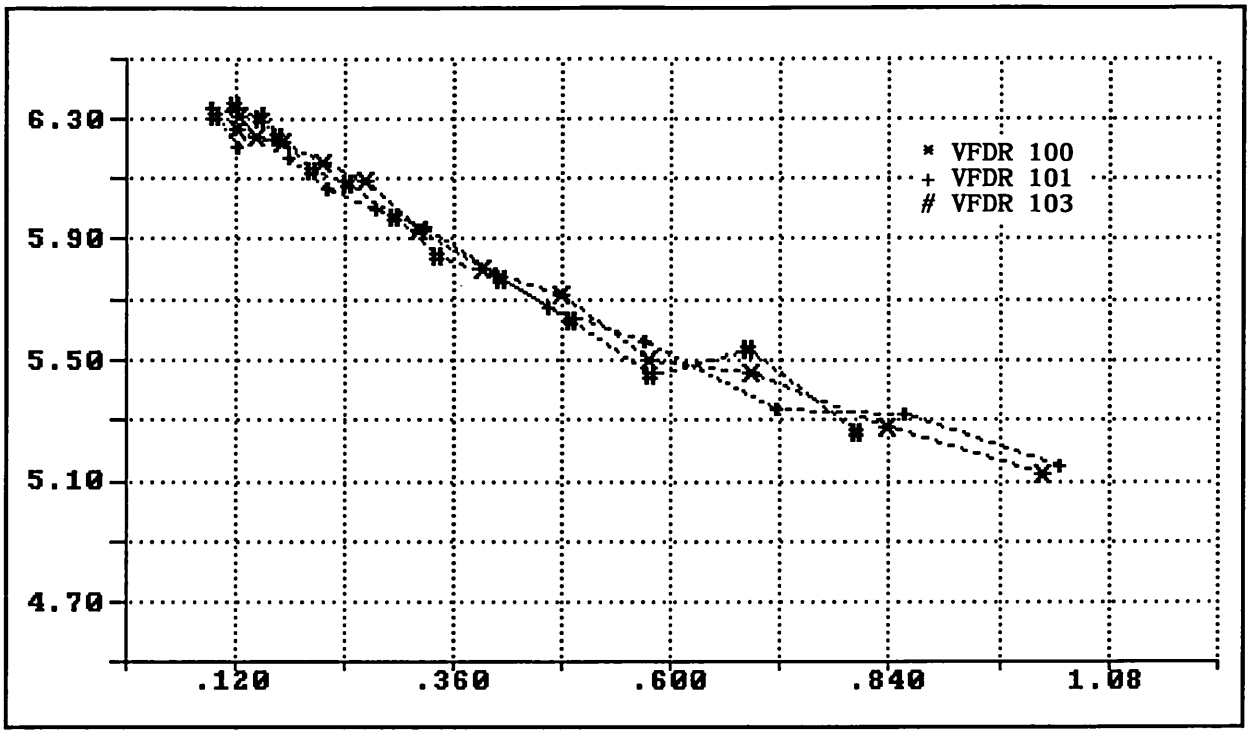
FIGURE 68b CHARACTERISATION OF FLUID 50LV/L35156



Temperature 30 C
Gap 0.763 mm

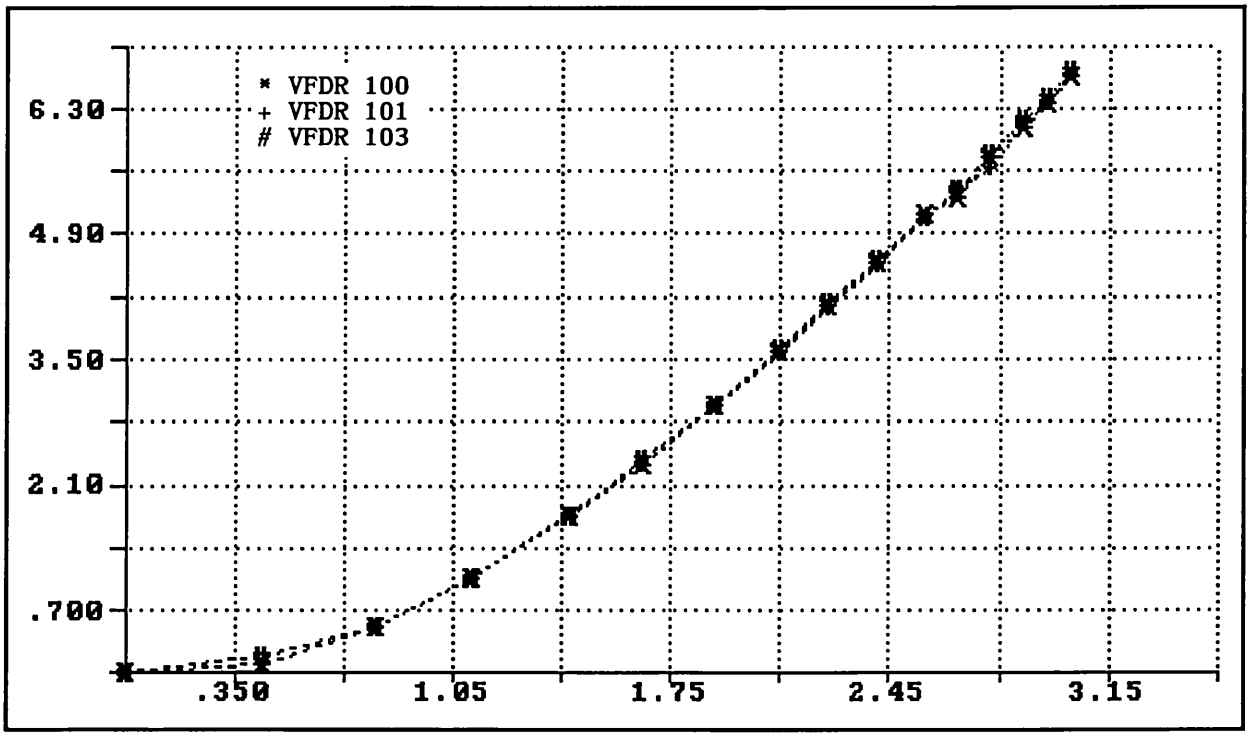
X Axis kv/mm
Y Axis kPa

FIGURE 69a REPRODUCIBILITY OF FLOW DATA



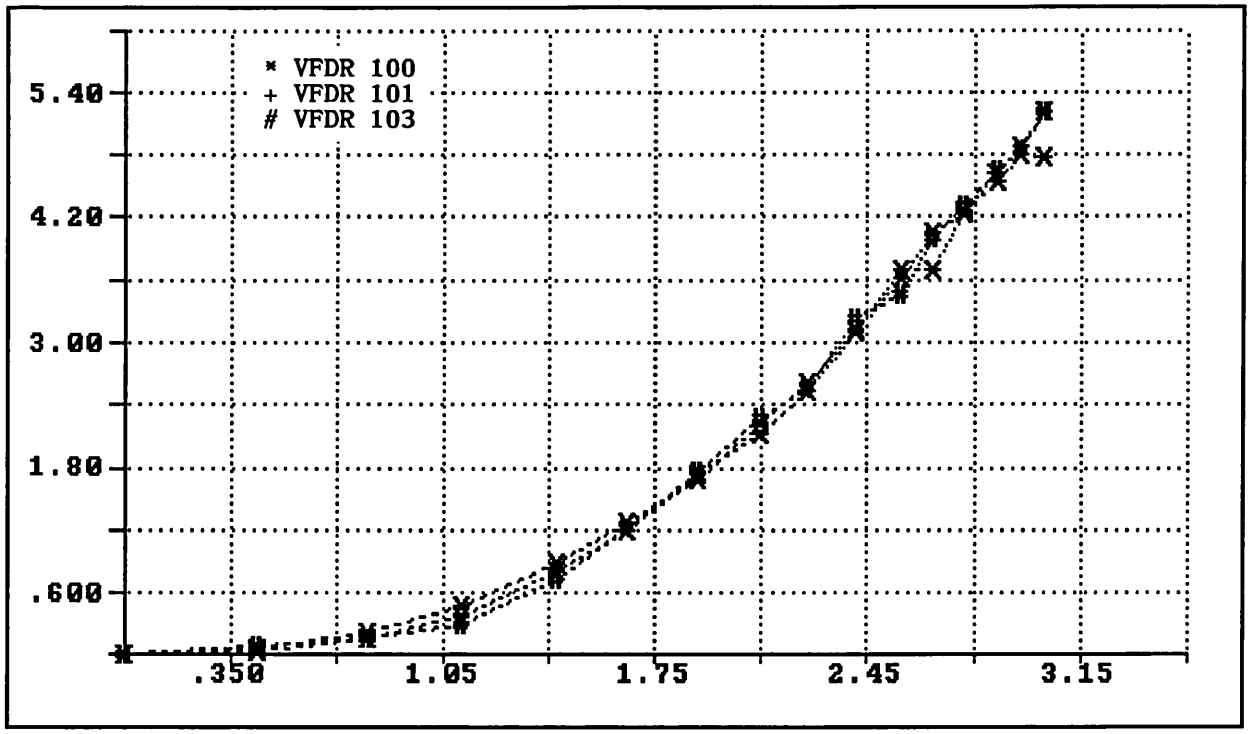
Fluid	50LV/L35180	X Axis 1*e4 s-1
Field	2.95 kV/mm	Y Axis kPa
Gap	0.763 mm	Temperature 30 C

FIGURE 69b REPRODUCIBILITY OF FIT TO ZERO SHEAR RATE INTERCEPT



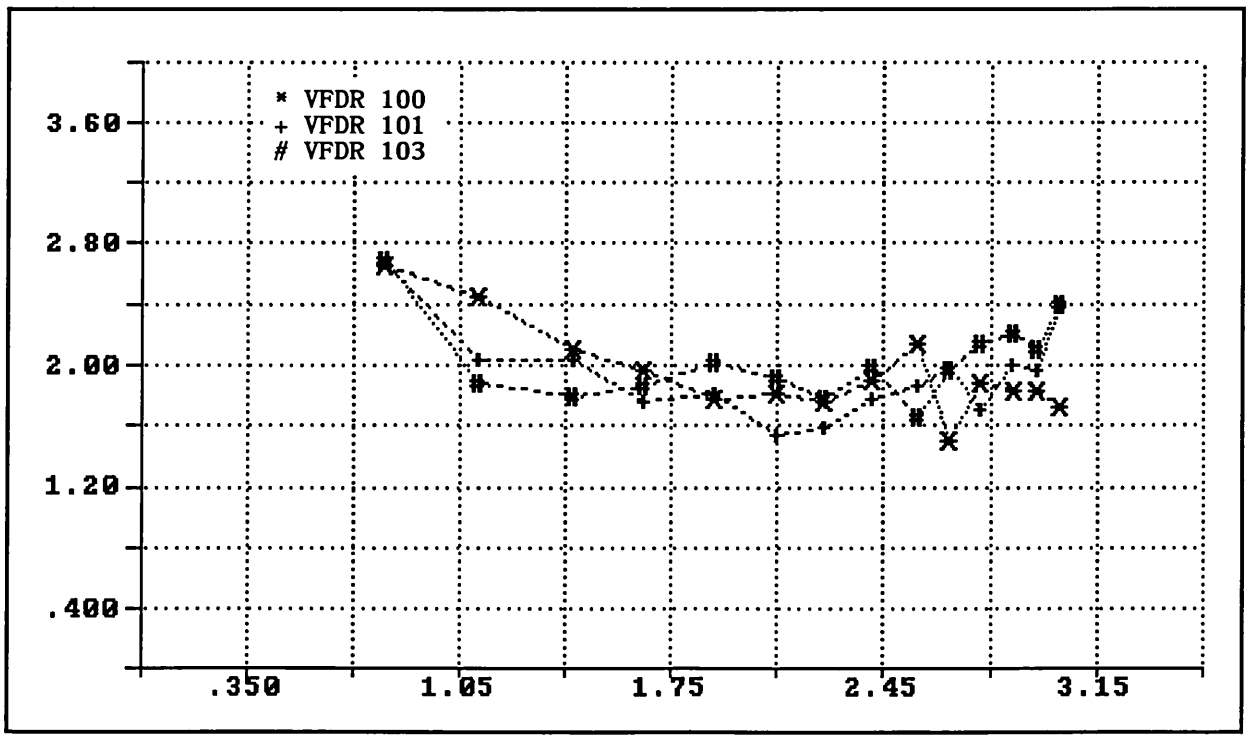
Fluid	50LV/L35180	X Axis kV/mm
Field	2.95 kV/mm	Y Axis kPa
Gap	0.763 mm	Temperature 30 C

FIGURE 70a REPRODUCIBILITY OF FIT TO INFINITE SHEAR RATE INTERCEPT



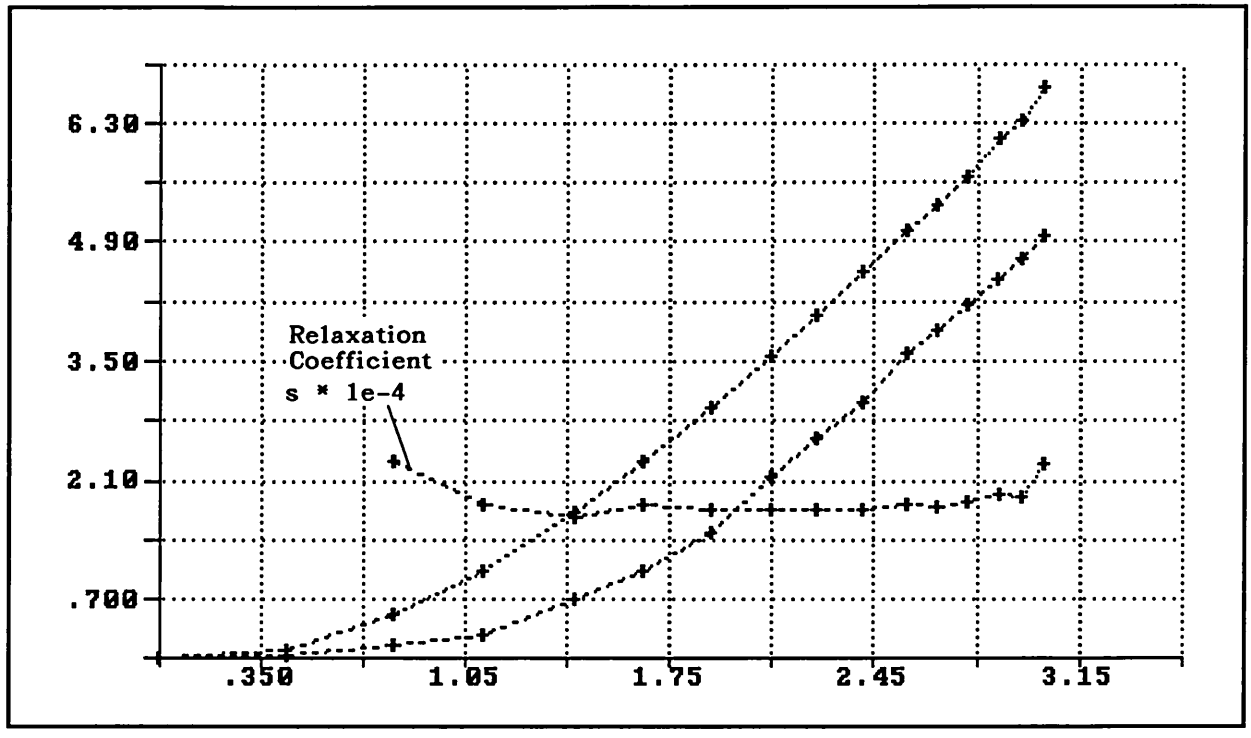
Fluid	50LV/L35180	X Axis kV/mm
Field	2.95 kV/mm	Y Axis kPa
Gap	0.763 mm	Temperature 30 C

FIGURE 70b REPRODUCIBILITY OF FIT TO RELAXATION COEFFICIENT



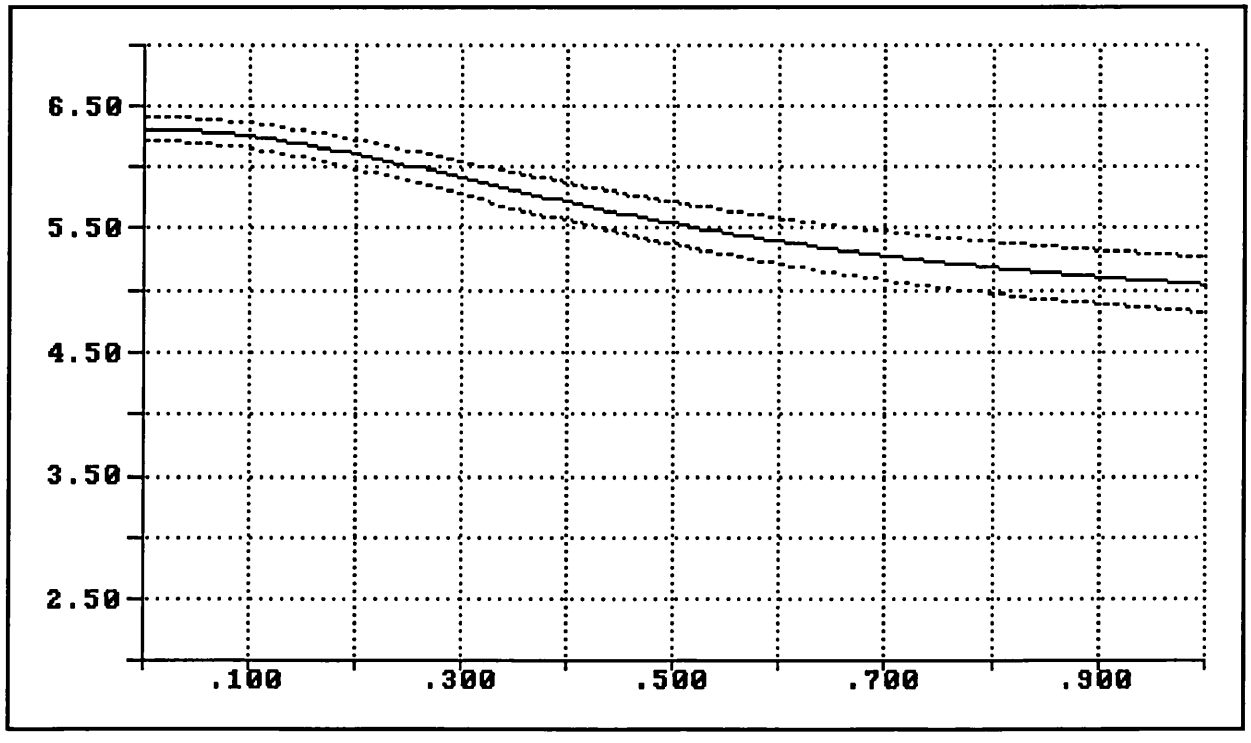
Fluid	50LV/L35180	X Axis kV/mm
Field	2.95 kV/mm	Y Axis s * 1e-4
Gap	0.763 mm	Temperature 30 C

FIGURE 71a MEAN CHARACTERISATION OF FLUID USING SIX SETS OF DATA



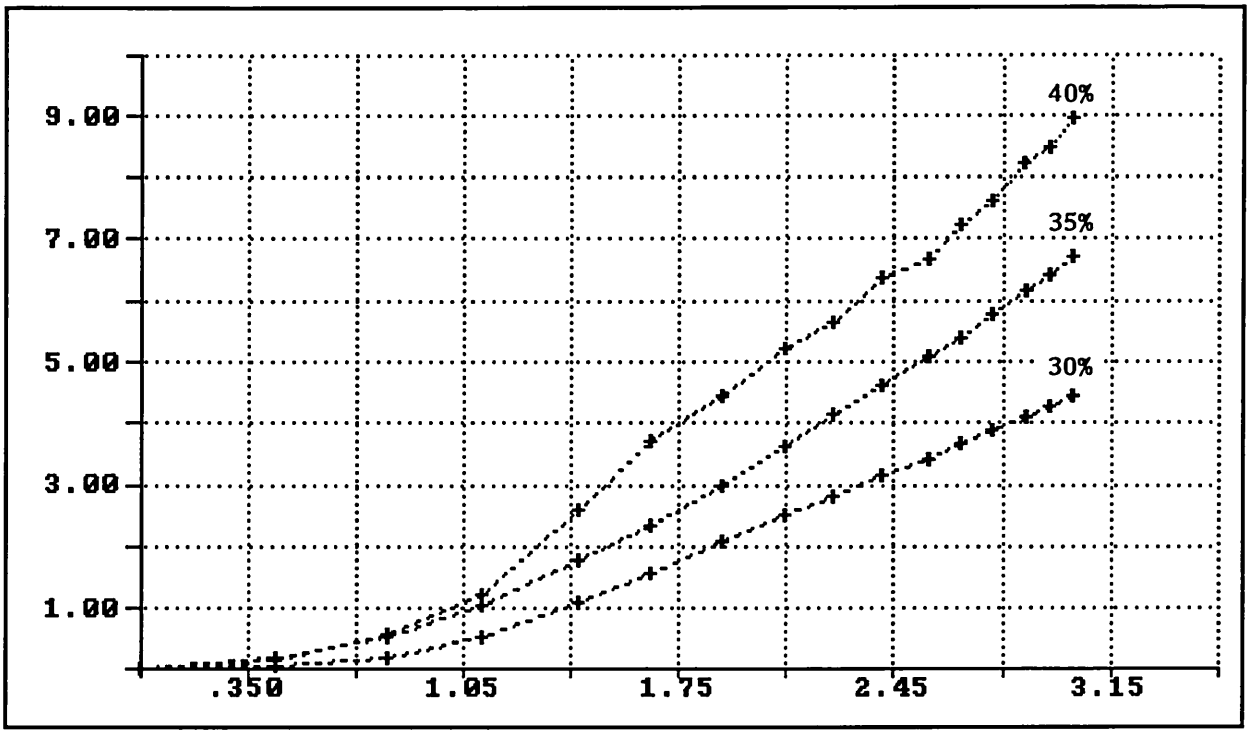
Fluid	50LV/L35180	X Axis kV/mm
Field	2.95 kV/mm	Y Axis kPa + sec
Gap	0.763 mm	Temperature 30 C

FIGURE 71b 95% CONFIDENCE LIMITS ON MODEL



Fluid	50LV/L35180	X Axis 1*e4 s-1
Field	2.95 kV/mm	Y Axis kPa
Gap	0.763 mm	Temperature 30 C

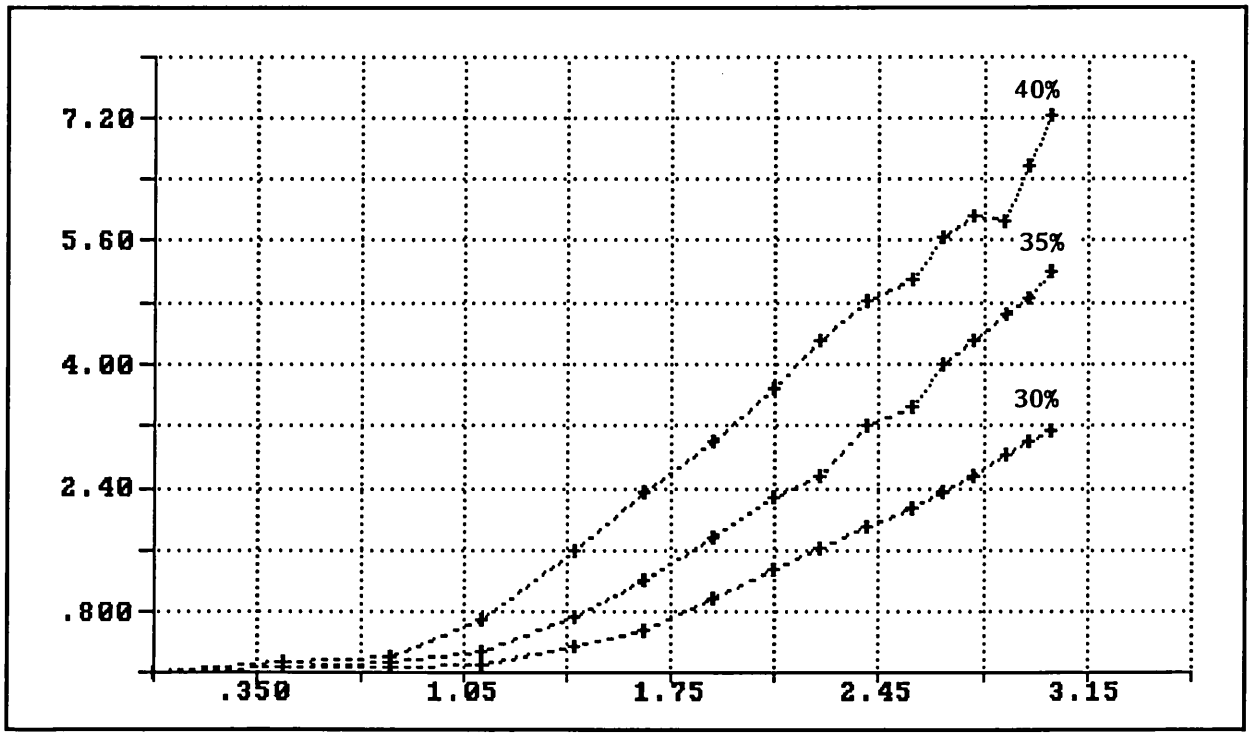
FIGURE 72a ZERO SHEAR RATE INTERCEPT FOR THREE VOLUME FRACTIONS



Fluids 50LV Based
Temperature 30 C
Gap 0.763 mm

X Axis kV/mm
Y Axis kPa
Flow Rig

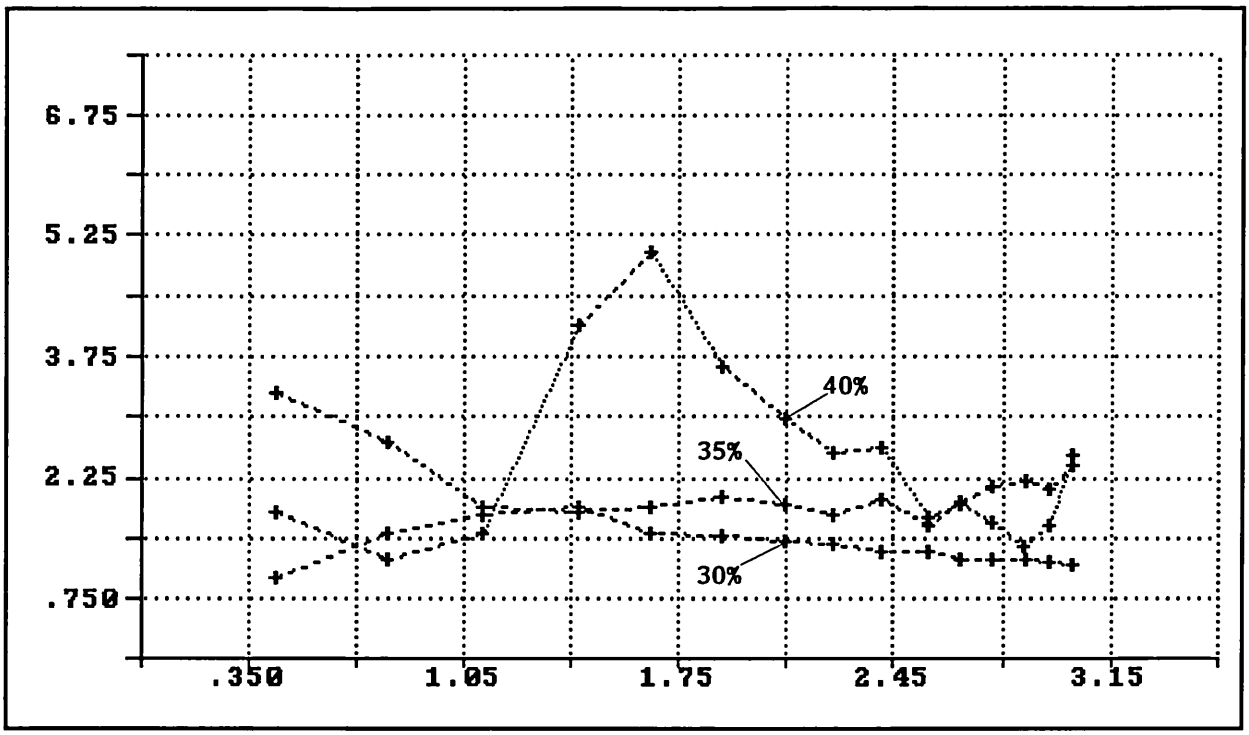
FIGURE 72b INFINITE SHEAR RATE INTERCEPT FOR THREE VOLUME FRACTIONS



Fluids 50LV Based
Temperature 30 C
Gap 0.763 mm

X Axis kV/mm
Y Axis kPa
Flow Rig

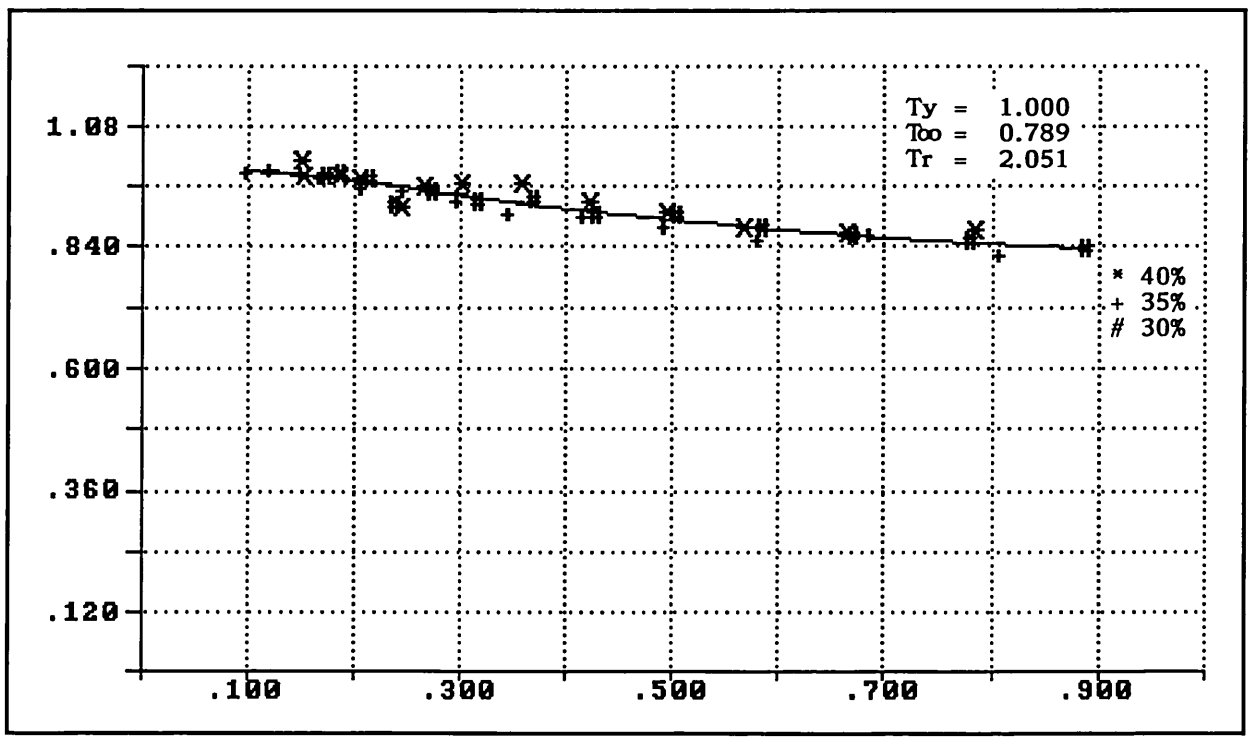
FIGURE 73a RELAXATION COEFFICIENT FOR THREE VOLUME FRACTIONS



Fluids 50LV Based
Temperature 30 C
Gap 0.763 mm

X Axis kV/mm
Y Axis s *1e-4
Flow Rig

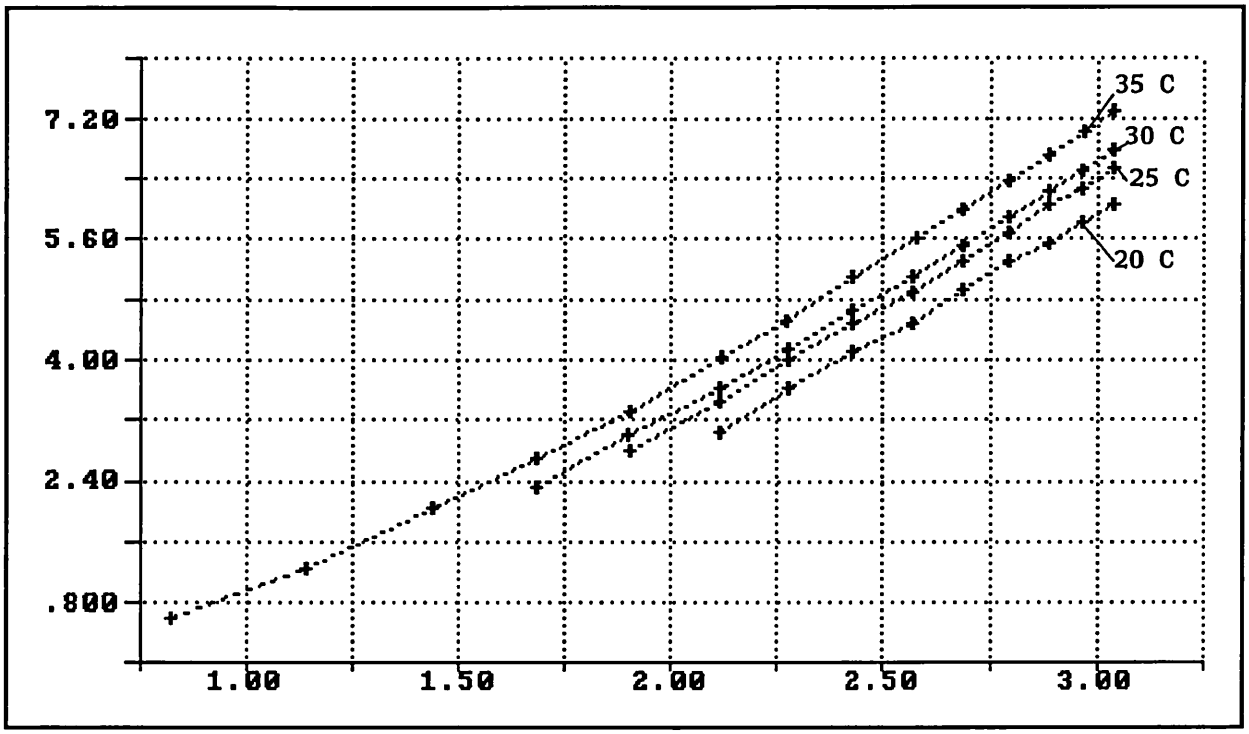
FIGURE 73b FIT OF MODEL TO NORMALISED VOLUME FRACTION DATA



Fluids 50LV Based
Temperature 30 C
Gap 0.763 mm

X Axis kV/mm
Y Axis kPa Norm
Flow Rig

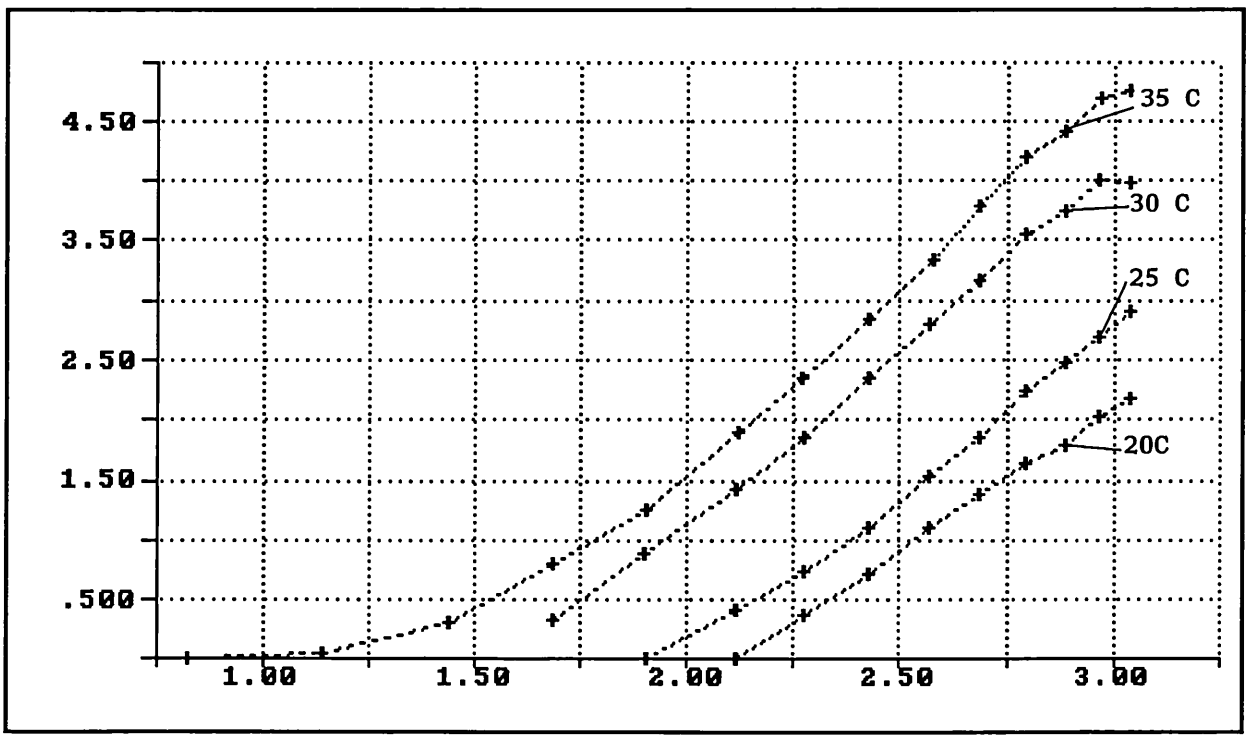
FIGURE 74a ZERO SHEAR RATE INTERCEPT AT DIFFERENT TEMPERATURES



Fluid 50LV/L35156
Temperature 30 C
Gaps Three Used

X Axis kV/mm
Y Axis kPa
Flow Rig

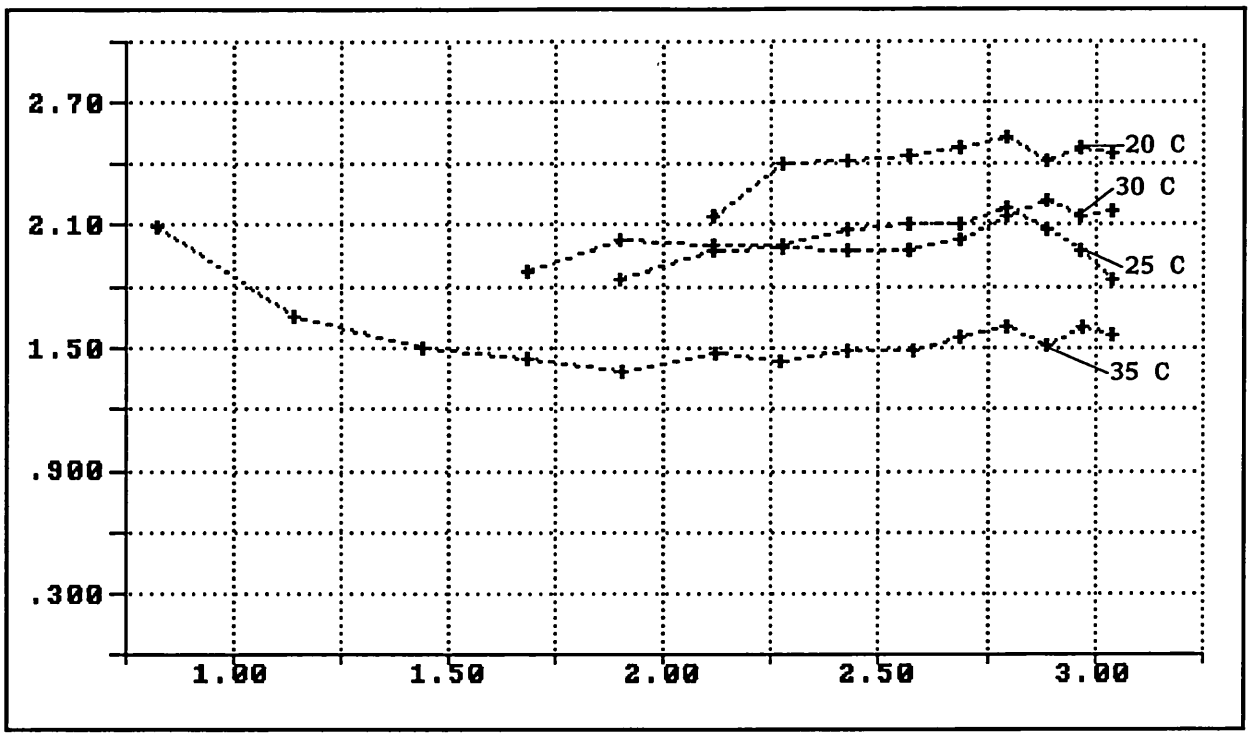
FIGURE 74b INFINITE SHEAR RATE INTERCEPT AT FOUR TEMPERATURES



Fluid 50LV/L35156
Temperature 30 C
Gaps Three Used

X Axis kV/mm
Y Axis kPa
Flow Rig

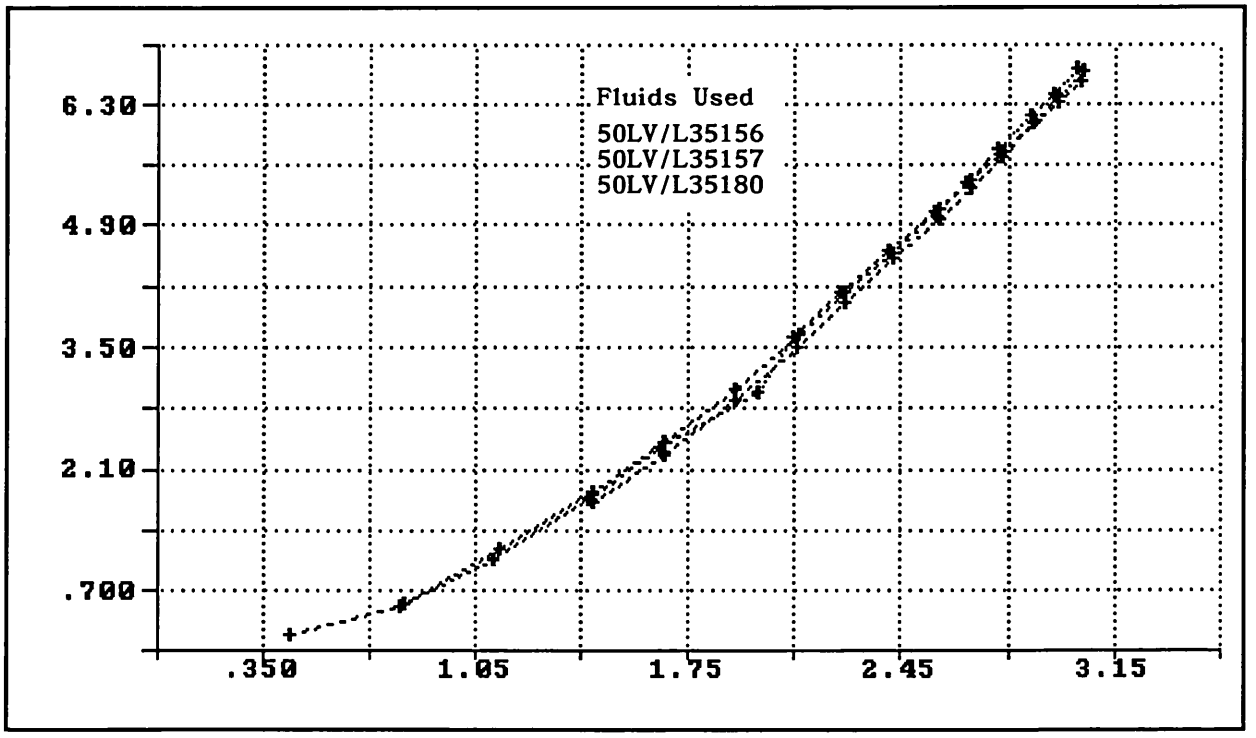
FIGURE 75a RELAXATION COEFFICIENT AT DIFFERENT TEMPERATURES



Fluid 50LV/L35156
Temperature 30 C
Gaps Three Used

X Axis kV/mm
Y Axis s *1e-4
Flow Rig

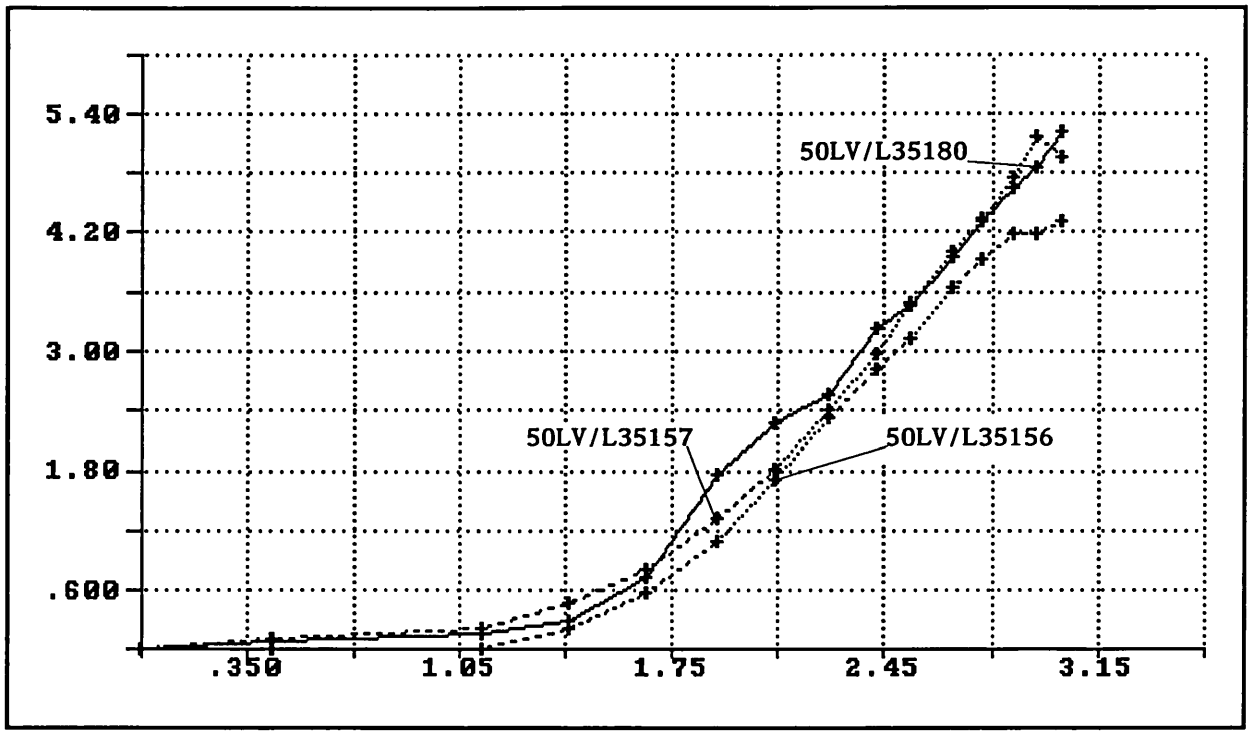
FIGURE 75b ZERO SHEAR RATE INTERCEPT FOR THREE FLUIDS



Fluids 50LV Based
Temperature 30 C
Gap 0.763 mm

X Axis kV/mm
Y Axis kPa
Flow Rig

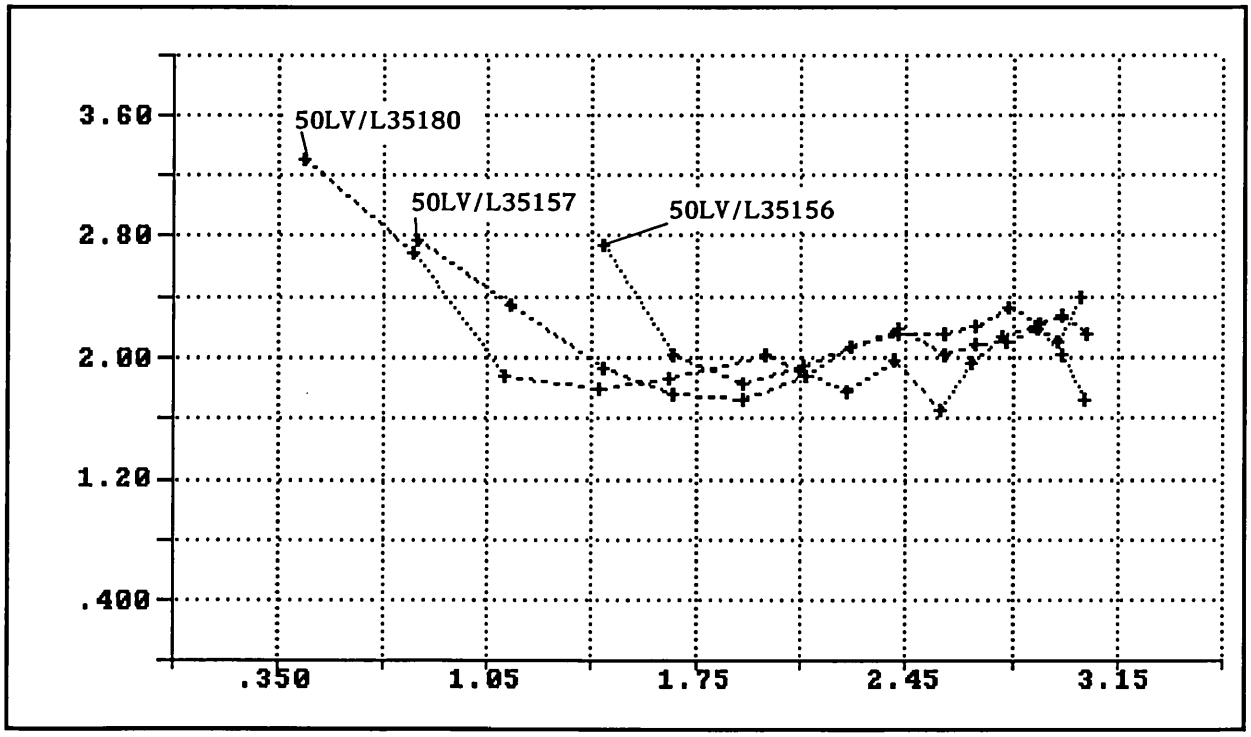
FIGURE 76a INFINITE SHEAR RATE INTERCEPT FOR THREE FLUIDS



Fluids 50LV Based
Temperature 30 C
Gaps Three Used

X Axis kV/mm
Y Axis kPa
Flow Rig

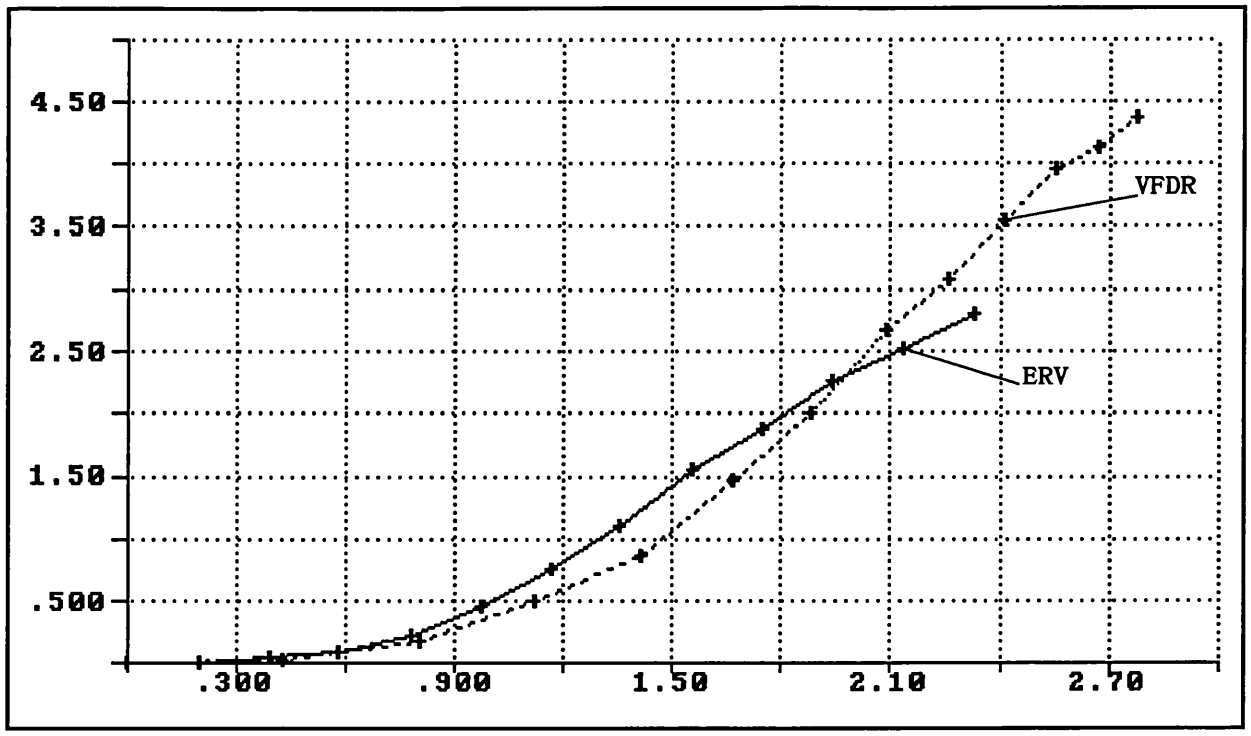
FIGURE 76b RELAXATION COEFFICIENT FOR THREE FLUIDS



Fluids 50LV Based
Temperature 30 C
Gaps Three Used

X Axis kV/mm
Y Axis s *1e-4
Flow Rig

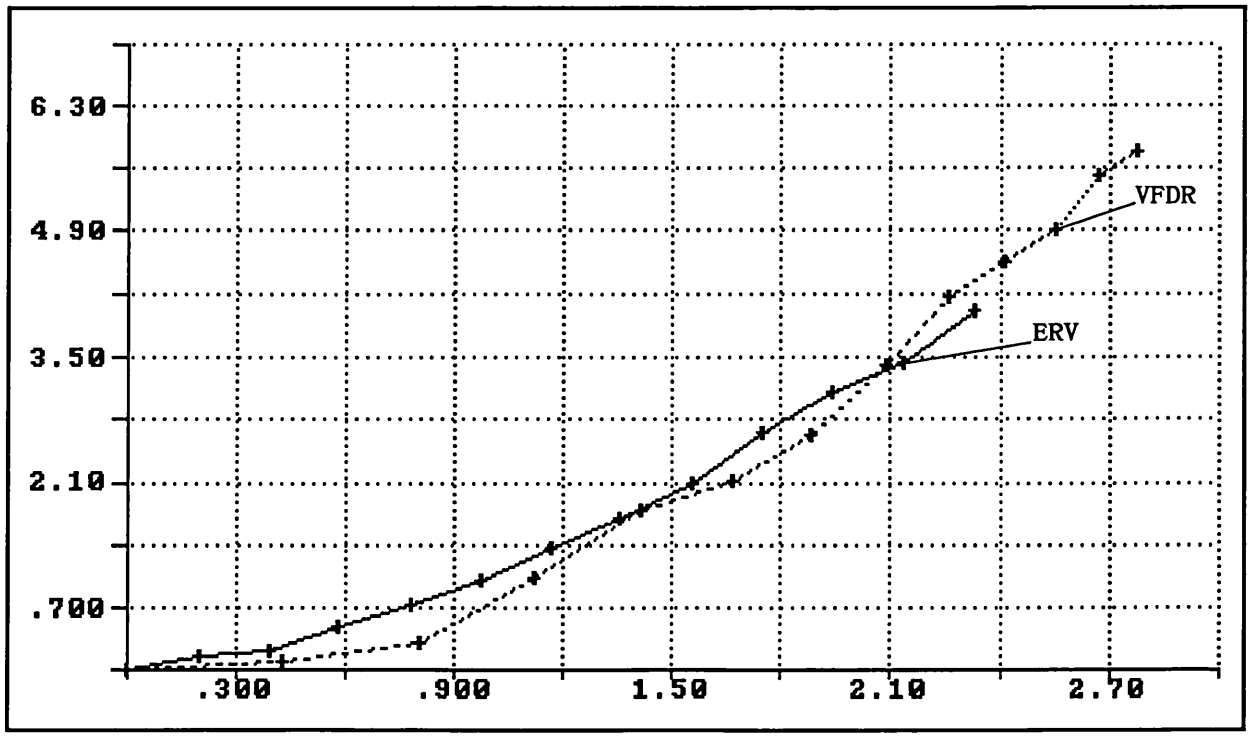
FIGURE 77a COMPARISON OF SHEAR STRESS FROM VFDR AND ERV



Fluid 50LV/L35180
Temperature 30 C

X Axis kV/mm
Y Axis kPa

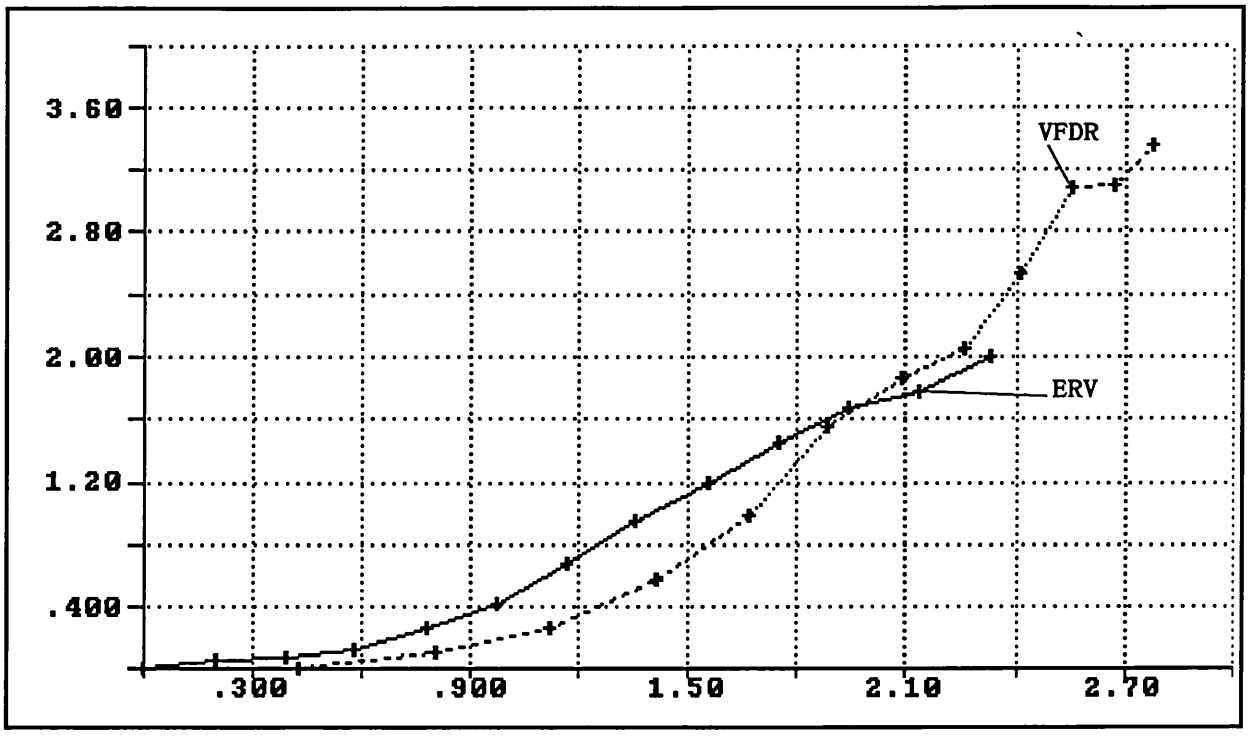
FIGURE 77b COMPARISON OF SHEAR STRESS FROM VFDR AND ERV



Fluid 50LV/L40180
Temperature 30 C

X Axis kV/mm
Y Axis kPa

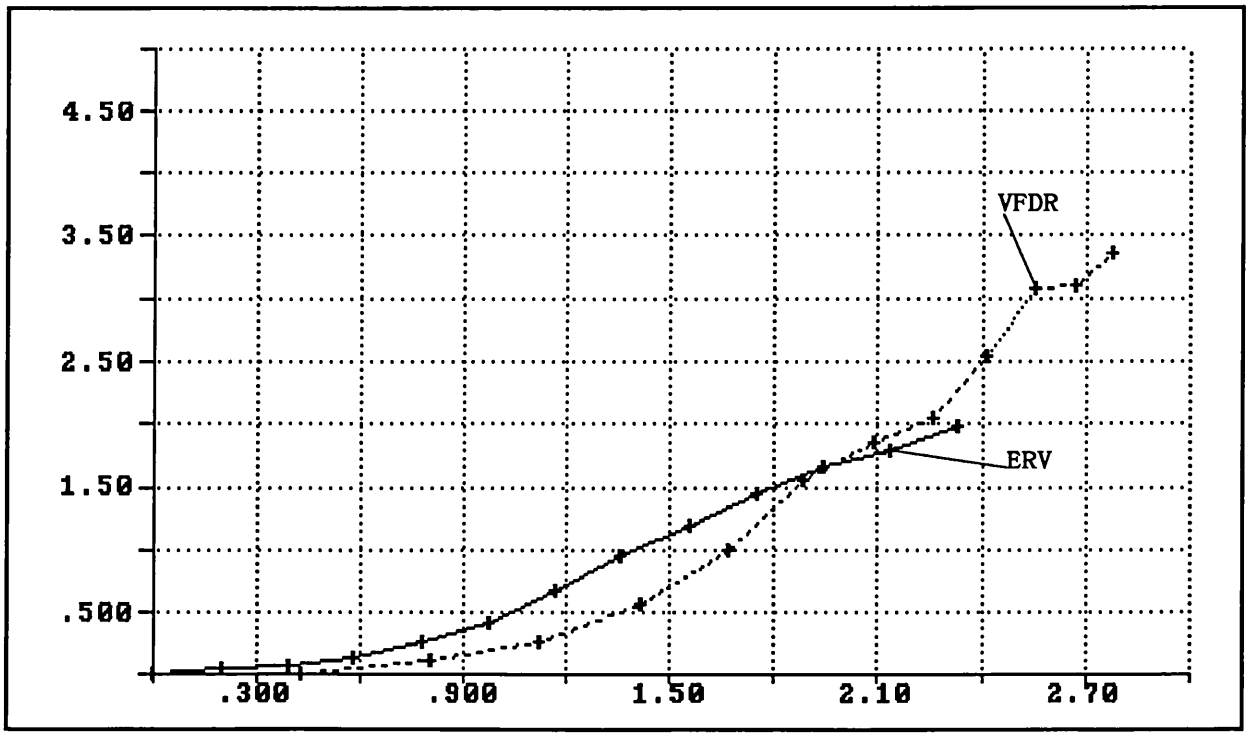
FIGURE 78a COMPARISON OF SHEAR STRESS FROM VFDR AND ERV



Fluid 50LV/L30180
Temperature 30 C

X Axis kV/mm
Y Axis kPa

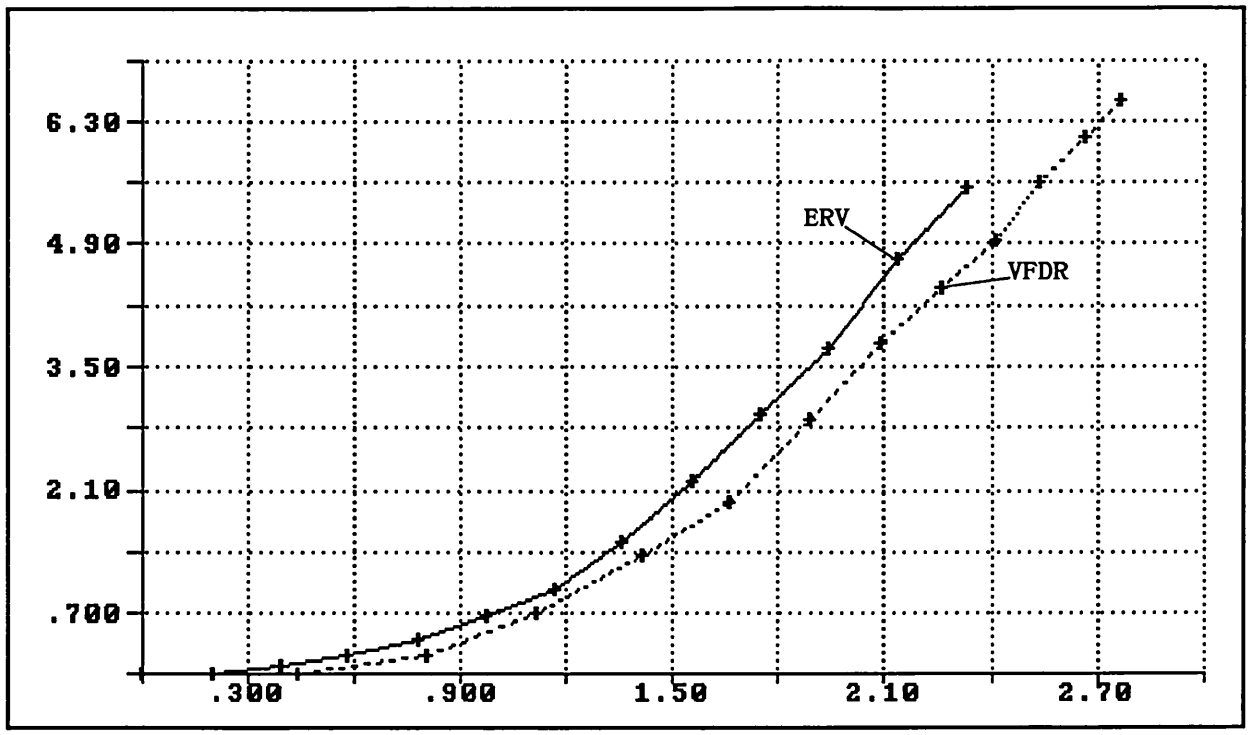
FIGURE 78b COMPARISON OF SHEAR STRESS FROM VFDR AND ERV



Fluid 50LV/L35180
Temperature 20 C

X Axis kV/mm
Y Axis kPa

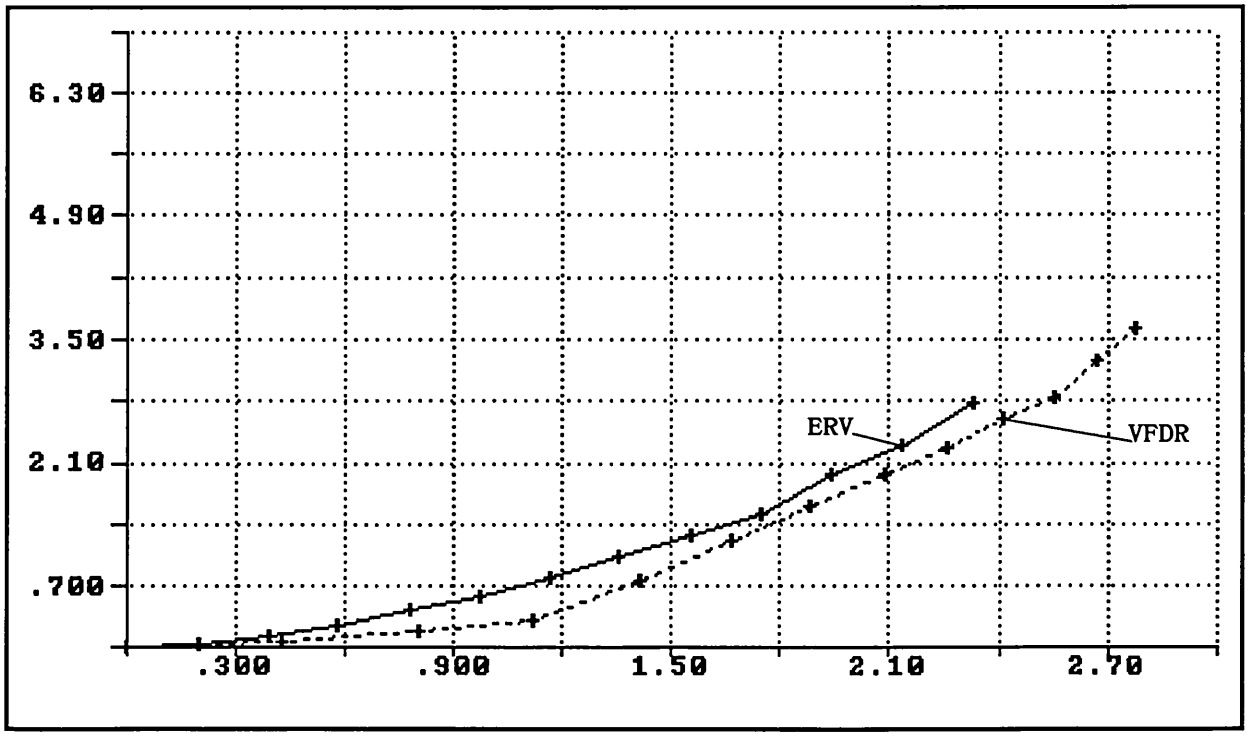
FIGURE 79a COMPARISON OF SHEAR STRESS FROM VFDR AND ERV



Fluid 50LV/L40180
Temperature 20 C

X Axis kV/mm
Y Axis kPa

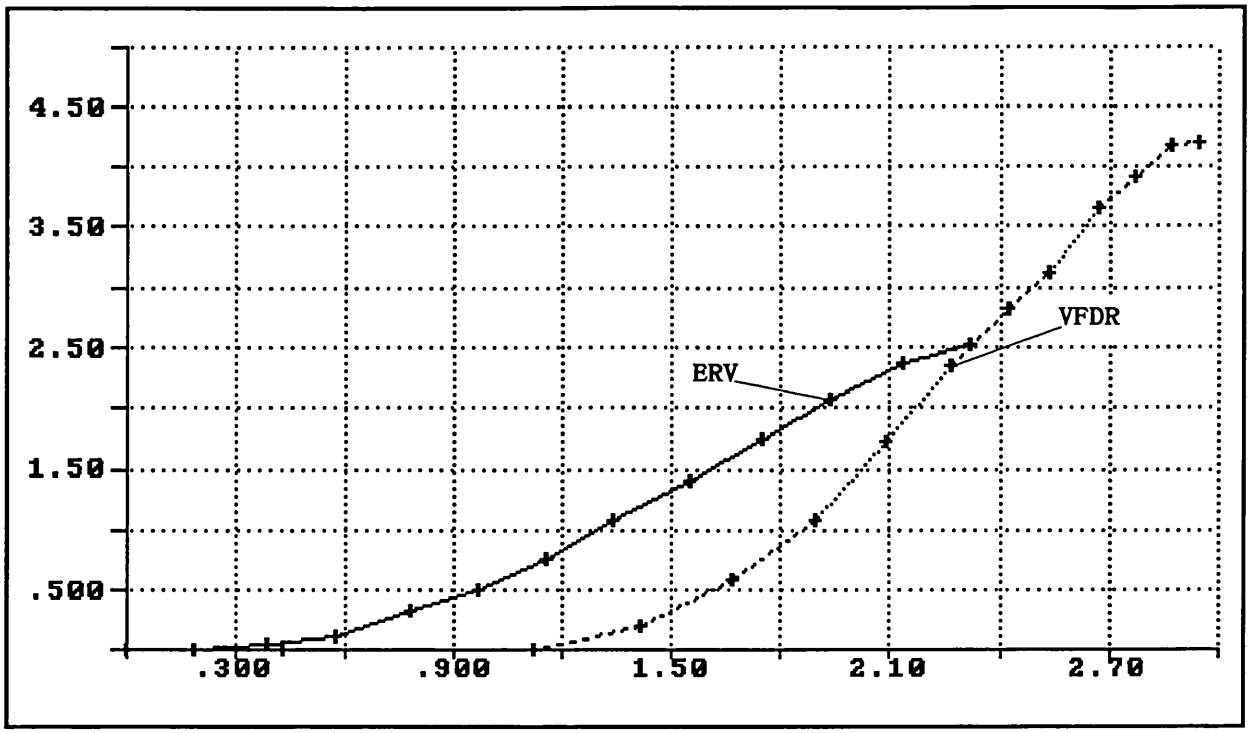
FIGURE 79b COMPARISON OF SHEAR STRESS FROM VFDR AND ERV



Fluid 50LV/L40180
Temperature 10 C

X Axis kV/mm
Y Axis kPa

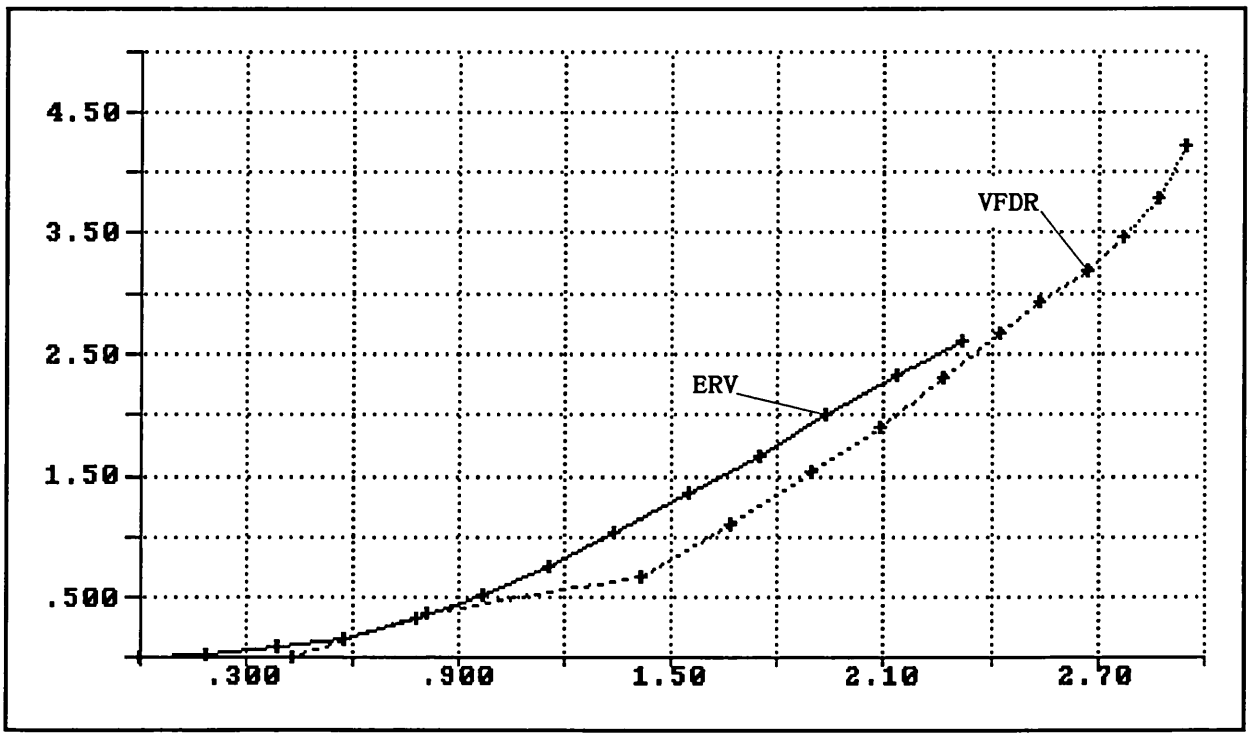
FIGURE 80a COMPARISON OF SHEAR STRESS FROM VFDR AND ERV



Fluid 50LV/L35156
Temperature 30 C

X Axis kV/mm
Y Axis kPa

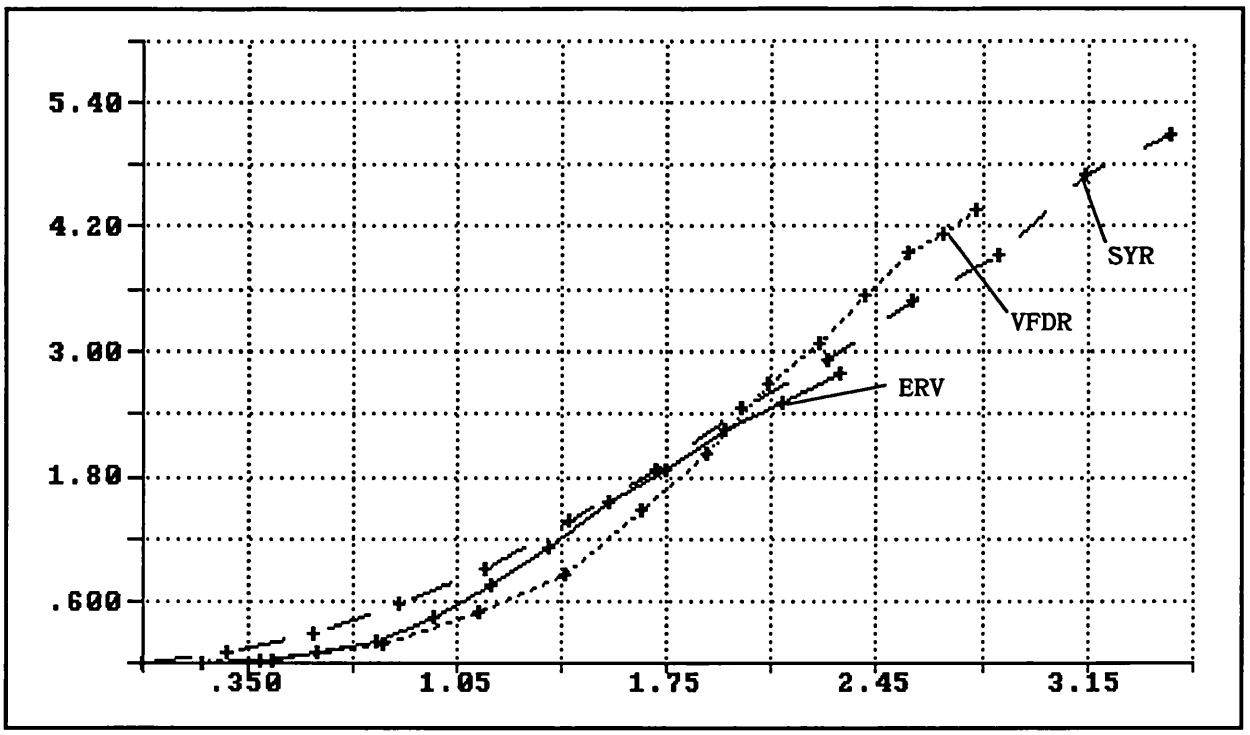
FIGURE 80b COMPARISON OF SHEAR STRESS FROM VFDR AND ERV



Fluid 50LV/L35135
Temperature 30 C

X Axis kV/mm
Y Axis kPa

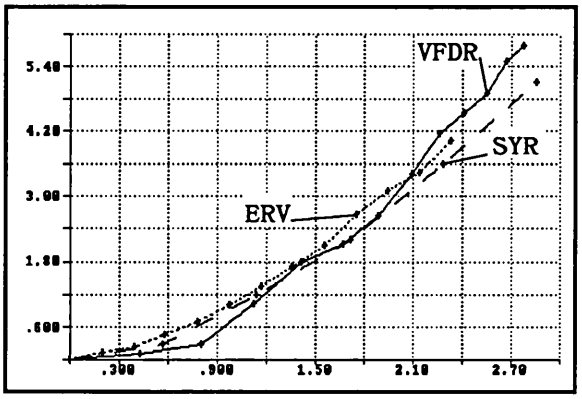
FIGURE 81a COMPARISON OF SHEAR STRESS FROM THREE TEST RIGS



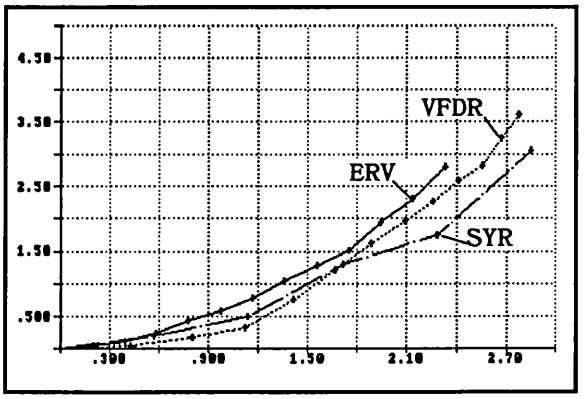
Fluid 50LV/L35180
Temperature 30 degC

X Axis kV/mm
Y Axis kPa

FIGURE 81b and 81c COMPARISON OF SHEAR STRESS FROM THREE TEST RIGS

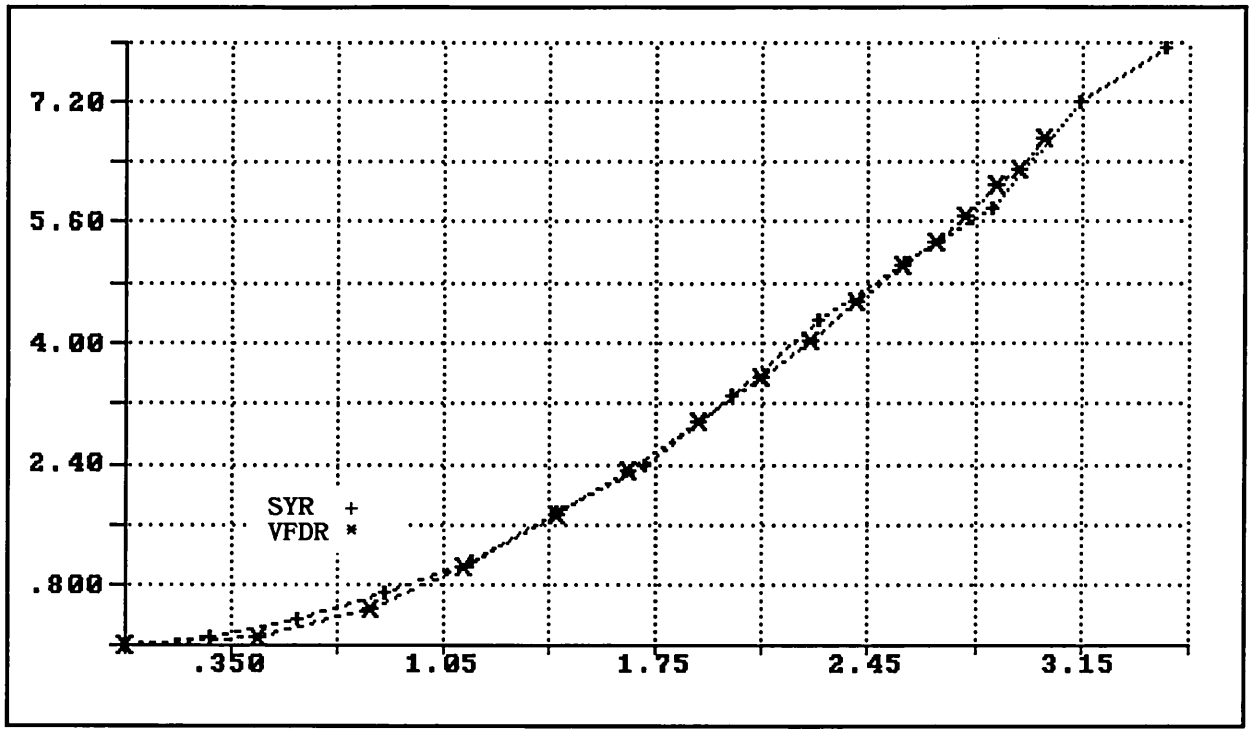


Fluid 50LV/L40180
Temperature 30 degC



Fluid 50LV/L35135
Temperature 30 degC

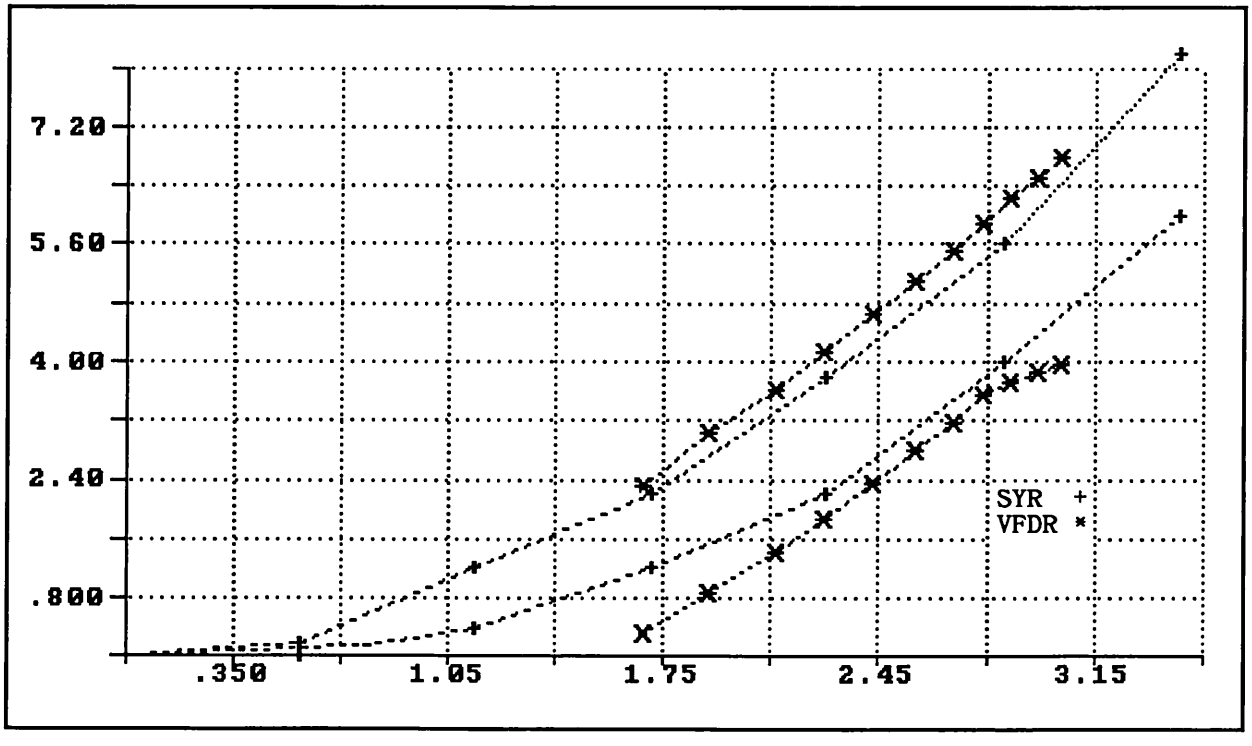
FIGURE 82a ZERO SHEAR STRESS and STATIC YIELD STRESS versus FIELD STRENGTH



Fluid 50LV/L35180
Temperature 30 C

X Axis kV/mm
Y Axis kPa

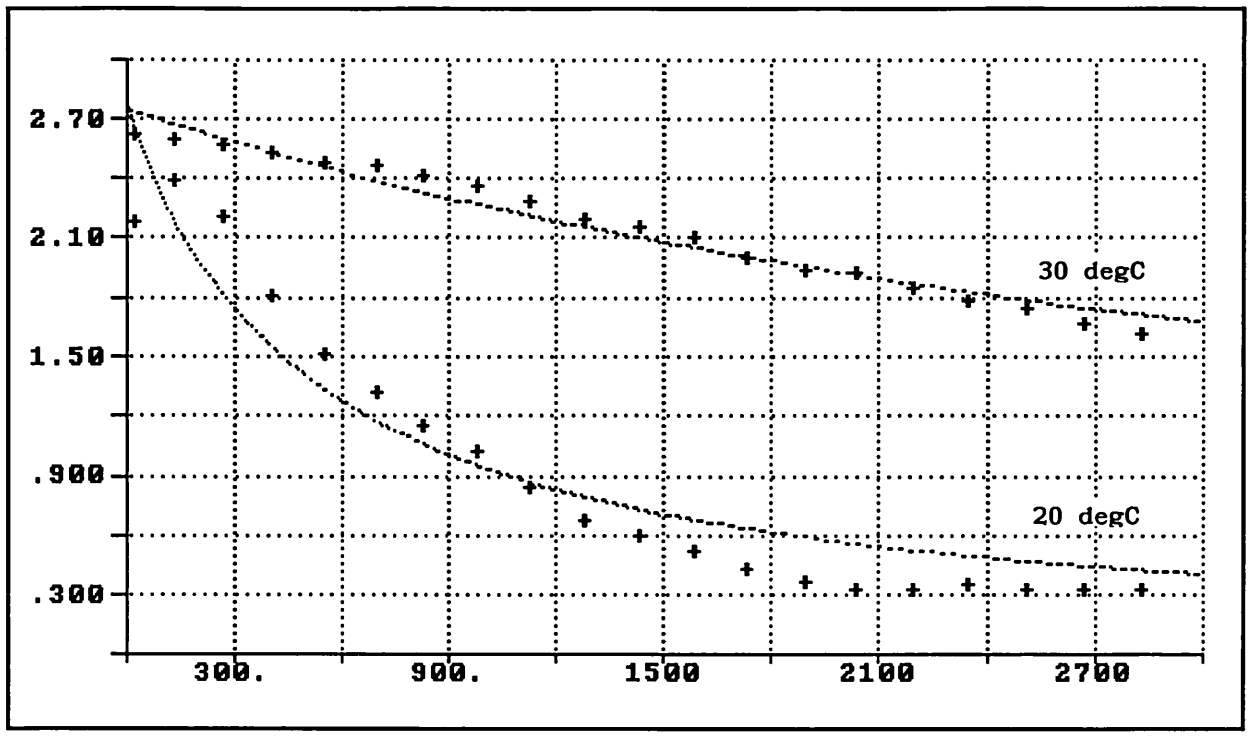
FIGURE 82b SHEAR STRESS PLOTS FOR VFDR and SYR



Fluid 50LV/L35156
Temperature 30 C

X Axis kV/mm
Y Axis kPa

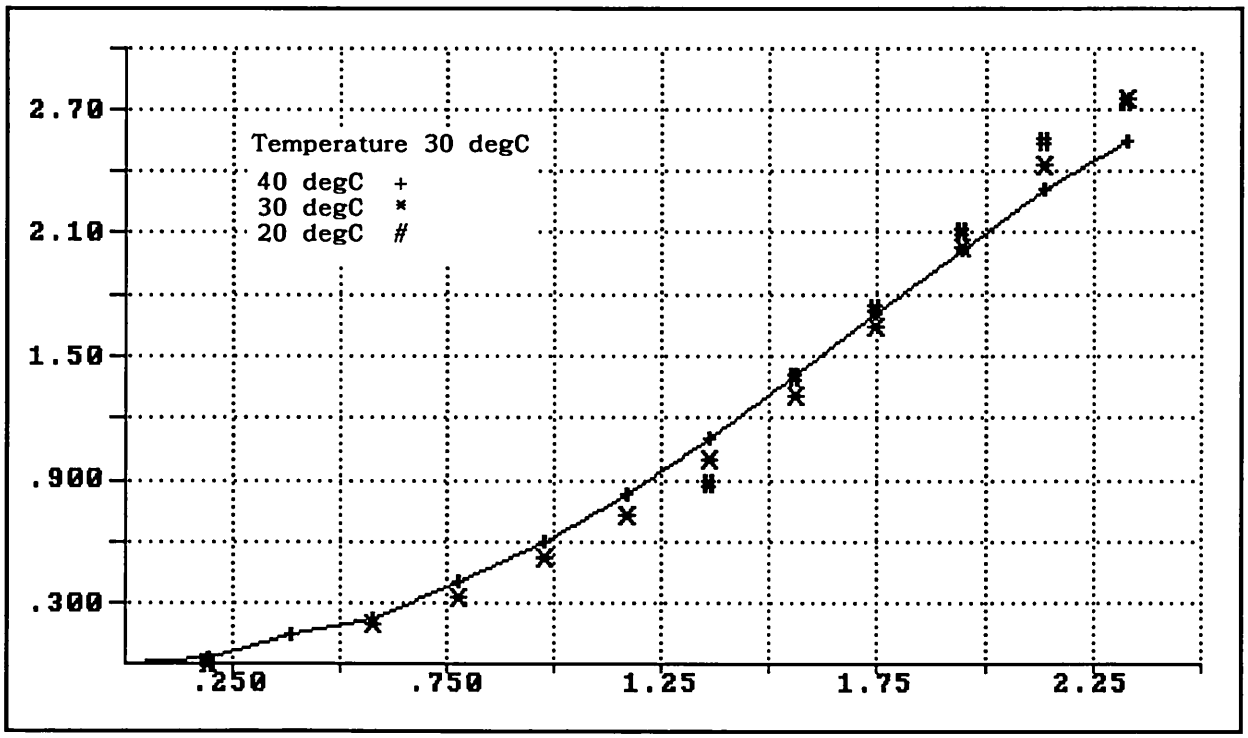
FIGURE 93a FIT OF EXCESS SHEAR STRESS DATA versus SHEAR RATE



Fluid 50LV/L35135
Field 2.34 kV/mm

X Axis sec-1
Y Axis kPa

FIGURE 93b FIT OF EXCESS SHEAR STRESS versus FIELD STRENGTH



Fluid 50LV/L35135

X Axis kV/mm
Y Axis kPa

FIGURE 94a STRUCTURAL PARAMETER "a" versus FIELD STRENGTH

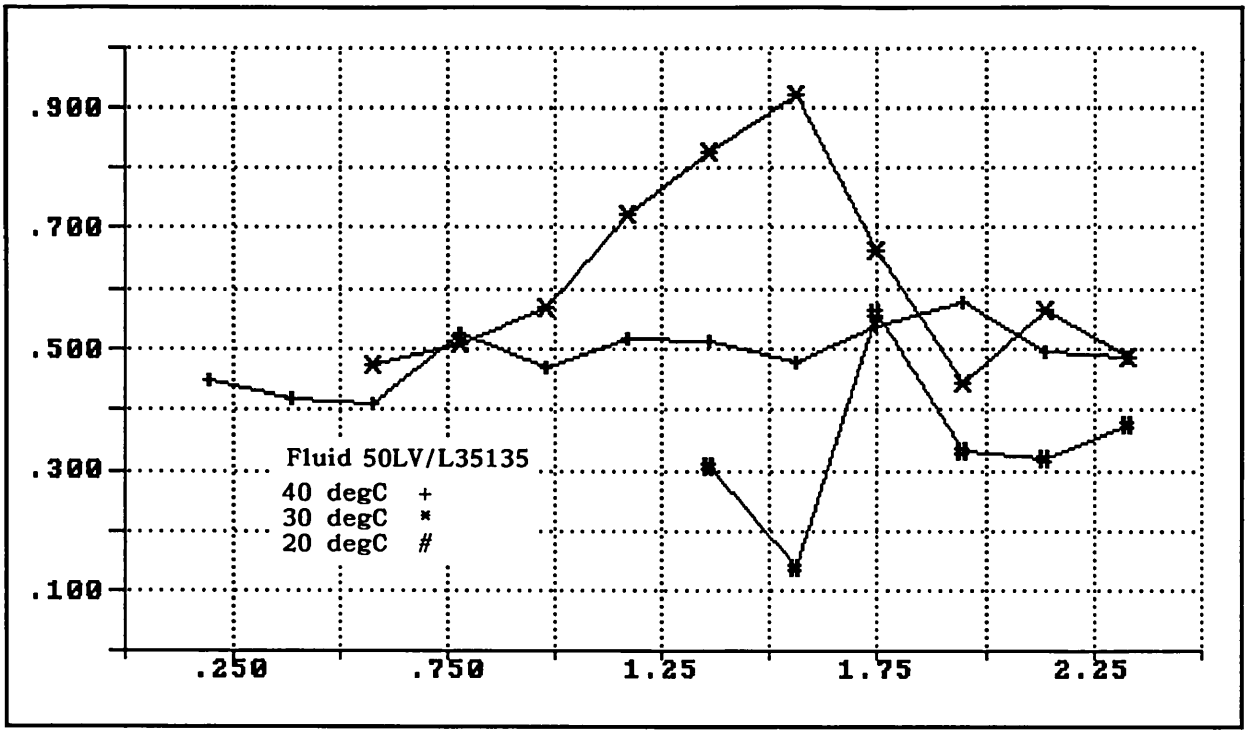


FIGURE 94b STRUCTURAL PARAMETER "b" versus FIELD STRENGTH

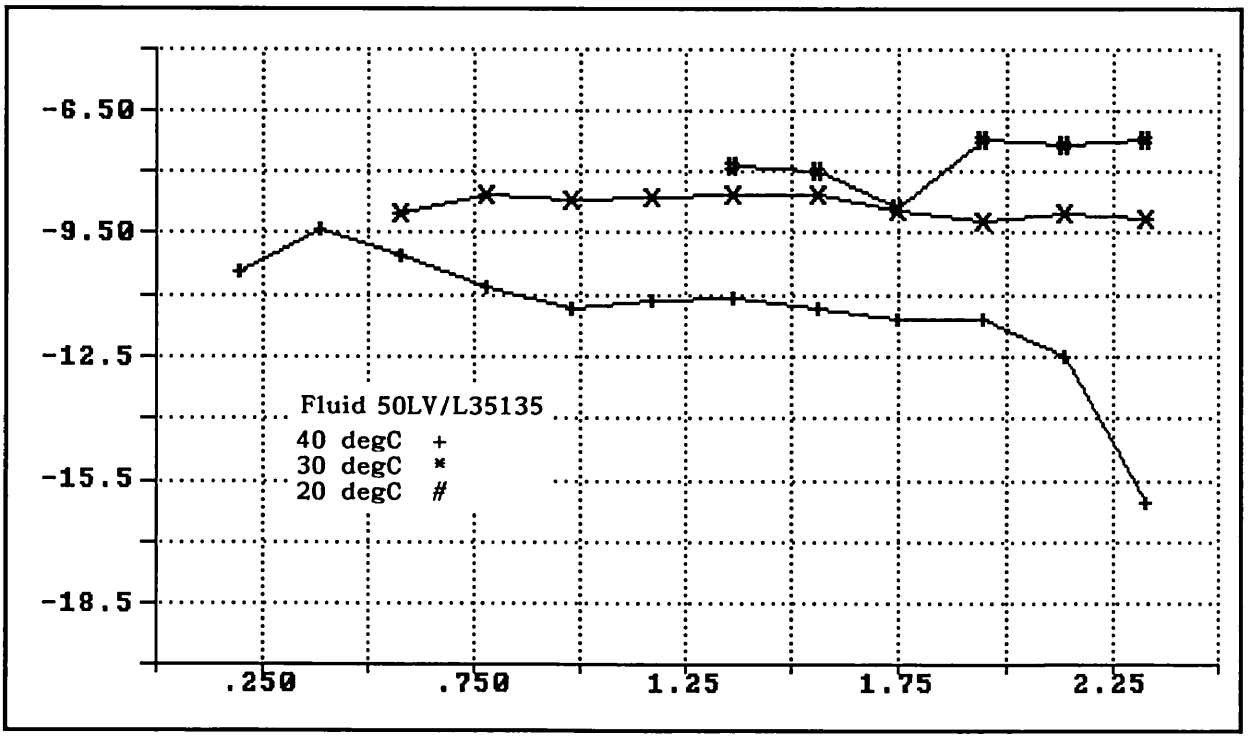
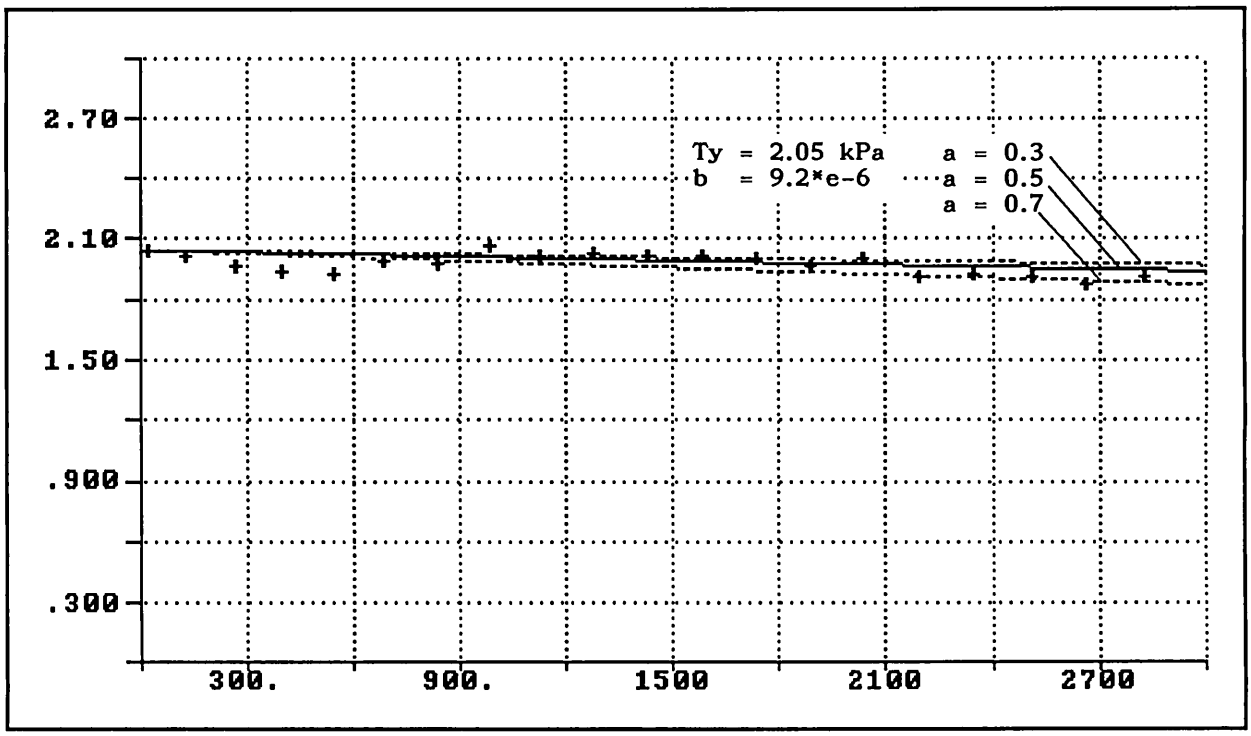


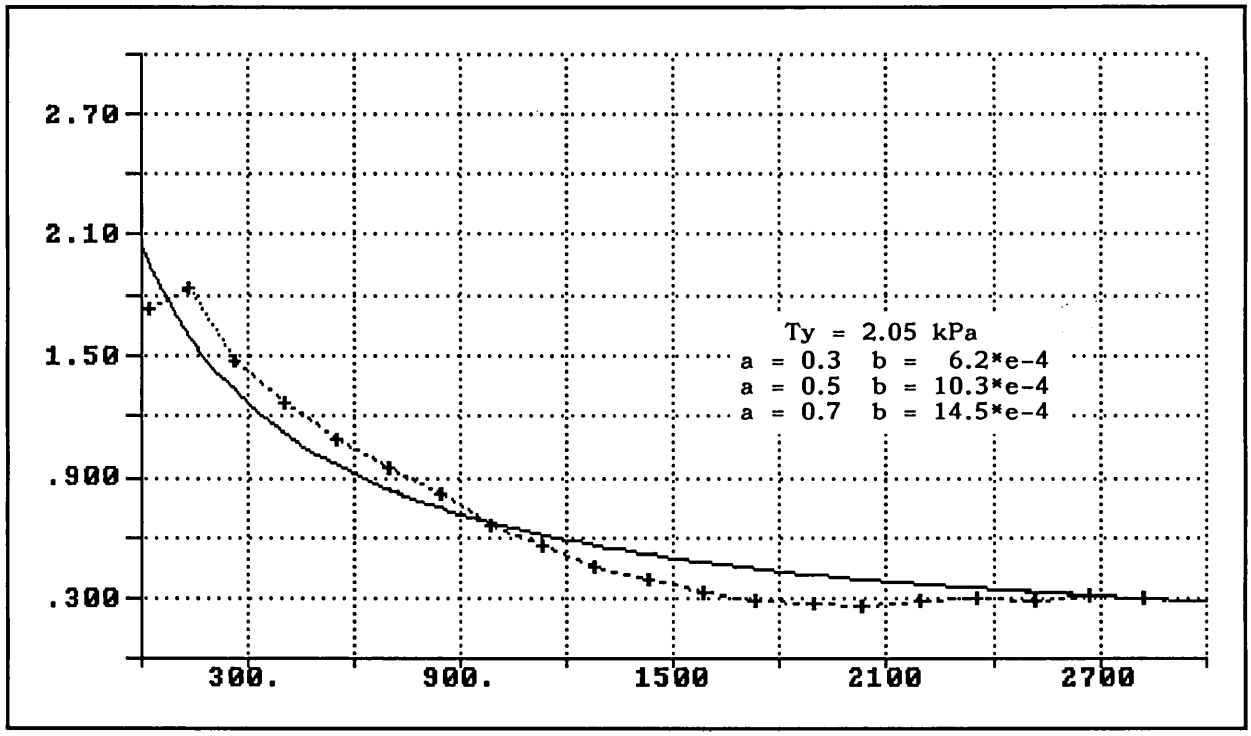
FIGURE 95a INFLUENCE OF STRUCTURAL PARAMETER ON FIT TO DATA



Fluid 50LV/L35135
Temperature 40 degC
Field 1.95 kV/mm

X Axis sec-1
Y Axis kPa
E.R.V.

FIGURE 95b INFLUENCE OF STRUCTURAL PARAMETER ON FIT TO DATA



Fluid 50LV/L35135
Temperature 20 degC
Field 1.95 kV/mm

X Axis sec-1
Y Axis kPa
E.R.V.